

Dissertation zur Erlangung des Doktorgrades der Fakultät Chemie und Pharmazie der  
Ludwig-Maximilians-Universität München

# Structural insights into bacterial ribosome rescue using cryo-EM



Claudia Müller  
aus Frankfurt am Main, Deutschland  
**2020**

## **Erklärung**

Diese Dissertation wurde im Sinne von §7 der Promotionsordnung vom 28. November 2011 von Herrn Prof. Dr. Daniel Wilson betreut.

## **Eidesstattliche Versicherung**

Diese Dissertation wurde eigenständig und ohne unerlaubte Hilfe erarbeitet.

Hamburg, den 10. Juni 2020

---

Claudia Müller

Dissertation eingereicht am 17. Juni 2020

1. Berichterstatter: Herr Prof. Dr. Daniel Wilson
2. Berichterstatter: Herr Prof. Dr. Roland Beckmann

Datum der Mündlichen Prüfung: 13. Juli 2020

## Table of Contents

Acknowledgements.....	I
List of original Publications.....	II
Contributions Report.....	III
List of abbreviations .....	IV
Summary.....	VII
1     Introduction.....	1
1.1     Structure of prokaryotic ribosomes.....	1
1.2     Translation cycle of prokaryotes .....	3
1.2.1     Translation Initiation.....	5
1.2.2     The Elongation Cycle .....	9
1.2.3     Translation Termination.....	22
1.2.4     Ribosome Recycling .....	29
1.3     Ribosome Rescue in Bacteria.....	31
1.4     Proline-rich antimicrobial peptides .....	47
2     Objective of these studies: Structural insights into bacterial ribosome rescue .....	55
3     Cumulative Thesis: Summary of Publications.....	57
3.1     Publication 1: Structural basis for ArfA-RF2-mediated translation termination on mRNAs lacking stop codons.....	57
3.2     Publication 2: Structural Basis for Ribosome Rescue in Bacteria .....	58
3.3     Publication 3: Mechanism of Ribosome Rescue by Alternative Ribosome Rescue Factor B.....	58
3.4     Publication 4: Release factor-dependent ribosome rescue by BrfA in the Gram-positive bacterium <i>Bacillus subtilis</i> .....	59
4     Discussion and Outlook .....	60
4.1     Alternative ribosome rescue factor A.....	60
4.2     Alternative ribosome rescue factor B.....	63

---

## Table of Contents

4.3	<i>Bacillus</i> ribosome recue factor A .....	68
4.4	Conclusion and Outlook.....	76
5	References.....	80
6	Publications.....	109

## Acknowledgements

First of all, I want to thank Prof. Daniel N. Wilson for giving me the opportunity to do my PhD studies in his lab. Thank you for your support, advice and patience during the last years. Also thank you for accepting my “owly-like” working rhythm even during tour de forces. I enjoyed working in your lab and actually missed modelling while writing the thesis.

Furthermore, I would like to thank Prof. Roland Beckmann for sharing chemicals, equipment and most importantly the Titan, as well as processing platforms with us. I would like to take the opportunity to thank the cryo-EM team including Dr. Otto Berninghausen, Susanne Rieder and Charlotte Ungewickell for preparing grids and collecting datasets. Furthermore, I would like to thank Dr. André Heuer, Dr. Thomas Becker and Lukas Kater for taking care of the cluster and computational issues, as well as André, Katharina Braununger and Hanna Kratzat for organisation of parties and events, Heidemarie Sieber, Andrea Gilmozzi and Joana Musial for keeping the lab stocked and organised. Thanks to the whole Beckmann group for sharing experience, support and great times at parties and conferences.

I want to thank Dr. Michael Graf and Dr. Paul Huter again for supervising me during my master thesis and Paul also for helping me getting started in cryo-EM. Thanks to Michael, Dr. Bertrand Beckert, Timm Koller and Caillan Crowe McAuliffe for taking care of the workstations. Additionally, I want to thank Daniela Hess-Otto, Katrin Möller and Tatjana Claußen for organisation of the lab, orders, solving organisational problems and providing help wherever they can, as well as Dr. Patrick Ziegelmüller and Dr. Meriem Rezgaoui for taking care of the practicals. Furthermore, I want to thank all present and former members of the Wilson lab, namely Dr. Stefan Arenz, Dr. Daniel Sohmen, Michael, Paul, Dr. Fabian Nguyen, Dr. Maha Abdelshahid, Karoline Raulf, Maximiliane Wieleand, Agnieszka Pochopien-Pobel, Timm, Caillan and Bertrand, as well as our guest scientists Dr. Mario Mardirossian, Dr. Hani Zaher and Tony Bougas for the great atmosphere in the lab, discussions and fun times during breaks, conferences and parties, with special thanks to Maxi and Aga.

Furthermore, I want to thank my students Julia Boshart, Max Berger and Nestor Pryszlak for their encouragement and great work. Max additionally for saving me many hours in the lab during his Hiwi job and also thanks to our former Hiwis Sabine Oganesian and Lorenzo Schwerdtfeger (hope I remember the spellings correctly).

Finally, I want to thank my family and friends, for always being supportive and caring, which is especially true for my parents.

## List of original Publications

### Publication 1

Huter, P.\*, **Müller, C.\***, Beckert, B., Arenz, S., Berninghausen, O., Beckmann, R., and Wilson, D.N. (2017). Structural basis for ArfA-RF2-mediated translation termination on mRNAs lacking stop codons. *Nature* 541, 546-549.

### Publication 2

Huter, P., **Müller, C.**, Arenz, S., Beckert, B., and Wilson, D.N. (2017). Structural Basis for Ribosome Rescue in Bacteria. *Trends Biochem Sci* 42, 669-680.

### Publication 3

Chan, K.H., Petrychenko, V., **Müller, C.**, Maracci, C., Holtkamp, W., Wilson, D.N., Fischer, N., and Rodnina, M.V. (accepted). Mechanism of Ribosome Rescue by Alternative Ribosome-Rescue Factor B. *Nature Communications*.

### Publication 4

Shimokawa-Chiba, N.\*, **Müller, C.\***, Fujiwara, K., Beckert, B., Ito, K., Wilson, D.N., and Chiba, S. (2019). Release factor-dependent ribosome rescue by BrfA in the Gram-positive bacterium *Bacillus subtilis*. *Nature Communications* 10, 5397.

### Publications not included in the thesis:

### Publication 5

Mardirossian, M., Barriere, Q., Timchenko, T., **Müller, C.**, Pacor, S., Mergaert, P., Scocchi, M., and Wilson, D.N. (2018). Fragments of the Nonlytic Proline-Rich Antimicrobial Peptide Bac5 Kill *Escherichia coli* Cells by Inhibiting Protein Synthesis. *Antimicrob Agents Chemother* 62, e00534-00518.

### Publication 6

Mardirossian, M., Pérébaskine, N., Benincasa, M., Gambato, S., Hofmann, S., Huter, P., **Müller, C.**, Hilpert, K., Innis, C.A., Tossi, A., et al. (2018). The Dolphin Proline-Rich Antimicrobial Peptide Tur1A Inhibits Protein Synthesis by Targeting the Bacterial Ribosome. *Cell Chemical Biology* 25, 530-539.e537.

## Contributions Report

This dissertation comprises the work, which was performed during my PhD research from February 2016 till June 2020 in the lab and under supervision of Prof. Daniel N. Wilson at the Gene Center of the Ludwig-Maximilians University Munich and the Institute of Biochemistry and Molecular Biology at the University of Hamburg. Most projects were done in collaboration with scientists from the labs of Roland Beckmann (Munich, Germany), Shinobu Chiba (Kyoto, Japan), Niels Fischer and Marina V. Rodnina (both Göttingen, Germany).

### **Publication 1 (Huter et al., 2017)**

The publication describes the mechanism of ribosome rescue of a non-stop complex by alternative ribosome rescue factor A and release factor 2. I purified both factors, tested their activity and bound them to the non-stop complex for cryo-EM. Furthermore, I was involved in sample preparation, processing of the cryo-EM dataset, manuscript preparation and preparation of supplementary figures 1, 5 and 6.

### **Publication 2 (Huter et al., 2017)**

This publication reviews the mechanism of ribosome rescue systems known to that date, with focus on ArfA. Similarities, differences and known biochemical data were discussed. I was involved in preparation of the manuscript, as well as figures 4 and 6.

### **Publication 3 (Chan et al., accepted)**

The publication illustrates the mode of action of ArfB on the *Escherichia coli* ribosome in dependence of the mRNA length kinetically and structurally. I was involved in processing and modelling of the P+0 dataset.

### **Publication 4 (Shimokawa-Chiba et al., 2019)**

This publication comprises the identification and characterisation of a new ribosome rescue factor in *Bacillus subtilis*, termed *Bacillus* ribosome rescue factor A, which cooperates with release factor 2. The factor is characterised biochemically and structurally. I prepared the sample for cryo-EM and was involved in processing and building models for both factors, as well as modelling and refinement of the whole complex. Furthermore, I was involved in the interpretation of the data, manuscript preparation and preparation of main figures 4, 5 and 6, as well as supplementary figures 2 and 3. Additionally, I prepared supplementary figure 5 till 8.

## List of abbreviations

A	adenine
aa	amino acid
aa-tRNA	aminoacyl-tRNA
Ala	alanine
AMP	antimicrobial peptide
Api	apidaecin
ArfA	alternative ribosome rescue factor A
ArfB	alternative ribosome rescue factor B
ArfT	alternative ribosome rescue factor T
Arg/R	arginine
A-site/-tRNA	acceptor site/tRNA
ASL	anticodon stem loop
ATP	adenosine-5'-triphosphate
bp	base pair
BrfA	<i>Bacillus</i> ribosome rescue factor A
<i>B. subtilis</i>	<i>Bacillus subtilis</i>
C	cytosine
CTD	C-terminal domain
cryo-EM	cryo electron microscopy
DC	decoding center
DNA	deoxyribonucleic acid
EC	elongation complex
<i>E. coli</i>	<i>Escherichia coli</i>
EF-G	translation elongation factor GTPase
EF-Tu	translation elongation factor thermo unstable
E-site/-tRNA	exit site/tRNA
fMet	formyl-methionine
G	guanine
GGQ-motif	glycine-glycine-glutamine motif
Gln	glutamine
GTP	guanosine-5'-triphosphate

GTPase	guanosine-5'-triphosphatase
h#	helix # of the small ribosomal subunit
H#	helix # of the large ribosomal subunit
<i>H. marismortui</i>	<i>Haloarcula marismortui</i>
IC	initiation complex
IF	initiation factor
kDa	kilodalton
KSIE	kinetic solvent isotope effect
LSU	large ribosomal subunit
Lys	lysine
MDa	megadalton
MIC	minimal inhibitory concentration
mRNA	messenger RNA
NTD	N-terminal domain
ORF	open reading frame
P <sub>i</sub>	inorganic phosphate
PIC	pre-initiation complex
POST	post-translocation
PoTC	post-termination complex
PrAMP	proline-rich antimicrobial peptide
PRE	pre-translocation
P-site/-tRNA	peptidyl site/tRNA
PTC	peptidyl transferase center
RF	peptide chain release factor
RNA	ribonucleic acid
RNC	ribosome nascent chain complex
rProtein	ribosomal protein
RRF	ribosome recycling factor
rRNA	ribosomal RNA
SD-sequence	Shine-Dalgarno sequence
SRC	stalled ribosome complex
SRL	sarcin-ricin loop
SSU	small ribosomal subunit

T	thymine
tmRNA	transfer-messenger RNA
tRNA	transfer RNA
<i>T. thermophilus</i>	<i>Thermus thermophilus</i>
U	uracil
UTP	uracil-5 <sup>c</sup> -triphosphate
wt	wild-type

## Summary

The ribosome is a ribonucleoprotein complex, which translates the genetic information stored in the mRNA in form of codons into a protein. It consists of a large and a small subunit, which form the bacterial 70S ribosome during initiation of translation. In subsequent elongation the polypeptide chain is extended until a stop-codon marks the end of the open reading frame. During the following termination the newly synthesised protein is released from the ribosome by release factor 1 or 2. Afterwards, the ribosome is recycled into subunits and returns to the pool of free subunits that can engage a new round of translation.

Prolonged stalling of the 70S ribosome at any step of the translation cycle can induce cleavage of the mRNA directly in the A-site of the ribosome, leaving so-called non-stop complexes. Accumulation of non-stop complexes depletes ribosomes from the pool of free subunits, which lastly inhibits translation and leads to cell death. Hence, bacteria have evolved specialized mechanisms that recognise and resolve non-stop complexes. The major and best characterised ribosome rescue mechanism is *trans*-translation, which is found in all known bacterial genomes. However, some bacteria have additional backup mechanisms that ensure survival when *trans*-translation is overwhelmed or defective. Using cryo-electron microscopy we investigated the mechanisms of ribosome rescue by the backup systems. First, we obtained a reconstruction of alternative ribosome rescue factor A (ArfA) and release factor 2 on a non-stop complex. Our structure shows that ArfA monitors the mRNA entry channel on the SSU with its C-terminus, while the N-terminus mediates recruitment and activation of release factor 2 in a stop-codon independent manner. This leads to release of the nascent chain from the tRNA and recycling of the ribosome. Furthermore, we investigated the mechanism of alternative ribosome rescue factor B (ArfB) regarding the mRNA length. ArfB can perform hydrolysis itself and the activity decreases with increasing length of the mRNA overhang. Our results show that ArfB binds to non-stop ribosomes without mRNA overhang and with nine mRNA nucleotides occupying the mRNA entry channel in the same way and that the mRNA overhang has moved out of the tunnel. Lastly, we obtained a structure of a recently identified backup mechanism of *Bacillus subtilis*, termed *Bacillus* ribosome rescue factor A (BrfA), which represents the first backup mechanism in a Gram-positive bacterium. BrfA specifically cooperates with *B. subtilis* release factor 2. As evident from our reconstruction, BrfA recruits release factor 2 in a similar manner compared to ArfA, but differs regarding the activation mechanism.

## 1 Introduction

The hypothesis of the central dogma of biochemistry was proposed almost sixty years ago and describes the workflow of genetic information maintenance and expression. The genetic information is stored in long DNA (deoxyribonucleic acid) polymers in the form of genes and the process of DNA replication, by a DNA-dependent DNA-polymerase, facilitates the preservation of the information. Two sequential steps achieve gene expression, namely transcription and translation. During transcription the gene sequence of the DNA is transcribed by a DNA-dependent RNA-polymerase into ribonucleic acid (RNA). RNA molecules have various functions in the cell, for instance they can act as scaffolds or adapters, regulate gene expression or even carry out enzymatic reactions by themselves (ribozymes). One category of RNAs is messenger RNA (mRNA), which is translated into an amino acid polymer, called protein, in the second step of gene expression by a macromolecular machine, the ribosome. During translation the ribosome reads the universal genetic code of the mRNA, which is composed of base triplets, and adds the cognate amino acids one after another to the nascent polypeptide chain. In this process, transfer RNAs (tRNAs) serve as adapters for amino acids (aa) and enable code deciphering. The end of the coding sequence is defined by a stop codon and leads to the release of the protein from the ribosome. There are certain cases where no in-frame stop codon is present and prokaryotic and eukaryotic cells have evolved different strategies to cope with this situation. Furthermore, translation is a critical process in the cell and higher eukaryotes have developed defence mechanisms against bacterial infections that also target the ribosome. Although the function and basic architecture of the ribosome is conserved in all three domains of life, there are species-specific differences and the ribosome-targeting defence mechanisms of eukaryotes affect not all bacteria to the same extend.

### 1.1 Structure of prokaryotic ribosomes

Prokaryotic ribosomes consist of two subunits, the 50S subunit (large subunit, LSU; 60S in eukaryotes) and the 30S subunit (small subunit, SSU; 40S in eukaryotes). Both ribosomal subunits associate to build the fully assembled 2.5 megadalton (MDa) 70S ribosome (80S in eukaryotes; Figure 1a). Each subunit consists of ribosomal RNA (rRNA) and ribosomal proteins (rProteins). While the intersubunit interface is predominantly composed of rRNA, the rProteins reside on the surface of the subunits and have long extensions that reach into the

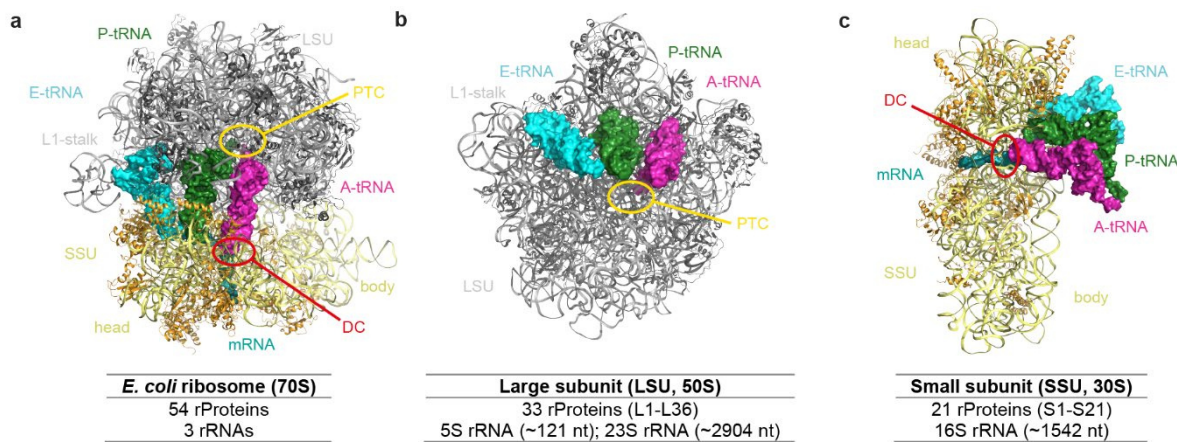


**Figure 1: Structure of the Prokaryotic Ribosome.** (a) 70S complex of the prokaryotic ribosome with mRNA (teal) and tRNAs (A-tRNA, pink; P-tRNA, green; E-tRNA, cyan), LSU: large ribosomal subunit (23S rRNA, gray70; ribosomal proteins, gray30), SSU: small ribosomal subunit (16S rRNA, yellow; ribosomal proteins, orange), PTC: peptidyl transferase center, DC: decoding center. (b) Intersubunit interface view of the 50 S subunit with bound tRNAs. (c) View from the A-site on the 30S subunit with mRNA and tRNAs. The figure was prepared using PDBID 5JTE (Arenz et al., 2016).

subunits. The LSU consists of 5S rRNA (~120 nucleotides), 23S rRNA (~2,900 nucleotides) and about 30 rProteins (Figure 1b), whereas the SSU is composed of 16S rRNA (~1,500 nucleotides) and around 20 rProteins (Figure 1c). The subunits have different tasks during the translational cycle: the SSU binds the mRNA in an inter-domain cleft between head and body, and harbours the decoding center (DC), where the message stored in the mRNA is decrypted with the help of tRNAs. The LSU harbours the peptidyl transferase center (PTC), which is the catalytic center for the main reactions of protein synthesis, peptide bond formation and peptide release. The PTC (and also the DC) consists predominantly of rRNA, which lead to the suggestion that the ribosome is not only a macromolecular machine but also a ribozyme (Ban et al., 2000; Nissen et al., 2000; Schmeing et al., 2002). In the vicinity of 8-10 Angstroms (Å) to the PTC is only the N-terminus of rProtein L27 (Voorhees et al., 2009). L27 is not essential in *Escherichia coli* (*E. coli*), although deletion of L27 or even truncation of the N-terminus results in a severely decreased growth rate and reduction of the PTC function (Wower et al., 1998; Maguire et al., 2005). This is supported by a structural study, which concludes that L27 is involved in proper positioning of the tRNA and a proton wire mechanism permitting peptide bond formation (Polikanov et al., 2014). However, a kinetic study showed that deletion of L27 had only little effect on peptide bond formation (Maracci et al., 2015).

The distance between the DC and the PTC is spanned by tRNAs, which possess an anticodon that specifically recognizes the codon of the mRNA in the DC, and carry the cognate amino acid (Carter et al., 2000; Schluenzen et al., 2000; VanLoock et al., 2000; Ogle et al., 2001; Yusupova et al., 2001). The ribosome harbours three tRNA binding sites and after initiation where the initiator tRNA is placed in the P-site, the tRNAs move sequentially from the acceptor

site (A-site) to the peptidyl site (P-site) and eventually to the exit site (E-site). Incoming aminoacyl-tRNA (aa-tRNA) is delivered to the ribosomal A-site, harbouring the DC in the SSU and the A-site part of the PTC in the LSU. The nascent polypeptide chain is attached to the peptidyl-tRNA (P-tRNA), which is temporary bound to the P-site. For peptide bond formation the A- and P-site tRNAs come in close proximity within the PTC. After peptide bond formation the ribosome engages hybrid states, tRNAs move to the next site during translocation mediated by EF-G and deacylated tRNA leaves the ribosome *via* the E-site (Yusupov et al., 2001; Schuwirth et al., 2005; Selmer et al., 2006). The end of the nascent polypeptide is marked by a stop-codon, which is not recognized by a tRNA, instead a release factor binds to the A-site and hydrolyses the polypeptide from the P-tRNA (reviewed by Schmeing and Ramakrishnan (2009)).

## 1.2 Translation cycle of prokaryotes

The translation cycle in all three domains of life is divided into four major steps: initiation, elongation, termination and recycling. Not all translation factors involved in the cycle are homologous to each among the different domains of life. Translation initiation in eukaryotes in particular is more complex and involves additional factors compared to bacterial initiation. Furthermore, eukaryotic/archaeal and prokaryotic peptide chain release factors are evolutionary unrelated, and with respect to this the recycling mechanism differs as well.

Successful protein synthesis in bacteria is dependent on the exact definition of the open reading frame (ORF) of the protein, as well as efficient translation, which includes proper charging of tRNA with amino acids by aminoacyl-tRNA synthetases. The ORF of a bacterial protein is defined in its mRNA by a start codon (usually AUG) and one of the three stop codons (UAA, UAG or UGA), with the actual coding sequence embedded in between as nucleotide triplets (codons). The mRNA is read by the ribosome from the 5' to the 3' end and can have regulatory elements in the 5' and/or 3' untranslated regions (UTR). One example is the Shine-Dalgarno (SD) sequence present in many prokaryotic mRNAs four to seven nucleotides upstream of the start codon in the 5' UTR (Shine and Dalgarno, 1974; Chen et al., 1994). During translation initiation placement of the start codon into the P-site of the SSU is aided by the SD sequence. Before association of the LSU the initiator tRNA ( $tRNA_i^{fMet}$ ) is recruited to the P-site and pairs with the start codon. The initiator tRNA carries a formylated methionine (fMet), which will be the first amino acid (aa) of the new polypeptide. The formylation distinguishes the methionine (Met) from ordinary Met used in subsequent elongation, where the polymerization of the

polypeptide occurs. During each round of elongation one amino acid is added C-terminally to the nascent polypeptide chain by the ribosome with a translational rate of ~4-22 aa per second (Sørensen and Pedersen, 1991; Proshkin et al., 2010; Wohlgemuth et al., 2010). Assuming an average length of about 300 aa for an *E. coli* protein (Netzer and Hartl, 1997; Allan Drummond and Wilke, 2009), the production of the protein takes only 14-75 s. Translation termination occurs when one of the three stop codons enter the ribosomal A-site. The codon is recognized by a peptide chain release factor (RF), which hydrolyses the nascent polypeptide from the P-tRNA. Subsequent recycling involves splitting of the subunits, as well as dissociation of mRNA

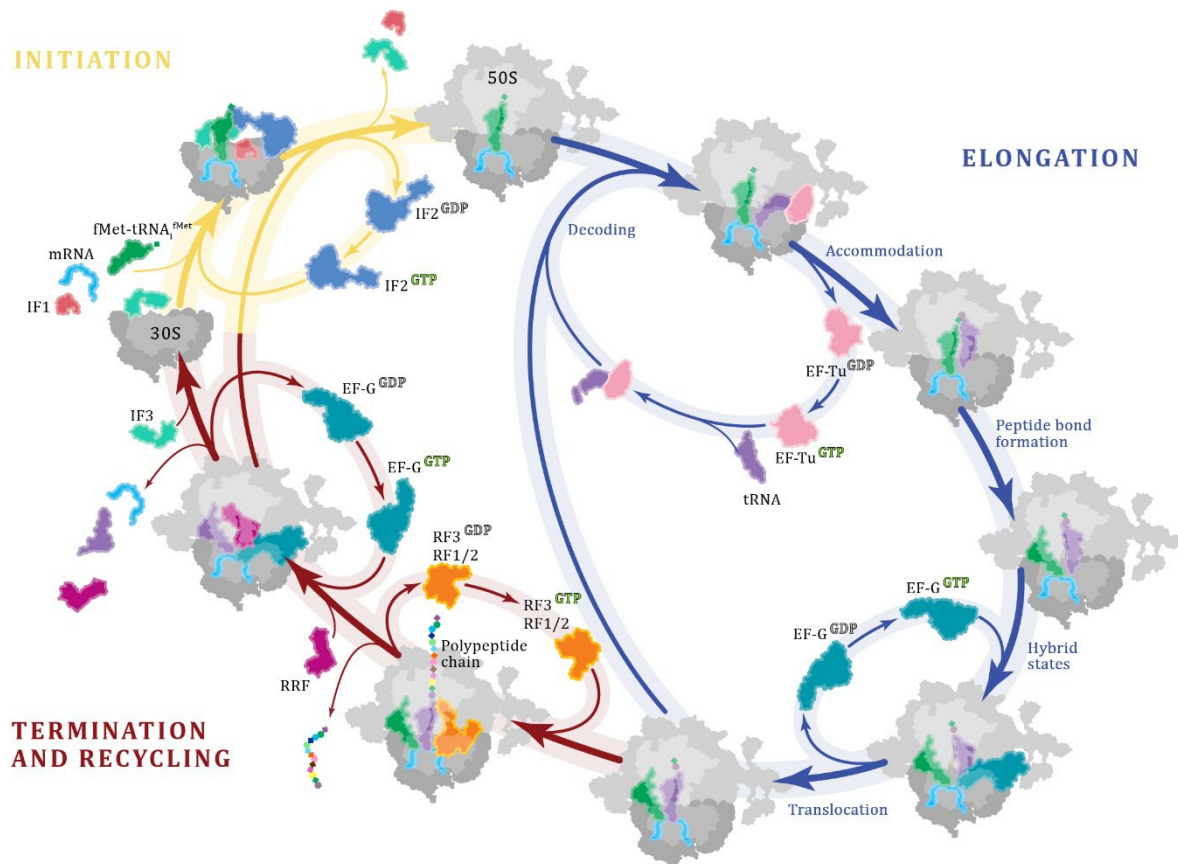


**Figure 2: Schematic overview of the bacterial translation cycle.** In bacterial translation initiation the mRNA binds to the 30S subunit and the start codon is placed in the P-site. Subsequent binding and proper placement of the initiator tRNA to the P-site involves three initiation factors (IF1-3). The initiator tRNA (tRNA<sub>i</sub><sup>fMet</sup>) carries a formylated methionine (fMet), which will be the first amino acid (aa) of the new polypeptide. Joining of the LSU leads to the 70S initiation complex (IC) formation and dissociation of the IFs, allowing the complex to enter the first round of elongation. The first stage of elongation is decoding of the codon in the A-site by an aminoacyl-tRNA (aa-tRNA), which is delivered to the ribosome by elongation factor (EF) Tu. EF-Tu leaves upon codon recognition and the tRNA accommodates to the PTC. The following peptide bond formation adds the second aa C-terminally to the nascent polypeptide chain, resulting in the A-tRNA carrying both aa and a deacylated tRNA in the P-site. The ribosome can now engage hybrid states, where the SSU rotates relatively to the LSU, which leads to shifting of the tRNA to the next site on the LSU, but not on the SSU. The translocation factor EF-G binds to the hybrid state and moves the tRNAs to the next site of the SSU, concurrently the mRNA is shifted by three nucleotides, which corresponds to one codon. The resulting complex has a deacylated tRNA in the E-site, a tRNA carrying the nascent polypeptide in the P-site and an unoccupied A-site with the following codon. This complex can now enter a new round of elongation. In this way one amino acid after another is added to the peptide chain until a stop codon enters the A-site. The stop codon serves as termination signal and is recognized by class I release factor (RF) 1 or 2, which hydrolyzes the bond between the tRNA and the completed polypeptide. Dissociation of class I RFs is enhanced by the class II release factor RF3. The ribosomal subunits are recycled for a new round of translation by splitting, which is carried out by the ribosome recycling factor (RRF) together with EF-G. Re-association of the subunits is prevented by binding of IF3 to the SSU, which links recycling and initiation. The figure was adapted from Sohmen et al. (2009).

and tRNA, which enables the subunits to participate in a new translation cycle. In the next chapters the individual steps of the bacterial translation cycle will be described further.

### 1.2.1 Translation Initiation

Translation initiation is the most regulated phase of the translational cycle and is the rate limiting step (Laursen et al., 2005). During initiation the fMet-tRNA<sub>i</sub><sup>fMet</sup> and the correct start codon within the mRNA have to be positioned in the P-site of the SSU (Seong and RajBhandary, 1987a; Allen et al., 2005; Julian et al., 2011; Hussain et al., 2016). The selection of the start site depends on several properties of the mRNA around the start site. One major influence is the accessibility, which depends on the mRNA secondary structure. Biochemical experiments and predictions of mRNA secondary structures indicate that the mRNA is less structured in initiation regions (de Smit and van Duin, 1990; Kudla et al., 2009; Scharff et al., 2011; Bentle et al., 2013; Goodman et al., 2013; Bhattacharyya et al., 2018; Mustoe et al., 2018). Furthermore, A/U-rich regions in the 5'-untranslated region (UTR) interact with rProtein S1 and are recognised as well as recruited to the ribosome in this manner (Boni et al., 1991; Sengupta et al., 2001; Byrgazov et al., 2015). An additional crucial element in canonical mRNAs is the Shine-Dalgarno (SD) sequence, which is also located in the 5'-UTR and base pairs with the 3'-end of the 16S rRNA (anti-SD-sequence (Shine and Dalgarno, 1974)), an interaction that strongly enhances the initiation rate (de Smit and van Duin, 1994; Hockenberry et al., 2017; Saito et al., 2020). Despite the universal conservation of the anti-SD sequence in the 16S rRNA only 54% of *E. coli* and 78% of *Bacillus subtilis* mRNAs contain a SD sequence (Nakagawa et al., 2010; Nakagawa et al., 2017). In Bacteroidetes and Cyanobacteria the prevalence of the SD-sequence is very low or even zero. Recently it was shown that in the Bacteroidetes *Flavobacterium johnsoniae*, which does not have a SD-sequence in the 5'-UTR, A-rich regions around the start codon are abundant instead (Nakagawa et al., 2017; Baez et al., 2019). Subsequently, A-rich regions were also found genome-wide to surround the SD-sequence and the start codon in *E. coli* (Baez et al., 2019; Saito et al., 2020). With respect to the recognition of A/U-rich regions by rProtein S1 (Boni et al., 1991; Sengupta et al., 2001; Byrgazov et al., 2015), it was suggested that the part of the A-rich region in the *E. coli* 5'-UTR interacts with rProtein S1 as well (Baez et al., 2019; Saito et al., 2020).

The formation of the elongation competent 70S initiation complex (70S IC) is achieved through a 30S pre-initiation complex (30S PIC) and 30S initiation complex (30S IC) (Gualerzi and Pon,

1990; Laursen et al., 2005; Simonetti et al., 2008). The 30S PIC and 30S IC are composed of the 30S subunit, fMet-tRNA<sub>i</sub><sup>fMet</sup>, mRNA and the initiation factors (IF) 1, 2 and 3. IF1 and IF2 are universally existent, while the phylogenetic distribution of IF3 is restricted to a subset of bacteria and plastids, such as mitochondria (Sørensen et al., 2001; Koc and Spremulli, 2002). Upon 50S subunit joining, the IFs dissociate and the fMet-tRNA<sub>i</sub><sup>fMet</sup> accommodates into the P-site of the LSU thereby establishing the active 70S IC, which is primed for the first round of elongation (Laursen et al., 2005; Marshall et al., 2009; Milón and Rodnina, 2012).

During formation of the 30S PIC the fMet-tRNA<sub>i</sub><sup>fMet</sup> is recruited to the SSU. The initiator tRNA<sub>i</sub><sup>fMet</sup> itself has structural determinants in the anticodon stem and the acceptor stem that distinguishes it from elongator tRNA<sup>Met</sup> (RajBhandary, 1994). Compared to the elongator tRNA<sup>Met</sup> the 1:72 Watson-Crick base pair in the acceptor stem of initiator tRNA<sub>i</sub><sup>fMet</sup> is missing (Dube et al., 1968; Woo et al., 1980). This is the major determinant for the *N*-formylation of Met-tRNA<sub>i</sub><sup>fMet</sup> to fMet-tRNA<sub>i</sub><sup>fMet</sup> by methionyl-tRNA transformylase (Lee et al., 1991; Lee et al., 1992; Schmitt et al., 1998). The formylation of fMet-tRNA<sub>i</sub><sup>fMet</sup> is monitored by IF2 upon recruitment to 30S PIC (Sundari et al., 1976; Wu and RajBhandary, 1997; Allen et al., 2005). The anticodon stem of tRNA<sub>i</sub><sup>fMet</sup> contains three conserved consecutive G:C base pairs, which renders the anticodon loop less flexible compared to elongator tRNA<sup>Met</sup> (Dube et al., 1968; Woo et al., 1980; Seong and RajBhandary, 1987a). The G:C base pairs are important for targeting the fMet-tRNA<sub>i</sub><sup>fMet</sup> to the P-site of the SSU and are recognized indirectly by IF3 (Seong and RajBhandary, 1987b; Dallas and Noller, 2001; Hussain et al., 2016).

The A-site within the 30S pre-initiation complex is occupied by the smallest of the three initiation factors, namely IF1 (Figure 3a-c) (Carter et al., 2001). IF1 belongs to the oligonucleotide binding fold protein family (Sette et al., 1997) and interacts with the decoding bases A1492 and A1493 in helix 44 (h44) and the G530-loop of the 16S rRNA. Furthermore, IF1 binds to ribosomal protein S12 (Carter et al., 2001). This binding site overlaps with binding of tRNA to the A-site so that their binding is prevented during the initiation phase (Laursen et al., 2005). IF1 serves also as an anchor point for IF2 and IF3, thereby enhancing their activity (Pon and Gualerzi, 1984; Milon et al., 2012; Hussain et al., 2016).

The recruitment of the fMet-tRNA<sub>i</sub><sup>fMet</sup> to the 30S PIC is aided by IF2, which is the largest initiation factor and a translational guanosine-5'-triphosphatase (trGTPase) (Pon et al., 1985; Milon et al., 2010). It has six domains in *E. coli*, which are termed domain I-VI (Mortensen et al., 1998). The N-terminal domains I-III are less conserved between species and differ in amino acid composition, as well as in length (Laursen et al., 2005). Their function varies depending on length, as well as organism and they are dispensable for translation initiation (Caserta et al.,

2006; Simonetti et al., 2013). In contrast, the C-terminal domains are involved in initiation and are conserved, with domain IV, the G-domain, displaying the highest conservation (Sørensen et al., 2001). The G-domain characterizes IF2 as trGTPase and is homologous to other GTPases participating in later stages of translation, like elongation factor Tu (EF-Tu) or release factor 3 (RF3). The GTPases associate with the ribosome in the GTP- bound state and their hydrolase activity is dependent on the LSU (reviewed by Maracci and Rodnina (2016)). Domain V anchors IF2 to the SSU and IF1 (Figure 3a, c) (Simonetti et al., 2013). Domain VI is further divided in two subdomains (Laursen et al., 2005), VI-1 and VI-2. Domain VI-2 interacts with the CCA-end of fMet-tRNA<sub>i</sub><sup>fMet</sup> and the fMet moiety (Allen et al., 2005; Myasnikov et al., 2005; Simonetti et al., 2013; Hussain et al., 2016). This protects fMet-tRNA<sub>i</sub><sup>fMet</sup> from spontaneous deacylation and discriminates against non-formylated initiator, as well as elongator tRNAs during recruitment of fMet-tRNA<sub>i</sub><sup>fMet</sup> to the 30S PIC (Sundari et al., 1976; Petersen et al., 1979; Wu and RajBhandary, 1997; Milon et al., 2012; Caban et al., 2017). Domain VI-1, parts of domain IV and fMet-tRNA<sub>i</sub><sup>fMet</sup> provide the surface for 50S subunit docking subsequent to fMet-tRNA<sub>i</sub><sup>fMet</sup> accommodation to the SSU P-site (Figure 3c)(Hussain et al., 2016; Sprink et al., 2016; Ge et al., 2018; Kaledhonkar et al., 2019).

IF3 is involved in start codon recognition, specific selection of initiator tRNA, monitoring of the codon:anticodon interaction and prevents premature LSU association (Gualerzi et al., 1977; Hartz et al., 1990; La Teana et al., 1995; Sacerdot et al., 1996; Antoun et al., 2006; Milon et al., 2008). It has two globular domains, which are located N- and C-terminally (NTD and CTD) and are connected *via* a mostly helical linker. IF3 is flexible and adopts several conformations, which are proposed to represent different stages during 30S pre- and initiation complex maturation (Figure 3a, b) (Hussain et al., 2016). Initially the NTD binds next to the platform of the SSU, while the CTD interacts with IF1 and is positioned near the P-site to discriminate against elongation tRNAs and monitor codon:anticodon interaction (Figure 3a, PIC II). Upon binding of fMet-tRNA<sub>i</sub><sup>fMet</sup> the NTD detaches from the 30S platform and contacts the elbow region of the tRNA (Figure 3a, PIC III). Accommodation of fMet-tRNA<sub>i</sub><sup>fMet</sup> to the P-site forces the CTD of IF3 to bind further away from the P-site, where it has no longer contact with IF1 or the anti-codon stem loop (ASL) of fMet-tRNA<sub>i</sub><sup>fMet</sup>, while the NTD stays attached to the elbow and moves together with the accommodating tRNA (Figure 3a, 30S IC). In all up to day reported structures and conformations of IF3 block one or more important connection points between the SSU and the LSU of the ribosome (Allen et al., 2005; Julian et al., 2011; Hussain

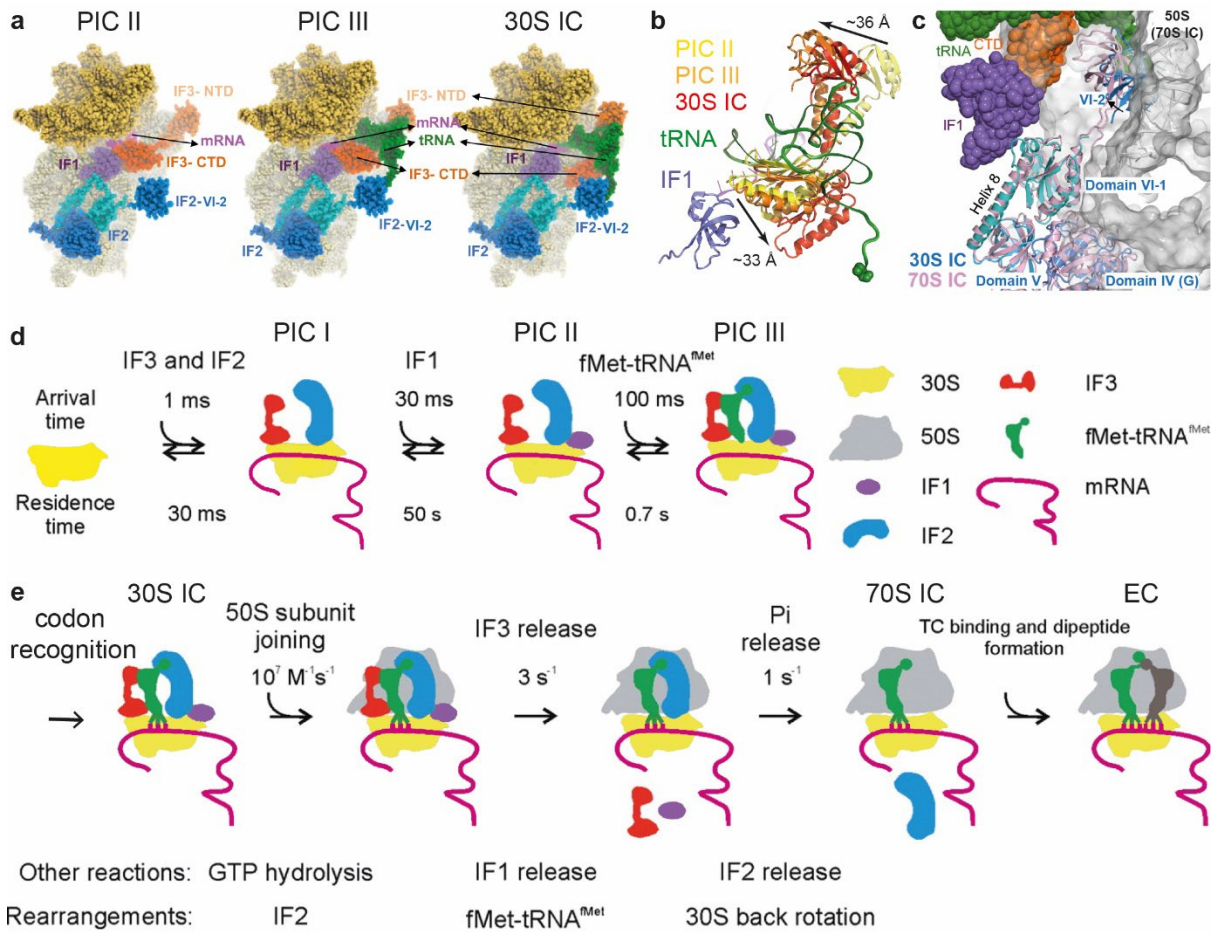


**Figure 3: Overview of Bacterial initiation.** (a) Binding of initiation factors to the SSU during PIC to 30S IC transition (IF1, purple; IF2, blue; IF3, red; mRNA magenta; SSU, yellow). (b) Structural rearrangement of IF3 in different stages of initiation (PIC II, yellow, PDBID 5LMP; PIC III, orange, PDBID 6LMT; 30S IC, red, fMet-tRNA green, IF1 purple, PDBID 5LMV), the fMet moiety of the tRNA is shown as spheres. (c) Superimposition of IF2 in the 30S IC (blue, PDBID 5LMV) and the 70S IC (pink, PDBID 3JCJ). (d) Kinetics of 30S IC formation, the mRNA (magenta) can bind at any time in this stage. (e) Kinetic representation of the progression to the 70S IC, with transition to an elongation complex (EC) by delivery of an aa-tRNA to the A-site in form of a ternary complex (TC). Figures a-c modified from Hussain et al. (2016), figures d and e were adapted with modifications from Milón and Rodnina (2012).

et al., 2016). This explains how IF3 prevents premature subunit association, and it is not known yet if IF3 has to leave before subunit association or if it adopts an unobserved conformation that does not overlap with the 50S subunit (Milón et al., 2008; Goyal et al., 2015; Hussain et al., 2016).

IFs bind to the SSU in a preferred sequence, with IF2 and IF3 binding first, followed by IF1, and finally the recruitment of fMet-tRNA<sub>i</sub><sup>fMet</sup> takes place (Figure 3d) (Milón et al., 2012). While the association of the mRNA can take place at any time point during 30S PIC assembly and is dependent on the concentration, as well as the accessibility of the ribosomal-binding site of the given mRNA (Studer and Joseph, 2006; Kudla et al., 2009; Milón et al., 2012). The transition from the 30S PIC to the 30S IC is marked by a movement of the head closer to the body, which facilitates stable mRNA binding, codon:anticodon interaction and accommodation of the fMet-tRNA<sub>i</sub><sup>fMet</sup> ASL to the P-site of the SSU (Figure 3e) (Milón et al., 2012; Hussain et

al., 2016). Initially reversible joining of the LSU is promoted by the surface provided by fMet-tRNA<sub>i</sub><sup>fMet</sup> and IF2 (Hussain et al., 2016; Sprink et al., 2016; Ge et al., 2018; Kaledhonkar et al., 2019). The association of the subunits leads to GTP hydrolysis to GDP and inorganic phosphate (P<sub>i</sub>) by IF2, as well as dissociation of IF1 and probably IF3, which in turn enables the formation of intersubunit bridges and stabilization of the 70S IC (Myasnikov et al., 2005; Milon et al., 2008; Goyal et al., 2015; Hussain et al., 2016; Kaledhonkar et al., 2019). The 70S IC displays a semi-rotated intersubunit conformation, with the fMet-tRNA<sub>i</sub><sup>fMet</sup> in the peptidyl/initiation (P/I) state (Allen et al., 2005; Sprink et al., 2016; Kaledhonkar et al., 2019). In this state the ASL is harboured in the P-site of the 30S subunit, while the CCA-end fMet-tRNA<sub>i</sub><sup>fMet</sup> is associated with IF2. The contact between the acceptor end of fMet-tRNA<sub>i</sub><sup>fMet</sup> and IF2 is lost upon P<sub>i</sub> release from IF2. Concurrently IF2 dissociates from the ribosome, leading to back-rotation of the 30S subunit into a non-rotated intersubunit conformation and accommodation of the CCA-end to the P-site of the LSU (Myasnikov et al., 2005; Milon et al., 2008; Goyal et al., 2015; Kaledhonkar et al., 2019). The charged initiator fMet-tRNA<sub>i</sub><sup>fMet</sup> is now in the P/P state and the vacant ribosomal A-site is able to bind the first elongator tRNA, which marks the passage to the elongation cycle (Goyal et al., 2015; Kaledhonkar et al., 2019).

### 1.2.2 The Elongation Cycle

During elongation the actual polypeptide is synthesized. In contrast to initiation, termination and recycling the elongation cycle is conserved among all domains of life. Three steps characterize the elongation cycle: decoding, peptide bond formation and translocation. Starting with decoding, which requires an elongation-competent ribosome, with a P-site tRNA and an empty A-site emerging from initiation or a previous elongation cycle. In bacteria, the next aminoacyl-tRNA (aa-tRNA) is delivered to the ribosome in the so-called ternary complex, consisting of the aa-tRNA, the trGTPase EF-Tu and GTP. Initially, the codon in the A-site is sampled and non-cognate ternary complexes are rejected, whereas the cognate aa-tRNA is accepted, which leads to GTP hydrolysis by EF-Tu and accommodation of the tRNA to the PTC. In the PTC peptide bond formation takes place, during which fMet or the nascent polypeptide chain is transferred from the P-site tRNA to the amino acid of the A-site tRNA. Subsequently to peptide bond formation the ribosome oscillates between the non-rotated and the rotated state, with tRNAs in classical A/A and P/P states or hybrid A/P and P/E states, respectively. For the next cycle of elongation to occur, the tRNAs have to move entirely to the

next site, and additionally the mRNA needs to be shifted by one codon. Both is achieved during translocation, which is promoted by binding of the trGTPase EF-G to the oscillating PRE-translocation ribosome. The resulting POST-translocation ribosome is non-rotated with tRNAs in the classical P/P- and E/E-state and an empty A-site, which renders it elongation competent and primed for the following decoding event. The elongation cycle proceeds until a stop-codon enters the A-site and engages the ribosome for termination, followed by recycling.

The most critical steps during elongation are selection of the correct aa-tRNA while decoding and maintenance of the ORF in the course of translocation. These steps, as well as the main reaction catalysed by the ribosome, peptide bond formation, will be explained in the following sections.

**Decoding** links the information stored in the mRNA to the amino acid sequence of the peptide by comparison of the mRNA codon with the anticodon of incoming aa-tRNAs. Initially EF-Tu·GTP·aa-tRNA ternary complexes are recruited to the elongation competent ribosome independently of the A-site codon by interaction with the rProteins L7/L12 in the T tRNA conformation (Figure 4a, b, panel 2) (Wieden et al., 2001; Kothe et al., 2004; Diaconu et al., 2005). EF-Tu consists of three domains: domain I is the G-domain, responsible for binding and hydrolysing GTP, while domain II and III in the GTP form of EF-Tu sandwich the aminoacylated CCA-end of the tRNA, whereas the ASL is free to interact with the anticodon (Nissen et al., 1995; Nissen et al., 1999; Loveland et al., 2017). *E. coli* ribosomes harbour four copies of L7/L12 and each of them might be associated with a ternary complex for rapid codon sampling (Diaconu et al., 2005; Mustafi and Weisshaar, 2018). The codon sampling is considered as the first of two proofreading steps during decoding (Figure 4c) and scans one codon per 1-2 ms (Thompson and Stone, 1977; Gromadski and Rodnina, 2004; Mustafi and Weisshaar, 2018). Importantly, only non-cognate ternary complexes are rejected and dissociate from the ribosome, while cognate ternary complexes are accepted. A small portion of near-cognate complexes, which mimic Watson-Crick base pairing by tautomerization can escape the initial selection and proceed like cognate ternary complexes (Figure 4a, b) (Pape et al., 1999; Gromadski and Rodnina, 2004; Wohlgemuth et al., 2010; Rozov et al., 2015; Rozov et al., 2016a; Rozov et al., 2016b; Loveland et al., 2017; Fislage et al., 2018; Rozov et al., 2018). During the codon recognition the SSU is in an open conformation and the tRNA is in the A\*/T state (Figure 4a, b, panel 3), which indicates that the tRNA is bent towards the A-site for sampling, but has not yet established Watson-Crick base pairing with the mRNA codon, while the CCA-end is associated with EF-Tu (Loveland et al., 2017; Fislage et al., 2018). Sampling

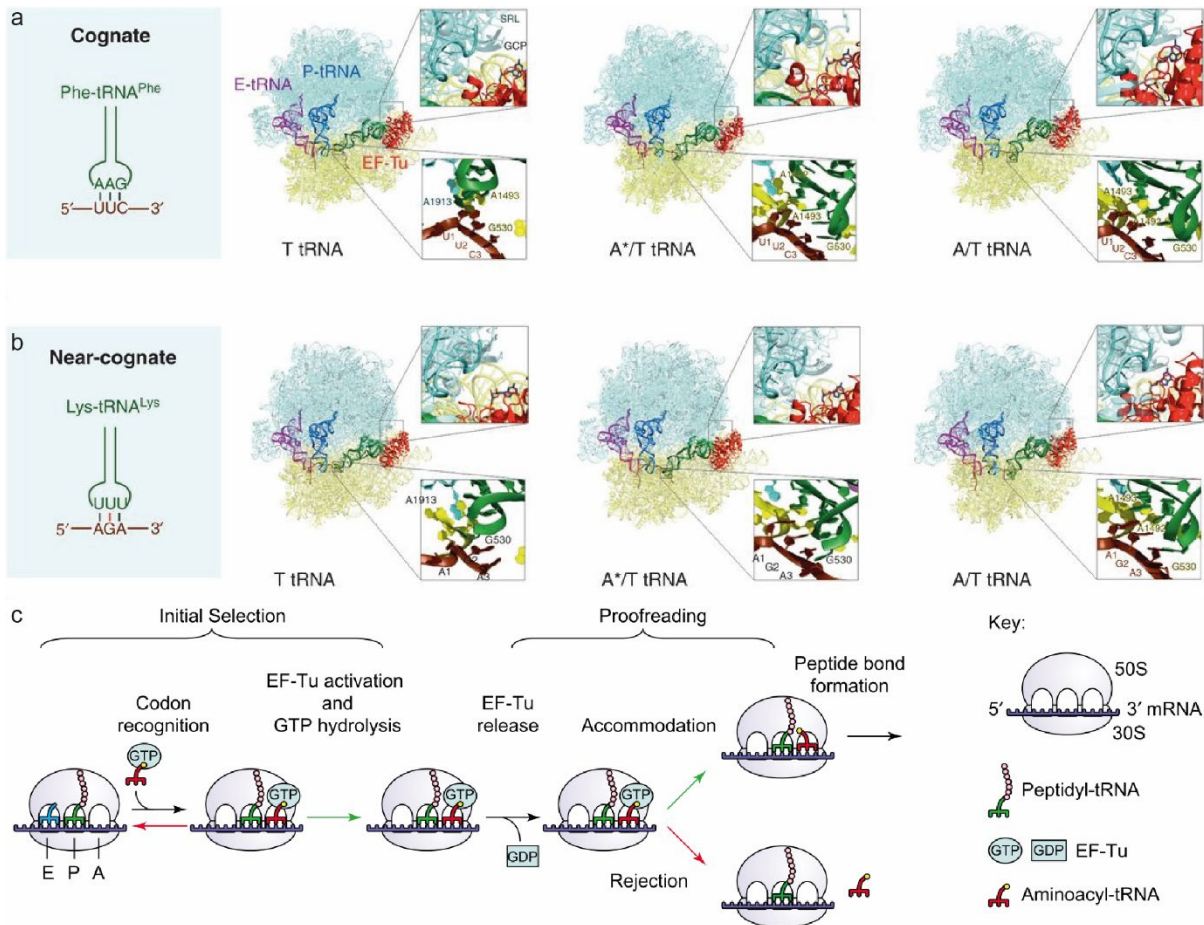


**Figure 4: Mechanism of initial selection of tRNAs and decoding.** (a) Schematic representation of decoding. Rearrangements and decoding intermediates of a cognate tRNA (b) and non-cognate tRNA (c) according to Loveland et al. (2017). Panel two depicts initial binding of the ternary complex, the anticodon is unpaired (lower inlet) and EF-Tu is not accommodated to the GAC (lower inlet). GCP, nonhydrolyzable GDP-CP. In panel three the codon:anticodon interaction is established, but the SSU is in an open conformation and EF-Tu does not interact with the SRL. In panel four the SSU is closed and EF-Tu is accommodated in the GAC. Figure (a) and (b) were adapted from Rodnina (2018), and (c) from Ogle et al. (2003).

by the ribosome is carried out by the decoding bases, namely 16S rRNA bases A1492 and A1493 of helix 44 (h44) in the SSU body, as well as G530 from the G530-loop in the shoulder of the SSU and A1913 of H69 of the 23S rRNA (*E. coli* numbering is used throughout the thesis) (Ogle et al., 2001; Loveland et al., 2017; Fislage et al., 2018). The decoding bases flip between their OFF and ON states. In the OFF state A1492 and A1493 reside inside h44, A1913 stacks on A1492 and G530 is in *syn*-conformation, while in the ON position A1492 and A1493 flip out of h44, G530 is in *anti*-conformation and A1913 shifts out of h44. The ON conformation establishes a hydrogen-bond network with the minor groove of the codon:anticodon helix and the ASL of the tRNA in order to verify Watson-Crick base pairing. More precisely, A1913 interacts with the ASL, A1493 and G530 monitor the first codon position, whereas A1492 and G530 verify the second position of the codon (Ogle et al., 2001; Loveland et al., 2017; Fislage et al., 2018). The third codon position is not monitored strictly

by the ribosome and allows Wobble base pairing. This allows reading of multiple redundant codons by one tRNA and is the reason that the genetic code is degenerated (Crick, 1966). Once the hydrogen bond network is tightly formed the tRNA is accepted. This is accompanied by closure of the small subunit, as the head and the shoulder move towards each other, which also brings the shoulder closer to the body (Ogle et al., 2001; Ogle et al., 2002; Loveland et al., 2017; Fislage et al., 2018). The domain closure embeds the tRNA deeper into the A-site facilitating the A/T-state (Figure 4a, b, panel 4). EF-Tu, which is associated with the shoulder throughout decoding, is guided to the GTPase activating center (GAC) on the LSU by the shoulder movement (Stark et al., 1997; Loveland et al., 2017; Fislage et al., 2018). The GAC acts like a GTPase activating protein (GAP) for trGTPases and consists of the sarcin-ricin-loop (SRL, H95) of the 23S rRNA, as well as the rProteins L10 and L7/L12 (Moazed et al., 1988; Kothe et al., 2004; Schmeing et al., 2009; Voorhees et al., 2010). Conformational changes in EF-Tu during domain closure place a histidine (His84 in *E. coli* EF-Tu) residue in switch II of the G-domain close to A2662 of the SRL (Voorhees et al., 2010; Loveland et al., 2017; Fislage et al., 2018). The G-domain and the His are conserved in all trGTPases indicating a similar GTP hydrolysis mechanism for different trGTPases in all domains of life, (Noller, 1984; Gutell et al., 1993; Leipe et al., 2002; Spahn et al., 2004; Voorhees et al., 2010; Maracci and Rodnina, 2016). Consistently, the GAC is conserved across all kingdoms. Hydrogen bonding between the His and A2662 leads to activation of the GTPase activity. The His is involved in coordinating a water molecule, which is necessary for the nucleophilic attack on the  $\gamma$ -phosphate of GTP (Cool and Parmeggiani, 1991; Daviter et al., 2003; Voorhees et al., 2010; Loveland et al., 2017; Fislage et al., 2018). The hydrolysis mechanism for EF-Tu based on biochemical and theoretical reaction simulation propagates *via* a substrate-assisted mechanism, in which one oxygen of the  $\gamma$ -phosphate group abstracts one hydrogen from the water and the resulting hydroxide anion performs the nucleophilic attack on the  $\gamma$ -phosphate in a concerted manner (Daviter et al., 2003; Adamczyk and Warshel, 2011; Ram Prasad et al., 2013; Wallin et al., 2013; Maracci et al., 2014). EF-Tu·GDP·Pi·aa-tRNA changes its conformation upon Pi release, which decreases the affinity for the ribosome and the tRNA. Consequently, EF-Tu·GDP releases the CCA-end of the tRNA, the tRNA detaches from EF-Tu and accommodates to the PTC (Pape et al., 1998; Pape et al., 1999; Kothe and Rodnina, 2006). Subsequently, EF-Tu dissociates from the ribosome (Morse et al., 2020). tRNA accommodation to the A-site of the LSU, places the CCA-end in the PTC for following peptide bond formation (Pape et al., 1998; Pape et al., 1999; Gromadski and Rodnina, 2004).

As mentioned earlier not all near-cognate tRNAs are rejected during decoding, although

GTPase activation is 100-fold faster for cognate than near-cognate tRNAs, a minor fraction of non-cognate tRNAs promotes domain closure and GTP hydrolysis by EF-Tu (Pape et al., 1998; Pape et al., 1999; Zhang et al., 2015a; Loveland et al., 2017; Fislage et al., 2018). Since the ribosome only monitors the geometry of the codon:anticodon helix, near-cognate aa-tRNAs fulfilling this criterion proceed to EF-Tu GTPase activation, but accommodation to the PTC is slower in kinetic studies, while tRNA dissociation increases (Pape et al., 1998; Pape et al., 1999; Demeshkina et al., 2013; Rozov et al., 2015; Rozov et al., 2016a; Rozov et al., 2016b). This observation indicates a second proofreading step, with a yet unknown mechanism (Figure 4c) (Pape et al., 1999; Geggier et al., 2010; Ieong et al., 2016). It has been shown recently that tRNAs that are unsuccessful in peptide bond formation can bind to EF-Tu·GTP from solution during the proofreading step, thus the ternary complex can be formed on the ribosome (Morse et al., 2020). With regard to this, multiple rounds of GTP hydrolysis can take place during proofreading. Near-cognate tRNAs which also escape the proofreading during accommodation will be included in the peptide. However, since the fidelity of decoding is  $10^3$  or higher an average *E. coli* protein of 300 aa is synthesised most likely error-free (Netzer and Hartl, 1997; Allan Drummond and Wilke, 2009; Wohlgemuth et al., 2010; Manickam et al., 2014).

**Peptide Bond Formation** is the main reaction catalysed by the ribosome and describes the polymerisation of amino acids into a polypeptide chain. The reaction takes place in the peptidyl transferase center (PTC) in the highly conserved domain V of the 23S rRNA. This already implies that the PTC is mainly composed of rRNA, which characterises the ribosome as a ribozyme (Ban et al., 2000; Nissen et al., 2000; Hansen et al., 2002). The closest rProtein to the PTC in bacteria with 8-10 Å distance is the N-terminal tail of bL27 (Voorhees et al., 2009; Polikanov et al., 2014). The 50S subunit is able to catalyse the reaction even without the SSU or additional translation factors, requiring only tRNAs or tRNA fragments (Monro, 1967; Maden and Monro, 1968; Schmeing et al., 2002; Wohlgemuth et al., 2006). The ribosome was suggested to function as an entropic trap that places the CCA-end of the P-tRNA, carrying fMet or the nascent chain and the incoming aa-tRNA optimally for the reaction to occur. This accelerates the peptidyl transfer by aminolysis from the P-site tRNA onto the amino acid of the A-site tRNA  $10^5$ - $10^7$ -fold compared to the reaction in solution (Sievers et al., 2004). The aminolysis is initiated by a nucleophilic attack of the  $\alpha$ -amino group of the aminoacyl-tRNA in the A-site onto the carbonyl carbon of the ester group connecting the nascent polypeptide with the P-site tRNA (Nissen et al., 2000). The positioning of the CCA-end in the P-site is facilitated by Watson-Crick base pairing of the nucleotides C74 and C75 with G2551 and

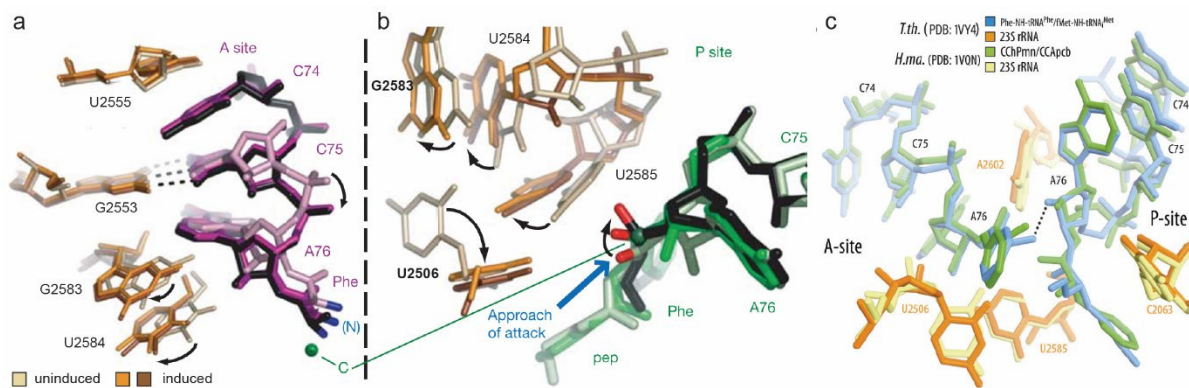


**Figure 5: Induced-fit of the peptidyl transferase center upon binding of substrates for peptide bond formation.** (a) Interaction of substrate analogues with the A-loop of the 23S rRNA and switch (arrows) of the A-site from uninduced to induced in response to binding of substrate analogues. The position of the carbonyl carbon is indicated. (b) Progression of the induced-fit by disruption of the G2583-U2506 Wobble base pair (bold) and position of substrate analogues in the P-site. (c) Comparison of the induced PTC upon binding of tRNAs (tRNAs, blue and 23S rRNA, orange) or substrate analogues (analogues, green and 23S rRNA, yellow). 23S rRNA base and tRNA backbone movements are indicated by black arrows. Hydrogen bonds are displayed as black dotted lines. Figure (a) and (b) modified from Schmeing et al. (2005b) and (c) from Polikanov et al. (2014).

G2552 within the P-loop (H80) of the 23S rRNA, respectively, while A76 forms hydrogen bonds (H-bonds) with A2450 and stacks on the ribose of A2451. The stabilization of the CCA-end of the aa-tRNA is mediated by the A-loop (H92) of the 23S rRNA, in particular C74 stacks on U2555 and C75 forms a Watson-Crick base pair with G2553 (Figure 5a). A76 attaches *via* an A-minor motif to G2583, this is propagated to the G2583-U2506 Wobble base pair, which is disrupted thereupon (Figure 5b). Furthermore, the bases U2584 and U2585 shift upon disruption of the Wobble base pair. U2585 shields the peptidyl-tRNA in the P-site from premature hydrolysis in the absence of an A-site tRNA, while its relocation exposes the ester bond of the peptidyl-tRNA for the nucleophilic attack by the  $\alpha$ -amino group of the A-site tRNA. Additionally, A2602 moves between the CCA-ends of the A- and P-site tRNA (Figure 5c) (Nissen et al., 2000; Hansen et al., 2002; Schmeing et al., 2005a; Schmeing et al., 2005b; Voorhees et al., 2009; Polikanov et al., 2014). Overall, the binding of the aa-tRNA to the A-site leads to a shift in the PTC from an uninduced to an induced conformation.

The reaction mechanism of peptide bond formation is a matter of ongoing discussion. Initially, acid-base catalysis was proposed on the structure of CCA-end analogues in complex with the LSU of the archaeon *Haloarcula marismortui* (Nissen et al., 2000). In this case, the 23S rRNA nucleotide A2451, in particular the N3 atom, which is in H-bond distance to the  $\alpha$ -amino group of the aa-tRNA should act as general base. This was challenged by a mutation and deletion analysis, which indicated that A2451 is dispensable for the reaction (Polacek et al., 2001; Youngman et al., 2004; Erlacher et al., 2005). Moreover, it was shown that the exchange of the 2'-OH group of A2451 to -H or -OCH<sub>3</sub> reduces the rate of peptidyl transfer 10- to 50-fold and that transpeptidation is pH independent, altogether these findings contradict an acid-base

catalysis (Erlacher et al., 2005; Bieling et al., 2006; Erlacher et al., 2006; Lang et al., 2008). Afterwards two proton relay models were suggested (Figure 6), which include water molecules found in a subsequent crystal structure of the *H. marismortui* LSU with substrate, as well as transition state analogues (Schmeing et al., 2005a) and a crystal structure of *Thermus thermophilus* 70S ribosomes with tRNAs in the P- and A-site in the preattack and postcatalysis state (Polikanov et al., 2014). Both models include one water that is involved in the movement of three protons, which is consistent with kinetic solvent isotope effect studies (Kuhlenkoetter et al., 2011). Both proton relays involve the 2'-OH group of A76 of the P-tRNA that has been shown to promote transpeptidation, since its replacement to-H decreased the rate of peptide bond formation 100-fold (Dorner et al., 2003; Weinger et al., 2004; Zaher et al., 2011). Additionally, the models include a tetrahedral intermediate of the carbonyl carbon, leading to a negative charge on the carbonyl oxygen (oxyanion) during the rate limiting transition state. The formation of the tetrahedral intermediate in both models is in agreement with the absence of building up a positive charge on the attacking  $\alpha$ -amino group as implied by kinetic isotope effect data and the close to zero Brønsted coefficient (Kingery et al., 2008). In contrast, the models disagree on the rate limiting transition state formed during peptidyl transfer.

The crystal structure of the *H. marismortui* LSU lead to the suggestion of a concerted eight-membered proton shuttle (Schmeing et al., 2005a), in which the nucleophilic attack of the  $\alpha$ -amino group onto the carbonyl carbon involves an eight-membered transition state. In the transition state the proton from the  $\alpha$ -amino group is accepted by the 2'-OH group of A76 that simultaneously donates its proton to the 3'-OH group of the P-tRNA *via* a water molecule (Figure 6a).

The higher resolution of the *T. thermophilus* 70S structures allowed a more sophisticated view on the PTC before and after peptide bond formation, as well as a more precise localisation of water molecules (Polikanov et al., 2014). The PTC was shown to be rather rigid, with water molecules coordinated by H-bonding with the 23S rRNA and the tRNAs. In particular, one water molecule (W1) interacts with the phosphate backbone of A-tRNA nucleotide A76, N6 of A2602 and the 2'-OH group of A2451 of the 23S rRNA, as well as the N-terminal amino group of L27. N1 of A2602 and the 2'-OH group of U2584 contact a second water molecule (W2) and a third water molecule (W3) is coordinated by the 2'-OH-groups of A76 of the P-tRNA and C2063. W2 and W3 were already identified in the complex of the *H. marismortui* LSU with substrate or transition state analogues and were proposed to stabilise the oxyanion and participate in the proton shuttle mechanism, respectively (Schmeing et al., 2005a). On the contrary, W3 was found at different positions in the preattack structure of the *T. thermophilus*

70S and was therefore excluded from participating in the proton wire (Polikanov et al., 2014). Rather, the abstraction of a proton from the attacking  $\alpha$ -amino group in the A-site should be mediated by a concerted proton wire from W1 *via* the 2'-OH groups of A2451 and P-tRNA A76. A partial negative charge of the oxygen of W1, facilitated by the basic character of the N-terminal  $\alpha$ -amino group of bL27 and the negative charge of the phosphate backbone of A-tRNA nucleotide A76 favours the start of the proton wire (Figure 6b). The resulting tetrahedral intermediate of the carbonyl carbon, containing the oxyanion is also stabilised by W2 in this model. In accordance with kinetic isotope effect studies (Hiller et al., 2011), rapid breakdown of the tetrahedral intermediate occurs in a second step and is promoted by the ribosome. Fast breakdown prevents premature translation termination by hydrolysis. This breakdown uses the negative charge of the oxyanion and the partial positive charge of the W1 oxygen to transfer a proton to W3 by inverting the direction of the proton wire (Polikanov et al., 2014).

The advantage of the proton wire over the proton shuttle is the favourable geometry for proton transfer, albeit the role of bL27 has been questioned (Maracci et al., 2015). Earlier studies

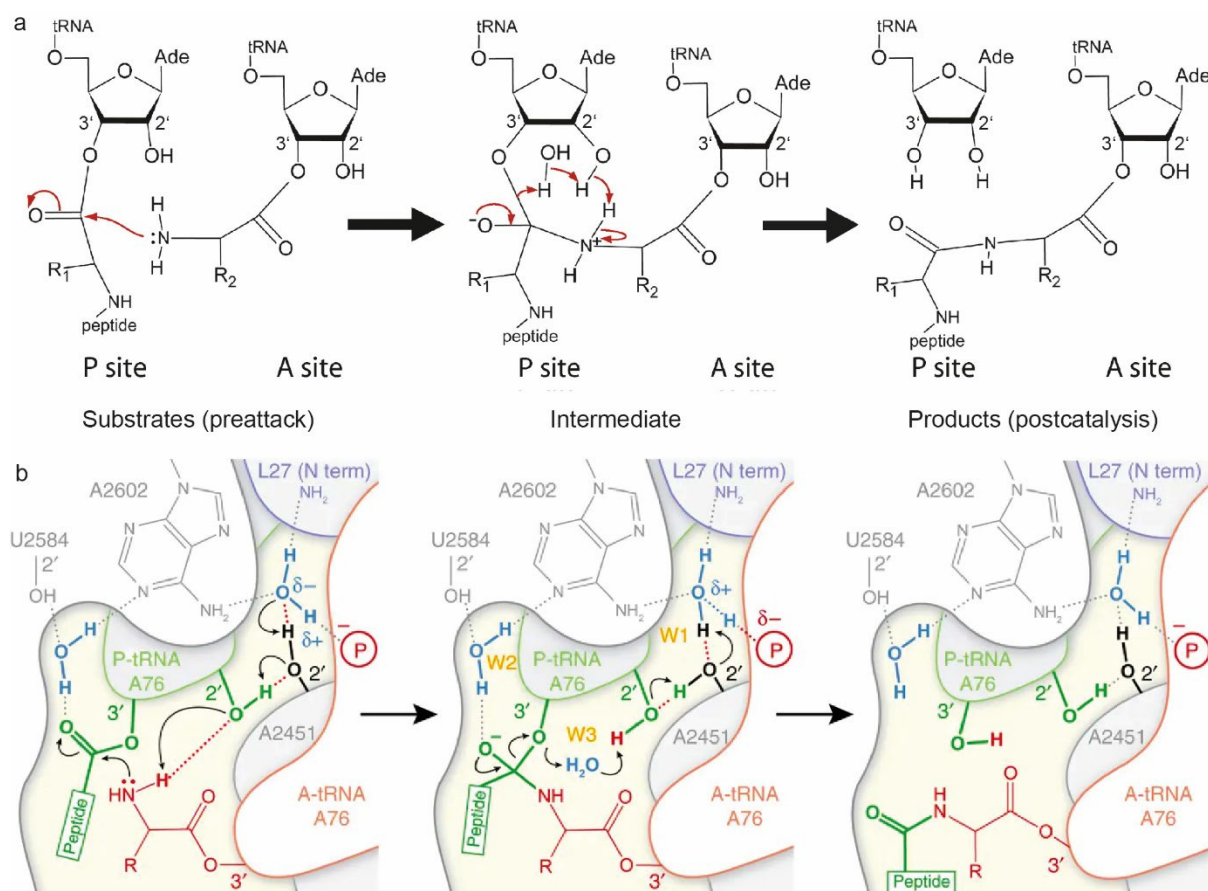


**Figure 6: Overview of possible reaction mechanism during peptide bond formation.** (a) Eight-membered proton shuttle (Schmeing et al., 2005a). (b) Proton wire (Polikanov et al., 2014). Both mechanisms lead to the formation of the tetrahedral intermediate due to nucleophilic attack of the  $\alpha$ -amino group in the A-site to the carbonyl carbon in the P-site. Breakdown of the intermediate *via* different proton transfer routes lead to the transfer of the peptide from the P-tRNA to the  $\alpha$ -amino group of the amino acid attached to the A-tRNA.

indicated that deletion of 3-6 N-terminal residues of bL27 reduced the peptide bond formation rate (Maguire et al., 2005). Additionally, bL27 was found to stabilize the P-and A-site tRNA and was thus suggested to take part in optimal substrate positioning (Voorhees et al., 2009; Polikanov et al., 2014). In contrast, the study by Maracci et al. (2015) found that deletion of bL27 had only a marginal effect on peptidyl transfer rate, but the extent of peptide bond formation was reduced by 20 %. Furthermore, it is not clear if the proton wire is applicable in eukaryotes and archaea, since bL27 is only conserved in bacteria (Ban et al., 2014). In a structure of the wheat-germ ribosome it has been shown that a conserved loop of L10e (uL16) reaches towards the PTC in eukaryotes instead (Armache et al., 2010), but the contribution of the loop to peptide bond formation has not been investigated yet and the loop was flexible in the *H. marismortui* LSU structures (Ban et al., 2000; Nissen et al., 2000; Hansen et al., 2002; Schmeing et al., 2005a; Schmeing et al., 2005b). In conclusion, the part of proteins in peptide bond formation, the conservation of the mechanism between prokaryotes and eukaryotes, as well as the mechanism itself are still not fully understood and further kinetic, biochemical and structural analysis is required.

**Translocation** describes the process of moving the mRNA by one codon, as well as the movement of peptidyl-tRNA and deacylated tRNA from the A- and P-site to the P- and E-site, respectively. Additionally, the ribosome is transformed from a dynamic PRE- to the rather static POST-translocation state, which can participate in a new round of elongation. It has been shown that after peptide bond formation the ribosome alternates between the classical and the rotated (or hybrid) state driven by thermal energy with a rate of ~40 oscillations per second (Moazed and Noller, 1989; Blanchard et al., 2004; Agirrezabala et al., 2008; Cornish et al., 2008; Chen et al., 2011; Chen et al., 2013a; Adio et al., 2015; Sharma et al., 2016). In the latter, the 30S subunit was found to be rotated approximately 6° counter clockwise in comparison to the 50S subunit, and the 30S head was swivelled by 6° (Frank and Agrawal, 2000; Agirrezabala et al., 2008; Julian et al., 2008; Agirrezabala et al., 2012; Chen et al., 2013b; Tourigny et al., 2013). Also, the tRNAs engaged hybrid states upon rotation: while the ASLs remain in the A- and P-site on the SSU, the acceptor stems switch to the P- and E-site in the LSU, resulting in A/P- and P/E-hybrid states. In addition, the L1 stalk of the LSU was rotated towards the E-site by 30° into its closed position where it contacts the 30S head and the P/E-tRNA in the elbow region. Translocation by spontaneous rotation is extremely slow (Gavrilova and Spirin, 1971; Fredrick and Noller, 2003; Shoji et al., 2006). Productive translocation needs GTP and EF-G, a translational GTPase consisting of five domains (Figure

7a, b), which shares the conserved G-domain (domain I), harbouring the for GTP-hydrolysis important His (His92 in EF-G) and domain II with other trGTPases, whereas domains III-V are characteristic for EF-G (Nishizuka and Lipmann, 1966; Åvarsson et al., 1994; Czworkowski et al., 1994; Rodnina et al., 1997; Chen et al., 2013b; Cunha et al., 2013; Pulk and Cate, 2013; Tourigny et al., 2013; Adio et al., 2015). Productive translocation is also dependent on ribosomal intersubunit rotations since inhibition of intersubunit flexibility by reversible crosslinking of the subunits also inhibited translocation, which was restored as soon as the crosslink was removed (Horan and Noller, 2007). EF-G·GTP accelerates the translocation rate by four orders of magnitude compared to spontaneous translocation and GTP hydrolysis increases the rate additionally by 40-fold (Rodnina et al., 1997; Munro et al., 2010). EF-G can adopt a compact and an elongated conformation (Figure 7a, b). According to single-molecule FRET studies free-EF-G prefers the compact state, while ribosome-bound EF-G preferentially engages the elongated conformation (Salsi et al., 2015). However, in a crystal structure of the PRE-translocation state EF-G was found in the compact state on the ribosome (Figure 7c) (Lin et al., 2015). The compact state might be the initial binding conformation but could also be accounted for by the crystallisation method, since EF-G was fused to rProtein L9 of the neighbouring ribosome to engage crystallisation and the compact conformation on the ribosome was only reproduced using the same method (Zhou et al., 2019a), whereas in all other crystal and cryo-EM structures of EF-G on the ribosome EF-G was found in the extended conformation. Overall, the extended conformation resembles the structure of EF-Tu·GTP·tRNA ternary complex, with domain IV of EF-G mimicking the ASL of the tRNA (Åvarsson et al., 1994; Czworkowski et al., 1994; Nissen et al., 1995). Domain IV was found to bind initially in a cleft between the head and the body of the SSU right next to the A-site,

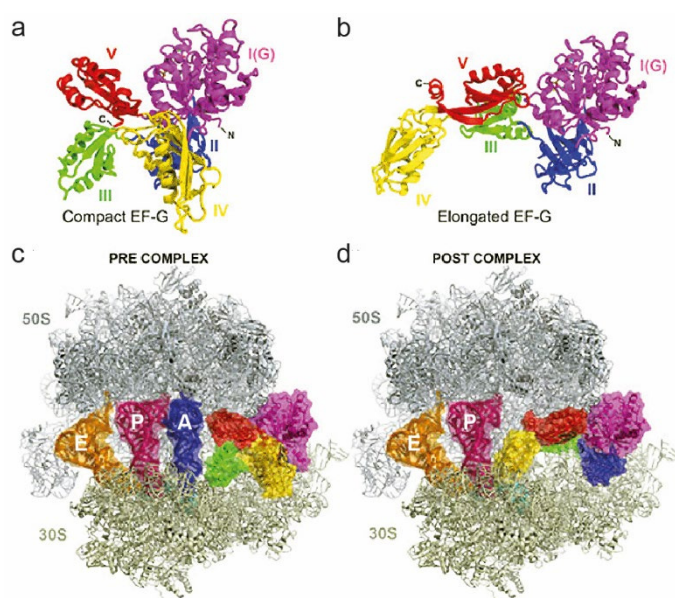


**Figure 7: Domain structure and conformational reorganisation of EF-G.** (a-b) EF-G in the compact and elongated form, with domain I (G-domain) in magenta, domain II in blue, domain III in green, domain IV in yellow and domain V in red. (c) compact EF-G on the non-rotated ribosome (Lin et al., 2015). The 50S subunit is depicted in grey and the 30S subunit in pale yellow. The tRNAs are in classical A- (blue), P- (hot pink) and E- (orange) states. (d) Non-rotated complex after translocation with EF-G in the elongated conformation. Domain IV of EF-G (yellow) is located in the A-site of the 30S subunit. The figure was modified from Noller et al. (2017).

contacting the ASL of the A-tRNA (Brilot et al., 2013). Binding of EF-G to the ribosomal GAC is mediated *via* the L7/L12 stalk in a similar manner to EF-Tu (Diaconu et al., 2005; Helgstrand et al., 2007). The binding can occur at any stage during spontaneous rotation and facilitates the hybrid state, which was found to be the preferential substrate for translocation by EF-G (Spiegel et al., 2007; Chen et al., 2011; Chen et al., 2013a; Adio et al., 2015; Belardinelli et al., 2016a). GTP hydrolysis is activated subsequent to association with the ribosome and several crystal, as well as cryo-EM, structures of the PRE-state support the hypothesis that the activation mechanism is similar between EF-G and EF-Tu (Bourne et al., 1991; Mohr et al., 2002; Brilot et al., 2013; Chen et al., 2013b; Pulk and Cate, 2013; Tourigny et al., 2013; Lin et al., 2015; Belardinelli et al., 2016a). The main questions of translocation are how the ASLs move from one site to the next, how the mRNA is shifted, how do ribosome motions influence translocation and what role does EF-G play in the process?

The first all-atom structure of the *E. coli* ribosome revealed a 13 Å constriction between the P- and E-site in the classical state, which hinders the ~22 Å wide anticodon stem of the tRNA to move from the P- to the E-site (Schuwirth et al., 2005). The constriction is formed by the 16S nucleotides G1338-U1341 of the head and A790 of the platform. Based on the comparison with a cryo-EM reconstruction of the yeast 80S ribosome in complex with the eukaryotic EF-G homologue eEF2 and the translocation inhibitor sardorin (Spahn et al., 2004), in which a swivel of the head opened the lock, Schuwirth et al. (2005) proposed a similar mechanism for the prokaryotic ribosome. This was confirmed by a cryo-EM and crystal structures of *E. coli* and *T. thermophilus* 70S ribosomes in complex with EF-G with or without fusidic acid (Ratje et al., 2010; Ramrath et al., 2013; Zhou et al., 2013, 2014; Macé et al., 2018). The authors observed an uncoupling of the head and body rotation of the 30S subunit during an intermediate state ( $\text{TI}^{\text{POST}}$ ) during translocation of tRNAs. In the  $\text{TI}^{\text{POST}}$  the intersubunit rotation was 3-5°, while the head domain was swivelled by 18-21°, which is a back rotation of the body and a forward movement of the head compared to the hybrid state. Fluorescence stopped-flow kinetics, single-molecule polarized total internal reflection fluorescence microscopy and force measurements using optical-tweezers indicated that the uncoupling is facilitated by a power stroke of 13-85 piconewton as consequence of GTP hydrolysis by EF-G and EF-G·GDP·P<sub>i</sub> is present during the intermediate states of translocation (Yao et al., 2013; Liu et al., 2014b; Chen et al., 2016; Yin et al., 2019). In the structures EF-G·GDP is present and rearrangements of EF-G·GDP due to P<sub>i</sub> release were blocked by fusidic acid (Ratje et al., 2010; Ramrath et al., 2013; Zhou et al., 2013). The acceptor stems in the  $\text{TI}^{\text{POST}}$  were fully translocated to the P- and E-site, as seen in the hybrid state. Additionally, rotation of the head domain opened the

constriction and the tRNA ASLs stayed partly attached to their A- and P-site contacts with the head, whereas they had established contacts with the P- and E-site on the body. Thus, the state is referred to as chimeric hybrid states with the annotation ap/P and pe/E, respectively. Additionally, a third chimeric hybrid state of the tRNA departing the A-site was found by adding neomycin to inhibit the finalisation of translocation (Zhou et al., 2014). In this chimeric hybrid state the acceptor stem contacted the A- and P-loops of the PTC, while the ASL is in the ap-state, hence the state is termed ap/ap.

During head swivelling, accompanied by formation of the chimeric hybrid states the P-tRNA follows the movement of the head into the pe-state on the SSU, while the A-tRNA moves even further towards the P-site, in consequence the tRNAs are closer than in the classical or hybrid state (Ramrath et al., 2013; Zhou et al., 2014). This is probably accounted to domain IV of EF-G, which reaches into the A-site and forms interactions with the ap/P-tRNA ASL, mRNA and rRNA elements, like h44 and H69 at the decoding center. Furthermore, the tip of EF-G domain VI harbours two conserved loops, which insert into the minor groove of the codon-anticodon helix. In accordance, the importance of loop I and II was demonstrated by time-resolved puromycin reactivity assays, *in vitro* translation assays, translocation assays and chemical footprinting with insertion and deletion mutations, as well as single amino acid mutations, since the mutations decreased the rate of tRNA translocation (Rodnina et al., 1997; Martemyanov et al., 1998; Savelbergh et al., 2000; Liu et al., 2014a). The loops were further suggested to weaken and replace the minor groove interactions of the decoding bases A1492, A1493 and G530 with the codon:anticodon minihelix, which should flatten the energy barrier for translocation (Gao et al., 2009; Khade and Joseph, 2011; Liu et al., 2014a; Adio et al.,

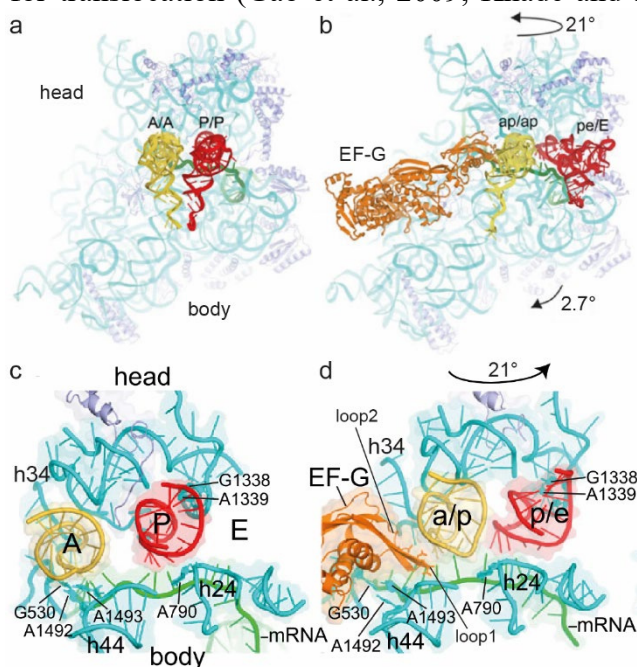


**Figure 8: Comparison of the 30S subunit in the classical state and the intermediate state of translocation.** (a) overview of the classical state on the 30S subunit (16S rRNA, cyan; rProteins, blue) with A/A-tRNA in yellow and P/P-tRNA in red. (b) chimeric hybrid state with tRNAs in ap/ap (yellow) and pe/E (red) -states. The head of the 30S subunit is rotated by 21° and the 30S subunit is rotated 2.7° with respect to the 50S subunit. The overall binding position of EF-G (orange) is shown. (c) View on the A-, P- and E-site of the 30S subunit in the classical state. The constriction between the head nucleotides G1338-A1339 and nucleotide A790 of the body is closed. The mRNA is shown in green. (d) Closeup view onto the ribosomal sites in the intermediate state. The gate between G1338-A1339 and A790 is opened by the rotation of the head. The ASLs are associated with elements of the A-site at the head and P-site at the body (a/p) or with the P-site in the head and E-site of the body (p/e), respectively. EF-G protrudes towards the a/p-ASL and interacts with the codon:anticodon helix. The figures were adapted from Zhou et al. (2014, 2019b)

2015). In addition, loop I was proposed to prevent backward slippage of the ap/P-tRNA-mRNA complex (Ramrath et al., 2013). Recent crystal structures and kinetic measurements support a role in reading frame maintenance for EF-G (Peng et al., 2019; Zhou et al., 2019b). The ribosome might be naturally -1 frameshift-prone during spontaneous translocation or slippery sequences in the absence of EF-G. While the presence of wild-type (wt) EF-G reduced the frameshifting, mutations in the tip of loop I or loop II could not prevent slippage. These findings indicate that domain IV of EF-G prevents the slide of the tRNA into the -1 frame during translocation from the A- to the P-side by restriction of the tRNA movement and preserving the codon:anticodon interaction. Furthermore, retention and stabilisation of the codon:anticodon interaction would lead to translocation of the mRNA along with the tRNA. For full translocation of the ASLs of the tRNAs from ap/P and pe/E hybrid states to classical P/P and E/E states (POST-state) to occur, the head and the body need to rotate back in a clockwise movement into their non-rotated positions. During this phase the interactions between EF-G and the ap/P-tRNA are likely preserved and domain IV accompanies the tRNA to the P-site, as the interactions are maintained from the PRE-state (Brilot et al., 2013; Chen et al., 2013b; Pulk and Cate, 2013; Tourigny et al., 2013) over intermediate states (Ramrath et al., 2013; Zhou et al., 2014) to the POST-state (Gao et al., 2009). Concurrently,  $P_i$  release by EF-G occurs, which could facilitate a second power stroke that pushes the ap/P-tRNA in place (Liu et al., 2014b; Belardinelli et al., 2016a; Chen et al., 2016). Alternatively, the back-rotation of the SSU and accommodation of tRNAs could proceed *via* a Brownian ratchet mechanism, which is supported by the finding that translocation can be accomplished although  $P_i$  release is impaired (Savelsbergh et al., 2005; Chen et al., 2016). In this case, Domain IV of EF-G would act as a resilient obstruction, preventing frameshifting and/or backward movement of the tRNAs along with the head (Gao et al., 2009; Ramrath et al., 2013; Zhou et al., 2014; Rodnina et al., 2019). In the late stage of back-rotation the E-tRNA can already leave the ribosome (Belardinelli et al., 2016a; Belardinelli et al., 2016b). Also, structural rearrangement of EF-G-GDP after  $P_i$  release facilitates a significantly lower affinity of EF-G for the ribosome and as a result EF-G dissociates, which marks the end of the translocation process and leaves the ribosome in the non-rotated POST-state (Savelsbergh et al., 2005; Belardinelli et al., 2016a). The POST-state is also characterised by a vacant A-site and depending on the A-site codon the ribosome can participate in a new round of the elongation cycle or enter into the translation termination phase.

Further structural data obtained by time-resolved cryo-EM and FRET experiments indicate that many more states exist along the process of translocation and the combination of kinetic data

and structural snapshots delivered a general overview of the translocation mechanism (Fischer et al., 2010; Holtkamp et al., 2014; Adio et al., 2015; Belardinelli et al., 2016a). Nevertheless, the detailed structural mechanism is not entirely described yet and molecular dynamic simulations indicate a relatively flat energy landscape in some areas, so that smooth transitions between different states may exist and completion of the structural data will be challenging (Whitford et al., 2013; Whitford and Sanbonmatsu, 2013; Holtkamp et al., 2014).

### 1.2.3 Translation Termination

The nascent polypeptide chain protrudes through the exit tunnel in the 50S subunit during elongation until a stop codon (UAA, UAG or UGA) encounters the A-site (Brenner et al., 1965; Brenner et al., 1967; Weigert et al., 1967). The stop codon signals the end of the ORF and the elongation cycle, as well as the transition to translation termination. Class I release factors (RFs) recognize the stop codon and hydrolyse the ester bond between the polypeptide chain and P-site tRNA (Capecci, 1967; Caskey et al., 1968). As a result, the synthesised protein is released from the ribosome. The dissociation of class I RFs is accelerated by class II RFs, which belong to the group of translational GTPases (Bourne et al., 1991; Frolova et al., 1996; Freistroffer et al., 1997). The termination factors are not conserved between eukaryotes/archaea and bacteria (Vestergaard et al., 2001; Burroughs and Aravind, 2019). While eukaryotes and archaea possess one class I RF (e/aRF1) that recognises all three stop codons and is delivered to the ribosome by the class II RF (e/aRF3) (Konecki et al., 1977; Zhouravleva et al., 1995; Dontsova et al., 2000; Hauryliuk et al., 2006; Mitkevich et al., 2006), bacteria have two class I RFs (RF1 and RF2) that read the stop codons in an overlapping manner (RF1: UAA, UAG; RF2: UAA, UGA) (Scolnick et al., 1968). The bacterial class I RFs bind independently of the class II RF3 to the ribosome (Goldstein and Caskey, 1970; Freistroffer et al., 1997). In contrast, a Gly-Gly-Gln (GGQ) -motif, which is necessary for peptide hydrolysis evolved convergently and is conserved in all class I RFs (Frolova et al., 1999; Seit-Nebi et al., 2001; Mora et al., 2003).

Bacterial RFs are composed of four domains (Figure 9a): The N-terminal domain 1 builds a three-helix bundle. Domains 2 and 4 fold into a superdomain, which is responsible for decoding, while domain 3 has a long helix ( $\alpha$ 7) and harbours a loop containing a short helix followed by the GGQ-motif (Vestergaard et al., 2001; Shin et al., 2004; Zoldak et al., 2007). In a crystal structure of isolated RF2 the decoding elements and the GGQ-motif were found

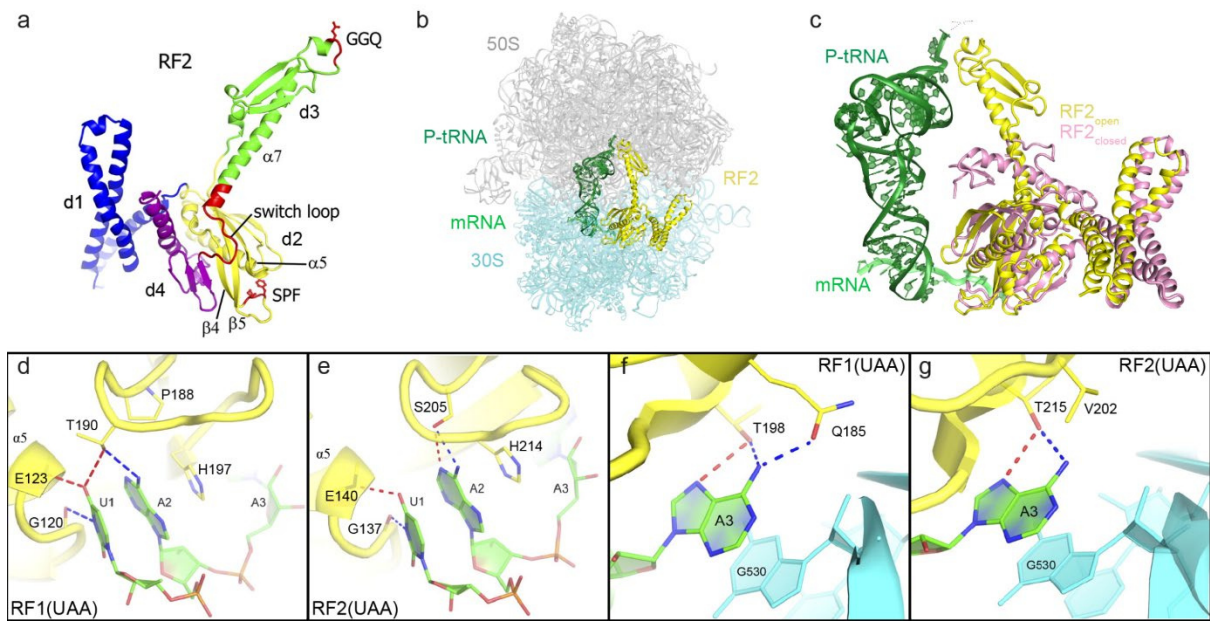


**Figure 9: Structure and binding of class I release factor 2 and decoding of the UAA stop codon by class I release factors.** (a) Overview of the domain structure and features of RF2 (Korostelev et al., 2008). Domain 1 (d1), dark blue; domain 2 (d2), yellow; domain 3 (d3), green; domain 4 (d4), purple; SPF-motif (SPF), red; GQQ-motif (GQQ), red; helix  $\alpha$ 5 ( $\alpha$ 5);  $\beta$ -strands 4 and 5 ( $\beta$ 4,  $\beta$ 5). (b) Binding of RF2 (yellow, PDBID 6OUO) to the ribosome (50S subunit, grey; 30S subunit, cyan) in the open conformation. P-tRNA (forest green) and mRNA (green) are depicted (Fu et al., 2019). (c) Comparison of the closed (RF2<sub>closed</sub>, pink, PDBID 6OST) and open (RF2<sub>open</sub>, yellow, PDBID 6OUO) conformation of RF2 on the ribosome (Fu et al., 2019). P-tRNA and mRNA are shown for reference. (d)-(g) decoding of the UAA stop codon by RF1 (Laurberg et al., 2008) and RF2 (Korostelev et al., 2008). Potential hydrogen bonds are indicated by red and blue dashed lines. Figure (a) and (d)-(g) were adapted from Korostelev (2011).

only  $\sim$ 20 Å apart (Vestergaard et al., 2001), whereas the distance between the decoding center and the PTC is approximately 73 Å (Rawat et al., 2003; Zoldak et al., 2007). This raised the question on how the GQQ-motif can fulfil hydrolysis in the PTC. Subsequent cryo-EM (11-14 Å) and crystal structures (6-7 Å) revealed that the RFs engage an open conformation on the ribosome, with the tip of domain 3 reaching towards the A-site of the PTC (Figure 9b) (Klaholz et al., 2003; Rawat et al., 2003; Petry et al., 2005; Rawat et al., 2006). Domain 1 bound near the head on the SSU and close to the GTPase associated center on the LSU, whereas the superdomain 2/4 was accommodated in the DC. The structural difference between the closed and the open conformation lead to the conclusion that RF1/2 undergo a large transition upon binding to the ribosome and stop codon recognition. While small-angle X-ray scattering (SAXS) measurements of *E. coli* RF1 and *T. thermophilus* RF2 indicated that the RFs can sample between the closed and the open conformation in solution and did not exclude binding to the ribosome in the open conformation (Vestergaard et al., 2005; Zoldak et al., 2007), transition metal ion FRET experiments with *E. coli* RF1 support this hypothesis (Trappl and Joseph, 2016). Recently, a time-resolved cryo-EM study (3.3-3.9 Å) identified the closed conformation of *E. coli* RF1 and RF2 on the ribosome (Figure 9c) (Fu et al., 2019). Moreover, the proportion of closed RF decreased over time, while the open, accommodated state increased

as the stop codon was recognised. The mechanism of stop codon recognition had been identified previously by crystal structures (3.5–3.0 Å) of the RFs on the ribosome (Figure 9d–g) (Korostelev et al., 2008; Laurberg et al., 2008; Weixlbaumer et al., 2008b; Korostelev et al., 2010). Both RFs monitor the first base (U1) of all three stop codons with the N-terminus of helix  $\alpha$ 5 (Figure 9d, e). The backbone interaction of the base of helix  $\alpha$ 5 restricts the base selection to an U in the first position, and further the interaction mimicking A:U Watson-Crick base pairing. The specificity for the UAG and UGA stop codons was found to be mediated by a Pro-x-Thr (PxT; x usually Ala or Val)-motif in RF1 and a Ser-Pro-Phe (SPF)-motif in RF2 (Ito et al., 2000; Scarlett et al., 2003), which is harboured in a loop connecting the  $\beta$ -strands  $\beta$ 4 and  $\beta$ 5 of domain 2 (Figure 9a, d, e) (Vestergaard et al., 2001; Shin et al., 2004; Zoldak et al., 2007). While the Pro- residues ensure proper conformation of the loop, the Thr190 of the PxT- and the Ser205 of the SPF-motif are involved in codon selection (Korostelev et al., 2008; Laurberg et al., 2008; Weixlbaumer et al., 2008b; Korostelev et al., 2010; Fu et al., 2019). The Thr190 of the PxT-motif discriminates against a G, U or C in the second codon position by a bifurcated H-bond between O4 of U1 and the N6-amino group of A2 (Figure 9d). In contrast, Ser205 of the RF2 SPF-motif can rotate to form a H-bond with the N6-amino group of an A2 or the N1-amino group of G2 (Figure 9e), enabling RF2 to decode both A and G in the second position. The third codon position is not monitored by the tripeptide-motifs, instead a part of the decoding loop inserts after the second base due to stacking of a conserved His (RF1: His197, RF2: His214) on to the second codon base (Figure 9d, e). This interaction was found to be necessary for proper binding of RF1 to the DC and stimulation of peptide release (Field et al., 2010). Additionally, the RF1 decoding loop contains Gln185 and Thr198, while the Thr is conserved in RF2 (Thr215), the Gln is substituted by the hydrophobic Val202 (Figure 9f, g) (Korostelev et al., 2008; Laurberg et al., 2008; Weixlbaumer et al., 2008b; Korostelev et al., 2010). The Thr can donate a H-bond to N7 of the Hoogsteen edge of an A3 in both RFs (Figure 9f, g), while Gln185 of RF1 can receive or donate an additional H-bond to the N7-amino group of an A3 or the keto group of a G3 and allows decoding of either nucleotide for RF1 (Figure 9f). In contrast, Val202 of RF2 cannot form H-bonds, which restricts RF2 to an A in the third position (Figure 9g). Thus, the near-cognate UGG codon is excluded due to discrimination against a G by RF1 in the second codon position and by RF2 in the third position. The RFs also make additional contacts with the mRNA, since bases following the stop codon determine the termination efficiency of stop codons and mutations of single amino acids render RF2 inactive (Poole et al., 1995; Ito et al., 1998; Poole et al., 1998). Furthermore, the conserved bases in the decoding center, A1913 of H69, A1492 and A1493 of h44, as well as G530, adopt a defined

conformation to allow termination to occur (Figure 10a) (Korostelev et al., 2008; Laurberg et al., 2008; Weixlbaumer et al., 2008b; Korostelev et al., 2010; Fu et al., 2019). A1493 remains flipped-in into h44 (OFF-position), this provides space for the RF to bind, since the flipped-out ON-position seen with cognate tRNAs would clash with the RF. A1913 inserts into h44 and stacks on A1493, which stabilises the position of A1493. On the other hand, A1942 and G530 are in their ON-conformation and form H-bonds with each other. G530 is also involved in determination of the third base of the stop codon (Figure 9f, g and Figure 10a). The third stop codon base stacks on G530, the stronger stacking interaction of purines disfavours pyrimidines in the third position, whereas A1942 together with further elements of the DC and the RF stabilize the so-called switch loop of the RF (Figure 10a). The switch loop connects the C-terminal end of helix  $\alpha$ 7 of domain 3 with domain 4 and undergoes an unstructured to structured transition upon stop codon recognition that extends and re-orientates helix  $\alpha$ 7. The transition is supported by a pocket built up by domain 2 of the RF, rProtein S12 (not depicted in Figure 10a), A1492 and A1493 of h44, G530 of the G530-loop as well as A1913-U1915 of H69. Based on the structural data it was proposed that the unstructured to structured transition facilitates the open conformation of the RF, which would link the decoding of the stop codon and placement of the GGQ-motif into the PTC for hydrolysis (Korostelev et al., 2008; Laurberg et al., 2008; Korostelev et al., 2010; Fu et al., 2019). Indeed, shortening of the switch loop of RF1 by three residues resulted in a three-fold decrease of the peptide release rate and a rate-limiting step for the reaction, which further supports the role of the switch loop during termination (Korostelev et al., 2010). Furthermore, the theory is supported by the time-resolved cryo-EM study by Fu et al. (2019), since the ordered form of the switch loop was observed in parallel with the open conformation

Upon placement of the GGQ-(RF1-G233G234Q235; RF2-G250G251Q252) motif in the PTC, the motif is preceded by a short helix (Korostelev et al., 2008; Laurberg et al., 2008; Weixlbaumer et al., 2008b; Jin et al., 2010; Korostelev et al., 2010; Fu et al., 2019) that is not present in the structures of the isolated RFs (Vestergaard et al., 2001; Shin et al., 2004; Zoldak et al., 2007). Simultaneously, the PTC switches from an uninduced to an induced conformation, exposing the carbonyl ester bond of the peptidyl-tRNA for nucleophilic attack from the oxygen of a water molecule. Crystal structures of the RFs on the ribosome revealed that the induced state of the PTC is slightly different from the induced state by an A-tRNA binding (Figure 10b) (Korostelev et al., 2008; Laurberg et al., 2008; Weixlbaumer et al., 2008b; Jin et al., 2010; Korostelev et al., 2010; Fu et al., 2019). A2602 is buried in a pocket of the RF and might help positioning the GGQ-motif, while U2506 and U2585 would clash with the RF and thus adopt

a different conformation (Figure 10b). The importance of the GQG-motif for peptide hydrolysis was first studied by mutational analysis in eRF1, which showed that substitution of either Gly lead to complete loss of the hydrolysis activity (Frolova et al., 1999). Surprisingly, replacement of the Gln to a third Gly (GGG) reduced the activity by ~50%, while conservative mutations to asparagine, aspartic acid or glutamic acid retained only ~20% activity and mutation to hydrophobic residues (alanine or isoleucine) reduced the activity >90% (Seit-Nebi et al., 2001). A contradictory finding was obtained for *E. coli* RF1 and RF2 using time-resolved peptide release assays. As seen for eRF1 the amount of released peptide was close to zero using a RF2-GAQ mutant (Zavialov et al., 2002). Based on this and the crystal structures it was proposed that both Gly are necessary to enable the flexibility needed for the placement of the loop into the PTC, since it can adopt backbone conformations that are not allowed for other amino acids. In contrast to eRF1, the RF1 and RF2 GGA-mutants were merely slower than the wild-type (Zavialov et al., 2002; Korostelev et al., 2008). The observation that the Gln itself seemed to be replaceable, not to be the sole coordination partner for the water needed for hydrolysis, as well as the conformation of the main-chain in crystal structures, lead to the proposal that the backbone amide of the Gln rather than the sidechain is involved in coordination of the water. This was further supported by substituting the Gln with proline (lacking a primary amine), which lead to a complete loss of hydrolysis activity even with extended incubation times of

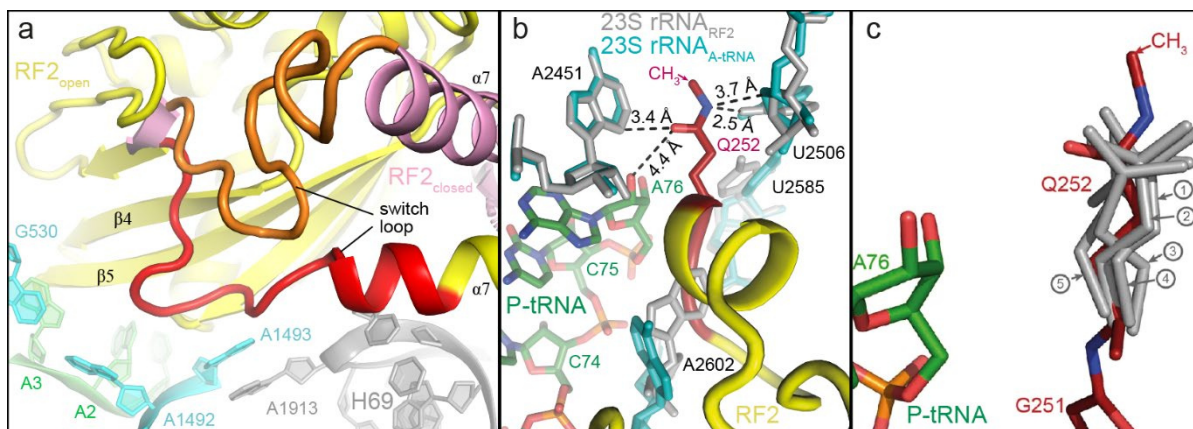


**Figure 10: Conformations of the RF2 switch loop, the decoding center, the peptidyl transferase center and the GQG-motif.** (a) Comparison of the switch loop of RF2 in the closed (RF2<sub>closed</sub>, pink; switch loop, orange; PDBID 6OST) and open (RF2<sub>open</sub>, yellow; switch loop, red; PDBID 6OUO) conformation (Fu et al., 2019). Due to the transition of the switch loop helix  $\alpha 7$  ( $\alpha 7$ ) is extended by ~2 turns (red) in the open conformation. The conformation of the decoding bases G530, A1492 and A1493 of the 16S rRNA (cyan), as well as A1913 in helix 69 (H69) of the 23S rRNA (grey) is shown. mRNA, green. (b) Conformation of the methylated Gln252 (Q252) within the GQG-motif (red) of RF2 (yellow) in the PTC (23S rRNA<sub>RF2</sub>, grey) (PDBID 6C51 (Zeng and Jin, 2018)). Distances between the PTC nucleotides and methylated N5-imino group or the carbonyl oxygen are shown as black dashed lines. Furthermore, comparison of the PTC induced states of 23S rRNA nucleotides A2451, U2506 and U2585 upon binding of RF2 (23S rRNA<sub>RF2</sub>, grey, PDBID 6C51 (Zeng and Jin, 2018)) or A-tRNA (23S rRNA<sub>A-tRNA</sub>, teal, PDBID 1VY4 (Polikanov et al., 2014)). P-tRNA, forest green. (c) Overlay of the conformation of unmethylated Gln252 (grey) from various termination complexes (RF2/UAA, ①, PDBID 4V67 (Korostelev et al., 2008); RF1/UAG, ②, PDBID 4V7P (Korostelev et al., 2010); RF1/UAA, ③, PDBID 4V63 (Laurberg et al., 2008); RF2/UGA, ④, PDBID 4V5E (Weixlbaumer et al., 2008b); RF2/UAA, ⑤, PDBID 4V5J (Jin et al., 2010)) with the conformation of methylated Gln252 (PDBID 6C51 (Zeng and Jin, 2018)). Figure (c) was adapted from Zeng and Jin (2018).

30 min (Korostelev et al., 2008; Santos et al., 2013). The crystal structure of RF2-GGP on the ribosome revealed that the effect is not based on a distortion of the backbone by the pyrrolidin ring of proline that connects the nitrogen of the backbone and the  $\alpha$ -carbon carrying the carboxyl group (Santos et al., 2013). Rather, compared to other amino acids the backbone (secondary) amide of proline cannot donate a H-bond to the carbonyl-oxygen of the peptidyl-tRNA due to its exceptional structure. This was proposed to lead to a failure in stabilising a possible negative charge building up on the carbonyl-oxygen during hydrolysis. Another finding regarding the GGQ-motif is that the methylation of Gln N5 enhances the peptide release and it was suggested by computational analysis and crystal structures that methylation increases the packing of the Gln between the 23S rRNA nucleotides A2451, U2585 and the ribose of U2506 (Mora et al., 2007; Trobro and Aqvist, 2007; Graille et al., 2012; Pierson et al., 2016). A recent crystal structure of methylated RF2 in a post-termination complex supports this suggestion and indicates stabilisation of the Gln by H-bonding with 23S nucleotides U2506 and A2451 *via* the methylated N5-imino group and the carbonyl oxygen of the Gln sidechain, respectively (Figure 10b) (Zeng and Jin, 2018). Additionally, the methyl group on N5 of the Gln sidechain provides increased van der Waals interactions with A2451 and U2506 of the 23S rRNA. This should further stabilise the Gln in a certain position and facilitate efficient hydrolysis (Figure 10c). Compared to peptide bond formation the mechanism of hydrolysis is less known. For example, the exact position of the attacking water has not been observed yet (Jin et al., 2010; Zeng and Jin, 2018). However, the transition state should also proceed *via* a tetrahedral intermediate with an oxyanion on the carbonyl carbon and involve the 2'-OH group of A76 of the P-tRNA (Trobro and Aqvist, 2007; Brunelle et al., 2008; Jin et al., 2010). The latter is supported by a study that replaced the 2'-OH with hydrogen or fluorine, which significantly reduced the rate of peptide release (Brunelle et al., 2008). In contrast to peptide bond formation, only one proton on is transferred during hydrolysis based on kinetic solvent isotope effect measurements and computer simulations (Trobro and Aqvist, 2009; Kuhlenkoetter et al., 2011). The different proton transfer numbers indicate that the PTC is able to catalyse at least two different reactions (Rodnina, 2013), which will be subject of further structural, kinetic, computational and biochemical studies.

After peptide chain release, the dissociation of class I RFs is promoted by the class II RF RF3 (Goldstein and Caskey, 1970; Freistroffer et al., 1997). Thereby, RF1 is more dependent on RF3 than RF2, which has a higher dissociation rate (Adio et al., 2018). RF3 is a translational GTPase consisting of three domains, of these the first domain (domain I) is the conserved G-domain (Gao et al., 2007a; Kihira et al., 2012; Zhou et al., 2012). In contrast to other trGTPases

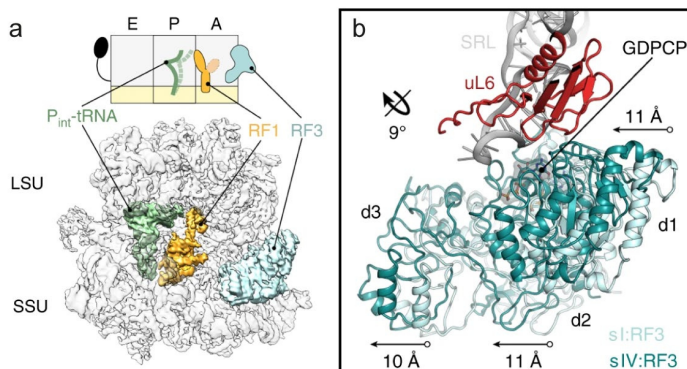


**Figure 11: Accommodation of class II release factor RF3 to the GTPase activating center.**  
 (a) Overview of the binding sites of RF1 (yellow) and RF3 (pale cyan) on the ribosome (grey) with tRNA in an intermediate state ( $P_{int}$ -tRNA, green).  
 (b) An intersubunit rotation of  $9^\circ$  facilitates the approach of RF3 (before rotation, pale cyan; after rotation teal) to the sarcin-ricin loop (SRL, grey) of the 23 S rRNA. The G-domain (domain 1, d1) and 2 (d2) move 11 Å and domain 3 (d3) 10 Å upon rotation. The figure was adapted from Graf et al. (2018).

RF3 has a 4-times higher affinity for GDP than GTP and it has been found that the ribosome can act as guanine nucleotide exchange factor upon RF3·GDP binding (Zavialov et al., 2001; Koutmou et al., 2014; Peske et al., 2014). However, in the cell the excess of GTP over GDP would lead to RF3 being predominantly associated with GTP (Bennett et al., 2009; Peske et al., 2014). Binding of RF3·GTP can occur to pre- and post-termination complex (i.e. before and after peptide release) and even in the absence of a class I RF (Freistroffer et al., 1997; Koutmou et al., 2014; Peske et al., 2014; Adio et al., 2018). Initial cryo-EM and crystal structures of *E. coli* RF3 on *E. coli* as well as *T. thermophilus* ribosomes utilised the latter phenomenon and depicted the conformational changes, which presumably initiate dissociation of class I RFs (Klaholz et al., 2004; Gao et al., 2007a; Zhou et al., 2012). Recently, the mechanism of *E. coli* RF1 release by RF3 was described by an ensemble cryo-EM study of both factors bound to the ribosome (Graf et al., 2018). Surprisingly, RF3 does not contact RF1 directly (Figure 11a), rather it facilitates an intersubunit rotation up to  $10^\circ$ , accompanied by a maximal head swivel of  $4^\circ$  that destabilises RF1 and promotes its dissociation. During the rotation the P-tRNA moves into the P/E-site over several intermediates. Overall, the rotations induced by RF3 are similar to the movements observed with EF-G during translocation (Klaholz et al., 2004; Gao et al., 2007a). This hints towards a general mechanism involving ribosome rotation during the operation of RF3 in termination and EF-G in translocation. As seen in the previous crystal structures of RF3 on the ribosome (Gao et al., 2007a; Zhou et al., 2012), domain II and III establish contacts with rProtein S12 and h5 as well as h15 of the 16S rRNA throughout the rotational process (Graf et al., 2018). In contrast, domain I of RF3 is initially not placed in the GAC, which prevents the interaction of the key histidine (His92) with the SRL (Figure 11b). The intersubunit rotation facilitates a 11 Å movement of domain I, placing it closer to the SRL, which leads to accommodation of domain I to the GAC and enables GTP-hydrolysis (Figure 11b) (Zhou et al., 2012; Graf et al., 2018). This indicates that the active form of RF3 is GTP bound, which is different compared to EF-Tu and EF-G, which act in the GTP and GDP·Pi-bound form, whereas Pi release promotes their dissociation. It has been

discussed that GTP hydrolysis by RF3 is only necessary for dissociation, but the exact role and kinetics are still elusive (Peske et al., 2014; Adio et al., 2018). Also, further structural studies regarding the dissociation and nucleotide state will be needed to fully understand the mechanism of RF3.

#### 1.2.4 Ribosome Recycling

Translation termination leaves the ribosome with an mRNA and a deacylated tRNA in the P-site (post-termination complex, PostTC). In this state the ribosome cannot enter a new round of protein synthesis, unless the tRNA and the mRNA have been removed. Already in 1964 James Watson suggested based on studies in the early sixties that ribosomes might split into subunits for the purpose of encountering a new translation cycle after termination (Watson, 1964). A few years later it was demonstrated by heavy isotope labelling and sucrose density gradient centrifugation that *E. coli* ribosomes do exchange subunits (Mangiarotti and Schlessinger, 1967; Schlessinger et al., 1967; Kaempfer, 1968; Kaempfer et al., 1968). Further kinetic experiments with cell extracts indicated that ribosomes split into subunits once during every translation cycle (Guthrie and Nomura, 1968; Kaempfer, 1968; Kaempfer and Meselson, 1969). It was found subsequently that initiation factor 3 (initially called dissociation factor) is involved in ribosome dissociation into subunits (Subramanian et al., 1968; Subramanian et al., 1969; Sabol et al., 1970; Subramanian and Davis, 1970). Additionally, an essential new factor, the ribosome recycling factor (RRF, initially ribosome releasing factor) was discovered and found to split ribosomes in concert with EF-G in a GTP dependent manner (Hirashima and Kaji, 1970, 1972, 1973; Subramanian and Davis, 1973; Ogawa and Kaji, 1975; Kaziro, 1978; Janosi et al., 1994; Zavialov et al., 2005). Albeit EF-G action should differ from translocation mode, since most steps in translocation can be performed with a non-hydrolysable GTP-analogue, whereas subunit dissociation requires GTP, as well as GTP hydrolysis (Rodnina et al., 1997; Karimi et al., 1999; Hirokawa et al., 2005; Peske et al., 2005; Zavialov et al., 2005). Moreover, recycling does not involve mRNA movement, i.e. translocation of the tRNA-mRNA complex (Peske et al., 2005).

The crystal structure of isolated RRF from *E. coli* and three additional organisms showed an overall L-shape and a two-domain structure (Selmer et al., 1999; Kim et al., 2000; Toyoda et al., 2000; Nakano et al., 2003). Domain I forms a three helix bundle, whereas domain II has  $\beta/\alpha/\beta$ -topology, both domains are connected by two linkers. Comparison of the crystal structures with the solution structure of RRF, as well as NMR relaxation experiments showed

that the linkers are flexible (Yoshida et al., 2001; Yoshida et al., 2003). Further mutational analysis of the linker region indicated that the flexibility is functionally relevant (Toyoda et al., 2000). Despite the L-shape of RRF it was initially shown by hydroxyl radical probing that the binding site in the ribosomal A-site of RRF differs from the binding site of A-tRNA (Lancaster et al., 2002). This was supported by several cryo-EM and crystal structures of RRF bound to the ribosome or the 50S subunit (Agrawal et al., 2004; Gao et al., 2005; Wilson et al., 2005; Dunkle et al., 2011). In the structures, domain II bound on top of rProtein S12 close to the A-site. Although RRF did not sink into the DC it can contact bridge B2a, which is formed by 16S rRNA h44 and A1913 of 23S rRNA H69. The tip of RRF domain I was found to bind to the 50S subunit in the intersubunit space at the central protuberance, close to rProtein L5 and contacting the P-loop of the PTC. This conformation would clash with a P/P-tRNA, and in accordance binding of RRF facilitates the rotated state of the ribosome with the tRNA in the P/E-hybrid state (Gao et al., 2005; Sternberg et al., 2009; Dunkle et al., 2011; Fu et al., 2016; Prabhakar et al., 2017). Kinetic studies indicate that RRF binds first followed by EF-G, proving in conclusion that the structures of RRF on the 70S ribosome in the absence of EF-G are physiologically relevant (Borg et al., 2016; Prabhakar et al., 2017). It has been proposed that the binding of EF-G in this state is similar to binding to the ribosome in the pre-translocation state (Agrawal et al., 2004; Gao et al., 2005; Wilson et al., 2005; Weixlbaumer et al., 2007). Unfortunately, the first cryo-EM structure of both factors on the 70S ribosome has been questioned regarding its physiological relevance. The complex was formed by binding *T. thermophilus* RRF and *E. coli* EF-G to the *E. coli* ribosome (Yokoyama et al., 2012). *In vitro* and *in vivo* experiments indicate that this heterologous combination does not have recycling activity (Toyoda et al., 2000; Ito et al., 2002; Raj et al., 2005), rendering the interpretation of the structural data difficult. A recent crystal structure by Zhou et al. (2019a) obtained both factors on the ribosome, but EF-G was in the debatable closed state (cf. translocation), which can be an initial binding state of EF-G, but did not provide further insight in the interaction between RRF, EF-G and the ribosome. In contrast, a 9 Å cryo-EM reconstruction of both factors in a post-splitting complex (i.e. bound to the 50S subunit) showed that RRF domain II and its hinge region interact with domain III and IV of EF-G, while EF-G domain I was associated with the GAC (Gao et al., 2007b). Furthermore, a time-resolved cryo-EM study using *E. coli* ribosomes and factors obtained low resolution (7.4-18 Å) intermediate steps of ribosome recycling and arranged the states based on a previous kinetic study (Borg et al., 2016; Fu et al., 2016). The study confirms the interaction between domain II of RRF and EF-G domains III and IV. Moreover, upon binding of EF-G the interaction between rProtein S12 and

RRF domain II was lost, and as a result domain II of RRF was found close to the intersubunit bridge B2a. This indicates that the concerted action of RRF and EF-G disrupts the intersubunit bridge, as already suggested based on previous cryo-EM and crystal structures (Agrawal et al., 2004; Gao et al., 2005; Wilson et al., 2005; Gao et al., 2007b; Weixlbaumer et al., 2007; Dunkle et al., 2011; Yokoyama et al., 2012). After dissociation of the ribosome into subunits the RRF and EF-G remained associated with the 50S subunit, whereas the tRNA was found in both, the 50S E-site and 30S P-site. In contrast, the mRNA was still bound to the 30S subunit, additionally IF3 was associated with the SSU (Fu et al., 2016). The action of IF3, as well as the dissociation of mRNA and tRNA remains a controversial subject. IF3 was found to promote dissociation of mRNA and tRNA from the 30S subunit (Karimi et al., 1999; Prabhakar et al., 2017). By contrast, it was also proposed that the association of mRNA and tRNA with the 30S is due to the SD-sequences of the short model mRNAs and dissociation of both actually occur before splitting, with the mRNA leaving first, followed by the tRNA (Chen et al., 2017). In the latter, the only task of IF3 would be to prohibit (re-)binding of the 50S subunit, which is generally necessary after subunit dissociation (Hirokawa et al., 2005; Peske et al., 2005; Prabhakar et al., 2017). Furthermore, IF3 connects ribosome recycling, the end of the translation cycle to initiation, the start of a new round of protein synthesis.

### 1.3 Ribosome Rescue in Bacteria

Ribosomes that stall on an mRNA lacking a stop codon (non-stop mRNA) cannot continue elongation or be terminated, since the mRNA ends in the P-site and there is no codon available in the A-site of the ribosome. There are various events that lead to the formation of non-stop ribosomal complexes in bacteria (Figure 1). For example readthrough of the stop codon (nonsense suppression), miscoding inducing drugs or non-programmed frameshifting can lead to the lack of an in-frame stop codon and translation of the mRNA until the 3'-end is reached (Abo et al., 2002; Ueda et al., 2002). Another reason is premature transcription termination, which leads to incomplete or truncated mRNA. Since translation of an mRNA can be initiated before transcription is finished the ribosome would end up in a non-stop complex if transcription terminates prematurely. However, the processivity of RNA polymerase is high and these events are likely to be rare (Nudler et al., 1996). Furthermore, truncated mRNAs can be generated by chemical or physical damage, as well as the activity of RNases during mRNA turnover, which is mostly carried out by 3'-5' exonucleases (Bandyra and Luisi, 2013).

Exonucleolytic cleavage of the stop codon of an actively translated mRNA would lead to the formation of a non-stop complex. Additionally prolonged ribosome stalling on intact mRNAs, due weak termination sequences or rare codon stretches can induce RNase II dependent mRNA cleavage in the ribosome A-site, directly leading to non-stop complexes (Hayes and Sauer, 2003; Sunohara et al., 2004b; Li et al., 2006; Li et al., 2007; Garza-Sánchez et al., 2009). Truncated mRNAs are also part of the bacterial stress response. For example, nutrient starvation induces endonuclease toxins, like RelE (Christensen et al., 2001; Pedersen et al., 2003). RelE is part of the RelBE toxin-antitoxin system, RelB (antitoxin) and RelE (toxin) are associated and inactive under normal conditions. Whereas upon starvation RelB is degraded and the endonuclease RelE is activated (Christensen et al., 2001). RelE then creates non-stop complexes by cleaving the mRNA in the A-site of the ribosome (Pedersen et al., 2003; Neubauer et al., 2009). Generation of non-stop complexes during starvation is likely a general mechanism to temporarily reduce the energy consumption, since protein production consumes ~50% of energy in growing *E. coli* cells (Russell and Cook, 1995; Pedersen et al., 2003; Garza-Sánchez et al., 2008). However, the non-stop complexes need to be resolved when starvation

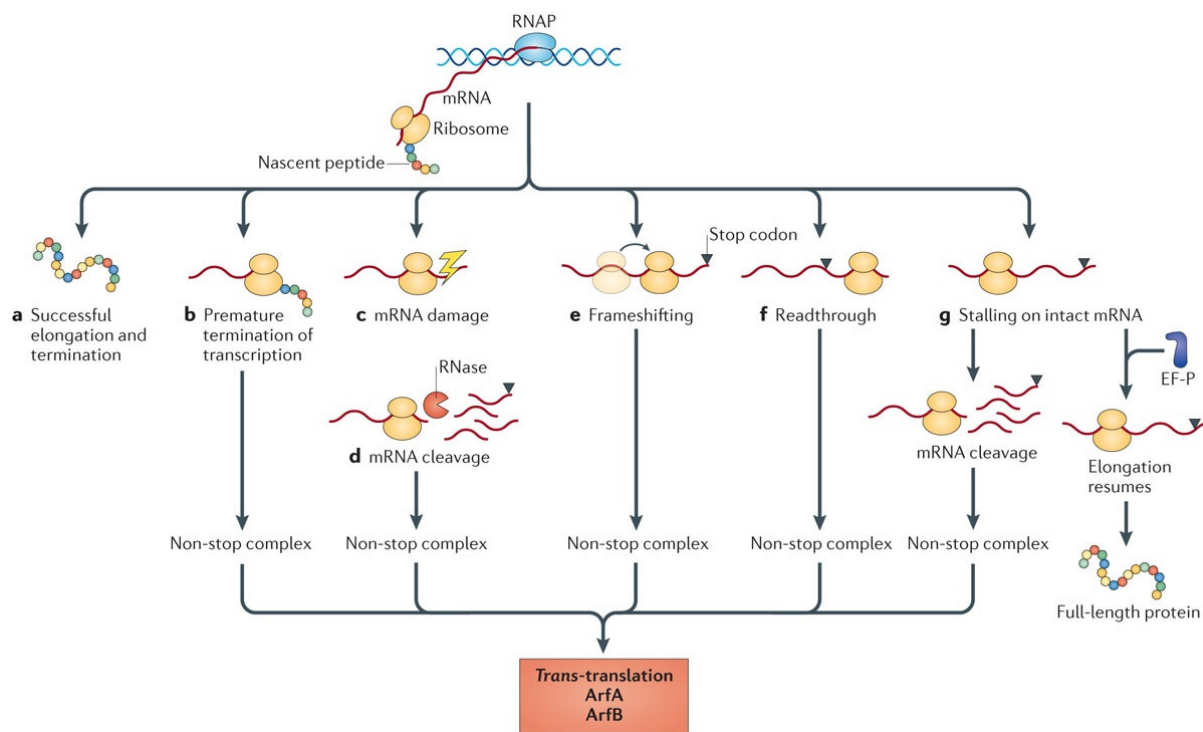


**Figure 12: Events of translational stalling leading to non-stop complexes and ribosome rescue.** Prokaryotic ribosomes can initiate translation while the mRNA is transcribed by RNA polymerase (RNAP). This event can lead to successful protein production (a) or to a non-stop complex, due to premature transcription termination (b). Further events producing non-stop complexes are damage of the mRNA (c), cleavage of the mRNA (d), frameshifting (e) and readthrough of the stop codon. Stalling on an intact mRNA can lead to mRNA cleavage and a non-stop complex or can be resolved and translation resumes. mRNAs containing certain proline motifs need the assistance of EF-P to continue translation (Starosta et al., 2014b; Huter et al., 2017a). Non-stop complexes are primarily subjected to *trans*-translation, if *trans*-translation is overwhelmed or absent alternative ribosome rescue factor (Arf) A or B can relieve the non-stop complex instead. The figure was adapted from Keiler (2015).

is alleviated. Measurements of non-stop complexes of growing *E. coli* cells indicate that ~2-4 % of peptidyl tRNAs are not hydrolysed, referring to frequent occurrence of non-stop complexes under normal conditions (Ito et al., 2011). Bacteria have evolved mechanisms to rescue the non-stop complexes, otherwise ribosomes stalled on non-stop mRNA are removed from the pool of ribosomes, as a consequence protein production of the cell diminishes and has toxic effects for the cell (Keiler et al., 1996; Karzai et al., 1999; Moore and Sauer, 2005; Chadani et al., 2010; Chadani et al., 2011b; Goralski et al., 2018; Shimokawa-Chiba et al., 2019). The major pathway, identified in >99% of bacterial genomes is *trans*-translation, which is mediated by transfer-messenger RNA (tmRNA, formerly 10S, 10Sa RNA or *ssrA* RNA) and small protein B (SmpB) (Tu et al., 1995; Keiler et al., 1996; Karzai et al., 1999; Hudson et al., 2014). The complex of tmRNA and SmpB mimics the structure of tRNA, which allows it to be charged with alanine, and to bind to the ribosomal A-site (Komine et al., 1994; Ushida et al., 1994). The messenger-part of tmRNA encodes a short reading frame, followed by a stop codon (Keiler et al., 1996). The ribosome resumes translation on the messenger-part, terminates on the stop codon and is recycled eventually (Keiler et al., 1996; Rae et al., 2019). The mRNA and the nascent peptide originating from the non-stop complex are targeted for degradation by means of *trans*-translation, so that all components of the non-stop complex are recycled or removed during the process (Keiler et al., 1996; Yamamoto et al., 2003). In some pathogenic bacteria, like *Neisseria gonorrhoeae* or *Mycobacterium tuberculosis*, *trans*-translation is essential, while others have developed protein-based alternative ribosome rescue factors (Arf) (Huang et al., 2000; Keiler and Feaga, 2014; Personne and Parish, 2014). ArfA recruits RF2 to hydrolyse the nascent polypeptide chain from the P-site tRNA, whereas ArfB harbours a GGQ-motif and can perform hydrolysis itself (Chadani et al., 2010; Chadani et al., 2011b; Handa et al., 2011; Chadani et al., 2012). The phylogenetic distribution of ArfA is restricted to a subset of  $\beta$ - and  $\gamma$ -proteobacteria, while ArfB has a wider distribution of 34 % in representatively sequenced bacterial genomes (Schaub et al., 2012; Feaga et al., 2014a). In *Francisella tularensis* and *B. subtilis* *trans*-translation is not essential, but both have no apparent Arf homologue and it was speculated that this could hint towards further alternative ribosome rescue systems (Shin and Price, 2007; Svetlanov et al., 2012; Keiler and Feaga, 2014). This was supported by recent studies, which identified ArfT in *F. tularensis* and *Bacillus* ribosome rescue factor A (BrfA) in *B. subtilis* (Goralski et al., 2018; Shimokawa-Chiba et al., 2019). Like ArfB, ArfT has a broader phylogenetic distribution (Burroughs and Aravind, 2019). Interestingly, ArfT cooperates with RF1 and RF2 for hydrolysis of the nascent chain (Goralski et al., 2018). BrfA is likely limited to the *Bacillus* genus and exclusively recruits RF2, hence

BrfA has some similarities but also differences to ArfA (Shimokawa-Chiba et al., 2019). Due to the little knowledge about ArfT it will not be included in the following sections, while the residual ribosome rescue mechanisms will be elucidated in greater detail.

**Trans-translation** is the major pathway of ribosome rescue in bacteria and is mediated by the ribonucleoprotein complex of tmRNA and SmpB. tmRNA was already discovered in 1979 as one of the stable RNAs in *E. coli* (Ray and Apirion, 1979), but its function and the cooperation with SmpB was described later in the 90s (Tu et al., 1995; Keiler et al., 1996; Karzai et al., 1999). Subsequently, tmRNA was named after its properties, as it contains a tRNA-like and a mRNA-like domain, connected by several pseudoknots (Figure 13a) (Atkins and Gesteland, 1996; Felden et al., 1996). Usually tmRNA is a single RNA molecule of approximately 360 nucleotides, but in some bacterial species tmRNA is composed of two RNA chains (Williams and Bartel, 1996; Keiler et al., 2000). However, the secondary structure and the function are conserved throughout bacteria. In single molecule tmRNAs the tRNA-like domain (TLD) consists of the 5'- and 3'-ends (Figure 13a), which fold into a secondary structure that resembles tRNA<sup>Ala</sup> without the ASL (Komine et al., 1994; Ushida et al., 1994; Gutmann et al., 2003; Ramrath et al., 2012). This allows recognition and charging of the 3'-CCA end of the TLD with alanine by the canonical alanyl-tRNA synthetase (Komine et al., 1994). Moreover, the binding affinity of EF-Tu for the TLD and tRNAs is comparable (Rudinger-Thirion et al., 1999; Barends et al., 2000). tmRNA binds to SmpB with high affinity, which occupies the space of the missing ASL and is required for *trans*-translation (Karzai et al., 1999; Gutmann et al., 2003; Cheng et al., 2010; Weis et al., 2010a; Neubauer et al., 2012). SmpB is a protein of ~160 amino acids with a globular N-terminal domain and a C-terminal tail, which is unstructured in solution (Dong et al., 2002). The formation of the tmRNA·SmpB complex stabilises the secondary structure of tmRNA and advances the interaction with alanyl-tRNA synthetase (Karzai et al., 1999; Wiegert and Schumann, 2001; Keiler and Shapiro, 2003). The mRNA-like domain (MLD) harbours the ‘tag reading frame’, which encodes a short degradation tag (‘tag peptide’) that is added C-terminally to the nascent protein and varies in length (8-35 amino acids) in different species (Figure 13a) (Komine et al., 1994; Tu et al., 1995; Felden et al., 1996; Williams and Bartel, 1996; Keiler et al., 2000). The first alanine of the tag peptide (AANDENYALAA in *E. coli*) is not encoded in the tag reading frame, instead it is the alanine attached to the TLD (Tu et al., 1995; Keiler et al., 1996). The tag reading frame differs from an ORF, since it does not include a start codon, however it ends with a stop codon (UAA) (Figure 13a) (Williams et al., 1999).

Biochemical and structural data acquired over the last three decades paint a good picture over the mechanism of *trans*-translation. The ribonucleoprotein complex of tmRNA·SmpB is delivered to the A-site of the ribosome in a quaternary complex with EF-Tu·GTP (Figure 13b) (Rudinger-Thirion et al., 1999; Barends et al., 2000; Valle et al., 2003; Fu et al., 2010; Weis et al., 2010b; Neubauer et al., 2012). Upon binding, the C-terminal tail of SmpB probes the mRNA entry channel (Neubauer et al., 2012) and *in vitro* assays imply that *trans*-translation is reduced by mRNAs extending beyond the decoding center (Hayes and Sauer, 2003; Ivanova et al., 2004; Moore and Sauer, 2005). Additionally, comparison of the path of a full-length mRNA and SmpB indicate a severe clash between both, which also suggests that the preferred substrate for *trans*-translation is a non-stop complex with an empty mRNA entry channel (Neubauer et al., 2012; Huter et al., 2017b). The C-terminal tail of SmpB attaches to the surrounding 16S rRNA of the mRNA entry channel *via* positively charged residues and motifs, and engages an  $\alpha$ -helical conformation on the ribosome. One conserved stretch is the DKR-motif (Asp137Lys138Arg139 in *E. coli*). Albeit single mutations in the motif had only a marginal effect, the substitution of all three residues to alanine eliminated *trans*-translation activity *in vitro* and *in vivo* (Sundermeier et al., 2005; Miller et al., 2011). Moreover, truncation of the C-terminal tail lead to a similar effect (Jacob et al., 2005; Sundermeier et al., 2005). In both cases the association with the ribosome was not abolished, but the tagging activity was strongly inhibited, indicating that the interactions are required mechanistically and are not redundant. The globular domain and the upper part of the C-terminal tail of SmpB bind to the decoding center *via* positively charged residues, which are in H-bond distance to the 16S rRNA (Neubauer et al., 2012). Furthermore, conserved aromatic residues of SmpB stack on the decoding bases G530 and A1493, whereas A1492 remains flipped into h44 (OFF- state) and stacks with A1913 of H69. Mutations of the decoding bases (G530A, A1492G or A1493G) were found to reduce the activity of *trans*-translation only twofold, whereas accommodation of aa-tRNA to the PTC was reduced  $\sim$ 1000-fold (Miller et al., 2011). Hence, the binding of tmRNA·SmpB based on the stacking interactions is less dependent on the identity of the base than on the stabilisation and monitoring of the codon:anticodon interaction by H-bonds during decoding (Ogle et al., 2001; Ogle et al., 2002; Neubauer et al., 2012). Overall, the conformation of the TLD and SmpB in the tmRNA·SmpB·EF-Tu·GTP quaternary complex in the A-site is similar to the A/T-state of aa-tRNA·EF-Tu·GTP during decoding (Figure 13b) (Schmeing et al., 2009; Neubauer et al., 2012). The pseudoknots of tmRNA were found to be wrapped around the head of the SSU (Valle et al., 2003; Fu et al., 2010; Neubauer et al., 2012). Thereby, pseudoknot 2 and helix 5 of tmRNA are bound close to the entrance of the mRNA channel (Fu

et al., 2010). These interactions remain throughout *trans*-translation, act as flexible hinge and anchor tmRNA to the ribosome, whereas the rest of the pseudoknots change their position during the process (Rae et al., 2019). In contrast to the release of the CCA-end of aa-tRNAs from EF-Tu during elongation, kinetic studies indicate that the process for tmRNA·SmpB is independent of GTP hydrolysis (Kurita et al., 2014b; Miller and Buskirk, 2014), although EF-Tu localises to the GAC in both cases (Schmeing et al., 2009; Neubauer et al., 2012). The release of the TLD of tmRNA from EF-Tu and the role of GTP hydrolysis in this regard need to be further evaluated in future experiments.

After accommodation of the TLD to the A-site of the PTC transpeptidation occurs and the nascent polypeptide chain is transferred from the P-site tRNA to the alanine that is attached to the TLD of tmRNA·SmpB (Figure 13c) (Tu et al., 1995; Keiler et al., 1996; Fu et al., 2010; Weis et al., 2010a; Ramrath et al., 2012). Translocation of tmRNA·SmpB is also assisted by

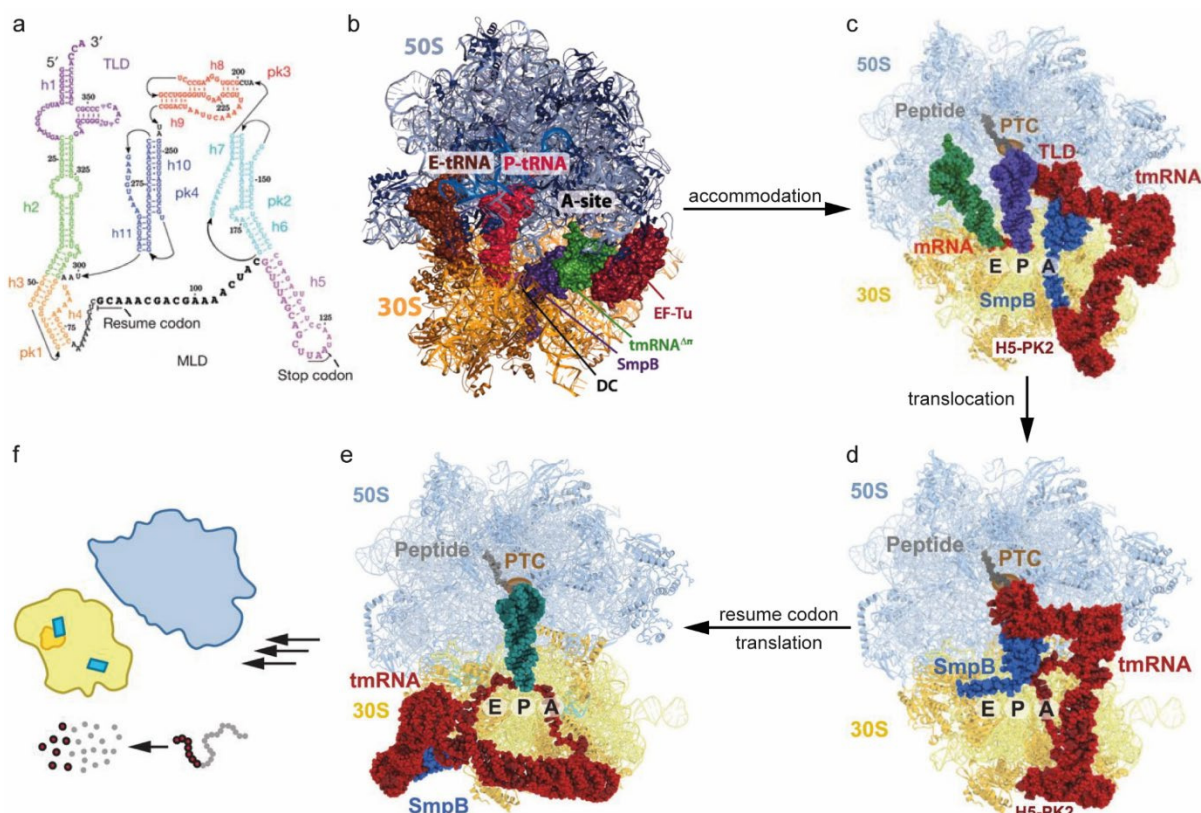


**Figure 13: Rescue of non-stop complexes by trans-translation.** (a) Overview of the *E. coli* tmRNA secondary structure. h, helix; pk, pseudoknot. (b) A fragment of tmRNA is bound to the A-site of the ribosome as part of the tmRNA·SmpB·EF-Tu·GTP quaternary complex. tmRNA·SmpB resembles the A/T-state of tRNAs during decoding and the C-terminal tail of SmpB occupies the empty mRNA entry channel in the helical conformation (PDBID 4V8Q). (c) The TLD of tmRNA has accommodated to the PTC and tmRNA·SmpB mimics the A/A-state of an A-site bound aa-tRNA (PDBID 6Q97). Helix 5 (H5) and pseudoknot 2 (PK2) bind close to the entrance of the mRNA channel. Peptidyl transfer from the P-site tRNA to the TLD of tmRNA takes place. (d) Translocation of tmRNA·SmpB to the P-site has occurred (PDBID 6Q98). The C-terminal tail of SmpB extends into the E-site and the mRNA, as well as E-site tRNA were expelled. The resume codon of tmRNA is placed in the A-site and the MLD passed through the A-site latch and is bound to the mRNA entry channel. (e) After decoding of the resume codon by a cognate tRNA and peptidyl transfer, translocation moves tmRNA·SmpB past the E-site, thereby the MLD is fully loaded to the mRNA channel (PDBID 6Q9A). (f) After translation of the tag reading frame termination and ribosome recycling occur. The tagged peptide is degraded by proteases. Figure a was adapted from Ramrath et al. (2012) and b from Neubauer et al. (2012). Figure c-f were modified from Rae et al. (2019).

EF-G. A cryo-EM study showed that domain IV of EF-G binds next to the globular domain of SmpB (Ramrath et al., 2012). As in translocation of A- and P-site tRNAs, the tmRNA·SmpB complex and the tRNA were in ap/P and pe/E chimeric hybrid states, respectively. During translocation the MLD has to be loaded into the mRNA channel, therefore it has to pass the A-site (or 30S) latch between h34 of the head and the G530-loop of the body (Ramrath et al., 2012; Rae et al., 2019). Ramrath et al. (2012) suggested that the latch opens by an ‘unique extra-large swivel of the 30S head’, which includes an additional incline of the head besides the swivel observed during canonical translocation. In the POST-translocation ribosome, the TLD and SmpB were located in the P-site, with the C-terminal helix of SmpB extending towards the E-site (Figure 13d) (Rae et al., 2019). The first (resume) codon of the MLD was placed in the A-site. Cryo-EM and mutational studies indicate that the first 5 bases upstream of the MLD interact with SmpB, which is important for proper placement of the resume codon (Lee et al., 2001; Konno et al., 2007; Rae et al., 2019). Subsequently a cognate tRNA binds to the resume codon, leading to peptide bond formation and translocation. Rae and co-workers found the TLD and SmpB beyond the E-site after the second translocation step (Figure 13e) and concluded that the complex would clash with the ribosome in the E-site, hence tmRNA·SmpB would not mimic a tRNA in the E-site (Rae et al., 2019). During the second translocation the MLD is fully loaded into the mRNA channel by passing through a second latch (E-site latch) between protein uS7 of the head, as well as uS11 and the 16S rRNA nucleotide G693 of the body. If an ‘extra-large swivel’ of the head domain during the second translocation accompanies the loading is not clear yet.

Afterwards translation continues on the MLD, adding the tag peptide to the nascent polypeptide chain, until the stop codon (usually UAA) at the end of the tag reading frame enters the A-site (Tu et al., 1995; Keiler et al., 1996). Subsequent termination and ribosome recycling occur (Figure 13f). The tag peptide added to the polypeptide by *trans*-translation is recognized by several proteases, like ClpXP, ClpAP and Lon, which promotes rapid degradation of the peptide chain (Gottesman et al., 1998; Flynn et al., 2001; Choy et al., 2007). Additionally, the defective mRNA is targeted for degradation by ribonuclease R (RNase R), which is required for mRNA decay and is enriched in non-stop complexes (Mehta et al., 2006; Richards et al., 2006; Ge et al., 2010; Venkataraman et al., 2014a; Venkataraman et al., 2014b). Recruitment of RNase R is mediated by the 3'-end of the tmRNA tag reading frame. The mechanism of the recruitment is not known yet, but mutations in the 3'-end region of the MLD prohibit the targeting of RNase R (Venkataraman et al., 2014b). Furthermore, the mechanism of handing over the mRNA from the non-stop complex to RNase R still needs to be elucidated. According

to Rae et al. (2019) the mRNA is already ejected during the first translocation step. RNase R is a 3'-5' exonuclease and the 3'-end of the mRNA remains inside the ribosome until its ejection. The recruitment of RNase R to the pre-translocation non-stop complex would bring RNase R in close proximity to the target mRNA prior to ejection, which could be one way to promote degradation (Keiler, 2015).

The degradation of the polypeptide and the mRNA is an advantage of tmRNA over the backup mechanisms (Hudson et al., 2014). However, resolving the non-stop complexes by backup mechanisms ensures the survival of the bacterial cell in absence of *trans*-translation (Feaga et al., 2014a; Keiler and Feaga, 2014), but leads to different phenotypes, particularly under stress conditions, depending on the species. For instance, deletion of *trans*-translation in *E. coli* leads to increased sensitivity to antibiotic stress, whereas *B. subtilis* is rendered temperature sensitive and *Francisella tularensis* displayed virulence defects (Abo et al., 2002; Shin and Price, 2007; Svetlanov et al., 2012; Li et al., 2013).

**Alternative ribosome rescue factor A (ArfA, former YhdL)** was discovered in a synthetic lethality screen in *E. coli* with deletion of the *ssrA* gene, which encodes tmRNA (Chadani et al., 2010). The study showed that ArfA is essential in the absence of tmRNA, i.e. *trans*-translation, and *vice versa*. Furthermore, tmRNA encoding a degradation deficient tag peptide was able to relieve the synthetic lethal phenotype, supporting that resolving non-stop complexes is essential for viability, rather than degradation of the defective peptide. ArfA expression was found to be dependent on *trans*-translation (Garza-Sanchez et al., 2011; Schaub et al., 2012). The *arfA* gene encodes 72 amino acids, but contains a stem loop structure, which can cause premature transcription termination or serves as target for specific cleavage by RNase III, leading to a non-stop mRNA in either case (Figure 14a) (Chadani et al., 2011a; Garza-Sanchez et al., 2011; Schaub et al., 2012). Even if full-length *arfA* mRNA and ArfA protein is produced occasionally the C-terminal amino acids are highly hydrophobic, rendering full-length ArfA aggregation prone and unstable with a short half-life of 1.6 minutes (Figure 14a) (Chiti, 2006; Chadani et al., 2011a). However, the majority of ArfA translation originates from truncated mRNA, which ends up in a non-stop complex and is subjected to *trans*-translation (Figure 14a) (Chadani et al., 2011a; Garza-Sanchez et al., 2011; Schaub et al., 2012). Only if *trans*-translation is defective or overwhelmed the C-terminally truncated ArfA escapes from the ribosome (Figure 14b). The truncated ArfA (referred to as ArfA afterwards) usually lacks the last 17-18 amino acids and maintains activity (Chadani et al., 2010; Chadani et al., 2011a; Garza-Sanchez et al., 2011; Schaub et al., 2012). This indicates that the terminal

amino acids are mainly important for regulation and not for activity, which is in line with their poor conservation (Chadani et al., 2011a; Garza-Sanchez et al., 2011; Schaub et al., 2012). The production of ArfA from truncated mRNA and thus the regulation by *trans*-translation indicates that it is indeed a backup mechanism for *trans*-translation.

In a cell extract-based translation assay ArfA was able to release a truncated peptide produced by a model non-stop mRNA, while the identified ArfA(A18T), which caused the synthetic lethal phenotype, had no release activity (Chadani et al., 2010). In follow up studies, it was shown that ArfA could not release the peptide itself, instead release activity was specifically dependent on canonical RF2 (Chadani et al., 2012; Shimizu, 2012). Furthermore, ArfA and also ArfA(A18T) were able to bind to the non-stop complex and to recruit RF2, indicating that ArfA(A18T) fails to activate RF2 hydrolysis (Shimizu, 2012). Interestingly, the release activity of ArfA/RF2 was independent of the SPF-motif, which suggests that ArfA does not mimic a stop codon. In contrast, the GQQ-motif was essential as in canonical termination (Chadani et al., 2012).

ArfA was found to be associated with isolated 50S subunits, which could demonstrate an initial binding site even in the absence of the 30S subunit (Chadani et al., 2010; Kurita et al., 2014a). However, ArfA binding was mapped to the 30S subunit by hydroxyl radical probing using a non-stop complex as substrate (Kurita et al., 2014a). Moreover, the pattern of the map partly

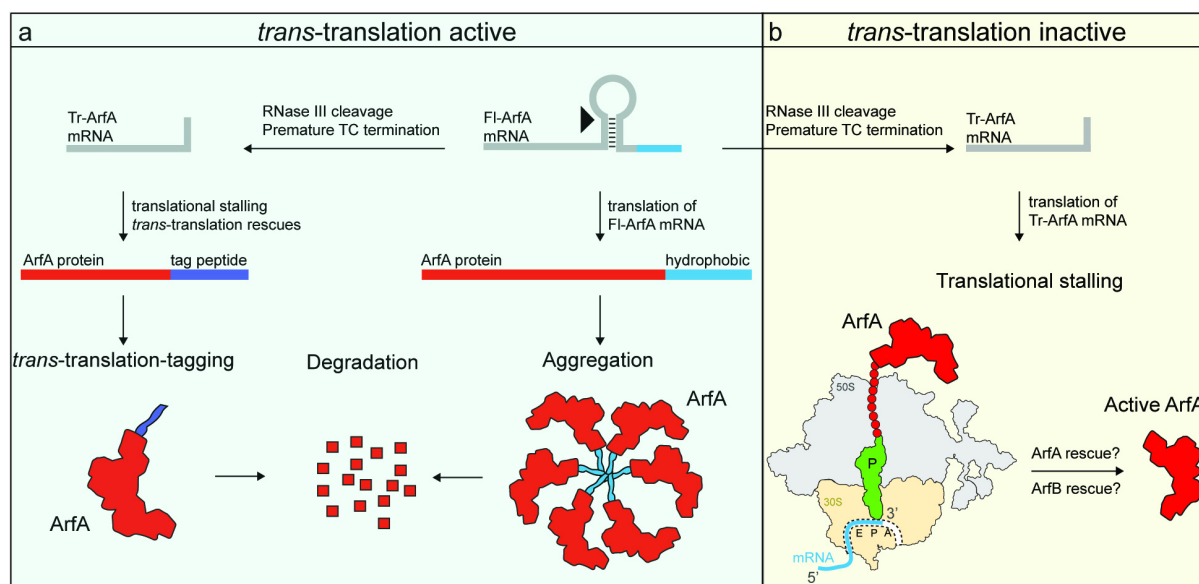


**Figure 14: Expression of ArfA is regulated via *trans*-translation.** (a) Full-length (Fl) ArfA mRNA (grey) harbours a stem loop structure, which can be targeted by RNase III. The stem loop can also cause premature transcription (TC) termination during transcription of the *arfA* gene. RNase III cleavage and premature TC termination lead to truncated (Tr) ArfA mRNA. As consequence ArfA protein (red) is tagged by *trans*-translation (tmRNA-tag, purple) during translation and degraded subsequently. Fl-ArfA mRNA encodes a C-terminal hydrophobic stretch (blue), so that occasional translation of Fl-ArfA protein leads to aggregation and degradation. (b) If *trans*-translation is overwhelmed or inactive translation of Tr-ArfA mRNA leads to translational stalling. Tr-ArfA protein, which is the active form of ArfA, could initially be released by free ArfA, ArfB or spontaneous hydrolysis, afterwards Tr-ArfA accedes ribosome rescue of non-stop complexes. The figure was adapted from Huter et al. (2017b).

changed with respect to RF2 presence. In particular, the pattern of the C-terminus was unchanged and mapped binding to the mRNA entry channel in an overlapping position to SmpB, indicating that ArfA monitors the mRNA entry channel. The N-terminal interactions around the decoding center altered when RF2 was bound and suggested the induction of a stable productive conformation for both, ArfA and RF2. Five cryo-EM structures provided detailed insight into the rescue mechanism by ArfA and RF2 recruitment to non-stop complexes (James et al., 2016; Demo et al., 2017; Huter et al., 2017c; Ma et al., 2017; Zeng et al., 2017). Despite the distinct approaches to generate the non-stop complexes with ArfA and RF2 the overall results are similar, which will be further described in this section. Differences will be outlined and discussed in the discussion section.

In all studies C-terminally truncated ArfA was used, which was shortened by 12 (James et al., 2016; Demo et al., 2017) or 17 amino acids (Huter et al., 2017c; Ma et al., 2017; Zeng et al., 2017). Despite the different ArfA length of 55-60 residues the electron density only allowed modelling of 46-48 amino acids due to flexibility of the very C-terminus. This suggests that these residues are less important for association with the ribosome and is in agreement with their poor conservation (Chadani et al., 2011a; Garza-Sanchez et al., 2011; Schaub et al., 2012). The position of the C-terminus within the mRNA entry channel is consistent with the data from the aforementioned hydroxyl radical probing and overlaps with the path of a full-length mRNA (Figure 15a), which further supports the hypothesis that the C-terminus of ArfA monitors the mRNA entry channel (Kurita et al., 2014a; James et al., 2016; Demo et al., 2017; Huter et al., 2017c; Ma et al., 2017; Zeng et al., 2017). In contrast to the defined path of the  $\alpha$ -helical tail of SmpB (Neubauer et al., 2012) the C-terminus of ArfA forms a loop that obstructs the mRNA entry channel (Figure 15a) (James et al., 2016; Demo et al., 2017; Huter et al., 2017c; Ma et al., 2017; Zeng et al., 2017). This could explain the difference in the ability to act on non-stop complexes with extension of the mRNA past the P-site. While *trans*-translation was shown to act on complexes with more than nine nucleotides downstream of the P-site, the activity of ArfA is strongly reduced by more than three nucleotides (Ivanova et al., 2004; Asano et al., 2005; Shimizu, 2012; Kurita et al., 2014b; Zeng and Jin, 2016). This is in agreement with the structural data, showing that the ArfA C-terminus allows maximal three nucleotides in the decoding center (James et al., 2016; Demo et al., 2017; Huter et al., 2017c; Ma et al., 2017; Zeng et al., 2017). Similar to SmpB, ArfA binds to the mRNA entry channel *via* H-bonding of positively charged amino acids with the 16S rRNA in a redundant manner, so that single mutations do not interfere with binding (Sundermeier et al., 2005; Miller et al., 2011; Kurita et al., 2014a; Ma et al., 2017; Zeng et al., 2017). By contrast shortening ArfA by 32 C-terminal

amino acids, leaving only 40 amino acids of ArfA, abolished rescue activity (Chadani et al., 2011a), indicating that removing positively charged stretches cannot be compensated for and reduces binding to the mRNA entry channel.

James et al. and Demo et al. were able to observe the recruitment of RF2 in the closed conformation (Figure 15b and c) using different approaches (James et al., 2016; Demo et al., 2017). While for Korostelev and co-workers the closed conformation appeared as a subset of their dataset (Demo et al., 2017), Ramakrishnan and co-workers formed two additional complexes with ArfA(A18T) and *T. thermophilus* RF2 (James et al., 2016), respectively. Comparison of the closed conformation of RF2 upon stop-codon recognition or recruitment by ArfA based on the alignment of the 16S rRNA showed that RF2 is in the same overall conformation in either case (James et al., 2016; Demo et al., 2017; Fu et al., 2019). The ArfA residues glutamine 27 (Q27) till glutamic acid 30 (E30) mediate the recruitment of RF2 by augmenting a  $\beta$ -strand to  $\beta$ -strand  $\beta$ 5 of the  $\beta$ -sheet formed by the superdomain 2/4 of RF2 (Figure 15c). Additionally, phenylalanine 25 (F25) of ArfA implements further hydrophobic

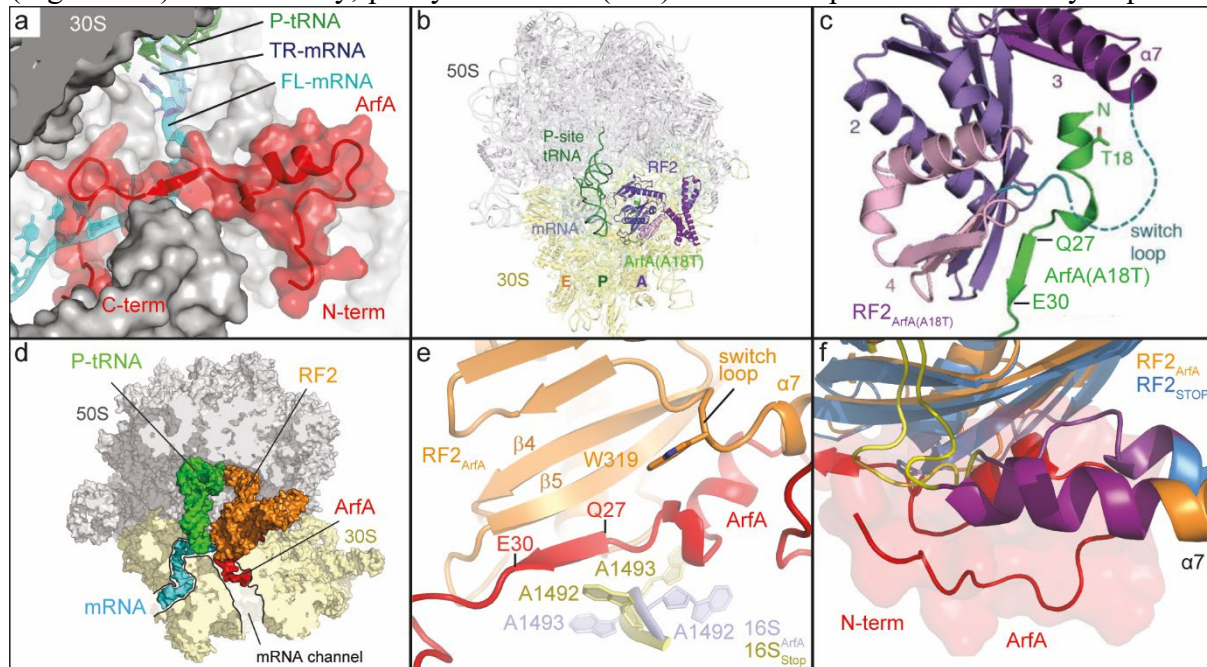


**Figure 15: Interactions of ArfA and ArfA(A18T) with RF2 and a non-stop complex.** (a) ArfA (red) is bound to the mRNA entry channel of the 30S subunit (grey) of a non-stop complex with P-site tRNA (green) and truncated mRNA (TR-mRNA, dark blue) (PDBID 5MGP (Huter et al., 2017c)). Full-length mRNA (FL-mRNA, blue, PDBID 4V6F (Jenner et al., 2010)) was superimposed. (b) Overview of ArfA(A18T) (light green), RF2 (shades of purple, according to domains) in the closed conformation and P-site tRNA (green) on the non-stop complex (PDBID 5MDW (James et al., 2016)). (c) Closeup onto the recruitment of RF2 ( $RF2_{ArfA(A18T)}$ ), shades of purple according to domains, domains are numbered by ArfA(A18T) (light green) by donation of a  $\beta$ -strand, the N-terminus and the switch loop of RF2 are unstructured (PDBID 5MDW (James et al., 2016; Seefeldt et al., 2016)). (d) Overview of ArfA and open RF2 (orange) bound to a non-stop complex (PDBID 5MGP (Huter et al., 2017c)). P-site tRNA and mRNA are shown, the mRNA channel is indicated as well. (e) Conformation of the RF2 switch loop in presence of ArfA (PDBID 5MGP (Huter et al., 2017c)). The augmentation of the  $\beta$ -sheet of RF2 by ArfA was maintained. The conformation of the 16S rRNA decoding bases A1492 and A1493 with ArfA ( $16S_{ArfA}$ , pale blue) and upon stop codon recognition ( $16S_{stop}$ , yellow) is shown. (f) The ordered ArfA N-terminus supports an additional extension (purple) of  $\sim 2$  turns of RF2 helix  $\alpha$ 7 ( $RF2_{ArfA}$ , orange, PDBID 5MGP (Huter et al., 2017c)) compared to the extension observed during stop codon recognition ( $RF2_{stop}$ , blue, PDBID 4V5E (Weixlbaumer et al., 2008b)). Figure a and f were modified from Huter et al. (2017c), b and c from James et al. (2016) and d and e from Huter et al. (2017b).

interactions with the  $\beta$ -strands  $\beta 4$  and  $\beta 5$  within the superdomain 2/4 of RF2 (James et al., 2016; Demo et al., 2017). The latter hydrophobic interactions are not conserved in RF1 providing an explanation for the specific binding of RF2 by ArfA (Shimizu, 2012; James et al., 2016; Huter et al., 2017c). The upper middle part of ArfA (residue 15-26) contains a short  $\alpha$ -helix (residue 15-24) and establishes initial interactions with the 16S rRNA at the decoding center. The N-terminus of ArfA (amino acids 1-14) and the switch loop of RF2 are flexible in these structures (Figure 15c) (James et al., 2016; Demo et al., 2017).

In contrast the switch loop and the N-terminus of ArfA are ordered when the open conformation of RF2 is established (Figure 15d and e) (James et al., 2016; Demo et al., 2017; Huter et al., 2017c; Ma et al., 2017; Zeng et al., 2017). As for canonical termination this supports that the switch loop is important for the closed to open transition (James et al., 2016; Demo et al., 2017; Fu et al., 2019). Overall, the open conformation in the presence of ArfA resembles the open conformation during termination, with domain 3 of RF2 reaching towards the PTC and accommodating the GGQ-motif for hydrolysis (Figure 15d) (James et al., 2016; Demo et al., 2017; Huter et al., 2017c; Ma et al., 2017; Zeng et al., 2017). One difference is a shift of the decoding loop due to the  $\beta$ -strand addition to the superdomain 2/4 (Huter et al., 2017c). ArfA does not interact with the SPF-motif, which is consistent with biochemical data indicating that mutation of the motif does not influence rescue by ArfA (James et al., 2016; Demo et al., 2017; Huter et al., 2017c; Zeng et al., 2017). Thus, ArfA does not mimic a stop codon in order to initiate the open conformation of RF2, rather ArfA provides the platform for the conformational change itself. In comparison to the closed conformation, ArfA and RF2 pack more tightly against the decoding center, which adopts a similar conformation as seen with SmpB, but is different from the conformation during stop codon recognition (Figure 15e) (James et al., 2016; Demo et al., 2017; Huter et al., 2017b). The stacking of ArfA E30 onto the 16S rRNA nucleotide G530 is maintained from the closed conformation and G530 is in the anti- or ON-state, A1493 flips out of h44, while A1492 is flipped into h44 and stacks of A1913 of H69 of the 23S rRNA (James et al., 2016; Demo et al., 2017; Huter et al., 2017c; Ma et al., 2017; Zeng et al., 2017). The tight packing between the decoding center and ArfA, as well as RF2, supports the structuring of the N-terminus of ArfA. The N-terminus loops back towards the decoding center (Figure 15f) where it interacts with rProtein S12. The turn of the ArfA N-terminus is coordinated by C1914 of H69. In this conformation the loop runs antiparallel to the  $\alpha$ -helix of ArfA and packs against A18 in the helical region. The mutation A18T prevents this interaction, explaining the inactivity of ArfA(A18T) (compare Figure 15c, e and f) (James et al., 2016). The structuring of the ArfA N-terminus builds up a hydrophobic pocket of the ArfA

residues leucine 19 (L19), leucine 24 (L24) and phenylalanine 25 (F25), as well as phenylalanine 217 (F217) and valine 198 (V198) of RF2 (James et al., 2016; Demo et al., 2017; Huter et al., 2017c; Ma et al., 2017; Zeng et al., 2017). Within the pocket resides tryptophan 319 (W319) of the RF2 switch loop, which stacks on A1492 during canonical termination (Korostelev et al., 2008; Weixlbaumer et al., 2008a; James et al., 2016; Demo et al., 2017; Huter et al., 2017c; Ma et al., 2017; Zeng et al., 2017). As in termination, helix  $\alpha$ 7 is extended by an unstructured to structured transition of the switch loop, but ArfA promotes formation of a longer helical segment (Figure 15f). However, during both events the interactions of W319 and the extension of helix  $\alpha$ 7 are proposed to induce the open conformation of RF2. Despite the conservation of W319 in *Thermus thermophilus*, which does not have an *arfA* gene, other residues of the switch loop are not conserved and would lead to steric clashes with ArfA (James et al., 2016). On the other hand, W319 and the switch loop itself are not conserved in RF1, both excludes interaction with ArfA and provides an additional explanation for the specificity of ArfA for RF2 (James et al., 2016; Huter et al., 2017c).

Analogous to termination, placement of the GGQ-motif into the PTC leads to induction and exposition of the ester bond between the P-site tRNA and the peptide for hydrolysis (James et al., 2016; Demo et al., 2017; Huter et al., 2017c; Ma et al., 2017; Zeng et al., 2017). Furthermore, methylation of Q252 enhanced peptide release during termination and ribosome rescue by ArfA/RF2 and the methylation promoted a distinct conformation of Q252 in both cases (Zeng and Jin, 2016; Zeng and Jin, 2018). In contrast to termination, the dissociation of RF2 was not accelerated by RF3 during ArfA mediated rescue (Zeng and Jin, 2016). The reasons for this difference, as well as the dissociation mechanism are still unknown and might be subject of future studies. Finally, ribosome recycling occurs and the ribosome is returned to the pool of free subunits and can participate in a new translation cycle.

**Alternative ribosome rescue factor B (ArfB, former YaeJ)** was identified as a multicopy suppressor upon deletion of *trans*-translation and ArfA in *E. coli*, and was additionally shown to hydrolyse peptidyl-tRNA on non-stop complexes *in vivo* and *in vitro* (Chadani et al., 2011b; Handa et al., 2011). Deletion of *trans*-translation and ArfA is synthetically lethal in *E. coli* despite a chromosomal *arfB* gene, hence the physiological role of ArfB is not clear yet. By contrast, in *Caulobacter crescentus* ArfB of chromosomal origin ensures survival and is essential in the absence of *trans*-translation. Also, most eukaryotes have an ArfB homologue, which is targeted to mitochondria, whereas ArfA is not found in eukaryotes and *trans*-translation is only conserved in mitochondria of some protists (Duarte et al., 2012). Best

characterised is the homologue of human mitochondria, named immature colon carcinoma transcript-1 (ICT1), which is essential for cell viability (Handa et al., 2010; Richter et al., 2010; Feaga et al., 2016). Although ICT1 was identified to be integrated into the LSU of the mitochondrial ribosome (mitochondrial large subunit protein 58, MRPL58, also mL62) it rescues *E. coli* and mammalian mitochondrial non-stop complexes *in vitro* (Richter et al., 2010; Koc et al., 2013; Akabane et al., 2014; Brown et al., 2014; Greber et al., 2014a; Greber et al., 2014b; Kogure et al., 2014; Feaga et al., 2016). ArfB and ICT1 are functionally interchangeable *in vivo*, since ICT1 can complement the synthetic lethal phenotype of double deletion of ArfB and *trans*-translation in *Caulobacter crescentus*, and plasmid derived ArfB supports viability of human cells upon ICT1 knock-down (Feaga et al., 2016). However, if ICT1 or another putative mitochondrial peptidyl-hydrolase releases non-stop complexes in mitochondria is still a matter of discussion (Richter et al., 2010; Duarte et al., 2012; Akabane et al., 2014; Chrzanowska-Lightowers and Lightowers, 2015; Takeuchi and Nierhaus, 2015; Ayyub et al., 2020).

ArfB consists of 140 amino acids, and has an N-terminal domain (residue 1-100) and a C-terminal tail (residue 115-140), connected *via* a ~12 amino acid long flexible linker (Figure 16a) (Gagnon et al., 2012; Chan et al., accepted). The N-terminal domain is homologous to domain 3 of bacterial class I RFs, including a GGQ-motif, whereas further class I RF domains, like the codon recognition superdomain 2/4, are absent (Figure 16a) (Singarapu et al., 2008; Chadani et al., 2011b; Gagnon et al., 2012; Kogure et al., 2014; Chan et al., accepted). As for class I RFs mutation of the GGQ (G25G26Q27)-motif abolished peptidyl-tRNA hydrolysis activity (Korostelev et al., 2008; Chadani et al., 2011b; Handa et al., 2011; Santos et al., 2013). The C-terminal tail has some similarities to the C-terminal tail of SmpB, as it contains positively charged amino acids, stays unstructured in solution and engages an  $\alpha$ -helical conformation upon binding to the ribosome (Chadani et al., 2011b; Gagnon et al., 2012; Kogure

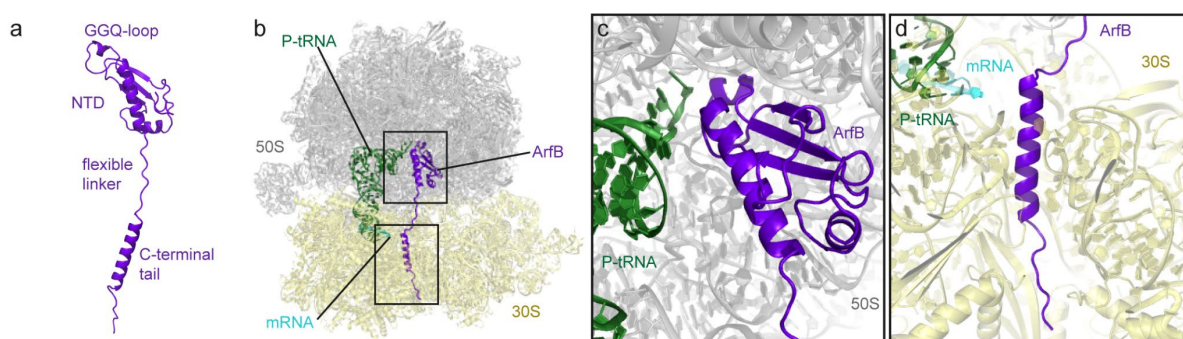


**Figure 16: Interaction of ArfB with non-stop ribosomal complexes.** (a) Overview of the secondary structure of ArfB (purple). NTD, N-terminal domain. (b) ArfB bound to the A-site of the non-stop complex. 50S subunit, grey; 30S subunit, yellow; P-site tRNA, P-tRNA, green; mRNA, cyan. Boxes indicate the enlarged views of the ArfB NTD in the PTC (c) and the helical C-terminal tail in the mRNA entry channel (d). PDBID 6YSS (Chan et al., accepted).

et al., 2014; Chan et al., accepted). Sucrose density gradient centrifugation showed that ArfB is associated with 70S ribosomes, as well as polysomes (Chadani et al., 2011b; Handa et al., 2011), and that removing 10 C-terminal residues abolished binding to the ribosome (Handa et al., 2011). Further mutational analysis showed that mutating three positively charged residues to alanine already severely decreased binding affinity for the ribosome (Kogure et al., 2014). By contrast, the single mutations in the C-terminal tail or removal of two amino acids from the linker did not influence binding to the ribosome, although hydrolysis activity was lost as a consequence.

The crystal and cryo-EM structures of *E. coli* ArfB on the *T. thermophilus* and *E. coli* ribosome, respectively, showed that the N-terminal domain is accommodated to the PTC, while the C-terminal tail binds to the mRNA entry channel (Figure 16b, c and d) (Gagnon et al., 2012; Chan et al., accepted). The position of the tail overlaps with the path of a full-length mRNA, as well as with C-terminal tail of SmpB and the C-terminus of ArfA, indicating that all systems monitor the channel (Gagnon et al., 2012; Neubauer et al., 2012; James et al., 2016; Demo et al., 2017; Huter et al., 2017c; Zeng et al., 2017; Chan et al., accepted). As for *trans*-translation, the release activity decreased with increasing length of the mRNA, with a significant drop for mRNAs with more than six-nine nucleotides downstream of the P-site (Ivanova et al., 2004; Feaga et al., 2016). This indicates that the mRNA and the C-terminal tails compete for binding to the mRNA channel, which was supported by a recent study (Chan et al., accepted). Why this is not the case for ArfA, which has a stricter mRNA length dependency (Ivanova et al., 2004; Asano et al., 2005; Shimizu, 2012; Kurita et al., 2014b; Zeng and Jin, 2016), is not clear yet, but could be assigned to the different structural properties (James et al., 2016; Demo et al., 2017; Huter et al., 2017c; Zeng et al., 2017).

The decoding center adopts a certain conformation due to interaction with ArfB (Gagnon et al., 2012; Chan et al., accepted). 16S rRNA nucleotide G530 is in *anti*-conformation, but the positioning differs from the ON-conformation seen with an A-tRNA (Gagnon et al., 2012; Huter et al., 2017b). Nucleotides A1492 and A1493 of 16S rRNA h44 are flipped into the helix or stack on A1913 of 23S rRNA H69, respectively. Proline 110 of ArfB stacks onto A1493 and was proposed to act as a 'hinge', restricting the movement of the tail on one side while allowing movement and accommodation of the N-terminal domain on the other (Gagnon et al., 2012). However, the proline is not conserved throughout ArfB proteins, and can be mutated to alanine without loss of activity, instead arginine 105 seems to be an important for the activity of ArfB (Kogure et al., 2014). Indeed, the sidechain stacks on U1915 of 23S rRNA H69, while C1914, which usually stacks on U1915 (e.g. during termination (Korostelev et al., 2008; Laurberg et

al., 2008; Weixlbaumer et al., 2008b; Korostelev et al., 2010), when A-site tRNA (Arenz et al., 2016), ArfA/RF2 (James et al., 2016; Demo et al., 2017; Huter et al., 2017c; Ma et al., 2017; Zeng et al., 2017) or SmpB-tmRNA (Rae et al., 2019) is present, respectively) flips out of H69 (Gagnon et al., 2012; Chan et al., accepted). Eventually, the N-terminal domain is placed in the A-site of the LSU and accommodates into the PTC, which is induced upon binding of the N-terminal domain (Gagnon et al., 2012; Chan et al., accepted). The GGQ-motif adopts an analogous conformation to the GGQ-motif of bacterial class I RFs and mediates hydrolysis of the ester bond between the peptide and the P-tRNA. The dissociation mechanism of ArfB is still unknown, as for ArfA the ribosome is finally recycled and the subunits can take part in translation initiation.

**Bacillus ribosome rescue factor A (BrfA, previously YqkK)** was identified in a synthetic lethality screen in *B. subtilis* deleted in *trans*-translation (Shimokawa-Chiba et al., 2019). The *brfA* gene encodes 72 amino acids, but contains a rho-independent transcription terminator before the stop codon. Using a reporter construct with a *lacZ* gene downstream to *brfA* variants it was shown that transcription termination and subsequent degradation by *trans*-translation occurred using the wild-type construct. Additionally, disruption of the terminator by synonymous mutation, as well as deletion of the terminator region lead to LacZ expression. Hence, BrfA is likely expressed from a truncated mRNA, regulated by *trans*-translation in a similar fashion to ArfA, and the active BrfA protein consists of ~62 amino acids.

Furthermore, BrfA was shown to cooperate with RF2 in the course of rescue of non-stop complexes *in vitro* (Shimokawa-Chiba et al., 2019). The release activity was dependent on the GGQ-motif of RF2, whereas the SPF-motif of the decoding loop was dispensable. This indicates that BrfA doesn't mimic a stop codon and hydrolysis activity of RF2 is activated in a different fashion. BrfA can support peptidyl-tRNA hydrolysis by *B. subtilis* RF2 on *B. subtilis* and *E. coli* ribosomes, whereas ArfA and *E. coli* RF2 only act on *E. coli* non-stop complexes. Additionally, RF2 is not interchangeable between both systems, indicating that the systems are adapted to the corresponding species. The low interspecies compatibility is in accordance with the late origin of the systems and the narrow phylogenetic distribution. Although BrfA and ArfA share the regulatory mechanism and are specific for RF2 of their respective species, the different phylogenetic distribution and the distinct amino acid composition hint towards an unrelated evolution of the systems (Shimokawa-Chiba et al., 2019).

The study also includes the cryo-EM structure of BrfA and *B. subtilis* RF2 of the *E. coli* ribosome, which illustrates further similarities and differences between rescue of non-stop

complexes by BrfA and ArfA. The structure of BrfA and *B. subtilis* RF2, as well as the comparison to ArfA and *E. coli* RF2 is elucidated in publication 3 (Shimokawa-Chiba et al., 2019) and the discussion section.

#### 1.4 Proline-rich antimicrobial peptides

Antimicrobial peptides (AMPs) are part of the innate immune system as initial defence against bacterial infections and are either continuously secreted into body fluids or induced as response to pathogen-sensing receptors (Zasloff, 2002). Most AMPs act against bacterial infections by a lytic mechanism, in which the bacterial membrane is permeabilised (Brogden, 2005). However, the mode of action is not limited to the bacterial membrane and AMPs can also have intracellular targets. Particularly, the subclass of proline-rich AMPs (PrAMPs) has been shown to target primarily bacterial translation, additionally the chaperone DnaK was identified as a secondary target (Casteels and Tempst, 1994; Brogden, 2005; Scocchi et al., 2009; Graf et al., 2017). Some of them also have a dual mechanism which depends on their concentration (Podda et al., 2006). At low concentrations the primary the intracellular target is inhibited, while at high concentrations the cell membrane is permeabilised additionally. PrAMPs are cationic peptides, which are enriched in the amino acids proline and arginine (Graf et al., 2017). So far PrAMPs have been found in some insects and crustaceans (arthropods), as well as in a few mammals (Figure 17) (Casteels et al., 1989; Gennaro et al., 1989; Casteels et al., 1990; Agerberth et al., 1991; Bulet et al., 1993; Cociancich et al., 1994; Chernysh et al., 1996; Schnapp et al., 1996; Huttner et al., 1998; Shamova et al., 1999; Schneider and Dorn, 2001; Stensvåg et al., 2008; Knappe et al., 2010; Mardirossian et al., 2018b), but not among humans or primates (Graf and Wilson, 2019). The synthesis of PrAMPs as inactive precursors is carried out in phagocyte progenitor cells by the eukaryotic ribosome (Zanetti et al., 1990; Zanetti et al., 1991; Graf et al., 2017; Graf and Wilson, 2019). The precursor peptides of mammals normally contain one peptide, while insect precursors can contain multiple copies and several isoforms of the peptide separated by an inactivating short spacer sequence (Zanetti et al., 1990; Bulet et al., 1993; Casteels-Josson et al., 1993; Xu et al., 2009; Graf et al., 2017). The precursor usually contains a pre- and a pro-sequence, which are both N-terminally of the PrAMP (pre-pro-peptide). The pre-sequence mediates targeting of the precursor to large granules and is cleaved upon import (Zanetti et al., 1990). The resulting pro-peptide is still inactive and needs to be activated by proteolytic cleavage of the pro-sequence, and in multicopy peptides the spacer has to be removed as well (Zanetti et al., 1991; Scocchi et al., 1992; Casteels-Josson et

al., 1993; Graf et al., 2017). The respective proteases are stored in separate granules (azurophil granules) (Zanetti et al., 1991). Upon bacterial infection both granules secrete their contents into the extracellular matrix, or the phagosome, which leads to maturation of the peptide and elaboration of their antimicrobial activity (Zanetti et al., 1991; Scocchi et al., 1992).

Because of their antimicrobial activity PrAMPs are candidates for the development of new antimicrobial drugs, which is of high interest considering the increasing number of bacterial resistances against drugs in use (Polikanov et al., 2018; Roncevic et al., 2019). Advantages of PrAMPs is their low cytotoxicity in cell culture and in mouse infection models, as well as their peptide nature, which does not lead to non-degradable metabolites (Knappe et al., 2010; Czihal et al., 2012; Berthold et al., 2013; Knappe et al., 2015; Knappe et al., 2019). The peptide nature is also the weakness of PrAMPs, since they are rapidly degraded by serum proteases of the treated organism and displayed short half-lives of maximal 2.5 h in mouse serum (Knappe et al., 2010; Knappe et al., 2011; Czihal et al., 2012; Berthold et al., 2013). Hence, efforts were made for apidaecin-1b from the honey bee (*Apis mellifera*) and oncocin from the milkweed bug (*Oncopeltus fasciatus*) to improve their serum stability by introduction of non-proteinogenic or D-amino acids and stabilisation of the termini (Knappe et al., 2010; Knappe et al., 2011; Czihal et al., 2012; Berthold et al., 2013; Bluhm et al., 2016). Most promising synthetic peptides amongst them were apidaecin137 (Api137), which has an N-terminal

		gu = N,N,N',N'-tetramethylguanidino; O = Ornithine; r = D-Arginine; X = unknown	[aa]	Organism
	Apidaecin-1b	G N N R P V Y I P Q P R P P H P R L	18	<i>Apis mellifera</i>
	Api137	g u - O N N R P V Y I P R P R P P H P R L - O H	18	synthetic
	Abaecin	Y V P L P N V P Q P G R R P F T F P G Q G P F N P K I K W P Q . .	34	<i>Apis mellifera</i>
	Drosocin	G K P R P Y S P R P T S H P R P I R V	19	<i>Drosophila melanog.</i>
Arthropods	Arasin 1	S R W P S P G R P R P F P G R P K P I F R P R P C	25	<i>Hyas araneus</i>
	PrAMP	X X V P Y P R P F P R P P I G P R P L P F P G G G R P . .	30	<i>Carcinus maenas</i>
	Oncocin	V D K P P Y L P R P P X P P R R I Y N N R	20	<i>Oncopeltus fasciatus</i>
	Onc112	V D K P P Y L P R P R P P R r I Y N r - N H <sub>2</sub>	19	synthetic
	Onc72	V D K P P Y L P R P R P P R O I Y N O - N H <sub>2</sub>	19	synthetic
	Metalnikowin-1	V D K P D Y R P R P R P P N M	15	<i>Palomena prasina</i>
	Pyrrhocorin	V D K G S Y L P R P T P P R P I Y N R N	20	<i>Pyrrhocoris apterus</i>
	Riptocin	V D K G G Y L P R P T P P R P V Y R S	>19	<i>Riptortus pedestris</i>
	bt_Bactenecin-7	R R I R P R P P R L P R P R P R P L P F P R P G P . .	60	<i>Bos taurus</i>
	ch_Bactenecin-7	R R L R P R P R P L P R P R P R P R P R S L P . .	60	<i>Capra hircus</i>
Mammals	oa_Bactenecin-7	R R L R P R P R P L P R P R P R P R P R S L P . .	60	<i>Ovis aries</i>
	PR-39	R R R P R P P Y L P R P R P P P F F P P R L P P R .	39	<i>Sus scrofa</i>
	Tur1A	R R I R F R P P Y L P R P G R R P R F P P P F P I . .	32	<i>Tursiops truncatus</i>
	bt_Bactenecin-5	R F R P P I R R P P I R P P F Y P P F R P P I R P . .	43	<i>Bos taurus</i>
	ch_Bactenecin-5	R F R P P I R R P P I R P P F N P P F R P P V R P . .	43	<i>Capra hircus</i>
	oa_Bactenecin-5	R F R P P I R R P P I R P P F R P P F R P P V R P . .	43	<i>Ovis aries</i>

**Figure 17: Sequence alignment of natural and synthetic PrAMPs.** Alignment of the amino acid sequence of PrAMPs derived from arthropods (grey) and mammals (blue). Identical residues are highlighted in black, and similar residues in cyan. O-glycosylation of threonine 11 of drosocin is indicated in blue. Amino acid 11 of oncocin is unknown and indicated by a bold "X". The number of amino acids [aa] corresponds to the mature peptide in the source organism, which are stated on the right. The figure was adapted from Graf and Wilson (2019).

protection by a tetramethylguanidino moiety followed by an ornithine residue, oncocin112 (Onc112), and oncocin72 (Onc72), which have a C-terminal amino group, furthermore arginine residues were exchanged to D-arginine or ornithine, respectively (Figure 17).

Regardless of the natural or synthetic origin of the PrAMPs, to reach their intracellular target in the bacterium the PrAMPs have to enter the cell. This has been shown to depend primarily on the bacterial inner membrane proteins SbmA and MdtM (Mattiuzzo et al., 2007; Krizsan et al., 2015). The cellular role of the SbmA transporter is still elusive, but it was shown to be the major importer of PrAMPs and deletion of the *sbmA* gene lead to decreased susceptibility against PrAMPs (Mattiuzzo et al., 2007; Runti et al., 2013; Paulsen et al., 2016). Additional deletion of the multidrug efflux pump MdtM further decreased the sensitivity to some PrAMPs in *E. coli* (Holdsworth and Law, 2012; Krizsan et al., 2015; Paulsen et al., 2016). Interestingly, the PrAMPs did enter the cell *via* MdtM, so that the effect was based on further reduced uptake (Krizsan et al., 2015).

The phylogenetic distribution of SbmA is not homogeneous, as homologues were found in various Gram-negative bacteria of distant relationships and not found in Gram-positive species (Graf et al., 2017). Among Gram-negative bacteria homologues of SbmA can be found in *Gamma-proteobacteria*, particularly in *Enterobacteriaceae*, which includes *E. coli* and *Klebsiella pneumoniae*, and *Pseudomonadales*, like *Acinetobacter baumannii*, further it is distributed in *Alpha-, Beta-,* and *Epsilon-proteobacteria*. While Gram-positive and Gram-negative species without a SbmA homologue, like *Pseudomonas aeruginosa*, are generally less susceptible towards PrAMPs, the susceptibility varies between SbmA containing species (Kolano et al., 2020). For example, *E. coli* displayed a minimal inhibitory concentration (MIC) of 4 mgL<sup>-1</sup> for Api137, *Klebsiella pneumoniae* showed a better susceptibility with a MIC of 2 mgL<sup>-1</sup>, while *Acinetobacter baumannii* had a highly increased MIC of 128 mgL<sup>-1</sup> (Kolano et al., 2020). The study also displayed the same trend for the MICs of Onc112, showing that *Acinetobacter baumannii* is less susceptible to PrAMPs, despite having a SbmA homologue and further factors, like off-target binding and/or affinity for the target, which can influence sensitivity to PrAMPs. However, both synthetic PrAMPs are promising candidates as new antimicrobial treatments, since they display low cytotoxicity in cell cultures and have been used successfully in murine infection models with *E. coli*, and *Klebsiella pneumoniae* (Czihal et al., 2012; Berthold et al., 2013; Knappe et al., 2015; Bluhm et al., 2016; Knappe et al., 2019). Structural and biochemical studies of several PrAMPs showed that they bind to the nascent polypeptide exit tunnel (NPET) (Figure 18) *via* interactions of arginine and aromatic residues and the 23S rRNA. Furthermore, PrAMPs can be divided in two classes (class I and class II)

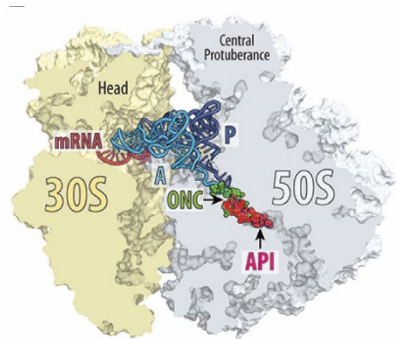


**Figure 18: PrAMPs bind to the nascent polypeptide exit tunnel.** Transverse section showing the binding of class II PrAMP Api137 (API, red) and class I PrAMP Onc112 (ONC, green) to the NPET of the ribosome (30S subunit, yellow, 50S subunit, pale blue). A-site tRNA (cyan), P-site tRNA (blue) and mRNA (magenta) are displayed for reference. The figure was adapted from Polikanov et al. (2018).

with respect to their translation inhibition mechanism (reviewed by Graf et al. (2017), Polikanov et al. (2018) and Graf and Wilson (2019)).

**Class I PrAMPs** identified so far are arasin 1, PrAMP, oncocin and its derivates, metalnikowin-1 (Met), pyrrhocoricin (Pyr), Ripocin, bactenecin-7 (Bac7), Tur1A and bactenecin-5 (Bac5) (Gennaro et al., 1989; Agerberth et al., 1991; Bulet et al., 1993; Cociancich et al., 1994; Chernysh et al., 1996; Schnapp et al., 1996; Huttner et al., 1998; Shamova et al., 1999; Schneider and Dorn, 2001; Stensvåg et al., 2008; Knappe et al., 2010; Mardirossian et al., 2018b). Compared to other PrAMPs (average ~25 aa) Bac7 has an increased length of 60 aa (Gennaro et al., 1989; Graf et al., 2017), which raised interest in investigating the difference (Benincasa et al., 2004). Subsequently, it was shown that the N-terminal aa 1-35 (Bac<sub>1-35</sub>) are sufficient to mediate the antimicrobial activity, without decrease in the MIC (Benincasa et al., 2004). Further truncation up to 16 residues (Bac<sub>1-16</sub>) only had marginal effects on the MIC, while leaving only 15 aa of Bac7 led to a complete loss of antimicrobial activity, due to impaired uptake (Benincasa et al., 2004; Guida et al., 2015). Removal of the first four N-terminal aa (Bac<sub>5-5</sub>) strongly reduced the MIC and was less inhibitory in *in vitro* translation assays (Benincasa et al., 2004). A similar effect was observed with an oncocin variant lacking two residues from the N-terminus (Gagnon et al., 2016), showing that the very N-terminal residues are involved in the mechanism of translation inhibition in class I PrAMPs. So far, the structures of Onc112, pyrrhocoricin (Pyr), metalnikowin-1 (Met), Bac<sub>1-16</sub> and Tur1A on the ribosome have been determined (Figure 19a) (Roy et al., 2015; Seefeldt et al., 2015; Gagnon et al., 2016; Seefeldt et al., 2016; Mardirossian et al., 2018b). The class I PrAMPs were shown to bind to the NPET in reverse orientation compared to a nascent polypeptide chain, i.e. from the middle of the peptide the C-terminus points towards the exit of the tunnel, while the N-terminus lies in PTC direction (Figure 19a). The residues of the very C-terminal residues were not resolved in each structure, which is in line with the C-terminal truncation experiments with Bac7, which led to the discovery of the Bac<sub>1-35</sub> and Bac<sub>1-16</sub> fragments (Benincasa et al., 2004; Roy et al., 2015; Seefeldt et al., 2015;

Gagnon et al., 2016; Seefeldt et al., 2016; Mardirossian et al., 2018b). On the ribosome the class I PrAMPs engage an elongated coil structure (Figure 19a) (Roy et al., 2015; Seefeldt et al., 2015; Gagnon et al., 2016; Seefeldt et al., 2016; Mardirossian et al., 2018b). Binding to the ribosome involves specific stacking and polar interactions with the NPET, which are partly conserved between class I PrAMPs. Alignment of class I PrAMPs indicates that they have a conserved ProArgPro (PRP)-motif and superimposition of the structures shows that the motif of the different class I PrAMPs binds to the ribosome in the same position and establishes the same interactions (Figure 19a) (reviewed by Graf et al. (2017) and Graf and Wilson (2019)). In particular, only the Arg (Arg9 in insects, Arg12 in mammals) residue establishes interactions by forming a H-bond with the 23S rRNA nucleotide U2584 and stacking on C2610. Furthermore, stacking of tyrosine 6 in insect class I PrAMPs onto C2452 is conserved *via* arginine 12 in mammals. Further interactions with the NPET are generally more specific for the respective class I PrAMP. *In vitro* translation assays indicated that class I PrAMPs inhibit the transition from initiation to elongation (Figure 19b-e) (Roy et al., 2015; Seefeldt et al., 2015; Gagnon et al., 2016; Seefeldt et al., 2016; Mardirossian et al., 2018b). This was supported by the structural data, which shows that the N-terminus of class I PrAMPs extends towards the PTC into the 50S A-site and thus overlaps with binding of the CCA-end of an A-site tRNA (Figure 19f-g), but does not interfere with binding of a P-site tRNA. With respect to this, formation of the 70S IC is possible, also the delivery of the aa-tRNA following the initiator tRNA could be allowed, but accommodation would be blocked and translation could not

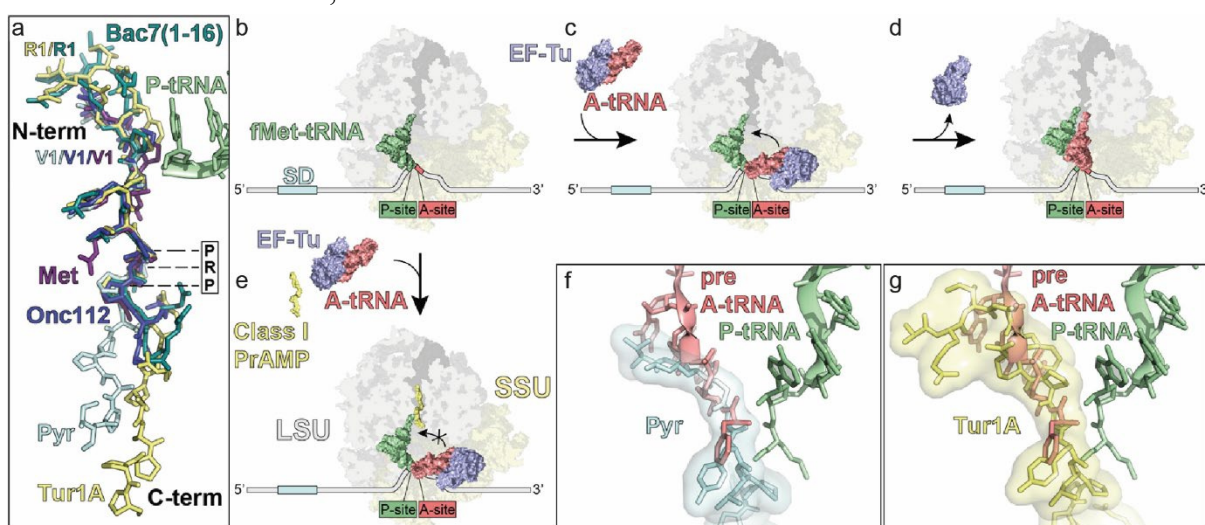


**Figure 19: Translation inhibition by class I PrAMPs.** (a) Superimposition of insect PrAMPs Met (purple), Onc112 (slate) and Pyr (cyan), as well as mammalian PrAMPs Bac7<sub>1-16</sub> and Tur1A (yellow) bound to the NPET (Roy et al., 2015; Seefeldt et al., 2015; Gagnon et al., 2016; Seefeldt et al., 2016; Mardirossian et al., 2018b). The conserved PRP-motif is indicated and P-site tRNA (green) is shown for reference. (b-d) Translation in the absence of PrAMPs starting with the 70S IC (b), followed by delivery of aa-tRNA (salmon) to the A-site by EF-Tu (light blue) (c) and accommodation of the aa-tRNA to the PTC, as well as dissociation of EF-Tu (d). (e) The presence of class I PrAMPs, like Tur1A, allows delivery of aa-tRNA to the A-site, but permits accommodation to the PTC. (f-g) Superimposition of an aa-tRNA accommodated to the A-site of the PTC with (f) Pyr (Gagnon et al., 2016) or (g) Tur1A (Mardirossian et al., 2018b). The figure was adapted from Graf and Wilson (2019).

proceed (Roy et al., 2015; Seefeldt et al., 2015; Gagnon et al., 2016; Seefeldt et al., 2016; Mardirossian et al., 2018b). Aligned on the PRP-motif, the N-terminus of mammalian class I PrAMPs is 3 residues longer than the N-terminus of insect class I PrAMPs (Figure 19f-g and Figure 17). This is consistent with the findings that removal of four N-terminal residues of Bac7 and two residues of Onc112 impair their function (Benincasa et al., 2004; Gagnon et al., 2016). The overall binding of class I PrAMPs is most likely not compatible with the simultaneous presence of a nascent polypeptide chain (Roy et al., 2015; Seefeldt et al., 2015; Gagnon et al., 2016; Seefeldt et al., 2016; Mardirossian et al., 2018b). With regard to this, binding of class I PrAMPs could occur in any situation with an unoccupied NPET, as after dissociation of the polypeptide chain during termination or in newly synthesised 50S subunits, maybe even in late stages of 50S biogenesis. Depending on the concentration of class I PrAMPs the whole pool of free 50S subunits could be compromised by binding of class I PrAMPs, which would be devastating for the bacterium. Despite the low sequence homology to other class I PrAMPs, Bac5 fragments were shown to also inhibit the transition from initiation to elongation (Mardirossian et al., 2018a; Mardirossian et al., 2019). Furthermore, competition assays indicate that Bac5 also binds to the NPET (Mardirossian et al., 2018a). However, it displayed species specific inhibition, as it inhibits *T. thermophilus* ribosomes poorly, while *E. coli* ribosomes are inhibited efficiently (Mardirossian et al., 2018a), which might indicate that Bac5 binding to the NPET differs from other class I PrAMPs and could be a further interesting lead compound with respect to development of new antimicrobial drugs.

**Class II PrAMPs** so far identified are apidaecin-1b and its derivate Api137. The cryo-EM structures of Api137 on the *E. coli* ribosome showed that Api137 binds to the NPET in an elongated coil structure as well, but has the same orientation as a nascent polypeptide chain (Figure 20a) (Florin et al., 2017; Graf et al., 2018). In particular, the N-terminus is directed towards the tunnel exit, whereby the last four residues were not resolved and the C-terminus binds to the A-site cleft of the PTC. In contrast to class I PrAMPs Api137 does not extend further into the A-site. Api137 binding to the NPET occurs primarily *via* stacking interactions of tyrosine 7 and 23S rRNA nucleotide A751, arginine 12 and nucleotide C2611, as well as histidine15 and nucleotide G2505 (Figure 20a). In addition, Api137 establishes H-bonds in the A-site cleft *via* arginine 17 (Figure 20b). Interestingly, the side chain and the backbone of arginine 17 are also in H-bonding distance to Gln235 of the GGQ-motif of RF1 (Figure 20b) (Florin et al., 2017; Graf et al., 2018). In accordance, *in vitro* translation assays showed that Api137 inhibits the turnover of RFs and mutational analysis indicated that exchange of

arginine17 to alanine drastically increases the MIC and reduces the affinity for the *E. coli* ribosome (Castle et al., 1999; Krizsan et al., 2014; Florin et al., 2017). Further H-bonds can be formed between the very C-terminus of leucine18 and the ribose of P-site tRNA nucleotide A76 (Figure 20c) (Florin et al., 2017; Graf et al., 2018). The importance of leucine18 is supported by reduced binding to *E. coli* ribosomes upon deletion (Krizsan et al., 2014). Additional deletion of arginine17 further reduced binding to *E. coli* ribosomes underlining the mechanistic involvement of both residues.

Similar to class I PrAMPs binding of Api137 and a nascent polypeptide chain to the NPET seems unlikely because of severe clashes (Florin et al., 2017; Graf et al., 2018). Furthermore, the interactions between Api137 and the P-site tRNA could only be established after peptidyl-tRNA hydrolysis. Mechanistically Api137 could enter the NPET from the tunnel exit subsequent to peptidyl-tRNA hydrolysis and dissociation of the polypeptide chain (Figure 20d-g) (Florin et al., 2017; Graf et al., 2018; Graf and Wilson, 2019). Api137 would then establish the interactions with the P-site tRNA and the RF, which hinders the dissociation of the RF. As

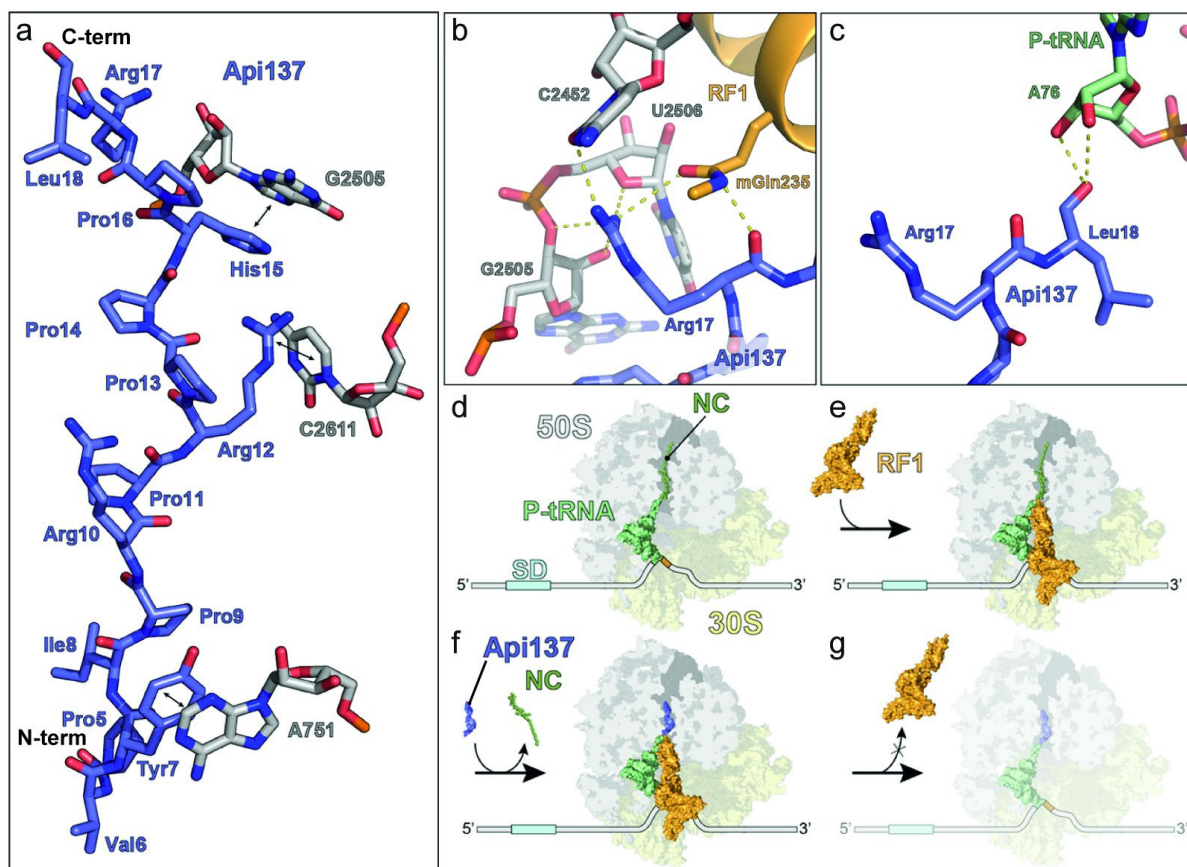


**Figure 20: Inhibition of translation by class II PrAMPs.** (a) Specific interactions of Api137 (blue) with 23S rRNA nucleotides of the NPET (grey) (Florin et al., 2017; Graf et al., 2018). (b-c) Potential H-bonds of Api137 with (b) 23S rRNA nucleotides and RF1 and (c) P-site tRNA (P-tRNA, green). (d-g) Translation of an ORF terminates when a stop codon encounters the A-site (d), subsequently a RF (RF1 (yellow) in this case) binds to the A-site and hydrolyses the nascent polypeptide chain (NC, green) from the P-site tRNA (green) (e). Afterwards Api137 binds to the NPET (f) and inhibits dissociation of the RF (g). The Figure was adapted from Graf and Wilson (2019).

a result the RFs would be depleted from the cell, this would inhibit termination of translation and leads to stalling with a stop codon in the A-site, which is in line with *in vitro* translation assays (Florin et al., 2017). Prolonged stalling could lead to cleavage of the mRNA in the A-site, which renders the stalled ribosomes to non-stop ribosomal complexes and targets them for ribosome rescue (Sunohara et al., 2002; Sunohara et al., 2004b). However, *trans*-translation and ArfA also depend on RFs (reviewed by Keiler (2015) and Huter et al. (2017b)), which would be less available when Api137 is present. Since termination of *trans*-translation happens canonically and the open conformation of RF2 by ArfA is very similar to the open conformation upon stop codon recognition (Williams et al., 1999; James et al., 2016; Demo et al., 2017; Huter et al., 2017c; Ma et al., 2017; Zeng et al., 2017), it is likely that also these systems are inhibited by Api137. With regard to the interaction with the conserved GGQ-motif, Api137 could also inhibit the turnover of other peptidyl-tRNA hydrolases, or the ArfB rescue system. This was supported by a recent study, which showed that also the turnover of ArfB is inhibited by Api137 and the established interactions are similar to the ones observed with RF1 (Florin et al., 2017; Graf et al., 2018; Chan et al., accepted).

## 2 Objective of these studies: Structural insights into bacterial ribosome rescue

Ribosomes stall at the 3'-end of mRNAs, if no in-frame stop codon is present. Due to the lack of a sense or a stop codon in the A-site elongation as well as termination cannot occur, leading to the accumulation of ribosomes in the form of non-stop complexes, requiring rescue by specialised factors and mechanisms. The general objective of our studies was to gain insights into the ribosome rescue mechanism of the different factors by high-resolution reconstructions of cryo-EM datasets obtained for the factor(s) bound to a non-stop complex.

The classical and well characterised ribosome rescue mechanisms comprise *trans*-translation, ArfA and ArfB. While *trans*-translation resumes translation on an inherent reading frame, that ends with a stop codon, ArfA specifically recruits RF2 to the non-stop complex and ArfB harbours its own GGQ-motif for direct peptidyl-tRNA hydrolysis (Keiler and Feaga, 2014; Starosta et al., 2014a; Himeno et al., 2015; Keiler, 2015). Structures for the *T. thermophilus* *trans*-translation system (Neubauer et al., 2012; Ramrath et al., 2012) and *E. coli* ArfB bound to the *T. thermophilus* ribosome (Gagnon et al., 2012) were already available, while structural data for ArfA was lacking. Therefore, our aim was to reveal the recruitment and activation of RF2 by ArfA using cryo-EM single particle reconstruction to generate a high-resolution reconstruction of both factors bound to a non-stop complex (**Publication 1**). Furthermore, we compared the obtained results with structures of the ArfA system attained by other groups and the available structures of the *trans*-translation and ArfB systems (**Publication 2**).

Although all three systems monitor the mRNA entry channel and prefer non-stop complexes, the systems can work on ribosomes harbouring an mRNA that extends past the P-site into the channel (Ivanova et al., 2004; Asano et al., 2005; Shimizu, 2012; Kurita et al., 2014b; Feaga et al., 2016; Zeng and Jin, 2016). Thereby, the systems exhibit different specificities for the mRNA length. While ArfA only allows three nucleotides past the P-site, *trans*-translation and ArfB can operate on complexes with an mRNA extending nine nucleotides past the P-site. However, the rescue mechanism of non-stop complexes is not known. Hence, aim of the study was to elucidate this further for ArfB. In that regard, we bound ArfB to *E. coli* non-stop complexes with nine or zero mRNA nucleotides past the P-site, prevented dissociation of ArfB using Api137 and determined high-resolution cryo-EM structures (**Publication 3**).

Ribosome rescue is essential in bacteria, and while *trans*-translation is found in all today known bacterial genomes, ArfA and ArfB are less prevalent and usually serve as backup systems (Keiler and Feaga, 2014). Deletion of all systems usually leads to synthetic lethality. However,

some bacteria, like *B. subtilis* and *Francisella tularensis*, have no apparent ArfA or ArfB homologue and *trans*-translation can be deleted. This indicates the existence of further ribosome rescue systems. Indeed, an alternative ribosome rescue factor was recently identified in *Francisella tularensis* and termed ArfT (Goralski et al., 2018). Aim of our study was to determine the cryo-EM structure of a new alternative ribosome rescue factor identified in *B. subtilis* (*Bacillus* ribosome rescue factor A, BrfA), which also cooperates with RF2 (**Publication 4**). Furthermore, we compared the mechanism of ArfA and BrfA regarding interaction with the ribosome, the recruitment and activation of RF2. Characterisation of the mentioned ribosome rescue mechanisms is of high interest, because the systems can serve as target for the development of new antibiotics, which is desirable with respect to the rapidly increasing number of bacterial strains with resistances against clinically used antibiotics.

### 3 Cumulative Thesis: Summary of Publications

#### 3.1 Publication 1: Structural basis for ArfA-RF2-mediated translation termination on mRNAs lacking stop codons

Paul Huter\*, Claudia Müller\*, Bertrand Beckert, Stefan Arenz, Otto Berninghausen, Roland Beckmann and Daniel N. Wilson

*Nature* 541, 546-549 (2017)

Ribosomes that reach the 3'-end of an mRNA cannot proceed with elongation or termination, since no codon resides in the decoding site. Hence, the ribosomes get stuck and end up in so-called non-stop complexes. This event has been estimated to occur on ~2-4 % of translating ribosomes in *E. coli*, indicating that non-stop complexes are frequent (Ito et al., 2011). Bacteria have evolved specialised mechanisms to rescue these non-stop complexes and deletion of all rescue mechanisms lead to synthetic lethality (reviewed by Keiler (2015) and Himeno et al. (2015)). The rescue mechanisms comprise *trans*-translation, which is mediated by tmRNA and SmpB, as well as ArfA (in cooperation with RF2) and ArfB. While structures of tmRNA·SmpB and ArfB bound to non-stop complexes have been determined, such information was missing for ArfA. To illuminate the interplay between ArfA, RF2 and the ribosome we generated a non-stop complex with ArfA and RF2 bound to it. Subsequently, the sample was subjected to analysis by cryo-EM and a reconstruction of 3.1 Å was obtained. The structure shows that ArfA binds in the decoding center and monitors the mRNA entry channel with the C-terminus. Thereby the C-terminus occupies the path that is usually taken by a full-length mRNA. The N-terminus ahead of the decoding center turns by 180° and loops back to the decoding center. The turn is coordinated by the 23S rRNA nucleotide C1914 and represents the only contact with the LSU. ArfA serves as platform for binding of RF2 to the non-stop complex. RF2 is recruited by ArfA *via* addition of a β-strand to the β-sheet of the RF2 superdomain 2/4. The overall conformation of RF2 is similar to the open conformation observed during termination. Interestingly, the open conformation is not induced by interaction of ArfA with the SPF-motif in the decoding loop of RF2. Instead, ArfA, RF2 itself and rProtein S12 stabilise a unique conformation of the RF2 switch loop that extends RF2 helix α7 by several turns. This directs domain 3 of RF3, which harbours the GGQ-motif necessary for peptidyl-tRNA hydrolysis, towards the PTC. Thus, ArfA recruits and activates RF2 in a codon-independent manner.

### 3.2 Publication 2: Structural Basis for Ribosome Rescue in Bacteria

Paul Huter, Claudia Müller, Stefan Arenz, Bertrand Beckert and Daniel N. Wilson  
*Trends in Biochemical Sciences* 42, 669-680 (2017)

When ribosomes translate to the 3'-end of an mRNA translation cannot continue and the ribosomes stall as non-stop complexes. These non-stop complexes are rescued by *trans*-translation, ArfA or ArfB. *Trans*-translation is found in all today sequenced bacterial genomes and serves as the major ribosome rescue mechanism. ArfA and ArfB are backup mechanisms in some bacteria and fulfil the task if *trans*-translation is overwhelmed or defect. *Trans*-translation is performed by tmRNA in complex with SmpB. While SmpB mediates binding to the non-stop complex, tmRNA encodes a short reading frame on which translation is resumed. The reading frame adds a degradation tag to the nascent polypeptide chain and ends with a stop codon, hence canonical termination occurs. ArfA specifically recruits RF2 for peptidyl-tRNA hydrolysis, while ArfB harbours a GGQ-motif and can hydrolyse the nascent chain from the tRNA itself. Based on our previous cryo-EM structure of ArfA and RF2 bound to a non-stop complex and ArfA/RF2 structures from other groups, as well as available structures of tmRNA·SmpB and ArfB we compare the mechanisms of the rescue systems. We highlight that ArfA, ArfB and SmpB probe the mRNA entry channel with their C-terminus and that the C-termini overlap with the path of a full-length mRNA. Furthermore, each system induces a distinct conformation of the decoding center.

### 3.3 Publication 3: Mechanism of Ribosome Rescue by Alternative Ribosome Rescue Factor B

Kai-Hsin Chan, Valentin Petrychenko, Claudia Müller, Cristina Maracci., Wolf Holtkamp, Daniel N. Wilson, Niels Fischer and Marina V. Rodnina  
*Nature Communications* (accepted)

ArfB is one of the ribosome rescue mechanisms, which resolves ribosomes stalled on the 3'-end of mRNAs. Although ArfB is more efficient on complexes that have an empty mRNA entry channel, it has been shown that ArfB can act on complexes with longer mRNAs (Feaga et al., 2016). The mechanism behind this is still unknown and we approached this subject by a combination of rapid kinetics and cryo-EM, which provides a deeper insight in multistep ribosome rescue by ArfB. Our kinetic experiments show that ArfB binds to ribosomes regardless of the mRNA length and that the difference results from an extended engagement step observed

with longer mRNAs. During the engagement step the C-terminus of ArfB establishes interactions within the mRNA entry channel, which enable the peptidyl-tRNA hydrolysis activity of ArfB. Comparison of our cryo-EM datasets of non-stop complexes with zero and nine mRNA nucleotides in the mRNA entry channel show that ArfB binds to both complexes in the same way, since the mRNA overhang shifted out of the channel. This indicates that the extended engagement step with longer mRNAs originates from a movement of the mRNA, which permits binding of the ArfB C-terminus.

### 3.4 Publication 4: Release factor-dependent ribosome rescue by BrfA in the Gram-positive bacterium *Bacillus subtilis*

Naomi Shimokawa-Chiba\*, Claudia Müller\*, Keigo Fujiwara, Bertrand Beckert, Koreaki Ito, Daniel N. Wilson and Shinobu Chiba

*Nature Communications* 10, 5397 (2019)

The rescue of non-stop complexes is essential in bacteria. The main ribosome rescue mechanism is *trans*-translation, which is found in all sequenced bacterial genomes (Keiler and Feaga, 2014). Some Gram-negative bacteria have evolved backup mechanisms for *trans*-translation, like ArfA and ArfB. The Gram-positive bacterium *Bacillus subtilis* has no apparent homologue of either backup mechanism. However, deletion of *trans*-translation does not lead to synthetic lethality, which indicated that an unknown backup system could exist in *B. subtilis*. Here we identify and characterise a new ribosome rescue factor in *B. subtilis*, termed BrfA. Our biochemical experiments show that BrfA, as ArfA, specifically recruits RF2 to the non-stop complex. BrfA can rescue non-stop complexes from *B. subtilis* and *E. coli* if *B. subtilis* RF2 is provided. Thus, we used the same non-stop complex as before for ArfA for analysis by cryo-EM, which lead to a reconstruction of 3.1 Å. Our structure shows that BrfA binds to the decoding center as well and, as other ribosome rescue mechanisms monitors the mRNA entry channel with its C-terminus. BrfA has an N-terminal helix (α1) which interacts with SSU h44 and LSU H71 at the intersubunit space, additionally arginine 25 stacks on U1915 of LSU H69. Hence, BrfA has more contacts with the LSU compared to ArfA. BrfA also recruits RF2 *via* addition of a β-strand to the β-sheet formed by the RF2 superdomain 2/4. However, ArfA and BrfA facilitate the open conformation of RF2 by a different mechanism.

## 4 Discussion and Outlook

The structures of the ribosome rescue systems provided an overview of the mechanistic background, as well as similarities and differences between the systems. These will be highlighted in this section and the main focus of the discussion will be on ArfA/RF2, ArfB and BrfA/RF2.

### 4.1 Alternative ribosome rescue factor A

As mentioned in the introduction the five cryo-EM structures of the *E. coli* system ArfA and RF2 on the homologous ribosome lead to congruent results for the closed and the open conformation, besides different approaches to generate the complexes (James et al., 2016; Demo et al., 2017; Huter et al., 2017c; Ma et al., 2017; Zeng et al., 2017). Four studies generated the non-stop complex using a short mRNA containing a SD-sequence and a start codon in optimal spacing, placing the start codon in the P-site whereas the A-site and the mRNA entrance tunnel were vacant (James et al., 2016; Demo et al., 2017; Ma et al., 2017; Zeng et al., 2017). The non-stop complex was incubated with deacylated tRNA<sup>fMet</sup> or non-hydrolysable fMet-NH-tRNA<sup>fMet</sup> and C-terminal truncated ArfA, as well as RF2. Zeng et al. (2017) used methylated RF2, but were not able to draw conclusions regarding the conformation of the methylated GGQ-motif and collected later on a second dataset (Zeng and Jin, 2018), which did not differ regarding the overall conformation of ArfA and RF2, and provided the information described in the introduction. Reconstruction of the cryo-EM datasets lead to one major population of ArfA, RF2 in the open conformation and P-tRNA bound to the 70S ribosome (James et al., 2016; Demo et al., 2017; Ma et al., 2017; Zeng et al., 2017). In contrast to the other complexes James et al. (2016) did not find an E-tRNA, due to usage of non-hydrolysable fMet-NH-tRNA<sup>fMet</sup>, which has a low affinity for the E-site because of the attached amino acid. Whereas non-cognate deacylated tRNA<sup>fMet</sup> bound to the E-site in the other complexes in consequence of the intrinsic affinity of the E-site for deacylated tRNA (Rheinberger et al., 1981; Grajevskaja et al., 1982; Yusupov et al., 2001; Schmeing et al., 2003; Demo et al., 2017; Ma et al., 2017; Zeng et al., 2017). However, the presence or absence of E-tRNA did not influence ArfA and RF2 binding or the rescue mechanism. Demo et al. (2017) additionally found a second major subpopulation with RF2 in the closed conformation together with ArfA and P-tRNA on the ribosome using this approach. In their dataset the occupancy of the closed and open RF2 subpopulations after removal of non-aligning particles was 43% and

34%.

Huter et al. (2017c) generated the non-stop complex by *in vitro* translation of a truncated *nlpD* version with engineered N-terminal His-tag. The tag was used to purify the non-stop complex, which was programmed with peptidyl-tRNA<sup>Pro</sup> in the P-site, while the mRNA entry channel was empty. This approach created a more natural substrate for ribosome rescue compared to the other complexes because it is stalled on an *E. coli* gene and the P-tRNA carries a nascent chain. The non-stop complexes were incubated with hydrolysis deficient RF2-GAQ and C-terminally truncated ArfA. Reconstruction and sorting revealed two major subpopulations of 50% and 39% after exclusion of non-aligning particles containing ArfA together with open RF2-GAQ. The subpopulations only differed in the absence or presence of E-tRNA, also in this case no difference regarding ArfA-supported rescue was observed between the subpopulations.

Notably, no non-stop complex with only ArfA bound was obtained by the different strategies, even not after sorting of the datasets, which indicates the high effectiveness of ArfA in recruiting RF2 to the ribosome (James et al., 2016; Demo et al., 2017; Huter et al., 2017c; Ma et al., 2017; Zeng et al., 2017). With regard to the state of the complex, using RF2-GAQ or non-hydrolysable fMet-NH-tRNAf<sup>Met</sup> represent pre-hydrolysis complexes, whereas complexes with deacylated tRNA<sup>fMet</sup> mimic the post-hydrolysis state. Recently, a cryo-EM study reported rearrangement of the GGQ-motif containing loop/helix combination in RF2 domain 3 into a  $\beta$ -hairpin within the PTC after peptide hydrolysis during termination on a stop codon, which was accompanied by relocation of the CCA-end of the P-tRNA out of the PTC (Svidritskiy et al., 2019). This was not described for the complexes mimicking post-hydrolysis complexes (Demo et al., 2017; Ma et al., 2017; Zeng et al., 2017). Rather, in all obtained non-stop complexes with ArfA and open RF2 the GGQ-loop was in the activated loop/helix combination, leading to the same conclusions despite the different hydrolysis state (James et al., 2016; Demo et al., 2017; Ma et al., 2017; Zeng et al., 2017). The difference between the post-hydrolysis complexes by Svidritskiy et al. (2019) and of Demo et al. (2017), Ma et al. (2017) and Zeng et al. (2017) might be a consequence of different incubation times and/or temperatures. While the former was incubated for 30 minutes at room temperature, the non-stop complexes were incubated at 37°C and quickly frozen for storage or applied to the cryo-EM grid. The  $\beta$ -hairpin of the GGQ-loop could be a conformation formed due to the lower temperature or a transient intermediate upon subunit rotation, because  $\beta$ -hairpin formation was associated with head swivelling and intersubunit rotation. Movement of the head and body of  $\sim 2^\circ$  each was only observed by Zeng et al. (2017), but without rearrangement of RF2 and P-tRNA, which could also indicate a

difference between termination and ribosome rescue by ArfA/RF2.

As mentioned earlier James et al. (2016) and Demo et al. (2017) observed the closed conformation of RF2 on the ribosome in the presence of ArfA by using different approaches. James et al. (2016) prepared two additional complexes one with ArfA(A18T) and one with *T. thermophilus* RF2 (see introduction). Whereas Demo et al. (2017) obtained the closed conformation as major subpopulation by incubating the non-stop complex with deacylated tRNA<sup>fMet</sup>, C-terminally truncated ArfA and RF2 (see above and introduction). This raises the question on why the other groups did not observe this and if this accounted for by differences in data processing or the complex formation conditions. Indeed, two different software packages or a combination of them was used for processing. The RELION software package was used by three groups (James et al., 2016; Ma et al., 2017; Zeng et al., 2017), Demo et al. (2017) used FREALIGN and Huter et al. (2017c) started in RELION, while sorting and refinement was performed in FREALIGN. During initial classification steps in RELION Ma et al. (2017) and Zeng et al. (2017) discarded 68% and 65% of their initially picked particles, respectively. Zeng et al. (2017) state that non-ribosomal particles, as well as 50S and 30S subunits were removed. However, more detailed information about the steps, classes and respective particle numbers are necessary to make assumptions if the closed state of RF2 can be found in the discarded particles. Notably, Zeng et al. (2017) obtained two different conformations of the ribosome with RELION, with respect to this both software packages are capable to sort out conformations and cannot account for the additional state found by Demo et al. (2017). James et al. (2016) only removed non-ribosomal particles by 2D classification in RELION and 82% of ribosomal particles contained ArfA, as well as RF2 in the open conformation and was analysed further. Because of the high proportion of used particles it seems unlikely that a subpopulation with closed RF2 was overlooked. Demo et al. (2017) and Huter et al. (2017c) used all particles for 3D classification without prior removal of non-ribosomal particles. However, both datasets contained ~60% non-stop complexes with ArfA and RF2 or RF2-GAQ, respectively. Demo et al. (2017) already observed both RF2 conformations in this initial sorting step, whereas Huter et al. (2017c) observed only the open conformation, as additional analysis did not reveal the closed conformation in our dataset. Thus, sorting of both datasets with the same software lead to distinctive results regarding RF2 conformation. This further hints towards a difference in complex preparation accounting for the major subpopulation of the RF2 closed conformation in the dataset of Demo et al. (2017). Various factors, like ion concentrations, grid preparation procedure or protein tags could have contributed. For example, Mg<sup>2+</sup> ions have an impact on the flexibility of the ribosome, high

$Mg^{2+}$  concentrations lead to more rigidity (Yamamoto et al., 2010). With respect to this the  $Mg^{2+}$  concentration (20mM) used by Demo et al. (2017) was by far the highest and lies in the less flexible range. This might have caused an extended transition time from the closed to the open conformation and thus reduced the accommodation of RF2 domain 3. Additionally, Demo et al. (2017) let the sample cool down to room temperature after incubation at 37°C and stored the complex at -80°C before grid preparation, whereas all other groups mixed and incubated the samples right before grid preparation. Especially the freezing and thawing cycle could have influenced the sample of Demo et al. (2017) and have led to the closed conformation of RF2. Another aspect is the N-terminal His-tag, which was included in the ArfA protein of Huter et al. (2017c) and Demo et al. (2017), while the other groups removed the tags in the course of protein purification. Although both groups confirmed the activity of their protein biochemically, the N-terminal tag could have facilitated the closed conformation of RF2 in the case of Demo et al. (2017) but not for Huter et al. (2017c). The difference in the used ArfA proteins lies in an additional protease cleavage site inserted between the tag and ArfA by Huter et al. (2017c), which might have prevented stabilization of the closed conformation. However, the N-terminus of ArfA, which included the tag was flexible in the subset with the closed RF2 conformation from Demo et al. (2017), hence an influence of the N-terminal His-tag seems unlikely. Further factors might have favoured formation of the closed conformation of RF2 in the sample of Demo et al. (2017) and the high occurrence hints towards the experimental conditions influencing the accommodation of RF2. In the meantime, the closed conformation of RF2 was identified as physiological intermediate during termination by time-resolved cryo-EM (Fu et al., 2019). This renders the reason for the influence on the conformation even more interesting with respect to identification of further transient conformations.

## 4.2 Alternative ribosome rescue factor B

The recent study about ArfB binding to the *E. coli* ribosome with regard to the mRNA length led to a deeper insight into the interaction of ArfB with the ribosome (Chan et al., accepted). As previously reported (Shimizu, 2012; Feaga et al., 2016), the hydrolysis activity of ArfB decreases with increasing length of the mRNA, with a significant drop for more than nine nucleotides (Chan et al., accepted). Interestingly, ArfB was able to bind to the ribosome regardless of the mRNA length, but showed an extended ‘engagement step’ on long mRNAs, which lead to delayed activation of the ArfB hydrolysis activity (Chan et al., accepted). Similar findings were also reported for the quaternary complex of tmRNA·SmpB·EF-Tu GTP, which

delivers tmRNA·SmpB to the ribosome during *trans*-translation and the ArfA/RF2 system (Kurita et al., 2014a; Kurita et al., 2014b), which could indicate that also these systems proceed *via* an engagement step after initial binding. Interestingly, SmpB was even able to activate GTP hydrolysis by EF-Tu in the quaternary complex regardless of the mRNA length and ArfA could recruit RF2 to a complex with 21 nucleotides past the P-site. Both events are suggested to depend on interactions with the decoding center (Miller and Buskirk, 2014; James et al., 2016; Demo et al., 2017; Huter et al., 2017c; Ma et al., 2017; Zeng et al., 2017), which is right above the mRNA entry channel where engagement takes place. Activation of the hydrolysis activity of EF-Tu during *trans*-translation is mediated by a stacking interaction of His136 of SmpB with the decoding base G530 of the 16SrRNA (Miller et al., 2011; Miller and Buskirk, 2014). This indicates that at least SmpB has already access to the decoding center in the initial binding phase. While recruitment of RF2 by ArfA is mediated by donation of a  $\beta$ -strand to the superdomain 2/4 of RF2 and residue E30 with the ArfA  $\beta$ -strand interacts also with G530, RF2 is further recruited *via* hydrophobic interactions (James et al., 2016; Demo et al., 2017; Huter et al., 2017c; Ma et al., 2017; Zeng et al., 2017) and it is not known which interactions are already established during initial recruitment.

However, it is not completely clear yet what causes the difference in the mRNA length dependency between ArfA, which causes the decline of hydrolysis activity when more than three nucleotides extend past the P-site (Shimizu, 2012; Kurita et al., 2014a; Zeng and Jin, 2016). Similarly, for *trans*-translation, as well as for ArfB the hydrolysis activity has been shown to decrease when mRNAs extend nine nucleotides past the P-site (Ivanova et al., 2004; Shimizu, 2012; Feaga et al., 2016; Chan et al., accepted). While superimposition of ArfA and full length mRNA is in line with the kinetic data and indicates a clash between ArfA and the third nucleotide past the P-site (James et al., 2016; Demo et al., 2017; Huter et al., 2017c; Ma et al., 2017; Zeng et al., 2017), SmpB and ArfB collide with the fourth and the second nucleotide following the P-site, respectively (Gagnon et al., 2012; Neubauer et al., 2012). According to Chan et al. (accepted) the C-terminal tail of ArfB establishes interactions with the mRNA entry channel during the engagement step and this is slower for long mRNAs probably because the mRNA has to be displaced for ArfB binding to occur. In accordance, the cryo-EM structure of ArfB on the *E. coli* ribosome with an mRNA extending nine nucleotides past the P-site shows that the mRNA was displaced from the mRNA entry channel and was flexible after the P-site codon (Chan et al., accepted). Furthermore, the interactions between ArfB and the ribosome were identical with the ones formed on a complex with an mRNA extending zero nucleotides past the P-site (Chan et al., accepted). Nevertheless, the hypothesis

raises the question if the unstructured ArfB C-terminus and the mRNA can coexist in the mRNA entry channel in the early phase of the engagement step, and further if the mRNA is actively displaced by formation of the interactions between ArfB and the ribosome and/or by the associated transition of the ArfB C-terminal tail into an  $\alpha$ -helix. The questions can be expanded to the *trans*-translation system, because the C-terminal tail of SmpB is also unstructured in solution and forms an  $\alpha$ -helix upon binding to the mRNA entry channel (Dong et al., 2002; Neubauer et al., 2012; Rae et al., 2019). The transition of the SmpB C-terminal tail into an  $\alpha$ -helix has been shown to be necessary for the activation of tagging during *trans*-translation (Miller et al., 2011), but it has not been investigated yet if longer mRNAs prolong the transition time. The extended engagement step for ArfB with longer mRNAs (Chan et al., accepted) could also occur due to an occasional event, in which the mRNA loops out of the channel, the ArfB C-terminus could then rapidly bind to the mRNA entry channel and establish the helix. However, this should only be likely until a certain length of the mRNA and besides the rate of hydrolysis was reduced 100-fold, it was not completely abolished on complexes with a mRNA extending 99 nucleotides past the P-site (Chan et al., accepted). For such a long mRNAs looping out of the mRNA entry channel is improbable because of mRNA secondary structures. Assuming that the transition of the ArfB C-terminus is also necessary for the activation of peptidyl-tRNA hydrolysis by the ArfB-NTD, the activity on complexes with 99 nucleotides past the P-site could also imply that even the ArfB C-terminal tail in the  $\alpha$ -helical conformation and the mRNA could coexist in the mRNA entry channel. The similarity in the length dependency for SmpB and ArfB would then arise from the formation of a C-terminal helix and the defined path of the helix, which could allow co-residing of the helix and the mRNA in the mRNA entry channel, as well as establishment of interactions needed for the progress of the respective system. Furthermore, because ArfA does not form an  $\alpha$ -helix the different length dependency for ArfA could be explained by the distinct structure of its C-terminus. The C-terminus of ArfA remains a loop within the mRNA entry channel, which rather blocks the channel and with regard to this only three nucleotides can be accommodated after the P-site.

For BrfA/RF2 the mRNA length dependency and ribosome binding have not been investigated biochemically yet. However, the binding of BrfA helix  $\alpha$ 1 to h44 of the SSU and H71 of the LSU, as well as BrfA helix  $\alpha$ 2 to 23S rRNA H69 (Shimokawa-Chiba et al., 2019), could promote binding independent of the mRNA length and may support an engagement step. Regarding the mRNA length dependency, it is very difficult to make assumptions, since BrfA shares structural features with ArfB and SmpB, as well as ArfA. Comparable to ArfA, the C-

terminus of BrfA clashes with the third nucleotide past the P-site and has a dipeptide (LysHis)-motif, which interacts in the same way with the 16S rRNA in both systems (Shimokawa-Chiba et al., 2019). Additionally, BrfA harbours an  $\alpha$ -helix (helix  $\alpha$ 3) that is shorter than the helices of ArfB and SmpB and rather blocks the tunnel. In this regard, further kinetic and biochemical data is needed to further elucidate the initial steps of the BrfA/RF2 system.

Another interesting point shown by Chan et al. (accepted) is that the turnover of ArfB, but not the peptidyl-tRNA hydrolysis activity, is inhibited by the PrAMP Api137. This had been reported previously for bacterial class I RFs (Florin et al., 2017; Graf et al., 2018). In consequence, the RF was trapped on the ribosome, which was used for analysis by cryo-EM. Since the turnover of ArfB was also inhibited (Chan et al., accepted), the same strategy used to stabilise ArfB on the ribosomal complex was employed. The used complex was composed of an mRNA extending zero or nine nucleotides past the P-site and P-site tRNA. As mentioned above, analysis of the datasets showed that the conformation of ArfB was identical because, as mentioned above, the overhang of nine nucleotides was displaced from the mRNA entry channel. Additionally, binding of Api137 to the ribosome and the interactions between ArfB and Api137 were identical to the ones observed with RF1 in the previous cryo-EM structures (Florin et al., 2017; Graf et al., 2018; Chan et al., accepted). Regarding this, Api137 could inhibit all bacterial peptidyl-tRNA hydrolases containing a GGQ-motif and also RF-dependent ribosome rescue systems, like ArfA/RF2, BrfA/RF1, ArfT/RF1 and ArfT/RF2. Since the GGQ-motif is universally conserved and the contacts between Api137 and the ribosome mostly involve conserved rRNA bases within the PTC and the peptide exit tunnel, it has the potential to inhibit translation across the domains of life (Frolova et al., 1999; Seit-Nebi et al., 2001; Zavialov et al., 2002; Mora et al., 2003; Shaw and Green, 2007; Florin et al., 2017; The Rnacentral Consortium, 2018; Graf and Wilson, 2019). This would render Api137 an interesting tool to investigate translation termination. Moreover, Api137 is also a prime candidate as antimicrobial agent against Gram-negative bacteria, which actively take up PrAMPs mainly *via* the SbmA transporter (see introduction) that is not found in Gram-positive bacteria (Mattiuzzo et al., 2007; Graf et al., 2017). Additional inhibition of human cytosolic or mitochondrial translation would increase cytotoxicity during treatment, which could be problematic regarding the use of Api137 as an antimicrobial agent. However, it is difficult to predict inhibition of different species by PrAMPs. For example, according to competition assays the bovine PrAMPs Bac5 and Bac7 should have an overlapping binding site (Mardirossian et al., 2018a). Nevertheless, while Bac7 inhibits translation of *E. coli* and *T. thermophilus*, Bac5 displays species-specific inhibition and did not inhibit *T. thermophilus*.

translation very well, whereas *E. coli* translation was inhibited effectively (Mardirossian et al., 2018a). Furthermore, a recent study determined the dissociation constant ( $K_d$ ) of Api137 from isolated 70S ribosomes and its minimal inhibitory concentration (MIC) of four human pathogens and the dissociation varied between species (Kolano et al., 2020). Compared to *E. coli* ribosomes ( $K_d=379$  nM) the  $K_d$  of pathogens *Klebsiella pneumoniae* and *Pseudomonas aeruginosa* was even lower, with 155 nM and 257 nM, respectively. In contrast, for ribosomes of *Acinetobacter baumannii* and *Staphylococcus aureus*, which is the only Gram-positive bacterium in the study, a higher  $K_d$  of 2 493 nM and 13 079 nM was determined. Interestingly, the MIC did not correlate with the  $K_d$ , as *E. coli* and *Klebsiella pneumoniae* had a low MIC of 2 and 4 mgL<sup>-1</sup>, while the MIC of *Acinetobacter baumannii*, *Pseudomonas aeruginosa* and *Staphylococcus aureus* was increased 31-fold or higher, compared to *E. coli*. The findings indicate that Api137 displays species specific inhibition and that the affinity of Api137 for ribosomes varies from species to species and that Api137 is mainly active against *Enterobacteriaceae*, like *Escherichia* and *Klebsiella* with respect to the MIC (Kolano et al., 2020). In conclusion, the activity and effectiveness of Api137 against different species and among species from various kingdoms needs to be tested individually. Even if Api137 would inhibit human translation in the cytosol or mitochondria, it is not clear yet if it can pass the cell membrane(s) to enter the cytosol and the mitochondrial matrix to reach the ribosomes. In this regard, a recent study in mice used Api137 successfully against an *E. coli* infection model (Knappe et al., 2019). The potency of Api137 treatment was greatly improved by continuous subcutaneous delivery (67% survival), because Api137 exhibited a short half-life of <30 min using single injections (33% survival) due to proteolytic degradation. This shows that rather the stability than cytotoxicity of Api137 is the major challenge for its usage as an antimicrobial drug. Although, the stability of Api137 was already improved compared to the wildtype apidaecin-1b by exchanging the N-terminal asparagine to an ornithine residue conjugated with a tetramethylguanidino moiety (Berthold et al., 2013), the stability could be further improved for more convenient treatment, for instance by additional introduction of D-amino acids (Kolano et al., 2020). Nonetheless, Api137 is a very promising compound for the treatment of infections with Gram-negative bacteria, especially of the *Enterobacteriaceae* family (Knappe et al., 2019; Kolano et al., 2020).

### 4.3 *Bacillus* ribosome rescue factor A

Our recent cryo-EM structure of *B. subtilis* BrfA and *B. subtilis* RF2 on the *E. coli* non-stop ribosomal complex shed light into the mechanism of ribosome rescue by the BrfA/RF2 system (Shimokawa-Chiba et al., 2019). Since BrfA and *B. subtilis* RF2 are able to promote peptidyl-tRNA hydrolysis on *E. coli* non-stop ribosomal complexes the same approach as for cryo-EM structure determination of the *E. coli* ArfA/RF2 system, which used the truncated *nlpD* ORF as template for non-stop complex generation (Huter et al., 2017c), was applied. Additionally, a similar set-up for complex formation was used by incubating the non-stop complex with BrfA and a hydrolysis deficient RF2 variant, in which the glutamine of the GGQ-motif was mutated to proline (GGP) (Korostelev et al., 2008; Santos et al., 2013).

The acquired cryo-EM dataset was analysed with RELION 3 and showed only one major population with stoichiometric binding of BrfA and RF2 in the open conformation to the non-stop complex. Substoichiometric binding of RF2-GGP to the non-stop complex may indicate that BrfA is less effective than ArfA in recruiting the RF, at least regarding *E. coli* ribosomes. Since substoichiometric occupancy was not found the datasets of the ArfA/RF2 system (James et al., 2016; Demo et al., 2017; Huter et al., 2017c; Ma et al., 2017; Zeng et al., 2017) or our BrfA dataset (Shimokawa-Chiba et al., 2019), both factors seem to recruit RF2 with high affinity. The closed conformation was not found in the BrfA dataset, hence BrfA efficiently activated the open conformation of RF2. The overall conformation of RF2 is similar in the structure of the BrfA/RF2 and the ArfA/RF2 system, in both the catalytic domain 3 of RF2 is directed towards the PTC (James et al., 2016; Demo et al., 2017; Huter et al., 2017c; Ma et al., 2017; Zeng et al., 2017; Shimokawa-Chiba et al., 2019). The GGP-motif variation of RF2 was previously found to adopt the same conformation in the PTC as the wild type GGQ-motif in a crystal structure of *T. thermophilus* RF2-GGP decoding a stop-codon on the corresponding ribosome (Santos et al., 2013). In contrast, in our cryo-EM structure the motif is rather flexible, which might indicate that the GGP-variation needs the longer timeframe of crystallisation to establish the conformation. Another possibility is that the adjustment of *B. subtilis* RF2 to the *B. subtilis* ribosome influenced the accommodation of domain 3 to the PTC, which is supported by the lower activity of BrfA/RF2 on *E. coli* ribosomes and the lower resolution of domain 3 in comparison to the ArfA/RF2 structures (James et al., 2016; Demo et al., 2017; Huter et al., 2017c; Ma et al., 2017; Zeng et al., 2017; Shimokawa-Chiba et al., 2019). However, comparison of the hydrolysis activity of BrfA/RF2 and ArfA/RF2 on the corresponding non-stop complex indicates that BrfA/RF2 is generally less active (Shimokawa-Chiba et al., 2019).

This is supported by the higher flexibility of the switch loop in the BrfA/RF2 structure compared to the ArfA/RF2 structures (James et al., 2016; Demo et al., 2017; Huter et al., 2017c; Ma et al., 2017; Zeng et al., 2017; Shimokawa-Chiba et al., 2019). ArfA, RF2 and rProtein S12 establish a hydrophobic pocket in which Trp319 (*E. coli* numbering; Trp318 in *B. subtilis*) of the RF2 switch loop is tightly bound (Figure 21a), while BrfA mainly provides stacking of Trp319 on phenylalanine 31 (Figure 21b). Additional hydrophobic interactions with RF2 phenylalanine 217 (phenylalanine 216 in *B. subtilis*) and rProtein S12 leucine 46 might be possible, while phenylalanine 31 could be stabilised by valine 198 (valine 197 in *B. subtilis*) also *via* hydrophobic interaction (Figure 21b). In conclusion, the alternative mechanism of BrfA to induce the open conformation of RF2 might be less tight and lead to more flexibility in the switch loop and domain 3, although further influences cannot be ruled out, since the observation is primarily based on the structure and needs further biochemical support.

As observed for ArfA, recruitment of RF2 by BrfA is mediated *via* addition of a  $\beta$ -strand to the  $\beta$ -sheet of the superdomain 2/4, the  $\beta$ -strand of the rescue factor lies between RF2 and the decoding center (James et al., 2016; Demo et al., 2017; Huter et al., 2017c; Ma et al., 2017; Zeng et al., 2017; Shimokawa-Chiba et al., 2019). In comparison, ArfA and RF2 sink deeper into the decoding center as BrfA and RF2, hence the  $\beta$ -strand of BrfA and the superdomain 2/4 of RF2 are shifted approximately by 2 Å. ArfA is able to recruit heterologous RF2 from *T. thermophilus*, but is not able to stabilise the open conformation because of steric clashes with non-conserved residues of RF2 helix  $\alpha$ 7 (James et al., 2016; Huter et al., 2017c). Because of the conserved recruitment mechanism this is also possible for BrfA (Shimokawa-Chiba et al., 2019) and could provide a structure of pre-accommodated BrfA, as well as more insight into the activation of RF2. Another possibility would be to use a BrfA variant which can recruit

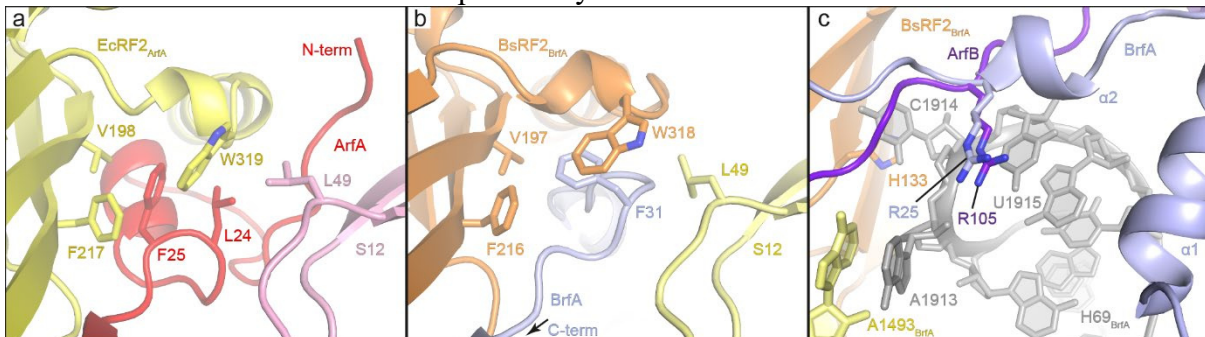


**Figure 21: Comparison of switch loop stabilisation by ArfA and BrfA, and interaction of ArfB and BrfA with H69.** (a) Hydrophobic pocket formed by leucine 24 (L24) and phenylalanine 25 (F25) of ArfA (red), valine 198 (V198) and phenylalanine 217 (F217) of *E. coli* RF2 ( $EcRF2_{ArfA}$ , yellow) and leucine 49 (L49) of rProtein S12 (S12, pink) (PDBID 5MGP (Huter et al., 2017c)). Tryptophan 319 (W319) of the RF2 switch loop lies in the center of the pocket. (b) Same view as (a) showing the stabilisation of W319 (W318 in *B. subtilis*) of *B. subtilis* RF2 ( $BsRF2_{BrfA}$ , orange) by stacking phenylalanine 31 of BrfA (pale blue) (PDBID 6SZS (Shimokawa-Chiba et al., 2019)). Hydrophobic interaction of W319 with F216 (F216 in *B. subtilis*) of *B. subtilis* RF2 and L49 of S12 (pale yellow) might contribute additionally. (c) Stacking of arginine 25 (R25) of BrfA and arginine 105 (R105) of ArfB (purple, PDBID 6YSS (Chan et al., accepted)) on U1915 of 23S rRNA helix 69 ( $H69_{BrfA}$ , grey). The PDBs were aligned based on the 16S rRNA.

*B. subtilis* RF2 but not activate it, similar to the usage of inactive ArfA(A18T) (James et al., 2016). Such a BrfA-variant has not been described yet. An interesting approach could entail the disruption of the stacking interaction of the conserved arginine 25 onto U1915 (Figure 21c), which would destabilise the BrfA region of residue 17 till 34, which includes the critical phenylalanine 31. The same stacking interaction was observed with the conserved residue arginine 105 within the ArfB linker region (Figure 21c) (Gagnon et al., 2012; Chan et al., accepted), which indicates a shared interaction mechanism between BrfA and ArfB with H69. Furthermore, mutation of ArfB arginine 105 to alanine reduced the activity of ArfB by ~80 % (Kogure et al., 2014), which raises the question if this would also apply for the mutation of BrfA arginine 25. Another possibility could be to inhibit binding of helix  $\alpha$ 1 to h44 of the 16S rRNA and H71 of the 23S rRNA by mutating lysines and arginines to alanine. However, this could lead to loss of binding of BrfA to the ribosome. Rather promising might be a mutation of serine 24 or serine 27 to a bulky residue, like tryptophan, which could induce a clash with helix  $\alpha$ 7 of RF2. Further mutation of proline 29 might be interesting, since it is partly conserved.

The structures of the ribosome rescue systems indicate that all systems bind to the mRNA entry channel *via* positively charged residues in the C-terminal region (Figure 22) (Neubauer et al., 2012; James et al., 2016; Demo et al., 2017; Huter et al., 2017c; Ma et al., 2017; Zeng et al., 2017; Rae et al., 2019; Chan et al., accepted). These residues are conserved within the respective protein (Figure 22). Furthermore, it has been shown that mutation of these positively charged residues in SmpB and ArfB inhibits activation of the following steps. As mentioned in the introduction triple mutation of the SmpB (Figure 22a) residues D137K138R139 prevents activation of the *trans*-transfer onto the TLD of tmRNA and thus progression of *trans*-translation (Sundermeier et al., 2005; Miller et al., 2011). In ArfB (Figure 22b) single mutations like K122A, K129A or R132A already reduced the activity severely. Mutations of the respective residues in ICT1 had the same dramatic effect, underlining the similarity of the proteins (Kogure et al., 2014). Interestingly the positively charged residues cluster to one side of the helix, which is directed towards the body of the 30S subunit (Figure 22b). In ArfA (Figure 22c) a mutational analysis showed that every residue could be substituted to cysteine and only the mutation of lysine 34 (K34C) led to a ~30% decrease of the hydrolysis activity (Kurita et al., 2014a). In a follow-up study it was shown that the hydrolysis rate was reduced for the mutation K34C by ~50%, however, the reduction was even more severe for mutation of tyrosine 39 (~70% reduction) or arginine 41 (~85% reduction) to cysteine (Ma et al., 2017). The cysteine mutation of tyrosine 39 or arginine 41 did not influence the activity in the former

study probably because of the longer incubation time, hence the endpoint of the reaction was represented and the reduced hydrolysis rate was not detected. Nevertheless, in both studies other single mutations in ArfA were redundant (Kurita et al., 2014a; Ma et al., 2017). However, C-terminal truncation of ArfA to 40 remaining residues did not support growth upon deletion

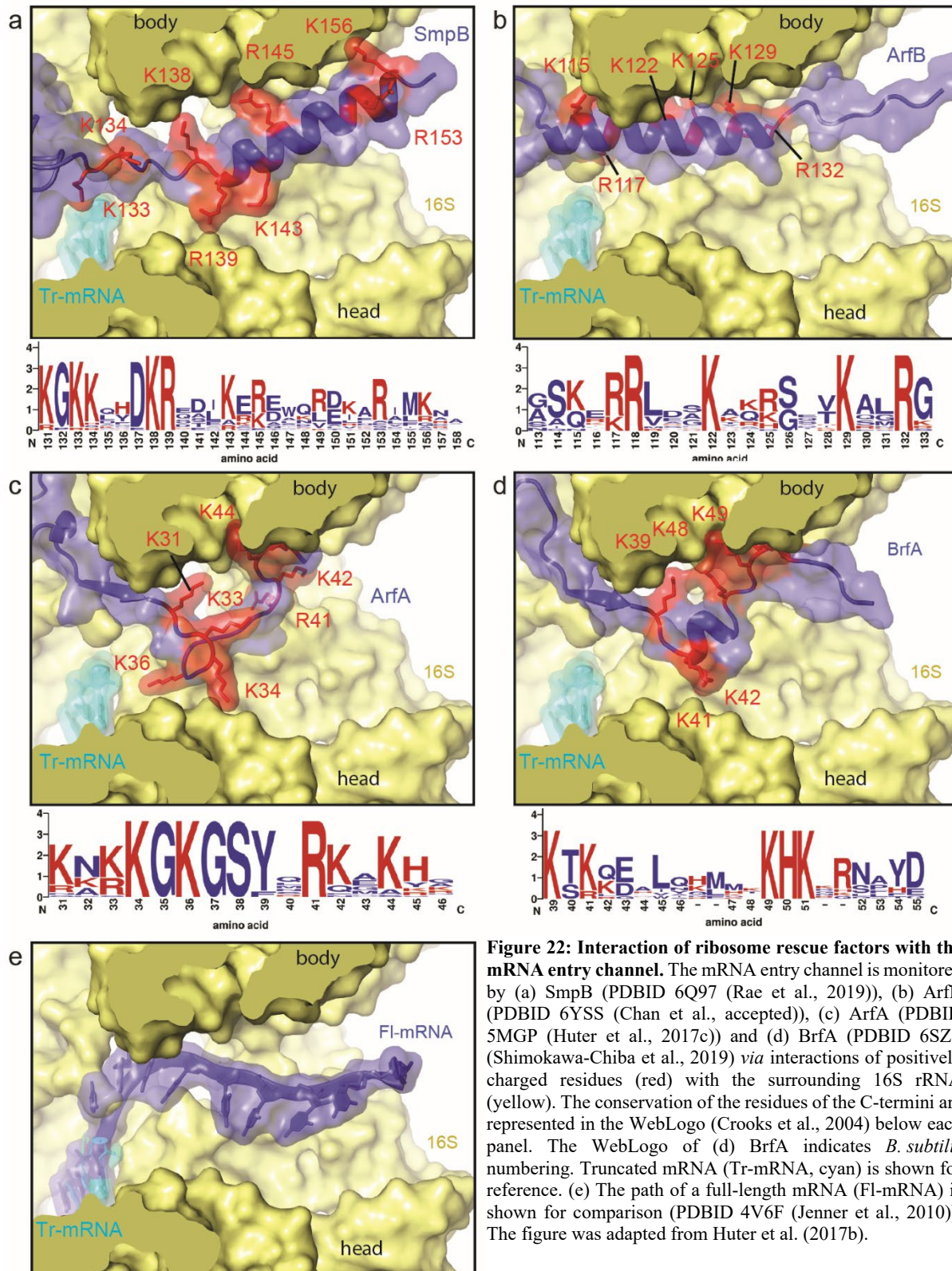


**Figure 22: Interaction of ribosome rescue factors with the mRNA entry channel.** The mRNA entry channel is monitored by (a) SmpB (PDBID 6Q97 (Rae et al., 2019)), (b) ArfB (PDBID 6YSS (Chan et al., accepted)), (c) ArfA (PDBID 5MGP (Huter et al., 2017c)) and (d) BrfA (PDBID 6S2S (Shimokawa-Chiba et al., 2019) via interactions of positively charged residues (red) with the surrounding 16S rRNA (yellow). The conservation of the residues of the C-termini are represented in the WebLogo (Crooks et al., 2004) below each panel. The WebLogo of (d) BrfA indicates *B. subtilis* numbering. Truncated mRNA (Tr-mRNA, cyan) is shown for reference. (e) The path of a full-length mRNA (Fl-mRNA) is shown for comparison (PDBID 4V6F (Jenner et al., 2010)). The figure was adapted from Huter et al. (2017b).

of *trans*-translation in *E. coli* (Chadani et al., 2011a). This rather indicates that removal of positively charged patches, like Arg41Lys42Gly43Lys44, might reduce the engagement of ArfA with the mRNA entry channel and/or the activation of RF2, what would in turn diminish the hydrolysis activity.

Mutational analysis of the BrfA C-terminus is not available yet, but based on our cryo-EM structure and the alignment of BrfA from different *Bacillus* species suggestions can be made (Figure 22d) (Shimokawa-Chiba et al., 2019). The conserved lysine 39 (Lys39), which follows the  $\beta$ -strand, putatively H-bonds with N4 of nucleotide C518 of the 16S rRNA, which is sandwiched between G529 and G530. Further H-bonds are possible with the oxygens of the backbone phosphate of G529, as well as with O6 or N7 of G530. The interactions between Lys39 and the 16S rRNA are probably involved in proper placement of the  $\beta$ -strand, hence mutation could influence recruitment of RF2. The following serine 40 (Ser40) is in H-bond distance to the sidechain of RF2 arginine 211 and alternatively, an H-bond with C1397 of the 16S rRNA is possible when the sidechain is rotated. This hints towards the sidechain having a different rotational state in dependence of the presence or absence of RF2 and thus could be involved in recruitment or placement of RF2. Ser40 is not conserved throughout BrfA and a threonine is more common in this position (Figure 22d) (Shimokawa-Chiba et al., 2019). However, both amino acids can participate in H-bonding *via* the hydroxyl group of the respective sidechain and seem to be interchangeable in this position. A mutation to alanine would disrupt H-bonding in this position, whereas bulky amino acids, like phenylalanine, would lead to clashes with C1397 and arginine 211. Both variants could interfere with BrfA binding and/or recruitment, as well as activation of RF2. Nevertheless, compensating stacking interactions cannot be excluded for aromatic sidechains. Ser40 is also the first amino acid of helix  $\alpha$ 3 of BrfA. Lysine 41 can form H-bonds with the surrounding 16S rRNA in different sidechain conformations, but not with rProtein S3, since the hydrophobic isoleucine 162 (Ile162) cannot form H-bonds. The following lysine 42 can H-bond with the 16S rRNA or rProtein S5. Both lysine residues could compensate each other regarding binding and mechanism of BrfA, hence it is possible that only double mutation of them would show an effect. Lysine 42 is less conserved than lysine 41, with glutamine and arginine commonly found in position 42. This indicates that medium and long sidechains with the ability to form H-bonds are sufficient in this position. In contrast, in position 41 a long sidechain, like lysine or arginine is preferred to span the hydrophobic Ile162 of rProtein S3 and to form H-bonds. The following glutamic acid (Glu43) H-bonds with N4 of C1397 of the 16S rRNA and the backbone amide of Ser40, which indicates that the residue could be important for binding of

BrfA to the ribosome and establishment of the secondary structure. The hydrophobic residues isoleucine 44 and leucine 45 are directed towards Ile162 of rProtein S3 and render helix  $\alpha$ 3 amphipathic in this region. Leucine 45 is more conserved than isoleucine 44, however in either case the hydrophobicity is conserved, with exceptions for isoleucine 44 for example in *Bacillus nakamurai*, *Bacillus haynesii* and *Bacillus populi*, which have an arginine, glutamic acid or a lysine in this position, respectively. The reason for this is difficult to dissect based only on our cryo-EM structure and further structures and biochemical data will be necessary to draw conclusions on the effect of these residues in other *Bacillus* species. Probably, the flexibility of these sidechains allows suitable positioning despite the charge. The following asparagine 46 does not interact with the ribosome in our structure, rather it ends helix  $\alpha$ 3, although the backbone amide of lysine 47 participates in the helix. The asparagine is not conserved in position 46 and BrfA of most other *Bacillus* species has a glutamine in this position, which preferably forms helices (Chou and Fasman, 1974; Prevelige and Fasman, 1989). Additionally, the following amino acids are less conserved between *B. subtilis* and other *Bacillus* species (Figure 22d), like *Bacillus altitudinis* (Shimokawa-Chiba et al., 2019). In particular, a subgroup of *Bacillus* species in the alignment has a conserved motif of five amino acids (GlnHisMetMetLys) between lysine 45 and the lysine-histidine (KH)-motif, which is conserved throughout BrfA. The five amino acids preferably form helices (Chou and Fasman, 1974; Prevelige and Fasman, 1989), which indicates that helix  $\alpha$ 3 could be longer in these species. Also, further variations are possible, since other *Bacillus* species have the same distance between lysine 45 and the KH-motif, but the amino acids differ in this region (Figure 22d) (Shimokawa-Chiba et al., 2019). In contrast, *B. subtilis* has only three amino acids (Asn46Lys47Arg48) between lysine 45 and the KH (Lys49His50)-motif (Figure 22d). While Lys47 can form H-bonds with the backbone of the 16S rRNA, Arg48 stabilises the secondary structure of BrfA via H-bonds with the backbone oxygen of asparagine 52 and the hydroxyl group of tyrosine 54. The KH-motif binds in a pocket formed by the 16S rRNA nucleotides G505, A533, U534 and A535, as well as the backbone of C528 and G529. While Lys49 H-bonds with the backbone of G529, His50 stacks on U534 and is in H-bond distance to the backbone of G534. These residues and interactions are also conserved in ArfA (James et al., 2016; Demo et al., 2017; Huter et al., 2017c; Ma et al., 2017; Zeng et al., 2017; Shimokawa-Chiba et al., 2019). Until now only mutation of Lys49 (Lys44 in ArfA) to cysteine has been investigated in an *in vitro* peptidyl-tRNA hydrolysis assay (Kurita et al., 2014a), but no effect was detected, as aforementioned probably due to the long incubation time and thus measurement of the endpoint of the reaction. In the follow-up study, which measured the

hydrolysis rate, the KH-motif was not included (Ma et al., 2017). However, the conservation implicates a defined role for the motif, which has not been elucidated yet.

Despite the high conservation of lysine 51 in BrfA only weak H-bonds with the surrounding 16S rRNA could be formed (Shimokawa-Chiba et al., 2019), hence its role is difficult to predict. The following asparagine 52 is partly conserved among BrfA the *Bacillus* species, however some have two additional amino acids between lysine 51 and asparagine 52, hence the interactions with the mRNA entry channel may vary in this region. In our structure of *B. subtilis* BrfA asparagine 52 can form an H-bond with O4 of U534, while proline 53 does not interact with any element and provides the flexibility for tyrosine 54 to stack on phenylalanine 33 of rProtein S5. Aspartic acid 55 may H-bond with arginine 47 of rProtein S4, but BrfA is already quite flexible in this region. Further residues were not modelled due to the high flexibility of the residues 56-62.

In summary, every resolved residue of the BrfA C-terminus (residue 39-55) contributes to proper binding to the mRNA entry channel and presumably also to activation of RF2. To reveal if residues display redundancies and fully decipher the discrete role for each residue further biochemical data, like alanine scanning in combination with time-resolved *in vitro* peptidyl-tRNA hydrolysis analysis, is necessary.

Our study also investigated the activity of the BrfA/RF2 and the *trans*-translation system with ribosomes stalled by the *B. subtilis* MifM arrest sequence, which stalls specifically *B. subtilis* ribosomes (Sohmen et al., 2015; Shimokawa-Chiba et al., 2019). Arrest sequences usually serve the regulation of a downstream ORF and mediate stalling during their own translation by interaction with the NPET (Figure 23a) (reviewed by Ito and Chiba (2013); Arenz et al. (2014); Wilson et al. (2016)). In particular, arrest sequences interactions with the NPET occur from the PTC till the constriction formed by the rProteins L4 and L22, which influences the activity of the PTC probably *via* an allosteric relay (Figure 23a). As reported for ArfA/RF2, ArfB and *trans*-translation with respect to *E. coli* ribosomes stalled by the *E. coli* SecM arrest sequence (Garza-Sánchez et al., 2006; Chadani et al., 2012), the observed activity of BrfA/RF2 and *trans*-translation of MifM-stalled ribosomes was not above spontaneous peptidyl-tRNA hydrolysis (Shimokawa-Chiba et al., 2019). However, during stalling on arrest peptides the mRNA entry channel is usually occupied and the mRNA would be quite long, since another ORF follows downstream of the channel, both rendering arrest peptide stalled ribosomes a poor target for ribosome rescue mechanisms (Ivanova et al., 2004; Shimizu, 2012; Kurita et al., 2014a; Feaga et al., 2016; Zeng and Jin, 2016; Shimokawa-Chiba et al., 2019; Chan et al., accepted). By contrast, the inhibition of *trans*-translation regarding SecM-stalled ribosomes

was mainly due to binding of proline-tRNA<sup>Pro</sup> to the ribosomal A-site, which prevented binding of tmRNA·SmpB (Garza-Sánchez et al., 2006). In the absence of proline-tRNA<sup>Pro</sup> *trans*-translation was less inhibited by SecM stalling. Furthermore, mRNA cleavage in the A-site due to prolonged stalling was inhibited by the presence of proline-tRNA<sup>Pro</sup>. Nevertheless, degradation of the mRNA would be possible until the nucleases encounter the entry of the mRNA entry channel, which protects the mRNA from further cleavage (Sunohara et al., 2004a; Garza-Sánchez et al., 2006). The remaining mRNA would extend approximately 12-15 nucleotides past the P-site and equal a mRNA overhang in which *trans*-translation can still act (Ivanova et al., 2004). This explains the activity of *trans*-translation on SecM-stalled ribosomes in the absence of proline-tRNA<sup>Pro</sup>. The same principle could also apply to MifM arrest (Figure 23b), because stalling occurs on several sequential codons due to slow peptide bond formation with a sense codon in the A-site (Chiba and Ito, 2012), which allows binding of the cognate tRNA. Interestingly, biochemical experiments showed that introduction of a stop codon into the MifM arrest sequence did not lead to termination (Chiba and Ito, 2012). This was also observed for a further arrest peptide, called TnaC, which allowed peptide bond formation but specifically inhibited termination (Gong and Yanofsky, 2002). Superimposition of the structures of TnaC and MifM stalled ribosomes show a similar conformation for the 23S rRNA nucleotide A2602 (Figure 23c) (Seidelt et al., 2009; Bischoff et al., 2014; Sohmen et al., 2015),

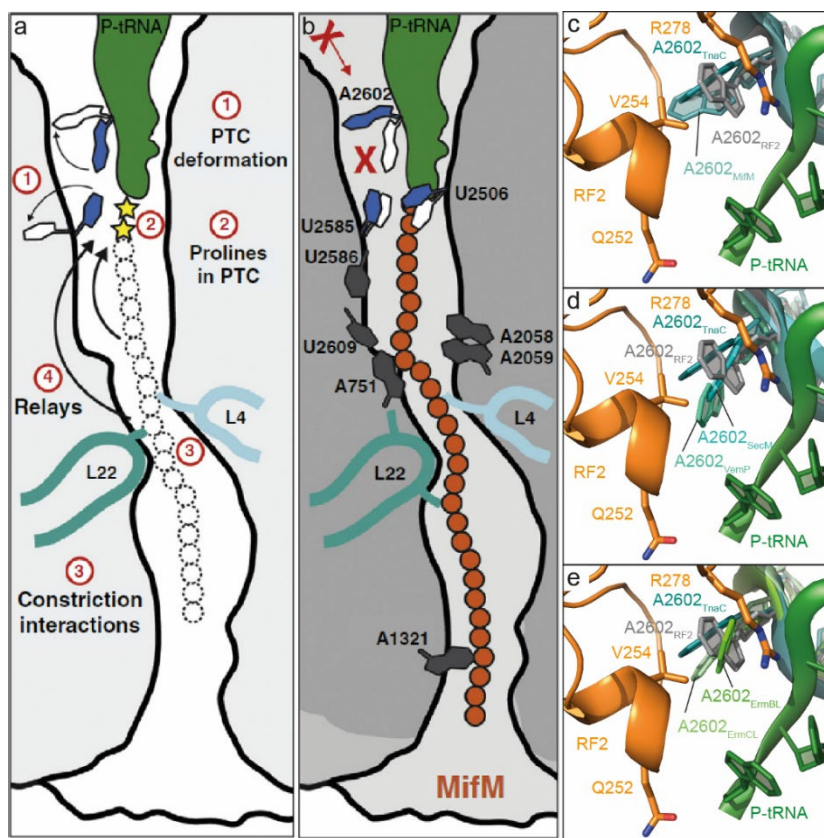


**Figure 23: Ribosome stalling by the arrest peptide MifM.** (a) Ribosome stalling can occur due to (1) rearrangement of the nucleotides of the PTC, (2) proline residues in the nascent polypeptide chain at the PTC or (3) interactions of the arrest peptide with the constriction formed by rProteins L4 and L22. (4) The constriction interactions are transmitted through the ribosome or the nascent chain and silence the PTC. (b) The scheme illustrates the interactions and PTC silencing by MifM. (c-e) Indicate the conformation of A2602 (c) during termination by RF2 (RF2, orange; A2602 grey; PDBID 5MDV (James et al., 2016)), or stalling by MifM (teal, PDBID 3J9W (Sohmen et al., 2015)), TnaC (deep teal, PDBID 4UY8 (Bischoff et al., 2014), (d) SecM (cyan, PDBID 3JBU (Zhang et al., 2015b; Feaga et al., 2016)), VemP (green cyan, PDBID 5NWY (Su et al., 2017)), (e) ErmBL (green, PDBID 5JU8 (Arenz et al., 2016)) or ErmCL (pale green, PDBID 3J7Z (Arenz et al., 2014)). P-site tRNA (forest, PDBID 3J9W) is shown for reference. Figure a-b were adapted from Wilson et al. (2016).

which usually supports binding of the GGQ-motif in domain 3 of RFs to the PTC (Figure 23c) (Korostelev et al., 2008; Laurberg et al., 2008; Weixlbaumer et al., 2008a; Korostelev et al., 2010). However, during stalling the conformation of A2602 is restricted and the induced state of the PTC upon RF binding is inhibited, hence accommodation of the GGQ-motif and subsequent peptidyl-tRNA hydrolysis are inhibited as well (Seidel et al., 2009; Bischoff et al., 2014; Sohmen et al., 2015). This could indicate that after occasional BrfA/RF2 binding and activation during MifM stalling, the adopted conformation A2602 may further inhibit BrfA/RF2 action by preventing accommodation of the GGQ-motif to the PTC. Whether specific inhibition of termination also occurs with *E. coli* SecM, ErmBL, *Staphylococcus aureus* ErmCL or VemP from *Vibrio alginolyticus* is not known yet, but superimposition of ribosome bound, open RF2 with the respective structure of the ribosome with SecM, ErmBL, ErmCL or VemP bound in the NPET also indicates conformations of A2602 that are incompatible with accommodation of the GGQ-motif (Figure 23d-e) (Arenz et al., 2014; Zhang et al., 2015b; Arenz et al., 2016; Su et al., 2017).

#### 4.4 Conclusion and Outlook

The structural and biochemical data obtained over the last decades shed light into ribosome rescue mechanisms in bacteria. Despite the apparent similarities between ArfA and BrfA involving regulation of expression by *trans*-translation, recruitment of RF2 and the KH-motif, the very low sequence similarity indicates that the systems evolved independently (Shimokawa-Chiba et al., 2019). This also holds true for *Francisella tularensis* ArfT, which is only ~40 amino acids in total (Goralski et al., 2018; Shimokawa-Chiba et al., 2019). In this regard further yet unidentified rescue mechanisms involving small proteins that can recruit and activate RFs could exist in other bacterial species. Identification of those could be rather difficult because the systems could possibly not be identified by sequence similarities and needs genetic screening in *trans*-translation deleted background. The mechanisms discussed so far also evolved independently from the eukaryotic ribosome-associated quality control (RQC) (Burroughs and Aravind, 2019), which resolves non-stop complexes and prolonged stalling of ribosomes (recently reviewed by (Joazeiro, 2019; Yan and Zaher, 2019). In brief, when a ribosome stalls the following ribosome(s) collides into the arrested (leading) ribosome. Stalling can occur for example on non-stop mRNAs or at inhibitory codon combinations, which adopt aberrant mRNA conformations in the A-site that are incompatible with decoding and thus lead to stalling (Tesina et al., 2020). The colliding ribosome is recognised and polyubiquitinylated

at rProtein uS10 in yeast by Hel2 (ZNF598 in mammals). The action of Hel2 is enhanced additionally by collision of three ribosomes (Matsuo et al., 2020). Ribosomes upstream of the collision site are recognized and polyubiquitylated by Not4 subunit of the Ccr4-Not complex and Hel2 at rProtein uS7. The mRNA is cleaved by Cue2 between the leading and the colliding ribosome and upstream of the collision site by further yet unidentified nucleases. In comparison to the prokaryotic ribosome rescue systems the former leading ribosome is split into subunits before release of the nascent polypeptide chain in an ubiquitinoylation and ATP-dependent manner by Dom34, Hbs1 and Rli1 (pelota, HBS1L or GTPBP2 and ABCE1 in mammals). This leads to an SSU (40S) with mRNA and an LSU (60S) carrying the nascent polypeptide chain associated with the previous P-site tRNA. Subsequently, the mRNA is degraded by Xrn1 (5'->3' degradation) and the exosome complex (3'->5' degradation). Nucleolytic cleavage of the mRNA by Xrn1 can already take place before splitting (Tesina et al., 2019). Xrn1 degradation of the mRNA is also enhanced on ribosomes upstream the collision site by the Ccr4-Not complex, which recognises vacant E-sites of stalled ribosomes, as well as the polyadenylation carried out previously by the Not4 subunit (Buschauer et al., 2020).

The obstructed 60S subunit is sensed by Rqc2 (NEMF in mammals), which triggers the assembly of the RQC complex, containing the E3-ubiquitin ligase Ltn1 and Rqc1 (Listerin and TCF25 in mammals). The RQC complex adds C-terminal alanine and threonine residues, a so-called CAT-tail, to the nascent polypeptide chain, while lysine residues emerging from the NPET are ubiquitylated by Ltn1. Interestingly, CAT-tails are added using aa-tRNAs in an SSU and mRNA independent way, in which the ASL of the tRNA interacts with Rqc2. Finally, the ubiquitylated nascent polypeptide is recognised by Cdc48 (VCP in mammals) and the CCA-end of the tRNA is cleaved by Vms1 (ANKZF1 in mammals), which releases the polypeptide from the tRNA in alternative way. The polypeptide is then extracted from the 60S subunit and stays associated with Cdc48, Ltn1 and Rqc2 until it is degraded by the proteasome. Whether the CCA-end of the tRNA is removed before degradation by further proteins or is hydrolysed spontaneously by cytosolic water is not known yet. Interestingly, the last universal common ancestor (LUCA) had an Rqc2 homologue as consequence Rqc2 homologues are found in all domains of life (Burroughs and Aravind, 2019; Lytvynenko et al., 2019). Recently, prokaryotic RQC was identified and described in *B. subtilis* (Lytvynenko et al., 2019). Similar to the eukaryotic RQC pathway, the prokaryotic homologue of Rqc2, termed RqcH, binds to the obstructed LSU and extends the nascent polypeptide chain with C-terminal alanine tails. After extraction of the polypeptide chain the alanine tails are recognized and degraded by the protease ClpXP. Double deletion of *trans*-translation and the *rqcH* gene was not synthetically

lethal under normal growth condition, but growth was strongly inhibited upon heat or antibiotic stress. The interplay between BrfA and RqcH is not investigated yet, but apparently BrfA was not able to suppress the growth defect upon stress. *Vice versa* RqcH was not able to overcome the synthetic lethality upon double deletion of *trans*-translation and the *brfA* gene (Shimokawa-Chiba et al., 2019). However, for the synthetic lethality screen the *brfA* gene was replaced by an antibiotic resistance gene, conferring resistance to erythromycin, and the use of the antibiotic during the screen might have stressed the cells, so that it could be possible that actually deletion of *trans*-translation, BrfA and RqcH is necessary to induce synthetic lethality in *B. subtilis*. This is supported by the CRISPR interference data, which shows synthetic lethality upon cold stress, but not at 37 °C, where only a strong growth defect was observed (Shimokawa-Chiba et al., 2019). However, to further elucidate the interplay between the three mechanisms additional experiments are needed.

Bacterial ribosome rescue mechanisms are a promising target for development of novel antibiotics, especially the systems that have no homologue in eukaryotes (i.e. *trans*-translation, ArfA, BrfA and ArfT). Since some bacteria possess more than one rescue system and all systems need to be targeted to reach lethality (Feaga et al., 2014b; Keiler and Feaga, 2014; Goralski et al., 2018; Lytvynenko et al., 2019; Shimokawa-Chiba et al., 2019), it would be convenient to target several mechanisms with one antibiotic. An antibiotic binding and blocking the mRNA entry channel would target *trans*-translation, ArfA, ArfB, BrfA and probably ArfT, additionally mRNA binding to the channel during initiation could be inhibited. In this regard, it has been shown that a synthetic peptide, which is equivalent to the C-terminal tail of SmpB inhibits binding of tmRNA·SmpB to the A-site of the ribosome, as well as peptidyl transfer to the TLD of tmRNA (Kurita et al., 2010). Since the peptide seems to bind to the mRNA entry channel itself its antimicrobial activity could be investigated. Furthermore, *trans*-translation is conserved in all today known bacterial genomes (Keiler and Feaga, 2014), thus it might affect a broad range of bacteria. The same strategy could be applied with synthetic peptides corresponding to the C-termini of ArfA, ArfB and BrfA. The brought distribution of ArfB also renders its C-terminal tail an interesting candidate for such investigations (Burroughs and Aravind, 2019). Furthermore, the KH-motif, which is conserved between ArfA and BrfA and displays conserved interactions with the mRNA entry channel (James et al., 2016; Demo et al., 2017; Huter et al., 2017c; Ma et al., 2017; Zeng et al., 2017; Shimokawa-Chiba et al., 2019), could indicate a binding of the C-termini of both systems to ribosomes of different species.

Also, specific inhibition of *trans*-translation for species, in which *trans*-translation is essential or in combination with other antimicrobial agents would be possible by the usage of an antisense DNA oligonucleotide to the gene encoding tmRNA (*ssrA* gene). This approach was already applied *in vitro* using an antisense oligonucleotide to the MLD of tmRNA, which blocked the activity of *trans*-translation (Hanes and Pluckthun, 1997). Furthermore, peptide aptamers were developed against *trans*-translation and ArfA of *Aeromonas veronii* and the expression of an aptamer against one of the systems from a plasmid led to reduced growth (Liu et al., 2016).

However, the challenge for usage of the approaches discussed above is their peptide or nucleotide nature, since both are prone to degradation by proteases and nucleases, respectively. As mentioned for PrAMPs, peptides corresponding to C-termini or aptamers could be stabilised by non-proteinogenic amino acids, like ornithine, or R-amino acids (Knappe et al., 2011; Berthold et al., 2013). DNA oligonucleotides are often stabilised by modification of the deoxyribose-phosphate backbone, for example in peptide nucleic acids the backbone is replaced by polyamide linkages (Karaki et al., 2019). Another challenge would be the uptake of the antimicrobial agents by the bacterial cell. Since the SbmA transporter can mediate import of peptides and peptide nucleic acids (Mattiuzzo et al., 2007; Ghosal et al., 2013), uptake of synthetic peptides and peptide nucleic acids could be restricted Gram-negative bacteria, which have a SbmA homologue (as seen for PrAMPs) (Graf et al., 2017; Graf and Wilson, 2019). Development of novel antimicrobial agents targeting RqcH could be difficult because of the homology to eukaryotic Rqc2 (Burroughs and Aravind, 2019; Lytvynenko et al., 2019). Non-conserved interaction sites with the ribosome could be one possibility, however structural and additional biochemical data will be necessary to identify such sites. Another option would be inhibition of other steps of bacterial RQC, which also need to be characterized further to make assumptions for targeting sites.

## 5 References

Abo, T., Ueda, K., Sunohara, T., Ogawa, K., and Aiba, H. (2002). SsrA-mediated protein tagging in the presence of miscoding drugs and its physiological role in *Escherichia coli*. *Genes to Cells* 7, 629-638.

Adamczyk, A.J., and Warshel, A. (2011). Converting structural information into an allosteric-energy-based picture for elongation factor Tu activation by the ribosome. *Proceedings of the National Academy of Sciences* 108, 9827.

Adio, S., Senyushkina, T., Peske, F., Fischer, N., Wintermeyer, W., and Rodnina, M.V. (2015). Fluctuations between multiple EF-G-induced chimeric tRNA states during translocation on the ribosome. *Nature Communications* 6, 7442.

Adio, S., Sharma, H., Senyushkina, T., Karki, P., Maracci, C., Wohlgemuth, I., Holtkamp, W., Peske, F., and Rodnina, M.V. (2018). Dynamics of ribosomes and release factors during translation termination in *E. coli*. *Elife* 7.

Ævarsson, A., Brazhnikov, E., Garber, M., Zheltonosova, J., Chirgadze, Y., al-Karadaghi, S., Svensson, L.A., and Liljas, A. (1994). Three-dimensional structure of the ribosomal translocase: elongation factor G from *Thermus thermophilus*. *EMBO J* 13, 3669-3677.

Agerberth, B., Lee, J.-Y., Bergman, T., Carlquist, M., Boman, H.G., Mutt, V., and JÖRnvall, H. (1991). Amino acid sequence of PR-39. *European Journal of Biochemistry* 202, 849-854.

Agirrezabala, X., Lei, J., Brunelle, J.L., Ortiz-Meoz, R.F., Green, R., and Frank, J. (2008). Visualization of the hybrid state of tRNA binding promoted by spontaneous ratcheting of the ribosome. *Mol Cell* 32, 190-197.

Agirrezabala, X., Liao, H.Y., Schreiner, E., Fu, J., Ortiz-Meoz, R.F., Schulten, K., Green, R., and Frank, J. (2012). Structural characterization of mRNA-tRNA translocation intermediates. *Proc Natl Acad Sci U S A* 109, 6094-6099.

Agrawal, R.K., Sharma, M.R., Kiel, M.C., Hirokawa, G., Booth, T.M., Spahn, C.M., Grassucci, R.A., Kaji, A., and Frank, J. (2004). Visualization of ribosome-recycling factor on the *Escherichia coli* 70S ribosome: functional implications. *Proc Natl Acad Sci U S A* 101, 8900-8905.

Akabane, S., Ueda, T., Nierhaus, K.H., and Takeuchi, N. (2014). Ribosome Rescue and Translation Termination at Non-Standard Stop Codons by ICT1 in Mammalian Mitochondria. *PLOS Genetics* 10, e1004616.

Allan Drummond, D., and Wilke, C.O. (2009). The evolutionary consequences of erroneous protein synthesis. *Nature Reviews Genetics* 10, 715.

Allen, G.S., Zavialov, A., Gursky, R., Ehrenberg, M., and Frank, J. (2005). The cryo-EM structure of a translation initiation complex from *Escherichia coli*. *Cell* 121, 703-712.

Antoun, A., Pavlov, M.Y., Lovmar, M., and Ehrenberg, M. (2006). How initiation factors tune the rate of initiation of protein synthesis in bacteria. *EMBO J* 25, 2539-2550.

Arenz, S., Bock, L.V., Graf, M., Innis, C.A., Beckmann, R., Grubmüller, H., Vaiana, A.C., and Wilson, D.N. (2016). A combined cryo-EM and molecular dynamics approach reveals the mechanism of ErmBL-mediated translation arrest. *Nature Communications* 7, 12026.

Arenz, S., Meydan, S., Starosta, Agata L., Berninghausen, O., Beckmann, R., Vázquez-Laslop, N., and Wilson, Daniel N. (2014). Drug Sensing by the Ribosome Induces Translational Arrest via Active Site Perturbation. *Molecular Cell* 56, 446-452.

Armache, J.-P., Jarasch, A., Anger, A.M., Villa, E., Becker, T., Bhushan, S., Jossinet, F., Habeck, M., Dindar, G., Franckenberg, S., *et al.* (2010). Localization of eukaryote-specific ribosomal proteins in a 5.5-Å cryo-EM map of the 80S eukaryotic ribosome. *Proceedings of the National Academy of Sciences* 107, 19754.

Asano, K., Kurita, D., Takada, K., Konno, T., Muto, A., and Himeno, H. (2005). Competition between trans-translation and termination or elongation of translation. *Nucleic Acids Res* 33, 5544-5552.

Atkins, J.F., and Gesteland, R.F. (1996). A case for trans translation. *Nature* 379, 769-771.

Ayyub, S.A., Gao, F., Lightowers, R.N., and Chrzanowska-Lightowers, Z.M. (2020). Rescuing stalled mammalian mitoribosomes – what can we learn from bacteria? *Journal of Cell Science* 133, jcs231811.

Baez, W.D., Roy, B., McNutt, Z.A., Shatoff, E.A., Chen, S., Bundschuh, R., and Fredrick, K. (2019). Global analysis of protein synthesis in *Flavobacterium johnsoniae* reveals the use of Kozak-like sequences in diverse bacteria. *Nucleic Acids Res* 47, 10477-10488.

Ban, N., Beckmann, R., Cate, J.H.D., Dinman, J.D., Dragon, F., Ellis, S.R., Lafontaine, D.L.J., Lindahl, L., Liljas, A., Lipton, J.M., *et al.* (2014). A new system for naming ribosomal proteins. *Current Opinion in Structural Biology* 24, 165-169.

Ban, N., Nissen, P., Hansen, J., Moore, P.B., and Steitz, T.A. (2000). The complete atomic structure of the large ribosomal subunit at 2.4 Å resolution. *Science* 289, 905-920.

Bandyra, K.J., and Luisi, B.F. (2013). Licensing and due process in the turnover of bacterial RNA. *RNA Biology* 10, 627-635.

Barends, S., Wower, J., and Kraal, B. (2000). Kinetic Parameters for tmRNA Binding to Alanyl-tRNA Synthetase and Elongation Factor Tu from *Escherichia coli*. *Biochemistry* 39, 2652-2658.

Belardinelli, R., Sharma, H., Caliskan, N., Cunha, C.E., Peske, F., Wintermeyer, W., and Rodnina, M.V. (2016a). Choreography of molecular movements during ribosome progression along mRNA. *Nature Structural & Molecular Biology* 23, 342-348.

Belardinelli, R., Sharma, H., Peske, F., Wintermeyer, W., and Rodnina, M.V. (2016b). Translocation as continuous movement through the ribosome. *RNA Biology* 13, 1197-1203.

Benincasa, M., Scocchi, M., Podda, E., Skerlavaj, B., Dolzani, L., and Gennaro, R. (2004). Antimicrobial activity of Bac7 fragments against drug-resistant clinical isolates. *Peptides* 25, 2055-2061.

Bennett, B.D., Kimball, E.H., Gao, M., Osterhout, R., Van Dien, S.J., and Rabinowitz, J.D. (2009). Absolute metabolite concentrations and implied enzyme active site occupancy in *Escherichia coli*. *Nature Chemical Biology* 5, 593-599.

Bentele, K., Saffert, P., Rauscher, R., Ignatova, Z., and Blüthgen, N. (2013). Efficient translation initiation dictates codon usage at gene start. *Molecular Systems Biology* 9, 675.

Berthold, N., Czihal, P., Fritsche, S., Sauer, U., Schiffer, G., Knappe, D., Alber, G., and Hoffmann, R. (2013). Novel Apidaecin 1b Analogs with Superior Serum Stabilities for Treatment of Infections by Gram-Negative Pathogens. *Antimicrobial Agents and Chemotherapy* 57, 402.

Bhattacharyya, S., Jacobs, W.M., Adkar, B.V., Yan, J., Zhang, W., and Shakhnovich, E.I. (2018). Accessibility of the Shine-Dalgarno Sequence Dictates N-Terminal Codon Bias in *E. coli*. *Mol Cell* 70, 894-905 e895.

Bieling, P., Beringer, M., Adio, S., and Rodnina, M.V. (2006). Peptide bond formation does not involve acid-base catalysis by ribosomal residues. *Nature Structural & Molecular Biology* 13, 423-428.

Bischoff, L., Berninghausen, O., and Beckmann, R. (2014). Molecular Basis for the Ribosome Functioning as an L-Tryptophan Sensor. *Cell Reports* 9, 469-475.

Blanchard, S.C., Kim, H.D., Gonzalez, R.L., Jr., Puglisi, J.D., and Chu, S. (2004). tRNA dynamics on the ribosome during translation. *Proc Natl Acad Sci U S A* 101, 12893-12898.

Bluhm, M.E.C., Schneider, V.A.F., Schäfer, I., Piantavigna, S., Goldbach, T., Knappe, D., Seibel, P., Martin, L.L., Veldhuizen, E.J.A., and Hoffmann, R. (2016). N-Terminal Ile-Orn- and Trp-Orn-Motif Repeats Enhance Membrane Interaction and Increase the Antimicrobial Activity of Apidaecins against *Pseudomonas aeruginosa*. *Frontiers in Cell and Developmental Biology* *4*, 39.

Boni, I.V., Isaeva, D.M., Musychenko, M.L., and Tzareva, N.V. (1991). Ribosome-messenger recognition: mRNA target sites for ribosomal protein S1. *Nucleic Acids Res* *19*, 155-162.

Borg, A., Pavlov, M., and Ehrenberg, M. (2016). Complete kinetic mechanism for recycling of the bacterial ribosome. *RNA* *22*, 10-21.

Bourne, H.R., Sanders, D.A., and McCormick, F. (1991). The GTPase superfamily: conserved structure and molecular mechanism. *Nature* *349*, 117-127.

Brenner, S., Barnett, L., Katz, E.R., and Crick, F.H.C. (1967). UGA: A Third Nonsense Triplet in the Genetic Code. *Nature* *213*, 449-450.

Brenner, S., Stretton, A.O.W., and Kaplan, S. (1965). Genetic Code: The 'Nonsense' Triplets for Chain Termination and their Suppression. *Nature* *206*, 994-998.

Brilot, A.F., Korostelev, A.A., Ermolenko, D.N., and Grigorieff, N. (2013). Structure of the ribosome with elongation factor G trapped in the pretranslocation state. *Proceedings of the National Academy of Sciences* *110*, 20994.

Brogden, K.A. (2005). Antimicrobial peptides: pore formers or metabolic inhibitors in bacteria? *Nature Reviews Microbiology* *3*, 238-250.

Brown, A., Amunts, A., Bai, X.-c., Sugimoto, Y., Edwards, P.C., Murshudov, G., Scheres, S.H.W., and Ramakrishnan, V. (2014). Structure of the large ribosomal subunit from human mitochondria. *Science* *346*, 718.

Brunelle, J.L., Shaw, J.J., Youngman, E.M., and Green, R. (2008). Peptide release on the ribosome depends critically on the 2' OH of the peptidyl-tRNA substrate. *RNA* *14*, 1526-1531.

Bulet, P., Dimarcq, J.L., Hetru, C., Lagueux, M., Charlet, M., Hegy, G., Van Dorsselaer, A., and Hoffmann, J.A. (1993). A novel inducible antibacterial peptide of *Drosophila* carries an O-glycosylated substitution. *Journal of Biological Chemistry* *268*, 14893-14897.

Burroughs, A.M., and Aravind, L. (2019). The Origin and Evolution of Release Factors: Implications for Translation Termination, Ribosome Rescue, and Quality Control Pathways. *Int J Mol Sci* *20*.

Buschauer, R., Matsuo, Y., Sugiyama, T., Chen, Y.-H., Alhusaini, N., Sweet, T., Ikeuchi, K., Cheng, J., Matsuki, Y., Nobuta, R., *et al.* (2020). The Ccr4-Not complex monitors the translating ribosome for codon optimality. *Science* *368*, eaay6912.

Byrgazov, K., Grishkovskaya, I., Arenz, S., Coudeville, N., Temmel, H., Wilson, D.N., Djinovic-Carugo, K., and Moll, I. (2015). Structural basis for the interaction of protein S1 with the *Escherichia coli* ribosome. *Nucleic Acids Res* *43*, 661-673.

Caban, K., Pavlov, M., Ehrenberg, M., and Gonzalez, R.L., Jr. (2017). A conformational switch in initiation factor 2 controls the fidelity of translation initiation in bacteria. *Nat Commun* *8*, 1475.

Capecchi, M.R. (1967). Polypeptide chain termination in vitro: isolation of a release factor. *Proc Natl Acad Sci U S A* *58*, 1144-1151.

Carter, A.P., Clemons, W.M., Brodersen, D.E., Morgan-Warren, R.J., Wimberly, B.T., and Ramakrishnan, V. (2000). Functional insights from the structure of the 30S ribosomal subunit and its interactions with antibiotics. *Nature* *407*, 340-348.

Carter, A.P., Clemons, W.M., Jr., Brodersen, D.E., Morgan-Warren, R.J., Hartsch, T., Wimberly, B.T., and Ramakrishnan, V. (2001). Crystal structure of an initiation factor bound to the 30S ribosomal subunit. *Science* 291, 498-501.

Caserta, E., Tomšić, J., Spurio, R., La Teana, A., Pon, C.L., and Gualerzi, C.O. (2006). Translation Initiation Factor IF2 Interacts with the 30 S Ribosomal Subunit via Two Separate Binding Sites. *Journal of Molecular Biology* 362, 787-799.

Caskey, C.T., Tompkins, R., Scolnick, E., Caryk, T., and Nirenberg, M. (1968). Sequential translation of trinucleotide codons for the initiation and termination of protein synthesis. *Science* 162, 135-138.

Casteels-Josson, K., Capaci, T., Casteels, P., and Tempst, P. (1993). Apidaecin multipeptide precursor structure: a putative mechanism for amplification of the insect antibacterial response. *EMBO J* 12, 1569-1578.

Casteels, P., Ampe, C., Jacobs, F., Vaeck, M., and Tempst, P. (1989). Apidaecins: antibacterial peptides from honeybees. *EMBO J* 8, 2387-2391.

Casteels, P., Ampe, C., Riviere, L., van Damme, J., Elicone, C., Fleming, M., Jacobs, F., and Tempst, P. (1990). Isolation and characterization of abaecin, a major antibacterial response peptide in the honeybee (*Apis mellifera*). *European Journal of Biochemistry* 187, 381-386.

Casteels, P., and Tempst, P. (1994). Apidaecin-Type Peptide Antibiotics Function through a Nonporeforming Mechanism Involving Stereospecificity. *Biochemical and Biophysical Research Communications* 199, 339-345.

Castle, M., Nazarian, A., Yi, S.S., and Tempst, P. (1999). Lethal Effects of Apidaecin on *Escherichia coli* Involve Sequential Molecular Interactions with Diverse Targets. *Journal of Biological Chemistry* 274, 32555-32564.

Chadani, Y., Ito, K., Kutsukake, K., and Abo, T. (2012). ArfA recruits release factor 2 to rescue stalled ribosomes by peptidyl-tRNA hydrolysis in *Escherichia coli*. *Mol Microbiol* 86, 37-50.

Chadani, Y., Matsumoto, E., Aso, H., Wada, T., Kutsukake, K., Sutou, S., and Abo, T. (2011a). trans-translation-mediated tight regulation of the expression of the alternative ribosome-rescue factor ArfA in *Escherichia coli*. *Genes Genet Syst* 86, 151-163.

Chadani, Y., Ono, K., Kutsukake, K., and Abo, T. (2011b). *Escherichia coli* YaeJ protein mediates a novel ribosome-rescue pathway distinct from SsrA- and ArfA-mediated pathways. *Mol Microbiol* 80, 772-785.

Chadani, Y., Ono, K., Ozawa, S., Takahashi, Y., Takai, K., Nanamiya, H., Tozawa, Y., Kutsukake, K., and Abo, T. (2010). Ribosome rescue by *Escherichia coli* ArfA (YhdL) in the absence of trans-translation system. *Mol Microbiol* 78, 796-808.

Chan, K.H., Petrychenko, V., Müller, C., Maracci, C., Holtkamp, W., Wilson, D.N., Fischer, N., and Rodnina, M.V. (accepted). Mechanism of Ribosome Rescue by Alternative Ribosome-Rescue Factor B. *Nature Communications*.

Chen, C., Cui, X., Beausang, J.F., Zhang, H., Farrell, I., Cooperman, B.S., and Goldman, Y.E. (2016). Elongation factor G initiates translocation through a power stroke. *Proceedings of the National Academy of Sciences* 113, 7515.

Chen, C., Stevens, B., Kaur, J., Cabral, D., Liu, H., Wang, Y., Zhang, H., Rosenblum, G., Smilansky, Z., Goldman, Yale E., *et al.* (2011). Single-Molecule Fluorescence Measurements of Ribosomal Translocation Dynamics. *Molecular Cell* 42, 367-377.

Chen, H., Bjerknes, M., Kumar, R., and Jay, E. (1994). Determination of the optimal aligned spacing between the Shine-Dalgarno sequence and the translation initiation codon of *Escherichia coli* mRNAs. *Nucleic Acids Res* 22, 4953-4957.

Chen, J., Petrov, A., Tsai, A., O'Leary, S.E., and Puglisi, J.D. (2013a). Coordinated conformational and compositional dynamics drive ribosome translocation. *Nat Struct Mol Biol* 20, 718-727.

Chen, Y., Feng, S., Kumar, V., Ero, R., and Gao, Y.-G. (2013b). Structure of EF-G-ribosome complex in a pretranslocation state. *Nature Structural & Molecular Biology* 20, 1077-1084.

Chen, Y., Kaji, A., Kaji, H., and Cooperman, B.S. (2017). The kinetic mechanism of bacterial ribosome recycling. *Nucleic Acids Res* 45, 10168-10177.

Cheng, K., Ivanova, N., Scheres, S.H.W., Pavlov, M.Y., Carazo, J.M., Hebert, H., Ehrenberg, M., and Lindahl, M. (2010). tmRNA-SmpB complex mimics native aminoacyl-tRNAs in the A site of stalled ribosomes. *Journal of Structural Biology* 169, 342-348.

Chernysh, S., Cociancich, S., Briand, J.-P., Hetru, C., and Bulet, P. (1996). The inducible antibacterial peptides of the Hemipteran insect *Palomena prasina*: Identification of a unique family of proline-rich peptides and of a novel insect defensin. *Journal of Insect Physiology* 42, 81-89.

Chiba, S., and Ito, K. (2012). Multisite Ribosomal Stalling: A Unique Mode of Regulatory Nascent Chain Action Revealed for MifM. *Molecular Cell* 47, 863-872.

Chiti, F. (2006). Relative Importance of Hydrophobicity, Net Charge, and Secondary Structure Propensities in Protein Aggregation. In *Protein Misfolding, Aggregation, and Conformational Diseases: Part A: Protein Aggregation and Conformational Diseases*, V.N. Uversky, and A.L. Fink, eds. (Boston, MA: Springer US), pp. 43-59.

Chou, P.Y., and Fasman, G.D. (1974). Prediction of protein conformation. *Biochemistry* 13, 222-245.

Choy, J.S., Aung, L.L., and Karzai, A.W. (2007). Lon Protease Degrades Transfer-Messenger RNA-Tagged Proteins. *Journal of Bacteriology* 189, 6564.

Christensen, S.K., Mikkelsen, M., Pedersen, K., and Gerdes, K. (2001). RelE, a global inhibitor of translation, is activated during nutritional stress. *Proceedings of the National Academy of Sciences* 98, 14328.

Chrzanowska-Lightowers, Z.M., and Lightowers, R.N. (2015). Response to "Ribosome Rescue and Translation Termination at Non-standard Stop Codons by ICT1 in Mammalian Mitochondria". *PLOS Genetics* 11, e1005227.

Cociancich, S., Dupont, A., Hegy, G., Lanot, R., Holder, F., Hetru, C., Hoffmann, J.A., and Bulet, P. (1994). Novel inducible antibacterial peptides from a hemipteran insect, the sap-sucking bug *Pyrrhocoris apterus*. *Biochemical Journal* 300, 567-575.

Cool, R.H., and Parmeggiani, A. (1991). Substitution of histidine-84 and the GTPase mechanism of elongation factor Tu. *Biochemistry* 30, 362-366.

Cornish, P.V., Ermolenko, D.N., Noller, H.F., and Ha, T. (2008). Spontaneous intersubunit rotation in single ribosomes. *Mol Cell* 30, 578-588.

Crick, F.H. (1966). Codon-anticodon pairing: the wobble hypothesis. *J Mol Biol* 19, 548-555.

Crooks, G.E., Hon, G., Chandonia, J.-M., and Brenner, S.E. (2004). WebLogo: A Sequence Logo Generator. *Genome Research* 14, 1188-1190.

Cunha, C.E., Belardinelli, R., Peske, F., Holtkamp, W., Wintermeyer, W., and Rodnina, M.V. (2013). Dual use of GTP hydrolysis by elongation factor G on the ribosome. *Translation (Austin)* 1, e24315.

Czihal, P., Knappe, D., Fritsche, S., Zahn, M., Berthold, N., Piantavigna, S., Müller, U., Van Dorpe, S., Herth, N., Binns, A., *et al.* (2012). Api88 Is a Novel Antibacterial Designer Peptide To Treat Systemic Infections with Multidrug-Resistant Gram-Negative Pathogens. *ACS Chemical Biology* 7, 1281-1291.

Czworkowski, J., Wang, J., Steitz, T.A., and Moore, P.B. (1994). The crystal structure of elongation factor G complexed with GDP, at 2.7 Å resolution. *EMBO J* 13, 3661-3668.

Dallas, A., and Noller, H.F. (2001). Interaction of translation initiation factor 3 with the 30S ribosomal subunit. *Mol Cell* 8, 855-864.

Daviter, T., Wieden, H.-J., and Rodnina, M.V. (2003). Essential Role of Histidine 84 in Elongation Factor Tu for the Chemical Step of GTP Hydrolysis on the Ribosome. *Journal of Molecular Biology* 332, 689-699.

de Smit, M.H., and van Duin, J. (1990). Secondary structure of the ribosome binding site determines translational efficiency: a quantitative analysis. *Proc Natl Acad Sci U S A* 87, 7668-7672.

de Smit, M.H., and van Duin, J. (1994). Translational initiation on structured messengers: Another role for the Shine-Dalgarno interaction. *Journal of Molecular Biology* 235, 173-184.

Demeshkina, N., Jenner, L., Westhof, E., Yusupov, M., and Yusupova, G. (2013). New structural insights into the decoding mechanism: translation infidelity via a G.U pair with Watson-Crick geometry. *FEBS Lett* 587, 1848-1857.

Demo, G., Svidritskiy, E., Madireddy, R., Diaz-Avalos, R., Grant, T., Grigorieff, N., Sousa, D., and Korostelev, A.A. (2017). Mechanism of ribosome rescue by ArfA and RF2. *Elife* 6.

Diaconu, M., Kothe, U., Schlunzen, F., Fischer, N., Harms, J.M., Tonevitsky, A.G., Stark, H., Rodnina, M.V., and Wahl, M.C. (2005). Structural basis for the function of the ribosomal L7/12 stalk in factor binding and GTPase activation. *Cell* 121, 991-1004.

Dong, G., Nowakowski, J., and Hoffman, D.W. (2002). Structure of small protein B: the protein component of the tmRNA-SmpB system for ribosome rescue. *EMBO J* 21, 1845-1854.

Dontsova, M., Frolova, L., Vassilieva, J., Piendl, W., Kisseelev, L., and Garber, M. (2000). Translation termination factor aRF1 from the archaeon *Methanococcus jannaschii* is active with eukaryotic ribosomes. *FEBS Letters* 472, 213-216.

Dorner, S., Panuschka, C., Schmid, W., and Barta, A. (2003). Mononucleotide derivatives as ribosomal P-site substrates reveal an important contribution of the 2'-OH to activity. *Nucleic Acids Research* 31, 6536-6542.

Duarte, I., Nabuurs, S.B., Magno, R., and Huynen, M. (2012). Evolution and Diversification of the Organellar Release Factor Family. *Molecular Biology and Evolution* 29, 3497-3512.

Dube, S.K., Marcker, K.A., Clark, B.F.C., and Cory, S. (1968). Nucleotide Sequence of N-Formyl-methionyl-transfer RNA. *Nature* 218, 232-233.

Dunkle, J.A., Wang, L., Feldman, M.B., Pulk, A., Chen, V.B., Kapral, G.J., Noeske, J., Richardson, J.S., Blanchard, S.C., and Cate, J.H.D. (2011). Structures of the Bacterial Ribosome in Classical and Hybrid States of tRNA Binding. *Science* 332, 981.

Erlacher, M.D., Lang, K., Shankaran, N., Wotzel, B., Hüttenhofer, A., Micura, R., Mankin, A.S., and Polacek, N. (2005). Chemical engineering of the peptidyl transferase center reveals an important role of the 2'-hydroxyl group of A2451. *Nucleic Acids Research* 33, 1618-1627.

Erlacher, M.D., Lang, K., Wotzel, B., Rieder, R., Micura, R., and Polacek, N. (2006). Efficient Ribosomal Peptidyl Transfer Critically Relies on the Presence of the Ribose 2'-OH at A2451 of 23S rRNA. *Journal of the American Chemical Society* 128, 4453-4459.

Feaga, H.A., Quickel, M.D., Hankey-Giblin, P.A., and Keiler, K.C. (2016). Human Cells Require Non-stop Ribosome Rescue Activity in Mitochondria. *PLoS Genet* 12, e1005964.

Feaga, H.A., Viollier, P.H., and Keiler, K.C. (2014a). Release of nonstop ribosomes is essential. *MBio* 5, e01916.

Feaga, H.A., Viollier, P.H., and Keiler, K.C. (2014b). Release of Nonstop Ribosomes Is Essential. *mBio* 5, e01916-01914.

Felden, B., Himeno, H., Muto, A., Atkins, J.F., and Gesteland, R.F. (1996). Structural organization of *Escherichia coli* tmRNA. *Biochimie* 78, 979-983.

Field, A., Hetrick, B., Mathew, M., and Joseph, S. (2010). Histidine 197 in release factor 1 is essential for a site binding and peptide release. *Biochemistry* 49, 9385-9390.

Fischer, N., Konevega, A.L., Wintermeyer, W., Rodnina, M.V., and Stark, H. (2010). Ribosome dynamics and tRNA movement by time-resolved electron cryomicroscopy. *Nature* 466, 329-333.

Fislage, M., Zhang, J., Brown, Z.P., Mandava, C.S., Sanyal, S., Ehrenberg, M., and Frank, J. (2018). Cryo-EM shows stages of initial codon selection on the ribosome by aa-tRNA in ternary complex with GTP and the GTPase-deficient EF-TuH84A. *Nucleic Acids Research* 46, 5861-5874.

Florin, T., Maracci, C., Graf, M., Karki, P., Klepacki, D., Berninghausen, O., Beckmann, R., Vazquez-Laslop, N., Wilson, D.N., Rodnina, M.V., *et al.* (2017). An antimicrobial peptide that inhibits translation by trapping release factors on the ribosome. *Nat Struct Mol Biol* 24, 752-757.

Flynn, J.M., Levchenko, I., Seidel, M., Wickner, S.H., Sauer, R.T., and Baker, T.A. (2001). Overlapping recognition determinants within the *ssrA* degradation tag allow modulation of proteolysis. *Proceedings of the National Academy of Sciences* 98, 10584.

Frank, J., and Agrawal, R.K. (2000). A ratchet-like inter-subunit reorganization of the ribosome during translocation. *Nature* 406, 318-322.

Fredrick, K., and Noller, H.F. (2003). Catalysis of ribosomal translocation by sparsomycin. *Science* 300, 1159-1162.

Freistroffer, D.V., Pavlov, M.Y., MacDougall, J., Buckingham, R.H., and Ehrenberg, M. (1997). Release factor RF3 in *E.coli* accelerates the dissociation of release factors RF1 and RF2 from the ribosome in a GTP-dependent manner. *EMBO J* 16, 4126-4133.

Frolova, L., Le Goff, X., Zhouravleva, G., Davydova, E., Philippe, M., and Kisseelev, L. (1996). Eukaryotic polypeptide chain release factor eRF3 is an eRF1- and ribosome-dependent guanosine triphosphatase. *RNA* 2, 334-341.

Frolova, L.Y., Tsivkovskii, R.Y., Sivolobova, G.F., Oparina, N.Y., Serpinsky, O.I., Blinov, V.M., Tatkov, S.I., and Kisseelev, L.L. (1999). Mutations in the highly conserved GGQ motif of class 1 polypeptide release factors abolish ability of human eRF1 to trigger peptidyl-tRNA hydrolysis. *RNA* 5, 1014-1020.

Fu, J., Hashem, Y., Wower, I., Lei, J., Liao, H.Y., Zwieb, C., Wower, J., and Frank, J. (2010). Visualizing the transfer-messenger RNA as the ribosome resumes translation. *EMBO J* 29, 3819-3825.

Fu, Z., Indrisiunaite, G., Kaledhonkar, S., Shah, B., Sun, M., Chen, B., Grassucci, R.A., Ehrenberg, M., and Frank, J. (2019). The structural basis for release-factor activation during translation termination revealed by time-resolved cryogenic electron microscopy. *Nat Commun* 10, 2579.

Fu, Z., Kaledhonkar, S., Borg, A., Sun, M., Chen, B., Grassucci, Robert A., Ehrenberg, M., and Frank, J. (2016). Key Intermediates in Ribosome Recycling Visualized by Time-Resolved Cryoelectron Microscopy. *Structure* 24, 2092-2101.

Gagnon, M.G., Roy, R.N., Lomakin, I.B., Florin, T., Mankin, A.S., and Steitz, T.A. (2016). Structures of proline-rich peptides bound to the ribosome reveal a common mechanism of protein synthesis inhibition. *Nucleic Acids Research* 44, 2439-2450.

Gagnon, M.G., Seetharaman, S.V., Bulkley, D., and Steitz, T.A. (2012). Structural basis for the rescue of stalled ribosomes: structure of YaeJ bound to the ribosome. *Science* *335*, 1370-1372.

Gao, H., Zhou, Z., Rawat, U., Huang, C., Bouakaz, L., Wang, C., Cheng, Z., Liu, Y., Zavialov, A., Gursky, R., *et al.* (2007a). RF3 induces ribosomal conformational changes responsible for dissociation of class I release factors. *Cell* *129*, 929-941.

Gao, N., Zavialov, A.V., Ehrenberg, M., and Frank, J. (2007b). Specific Interaction between EF-G and RRF and Its Implication for GTP-Dependent Ribosome Splitting into Subunits. *Journal of Molecular Biology* *374*, 1345-1358.

Gao, N., Zavialov, A.V., Li, W., Sengupta, J., Valle, M., Gursky, R.P., Ehrenberg, M., and Frank, J. (2005). Mechanism for the disassembly of the posttermination complex inferred from cryo-EM studies. *Mol Cell* *18*, 663-674.

Gao, Y.G., Selmer, M., Dunham, C.M., Weixlbaumer, A., Kelley, A.C., and Ramakrishnan, V. (2009). The structure of the ribosome with elongation factor G trapped in the posttranslocational state. *Science* *326*, 694-699.

Garza-Sánchez, F., Gin, J.G., and Hayes, C.S. (2008). Amino Acid Starvation and Colicin D Treatment Induce A-site mRNA Cleavage in *Escherichia coli*. *Journal of Molecular Biology* *378*, 505-519.

Garza-Sánchez, F., Janssen, B.D., and Hayes, C.S. (2006). Prolyl-tRNAPro in the A-site of SecM-arrested Ribosomes Inhibits the Recruitment of Transfer-messenger RNA. *Journal of Biological Chemistry* *281*, 34258-34268.

Garza-Sánchez, F., Schaub, R.E., Janssen, B.D., and Hayes, C.S. (2011). tmRNA regulates synthesis of the ArfA ribosome rescue factor. *Mol Microbiol* *80*, 1204-1219.

Garza-Sánchez, F., Shoji, S., Fredrick, K., and Hayes, C.S. (2009). RNase II is important for A-site mRNA cleavage during ribosome pausing. *Molecular Microbiology* *73*, 882-897.

Gavrilova, L.P., and Spirin, A.S. (1971). Stimulation of "non-enzymic" translocation in ribosomes by p-chloromercuribenzoate. *FEBS Lett* *17*, 324-326.

Ge, X., Mandava, C.S., Lind, C., Åqvist, J., and Sanyal, S. (2018). Complementary charge-based interaction between the ribosomal-stalk protein L7/12 and IF2 is the key to rapid subunit association. *Proceedings of the National Academy of Sciences* *115*, 4649.

Ge, Z., Mehta, P., Richards, J., and Karzai, A.W. (2010). Non-stop mRNA decay initiates at the ribosome. *Molecular Microbiology* *78*, 1159-1170.

Geggier, P., Dave, R., Feldman, M.B., Terry, D.S., Altman, R.B., Munro, J.B., and Blanchard, S.C. (2010). Conformational Sampling of Aminoacyl-tRNA during Selection on the Bacterial Ribosome. *Journal of Molecular Biology* *399*, 576-595.

Gennaro, R., Skerlavaj, B., and Romeo, D. (1989). Purification, composition, and activity of two bactenecins, antibacterial peptides of bovine neutrophils. *Infection and Immunity* *57*, 3142.

Ghosal, A., Vitali, A., Stach, J.E.M., and Nielsen, P.E. (2013). Role of SbmA in the Uptake of Peptide Nucleic Acid (PNA)-Peptide Conjugates in *E. coli*. *ACS Chemical Biology* *8*, 360-367.

Goldstein, J.L., and Caskey, C.T. (1970). Peptide Chain Termination: Effect of Protein S on Ribosomal Binding of Release Factors. *Proceedings of the National Academy of Sciences* *67*, 537.

Gong, F., and Yanofsky, C. (2002). Instruction of Translating Ribosome by Nascent Peptide. *Science* *297*, 1864.

Goodman, D.B., Church, G.M., and Kosuri, S. (2013). Causes and effects of N-terminal codon bias in bacterial genes. *Science* *342*, 475-479.

Goralski, T.D.P., Kirimanjeswara, G.S., and Keiler, K.C. (2018). A New Mechanism for Ribosome Rescue Can Recruit RF1 or RF2 to Nonstop Ribosomes. *MBio* 9.

Gottesman, S., Roche, E., Zhou, Y., and Sauer, R.T. (1998). The ClpXP and ClpAP proteases degrade proteins with carboxy-terminal peptide tails added by the SsrA-tagging system. *Genes & Development* 12, 1338-1347.

Goyal, A., Belardinelli, R., Maracci, C., Milon, P., and Rodnina, M.V. (2015). Directional transition from initiation to elongation in bacterial translation. *Nucleic Acids Res* 43, 10700-10712.

Graf, M., Huter, P., Maracci, C., Peterek, M., Rodnina, M.V., and Wilson, D.N. (2018). Visualization of translation termination intermediates trapped by the Apidaecin 137 peptide during RF3-mediated recycling of RF1. *Nat Commun* 9, 3053.

Graf, M., Mardirossian, M., Nguyen, F., Seefeldt, A.C., Guichard, G., Scocchi, M., Innis, C.A., and Wilson, D.N. (2017). Proline-rich antimicrobial peptides targeting protein synthesis. *Nat Prod Rep* 34, 702-711.

Graf, M., and Wilson, D.N. (2019). Intracellular Antimicrobial Peptides Targeting the Protein Synthesis Machinery. In *Adv Exp Med Biol*, pp. 73-89.

Graille, M., Figaro, S., Kervestin, S., Buckingham, R.H., Liger, D., and Heurgue-Hamard, V. (2012). Methylation of class I translation termination factors: structural and functional aspects. *Biochimie* 94, 1533-1543.

Grajevskaja, R.A., Ivanov, Y.V., and Saminsky, E.M. (1982). 70-S Ribosomes of *Escherichia coli* Have an Additional Site for Deacylated tRNA Binding. *European Journal of Biochemistry* 128, 47-52.

Greber, B.J., Boehringer, D., Leibundgut, M., Bieri, P., Leitner, A., Schmitz, N., Aebersold, R., and Ban, N. (2014a). The complete structure of the large subunit of the mammalian mitochondrial ribosome. *Nature* 515, 283-286.

Greber, B.J., Boehringer, D., Leitner, A., Bieri, P., Voigts-Hoffmann, F., Erzberger, J.P., Leibundgut, M., Aebersold, R., and Ban, N. (2014b). Architecture of the large subunit of the mammalian mitochondrial ribosome. *Nature* 505, 515-519.

Gromadski, K.B., and Rodnina, M.V. (2004). Kinetic determinants of high-fidelity tRNA discrimination on the ribosome. *Mol Cell* 13, 191-200.

Gualerzi, C., Risuleo, G., and Pon, C.L. (1977). Initial rate kinetic analysis of the mechanism of initiation complex formation and the role of initiation factor IF-3. *Biochemistry* 16, 1684-1689.

Gualerzi, C.O., and Pon, C.L. (1990). Initiation of mRNA translation in prokaryotes. *Biochemistry* 29, 5881-5889.

Guida, F., Benincasa, M., Zahariev, S., Scocchi, M., Berti, F., Gennaro, R., and Tossi, A. (2015). Effect of Size and N-Terminal Residue Characteristics on Bacterial Cell Penetration and Antibacterial Activity of the Proline-Rich Peptide Bac7. *Journal of Medicinal Chemistry* 58, 1195-1204.

Gutell, R.R., Gray, M.W., and Schnare, M.N. (1993). A compilation of large subunit (23S and 23S-like) ribosomal RNA structures: 1993. *Nucleic Acids Research* 21, 3055-3074.

Guthrie, C., and Nomura, M. (1968). Initiation of protein synthesis: a critical test of the 30S subunit model. *Nature* 219, 232-235.

Gutmann, S., Haebel, P.W., Metzinger, L., Sutter, M., Felden, B., and Ban, N. (2003). Crystal structure of the transfer-RNA domain of transfer-messenger RNA in complex with SmpB. *Nature* 424, 699-703.

Handa, Y., Hikawa, Y., Tochio, N., Kogure, H., Inoue, M., Koshiba, S., Güntert, P., Inoue, Y., Kigawa, T., Yokoyama, S., *et al.* (2010). Solution Structure of the Catalytic Domain of the Mitochondrial Protein ICT1 That Is Essential for Cell Vitality. *Journal of Molecular Biology* 404, 260-273.

Handa, Y., Inaho, N., and Nameki, N. (2011). YaeJ is a novel ribosome-associated protein in *Escherichia coli* that can hydrolyze peptidyl-tRNA on stalled ribosomes. *Nucleic Acids Res* *39*, 1739-1748.

Hanes, J., and Pluckthun, A. (1997). In vitro selection and evolution of functional proteins by using ribosome display. *Proc Natl Acad Sci U S A* *94*, 4937-4942.

Hansen, J.L., Schmeing, T.M., Moore, P.B., and Steitz, T.A. (2002). Structural insights into peptide bond formation. *Proc Natl Acad Sci U S A* *99*, 11670-11675.

Hartz, D., Binkley, J., Hollingsworth, T., and Gold, L. (1990). Domains of initiator tRNA and initiation codon crucial for initiator tRNA selection by *Escherichia coli* IF3. *Genes & Development* *4*, 1790-1800.

Hauryliuk, V., Zavialov, A., Kisseelev, L., and Ehrenberg, M. (2006). Class-1 release factor eRF1 promotes GTP binding by class-2 release factor eRF3. *Biochimie* *88*, 747-757.

Hayes, C.S., and Sauer, R.T. (2003). Cleavage of the A Site mRNA Codon during Ribosome Pausing Provides a Mechanism for Translational Quality Control. *Molecular Cell* *12*, 903-911.

Helgstrand, M., Mandava, C.S., Mulder, F.A., Liljas, A., Sanyal, S., and Akke, M. (2007). The ribosomal stalk binds to translation factors IF2, EF-Tu, EF-G and RF3 via a conserved region of the L12 C-terminal domain. *J Mol Biol* *365*, 468-479.

Hiller, D.A., Singh, V., Zhong, M., and Strobel, S.A. (2011). A two-step chemical mechanism for ribosome-catalysed peptide bond formation. *Nature* *476*, 236-239.

Himeno, H., Nameki, N., Kurita, D., Muto, A., and Abo, T. (2015). Ribosome rescue systems in bacteria. *Biochimie* *114*, 102-112.

Hirashima, A., and Kaji, A. (1970). Factor dependent breakdown of polysomes. *Biochem Biophys Res Commun* *41*, 877-883.

Hirashima, A., and Kaji, A. (1972). Factor-dependent release of ribosomes from messenger RNA. Requirement for two heat-stable factors. *J Mol Biol* *65*, 43-58.

Hirashima, A., and Kaji, A. (1973). Role of elongation factor G and a protein factor on the release of ribosomes from messenger ribonucleic acid. *J Biol Chem* *248*, 7580-7587.

Hirokawa, G.O., Nijman, R.M., Raj, V.S., Kaji, H., Igarashi, K., and Kaji, A. (2005). The role of ribosome recycling factor in dissociation of 70S ribosomes into subunits. *RNA* *11*, 1317-1328.

Hockenberry, A.J., Pah, A.R., Jewett, M.C., and Amaral, L.A. (2017). Leveraging genome-wide datasets to quantify the functional role of the anti-Shine-Dalgarno sequence in regulating translation efficiency. *Open Biol* *7*.

Holdsworth, S.R., and Law, C.J. (2012). Functional and biochemical characterisation of the *Escherichia coli* major facilitator superfamily multidrug transporter MdtM. *Biochimie* *94*, 1334-1346.

Holtkamp, W., Wintermeyer, W., and Rodnina, M.V. (2014). Synchronous tRNA movements during translocation on the ribosome are orchestrated by elongation factor G and GTP hydrolysis. *BioEssays* *36*, 908-918.

Horan, L.H., and Noller, H.F. (2007). Intersubunit movement is required for ribosomal translocation. *Proceedings of the National Academy of Sciences* *104*, 4881.

Huang, C., Wolfgang, M.C., Withey, J., Koomey, M., and Friedman, D.I. (2000). Charged tmRNA but not tmRNA-mediated proteolysis is essential for *Neisseria gonorrhoeae* viability. *EMBO J* *19*, 1098-1107.

Hudson, C.M., Lau, B.Y., and Williams, K.P. (2014). Ends of the line for tmRNA-SmpB. *Front Microbiol* *5*, 421.

Hussain, T., Llacer, J.L., Wimberly, B.T., Kieft, J.S., and Ramakrishnan, V. (2016). Large-Scale Movements of IF3 and tRNA during Bacterial Translation Initiation. *Cell* *167*, 133-144 e113.

Huter, P., Arenz, S., Bock, L.V., Graf, M., Frister, J.O., Heuer, A., Peil, L., Starosta, A.L., Wohlgemuth, I., Peske, F., *et al.* (2017a). Structural Basis for Polyproline-Mediated Ribosome Stalling and Rescue by the Translation Elongation Factor EF-P. *Mol Cell* *68*, 515-527 e516.

Huter, P., Muller, C., Arenz, S., Beckert, B., and Wilson, D.N. (2017b). Structural Basis for Ribosome Rescue in Bacteria. *Trends Biochem Sci* *42*, 669-680.

Huter, P., Muller, C., Beckert, B., Arenz, S., Berninghausen, O., Beckmann, R., and Wilson, D.N. (2017c). Structural basis for ArfA-RF2-mediated translation termination on mRNAs lacking stop codons. *Nature* *541*, 546-549.

Huttner, K.M., Lambeth, M.R., Burkin, H.R., Burkin, D.J., and Broad, T.E. (1998). Localization and genomic organization of sheep antimicrobial peptide genes. *Gene* *206*, 85-91.

Ieong, K.-W., Uzun, Ü., Selmer, M., and Ehrenberg, M. (2016). Two proofreading steps amplify the accuracy of genetic code translation. *Proceedings of the National Academy of Sciences* *113*, 13744.

Ito, K., Chadani, Y., Nakamori, K., Chiba, S., Akiyama, Y., and Abo, T. (2011). Nascentome analysis uncovers futile protein synthesis in *Escherichia coli*. *PLoS One* *6*, e28413.

Ito, K., and Chiba, S. (2013). Arrest Peptides: Cis-Acting Modulators of Translation. *Annual Review of Biochemistry* *82*, 171-202.

Ito, K., Fujiwara, T., Toyoda, T., and Nakamura, Y. (2002). Elongation Factor G Participates in Ribosome Disassembly by Interacting with Ribosome Recycling Factor at Their tRNA-Mimicry Domains. *Molecular Cell* *9*, 1263-1272.

Ito, K., Uno, M., and Nakamura, Y. (1998). Single amino acid substitution in prokaryote polypeptide release factor 2 permits it to terminate translation at all three stop codons. *Proc Natl Acad Sci U S A* *95*, 8165-8169.

Ito, K., Uno, M., and Nakamura, Y. (2000). A tripeptide 'anticodon' deciphers stop codons in messenger RNA. *Nature* *403*, 680-684.

Ivanova, N., Pavlov, M.Y., Felden, B., and Ehrenberg, M. (2004). Ribosome rescue by tmRNA requires truncated mRNAs. *J Mol Biol* *338*, 33-41.

Jacob, Y., Sharkady, S.M., Bhardwaj, K., Sanda, A., and Williams, K.P. (2005). Function of the SmpB Tail in Transfer-messenger RNA Translation Revealed by a Nucleus-encoded Form. *Journal of Biological Chemistry* *280*, 5503-5509.

James, N.R., Brown, A., Gordiyenko, Y., and Ramakrishnan, V. (2016). Translational termination without a stop codon. *Science* *354*, 1437-1440.

Janosi, L., Shimizu, I., and Kaji, A. (1994). Ribosome recycling factor (ribosome releasing factor) is essential for bacterial growth. *Proceedings of the National Academy of Sciences* *91*, 4249.

Jenner, L.B., Demeshkina, N., Yusupova, G., and Yusupov, M. (2010). Structural aspects of messenger RNA reading frame maintenance by the ribosome. *Nature Structural & Molecular Biology* *17*, 555-560.

Jin, H., Kelley, A.C., Loakes, D., and Ramakrishnan, V. (2010). Structure of the 70S ribosome bound to release factor 2 and a substrate analog provides insights into catalysis of peptide release. *Proceedings of the National Academy of Sciences* *107*, 8593.

Joazeiro, C.A.P. (2019). Mechanisms and functions of ribosome-associated protein quality control. *Nature Reviews Molecular Cell Biology* *20*, 368-383.

Julian, P., Konevega, A.L., Scheres, S.H., Lazaro, M., Gil, D., Wintermeyer, W., Rodnina, M.V., and Valle, M. (2008). Structure of ratcheted ribosomes with tRNAs in hybrid states. *Proc Natl Acad Sci U S A* *105*, 16924-16927.

Julian, P., Milon, P., Agirrezabala, X., Lasso, G., Gil, D., Rodnina, M.V., and Valle, M. (2011). The Cryo-EM structure of a complete 30S translation initiation complex from *Escherichia coli*. *PLoS Biol* 9, e1001095.

Kaempfer, R. (1968). Ribosomal subunit exchange during protein synthesis. *Proc Natl Acad Sci U S A* 61, 106-113.

Kaempfer, R., and Meselson, M. (1969). Studies of ribosomal subunit exchange. *Cold Spring Harb Symp Quant Biol* 34, 209-220.

Kaempfer, R.O.R., Meselson, M., and Raskas, H.J. (1968). Cyclic dissociation into stable subunits and re-formation of ribosomes during bacterial growth. *Journal of Molecular Biology* 31, 277-289.

Kaledhonkar, S., Fu, Z., Caban, K., Li, W., Chen, B., Sun, M., Gonzalez, R.L., and Frank, J. (2019). Late steps in bacterial translation initiation visualized using time-resolved cryo-EM. *Nature* 570, 400-404.

Karaki, S., Paris, C., and Rocchi, P. (2019). Antisense Oligonucleotides, A Novel Developing Targeting Therapy. In *Antisense Therapy*, S. Sharad, ed. (IntechOpen).

Karimi, R., Pavlov, M.Y., Buckingham, R.H., and Ehrenberg, M. (1999). Novel roles for classical factors at the interface between translation termination and initiation. *Mol Cell* 3, 601-609.

Karzai, A.W., Susskind, M.M., and Sauer, R.T. (1999). SmpB, a unique RNA-binding protein essential for the peptide-tagging activity of SsrA (tmRNA). *EMBO J* 18, 3793-3799.

Kaziro, Y. (1978). The role of guanosine 5'-triphosphate in polypeptide chain elongation. *Biochim Biophys Acta* 505, 95-127.

Keiler, K.C. (2015). Mechanisms of ribosome rescue in bacteria. *Nat Rev Microbiol* 13, 285-297.

Keiler, K.C., and Feaga, H.A. (2014). Resolving nonstop translation complexes is a matter of life or death. *J Bacteriol* 196, 2123-2130.

Keiler, K.C., and Shapiro, L. (2003). tmRNA Is Required for Correct Timing of DNA Replication in <em>Caulobacter crescentus</em>. *Journal of Bacteriology* 185, 573.

Keiler, K.C., Shapiro, L., and Williams, K.P. (2000). tmRNAs that encode proteolysis-inducing tags are found in all known bacterial genomes: A two-piece tmRNA functions in *Caulobacter*. *Proc Natl Acad Sci U S A* 97, 7778-7783.

Keiler, K.C., Waller, P.R., and Sauer, R.T. (1996). Role of a peptide tagging system in degradation of proteins synthesized from damaged messenger RNA. *Science* 271, 990-993.

Khade, P.K., and Joseph, S. (2011). Messenger RNA interactions in the decoding center control the rate of translocation. *Nature Structural & Molecular Biology* 18, 1300-1302.

Kihira, K., Shimizu, Y., Shomura, Y., Shibata, N., Kitamura, M., Nakagawa, A., Ueda, T., Ochi, K., and Higuchi, Y. (2012). Crystal structure analysis of the translation factor RF3 (release factor 3). *FEBS Letters* 586, 3705-3709.

Kim, K.K., Min, K., and Suh, S.W. (2000). Crystal structure of the ribosome recycling factor from *Escherichia coli*. *EMBO J* 19, 2362-2370.

Kingery, D.A., Pfund, E., Voorhees, R.M., Okuda, K., Wohlgemuth, I., Kitchen, D.E., Rodnina, M.V., and Strobel, S.A. (2008). An Uncharged Amine in the Transition State of the Ribosomal Peptidyl Transfer Reaction. *Chemistry & Biology* 15, 493-500.

Klaholz, B.P., Myasnikov, A.G., and Van Heel, M. (2004). Visualization of release factor 3 on the ribosome during termination of protein synthesis. *Nature* 427, 862-865.

Klaholz, B.P., Pape, T., Zavialov, A.V., Myasnikov, A.G., Orlova, E.V., Vestergaard, B., Ehrenberg, M., and van Heel, M. (2003). Structure of the *Escherichia coli* ribosomal termination complex with release factor 2. *Nature* 421, 90-94.

Knappe, D., Adermann, K., and Hoffmann, R. (2015). Oncocin Onc72 is efficacious against antibiotic-susceptible *Klebsiella pneumoniae* ATCC 43816 in a murine thigh infection model. *Peptide Science* 104, 707-711.

Knappe, D., Piantavigna, S., Hansen, A., Mechler, A., Binas, A., Nolte, O., Martin, L.L., and Hoffmann, R. (2010). Oncocin (VDKPPYLPRLPRPRPRRIYNR-NH2): A Novel Antibacterial Peptide Optimized against Gram-Negative Human Pathogens. *Journal of Medicinal Chemistry* 53, 5240-5247.

Knappe, D., Schmidt, R., Adermann, K., and Hoffmann, R. (2019). Continuous Subcutaneous Delivery of Proline-Rich Antimicrobial Peptide Api137 Provides Superior Efficacy to Intravenous Administration in a Mouse Infection Model. *Frontiers in Microbiology* 10, 2283.

Knappe, D., Zahn, M., Sauer, U., Schiffer, G., Sträter, N., and Hoffmann, R. (2011). Rational Design of Oncocin Derivatives with Superior Protease Stabilities and Antibacterial Activities Based on the High-Resolution Structure of the Oncocin-DnaK Complex. *ChemBioChem* 12, 874-876.

Koc, E., Cimen, H., Kumcuoglu, B., Abu, N., Akpinar, G., Haque, M., Spremulli, L., and Koc, H. (2013). Identification and characterization of CHCHD1, AURKAIP1, and CRIF1 as new members of the mammalian mitochondrial ribosome. *Frontiers in Physiology* 4, 183.

Koc, E.C., and Spremulli, L.L. (2002). Identification of mammalian mitochondrial translational initiation factor 3 and examination of its role in initiation complex formation with natural mRNAs. *J Biol Chem* 277, 35541-35549.

Kogure, H., Handa, Y., Nagata, M., Kanai, N., Guntert, P., Kubota, K., and Nameki, N. (2014). Identification of residues required for stalled-ribosome rescue in the codon-independent release factor YaeJ. *Nucleic Acids Res* 42, 3152-3163.

Kolano, L., Knappe, D., Volke, D., Sträter, N., and Hoffmann, R. (2020). Ribosomal target-binding sites of antimicrobial peptides Api137 and Onc112 are conserved among pathogens providing new lead structures to develop novel broad-spectrum antibiotics. *ChemBioChem* n/a.

Komine, Y., Kitabatake, M., Yokogawa, T., Nishikawa, K., and Inokuchi, H. (1994). A tRNA-like structure is present in 10Sa RNA, a small stable RNA from *Escherichia coli*. *Proceedings of the National Academy of Sciences* 91, 9223.

Konecki, D.S., Aune, K.C., Tate, W., and Caskey, C.T. (1977). Characterization of reticulocyte release factor. *Journal of Biological Chemistry* 252, 4514-4520.

Konno, T., Kurita, D., Takada, K., Muto, A., and Himeno, H. (2007). A functional interaction of SmpB with tmRNA for determination of the resuming point of trans-translation. *RNA* 13, 1723-1731.

Korostelev, A., Asahara, H., Lancaster, L., Laurberg, M., Hirschi, A., Zhu, J., Trakhanov, S., Scott, W.G., and Noller, H.F. (2008). Crystal structure of a translation termination complex formed with release factor RF2. *Proc Natl Acad Sci U S A* 105, 19684-19689.

Korostelev, A., Zhu, J., Asahara, H., and Noller, H.F. (2010). Recognition of the amber UAG stop codon by release factor RF1. *EMBO J* 29, 2577-2585.

Korostelev, A.A. (2011). Structural aspects of translation termination on the ribosome. *RNA* 17, 1409-1421.

Kothe, U., and Rodnina, M.V. (2006). Delayed Release of Inorganic Phosphate from Elongation Factor Tu Following GTP Hydrolysis on the Ribosome. *Biochemistry* 45, 12767-12774.

Kothe, U., Wieden, H.J., Mohr, D., and Rodnina, M.V. (2004). Interaction of helix D of elongation factor Tu with helices 4 and 5 of protein L7/12 on the ribosome. *J Mol Biol* 336, 1011-1021.

Koutmou, K.S., McDonald, M.E., Brunelle, J.L., and Green, R. (2014). RF3:GTP promotes rapid dissociation of the class 1 termination factor. *RNA* 20, 609-620.

Krizsan, A., Knappe, D., and Hoffmann, R. (2015). Influence of the yjiL-mdtM Gene Cluster on the Antibacterial Activity of Proline-Rich Antimicrobial Peptides Overcoming *Escherichia coli* Resistance Induced by the Missing SbmA Transporter System. *Antimicrob Agents Chemother* 59, 5992-5998.

Krizsan, A., Volke, D., Weinert, S., Sträter, N., Knappe, D., and Hoffmann, R. (2014). Insect-Derived Proline-Rich Antimicrobial Peptides Kill Bacteria by Inhibiting Bacterial Protein Translation at the 70 S Ribosome. *Angewandte Chemie International Edition* 53, 12236-12239.

Kudla, G., Murray, A.W., Tollervey, D., and Plotkin, J.B. (2009). Coding-sequence determinants of gene expression in *Escherichia coli*. *Science* 324, 255-258.

Kuhlenkoetter, S., Wintermeyer, W., and Rodnina, M.V. (2011). Different substrate-dependent transition states in the active site of the ribosome. *Nature* 476, 351-354.

Kurita, D., Chadani, Y., Muto, A., Abo, T., and Himeno, H. (2014a). ArfA recognizes the lack of mRNA in the mRNA channel after RF2 binding for ribosome rescue. *Nucleic Acids Res* 42, 13339-13352.

Kurita, D., Miller, M.R., Muto, A., Buskirk, A.R., and Himeno, H. (2014b). Rejection of tmRNA.SmpB after GTP hydrolysis by EF-Tu on ribosomes stalled on intact mRNA. *RNA* 20, 1706-1714.

Kurita, D., Muto, A., and Himeno, H. (2010). Role of the C-terminal tail of SmpB in the early stage of trans-translation. *RNA* 16, 980-990.

La Teana, A., Gualerzi, C.O., and Brimacombe, R. (1995). From stand-by to decoding site. Adjustment of the mRNA on the 30S ribosomal subunit under the influence of the initiation factors. *RNA* (New York, NY) 1, 772-782.

Lancaster, L., Kiel, M.C., Kaji, A., and Noller, H.F. (2002). Orientation of ribosome recycling factor in the ribosome from directed hydroxyl radical probing. *Cell* 111, 129-140.

Lang, K., Erlacher, M., Wilson, D.N., Micura, R., and Polacek, N. (2008). The Role of 23S Ribosomal RNA Residue A2451 in Peptide Bond Synthesis Revealed by Atomic Mutagenesis. *Chemistry & Biology* 15, 485-492.

Laurberg, M., Asahara, H., Korostelev, A., Zhu, J., Trakhanov, S., and Noller, H.F. (2008). Structural basis for translation termination on the 70S ribosome. *Nature* 454, 852-857.

Laursen, B.S., Sorensen, H.P., Mortensen, K.K., and Sperling-Petersen, H.U. (2005). Initiation of protein synthesis in bacteria. *Microbiol Mol Biol Rev* 69, 101-123.

Lee, C.P., Dyson, M.R., Mandal, N., Varshney, U., Bahramian, B., and RajBhandary, U.L. (1992). Striking effects of coupling mutations in the acceptor stem on recognition of tRNAs by *Escherichia coli* Met-tRNA synthetase and Met-tRNA transformylase. *Proceedings of the National Academy of Sciences* 89, 9262.

Lee, C.P., Seong, B.L., and RajBhandary, U.L. (1991). Structural and sequence elements important for recognition of *Escherichia coli* formylmethionine tRNA by methionyl-tRNA transformylase are clustered in the acceptor stem. *Journal of Biological Chemistry* 266, 18012-18017.

Lee, S., Ishii, M., Tadaki, T., Muto, A., and Himeno, H. (2001). Determinants on tmRNA for initiating efficient and precise trans-translation: Some mutations upstream of the tag-encoding sequence of *Escherichia coli* tmRNA shift the initiation point of trans-translation in vitro. *RNA* 7, 999-1012.

Leipe, D.D., Wolf, Y.I., Koonin, E.V., and Aravind, L. (2002). Classification and evolution of P-loop GTPases and related ATPases11Edited by J. Thornton. *Journal of Molecular Biology* 317, 41-72.

Li, J., Ji, L., Shi, W., Xie, J., and Zhang, Y. (2013). Trans-translation mediates tolerance to multiple antibiotics and stresses in *Escherichia coli*. *Journal of Antimicrobial Chemotherapy* *68*, 2477-2481.

Li, X., Yokota, T., Ito, K., Nakamura, Y., and Aiba, H. (2007). Reduced action of polypeptide release factors induces mRNA cleavage and tmRNA tagging at stop codons in *Escherichia coli*. *Molecular Microbiology* *63*, 116-126.

Li, X.I.A., Hirano, R., Tagami, H., and Aiba, H. (2006). Protein tagging at rare codons is caused by tmRNA action at the 3' end of nonstop mRNA generated in response to ribosome stalling. *RNA* *12*, 248-255.

Lin, J., Gagnon, Matthieu G., Bulkley, D., and Steitz, Thomas A. (2015). Conformational Changes of Elongation Factor G on the Ribosome during tRNA Translocation. *Cell* *160*, 219-227.

Liu, G., Song, G., Zhang, D., Zhang, D., Li, Z., Lyu, Z., Dong, J., Achenbach, J., Gong, W., Zhao, X.S., *et al.* (2014a). EF-G catalyzes tRNA translocation by disrupting interactions between decoding center and codon–anticodon duplex. *Nature Structural & Molecular Biology* *21*, 817-824.

Liu, P., Chen, Y., Wang, D., Tang, Y., Tang, H., Song, H., Sun, Q., Zhang, Y., and Liu, Z. (2016). Genetic Selection of Peptide Aptamers That Interact and Inhibit Both Small Protein B and Alternative Ribosome-Rescue Factor A of *Aeromonas veronii* C4. *Front Microbiol* *7*, 1228.

Liu, T., Kaplan, A., Alexander, L., Yan, S., Wen, J.-D., Lancaster, L., Wickersham, C.E., Fredrick, K., Noller, H., Tinoco, I., Jr., *et al.* (2014b). Direct measurement of the mechanical work during translocation by the ribosome. *eLife* *3*, e03406.

Loveland, A.B., Demo, G., Grigorieff, N., and Korostelev, A.A. (2017). Ensemble cryo-EM elucidates the mechanism of translation fidelity. *Nature* *546*, 113-117.

Lytvynenko, I., Paternoga, H., Thrun, A., Balke, A., Muller, T.A., Chiang, C.H., Nagler, K., Tsaprailis, G., Anders, S., Bischofs, I., *et al.* (2019). Alanine Tails Signal Proteolysis in Bacterial Ribosome-Associated Quality Control. *Cell* *178*, 76-90 e22.

Ma, C., Kurita, D., Li, N., Chen, Y., Himeno, H., and Gao, N. (2017). Mechanistic insights into the alternative translation termination by ArfA and RF2. *Nature* *541*, 550-553.

Macé, K., Giudice, E., Chat, S., and Gillet, R. (2018). The structure of an elongation factor G-ribosome complex captured in the absence of inhibitors. *Nucleic Acids Research* *46*, 3211-3217.

Maden, B.E.H., and Monro, R.E. (1968). Ribosome-Catalyzed Peptidyl Transfer. *European Journal of Biochemistry* *6*, 309-316.

Maguire, B.A., Beniaminov, A.D., Ramu, H., Mankin, A.S., and Zimmermann, R.A. (2005). A protein component at the heart of an RNA machine: the importance of protein l27 for the function of the bacterial ribosome. *Mol Cell* *20*, 427-435.

Mangiarotti, G., and Schlessinger, D. (1967). Polyribosome metabolism in *Escherichia coli*: II. Formation and lifetime of messenger RNA molecules, ribosomal subunit couples and polyribosomes. *Journal of Molecular Biology* *29*, 395-418.

Manickam, N., Nag, N., Abbasi, A., Patel, K., and Farabaugh, P.J. (2014). Studies of translational misreading in vivo show that the ribosome very efficiently discriminates against most potential errors. *RNA* *20*, 9-15.

Maracci, C., Peske, F., Dannies, E., Pohl, C., and Rodnina, M.V. (2014). Ribosome-induced tuning of GTP hydrolysis by a translational GTPase. *Proceedings of the National Academy of Sciences* *111*, 14418.

Maracci, C., and Rodnina, M.V. (2016). Review: Translational GTPases. *Biopolymers* *105*, 463-475.

Maracci, C., Wohlgemuth, I., and Rodnina, M.V. (2015). Activities of the peptidyl transferase center of ribosomes lacking protein L27. *RNA* *21*, 2047-2052.

Mardirossian, M., Barriere, Q., Timchenko, T., Muller, C., Pacor, S., Mergaert, P., Scocchi, M., and Wilson, D.N. (2018a). Fragments of the Nonlytic Proline-Rich Antimicrobial Peptide Bac5 Kill *Escherichia coli* Cells by Inhibiting Protein Synthesis. *Antimicrob Agents Chemother* *62*, e00534-00518.

Mardirossian, M., Pérébaskine, N., Benincasa, M., Gambato, S., Hofmann, S., Huter, P., Müller, C., Hilpert, K., Innis, C.A., Tossi, A., *et al.* (2018b). The Dolphin Proline-Rich Antimicrobial Peptide Tur1A Inhibits Protein Synthesis by Targeting the Bacterial Ribosome. *Cell Chemical Biology* *25*, 530-539.e537.

Mardirossian, M., Sola, R., Degasperi, M., and Scocchi, M. (2019). Search for Shorter Portions of the Proline-Rich Antimicrobial Peptide Fragment Bac5(1-25) That Retain Antimicrobial Activity by Blocking Protein Synthesis. *ChemMedChem* *14*, 343-348.

Marshall, R.A., Aitken, C.E., and Puglisi, J.D. (2009). GTP hydrolysis by IF2 guides progression of the ribosome into elongation. *Mol Cell* *35*, 37-47.

Martemyanov, K.A., Yarunin, A.S., Liljas, A., and Gudkov, A.T. (1998). An intact conformation at the tip of elongation factor G domain IV is functionally important. *FEBS Letters* *434*, 205-208.

Matsuo, Y., Tesina, P., Nakajima, S., Mizuno, M., Endo, A., Buschauer, R., Cheng, J., Shounai, O., Ikeuchi, K., Saeki, Y., *et al.* (2020). RQT complex dissociates ribosomes collided on endogenous RQC substrate SDD1. *Nature Structural & Molecular Biology* *27*, 323-332.

Mattiuzzo, M., Bandiera, A., Gennaro, R., Benincasa, M., Pacor, S., Antcheva, N., and Scocchi, M. (2007). Role of the *Escherichia coli* SbmA in the antimicrobial activity of proline-rich peptides. *Molecular Microbiology* *66*, 151-163.

Mehta, P., Richards, J., and Karzai, A.W. (2006). tmRNA determinants required for facilitating nonstop mRNA decay. *RNA* *12*, 2187-2198.

Miller, M.R., and Buskirk, A.R. (2014). An unusual mechanism for EF-Tu activation during tmRNA-mediated ribosome rescue. *RNA* *20*, 228-235.

Miller, M.R., Liu, Z., Cazier, D.J., Gebhard, G.M., Herron, S.R., Zaher, H.S., Green, R., and Buskirk, A.R. (2011). The role of SmpB and the ribosomal decoding center in licensing tmRNA entry into stalled ribosomes. *RNA* *17*, 1727-1736.

Milon, P., Carotti, M., Konevega, A.L., Wintermeyer, W., Rodnina, M.V., and Gualerzi, C.O. (2010). The ribosome-bound initiation factor 2 recruits initiator tRNA to the 30S initiation complex. *EMBO Rep* *11*, 312-316.

Milon, P., Konevega, A.L., Gualerzi, C.O., and Rodnina, M.V. (2008). Kinetic checkpoint at a late step in translation initiation. *Mol Cell* *30*, 712-720.

Milon, P., Maracci, C., Filonava, L., Gualerzi, C.O., and Rodnina, M.V. (2012). Real-time assembly landscape of bacterial 30S translation initiation complex. *Nat Struct Mol Biol* *19*, 609-615.

Milón, P., and Rodnina, M.V. (2012). Kinetic control of translation initiation in bacteria. *Critical Reviews in Biochemistry and Molecular Biology* *47*, 334-348.

Mitkevich, V.A., Kononenko, A.V., Petrushanko, I.Y., Yanvarev, D.V., Makarov, A.A., and Kisselov, L.L. (2006). Termination of translation in eukaryotes is mediated by the quaternary eRF1•eRF3•GTP•Mg<sup>2+</sup> complex. The biological roles of eRF3 and prokaryotic RF3 are profoundly distinct. *Nucleic Acids Research* *34*, 3947-3954.

Moazed, D., and Noller, H.F. (1989). Intermediate states in the movement of transfer RNA in the ribosome. *Nature* *342*, 142-148.

Moazed, D., Robertson, J.M., and Noller, H.F. (1988). Interaction of elongation factors EF-G and EF-Tu with a conserved loop in 23S RNA. *Nature* *334*, 362-364.

Mohr, D., Wintermeyer, W., and Rodnina, M.V. (2002). GTPase Activation of Elongation Factors Tu and G on the Ribosome. *Biochemistry* 41, 12520-12528.

Monro, R.E. (1967). Catalysis of peptide bond formation by 50 s ribosomal subunits from *Escherichia coli*. *Journal of Molecular Biology* 26, 147-151.

Moore, S.D., and Sauer, R.T. (2005). Ribosome rescue: tmRNA tagging activity and capacity in *Escherichia coli*. *Mol Microbiol* 58, 456-466.

Mora, L., Heurgue-Hamard, V., Champ, S., Ehrenberg, M., Kisseelev, L.L., and Buckingham, R.H. (2003). The essential role of the invariant GGQ motif in the function and stability in vivo of bacterial release factors RF1 and RF2. *Mol Microbiol* 47, 267-275.

Mora, L., Heurgue-Hamard, V., de Zamaroczy, M., Kervestin, S., and Buckingham, R.H. (2007). Methylation of bacterial release factors RF1 and RF2 is required for normal translation termination in vivo. *J Biol Chem* 282, 35638-35645.

Morse, J.C., Girodat, D., Burnett, B.J., Holm, M., Altman, R.B., Sanbonmatsu, K.Y., Wieden, H.-J., and Blanchard, S.C. (2020). Elongation factor-Tu can repetitively engage aminoacyl-tRNA within the ribosome during the proofreading stage of tRNA selection. *Proceedings of the National Academy of Sciences*, 201904469.

Mortensen, K.K., Kildsgaard, J., Moreno, J.M., Steffensen, S.A., Egebjerg, J., and Sperling-Petersen, H.U. (1998). A six-domain structural model for *Escherichia coli* translation initiation factor IF2. Characterisation of twelve surface epitopes. *Biochem Mol Biol Int* 46, 1027-1041.

Munro, J.B., Wasserman, M.R., Altman, R.B., Wang, L., and Blanchard, S.C. (2010). Correlated conformational events in EF-G and the ribosome regulate translocation. *Nat Struct Mol Biol* 17, 1470-1477.

Mustafi, M., and Weisshaar, J.C. (2018). Simultaneous Binding of Multiple EF-Tu Copies to Translating Ribosomes in Live *Escherichia coli*. *mBio* 9, e02143-02117.

Mustoe, A.M., Busan, S., Rice, G.M., Hajdin, C.E., Peterson, B.K., Ruda, V.M., Kubica, N., Nutiu, R., Baryza, J.L., and Weeks, K.M. (2018). Pervasive Regulatory Functions of mRNA Structure Revealed by High-Resolution SHAPE Probing. *Cell* 173, 181-195.e118.

Myasnikov, A.G., Marzi, S., Simonetti, A., Giuliodori, A.M., Gualerzi, C.O., Yusupova, G., Yusupov, M., and Klaholz, B.P. (2005). Conformational transition of initiation factor 2 from the GTP- to GDP-bound state visualized on the ribosome. *Nat Struct Mol Biol* 12, 1145-1149.

Nakagawa, S., Niimura, Y., and Gojobori, T. (2017). Comparative genomic analysis of translation initiation mechanisms for genes lacking the Shine-Dalgarno sequence in prokaryotes. *Nucleic Acids Res* 45, 3922-3931.

Nakagawa, S., Niimura, Y., Miura, K., and Gojobori, T. (2010). Dynamic evolution of translation initiation mechanisms in prokaryotes. *Proc Natl Acad Sci U S A* 107, 6382-6387.

Nakano, H., Yoshida, T., Uchiyama, S., Kawachi, M., Matsuo, H., Kato, T., Ohshima, A., Yamaichi, Y., Honda, T., Kato, H., *et al.* (2003). Structure and Binding Mode of a Ribosome Recycling Factor (RRF) from Mesophilic Bacterium. *Journal of Biological Chemistry* 278, 3427-3436.

Netzer, W.J., and Hartl, F.U. (1997). Recombination of protein domains facilitated by cotranslational folding in eukaryotes. *Nature* 388, 343-349.

Neubauer, C., Gao, Y.-G., Andersen, K.R., Dunham, C.M., Kelley, A.C., Hentschel, J., Gerdes, K., Ramakrishnan, V., and Brodersen, D.E. (2009). The Structural Basis for mRNA Recognition and Cleavage by the Ribosome-Dependent Endonuclease RelE. *Cell* 139, 1084-1095.

Neubauer, C., Gillet, R., Kelley, A.C., and Ramakrishnan, V. (2012). Decoding in the Absence of a Codon by tmRNA and SmpB in the Ribosome. *Science* *335*, 1366.

Nishizuka, Y., and Lipmann, F. (1966). The interrelationship between guanosine triphosphatase and amino acid polymerization. *Archives of Biochemistry and Biophysics* *116*, 344-351.

Nissen, P., Hansen, J., Ban, N., Moore, P.B., and Steitz, T.A. (2000). The structural basis of ribosome activity in peptide bond synthesis. *Science* *289*, 920-930.

Nissen, P., Kjeldgaard, M., Thirup, S., Polekhina, G., Reshetnikova, L., Clark, B.F., and Nyborg, J. (1995). Crystal structure of the ternary complex of Phe-tRNAPhe, EF-Tu, and a GTP analog. *Science* *270*, 1464-1472.

Nissen, P., Thirup, S., Kjeldgaard, M., and Nyborg, J. (1999). The crystal structure of Cys-tRNACys-EF-Tu-GDPNP reveals general and specific features in the ternary complex and in tRNA. *Structure* *7*, 143-156.

Noller, H.F. (1984). STRUCTURE OF RIBOSOMAL RNA. *Annual Review of Biochemistry* *53*, 119-162.

Noller, H.F., Lancaster, L., Mohan, S., and Zhou, J. (2017). Ribosome structural dynamics in translocation: yet another functional role for ribosomal RNA. *Quarterly Reviews of Biophysics* *50*, e12.

Nudler, E., Avetissova, E., Markovtsov, V., and Goldfarb, A. (1996). Transcription Processivity: Protein-DNA Interactions Holding Together the Elongation Complex. *Science* *273*, 211.

Ogawa, K., and Kaji, A. (1975). Requirement for Ribosome-Releasing Factor for the Release of Ribosomes at the Termination Codon. *European Journal of Biochemistry* *58*, 411-419.

Ogle, J.M., Brodersen, D.E., Clemons, W.M., Jr., Tarry, M.J., Carter, A.P., and Ramakrishnan, V. (2001). Recognition of cognate transfer RNA by the 30S ribosomal subunit. *Science* *292*, 897-902.

Ogle, J.M., Carter, A.P., and Ramakrishnan, V. (2003). Insights into the decoding mechanism from recent ribosome structures. *Trends in Biochemical Sciences* *28*, 259-266.

Ogle, J.M., Murphy, F.V., Tarry, M.J., and Ramakrishnan, V. (2002). Selection of tRNA by the ribosome requires a transition from an open to a closed form. *Cell* *111*, 721-732.

Pape, T., Wintermeyer, W., and Rodnina, M. (1999). Induced fit in initial selection and proofreading of aminoacyl-tRNA on the ribosome. *EMBO J* *18*, 3800-3807.

Pape, T., Wintermeyer, W., and Rodnina, M.V. (1998). Complete kinetic mechanism of elongation factor Tu-dependent binding of aminoacyl-tRNA to the A site of the *E.coli* ribosome. *EMBO J* *17*, 7490-7497.

Paulsen, V.S., Mardirossian, M., Blencke, H.-M., Benincasa, M., Runti, G., Nepa, M., Haug, T., Stensvåg, K., and Scocchi, M. (2016). Inner membrane proteins YgDD and SbmA are required for the complete susceptibility of *Escherichia coli* to the proline-rich antimicrobial peptide arasin 1(1-25). *Microbiology* *162*, 601-609.

Pedersen, K., Zavialov, A.V., Pavlov, M.Y., Elf, J., Gerdes, K., and Ehrenberg, M. (2003). The bacterial toxin RelE displays codon-specific cleavage of mRNAs in the ribosomal A site. *Cell* *112*, 131-140.

Peng, B.-Z., Bock, L.V., Belardinelli, R., Peske, F., Grubmüller, H., and Rodnina, M.V. (2019). Active role of elongation factor G in maintaining the mRNA reading frame during translation. *Science Advances* *5*, eaax8030.

Personne, Y., and Parish, T. (2014). *Mycobacterium tuberculosis* possesses an unusual tmRNA rescue system. *Tuberculosis* *94*, 34-42.

Peske, F., Kuhlenkoetter, S., Rodnina, M.V., and Wintermeyer, W. (2014). Timing of GTP binding and hydrolysis by translation termination factor RF3. *Nucleic Acids Res* *42*, 1812-1820.

Peske, F., Rodnina, M.V., and Wintermeyer, W. (2005). Sequence of steps in ribosome recycling as defined by kinetic analysis. *Mol Cell* *18*, 403-412.

Petersen, H.U., Røll, T., Grunberg-Manago, M., and Clark, B.F.C. (1979). Specific interaction of initiation factor IF2 of *E. coli* with formylmethionyl-tRNAfMet. *Biochemical and Biophysical Research Communications* *91*, 1068-1074.

Petry, S., Brodersen, D.E., Murphy, F.V.t., Dunham, C.M., Selmer, M., Tarry, M.J., Kelley, A.C., and Ramakrishnan, V. (2005). Crystal structures of the ribosome in complex with release factors RF1 and RF2 bound to a cognate stop codon. *Cell* *123*, 1255-1266.

Pierson, William E., Hoffer, Eric D., Keedy, Hannah E., Simms, Carrie L., Dunham, Christine M., and Zaher, Hani S. (2016). Uniformity of Peptide Release Is Maintained by Methylation of Release Factors. *Cell Reports* *17*, 11-18.

Podda, E., Benincasa, M., Pacor, S., Micali, F., Mattiuzzo, M., Gennaro, R., and Scocchi, M. (2006). Dual mode of action of Bac7, a proline-rich antibacterial peptide. *Biochimica et Biophysica Acta (BBA) - General Subjects* *1760*, 1732-1740.

Polacek, N., Gaynor, M., Yassin, A., and Mankin, A.S. (2001). Ribosomal peptidyl transferase can withstand mutations at the putative catalytic nucleotide. *Nature* *411*, 498-501.

Polikanov, Y.S., Aleksashin, N.A., Beckert, B., and Wilson, D.N. (2018). The Mechanisms of Action of Ribosome-Targeting Peptide Antibiotics. *Front Mol Biosci* *5*, 48.

Polikanov, Y.S., Steitz, T.A., and Innis, C.A. (2014). A proton wire to couple aminoacyl-tRNA accommodation and peptide-bond formation on the ribosome. *Nat Struct Mol Biol* *21*, 787-793.

Pon, C.L., and Gualerzi, C.O. (1984). Mechanism of protein biosynthesis in prokaryotic cells. *FEBS Letters* *175*, 203-207.

Pon, C.L., Paci, M., Pawlik, R.T., and Gualerzi, C.O. (1985). Structure-function relationship in *Escherichia coli* initiation factors. Biochemical and biophysical characterization of the interaction between IF-2 and guanosine nucleotides. *Journal of Biological Chemistry* *260*, 8918-8924.

Poole, E.S., Brown, C.M., and Tate, W.P. (1995). The identity of the base following the stop codon determines the efficiency of *in vivo* translational termination in *Escherichia coli*. *EMBO J* *14*, 151-158.

Poole, E.S., Major, L.L., Mannering, S.A., and Tate, W.P. (1998). Translational termination in *Escherichia coli*: three bases following the stop codon crosslink to release factor 2 and affect the decoding efficiency of UGA-containing signals. *Nucleic Acids Res* *26*, 954-960.

Prabhakar, A., Capece, M.C., Petrov, A., Choi, J., and Puglisi, J.D. (2017). Post-termination Ribosome Intermediate Acts as the Gateway to Ribosome Recycling. *Cell Reports* *20*, 161-172.

Prevelige, P., and Fasman, G.D. (1989). Chou-Fasman Prediction of the Secondary Structure of Proteins. In *Prediction of Protein Structure and the Principles of Protein Conformation*, G.D. Fasman, ed. (Boston, MA: Springer US), pp. 391-416.

Proshkin, S., Rahmouni, A.R., Mironov, A., and Nudler, E. (2010). Cooperation Between Translating Ribosomes and RNA Polymerase in Transcription Elongation. *Science* *328*, 504.

Pulk, A., and Cate, J.H.D. (2013). Control of Ribosomal Subunit Rotation by Elongation Factor G. *Science* *340*, 1235970.

Rae, C.D., Gordiyenko, Y., and Ramakrishnan, V. (2019). How a circularized tmRNA moves through the ribosome. *Science* *363*, 740-744.

Raj, V.S., Kaji, H., and Kaji, A. (2005). Interaction of RRF and EF-G from *E. coli* and *T. thermophilus* with ribosomes from both origins—insight into the mechanism of the ribosome recycling step. *RNA* *11*, 275-284.

RajBhandary, U.L. (1994). Initiator transfer RNAs. *Journal of Bacteriology* *176*, 547.

Ram Prasad, B., Plotnikov, N.V., Lameira, J., and Warshel, A. (2013). Quantitative exploration of the molecular origin of the activation of GTPase. *Proceedings of the National Academy of Sciences* *110*, 20509.

Ramrath, D.J.F., Lancaster, L., Sprink, T., Mielke, T., Loerke, J., Noller, H.F., and Spahn, C.M.T. (2013). Visualization of two transfer RNAs trapped in transit during elongation factor G-mediated translocation. *Proceedings of the National Academy of Sciences* *110*, 20964.

Ramrath, D.J.F., Yamamoto, H., Rother, K., Wittek, D., Pech, M., Mielke, T., Loerke, J., Scheerer, P., Ivanov, P., Teraoka, Y., *et al.* (2012). The complex of tmRNA–SmpB and EF-G on translocating ribosomes. *Nature* *485*, 526-529.

Ratje, A.H., Loerke, J., Mikolajka, A., Brünner, M., Hildebrand, P.W., Starosta, A.L., Dönhöfer, A., Connell, S.R., Fucini, P., Mielke, T., *et al.* (2010). Head swivel on the ribosome facilitates translocation by means of intra-subunit tRNA hybrid sites. *Nature* *468*, 713-716.

Rawat, U., Gao, H., Zavialov, A., Gursky, R., Ehrenberg, M., and Frank, J. (2006). Interactions of the Release Factor RF1 with the Ribosome as Revealed by Cryo-EM. *Journal of Molecular Biology* *357*, 1144-1153.

Rawat, U.B., Zavialov, A.V., Sengupta, J., Valle, M., Grassucci, R.A., Linde, J., Vestergaard, B., Ehrenberg, M., and Frank, J. (2003). A cryo-electron microscopic study of ribosome-bound termination factor RF2. *Nature* *421*, 87-90.

Ray, B.K., and Apirion, D. (1979). Characterization of 10S RNA: A new stable RNA molecule from *Escherichia coli*. *Molecular and General Genetics MGG* *174*, 25-32.

Rheinberger, H.J., Sternbach, H., and Nierhaus, K.H. (1981). Three tRNA binding sites on *Escherichia coli* ribosomes. *Proceedings of the National Academy of Sciences* *78*, 5310.

Richards, J., Mehta, P., and Karzai, A.W. (2006). RNase R degrades non-stop mRNAs selectively in an SmpB-tmRNA-dependent manner. *Molecular Microbiology* *62*, 1700-1712.

Richter, R., Rorbach, J., Pajak, A., Smith, P.M., Wessels, H.J., Huynen, M.A., Smeitink, J.A., Lightowers, R.N., and Chrzanowska-Lightowers, Z.M. (2010). A functional peptidyl-tRNA hydrolase, ICT1, has been recruited into the human mitochondrial ribosome. *EMBO J* *29*, 1116-1125.

Rodnina, M.V. (2013). The ribosome as a versatile catalyst: reactions at the peptidyl transferase center. *Current Opinion in Structural Biology* *23*, 595-602.

Rodnina, M.V. (2018). Translation in Prokaryotes. *Cold Spring Harb Perspect Biol* *10*.

Rodnina, M.V., Peske, F., Peng, B.Z., Belardinelli, R., and Wintermeyer, W. (2019). Converting GTP hydrolysis into motion: versatile translational elongation factor G. *Biol Chem* *401*, 131-142.

Rodnina, M.V., Savelsbergh, A., Katunin, V.I., and Wintermeyer, W. (1997). Hydrolysis of GTP by elongation factor G drives tRNA movement on the ribosome. *Nature* *385*, 37-41.

Roncevic, T., Puizina, J., and Tossi, A. (2019). Antimicrobial Peptides as Anti-Infective Agents in Pre-Post-Antibiotic Era? *Int J Mol Sci* *20*.

Roy, R.N., Lomakin, I.B., Gagnon, M.G., and Steitz, T.A. (2015). The mechanism of inhibition of protein synthesis by the proline-rich peptide oncocin. *Nature Structural & Molecular Biology* *22*, 466-469.

Rozov, A., Demeshkina, N., Khusainov, I., Westhof, E., Yusupov, M., and Yusupova, G. (2016a). Novel base-pairing interactions at the tRNA wobble position crucial for accurate reading of the genetic code. *Nat Commun* 7, 10457.

Rozov, A., Demeshkina, N., Westhof, E., Yusupov, M., and Yusupova, G. (2015). Structural insights into the translational infidelity mechanism. *Nat Commun* 6, 7251.

Rozov, A., Westhof, E., Yusupov, M., and Yusupova, G. (2016b). The ribosome prohibits the G\*U wobble geometry at the first position of the codon-anticodon helix. *Nucleic Acids Res* 44, 6434-6441.

Rozov, A., Wolff, P., Grosjean, H., Yusupov, M., Yusupova, G., and Westhof, E. (2018). Tautomeric G\*U pairs within the molecular ribosomal grip and fidelity of decoding in bacteria. *Nucleic Acids Res* 46, 7425-7435.

Rudinger-Thirion, J., Giegé, R., and Felden, B. (1999). Aminoacylated tmRNA from *Escherichia coli* interacts with prokaryotic elongation factor Tu. *RNA* 5, 989-992.

Runti, G., Lopez Ruiz, M.d.C., Stoilova, T., Hussain, R., Jennions, M., Choudhury, H.G., Benincasa, M., Gennaro, R., Beis, K., and Scocchi, M. (2013). Functional Characterization of SbmA, a Bacterial Inner Membrane Transporter Required for Importing the Antimicrobial Peptide Bac7(1-35). *Journal of Bacteriology* 195, 5343.

Russell, J.B., and Cook, G.M. (1995). Energetics of bacterial growth: balance of anabolic and catabolic reactions. *Microbiol Rev* 59, 48-62.

Sabol, S., Sillero, M.A., Iwasaki, K., and Ochoa, S. (1970). Purification and properties of initiation factor F3. *Nature* 228, 1269-1273.

Sacerdot, C., Chiaruttini, C., Engst, K., Graffe, M., Milet, M., Mathy, N., Dondon, J., and Springer, M. (1996). The role of the AUU initiation codon in the negative feedback regulation of the gene for translation initiation factor IF3 in *Escherichia coli*. *Molecular Microbiology* 21, 331-346.

Saito, K., Green, R., and Buskirk, A.R. (2020). Translational initiation in *E. coli* occurs at the correct sites genome-wide in the absence of mRNA-rRNA base-pairing. *eLife* 9, e55002.

Salsi, E., Farah, E., Netter, Z., Dann, J., and Ermolenko, D.N. (2015). Movement of Elongation Factor G between Compact and Extended Conformations. *Journal of Molecular Biology* 427, 454-467.

Santos, N., Zhu, J., Donohue, J.P., Korostelev, A.A., and Noller, H.F. (2013). Crystal structure of the 70S ribosome bound with the Q253P mutant form of release factor RF2. *Structure* 21, 1258-1263.

Savelsbergh, A., Matassova, N.B., Rodnina, M.V., and Wintermeyer, W. (2000). Role of Domains 4 and 5 in Elongation Factor G Functions on the Ribosome. *Journal of Molecular Biology* 300, 951-961.

Savelsbergh, A., Mohr, D., Kothe, U., Wintermeyer, W., and Rodnina, M.V. (2005). Control of phosphate release from elongation factor G by ribosomal protein L7/12. *EMBO J* 24, 4316-4323.

Scarlett, D.J., McCaughan, K.K., Wilson, D.N., and Tate, W.P. (2003). Mapping functionally important motifs SPF and GGQ of the decoding release factor RF2 to the *Escherichia coli* ribosome by hydroxyl radical footprinting. Implications for macromolecular mimicry and structural changes in RF2. *J Biol Chem* 278, 15095-15104.

Scharff, L.B., Childs, L., Walther, D., and Bock, R. (2011). Local Absence of Secondary Structure Permits Translation of mRNAs that Lack Ribosome-Binding Sites. *PLOS Genetics* 7, e1002155.

Schaub, R.E., Poole, S.J., Garza-Sanchez, F., Benbow, S., and Hayes, C.S. (2012). Proteobacterial ArfA peptides are synthesized from non-stop messenger RNAs. *J Biol Chem* 287, 29765-29775.

Schlessinger, D., Mangiarotti, G., and Apirion, D. (1967). The formation and stabilization of 30S and 50S ribosome couples in *Escherichia coli*. *Proceedings of the National Academy of Sciences* *58*, 1782.

Schluelzen, F., Tocilj, A., Zarivach, R., Harms, J., Gluehmann, M., Janell, D., Bashan, A., Bartels, H., Agmon, I., Franceschi, F., *et al.* (2000). Structure of functionally activated small ribosomal subunit at 3.3 angstroms resolution. *Cell* *102*, 615-623.

Schmeing, T.M., Huang, K.S., Kitchen, D.E., Strobel, S.A., and Steitz, T.A. (2005a). Structural insights into the roles of water and the 2' hydroxyl of the P site tRNA in the peptidyl transferase reaction. *Mol Cell* *20*, 437-448.

Schmeing, T.M., Huang, K.S., Strobel, S.A., and Steitz, T.A. (2005b). An induced-fit mechanism to promote peptide bond formation and exclude hydrolysis of peptidyl-tRNA. *Nature* *438*, 520-524.

Schmeing, T.M., Moore, P.B., and Steitz, T.A. (2003). Structures of deacylated tRNA mimics bound to the E site of the large ribosomal subunit. *RNA* *9*, 1345-1352.

Schmeing, T.M., and Ramakrishnan, V. (2009). What recent ribosome structures have revealed about the mechanism of translation. *Nature* *461*, 1234.

Schmeing, T.M., Seila, A.C., Hansen, J.L., Freeborn, B., Soukup, J.K., Scaringe, S.A., Strobel, S.A., Moore, P.B., and Steitz, T.A. (2002). A pre-translocational intermediate in protein synthesis observed in crystals of enzymatically active 50S subunits. *Nature Structural Biology* *9*, 225-230.

Schmeing, T.M., Voorhees, R.M., Kelley, A.C., Gao, Y.-G., Murphy, F.V., Weir, J.R., and Ramakrishnan, V. (2009). The Crystal Structure of the Ribosome Bound to EF-Tu and Aminoacyl-tRNA. *Science* *326*, 688.

Schmitt, E., Panvert, M., Blanquet, S., and Mechulam, Y. (1998). Crystal structure of methionyl-tRNAfMet transformylase complexed with the initiator formyl-methionyl-tRNAfMet. *EMBO J* *17*, 6819-6826.

Schnapp, D., Kemp, G.D., and Smith, V.J. (1996). Purification and Characterization of a Proline-Rich Antibacterial Peptide, with Sequence Similarity to Bactenecin-7, from the Haemocytes of the Shore Crab, *Carcinus Maenas*. *European Journal of Biochemistry* *240*, 532-539.

Schneider, M., and Dorn, A. (2001). Differential Infectivity of Two *Pseudomonas* Species and the Immune Response in the Milkweed Bug, *Oncopeltus fasciatus* (Insecta: Hemiptera). *Journal of Invertebrate Pathology* *78*, 135-140.

Schuwirth, B.S., Borovinskaya, M.A., Hau, C.W., Zhang, W., Vila-Sanjurjo, A., Holton, J.M., and Cate, J.H. (2005). Structures of the bacterial ribosome at 3.5 Å resolution. *Science* *310*, 827-834.

Scocchi, M., Lüthy, C., Decarli, P., Mignogna, G., Christen, P., and Gennaro, R. (2009). The Proline-rich Antibacterial Peptide Bac7 Binds to and Inhibits in vitro the Molecular Chaperone DnaK. *International Journal of Peptide Research and Therapeutics* *15*, 147-155.

Scocchi, M., Skerlavaj, B., Romeo, D., and Gennaro, R. (1992). Proteolytic cleavage by neutrophil elastase converts inactive storage proforms to antibacterial bactenecins. *European Journal of Biochemistry* *209*, 589-595.

Scolnick, E., Tompkins, R., Caskey, T., and Nirenberg, M. (1968). Release factors differing in specificity for terminator codons. *Proc Natl Acad Sci U S A* *61*, 768-774.

Seefeldt, A.C., Graf, M., Perebaskine, N., Nguyen, F., Arenz, S., Mardirossian, M., Scocchi, M., Wilson, D.N., and Innis, C.A. (2016). Structure of the mammalian antimicrobial peptide Bac7(1-16) bound within the exit tunnel of a bacterial ribosome. *Nucleic Acids Res* *44*, 2429-2438.

Seefeldt, A.C., Nguyen, F., Antunes, S., Perebaskine, N., Graf, M., Arenz, S., Inampudi, K.K., Douat, C., Guichard, G., Wilson, D.N., *et al.* (2015). The proline-rich antimicrobial peptide Onc112 inhibits translation by blocking and destabilizing the initiation complex. *Nat Struct Mol Biol* 22, 470-475.

Seidelt, B., Innis, C.A., Wilson, D.N., Gartmann, M., Armache, J.-P., Villa, E., Trabuco, L.G., Becker, T., Mielke, T., Schulten, K., *et al.* (2009). Structural Insight into Nascent Polypeptide Chain–Mediated Translational Stalling. *Science* 326, 1412.

Seit-Nebi, A., Frolova, L., Justesen, J., and Kisseelev, L. (2001). Class-1 translation termination factors: invariant GGQ minidomain is essential for release activity and ribosome binding but not for stop codon recognition. *Nucleic Acids Research* 29, 3982-3987.

Selmer, M., Al-Karadaghi, S., Hirokawa, G., Kaji, A., and Liljas, A. (1999). Crystal structure of *Thermotoga maritima* ribosome recycling factor: a tRNA mimic. *Science* 286, 2349-2352.

Selmer, M., Dunham, C.M., Murphy, F.V.t., Weixlbaumer, A., Petry, S., Kelley, A.C., Weir, J.R., and Ramakrishnan, V. (2006). Structure of the 70S ribosome complexed with mRNA and tRNA. *Science* 313, 1935-1942.

Sengupta, J., Agrawal, R.K., and Frank, J. (2001). Visualization of protein S1 within the 30S ribosomal subunit and its interaction with messenger RNA. *Proceedings of the National Academy of Sciences* 98, 11991.

Seong, B.L., and RajBhandary, U.L. (1987a). *Escherichia coli* formylmethionine tRNA: mutations in GGGCCC sequence conserved in anticodon stem of initiator tRNAs affect initiation of protein synthesis and conformation of anticodon loop. *Proceedings of the National Academy of Sciences* 84, 334.

Seong, B.L., and RajBhandary, U.L. (1987b). Mutants of *Escherichia coli* formylmethionine tRNA: a single base change enables initiator tRNA to act as an elongator in vitro. *Proceedings of the National Academy of Sciences* 84, 8859.

Sette, M., van Tilborg, P., Spurio, R., Kaptein, R., Paci, M., Gualerzi, C.O., and Boelens, R. (1997). The structure of the translational initiation factor IF1 from *E.coli* contains an oligomer-binding motif. *EMBO J* 16, 1436-1443.

Shamova, O., Brogden, K.A., Zhao, C., Nguyen, T., Kokryakov, V.N., and Lehrer, R.I. (1999). Purification and Properties of Proline-Rich Antimicrobial Peptides from Sheep and Goat Leukocytes. *Infection and Immunity* 67, 4106.

Sharma, H., Adio, S., Senyushkina, T., Belardinelli, R., Peske, F., and Rodnina, M.V. (2016). Kinetics of Spontaneous and EF-G-Accelerated Rotation of Ribosomal Subunits. *Cell Rep* 16, 2187-2196.

Shaw, J.J., and Green, R. (2007). Two distinct components of release factor function uncovered by nucleophile partitioning analysis. *Mol Cell* 28, 458-467.

Shimizu, Y. (2012). ArfA recruits RF2 into stalled ribosomes. *J Mol Biol* 423, 624-631.

Shimokawa-Chiba, N., Muller, C., Fujiwara, K., Beckert, B., Ito, K., Wilson, D.N., and Chiba, S. (2019). Release factor-dependent ribosome rescue by BrfA in the Gram-positive bacterium *Bacillus subtilis*. *Nature Communications* 10, 5397.

Shin, D.H., Brandsen, J., Jancarik, J., Yokota, H., Kim, R., and Kim, S.H. (2004). Structural analyses of peptide release factor 1 from *Thermotoga maritima* reveal domain flexibility required for its interaction with the ribosome. *J Mol Biol* 341, 227-239.

Shin, J.H., and Price, C.W. (2007). The SsrA-SmpB ribosome rescue system is important for growth of *Bacillus subtilis* at low and high temperatures. *J Bacteriol* 189, 3729-3737.

Shine, J., and Dalgarno, L. (1974). The 3'-terminal sequence of *Escherichia coli* 16S ribosomal RNA: complementarity to nonsense triplets and ribosome binding sites. *Proc Natl Acad Sci U S A* 71, 1342-1346.

Shoji, S., Walker, S.E., and Fredrick, K. (2006). Reverse translocation of tRNA in the ribosome. *Mol Cell* 24, 931-942.

Sievers, A., Beringer, M., Rodnina, M.V., and Wolfenden, R. (2004). The ribosome as an entropy trap. *Proc Natl Acad Sci U S A* 101, 7897.

Simonetti, A., Marzi, S., Billas, I.M.L., Tsai, A., Fabbretti, A., Myasnikov, A.G., Roblin, P., Vaiana, A.C., Hazemann, I., Eiler, D., *et al.* (2013). Involvement of protein IF2 N domain in ribosomal subunit joining revealed from architecture and function of the full-length initiation factor. *Proceedings of the National Academy of Sciences* 110, 15656.

Simonetti, A., Marzi, S., Myasnikov, A.G., Fabbretti, A., Yusupov, M., Gualerzi, C.O., and Klaholz, B.P. (2008). Structure of the 30S translation initiation complex. *Nature* 455, 416-420.

Singarapu, K.K., Xiao, R., Acton, T., Rost, B., Montelione, G.T., and Szyperski, T. (2008). NMR structure of the peptidyl-tRNA hydrolase domain from *Pseudomonas syringae* expands the structural coverage of the hydrolysis domains of class 1 peptide chain release factors. *Proteins: Structure, Function, and Bioinformatics* 71, 1027-1031.

Sohmen, D., Chiba, S., Shimokawa-Chiba, N., Innis, C.A., Berninghausen, O., Beckmann, R., Ito, K., and Wilson, D.N. (2015). Structure of the *Bacillus subtilis* 70S ribosome reveals the basis for species-specific stalling. *Nature Communications* 6, 6941.

Sohmen, D., Harms, J.M., Schlünzen, F., and Wilson, D.N. (2009). Enhanced SnapShot: Antibiotic Inhibition of Protein Synthesis II. *Cell* 139, 212-212.e211.

Sørensen, H.P., Hedegaard, J., Sperling-Petersen, H.U., and Mortensen, K.K. (2001). Remarkable Conservation of Translation Initiation Factors: IF1/eIF1A and IF2/eIF5B are Universally Distributed Phylogenetic Markers. *IUBMB Life* 51, 321-327.

Sørensen, M.A., and Pedersen, S. (1991). Absolute in vivo translation rates of individual codons in *Escherichia coli*: The two glutamic acid codons GAA and GAG are translated with a threefold difference in rate. *Journal of Molecular Biology* 222, 265-280.

Spahn, C.M.T., Gomez-Lorenzo, M.G., Grassucci, R.A., Jørgensen, R., Andersen, G.R., Beckmann, R., Penczek, P.A., Ballesta, J.P.G., and Frank, J. (2004). Domain movements of elongation factor eEF2 and the eukaryotic 80S ribosome facilitate tRNA translocation. *EMBO J* 23, 1008-1019.

Spiegel, P.C., Ermolenko, D.N., and Noller, H.F. (2007). Elongation factor G stabilizes the hybrid-state conformation of the 70S ribosome. *RNA* 13, 1473-1482.

Sprink, T., Ramrath, D.J.F., Yamamoto, H., Yamamoto, K., Loerke, J., Ismer, J., Hildebrand, P.W., Scheerer, P., Bürger, J., Mielke, T., *et al.* (2016). Structures of ribosome-bound initiation factor 2 reveal the mechanism of subunit association. *Science Advances* 2, e1501502.

Stark, H., Rodnina, M.V., Rinke-Appel, J., Brimacombe, R., Wintermeyer, W., and Heel, M.v. (1997). Visualization of elongation factor Tu on the *Escherichia coli* ribosome. *Nature* 389, 403-406.

Starosta, A.L., Lassak, J., Jung, K., and Wilson, D.N. (2014a). The bacterial translation stress response. *FEMS Microbiol Rev* 38, 1172-1201.

Starosta, A.L., Lassak, J., Peil, L., Atkinson, G.C., Virumae, K., Tenson, T., Remme, J., Jung, K., and Wilson, D.N. (2014b). Translational stalling at polyproline stretches is modulated by the sequence context upstream of the stall site. *Nucleic Acids Res* 42, 10711-10719.

Stensvåg, K., Haug, T., Sperstad, S.V., Rekdal, Ø., Indrevoll, B., and Styrvold, O.B. (2008). Arasin 1, a proline-arginine-rich antimicrobial peptide isolated from the spider crab, *Hyas araneus*. *Developmental & Comparative Immunology* 32, 275-285.

Sternberg, S.H., Fei, J., Prywes, N., McGrath, K.A., and Gonzalez, R.L., Jr. (2009). Translation factors direct intrinsic ribosome dynamics during translation termination and ribosome recycling. *Nat Struct Mol Biol* 16, 861-868.

Studer, S.M., and Joseph, S. (2006). Unfolding of mRNA Secondary Structure by the Bacterial Translation Initiation Complex. *Molecular Cell* 22, 105-115.

Su, T., Cheng, J., Sohmen, D., Hedman, R., Berninghausen, O., von Heijne, G., Wilson, D.N., and Beckmann, R. (2017). The force-sensing peptide VemP employs extreme compaction and secondary structure formation to induce ribosomal stalling. *eLife* 6, e25642.

Subramanian, A.R., and Davis, B.D. (1970). Activity of initiation factor F3 in dissociating *Escherichia coli* ribosomes. *Nature* 228, 1273-1275.

Subramanian, A.R., and Davis, B.D. (1973). Release of 70 S ribosomes from polysomes in *Escherichia coli*. *J Mol Biol* 74, 45-56.

Subramanian, A.R., Davis, B.D., and Beller, R.J. (1969). The ribosome dissociation factor and the ribosome-polysome cycle. *Cold Spring Harb Symp Quant Biol* 34, 223-230.

Subramanian, A.R., Ron, E.Z., and Davis, B.D. (1968). A factor required for ribosome dissociation in *Escherichia coli*. *Proc Natl Acad Sci U S A* 61, 761-767.

Sundari, R.M., Stringer, E.A., Schulman, L.H., and Maitra, U. (1976). Interaction of bacterial initiation factor 2 with initiator tRNA. *Journal of Biological Chemistry* 251, 3338-3345.

Sundermeier, T.R., Dulebohn, D.P., Cho, H.J., and Karzai, A.W. (2005). A previously uncharacterized role for small protein B (SmpB) in transfer messenger RNA-mediated trans-translation. *Proc Natl Acad Sci U S A* 102, 2316-2321.

Sunohara, T., Abo, T., Inada, T., and Aiba, H. (2002). The C-terminal amino acid sequence of nascent peptide is a major determinant of SsrA tagging at all three stop codons. *RNA* 8, 1416-1427.

Sunohara, T., Jojima, K., Tagami, H., Inada, T., and Aiba, H. (2004a). Ribosome Stalling during Translation Elongation Induces Cleavage of mRNA Being Translated in *Escherichia coli*. *Journal of Biological Chemistry* 279, 15368-15375.

Sunohara, T., Jojima, K., Yamamoto, Y., Inada, T., and Aiba, H. (2004b). Nascent-peptide-mediated ribosome stalling at a stop codon induces mRNA cleavage resulting in nonstop mRNA that is recognized by tmRNA. *RNA* 10, 378-386.

Svetlanov, A., Puri, N., Mena, P., Koller, A., and Karzai, A.W. (2012). *Francisella tularensis* tmRNA system mutants are vulnerable to stress, avirulent in mice, and provide effective immune protection. *Mol Microbiol* 85, 122-141.

Svidritskiy, E., Demo, G., Loveland, A.B., Xu, C., and Korostelev, A.A. (2019). Extensive ribosome and RF2 rearrangements during translation termination. *Elife* 8.

Takeuchi, N., and Nierhaus, K.H. (2015). Response to the Formal Letter of Z. Chrzanowska-Lightowers and R. N. Lightowers Regarding Our Article “Ribosome Rescue and Translation Termination at Non-Standard Stop Codons by ICT1 in Mammalian Mitochondria”. *PLOS Genetics* 11, e1005218.

Tesina, P., Heckel, E., Cheng, J., Fromont-Racine, M., Buschauer, R., Kater, L., Beatrix, B., Berninghausen, O., Jacquier, A., Becker, T., *et al.* (2019). Structure of the 80S ribosome-Xrn1 nuclease complex. *Nature Structural & Molecular Biology* 26, 275-280.

Tesina, P., Lessen, L.N., Buschauer, R., Cheng, J., Wu, C.C.-C., Berninghausen, O., Buskirk, A.R., Becker, T., Beckmann, R., and Green, R. (2020). Molecular mechanism of translational stalling by inhibitory codon combinations and poly(A) tracts. *EMBO J* 39, e103365.

The Rnacentral Consortium (2018). RNacentral: a hub of information for non-coding RNA sequences. *Nucleic Acids Research* 47, D221-D229.

Thompson, R.C., and Stone, P.J. (1977). Proofreading of the codon-anticodon interaction on ribosomes. *Proceedings of the National Academy of Sciences* *74*, 198.

Tourigny, D.S., Fernandez, I.S., Kelley, A.C., and Ramakrishnan, V. (2013). Elongation factor G bound to the ribosome in an intermediate state of translocation. *Science* *340*, 1235490.

Toyoda, T., Tin, O.F., Ito, K., Fujiwara, T., Kumasaka, T., Yamamoto, M., Garber, M.B., and Nakamura, Y. (2000). Crystal structure combined with genetic analysis of the *Thermus thermophilus* ribosome recycling factor shows that a flexible hinge may act as a functional switch. *RNA* *6*, 1432-1444.

Trappi, K., and Joseph, S. (2016). Ribosome Induces a Closed to Open Conformational Change in Release Factor 1. *J Mol Biol* *428*, 1333-1344.

Trobro, S., and Aqvist, J. (2007). A model for how ribosomal release factors induce peptidyl-tRNA cleavage in termination of protein synthesis. *Mol Cell* *27*, 758-766.

Trobro, S., and Aqvist, J. (2009). Mechanism of the translation termination reaction on the ribosome. *Biochemistry* *48*, 11296-11303.

Tu, G.-F., Reid, G.E., Zhang, J.-G., Moritz, R.L., and Simpson, R.J. (1995). C-terminal Extension of Truncated Recombinant Proteins in *Escherichia coli* with a 10Sa RNA Decapeptide. *Journal of Biological Chemistry* *270*, 9322-9326.

Ueda, K., Yamamoto, Y., Ogawa, K., Abo, T., Inokuchi, H., and Aiba, H. (2002). Bacterial SsrA system plays a role in coping with unwanted translational readthrough caused by suppressor tRNAs. *Genes to Cells* *7*, 509-519.

Ushida, C., Himeno, H., Watanabe, T., and Muto, A. (1994). tRNA-like structures in 10Sa RNAs of *Mycoplasma capricolum* and *Bacillus subtilis*. *Nucleic Acids Research* *22*, 3392-3396.

Valle, M., Gillet, R., Kaur, S., Henne, A., Ramakrishnan, V., and Frank, J. (2003). Visualizing tmRNA Entry into a Stalled Ribosome. *Science* *300*, 127.

VanLoock, M.S., Agrawal, R.K., Gabashvili, I.S., Qi, L., Frank, J., and Harvey, S.C. (2000). Movement of the decoding region of the 16 S ribosomal RNA accompanies tRNA translocation. *J Mol Biol* *304*, 507-515.

Venkataraman, K., Guja, K.E., Garcia-Diaz, M., and Karzai, A.W. (2014a). Non-stop mRNA decay: a special attribute of trans-translation mediated ribosome rescue. *Front Microbiol* *5*, 93.

Venkataraman, K., Zafar, H., and Karzai, A.W. (2014b). Distinct tmRNA sequence elements facilitate RNase R engagement on rescued ribosomes for selective nonstop mRNA decay. *Nucleic Acids Research* *42*, 11192-11202.

Vestergaard, B., Sanyal, S., Roessle, M., Mora, L., Buckingham, R.H., Kastrup, J.S., Gajhede, M., Svergun, D.I., and Ehrenberg, M. (2005). The SAXS Solution Structure of RF1 Differs from Its Crystal Structure and Is Similar to Its Ribosome Bound Cryo-EM Structure. *Molecular Cell* *20*, 929-938.

Vestergaard, B., Van, L.B., Andersen, G.R., Nyborg, J., Buckingham, R.H., and Kjeldgaard, M. (2001). Bacterial Polypeptide Release Factor RF2 Is Structurally Distinct from Eukaryotic eRF1. *Molecular Cell* *8*, 1375-1382.

Voorhees, R.M., Schmeing, T.M., Kelley, A.C., and Ramakrishnan, V. (2010). The mechanism for activation of GTP hydrolysis on the ribosome. *Science* *330*, 835-838.

Voorhees, R.M., Weixlbaumer, A., Loakes, D., Kelley, A.C., and Ramakrishnan, V. (2009). Insights into substrate stabilization from snapshots of the peptidyl transferase center of the intact 70S ribosome. *Nat Struct Mol Biol* *16*, 528-533.

Wallin, G., Kamerlin, S.C.L., and Åqvist, J. (2013). Energetics of activation of GTP hydrolysis on the ribosome. *Nature Communications* *4*, 1733.

Watson, J.D. (1964). THE SYNTHESIS OF PROTEINS UPON RIBOSOMES. *Bull Soc Chim Biol (Paris)* *46*, 1399-1425.

Weigert, M.G., Lanka, E., and Garen, A. (1967). Base composition of nonsense codons in *Escherichia coli*: The N2 codon UAA. *Journal of Molecular Biology* *23*, 391-400.

Weinger, J.S., Parnell, K.M., Dorner, S., Green, R., and Strobel, S.A. (2004). Substrate-assisted catalysis of peptide bond formation by the ribosome. *Nature Structural & Molecular Biology* *11*, 1101-1106.

Weis, F., Bron, P., Giudice, E., Rolland, J.-P., Thomas, D., Felden, B., and Gillet, R. (2010a). tmRNA-SmpB: a journey to the centre of the bacterial ribosome. *EMBO J* *29*, 3810-3818.

Weis, F., Bron, P., Rolland, J.-P., Thomas, D., Felden, B., and Gillet, R. (2010b). Accommodation of tmRNA-SmpB into stalled ribosomes: A cryo-EM study. *RNA* *16*, 299-306.

Weixlbaumer, A., Jin, H., Neubauer, C., Voorhees, R.M., Petry, S., Kelley, A.C., and Ramakrishnan, V. (2008a). Insights into translational termination from the structure of RF2 bound to the ribosome. *Science* *322*, 953-956.

Weixlbaumer, A., Jin, H., Neubauer, C., Voorhees, R.M., Petry, S., Kelley, A.C., and Ramakrishnan, V. (2008b). Insights into Translational Termination from the Structure of RF2 Bound to the Ribosome. *Science* *322*, 953.

Weixlbaumer, A., Petry, S., Dunham, C.M., Selmer, M., Kelley, A.C., and Ramakrishnan, V. (2007). Crystal structure of the ribosome recycling factor bound to the ribosome. *Nat Struct Mol Biol* *14*, 733-737.

Whitford, P.C., Blanchard, S.C., Cate, J.H., and Sanbonmatsu, K.Y. (2013). Connecting the kinetics and energy landscape of tRNA translocation on the ribosome. *PLoS Comput Biol* *9*, e1003003.

Whitford, P.C., and Sanbonmatsu, K.Y. (2013). Simulating movement of tRNA through the ribosome during hybrid-state formation. *The Journal of Chemical Physics* *139*, 121919.

Wieden, H.J., Wintermeyer, W., and Rodnina, M.V. (2001). A common structural motif in elongation factor Ts and ribosomal protein L7/12 may be involved in the interaction with elongation factor Tu. *J Mol Evol* *52*, 129-136.

Wiegert, T., and Schumann, W. (2001). SsrA-mediated tagging in *Bacillus subtilis*. *J Bacteriol* *183*, 3885-3889.

Williams, K.P., and Bartel, D.P. (1996). Phylogenetic analysis of tmRNA secondary structure. *RNA* *2*, 1306-1310.

Williams, K.P., Martindale, K.A., and Bartel, D.P. (1999). Resuming translation on tmRNA: a unique mode of determining a reading frame. *EMBO J* *18*, 5423-5433.

Wilson, D.N., Arenz, S., and Beckmann, R. (2016). Translation regulation via nascent polypeptide-mediated ribosome stalling. *Curr Opin Struct Biol* *37*, 123-133.

Wilson, D.N., Schluenzen, F., Harms, J.M., Yoshida, T., Ohkubo, T., Albrecht, R., Buerger, J., Kobayashi, Y., and Fucini, P. (2005). X-ray crystallography study on ribosome recycling: the mechanism of binding and action of RRF on the 50S ribosomal subunit. *EMBO J* *24*, 251-260.

Wohlgemuth, I., Beringer, M., and Rodnina, M.V. (2006). Rapid peptide bond formation on isolated 50S ribosomal subunits. *EMBO reports* *7*, 699-703.

Wohlgemuth, I., Pohl, C., and Rodnina, M.V. (2010). Optimization of speed and accuracy of decoding in translation. *EMBO J* *29*, 3701-3709.

Woo, N.H., Roe, B.A., and Rich, A. (1980). Three-dimensional structure of *Escherichia coli* initiator tRNA<sup>fMet</sup>. *Nature* *286*, 346-351.

Wower, I.K., Wower, J., and Zimmermann, R.A. (1998). Ribosomal protein L27 participates in both 50 S subunit assembly and the peptidyl transferase reaction. *J Biol Chem* 273, 19847-19852.

Wu, X.-Q., and RajBhandary, U.L. (1997). Effect of the Amino Acid Attached to Escherichia coli Initiator tRNA on Its Affinity for the Initiation Factor IF2 and on the IF2 Dependence of Its Binding to the Ribosome. *Journal of Biological Chemistry* 272, 1891-1895.

Xu, P., Shi, M., and Chen, X.-x. (2009). Antimicrobial Peptide Evolution in the Asiatic Honey Bee *Apis cerana*. *PLOS ONE* 4, e4239.

Yamamoto, T., Shimizu, Y., Ueda, T., and Shiro, Y. (2010). Mg<sup>2+</sup> Dependence of 70 S Ribosomal Protein Flexibility Revealed by Hydrogen/Deuterium Exchange and Mass Spectrometry. *Journal of Biological Chemistry* 285, 5646-5652.

Yamamoto, Y., Sunohara, T., Jojima, K., Inada, T., and Aiba, H. (2003). SsrA-mediated translational quality control plays a role in mRNA quality control by facilitating degradation of truncated mRNAs. *RNA* 9, 408-418.

Yan, L.L., and Zaher, H.S. (2019). How do cells cope with RNA damage and its consequences? *Journal of Biological Chemistry*.

Yao, L., Li, Y., Tsai, T.-W., Xu, S., and Wang, Y. (2013). Noninvasive Measurement of the Mechanical Force Generated by Motor Protein EF-G during Ribosome Translocation. *Angewandte Chemie International Edition* 52, 14041-14044.

Yin, H., Gavriliuc, M., Lin, R., Xu, S., and Wang, Y. (2019). Modulation and Visualization of EF-G Power Stroke During Ribosomal Translocation. *Chembiochem* 20, 2927-2935.

Yokoyama, T., Shaikh, T.R., Iwakura, N., Kaji, H., Kaji, A., and Agrawal, R.K. (2012). Structural insights into initial and intermediate steps of the ribosome-recycling process. *EMBO J* 31, 1836-1846.

Yoshida, T., Oka, S., Uchiyama, S., Nakano, H., Kawasaki, T., Ohkubo, T., and Kobayashi, Y. (2003). Characteristic domain motion in the ribosome recycling factor revealed by <sup>15</sup>N NMR relaxation experiments and molecular dynamics simulations. *Biochemistry* 42, 4101-4107.

Yoshida, T., Uchiyama, S., Nakano, H., Kashimori, H., Kijima, H., Ohshima, T., Saihara, Y., Ishino, T., Shimahara, H., Yoshida, T., et al. (2001). Solution Structure of the Ribosome Recycling Factor from *Aquifex aeolicus*. *Biochemistry* 40, 2387-2396.

Youngman, E.M., Brunelle, J.L., Kochaniak, A.B., and Green, R. (2004). The Active Site of the Ribosome Is Composed of Two Layers of Conserved Nucleotides with Distinct Roles in Peptide Bond Formation and Peptide Release. *Cell* 117, 589-599.

Yusupov, M.M., Yusupova, G.Z., Baucom, A., Lieberman, K., Earnest, T.N., Cate, J.H., and Noller, H.F. (2001). Crystal structure of the ribosome at 5.5 Å resolution. *Science* 292, 883-896.

Yusupova, G.Z., Yusupov, M.M., Cate, J.H., and Noller, H.F. (2001). The path of messenger RNA through the ribosome. *Cell* 106, 233-241.

Zaher, H.S., Shaw, J.J., Strobel, S.A., and Green, R. (2011). The 2'-OH group of the peptidyl-tRNA stabilizes an active conformation of the ribosomal PTC. *EMBO J* 30, 2445-2453.

Zanetti, M., Litteri, L., Gennaro, R., Horstmann, H., and Romeo, D. (1990). Bactenecins, defense polypeptides of bovine neutrophils, are generated from precursor molecules stored in the large granules. *Journal of Cell Biology* 111, 1363-1371.

Zanetti, M., Litteri, L., Griffiths, G., Gennaro, R., and Romeo, D. (1991). Stimulus-induced maturation of probactenecins, precursors of neutrophil antimicrobial polypeptides. *The Journal of Immunology* 146, 4295.

Zasloff, M. (2002). Antimicrobial Peptides in Health and Disease. *New England Journal of Medicine* 347, 1199-1200.

Zavialov, A.V., Buckingham, R.H., and Ehrenberg, M. (2001). A posttermination ribosomal complex is the guanine nucleotide exchange factor for peptide release factor RF3. *Cell* *107*, 115-124.

Zavialov, A.V., Hauryliuk, V.V., and Ehrenberg, M. (2005). Splitting of the Posttermination Ribosome into Subunits by the Concerted Action of RRF and EF-G. *Molecular Cell* *18*, 675-686.

Zavialov, A.V., Mora, L., Buckingham, R.H., and Ehrenberg, M. (2002). Release of peptide promoted by the GGQ motif of class 1 release factors regulates the GTPase activity of RF3. *Mol Cell* *10*, 789-798.

Zeng, F., Chen, Y., Remis, J., Shekhar, M., Phillips, J.C., Tajkhorshid, E., and Jin, H. (2017). Structural basis of co-translational quality control by ArfA and RF2 bound to ribosome. *Nature*.

Zeng, F., and Jin, H. (2016). Peptide release promoted by methylated RF2 and ArfA in nonstop translation is achieved by an induced-fit mechanism. *RNA* *22*, 49-60.

Zeng, F., and Jin, H. (2018). Conformation of methylated GGQ in the Peptidyl Transferase Center during Translation Termination. *Scientific Reports* *8*, 2349.

Zhang, J., Ieong, K.-W., Johansson, M., and Ehrenberg, M. (2015a). Accuracy of initial codon selection by aminoacyl-tRNAs on the mRNA-programmed bacterial ribosome. *Proceedings of the National Academy of Sciences* *112*, 9602.

Zhang, J., Pan, X., Yan, K., Sun, S., Gao, N., and Sui, S.-F. (2015b). Mechanisms of ribosome stalling by SecM at multiple elongation steps. *eLife* *4*, e09684.

Zhou, D., Tanzawa, T., Lin, J., and Gagnon, M.G. (2019a). Structural Basis for Ribosome Recycling by RRF and tRNA. *Nature Structural & Molecular Biology*.

Zhou, J., Lancaster, L., Donohue, J.P., and Noller, H.F. (2013). Crystal Structures of EF-G–Ribosome Complexes Trapped in Intermediate States of Translocation. *Science* *340*, 1236086.

Zhou, J., Lancaster, L., Donohue, J.P., and Noller, H.F. (2014). How the ribosome hands the A-site tRNA to the P site during EF-G–catalyzed translocation. *Science* *345*, 1188.

Zhou, J., Lancaster, L., Donohue, J.P., and Noller, H.F. (2019b). Spontaneous ribosomal translocation of mRNA and tRNAs into a chimeric hybrid state. *Proceedings of the National Academy of Sciences* *116*, 7813.

Zhou, J., Lancaster, L., Trakhanov, S., and Noller, H.F. (2012). Crystal structure of release factor RF3 trapped in the GTP state on a rotated conformation of the ribosome. *RNA* *18*, 230-240.

Zhouravleva, G., Frolova, L., Le Goff, X., Le Guellec, R., Inge-Vechtomov, S., Kisselev, L., and Philippe, M. (1995). Termination of translation in eukaryotes is governed by two interacting polypeptide chain release factors, eRF1 and eRF3. *EMBO J* *14*, 4065-4072.

Zoldak, G., Redecke, L., Svergun, D.I., Konarev, P.V., Voertler, C.S., Dobbek, H., Sedlak, E., and Sprinzl, M. (2007). Release factors 2 from *Escherichia coli* and *Thermus thermophilus*: structural, spectroscopic and microcalorimetric studies. *Nucleic Acids Res* *35*, 1343-1353.

## 6 Publications

### Accepted

Chan, K.H., Petrychenko, V., **Müller, C.**, Maracci, C., Holtkamp, W., Wilson, D.N., Fischer, N., and Rodnina, M.V. (accepted). Mechanism of Ribosome Rescue by Alternative Ribosome-Rescue Factor B. *Nature Communications*.

### 2019

Shimokawa-Chiba, N.\*, **Müller, C.\***, Fujiwara, K., Beckert, B., Ito, K., Wilson, D.N., and Chiba, S. (2019). Release factor-dependent ribosome rescue by BrfA in the Gram-positive bacterium *Bacillus subtilis*. *Nature Communications* *10*, 5397.

### 2017

Huter, P.\*, **Müller, C.\***, Beckert, B., Arenz, S., Berninghausen, O., Beckmann, R., and Wilson, D.N. (2017). Structural basis for ArfA-RF2-mediated translation termination on mRNAs lacking stop codons. *Nature* *541*, 546-549.

Huter, P., **Müller, C.**, Arenz, S., Beckert, B., and Wilson, D.N. (2017). Structural Basis for Ribosome Rescue in Bacteria. *Trends in Biochemical Sciences* *42*, 669-680.

\*these authors contributed equally to this work.

1 Peer review information: Nature Communications thanks the anonymous reviewers for their  
2 contribution to the peer review of this work. Peer reviewer reports are available.

3 **Mechanism of Ribosome Rescue by Alternative Ribosome-Rescue**

4 **Factor B**

5

6 Kai-Hsin Chan<sup>1</sup>, Valentyn Petrychenko<sup>2</sup>, Claudia Mueller<sup>3</sup>, Cristina Maracci<sup>1</sup>, Wolf Holtkamp<sup>1,4</sup>, Daniel  
7 N. Wilson<sup>3</sup>, Niels Fischer<sup>2\*</sup> and Marina V. Rodnina<sup>1\*</sup>

8

9 <sup>1</sup> Department of Physical Biochemistry, Max Planck Institute for Biophysical Chemistry, Am Fassberg  
10 11, 37077 Göttingen, Germany

11 <sup>2</sup> Department of Structural Dynamics, Max Planck Institute for Biophysical Chemistry, Am Fassberg  
12 11, 37077 Göttingen, Germany

13 <sup>3</sup> Institute for Biochemistry and Molecular Biology, University of Hamburg, Martin-Luther-King-Platz 6,  
14 20146 Hamburg, Germany

15 <sup>4</sup> Present address: Paul-Ehrlich-Institut, Paul-Ehrlich-Straße 51-59, 63225 Langen

16

17 \* Correspondence to: Niels Fischer (email: niels.fischer@mpibpc.mpg.de) and Marina V. Rodnina  
18 (email: rodnina@mpibpc.mpg.de)

19

20

21 **Abstract**

22 Alternative ribosome-rescue factor B (ArfB) rescues ribosomes stalled on non-stop mRNAs by  
23 releasing the nascent polypeptide from the peptidyl-tRNA. By rapid kinetics we show that ArfB  
24 selects ribosomes stalled on short truncated mRNAs, rather than on longer mRNAs mimicking  
25 pausing on rare codon clusters. In combination with cryo-EM we dissect the multistep rescue  
26 pathway of ArfB, which first binds to ribosomes very rapidly regardless of the mRNA length. The  
27 selectivity for shorter mRNAs arises from the subsequent slow engagement step, as it requires longer  
28 mRNA to shift to enable ArfB binding. Engagement results in specific interactions of the ArfB C-  
29 terminal domain with the mRNA entry channel, which activates peptidyl-tRNA hydrolysis by the N-  
30 terminal domain. These data reveal how protein dynamics translate into specificity of substrate  
31 recognition and provide insights into the action of a putative rescue factor in mitochondria.

32

33

34 **Introduction**

35 Rescue of ribosomes stalled on non-stop mRNAs is essential for most bacterial species<sup>1</sup>, and for  
36 mitochondrial translation in humans<sup>2,3</sup>. The lack of a stop codon causes ribosomes to stall at the 3'  
37 end of mRNAs, an event that is estimated to occur on 2-4% of translations in *Escherichia coli*<sup>4</sup>. The  
38 rescue systems tmRNA-SmpB, ArfA, and ArfB release the truncated translation product, allowing the  
39 ribosomes to be recycled for subsequent rounds of translation<sup>5</sup>. Among the rescue systems, only ArfB  
40 is able to induce polypeptide release independent of canonical termination factors<sup>6,7</sup>. ArfB is highly  
41 conserved among bacteria and has conserved homologs in eukaryotes from yeast to humans<sup>8</sup>. The  
42 eukaryotic homolog of ArfB, ICT1, is essential for cell viability and a candidate for non-stop ribosome  
43 rescue during translation in mitochondria<sup>2,3</sup>. Given the functional interchangeability and striking  
44 structural similarities between ArfB and ICT1<sup>9,10</sup>, studies of ArfB in bacteria may provide insights into  
45 how its homolog functions on the mitochondrial ribosome.

46 The cellular role of ArfB and the molecular mechanism of ArfB-mediated rescue are unclear.  
47 Under normal conditions in *E. coli*, ArfB appears redundant with tmRNA-SmpB and ArfA<sup>6</sup>. While  
48 tmRNA-SmpB and ArfA preferentially target ribosomes stalled on truncated mRNAs<sup>11-13</sup>, ArfB has  
49 been suggested to act on ribosomes stalled on mRNAs extending downstream past the P site<sup>7,14</sup>. If so,  
50 one potential function of ArfB could be to rescue ribosomes pausing on rare codon clusters<sup>7</sup>.  
51 However, another study indicated that ArfB does not rescue ribosomes stalled on longer mRNAs<sup>3</sup>.  
52 We note that the experimental conditions used in the two conflicting reports are similar in that they  
53 measured peptidyl-tRNA hydrolysis *in vitro* after long incubation times<sup>7</sup>, which does not probe the  
54 potential kinetic differences in ArfB activity.

55 The crystal structure of ArfB on the ribosome showed that ArfB consists of N- and C-terminal  
56 domains connected by a linker<sup>15</sup>. The globular N-terminal domain contains the conserved GGQ motif  
57 essential for catalysis of peptidyl-tRNA hydrolysis<sup>6,7</sup>. Its C-terminal tail, rich in positive residues, forms  
58 an  $\alpha$ -helix in the mRNA entry channel that would be incompatible with mRNA extending significantly  
59 past the P-site codon<sup>15</sup>. In solution, the linker region and at least parts of the C-terminal domain are

60 disordered giving rise to various orientations relative to the N-terminal domain<sup>10</sup>. Intrinsic disorder  
61 has been increasingly considered an important factor in understanding the dynamics of molecular  
62 recognition<sup>16-18</sup>. However, how the disordered regions of ArfB might contribute to recognition of its  
63 cellular targets is not known.

64 A comprehensive mutagenesis study identified ArfB residues that are important for ribosome  
65 binding and peptidyl-tRNA hydrolysis<sup>10</sup>. Remarkably, most of these essential amino acids are not  
66 located in the catalytic N-terminal domain, but in the C-terminal tail of ArfB. The crystal structure of  
67 ribosome-bound ArfB suggested that the C-terminal domain may function as a sensor for stalled  
68 ribosomes by inserting into the empty mRNA entry channel<sup>15</sup>, in apparent agreement with the  
69 mutational data. However, a detailed comparison of the structural and mutational data revealed  
70 dramatic discrepancies, as nearly all, except one, of the identified essential C-terminal ArfB residues  
71 were not involved in ribosome interactions in the crystal structure<sup>10,15</sup>, raising a question as to why  
72 these residues are crucial<sup>10</sup>.

73 In this study, we use a combination of rapid kinetics techniques and cryo-electron microscopy to  
74 dissect the kinetic and structural mechanism of ArfB action on the ribosome. The results provide  
75 insights into the physiologically-relevant targets of ArfB, establish a mechanistic model of ArfB-  
76 mediated ribosome rescue, and reveal the importance of ArfB dynamics in recognition of stalled  
77 ribosome complexes.

78

## 79 **Results**

### 80 **ArfB rescues ribosomes stalled on short truncated mRNAs**

81 We first used kinetic experiments in a fully reconstituted *in vitro* system to study whether the activity  
82 of ArfB depends on the length of the mRNA in the stalled ribosome complexes. We formed ribosome  
83 complexes with mRNAs of different length, let ribosomes translate the first two codons, and then  
84 stalled translation by omitting the aminoacyl-tRNA needed to decode the next codon. The resulting  
85 complexes contained [<sup>3</sup>H]fMet-[<sup>14</sup>C]Phe-tRNA<sup>Phe</sup> in the P site, no tRNA in the A site and an mRNA of

86 different lengths (0-99 nucleotides (nts)) extending past the P site, denoted as P+0 to P+99 (Fig. 1a).  
87 We rapidly mixed these stalled ribosomes with a large excess of purified ArfB and followed the time  
88 courses of peptidyl-tRNA hydrolysis by the quench-flow technique (Fig. 1b). When more than 9 nts of  
89 the mRNA extended past the P-site codon, the rate of hydrolysis reaction decreases sharply, by about  
90 15-fold (P+12) to 100-fold (P+99) (Fig. 1c), indicating that ArfB-mediated rescue is most efficient  
91 when the mRNA is short.

92 In the post-termination complex, the C-terminal domain of ArfB occupies the mRNA entry  
93 channel<sup>15</sup>, suggesting that mRNA extending past the P site inhibits ArfB-mediated ribosome rescue.  
94 To test whether a long mRNA overhang affects the selectivity of ArfB binding, we measured the  
95 steady-state parameters of the rescue pathway at conditions of ArfB turnover, i.e., at catalytic  
96 concentrations of ArfB and excess of the ribosomes. We chose the P+9 construct (i.e., with 9 nts  
97 extending past the P site), because this is the mRNA length for which we observe a significant, albeit  
98 reduced, ArfB activity. The Michaelis-Menten dependence of initial velocities yields the  $k_{cat}/K_M$  values  
99 of 0.04  $\mu\text{M}^{-1}\text{s}^{-1}$  and 0.003  $\mu\text{M}^{-1}\text{s}^{-1}$  for P+0 and P+9 complexes, respectively, indicating a 12-fold  
100 catalytic preference for ribosomes stalled on a shorter mRNA (Fig. 1d). The rate of ArfB turnover is  
101 quite low even for the P+0 complex, with  $k_{cat} = 0.01 \text{ s}^{-1}$ . RRF and EF-G, factors involved in post-  
102 termination ribosome recycling<sup>19</sup>, decrease ArfB residence time on the ribosome by up to 30%; RF3  
103 had very little effect (Fig. 1e).

104 A ribosome with a long mRNA presents a sense codon in the A site, which is much more likely to  
105 be read by a ternary complex EF-Tu–GTP–aminoacyl-tRNA, which is abundant in the cell, than recruit  
106 ArfB, which is expressed in only 0.5 copies per *E. coli* cell, in comparison to over 25,000 copies of  
107 RF1<sup>20</sup>. To study the effect of ternary complexes, we measured ArfB activity on ribosome complexes  
108 with [<sup>3</sup>H]fMet-tRNA<sup>fMet</sup> in the P site in the presence of EF-Tu–GTP–[<sup>14</sup>C]Phe-tRNA<sup>Phe</sup>, which is cognate  
109 for the second codon, using P+3 and P+33 mRNAs (Supplementary Fig. 1a). At high concentration,  
110 ArfB is able to impede dipeptide formation on P+3, but not on P+33 mRNA (Supplementary Fig. 1b),  
111 and, *vice versa*, ArfB-induced peptide release does not occur on P+33 complexes in the presence of

112 cognate ternary complex (Supplementary Fig. 1c). ArfB can release fMet from P+33 only when  
113 cognate ternary complexes are completely absent, e.g. in the presence of non-cognate ternary  
114 complex alone (EF-Tu–GTP–Val-tRNA<sup>Val</sup>) (Supplemental Fig. 1d).

115

116 **Structural mechanism of ribosome rescue by ArfB**

117 In order to understand how longer mRNAs affect ArfB-mediated rescue, we determined the cryo-EM  
118 structures of ArfB bound to P+0 and P+9 *E. coli* ribosome complexes (Fig. 2, Supplementary Fig. 2 and  
119 Supplementary Table 1). To stabilize ArfB on the ribosome, we used the antimicrobial peptide  
120 apidaecin-137 (Api137), which is known to trap canonical RFs on the ribosome<sup>21,22</sup>. Similarly to RFs,  
121 Api137 stalls ArfB after one round of peptide hydrolysis (Supplementary Fig. 2a). The cryo-EM  
122 particle images were sorted *in silico* for ArfB occupancy and ribosome conformation yielding cryo-EM  
123 maps for the major states of P+0 and P+9 complexes at 3.7 Å and 2.6 Å resolution, respectively  
124 (Supplementary Fig. 2c-e). The two structures are virtually identical within the error of resolution and  
125 depict ArfB bound to the ribosome in the post-hydrolysis state with Api137 and deacylated tRNA<sup>Phe</sup> in  
126 the P site (Fig. 2a). ArfB extends from the mRNA entry channel of the 30S subunit to the peptidyl  
127 transferase center on the 50S subunit. The N-terminal domain is bound to the A-site of the 50S  
128 subunit, whereas the C-terminal domain of ArfB folds into an  $\alpha$ -helix that occupies the A-site and  
129 mRNA entry channel on the 30S subunit. The absence of mRNA density past the P site codon in the  
130 P+9 state suggests that ArfB has displaced the mRNA 3' extension from the mRNA entry channel. The  
131 mRNA is intact under these conditions (Supplementary Fig. 2b), indicating that the A-site overhang  
132 must have become disordered to allow accommodation of ArfB into the mRNA entry channel.

133 In the PTC, Gln28 in the universally conserved catalytic GGQ motif of ArfB retains a conformation  
134 poised for peptidyl-tRNA hydrolysis, which is stabilized by interaction with Api137 (Supplementary  
135 Fig. 2c). The structural details of stalling by Api137 are very similar for ArfB and the canonical RFs<sup>21,22</sup>  
136 (Supplementary Fig. 2c). In both cases, Api137 mimics a nascent peptide chain in the post-hydrolysis  
137 state. Api137's C-terminal hydroxyl group interacts with the ribose hydroxyls at position A76 of the P-

138 site tRNA, thereby stabilizing the tRNA in the PTC. The penultimate Arg17 of Api137 traps the GQG  
139 motif in an active conformation via the guanidinium group that interacts with the side chain carbonyl  
140 group of Gln28.

141 The higher number of cryo-EM particles acquired for the P+9 complex allowed us to visualize  
142 additional intermediates of ribosome rescue: (i) a 3.1 Å map of the pre-hydrolysis complex prior to  
143 ArfB binding, with fMetPhe-tRNA<sup>Phe</sup> in the P-site, no Api137, and a clear density for the 9-nucleotide  
144 3' extension of the mRNA occupying the mRNA entry channel; and (ii) a 3.2 Å map of a minor fraction  
145 of ribosomes in a post-hydrolysis state with ArfB and Api137 bound and deacylated tRNA<sup>Phe</sup> in the  
146 hybrid P/E state (Supplementary Fig. 2f). Because the post-hydrolysis state is structurally very similar  
147 with P+0 and P+9 mRNAs, in the following we generally refer to the 2.6 Å cryo-EM structure of the  
148 P+9 complex as the major P/P post-hydrolysis state.

149

#### 150 **Essential ArfB–ribosome interactions**

151 The present 2.6 Å cryo-EM map shows how ArfB interacts with the ribosome in the post-hydrolysis  
152 complex. The density for ArfB, in particular in the C-terminal domain, is significantly better in the  
153 cryo-EM structure than in the previous crystal structure<sup>15</sup>, which allowed us to improve model  
154 accuracy, including register shifts in the N- and C-terminal domains (Supplementary Fig. 3a). In  
155 agreement with mutational data, the cryo-EM-based model shows that the essential residues Arg105,  
156 Arg118, Leu119, Lys122, Lys129, and Arg132 form intricate side chain contacts with the ribosomal  
157 RNA (rRNA), whereas most non-essential side chains that are not involved in any interactions are less  
158 well-resolved (Fig. 3a and Supplementary Fig. 3b). The essential positively charged amino acids  
159 interact via their guanidinium and ε-amino groups with negatively charged groups of 16S rRNA (and  
160 23S rRNA for Arg105), whereas the hydrophobic Leu119 stacks with its isobutyl group onto the  
161 guanine of G530. Moreover, the key functional residues, Lys129 and Arg132, also show the most  
162 intricate interactions. For instance, the side chain of Arg132 alone forms 6 non-covalent interactions;  
163 mutating Arg132 even to a Lys completely abolishes catalysis, whereas the binding to the ribosome is

164 reduced by 2-fold only<sup>10</sup>. Notably, the network of ArfB–16S rRNA interactions that we observe in the  
165 major P/P post-hydrolysis state appears to be very stable and persists upon 30S subunit rotation, as  
166 evident from the comparison with the minor P/E post-hydrolysis state (Fig. 3b).

167 To further understand the nature of the ArfB-ribosome interactions and probe them not only in  
168 the post-hydrolysis state revealed by the cryo-EM, but also in the pre-hydrolysis state, we studied the  
169 effect of monovalent (KCl) and divalent ( $MgCl_2$ ) ions on ArfB binding to P+0 and P+9 complexes (Fig.  
170 3c,d). To capture the factor in the pre-hydrolysis state, we used ArfB<sub>GAQ</sub>(Flu), a hydrolysis-deficient  
171 ArfB mutant (Gly27 to Ala), with a fluorescein attached at position 96 (Supplementary Fig. 4a-c).  
172 Binding to the ribosome is monitored as an increase of the fluorescein anisotropy. The binding is salt-  
173 sensitive, indicating that electrostatic interactions play an important role (Fig. 3d). However, at ionic  
174 strength within the physiological range<sup>23</sup> the binding of ArfB is not perturbed, as the inhibitory  
175 concentration  $IC_{50}$  for the P+0 complex is ~260 mM for KCl and ~40 mM for  $MgCl_2$ . Thus, ArfB binding  
176 is not mediated by unspecific electrostatic interactions, but rather by strong side chain-specific  
177 interactions such as those we observe in the cryo-EM structure. For the P+9 complex, the tendency is  
178 similar, but the  $IC_{50}$  value for  $Mg^{2+}$  is somewhat lower (~30 mM) than for the P+0 complex, indicating  
179 a difference in binding stabilities (Fig. 3d). We also measured the effect of  $Mg^{2+}$  on peptidyl-tRNA  
180 hydrolysis (Fig. 3e). At high ArfB concentrations, hydrolysis is not affected by  $Mg^{2+}$  demonstrating  
181 that  $Mg^{2+}$  ions do not affect the chemistry step itself. Taken together, our cryo-EM data and binding  
182 measurements, as well as the published mutagenesis data<sup>10</sup>, strongly suggest that the essential C-  
183 terminal residues of ArfB play a major role in specifically stabilizing the catalytically active state of the  
184 ArfB-ribosome complex.

185

#### 186 **Kinetics of ArfB initial binding followed by engagement**

187 Because ArfB attains very similar conformations on P+0 and on P+9 post-hydrolysis complexes, we  
188 sought to identify a potential mRNA discrimination step prior to hydrolysis. First, we monitored ArfB  
189 binding to the ribosome by fluorescence resonance energy transfer (FRET) using a donor-acceptor

190 pair with a fluorescein-labeled tRNA in the P site and a fluorescence quencher-labeled ArfB  
191 (ArfB(540Q)) (Fig. 4a); the respective ribosome complexes are denoted P+0(Flu), P+9(Flu), and  
192 P+30(Flu). The activity of the labeled components is not affected by fluorescence labeling  
193 (Supplementary Fig. 4d). The experiments were carried out at 20°C, because at 37°C the binding was  
194 too fast to measure by the stopped-flow technique.

195 Binding of ArfB(540Q) to P+0(Flu) (Supplementary Fig. 4e), P+9(Flu) (Fig. 4b) or P+30(Flu) results  
196 in fluorescence quenching due to proximity of the quencher to the fluorophore. To determine the  
197 association and dissociation rate constants, we measured the kinetics of binding at increasing  
198 concentrations of ArfB(540Q) in excess over a constant concentration of labeled ribosome complexes.  
199 Exponential fitting of the resulting time courses yields three distinct apparent rate constants,  
200 indicative of three binding phases (Fig. 4c and Supplementary Fig. 4e,f). With P+0, P+9, or P+30  
201 complexes, the predominant phase contributing up to 80% of the observed FRET change is very rapid;  
202 the two slower phases together contribute about 20% of the FRET change (Fig. 4c, Supplementary Fig.  
203 4e,f and Supplementary Table 2). In a simplest model, if the rapid phase reports on the association of  
204 ArfB to the ribosome, and the slower phases represent subsequent rearrangement steps, the  
205 concentration dependence of the apparent rate constants is expected to be linear for the rapid  
206 phase and hyperbolic for the slower phases. Surprisingly, this turned out not to be the case; rather,  
207 all three apparent rate constants increased linearly with concentration (Fig. 4c and Supplementary  
208 Fig. 4f), indicating that all phases reflect binding, albeit apparently for different ArfB populations. We  
209 then estimated the rate constants of binding ( $k_{ON}$ ) and dissociation ( $k_{OFF}$ ) for the predominant rapid  
210 phase, which represent the values for the majority of ArfB molecules (Fig. 4c). The binding is very  
211 rapid with  $k_{ON}$  of  $\sim 500 \mu\text{M}^{-1}\text{s}^{-1}$  for P+0 and  $\sim 300 \mu\text{M}^{-1}\text{s}^{-1}$  for P+9 and P+30. The initial binding complex  
212 is labile, with  $k_{OFF}$  of  $\sim 110 \text{ s}^{-1}$ ,  $\sim 140 \text{ s}^{-1}$ , and  $\sim 120 \text{ s}^{-1}$  for P+0, P+9, and P+30, respectively, which shows  
213 that the initial binding is independent of the mRNA length. The high values of the  $k_{ON}$  and  $k_{OFF}$   
214 independent of the mRNA length suggest a scanning step where ArfB rapidly binds to and can  
215 dissociate from ribosomes regardless of whether the mRNA entry channel is occupied or not.

216 To understand the nature of the rapid association step, we tested the effect of Mg<sup>2+</sup>  
217 concentrations (Supplementary Fig. 4g). We have chosen Mg<sup>2+</sup> rather than monovalent cations,  
218 because Mg<sup>2+</sup> disrupts rapid unspecific binding of IF3 to the ribosome<sup>24</sup>; binding of ArfB to the  
219 ribosome may be driven by similar interactions. However, ArfB association with the ribosome is not  
220 affected by high ion concentrations (Supplementary Fig. 4h), which suggests that the initial binding is  
221 not driven by electrostatic interactions.

222 Given that the initial binding is insensitive to the mRNA length, a subsequent step must account  
223 for the observed inhibition of peptidyl-tRNA hydrolysis with the long mRNAs (Fig. 1c). In a simplest  
224 model, the rate of the chemistry step itself may depend on the mRNA length, i.e. due to  
225 misalignment in the transition state. At saturating concentrations of ArfB, the rate of hydrolysis is  
226 ~0.15 s<sup>-1</sup> on P+0 complexes, and 0.06 s<sup>-1</sup> on P+9 complexes (Fig. 4d,e and Supplementary Fig. 4i). If  
227 the measured rate reflected the chemistry step, it is expected to be pH-dependent, as previous  
228 experiments on the kinetics of peptidyl-tRNA hydrolysis by RF1 and RF2 revealed a strong pH  
229 dependence of the reaction<sup>25,26</sup>. However, for the ArfB-catalyzed reaction, the hydrolysis rate is  
230 identical at pH 6.8, 7.4 and 8.0 for both P+0 and P+9 complexes (Supplementary Fig. 4j). This strongly  
231 suggests that hydrolysis is rate-limited by a step after initial binding, but preceding the chemistry  
232 step. The rate of this additional step, which we call an engagement step, depends on the mRNA  
233 length (Fig. 4e), whereas the subsequent chemistry step itself must be faster than engagement.

234 To measure the stability of ArfB binding to stalled ribosomes prior to peptidyl-tRNA hydrolysis  
235 we used ArfB<sub>GAQ</sub> and a FRET pair described above (Fig. 4f and Supplementary Fig. 4b). We formed  
236 complexes of ArfB<sub>GAQ</sub>(540Q) with P+0(Flu), P+9(Flu), or P+30(Flu), and then rapidly mixed them with a  
237 10-fold excess of unlabeled P+0 complexes. Fluorescence increase over time reports on the  
238 dissociation of ArfB<sub>GAQ</sub>(540Q) from the ribosome (Fig. 4f). Exponential fitting of the time courses  
239 (Methods) required a minimum of two dissociation steps, a slow one with a rate constant of 0.04 s<sup>-1</sup>  
240 (P+0), 0.07 s<sup>-1</sup> (P+9) or 0.1 s<sup>-1</sup> (P+30) and a faster one of about 0.4 s<sup>-1</sup>, i.e. the dissociation rates are  
241 similar for the three complexes (Supplementary Table 3). The difference is in the fraction of the slow

242 vs. fast steps, with about 80% of P+0 compared to 50%-40% of P+9 and P+30 complexes dissociating  
243 slowly, as indicated by the proportion of the fluorescence change amplitude for each step. The slowly  
244 dissociating population likely represents the complexes captured by cryo-EM; hence the similar  
245 conformation of P+0 and P+9. The population of complexes that dissociate more rapidly may  
246 represent either a step before the full engagement of ArfB, i.e. when not all interactions of ArfB with  
247 the ribosome are formed, or a heterogeneity within the ribosome complexes, with a larger  
248 proportion of rapidly dissociating complexes when the mRNA is long. As we cannot distinguish  
249 between these two possibilities, we report average dissociation rate constants of  $0.06\text{ s}^{-1}$ ,  $0.23\text{ s}^{-1}$ ,  
250 and  $0.33\text{ s}^{-1}$  for P+0, P+9, and P+30, respectively, which is a characteristic of the ensemble as a whole.  
251 In summary, our rapid kinetics analysis identifies an engagement step prior to peptidyl-tRNA  
252 hydrolysis that results in a selective stabilization and more rapid rescue reaction for those complexes  
253 that have a short truncated mRNA.

254

## 255 **Discussion**

256 Our rapid kinetics analysis shows that ribosomes stalled on short truncated mRNAs are the  
257 physiologically relevant substrate for ArfB-dependent rescue. The residual ArfB activity is  
258 substantially reduced when the mRNA exceeds the P-site codon by more than 6 nts. When the mRNA  
259 is long, ArfB is unable to compete with cognate ternary complexes and can rescue the ribosomes only  
260 if a cognate ternary complex is absent. This is, however, not a realistic scenario *in vivo*, because in  
261 bacteria the codon frequency correlates with aa-tRNA abundance, i.e. some aa-tRNA are rare but not  
262 missing. Even if aa-tRNA pools are exhausted, e.g. by starvation, the concentrations of rare tRNAs  
263 isoacceptors are less responsive to starvation conditions than those of abundant tRNAs<sup>27</sup>. Thus, at  
264 cellular concentrations, ArfB activity is too low to interfere with on-going translation of long mRNAs.  
265 We therefore conclude that a role for ArfB in rescuing ribosomes that pause at a rare codon cluster is  
266 unlikely; rather, ArfB acts on complexes containing an mRNA truncated just past the P site.

267 In the context of ribosome rescue in *E. coli*, the specific role of ArfB remains unclear, as ArfB has  
268 the same preference for ribosomes stalled on short mRNAs as tmRNA-SmpB and ArfA<sup>11-13</sup>. As  
269 suggested earlier, ArfB may be simply not as crucial in *E. coli* as in other species that lack one or both  
270 of the other rescue systems<sup>5</sup>. Notably, its human homolog ICT1 is the only rescue factor that is found  
271 in eukaryotic mitochondria<sup>8</sup>. The exact function of ICT1 is unclear, because it is also found as an  
272 integral protein of the large ribosomal subunit, mL62<sup>28,29</sup>. The activity of ICT1 as a peptidyl-tRNA  
273 hydrolase is essential for cell viability<sup>2,3</sup>, and some studies have proposed that ICT1 catalyzes  
274 termination on mitochondrial transcripts with non-canonical stop codons AGA and AGG<sup>30,31</sup>.  
275 Assuming that ArfB and ICT1 have a similar preference for mRNA with short overhangs, a role for  
276 termination seems unlikely, as the mRNAs in question extend 14 nucleotides past the A site<sup>32,33</sup>, a  
277 length at which ArfB activity is drastically reduced. On the other hand, mitochondrial mRNAs are  
278 polyadenylated, with polyadenylation playing transcript-dependent roles in regulating protein  
279 synthesis<sup>34,35</sup>. The sensitivity to mRNA length could create interesting opportunities for regulation of  
280 translation and mRNA stability in mitochondria by ICT1.

281 Our biochemical and structural data reveal the mechanism of ArfB-mediated ribosome-rescue. In  
282 combination with the reported solution structures of free ArfB, we propose a structural model  
283 explaining the rapid mRNA-independent initial binding and subsequent mRNA-dependent  
284 engagement step of ArfB. Structures of free ArfB<sup>10</sup> and of its human ortholog ICT1<sup>9</sup> determined by  
285 NMR indicate that in solution the linker and C-terminal domains of the two factors are largely  
286 disordered, whereas the structures of their catalytic N-terminal domains are similar to that in the  
287 ribosome-bound state and only the catalytic GGQ motif itself is disordered. The structure of the  
288 linker determines the relative orientation of the N- and C-terminal domains, indicating that in  
289 solution the molecule is highly dynamic due to the linker flexibility. To understand how this  
290 heterogeneous ensemble of conformers binds to the ribosome, in particular with an mRNA  
291 occupying the entry channel, we docked the structures of the NMR ensemble of free ArfB onto the  
292 P+9 complex using the N-terminal domain for orientation (Fig. 5a). The resulting model provides a

293 simple explanation for the kinetic data (Fig. 5b). If an ArfB molecule initially docks onto the ribosome  
294 through the contact between the ArfB N-terminal domain and the 50S subunit, the interdomain  
295 linker would be flexible enough to accommodate the C-terminal domain into the intersubunit space.  
296 The positively charged C-terminal tail may form unspecific interactions with the negatively charged  
297 ribosomal RNA backbone at this stage. Most importantly, such initial docking does not require the  
298 mRNA to move out of the entry channel, explaining why the rapid initial binding of ArfB is  
299 independent of the mRNA length. The theoretical encounter frequency<sup>36</sup> for ArfB and the ribosome is  
300  $\sim 9 \times 10^9 \text{ M}^{-1} \text{s}^{-1}$ , whereas the  $k_{\text{ON}}$  for the major fraction of ArfB molecules is  $5 \times 10^8 \mu\text{M}^{-1} \text{s}^{-1}$ . This  
301 difference may suggest that for a fraction of ArfB molecules ( $\sim 10\%$ ) arriving in an optimal orientation,  
302 the reaction is diffusion controlled, whereas the majority of molecules require several attempts  
303 before docking, which slows down the effective association. The remaining small fraction of ArfB  
304 molecules that bind even slower (Supplementary Fig. 4f) may arise from those ArfB conformations  
305 where the C-terminal domain clashes with the ribosome and is too slow to rearrange. At this step, no  
306 catalytic activation takes place in agreement with the disordered GGQ motif in the NMR structures.

307 In the subsequent engagement step, docking of the C-terminal tail into the mRNA channel  
308 requires movement of the A-site mRNA extension out of the channel, consistent with the notion that  
309 the engagement is substantially slower for a longer mRNA. However the rate of engagement is also  
310 low with the P+0 mRNA, which may be due to the slow ordering and accommodation of the ArfB C-  
311 terminal domain into the mRNA channel. The favorable enthalpic contribution of forming specific  
312 interactions with the ribosome may be offset by the entropic cost of folding of the C-terminal domain.  
313 In contrast to the initial binding, the engagement step is salt sensitive, suggesting an important role  
314 of electrostatic interactions. The pliability of the flexible linker region would allow the basic C-  
315 terminal domain to fit into the intersubunit space, possibly guided by electrostatic steering by the  
316 acidic phosphate backbone of the ribosome. ArfB C-terminal domain forms a network of hydrogen  
317 bonds and stacking interactions with key residues in the decoding center of the ribosome. Many of  
318 these interactions are electrostatic in nature and very stable at physiological salt concentrations.

319 Once ArfB has been fully accommodated into the mRNA channel, catalysis is rapid, in agreement with  
320 the similar structures for the P+0 and P+9 post-hydrolysis states. Previous work has shown that the  
321 N-terminal domain on its own cannot hydrolyze peptidyl-tRNA<sup>10</sup>. This is consistent with the key role  
322 of the ArfB interdomain linker in activating its hydrolytic activity; how exactly the folding and binding  
323 of the C-terminal domain activates peptidyl-tRNA hydrolysis more than 40 Å away remains unknown.

324 Our kinetic and structural data explain why ArfB is more active when the mRNA extension is  
325 short. The steady-state kinetic data indicate that the specificity of ArfB binding ( $k_{cat}/K_M$ ) is decreased  
326 by >10-fold when the mRNA extension post the P-site codon exceeds 9 nucleotides. The lower  
327 catalytic activity of ArfB is due to the slower engagement step and to a smaller fraction of molecules  
328 that are stabilized in the catalytically active conformation. Overall, ArfB follows the same strategy to  
329 select for the rescue substrates as ArfA–RF2<sup>37–41</sup>: they activate peptide release only after the mRNA-  
330 sensing domain is accommodated in the mRNA channel on the 30S subunit.

331 After peptidyl-tRNA hydrolysis and peptide release, the ArfB–ribosome complex adopts a  
332 rotated conformation with tRNA in a hybrid state. The flexible linker domain of ArfB allows both ArfB  
333 domains to retain their interactions with the 50S and 30S subunits. This may explain why turnover of  
334 ArfB is slow compared to other factors interacting with the ribosome: while rotation of the ribosomal  
335 subunits destabilizes RF1 and RF2 binding to the ribosome<sup>42</sup>, ArfB retains its tight interactions in the  
336 non-rotated and rotated state. The  $k_{cat}$  value of 0.01 s<sup>-1</sup> is much lower than the single-round  
337 hydrolysis rate of 0.15 s<sup>-1</sup> for the P+0 complex, suggesting that for short truncated mRNAs the overall  
338 ArfB cycle is limited by ArfB dissociation. The tight interactions that persist after peptide hydrolysis  
339 likely contribute to the slow dissociation rate, which may encompass the rates for unbinding as well  
340 as unfolding of the ArfB C-terminal domain. With the longer mRNA constructs, where the rate of  
341 hydrolysis is low, engagement of ArfB might become the rate-limiting step. The presence of recycling  
342 factors RRF and EF-G may accelerate turnover by precluding ArfB from unproductively binding to  
343 post-termination ribosomes. Whether additional factors are required to disengage the tight binding  
344 of ArfB to the ribosome after peptide release is unclear at present.

345 In conclusion, our studies show how protein dynamics contributes to molecular recognition and  
346 discrimination in a large ribonucleoprotein complex. The disordered linker region of ArfB helps the  
347 factor to rapidly dock and scan the state of the mRNA on the ribosome, and to select the right  
348 substrate. The linker also guides the C-terminal domain into its confined binding pocket in the mRNA  
349 entry channel and helps the factor to adjust to different ribosome conformations. Binding of the C-  
350 terminal domain is stabilized by specific electrostatic interactions that define the shape of ArfB in the  
351 complex and ultimately lead to catalytic activation of the GGQ motif in the N-terminal domain. Thus,  
352 flexibility allows ArfB to bind rapidly and non-specifically to its target first, followed by ordering of  
353 the C-terminal domain and formation of tight specific interactions, as has been suggested for  
354 dynamic, intrinsically disordered proteins<sup>18,43</sup>.

355 **Methods**

356 **Reconstitution of stalled ribosome complexes**

357 All experiments were carried out in HKM<sub>7</sub> buffer (50 mM HEPES pH 7.4, 30 mM KCl, 7 mM MgCl<sub>2</sub>)  
358 unless otherwise stated. 70S ribosomes from *E. coli* MRE600, IF1, IF2, IF3, EF-Tu, EF-G, RRF, f[<sup>3</sup>H]Met-  
359 tRNA<sup>fMet</sup>, [<sup>14</sup>C]Phe-tRNA<sup>Phe</sup>, and [<sup>14</sup>C]Phe-tRNA<sup>Phe</sup>(Flu) were prepared using published protocols<sup>44-46</sup>.  
360 [<sup>14</sup>C]Phe-tRNA<sup>Phe</sup>(Flu) is labeled with fluorescein at thioU8. Truncated mRNAs of varying length were  
361 *in vitro* transcribed using T7 RNA-polymerase from a T7 promoter on a DNA template derived from  
362 the *E. coli* *lepB* gene with the second codon mutated to encode phenylalanine, then purified over a  
363 HiTrap Q HP column.

364 Stalled ribosome complexes were prepared by translating the first two codons on truncated  
365 mRNAs using published protocols<sup>47,48</sup>. Briefly, 70S ribosomes were mixed with 1.5-fold excess of  
366 initiation factors, 3-fold excess of f[<sup>3</sup>H]Met-tRNA<sup>fMet</sup>, and 3-fold excess of mRNA in HAKM<sub>7</sub> buffer  
367 (HAKM<sub>7</sub> buffer supplemented with 70 mM NH<sub>4</sub>Cl) containing 1 mM dithiothreitol (DTT) and 1 mM GTP,  
368 and incubated for 45 min at 37°C. Initiation efficiency, determined by nitrocellulose filtration and  
369 scintillation counting using QuantaSmart (Perkin Elmer), was >90% for all mRNAs. Ternary complexes  
370 were formed with 3-fold excess of [<sup>14</sup>C]Phe-tRNA<sup>Phe</sup> or [<sup>14</sup>C]Phe-tRNA<sup>Phe</sup>(Flu) over ribosomes and 1.5  
371 μM EF-G, and a 2-fold excess of EF-Tu incubated with 1 mM GTP, 3 mM phosphoenolpyruvate (PEP),  
372 and 0.5 mg mL<sup>-1</sup> pyruvate kinase in HAKM<sub>7</sub> buffer for 15 min at 37° C. To form P+0 complexes,  
373 initiation complexes (IC) were mixed with ternary complex for 2 min at room temperature to  
374 translate the second codon. To form P+n complexes (n = 3, 6, 9, 12, 15, 24, 30, 99), the ribosomes  
375 were supplied with the same ternary complex so that the ribosome is stalled with the second codon  
376 of the mRNA in the P site. The resulting complexes were purified by ultracentrifugation over a  
377 cushion of 1.1 M sucrose in HAKM<sub>20</sub> buffer (HAKM<sub>7</sub> buffer containing 20 mM MgCl<sub>2</sub>). The pellets were  
378 resuspended in HAKM<sub>7</sub> buffer and quantified by liquid-liquid scintillation counting, then flash frozen  
379 and stored at -80°C. Dipeptide formation under these conditions was at least 80%.

380

381 **ArfB purification**

382 The sequence of the *yaeJ* gene encoding ArfB was cloned from *E. coli* K12 strain into a vector carrying  
383 an N terminal 6xHis tag followed by a SUMO tag. Overexpression and cell lysis were carried out using  
384 a published protocol<sup>15</sup>. Tagged ArfB was isolated from the cell lysate by incubation with Ni-IDA beads  
385 in buffer A (40 mM HEPES pH 7, 300 mM KCl, 7 mM MgCl<sub>2</sub>, and 10 mM β-mercaptoethanol) for 1 h at  
386 4°C. Following elution with buffer A supplemented with 600 mM imidazole, fractions containing ArfB  
387 were dialyzed into buffer A overnight at 4°C in the presence of Ulp1 protease to cleave the SUMO tag.  
388 Untagged ArfB was further purified via cation-exchange chromatography over a HiTrap HP SP column.  
389 ArfB concentration was determined by comparing SDS-PAGE band intensities to a standard curve  
390 generated by known amounts of IF3 that was run on the same gel. For fluorescence-labeled ArfB,  
391 amino acid residues at positions 96 and 112 were changed to cysteine, and labeled with a thiol-  
392 reactive fluorescein or ATTO540Q using established protocols<sup>46</sup>. Free dye was removed using a PD  
393 MidiTrap G-25 column (GE Healthcare). Labeling efficiency, estimated by absorbance measurements  
394 of the dye and SDS-PAGE based estimation of protein concentration, was approximately 60%.

395

396 **Hydrolysis assays**

397 Single-round peptidyl-tRNA hydrolysis were monitored by rapidly mixing P+O complexes and ArfB in a  
398 quenched-flow apparatus at 37°C. Released peptides were quantified using a published protocol<sup>21</sup>:  
399 at each time point, the reaction was stopped by adding a quenching solution of chilled 10%  
400 trichloroacetic acid (TCA) and 50% ethanol. The samples were kept on ice for 30 min, then the  
401 precipitated ribosomes and peptidyl-tRNA were spun down for 15 min at 16,000 x g at 4°C. The  
402 released peptides in the supernatant were quantified by liquid-liquid scintillation counting. Time  
403 courses were evaluated by exponential fitting in GraphPad Prism using one or two exponential terms,  
404 depending on the ArfB concentration used. For high ArfB concentrations, one exponential fitting was  
405 sufficient. At low ArfB compared to the ribosome concentration (Fig. 4d), the first reaction round was  
406 successful only on a fraction of ribosomes and the completion of the reaction required multiple

407 rounds of ArfB binding, which results in two-exponential behavior; of the two apparent rate  
408 constants, the faster represents the single-round rate constant.

409       Multiple turnover peptidyl-tRNA hydrolysis was measured at 37°C by incubating ArfB with at  
410 least 10-fold excess of stalled ribosome complex. At each time point, an aliquot of the mixture was  
411 quenched as described above. Initial velocity of the reaction was calculated as the slope of the linear  
412 fit of the time course, after subtracting background peptide drop-off, as measured in a parallel  
413 reaction without ArfB. Michaelis-Menten constants  $k_{cat}$ ,  $K_M$  and  $k_{cat}/K_M$  were calculated from the  
414 hyperbolic fit of initial velocity plotted against substrate concentration. To assess the effect of  
415 translation factors on ArfB turnover, the HKM<sub>7</sub> buffer was supplemented with 3 mM PEP, 1 mM GTP,  
416 and 1 mg mL<sup>-1</sup> pyruvate kinase. Initial velocities of the hydrolysis reaction were measured in the  
417 presence of RF3, RRF, and EF-G.

418

419 **ArfB activity assay in the presence of elongation factors**

420 To observe the interplay between ArfB and ongoing translation, initiation complexes termed P+3 and  
421 P+33 were prepared as described above, albeit without the addition of ternary complex. ArfB (0.3  
422  $\mu$ M or 2  $\mu$ M) was mixed with IC (0.5  $\mu$ M) and ternary complex (0.25  $\mu$ M EF-Tu, 1  $\mu$ M [<sup>14</sup>C]Phe-tRNA<sup>Phe</sup>,  
423 1 mg mL<sup>-1</sup> pyruvate kinase, 3 mM PEP, and 1 mM GTP) and incubated at 37°C for 120 s. Each reaction  
424 was run twice, with one sample quenched with 0.1x sample volume 5M potassium hydroxide (KOH)  
425 then hydrolyzed for 30 min at 37°C, and subsequently used to quantify the amount of dipeptides  
426 formed. The other sample was quenched with 500  $\mu$ L 10% TCA and 50% ethanol, and processed to  
427 quantify the amount of [<sup>3</sup>H]fMet released.

428       Dipeptides were quantified using a published protocol <sup>50</sup>. Briefly, the samples quenched with  
429 KOH were neutralized with acetic acid and analyzed by reversed phase HPLC (Chromolith RP8 100-4.6  
430 mm column, Merck), over a 0-65% acetonitrile gradient in 0.1% TFA. Fractions were analyzed by  
431 scintillation counting, with the fractions containing both <sup>3</sup>H and <sup>14</sup>C counts identified as dipeptide-  
432 containing fractions.

433 Hydrolysis in the presence of non-cognate ternary complex was measured at 37°C. Non-cognate  
434 ternary complex (TC) was formed for 15 min at 37°C with 10  $\mu$ M EF-Tu, 5  $\mu$ M Val-tRNA<sup>Val</sup>, 0.5 mg mL<sup>-1</sup>  
435 pyruvate kinase, 1.5 mM PEP, and 0.5 mM GTP (all concentrations reflect final concentrations in the  
436 experiment). TC was mixed with an equal volume of purified P+3 or P+33 in the presence of 0.1  $\mu$ M  
437 ArfB and 2  $\mu$ M ArfB, respectively. To assess the effect of translocation on hydrolysis, 2  $\mu$ M EF-G was  
438 also added to a set of samples. Aliquots were taken at time points up to 5 minutes, then processed to  
439 quantify the released peptides.

440

441 **Pre-steady state binding assays**

442 All stopped flow experiments were performed at 20°C, with an excitation wavelength of 465 nm and  
443 a KV500 cutoff filter (Schott), and using an SX-20MV stopped flow machine (Applied Photophysics).  
444 Fluorescence data was collected using Pro-Data SX (Applied Photophysics). For the binding reaction,  
445 equal volumes of ArfB(540Q) labeled at position 96 and P+0(Flu) complex were rapidly mixed to a  
446 final concentration of 0.05  $\mu$ M, 0.1  $\mu$ M, 0.2  $\mu$ M, 0.3  $\mu$ M, 0.4  $\mu$ M, and 0.5  $\mu$ M ArfB, and 0.015  $\mu$ M  
447 P+0(Flu) complex. Fluorescence quenching was recorded over time. For the pre-hydrolysis  
448 dissociation reaction, 0.2  $\mu$ M ArfB<sub>GAQ</sub>(540Q) was incubated with 0.03  $\mu$ M P+0(Flu) for 1 min at room  
449 temperature to form the complex, then rapidly mixed with an equal volume of 2  $\mu$ M unlabeled P+0  
450 complex. Recovery of fluorescence following dissociation of the quencher-labeled ArfB was recorded  
451 over time. The resulting time courses were fit with exponential equations using GraphPad Prism.  
452 Average dissociation rate constants were calculated by summation of the product of the apparent  
453 rate and the amplitude of each exponent. All fluorescence traces were then normalized by the  
454 highest level of fluorescence as extrapolated by the fit.

455 While the rates are clearly different for the P+0 and P+9 or P+30 complexes, we note that for  
456 technical reasons the dissociation rate constants were measured at 20°C, whereas the single- and  
457 multiple-turnover hydrolysis rates are measured at physiological temperature. Thus, the measured  
458 dissociation rates provide a lower limit to the values expected *in vivo*. Also the precise value for the

459 chemistry step is not known, as it is rate-limited by the preceding engagement step. These  
460 uncertainties prevent us from calculating the selectivity of ArfB from the elemental rate constants, as  
461 we previously have done for tRNA selection<sup>49</sup>.

462

463 **Equilibrium binding assays**

464 All binding experiments were carried out at 20°C. To assess the effect of salt concentration on ArfB  
465 binding, ArfB[Flu]-96C was allowed to bind to P+0 complexes in HK<sub>50</sub>M<sub>7</sub> buffer (HKM<sub>7</sub> buffer with 50  
466 mM KCl). Then, KCl was titrated into the sample, and the anisotropy value at each KCl concentration  
467 was recorded. A titration of the unbound protein was performed in parallel and the anisotropy  
468 values of about 0.2 subtracted; to account for light scattering, polarized light intensities of P+0  
469 complexes at each KCl concentration were also subtracted. The resulting curve was fit with a  
470 log(inhibitor) dose-response (variable slope) equation. Anisotropy was recorded using the  
471 FluorEssence software (Horiba).

472 The integrity of the ribosome-bound mRNA following ArfB binding was assayed using ribosome-  
473 nascent chain complexes labeled at the 3' end of mRNA with fluorescein (provided by Bee-Zen Peng,  
474 MPIbpc). We expect that if the mRNA were cleaved in the presence of ArfB, the anisotropy of the  
475 free 3' mRNA fragment must be significantly lower than that of the ribosome-bound mRNA. The  
476 complexes had a model dipeptide (fMetPhe-tRNA<sup>Phe</sup>) and 36 nucleotides of mRNA extending past the  
477 P site. Anisotropy of the attached dye was measured before and after incubation of 0.1 μM ArfB with  
478 0.01 μM ribosomal complex.

479

480 **Cryo-EM analysis**

481 For cryo-EM of ArfB-bound P+0 complexes, P+0 complexes (purified as described above) were diluted  
482 to 0.24 μM with HKM<sub>7</sub>+DDM-Buffer [50 mM Hepes pH 7.4, 30 mM KCl, 7 mM MgCl<sub>2</sub>, 0.1 % w/v  
483 Dodecyl-β-D-maltosid (DDM)]; ArfB was diluted to 3 μM using the same buffer. 2 μL of ribosome  
484 complex were supplemented with 0.4 μL ArfB and 0.33 μL Api137 (0.6 mM in 50 mM Hepes pH 7.2,

485 100 mM potassium acetate, 25 mM magnesium acetate; synthesized by NovoPro Biosciences Inc.)  
486 and filled up to 4  $\mu$ L with HKM,+DDM-Buffer leading to final concentrations of 0.12  $\mu$ M of P+0  
487 complex, 0.30  $\mu$ M ArfB (2.5-fold excess) and 50  $\mu$ M Api137. 3  $\mu$ L of the sample were applied to glow  
488 discharged Quantifoil R3/3 holey carbon supported copper grids covered with continuous carbon film.  
489 Grids were blotted for 2-3 s and vitrified using the Vitrobot Mark IV (ThermoFisher Eindhoven). Data  
490 collection was performed in movie mode - 10 frames at a dose of 2.5 electrons per  $\text{\AA}^{-2}$  per frame -  
491 with a Falcon II direct electron detector (ThermoFisher Eindhoven) on a Titan Krios electron  
492 microscope (ThermoFisher Eindhoven) at 300 kV, a pixel size of 1.084  $\text{\AA}$  and a defocus range from 1.1  
493 to 2.3  $\mu$ m using the semi-automated software EM-TOOLS (TVIPS GmbH).

494 For cryo-EM of ArfB-bound P+9 complexes, traces of sucrose were removed from P+9 complexes  
495 (purified as described above) using Zeba Spin Desalting Columns (7K MWCO, ThermoFisher). The  
496 complexes (0.4  $\mu$ M) were then incubated with ArfB (1.5  $\mu$ M) and Api137 (50  $\mu$ M) for 10 min at 37°C  
497 in buffer B (50 mM HEPES, 30 mM KCl, 7 mM MgCl<sub>2</sub>, pH 7.4). Cryo-EM grids were prepared by  
498 applying 5  $\mu$ L of the resulting complexes onto EM grids (Quantifoil 3.5/1  $\mu$ m, Jena) covered with pre-  
499 floated continuous carbon, manually blotted with filter paper (Whatman #1) and vitrified using a  
500 custom-made plunge-freezing device operated at 4 °C and 95% humidity. 4096 x 4096 image movie  
501 stacks - 40 frames per image,  $\sim$ 50  $\pm$  5 electrons per  $\text{\AA}^2$  total electron dose, 0.2 to 2.5  $\mu$ m defocus -  
502 were acquired in integration mode on a Falcon 3 direct detector (ThermoFisher Eindhoven) at 300kV  
503 acceleration voltage with a Titan Krios G1 microscope (ThermoFisher Eindhoven) equipped with a  
504 XFEG electron source (ThermoFisher Eindhoven) and a spherical aberration (Cs)-corrector (CEOS  
505 Heidelberg) using the software EPU 2.1 (ThermoFisher Eindhoven) for acquisition and CETCORPLUS  
506 4.6.9 (CEOS Heidelberg) for tuning of the Cs-corrector.

507 Data processing of images of P+0 and P+9 complexes was performed using a similar strategy for  
508 both data sets as described in the following. Image movie stacks were motion corrected using the  
509 software MCOR2<sup>51</sup>, CTF parameters were estimated using GCTF<sup>52</sup> and ribosome particle images were  
510 selected using GAUTOMATCH (K. Zhang, MRC-LMB, Cambridge). All subsequent cryo-EM image

511 processing was performed using RELION 2.1<sup>53</sup> and 3.0<sup>54</sup>. The two data sets represented mixtures of  
512 different ribosome populations and were therefore sorted computationally in a hierarchical manner  
513 (Supplementary Fig. 2d). First, ribosome particle images were sorted according to data quality by 2D  
514 classification and 3D classification at 3.252 Å per pixel (P+0) and 4.64 Å per pixel (P+9; step 1 and 2).  
515 All following steps were performed at the final pixel sizes of 1.07 Å (P+0) and 1.16 Å (P+9). The P+0  
516 data were subsequently classified according to ArfB occupancy by focused classification with signal  
517 subtraction (step 3) and by global classification according to ribosome conformation (step 4). The  
518 latter step resulted in three populations corresponding to different states of ribosome conformation:  
519 i) the non-ratcheted ground state, ii) an intermediate state of rotation and iii) a fully rotated  
520 ratcheted state. Due to the low particle numbers for the two rotated states, only particles of the  
521 major ground state were further processed. These particles were sorted again for presence of ArfB  
522 resulting in a homogenous particle population of ArfB-bound P+0 ribosome complexes (step 5) that  
523 was refined to a final resolution of about 3.7 Å (Supplementary Fig. 2e). For the P+9 data per-particle-  
524 motion correction was performed by RELION's Bayesian polishing approach in step 6 and the  
525 resulting particles were sorted by 3D classification according to global ribosome conformation (step  
526 7). The resulting two populations – one with ribosome particles in the ground state (non-rotated) and  
527 the other one with particles showing inter-subunit rotation (rotated) – were each further classified  
528 by focused classification with signal subtraction according to tRNA occupancy (for non-ratcheted  
529 population only, step 8) and/or ArfB occupancy (step 9). The three resulting homogenous ribosome  
530 particle populations were refined to high-resolution according to the gold-standard procedure and  
531 overall resolutions were determined using high-resolution noise substitution (Supplementary Fig. 2e).

532 For visualization and atomic model refinement all final maps were amplitude sharpened globally  
533 using PHENIX 1.16<sup>55</sup>. The two best-resolved cryo-EM maps – the P+9 post-hydrolysis state at 2.6 Å  
534 and the P+9 stalled complex at 3.1 Å – were resampled to a finer pixel size of 0.6525 Å for improved  
535 visualization and interpretation. We first created an atomic model for the highest-resolved 2.6 Å  
536 cryo-EM map. An initial model was built by rigid body fitting in ChimeraX 0.91<sup>56</sup> based on the

537 following structures: PDB 5AF1<sup>57</sup> for the *E. coli* 70S ribosome, PDB 4RB7<sup>58</sup> for tRNA<sup>Phe</sup>, PDB 5O2R<sup>21</sup> for  
538 Api137 and PDB 4V95<sup>15</sup> for ArfB. Parts of ArfB had to be re-built manually in WinCoot<sup>59</sup> 0.8.9.2 to fit  
539 our high-resolution density due to register shifts with respect to the reported model from the 3.2 Å  
540 crystal structure of *E. coli* ArfB bound to the *Thermus thermophilus* ribosome (PDB 4V95); register  
541 shifts – by one amino acid - occurred in the N-terminal domain (Ile2 to His7, Thr33 to Ser46) and all  
542 residues of the C-terminal domain starting from Arg112. Metal coordination and secondary structure  
543 restraints were prepared using initial models with phenix.ready\_set. Additional structural restraints  
544 were generated from hydrogen bond search in ChimeraX. Real space refinement was performed  
545 using phenix.real\_space\_refine with global minimization, simulated annealing, atomic displacement  
546 parameters and local grid search for 300 iterations limit and 5 macrocycles. Atomic model  
547 refinement of the remaining states (P+0 post-hydrolysis state, P+9 stalled complex and P+9 hybrid  
548 state) was based on the model of the P+9 post-hydrolysis state and performed in an analogous way.  
549 As an additional validation step we also refined the scrambled atomic models against one of the half  
550 maps and calculated FSCs of the resulting model against the second half map. To remove possible  
551 model bias, atomic models from the full-map refinement were scrambled by applying random shifts  
552 of 0.25 Å to all atomic positions beforehand. Modeling statistics are described in Table 1, FSC curves  
553 are depicted in Supplementary Fig. 2e.

554

## 555 **DATA AVAILABILITY**

556 Cryo-EM maps/associated coordinates of atomic models have been deposited in the Electron  
557 Microscopy Data Bank/Protein Data Bank with the following accession codes: PDB 6YSR  
558 [<https://doi.org/10.2210/pdb6YSR/pdb>] and EMD-10905  
559 [<https://www.ebi.ac.uk/pdbe/entry/emdb/EMD-10905>] (P+9 stalled complex), PDB 6YSS  
560 [<https://doi.org/10.2210/pdb6YSS/pdb>] and EMD-10906  
561 [<https://www.ebi.ac.uk/pdbe/entry/emdb/EMD-10906>] (P+9 post-hydrolysis), EMD-10907PDB 6YST  
562 [<https://doi.org/10.2210/pdb6YST/pdb>] and EMD-10907  
563 [<https://www.ebi.ac.uk/pdbe/entry/emdb/EMD-10907>] (P+9 tRNA hybrid state), PDB 6YSU  
564 [<https://doi.org/10.2210/pdb6YSU/pdb>] and EMD-10908  
565 [<https://www.ebi.ac.uk/pdbe/entry/emdb/EMD-10908>] (P+0 post-hydrolysis). Cryo-EM micrographs  
566 and particle images have been deposited in the EMPIAR database  
567 (<https://www.ebi.ac.uk/pdbe/emdb/empiar/>) with accession code EMPIAR-10443. The data  
568 supporting the findings of this study are available within the paper and its supplementary

569 information files, and available from the corresponding authors upon reasonable request. Source  
570 data are provided with this paper.

571

572 **References**

- 573 1. Keiler, K.C. & Feaga, H.A. Resolving nonstop translation complexes is a matter of life or death.  
574 *J Bacteriol* **196**, 2123-30 (2014).
- 575 2. Richter, R. et al. A functional peptidyl-tRNA hydrolase, ICT1, has been recruited into the  
576 human mitochondrial ribosome. *EMBO J* **29**, 1116-25 (2010).
- 577 3. Feaga, H.A., Quickel, M.D., Hankey-Giblin, P.A. & Keiler, K.C. Human Cells Require Non-stop  
578 Ribosome Rescue Activity in Mitochondria. *PLoS Genet* **12**, e1005964 (2016).
- 579 4. Ito, K. et al. Nascentome analysis uncovers futile protein synthesis in *Escherichia coli*. *PLoS*  
580 *One*, <https://doi.org/10.1371/journal.pone.0028413> (2011).
- 581 5. Huter, P., Muller, C., Arenz, S., Beckert, B. & Wilson, D.N. Structural Basis for Ribosome  
582 Rescue in Bacteria. *Trends Biochem Sci* **42**, 669-680 (2017).
- 583 6. Chadani, Y., Ono, K., Kutsukake, K. & Abo, T. *Escherichia coli* YaeJ protein mediates a novel  
584 ribosome-rescue pathway distinct from SsrA- and ArfA-mediated pathways. *Mol Microbiol* **80**,  
585 772-85 (2011).
- 586 7. Handa, Y., Inaho, N. & Nameki, N. YaeJ is a novel ribosome-associated protein in *Escherichia*  
587 *coli* that can hydrolyze peptidyl-tRNA on stalled ribosomes. *Nucleic Acids Res* **39**, 1739-48  
588 (2011).
- 589 8. Duarte, I., Nabuurs, S.B., Magno, R. & Huynen, M. Evolution and diversification of the  
590 organellar release factor family. *Mol Biol Evol* **29**, 3497-512 (2012).
- 591 9. Handa, Y. et al. Solution structure of the catalytic domain of the mitochondrial protein ICT1  
592 that is essential for cell vitality. *J Mol Biol* **404**, 260-73 (2010).
- 593 10. Kogure, H. et al. Identification of residues required for stalled-ribosome rescue in the codon-  
594 independent release factor YaeJ. *Nucleic Acids Res* **42**, 3152-63 (2014).
- 595 11. Ivanova, N., Pavlov, M.Y., Felden, B. & Ehrenberg, M. Ribosome rescue by tmRNA requires  
596 truncated mRNAs. *J Mol Biol* **338**, 33-41 (2004).
- 597 12. Kurita, D., Miller, M.R., Muto, A., Buskirk, A.R. & Himeno, H. Rejection of tmRNA.SmpB after  
598 GTP hydrolysis by EF-Tu on ribosomes stalled on intact mRNA. *RNA* **20**, 1706-14 (2014).
- 599 13. Kurita, D., Chadani, Y., Muto, A., Abo, T. & Himeno, H. ArfA recognizes the lack of mRNA in  
600 the mRNA channel after RF2 binding for ribosome rescue. *Nucleic Acids Res* **42**, 13339-52  
601 (2014).
- 602 14. Shimizu, Y. ArfA recruits RF2 into stalled ribosomes. *J Mol Biol* **423**, 624-31 (2012).

603 15. Gagnon, M.G., Seetharaman, S.V., Bulkley, D. & Steitz, T.A. Structural basis for the rescue of  
604 stalled ribosomes: structure of YaeJ bound to the ribosome. *Science* **335**, 1370-2 (2012).

605 16. Dyson, H.J. & Wright, P.E. Intrinsically unstructured proteins and their functions. *Nat Rev Mol  
606 Cell Biol* **6**, 197-208 (2005).

607 17. Mollica, L. et al. Binding Mechanisms of Intrinsically Disordered Proteins: Theory, Simulation,  
608 and Experiment. *Front Mol Biosci*, <https://doi.org/10.3389/fmolb.2016.00052> (2016).

609 18. Habchi, J., Tompa, P., Longhi, S. & Uversky, V.N. Introducing protein intrinsic disorder. *Chem  
610 Rev* **114**, 6561-88 (2014).

611 19. Gao, N. et al. Mechanism for the disassembly of the posttermination complex inferred from  
612 cryo-EM studies. *Mol Cell* **18**, 663-74 (2005).

613 20. Taniguchi, Y. et al. Quantifying *E. coli* proteome and transcriptome with single-molecule  
614 sensitivity in single cells. *Science* **329**, 533-8 (2010).

615 21. Florin, T. et al. An antimicrobial peptide that inhibits translation by trapping release factors  
616 on the ribosome. *Nat Struct Mol Biol* **24**, 752-757 (2017).

617 22. Graf, M. et al. Visualization of translation termination intermediates trapped by the  
618 Apidaecin 137 peptide during RF3-mediated recycling of RF1. *Nat Commun* **9**, 3053 (2018).

619 23. Cayley, S., Lewis, B.A., Guttman, H.J. & Record, M.T., Jr. Characterization of the cytoplasm of  
620 *Escherichia coli* K-12 as a function of external osmolarity. Implications for protein-DNA  
621 interactions in vivo. *J Mol Biol* **222**, 281-300 (1991).

622 24. Goyal, A., Belardinelli, R. & Rodnina, M.V. Non-canonical Binding Site for Bacterial Initiation  
623 Factor 3 on the Large Ribosomal Subunit. *Cell Rep* **20**, 3113-3122 (2017).

624 25. Kuhlenkoetter, S., Wintermeyer, W. & Rodnina, M.V. Different substrate-dependent  
625 transition states in the active site of the ribosome. *Nature* **476**, 351-4 (2011).

626 26. Indrisiunaite, G., Pavlov, M.Y., Heurgue-Hamard, V. & Ehrenberg, M. On the pH dependence  
627 of class-1 RF-dependent termination of mRNA translation. *J Mol Biol* **427**, 1848-60 (2015).

628 27. Elf, J., Nilsson, D., Tenson, T. & Ehrenberg, M. Selective charging of tRNA isoacceptors  
629 explains patterns of codon usage. *Science* **300**, 1718-22 (2003).

630 28. Brown, A. et al. Structure of the large ribosomal subunit from human mitochondria. *Science*  
631 **346**, 718-722 (2014).

632 29. Amunts, A., Brown, A., Toots, J., Scheres, S.H.W. & Ramakrishnan, V. Ribosome. The structure  
633 of the human mitochondrial ribosome. *Science* **348**, 95-98 (2015).

634 30. Akabane, S., Ueda, T., Nierhaus, K.H. & Takeuchi, N. Ribosome rescue and translation  
635 termination at non-standard stop codons by ICT1 in mammalian mitochondria. *PLoS Genet* **10**,  
636 e1004616 (2014).

637 31. Lind, C., Sund, J. & Aqvist, J. Codon-reading specificities of mitochondrial release factors and  
638 translation termination at non-standard stop codons. *Nat Commun* **4**, 2940 (2013).

639 32. Chrzanowska-Lightowlers, Z.M. & Lightowlers, R.N. Response to "Ribosome Rescue and  
640 Translation Termination at Non-standard Stop Codons by ICT1 in Mammalian Mitochondria".  
641 *PLoS Genet*, <https://doi.org/10.1371/journal.pgen.1005227> (2015).

642 33. D'Souza, A.R. & Minczuk, M. Mitochondrial transcription and translation: overview. *Essays  
643 Biochem* **62**, 309-320 (2018).

644 34. Rorbach, J., Nicholls, T.J. & Minczuk, M. PDE12 removes mitochondrial RNA poly(A) tails and  
645 controls translation in human mitochondria. *Nucleic Acids Res* **39**, 7750-63 (2011).

646 35. Nagaike, T., Suzuki, T., Katoh, T. & Ueda, T. Human mitochondrial mRNAs are stabilized with  
647 polyadenylation regulated by mitochondria-specific poly(A) polymerase and polynucleotide  
648 phosphorylase. *J Biol Chem* **280**, 19721-7 (2005).

649 36. Fersht, A. *Structure and mechanism in protein science: a guide to enzyme catalysis and  
650 protein folding*, (Macmillan, 1999).

651 37. James, N.R., Brown, A., Gordiyenko, Y. & Ramakrishnan, V. Translational termination without  
652 a stop codon. *Science* **354**, 1437-1440 (2016).

653 38. Ma, C. et al. Mechanistic insights into the alternative translation termination by ArfA and RF2.  
654 *Nature* **541**, 550-553 (2017).

655 39. Demo, G. et al. Mechanism of ribosome rescue by ArfA and RF2. *Elife* **6**(2017).

656 40. Zeng, F. et al. Structural basis of co-translational quality control by ArfA and RF2 bound to  
657 ribosome. *Nature* **541**, 554-557 (2017).

658 41. Huter, P. et al. Structural basis for ArfA-RF2-mediated translation termination on mRNAs  
659 lacking stop codons. *Nature* **541**, 546-549 (2017).

660 42. Adio, S. et al. Dynamics of ribosomes and release factors during translation termination in *E.*  
661 *coli*. *Elife* **7**(2018).

662 43. Shoemaker, B.A., Portman, J.J. & Wolynes, P.G. Speeding molecular recognition by using the  
663 folding funnel: the fly-casting mechanism. *Proc Natl Acad Sci U S A* **97**, 8868-73 (2000).

664 44. Rodnina, M.V. & Wintermeyer, W. GTP consumption of elongation factor Tu during  
665 translation of heteropolymeric mRNAs. *Proc Natl Acad Sci U S A* **92**, 1945-9 (1995).

666 45. Cunha, C.E. et al. Dual use of GTP hydrolysis by elongation factor G on the ribosome.  
667 *Translation (Austin)* **1**, e24315 (2013).

668 46. Milon, P. et al. Transient kinetics, fluorescence, and FRET in studies of initiation of translation  
669 in bacteria. *Methods Enzymol* **430**, 1-30 (2007).

670 47. Savelsbergh, A. et al. An elongation factor G-induced ribosome rearrangement precedes  
671 tRNA-mRNA translocation. *Mol Cell* **11**, 1517-23 (2003).

672 48. Rodnina, M.V., Savelsbergh, A., Katunin, V.I. & Wintermeyer, W. Hydrolysis of GTP by  
673 elongation factor G drives tRNA movement on the ribosome. *Nature* **385**, 37-41 (1997).

674 49. Rodnina, M.V., Gromadski, K.B., Kothe, U. & Wieden, H.J. Recognition and selection of tRNA  
675 in translation. *FEBS Lett* **579**, 938-42 (2005).

676 50. Doerfel, L.K. et al. EF-P is essential for rapid synthesis of proteins containing consecutive  
677 proline residues. *Science* **339**, 85-8 (2013).

678 51. Zheng, S.Q. et al. MotionCor2: anisotropic correction of beam-induced motion for improved  
679 cryo-electron microscopy. *Nat Methods* **14**, 331-332 (2017).

680 52. Zhang, K. Gctf: Real-time CTF determination and correction. *J Struct Biol* **193**, 1-12 (2016).

681 53. Kimanius, D., Forsberg, B.O., Scheres, S.H. & Lindahl, E. Accelerated cryo-EM structure  
682 determination with parallelisation using GPUs in RELION-2. *Elife*,  
683 <https://doi.org/10.7554/eLife.18722.001> (2016).

684 54. Zivanov, J. et al. New tools for automated high-resolution cryo-EM structure determination in  
685 RELION-3. *Elife*, <https://doi.org/10.7554/eLife.42166.001> (2018).

686 55. Liebschner, D. et al. Macromolecular structure determination using X-rays, neutrons and  
687 electrons: recent developments in Phenix. *Acta Crystallogr D Struct Biol* **75**, 861-877 (2019).

688 56. Goddard, T.D. et al. UCSF ChimeraX: Meeting modern challenges in visualization and analysis.  
689 *Protein Sci* **27**, 14-25 (2018).

690 57. Fischer, N. et al. Structure of the E. coli ribosome-EF-Tu complex at <3 Å resolution by Cs-  
691 corrected cryo-EM. *Nature* **520**, 567-70 (2015).

692 58. Polikanov, Y.S. et al. Amicoumacin a inhibits translation by stabilizing mRNA interaction with  
693 the ribosome. *Mol Cell* **56**, 531-40 (2014).

694 59. Brown, A. et al. Tools for macromolecular model building and refinement into electron cryo-  
695 microscopy reconstructions. *Acta Crystallogr D Biol Crystallogr* **71**, 136-53 (2015).

696

697 **ACKNOWLEDGMENTS**

698 We thank Olaf Geintzer, Vanessa Herold, Tessa Huebner, Sandra Kappler, Christina Kothe, Anna  
699 Pfeifer, Theresia Steiger, Franziska Hummel and Michael Zimmermann for expert technical assistance,  
700 Holger Stark for providing electron microscopy and computational resources and Mario Lüttich and  
701 Tobias Koske for support in high-performance computation. This research was supported by the Max  
702 Planck Society, the Leibniz Prize of the Deutsche Forschungsgemeinschaft to M.V.R. and a Deutsche  
703 Forschungsgemeinschaft grant (WI3285/6-1) to D.N.W.

704

705 **AUTHOR CONTRIBUTIONS**

706 K.-H. C. performed all biochemical experiments and prepared the cryo-EM sample, V.P., Cl.M. and  
707 N.F. performed the cryo-EM analysis, Cr.M., W.H., D.N.W, N.F. and M.V.R. designed the study, K.-H.C,  
708 Cr.M., N.F. and M.V.R wrote the paper with inputs from all authors.

709

710 **COMPETING INTERESTS**

711 The authors declare no competing interests.

712

713

714

715 **Figure legends**

716

717 **Fig. 1 | ArfB preferentially rescues ribosomes stalled on short mRNA.** **a**, Experimental assay for  
718 ArfB-mediated ribosome rescue. Ribosome complexes with mRNAs of different length are rapidly  
719 mixed with ArfB and the fraction of peptides released from tRNA by ArfB-dependent hydrolysis is  
720 quantified. PTC, peptidyl transferase center; DC, decoding center; NTD, N-terminal domain; CTD, C-  
721 terminal domain. Free ArfB is shown as ensemble of dynamic molecules<sup>10</sup>, the ribosome-bound ArfB  
722 is shown as in the X-ray structure<sup>15</sup>. **b**, Time courses of single-round peptidyl-tRNA hydrolysis at  
723 excess ArfB (1  $\mu$ M) over ribosome complexes (0.15  $\mu$ M). The mRNA length is indicated in number of  
724 nucleotides (nt) extending beyond the P site, from none (P+0) to 99 nt (P+99). Data represented as  
725 mean values of two biological replicates.. Solid lines are exponential fits. **c**, Rate of hydrolysis at  
726 increasing mRNA length. Error bars indicate the SEM of the exponential fits (**b**). **d**, Peptidyl-tRNA  
727 hydrolysis on P+0 and P+9 complexes at limiting ArfB concentrations. Initial velocity of the hydrolysis  
728 reaction is measured after mixing ArfB (0.02  $\mu$ M) with increasing concentrations of P+0 or P+9  
729 complexes. Solid lines are results of hyperbolic fitting. Error bars represent the SEM of three  
730 biological replicates. **e**, Effect of ribosome recycling factors on the duration of an ArfB catalytic cycle  
731 on P+0 complexes (0.2  $\mu$ M) mixed with catalytic amounts of ArfB (0.02  $\mu$ M) and excess of RF3 (0.5  
732  $\mu$ M), RRF (0.5  $\mu$ M) and EF-G (0.5  $\mu$ M). All experiments were carried out at 37°C.

733

734 **Fig. 2 | Structural intermediates of ribosome rescue by ArfB as visualized by cryo-EM.** For cryo-EM  
735 analysis, ArfB was stalled on the ribosome using the antibiotic Api137. **a**, Major states of ArfB-bound  
736 P+0 and P+9 complexes exhibit a striking structural similarity. Close-ups: Superposition of P+0 (lighter  
737 colors) and P+9 (darker colors) structures in the PTC (top) and the DC region (bottom). **b**, Stalled P+9  
738 complex with dipeptidyl-tRNA prior to ArfB binding. **c**, Post-hydrolysis P+9 complex with P/E hybrid  
739 tRNA. Note the lack of density for mRNA in the mRNA entry channel in the ArfB-bound P+9 states  
740 indicating a highly flexible 3' extension of mRNA versus the well-defined 3' extension in the vacant  
741 P+9 complex.

742

743 **Fig. 3 | Specific interactions with the ribosome stabilize ArfB in the active state.** **a**, ArfB residues  
744 known to be essential for ribosome rescue<sup>10</sup> form a network of interactions with the ribosome as  
745 seen in the P+9 cryo-EM structure. Panels 1, 2, 3 depict distinct regions in ArfB indicated in the  
746 schematic (left). **b**, Subunit rotation changes the position, but not the interactions of ArfB on the  
747 ribosome in the P+9 hybrid state cryo-EM structure. **c**, Experimental assay to measure the affinity of

748 ArfB binding to stalled ribosomes using the anisotropy change of fluorescein-labeled ArfB<sub>GAQ</sub>  
749 (ArfB<sub>GAQ</sub>(Flu)). **d**, Role of electrostatic interactions in ArfB binding to the ribosome. P+0 or P+9  
750 complexes (0.15  $\mu$ M) with ArfB(Flu) (0.05  $\mu$ M) at different KCl (left) or MgCl<sub>2</sub> (right) concentrations.  
751 IC<sub>50</sub> is ~260 mM for KCl and ~40 mM for MgCl<sub>2</sub> (P+0) or ~30 mM for MgCl<sub>2</sub> (P+9). The range of  
752 physiological ion concentrations is highlighted in gray (180 - 200 mM for K<sup>+</sup> and 2 - 3 mM for Mg<sup>2+</sup>; ref.  
753 <sup>23</sup>). Error bars indicate the SEM of three biological replicates, and the solid line are dose-response fits.  
754 **e**, Effect of Mg<sup>2+</sup> concentration on ArfB activity. P+0 and P+9 (0.1  $\mu$ M) were incubated with ArfB  
755 (1  $\mu$ M) for 5 min at 20°C. Error bars indicate the SEM of three biological replicates.

756

757 **Fig. 4 | A dynamic model of ArfB recruitment.** **a**, Experimental assay to monitor binding of ArfB to  
758 the ribosome in real time. P+n ribosome complexes containing fluorescein-labeled fMetPhe-tRNA<sup>Phe</sup>  
759 (P+n(Flu)) are mixed with quencher-labeled ArfB (ArfB(540Q)) and fluorescein quenching is  
760 monitored in real time in a stopped-flow apparatus. **b**, Time courses of ArfB binding with fixed  
761 concentration of P+9(Flu) (0.015  $\mu$ M) and increasing concentrations of ArfB(540Q) (0.05-0.5  $\mu$ M)  
762 (20°C). Lines indicate three-exponential fits. **c**, Kinetics of initial binding of ArfB(540Q) to P+0(Flu),  
763 P+9(Flu), and P+30(Flu) complexes. Plotted is the concentration dependence of the apparent rate  
764 constant ( $k_{app1}$ ) for the predominant association phase in panel b. Data represents the mean values of  
765 two biological replicates with up to six technical replicates each. The association ( $k_{ON}$ ) and  
766 dissociation ( $k_{OFF}$ ) rate constants are determined by linear fitting of the concentration dependence.  
767 Errors of  $k_{ON}$  and  $k_{OFF}$  values are SEM of the fit. **d**, Kinetics of peptidyl-tRNA hydrolysis. Time courses  
768 of hydrolysis with P+0 ribosome complex (0.15  $\mu$ M) and ArfB (0.2-2  $\mu$ M) (37°C). Data represented as  
769 mean values of two biological replicates. **e**, Comparison of peptidyl-tRNA hydrolysis rates on P+0 and  
770 P+9 complexes. Values are obtained by exponential fitting of the rapid phase of the hydrolysis time  
771 courses (**d** and Supplementary Fig. 4f). Error bars represent the SEM of the fit. **f**, Dissociation of ArfB  
772 from P+0, P+9, and P+30 complexes. The release of ArfB<sub>GAQ</sub>(540Q) (0.1  $\mu$ M) from the pre-hydrolysis  
773 complexes P+0(Flu), P+9(Flu), and P+30(Flu) (0.015  $\mu$ M) was initiated by rapid mixing with unlabeled  
774 P+0 complexes (1  $\mu$ M) (20°C).

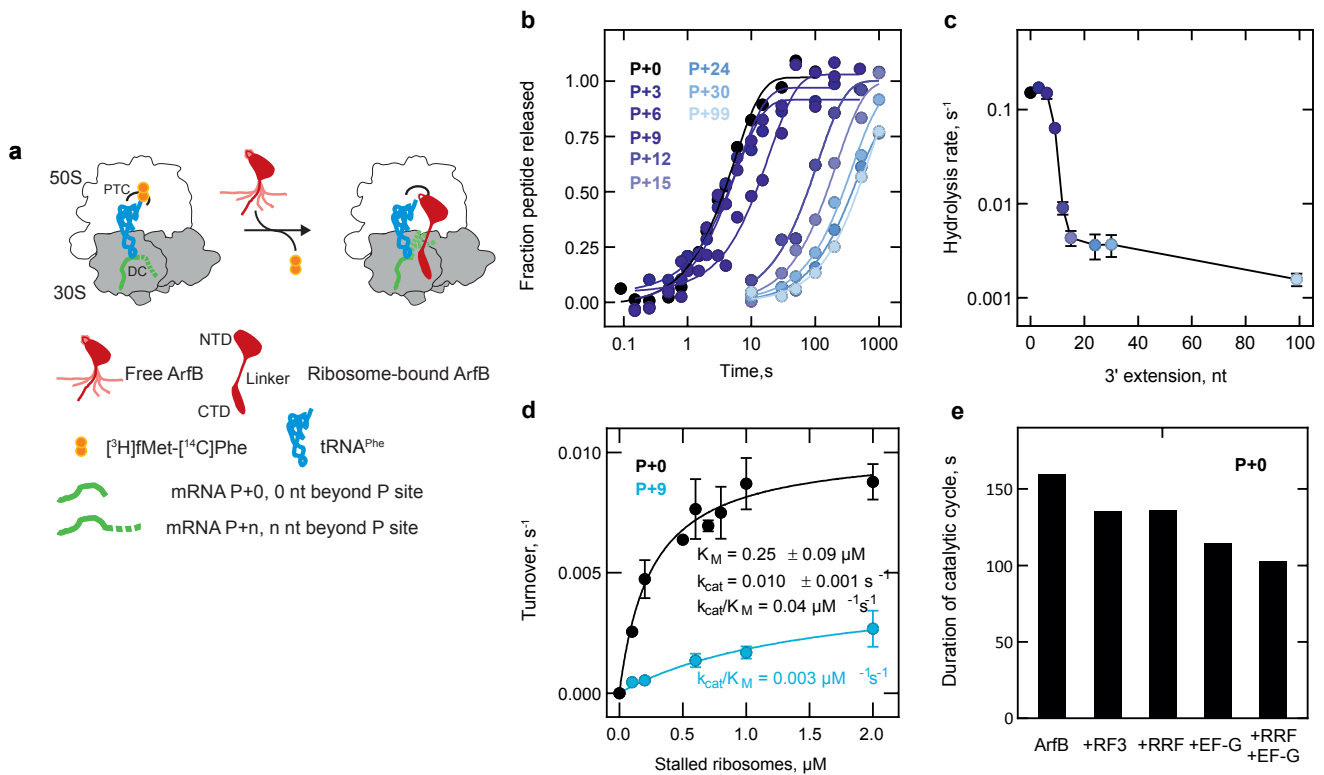
775

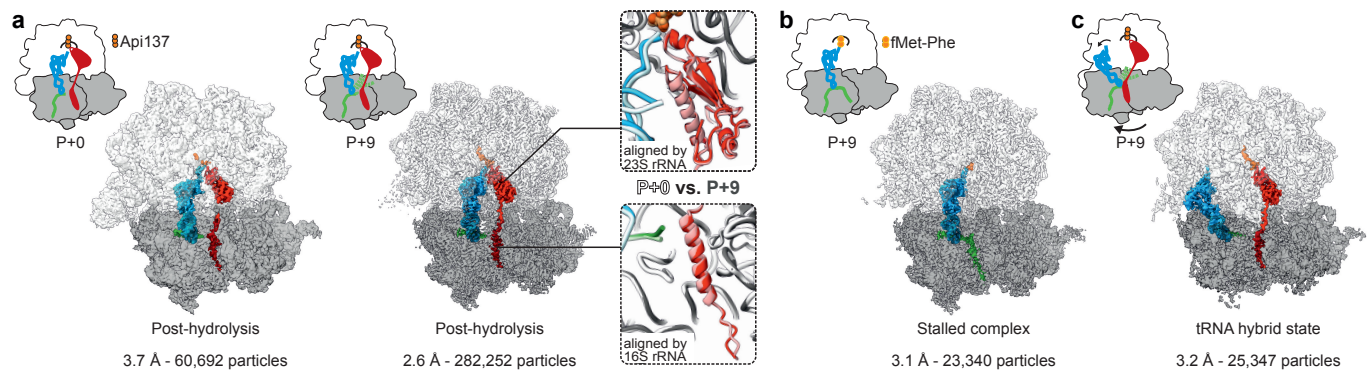
776 **Fig. 5 | Mechanism of ribosome rescue by ArfB based on rapid kinetics and cryo-EM data.** **a**, Model  
777 for initial binding of ArfB, based on the NMR ensemble of free ArfB<sup>10</sup> and cryo-EM structures of the  
778 P+9 ribosome-ArfB complex. 1, 2, 3 illustrate the key steps of the mechanism. **b**, Mechanism of ArfB  
779 action. 1, When the ribosome stalls on a truncated mRNA, ArfB can rapidly bind regardless of the  
780 mRNA length. Subsequent conformational rearrangement allow the factor to probe the mRNA entry  
781 channel; if there is mRNA extending past the P site, the mRNA must first move out of the mRNA entry

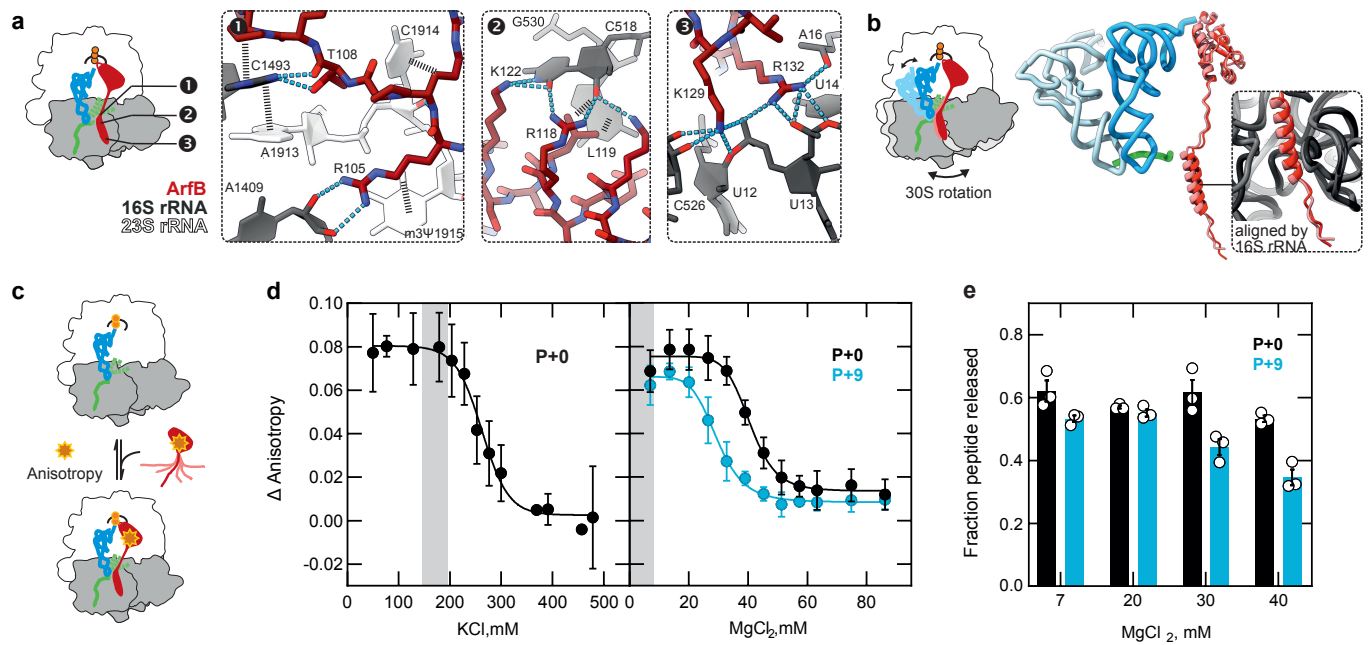
782 channel 2, a process that occurs more slowly with longer mRNAs. The binding and folding of the ArfB  
783 C-terminal domain results in the engagement of ArfB on the 30S subunit 3, which allows the rapid  
784 hydrolysis reaction to occur via the GQQ motif in the PTC, followed by peptide release, ribosome  
785 rotation and movement of the tRNA into the hybrid state, and ArfB dissociation.

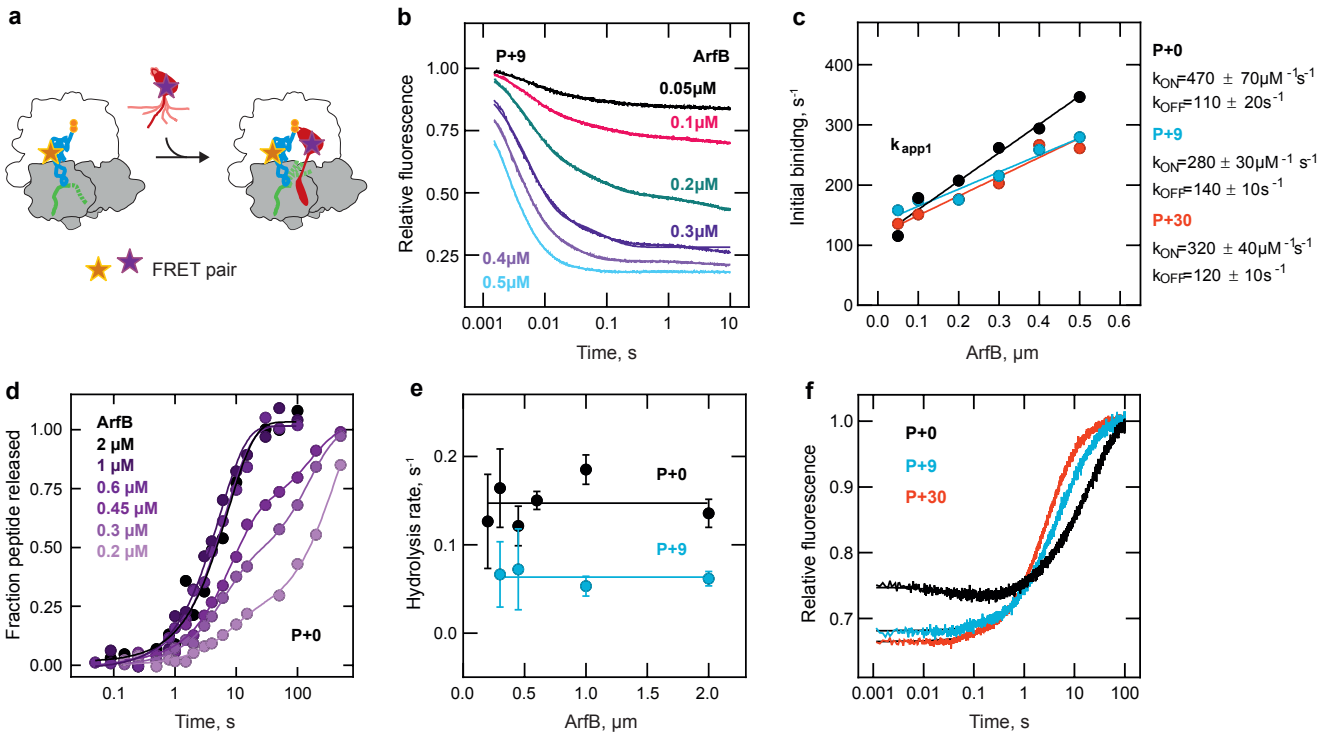
786

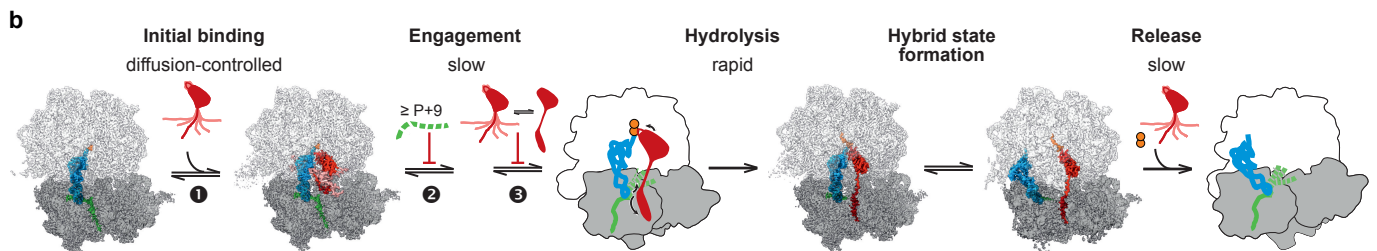
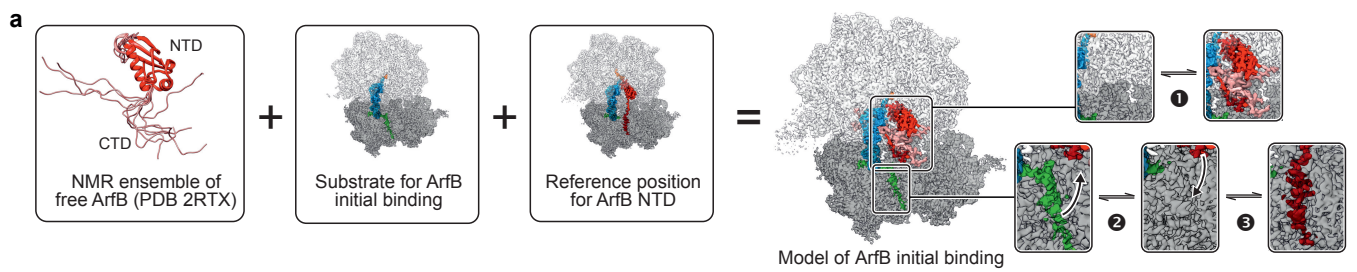
787











# Mechanism of Ribosome Rescue by Alternative Ribosome-Rescue

## Factor B - Supplementary Information

Kai-Hsin Chan<sup>1</sup>, Valentyn Petrychenko<sup>2</sup>, Claudia Mueller<sup>3</sup>, Cristina Maracci<sup>1</sup>, Wolf Holtkamp<sup>1,4</sup>, Daniel N. Wilson<sup>3</sup>, Niels Fischer<sup>2\*</sup> and Marina V. Rodnina<sup>1\*</sup>

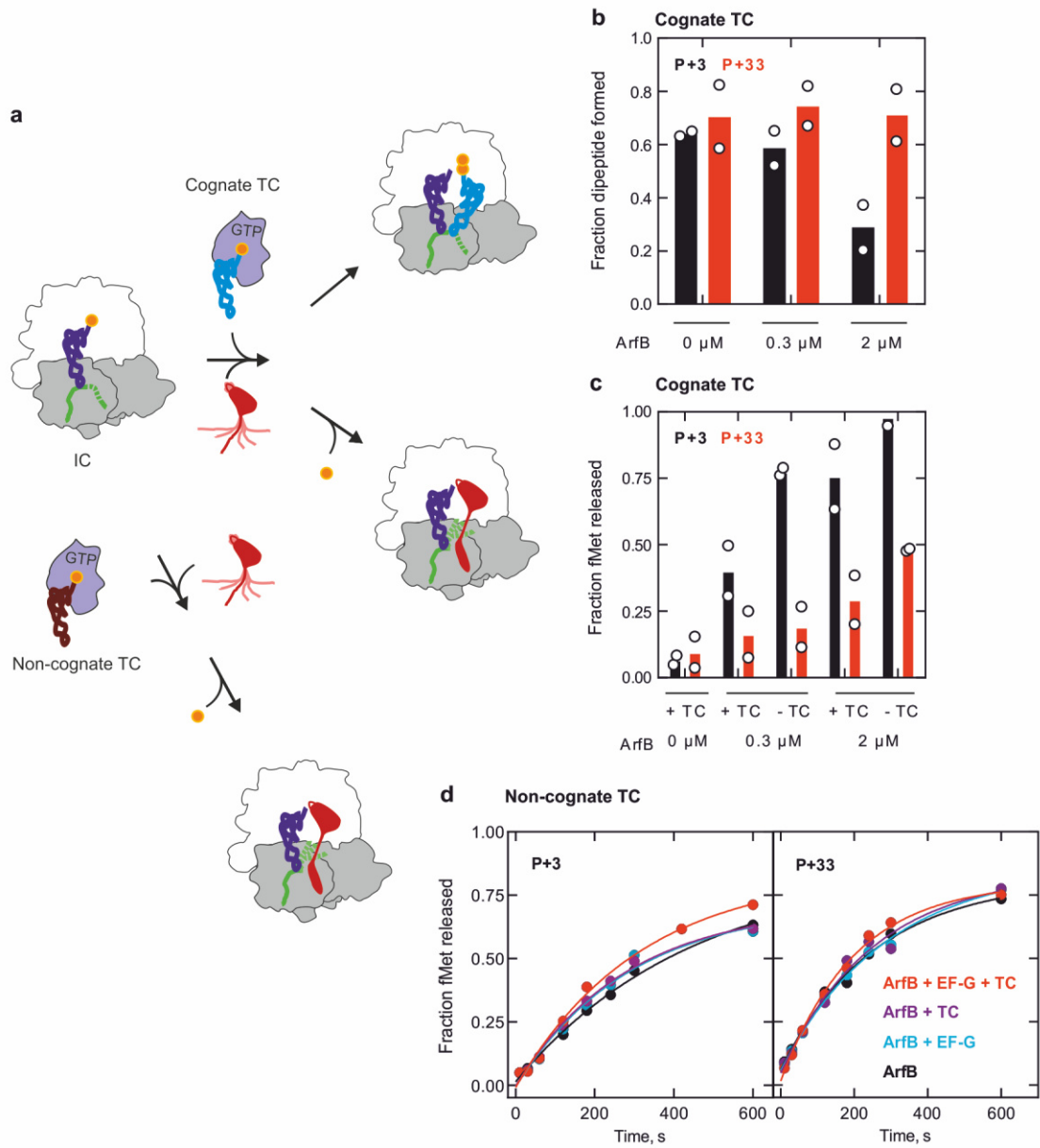
<sup>1</sup> Department of Physical Biochemistry, Max Planck Institute for Biophysical Chemistry, Am Fassberg 11, 37077 Göttingen, Germany

<sup>2</sup> Department of Structural Dynamics, Max Planck Institute for Biophysical Chemistry, Am Fassberg 11, 37077 Göttingen, Germany

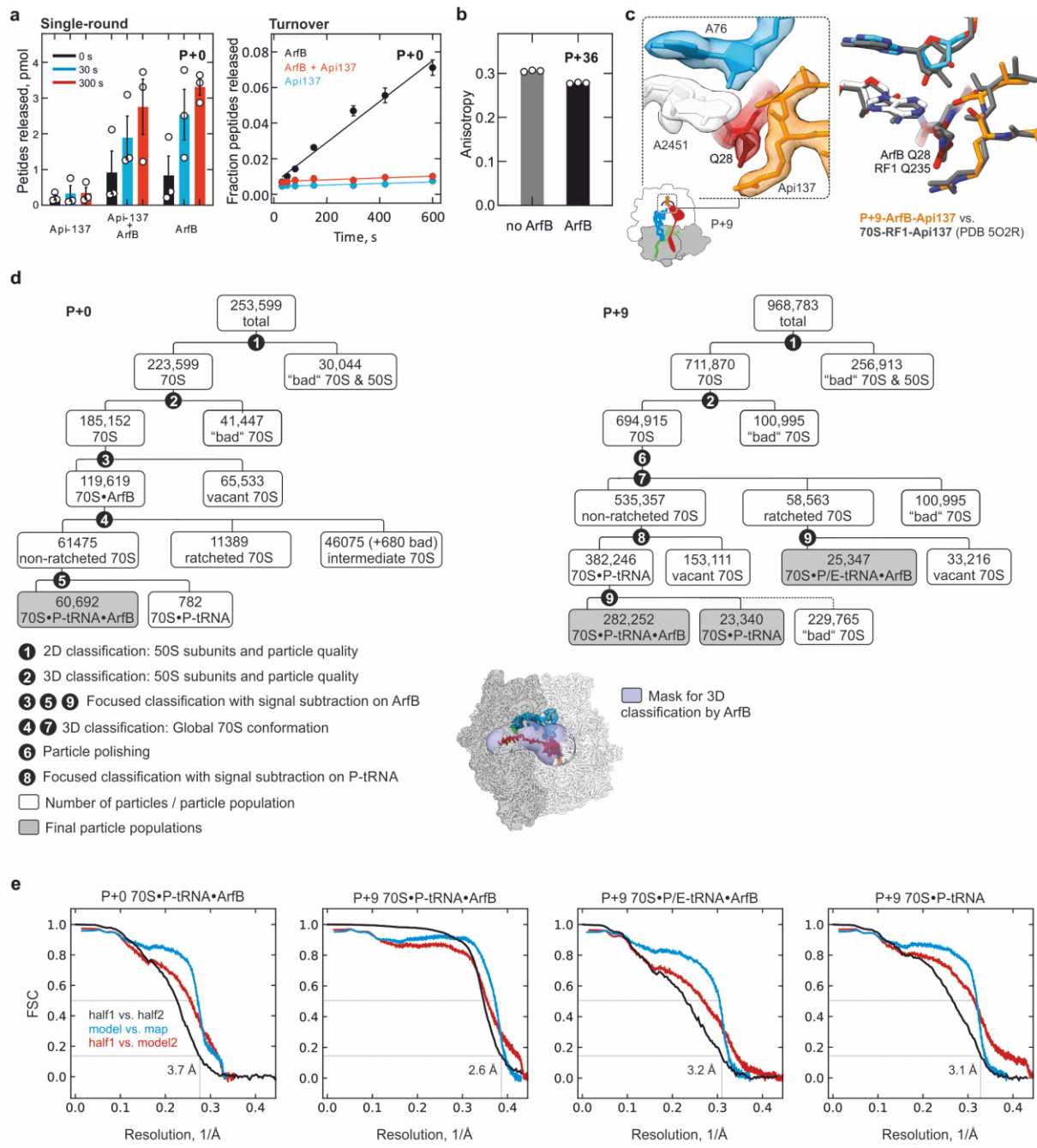
<sup>3</sup> Institute for Biochemistry and Molecular Biology, University of Hamburg, Martin-Luther-King-Platz 6, 20146 Hamburg, Germany

<sup>4</sup> Present address: Paul-Ehrlich-Institut, Paul-Ehrlich-Straße 51-59, 63225 Langen

\* Correspondence to: niels.fischer@mpibpc.mpg.de (ORCID 0000-0002-4609-4052) and rodnina@mpibpc.mpg.de (ORCID 0000-0003-0105-3879)

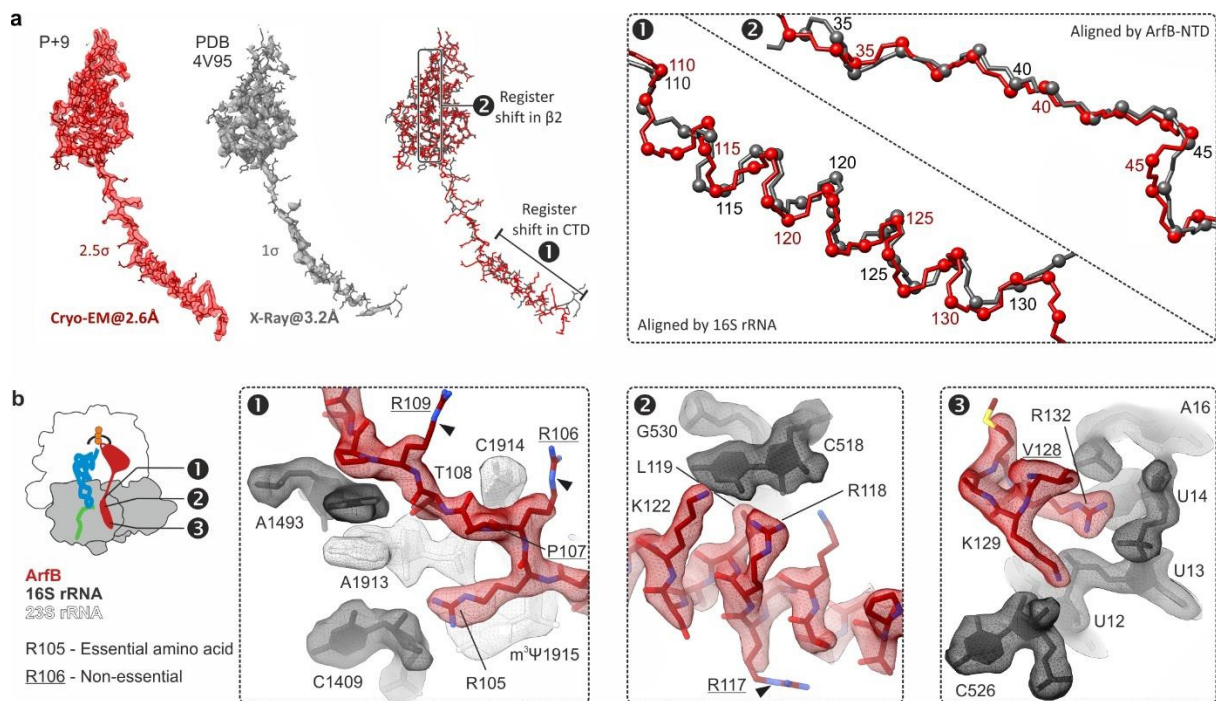


**Supplementary Figure 1 | Cognate ternary complexes (TC), but not non-cognate TC, compete with ArfB for binding to the ribosome.** **a**, Experimental assay to measure competition between ternary complexes and ArfB on ribosome complexes with P+3 or P+33 mRNAs and [<sup>3</sup>H]fMet-tRNA in the P site (IC). TC activity is monitored by dipeptide formation (f[<sup>3</sup>H]Met-[<sup>14</sup>C]Phe), ArfB activity by f[<sup>3</sup>H]Met release from f[<sup>3</sup>H]Met-tRNA<sup>fMet</sup>. **b, c**, Dipeptide formation (**b**) and ArfB-induced fMet release (**c**) on P+3 and P+33 initiation complex (IC, 0.5 μM) mixed with cognate EF-Tu–GTP–[<sup>14</sup>C]Phe-tRNA<sup>Phe</sup> (0.25 μM), and ArfB (0.3 or 2 μM). Data are presented as mean values from two biological replicates (white circles). **d**, ArfB-induced fMet-tRNA hydrolysis on P+3 and P+33 IC (0.5 μM) in the presence of ArfB (0.1 μM and 2 μM, respectively), non-cognate EF-Tu–GTP–Val-tRNA<sup>Val</sup> (5 μM) and EF-G (2 μM).

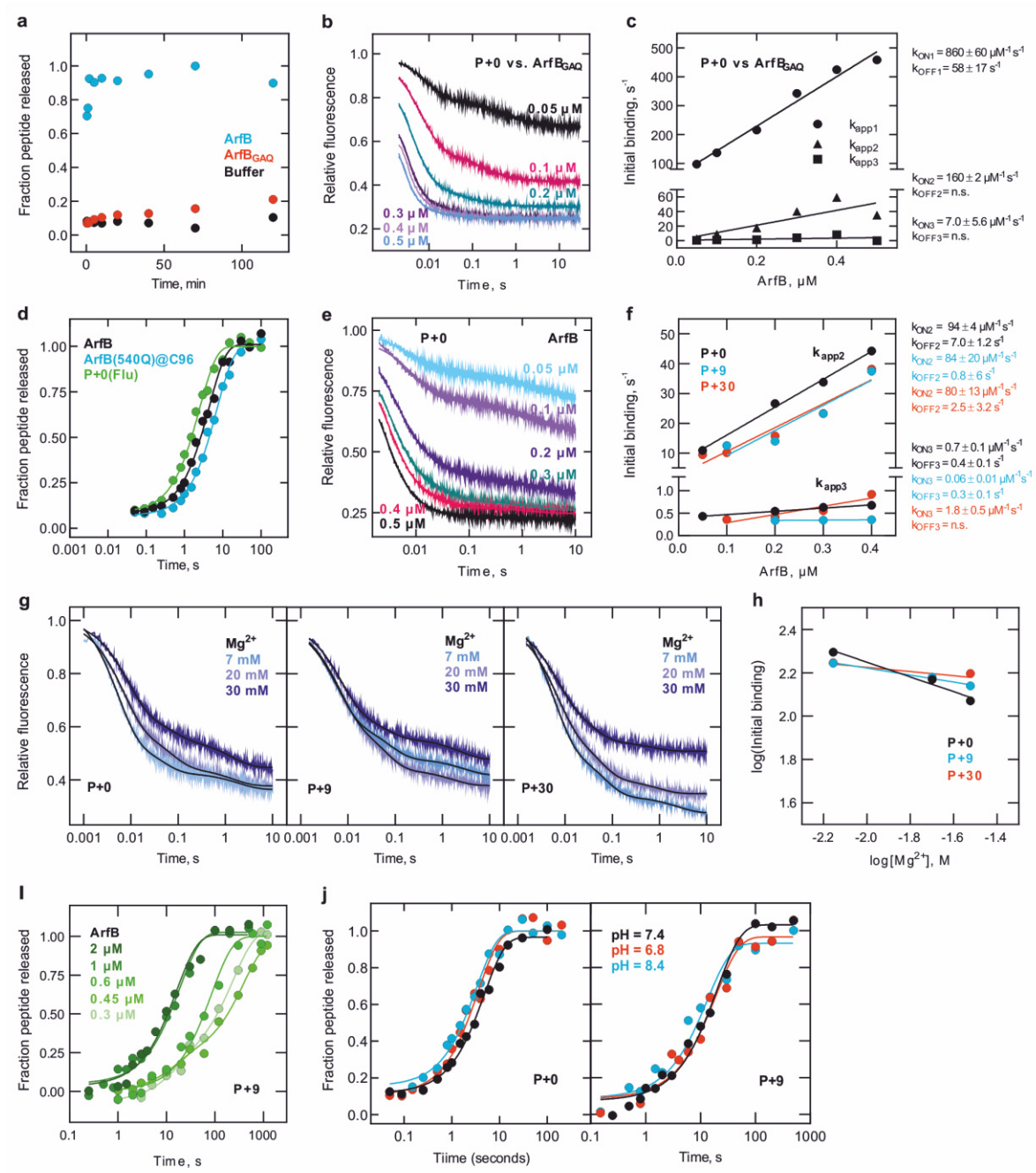


**Supplementary Figure 2 | Cryo-EM analysis of Api137-stalled ribosome–ArfB complexes. a,** Api137 traps ArfB on stalled ribosomes after one round of hydrolysis. Left: Single-round peptidyl-tRNA hydrolysis of P+0 complexes (0.1  $\mu$ M) by ArfB (1  $\mu$ M) in the presence or absence of Api137 (1  $\mu$ M). Right: Multiple-turnover peptidyl-tRNA hydrolysis on P+0 complexes (0.2  $\mu$ M) by ArfB (0.02  $\mu$ M) in the presence or absence of Api137 (1  $\mu$ M). Error bars represent the SEM of three biological replicates. **b,** mRNA remains intact after incubation with ArfB. Fluorescence anisotropy of fluorescein attached at the 3' end of ribosome-bound P+36 mRNA is shown before and after addition of ArfB (0.1  $\mu$ M) to P+36 ribosome complex (0.01  $\mu$ M). Error bars represent the SEM of three biological replicates (white circles). **c,** Api137 stalls ArfB and canonical release factors on the ribosome by a similar structural

mechanism. Left: Cryo-EM density of the PTC in the major P+9 post-hydrolysis state, rendered at  $3.5\sigma$ . Right: Corresponding interaction network of Api37 and the ribosome with ArfB vs. the network reported for RF1<sup>1</sup>. **d**, Sorting of P+0 complexes (left) and P+9 complexes (right) and the mask used for 3D classification for ArfB occupancy (lower right, transparent blue). See Methods for further details. **e**, Fourier-shell-correlation (FSC) curves of P+0 complexes (left) and P+9 complexes.



**Supplementary Figure 3 | Quality of the ArfB models.** **a**, Improved atomic model of the ribosome-ArfB complex from the present high-resolution 2.6 Å cryo-EM map. Left: Present cryo-EM density and model of ArfB in the P+9 post-hydrolysis complex, density rendered at 3.5 $\sigma$ . Middle: X-ray based density (2mF<sub>0</sub>-DF<sub>c</sub>) and corresponding model of ArfB in the 3.2 Å crystal structure of a post-hydrolysis complex<sup>2</sup>, density rendered at 1 $\sigma$ . Right: Superposition of the cryo-EM and X-ray based models reveals register shift between the models. Box: Close-ups of register shifts between the models for backbone regions as indicated by labels 1, 2 in the superposition; C $\alpha$  atoms are rendered as spheres with residue numbers. The register shift in the CTD starting at Arg112 affects all subsequent residues and their interactions with the ribosome. **b**, Cryo-EM densities for functionally important ArfB residues. Note the well-defined density for ArfB residues forming important interactions vs. the undefined densities (arrow-heads) for non-essential residues (underlined), which are not involved in tight interactions, in accordance with the functional data<sup>3</sup>. Panels 1, 2, 3 depict distinct regions in ArfB indicated in the schematic (left).



**Supplementary Figure 4 | Detailed characterization of ArfB initial binding and engagement steps.** **a**, ArfB<sub>GAQ</sub> is catalytically inactive at 20°C. ArfB, ArfB<sub>GAQ</sub> (1  $\mu$ M) or buffer were mixed with P+0 complex (0.1  $\mu$ M) and time courses of peptidyl-tRNA hydrolysis were measured. **b**, Time courses of initial binding are similar for ArfB<sub>GAQ</sub> and the catalytically active wild-type ArfB (compare to **e**). ArfB<sub>GAQ</sub>(540Q) (0.05-0.5  $\mu$ M) was rapidly mixed with P+0(Flu) complexes (0.015  $\mu$ M). **c**, Linear concentration dependence of the apparent rate constants for the binding of ArfB<sub>GAQ</sub> to P+0. Data are represented as mean values of two independent experiments with six technical replicates each. **d**, Labeled components used in binding experiments have the same activity in the peptidyl-tRNA hydrolysis reaction as unlabeled wild-type ArfB. Time courses of peptidyl-tRNA hydrolysis with the wt ArfB or

ArfB(540Q) labeled at position 96 (1  $\mu$ M) on P+0 (0.15  $\mu$ M), and of wt ArfB on P+0(Flu) complexes (37°C). Solid lines represent single-exponential fits. **e**, Time courses of ArfB binding to P+0. P+0(Flu) (0.015  $\mu$ M) was rapidly mixed with ArfB(540Q) (0.05-0.5  $\mu$ M). Solid lines indicate exponential fits with three exponential terms. **f**, Linear concentration dependence of the apparent rate constants for the intermediate and slow phases of ArfB binding to P+0, P+9, and P+30 complexes. **g**, Rapid initial binding of ArfB to the ribosome at increasing Mg<sup>2+</sup> concentrations. ArfB(540Q) (0.2  $\mu$ M) was rapidly mixed with P+0(Flu), P+9(Flu), or P+30(Flu) (0.015  $\mu$ M) at 7 mM, 20 mM, or 30 mM MgCl<sub>2</sub>. **h**, Effect of Mg<sup>2+</sup> on the apparent rate constant of the rapid association phase. Data represented as mean values of two independent experiments with six technical replicates each. **i**, Kinetics of peptidyl-tRNA hydrolysis on P+9 complexes. Time courses of hydrolysis with P+9 ribosome complex (0.15  $\mu$ M) and ArfB (0.3-2  $\mu$ M) (37°C). Data are represented as mean values of two independent experiments. **j**, ArfB-mediated peptidyl-tRNA hydrolysis is pH-independent. Time courses were measured at pH = 7.4, 6.8, or 8.4 with P+0 (left panel) and P+9 (right panel) complexes. ArfB (1  $\mu$ M) was rapidly mixed with stalled ribosomes (0.15  $\mu$ M) at 37°C.

**Supplementary Table 1. Cryo-EM structure determination.**

Ribosomal complex	P+0 70S•tRNA•ArfB•Api137	P+9 70S•tRNA•ArfB•Api137	P+9 70S•Phe-fMet-tRNA	P+9 70S•tRNA•ArfB•Api137
Ribosomal state	P+0 post-hydrolysis	P+9 post-hydrolysis	P+9 stalled complex	P+9 tRNA hybrid state
<b>Database entries</b>				
EMDB ID	10908	10906	10905	10907
PDB ID	6YSU	6YSS	6YSR	6YST
<b>Data collection</b>				
Microscope	Titan Krios	Titan Krios	Titan Krios	Titan Krios
Camera	Falcon II	Falcon III	Falcon III	Falcon III
Magnification	59.000	59.000	59.000	59.000
Voltage (kV)	300	300	300	300
Electron dose (e <sup>-</sup> /Å <sup>2</sup> )	25	50	50	50
Defocus range (μm)	1.2-2.3	0.2-2.5	0.2-2.5	0.2-2.5
Pixel size (Å)	1.072	1.16	1.16	1.16
<b>Cryo-EM reconstruction</b>				
Final resolution	3.7	2.6	3.1	3.2
Final particles (no.)	60.692	282.252	25.347	23.340
Point group symmetry	C1	C1	C1	C1
FSC-threshold	0.143	0.143	0.143	0.143
Resolution (Å)	3.7	2.6	3.1	3.2
Resolution metric	gold standard FSC	gold standard FSC	gold standard FSC	gold standard FSC
<b>Atomic model refinement</b>				
Final resolution (Å)	3.7	2.6	3.1	3.2
Cumulative RSCC (%) >0.8/>0.6/>0.4	84.80%/96.49%/98.79%	87.47%/95.28%/97.23%	80.50%/94.66%/97.31%	67.52%/93.74%/97.93%
Initial models used	5afi (70S) 4v95 (ArfB) 5O2R (Api137) 4RB7 (P-tRNA)	5afi (70S) 4v95 (ArfB) 5O2R (Api137) 4RB7 (P-tRNA)	5afi (70S) 4RB7 (P-tRNA)	5afi (70S) 4v95 (ArfB) 5O2R (Api137) 4RB7 (P-tRNA)
Molprobity score	2.41	2.05	2.15	2.45
Clashscore	20.23	10.58	12.11	20.46
<b>No. Atoms/No. Residues/RSCC</b>				
Total	146404/10675/0.85	147051/10751/0.86	145963/10607/0.83	146850/10748/0.81
Protein	46328/6030/0.84	46921/6105/0.86	45722/5954/0.82	46921/6105/0.78
Nucleic	99717/4645/0.87	99739/4646/0.87	99903/4653/0.85	99672/4643/0.83
ArfB	1078/140/0.75	1078/140/0.88	-	1078/140/0.84
<b>B-factors</b>				
Protein	77.38	36.20	63.65	96.08
Nucleotide	81.47	36.82	64.24	93.91
Ligands, Ions	54.69	23.40	43.02	60.77
<b>R.m.s. deviations</b>				
Bond lengths (Å)	0.007	0.007	0.006	0.007
Bond angles (°)	0.758	0.685	0.737	0.847
<b>Ramachandran plot</b>				
Favored (%)	87.72	91.50	89.74	86.10
Allowed (%)	12.10	8.08	9.88	13.49
Disallowed (%)	0.19	0.42	0.38	0.42

\*For model refinement, maps at ≤3.1 Å resolution were resampled to 512×512×512 pixels, corresponding to a pixel size of 0.6525 Å

**Supplementary Table 2. Summary of rate constants.**

	<b>P+0</b>	<b>P+9</b>	<b>P+30</b>
Hydrolysis rate, $s^{-1}$	$0.15 \pm 0.01$	$0.06 \pm 0.01$	$0.004 \pm 0.001$
Fast $k_{ON}$ , $\mu M^{-1}s^{-1}$	$470 \pm 70$	$280 \pm 30$	$320 \pm 40$
Fast $k_{OFF}$ , $s^{-1}$	$110 \pm 20$	$140 \pm 10$	$120 \pm 10$
Medium $k_{ON}$ , $\mu M^{-1}s^{-1}$	$94 \pm 4$	$84 \pm 20$	$80 \pm 13$
Medium $k_{OFF}$ , $s^{-1}$	$7.0 \pm 1.2$	$0.8 \pm 6$	$2.5 \pm 3.2$
Slow $k_{ON}$ , $\mu M^{-1}s^{-1}$	$0.7 \pm 0.1$	$0.06 \pm 0.01$	$1.8 \pm 0.5$
Slow $k_{OFF}$ , $s^{-1}$	$0.4 \pm 0.1$	$0.3 \pm 0.1$	n.s.
$k_{diss\ avg}$ , $s^{-1}$	$0.06 \pm 0.01$	$0.23 \pm 0.01$	$0.33 \pm 0.01$
$K_M$ , $\mu M$	$0.25 \pm 0.09$	n.d.	
$k_{cat}$ , $s^{-1}$	$0.010 \pm 0.001$	n.d.	

The hydrolysis rate is obtained by exponential fitting of single-round hydrolysis time courses (Fig. 4d,e). The  $k_{ON}$  and  $k_{OFF}$  values were calculated from the slope and Y-axis intercept, respectively, of the linear concentration dependence of the apparent rate constant of the rapid initial binding phase (Fig. 4c).  $k_{diss\_avg}$  is a weighted average dissociation rate constant of the ArfB-ribosome complex estimated from the time courses of Fig. 4f.  $K_M$  is the substrate concentration at which the reaction velocity reaches half-maximum and is calculated by hyperbolic fitting of the Michaelis-Menten titration (Fig. 5A).  $k_{cat}$  is calculated by dividing the maximum reaction velocity with the ArfB concentration in the reaction.

**Supplementary Table 3. Apparent rate constants of ArfB dissociation.**

	$k_{app}^1, s^{-1}$	$A_1$	$k_{app}^2, s^{-1}$	$A_2$
<b>P+0</b>	$0.41 \pm 0.01$	$0.21 \pm 0.02$	$0.04 \pm 0.01$	$0.79 \pm 0.02$
<b>P+9</b>	$0.41 \pm 0.01$	$0.47 \pm 0.01$	$0.07 \pm 0.01$	$0.53 \pm 0.01$
<b>P+30</b>	$0.47 \pm 0.01$	$0.61 \pm 0.01$	$0.10 \pm 0.01$	$0.39 \pm 0.01$

Apparent rate constants were obtained from the exponential fit of representative dissociation experiments with at least 6 technical replicates averaged. Values are averages with SEM of the fit.

## Supplementary References

1. Florin, T. et al. An antimicrobial peptide that inhibits translation by trapping release factors on the ribosome. *Nat Struct Mol Biol* **24**, 752-757 (2017).
2. Gagnon, M.G., Seetharaman, S.V., Bulkley, D. & Steitz, T.A. Structural basis for the rescue of stalled ribosomes: structure of YaeJ bound to the ribosome. *Science* **335**, 1370-2 (2012).
3. Kogure, H. et al. Identification of residues required for stalled-ribosome rescue in the codon-independent release factor YaeJ. *Nucleic Acids Res* **42**, 3152-63 (2014).

ARTICLE

<https://doi.org/10.1038/s41467-019-13408-7>

OPEN

# Release factor-dependent ribosome rescue by BrfA in the Gram-positive bacterium *Bacillus subtilis*

Naomi Shimokawa-Chiba<sup>1,3</sup>, Claudia Müller<sup>2,3</sup>, Keigo Fujiwara<sup>1</sup>, Bertrand Beckert<sup>2</sup>, Koreaki Ito<sup>1</sup>, Daniel N. Wilson<sup>2\*</sup> & Shinobu Chiba<sup>1\*</sup>

Rescue of the ribosomes from dead-end translation complexes, such as those on truncated (non-stop) mRNA, is essential for the cell. Whereas bacteria use *trans*-translation for ribosome rescue, some Gram-negative species possess alternative and release factor (RF)-dependent rescue factors, which enable an RF to catalyze stop-codon-independent polypeptide release. We now discover that the Gram-positive *Bacillus subtilis* has an evolutionarily distinct ribosome rescue factor named BrfA. Genetic analysis shows that *B. subtilis* requires the function of either *trans*-translation or BrfA for growth, even in the absence of proteotoxic stresses. Biochemical and cryo-electron microscopy (cryo-EM) characterization demonstrates that BrfA binds to non-stop stalled ribosomes, recruits homologous RF2, but not RF1, and induces its transition into an open active conformation. Although BrfA is distinct from *E. coli* ArfA, they use convergent strategies in terms of mode of action and expression regulation, indicating that many bacteria may have evolved as yet unidentified ribosome rescue systems.

<sup>1</sup> Faculty of Life Sciences and Institute for Protein Dynamics, Kyoto Sangyo University, Motoyama, Kamigamo, Kita-Ku, Kyoto 603-8555, Japan. <sup>2</sup> Institute for Biochemistry and Molecular Biology, University of Hamburg, Martin-Luther-King-Platz 6, 20146 Hamburg, Germany. <sup>3</sup>These authors contributed equally: Naomi Shimokawa-Chiba, Claudia Müller. \*email: [Daniel.Wilson@chemie.uni-hamburg.de](mailto:Daniel.Wilson@chemie.uni-hamburg.de); [schiba@cc.kyoto-su.ac.jp](mailto:schiba@cc.kyoto-su.ac.jp)

Faithful translation requires accurate initiation, elongation, and termination. In translation termination, the stop codon situated in the A-site of the ribosome recruits a release factor (RF), which then hydrolyzes the peptidyl-tRNA ester bond to release the polypeptide product from the ribosome. In bacteria, RF1 recognizes UAA and UAG while RF2 recognizes UAA and UGA through their PxT and SPF codon recognition motifs, respectively<sup>1</sup>. These RFs contain the hydrolysis active site motif, GGQ, for catalysis. Polypeptide release is then followed by dissociation of the ribosome from mRNA into the small and large subunits by a process mediated by ribosome recycling factor and elongation factor G<sup>2</sup>.

However, the termination/recycling event can be perturbed when mRNA has aberrant features, one of which is the absence of an in-frame stop codon. The mRNA lacking a stop codon, called a non-stop mRNA, causes stalling of the ribosome at the 3' end because recruitment of RFs to the ribosome requires the interaction of a stop codon recognition motif of the RF with a cognate stop codon. Since the role of termination is not only to define the end of the protein but also to recycle the ribosome for the next round of translation initiation, a failure in termination lowers the cellular capacity of protein synthesis, unless dealt with by the cellular quality control mechanisms. Indeed, a loss of function in the quality control machinery leads to an accumulation of dead-end translation products, which was estimated to represent ~2–4% of the translation products in *Escherichia coli*<sup>3</sup>, and results in lethality<sup>4,5</sup>.

Living organisms have evolved mechanisms that resolve non-productive translation complexes produced by ribosome stalling on non-stop mRNAs. Such quality control is also called ribosome rescue. In eukaryotic cells, like yeast, the Dom34/Hbs1 complex, together with Rli1, mediates ribosome rescue on truncated mRNAs<sup>4,6,7</sup>. In bacteria, two distinct mechanisms operate in the resolution of non-stop nascent chain-ribosome complexes, *trans*-translation and stop-codon-independent peptide release from the ribosome<sup>4,5,8,9</sup>. The latter mechanism can further be classified into two classes, RF-dependent and RF-independent. The crucial player in *trans*-translation is the *transfer*-messenger RNA (tmRNA), which is encoded by *ssrA*. tmRNA cooperates with SmpB, which mediates ribosomal accommodation of tmRNA at the ribosomal A-site<sup>10,11</sup>. The tmRNA is composed of tRNA- and mRNA-like domains. The former can be charged with alanine, which then accepts the non-stop peptide and is elongated further according to the mRNA-like coding function of tmRNA until the built-in stop codon is reached. The result is the formation of the non-stop polypeptide bearing an extra *ssrA*-encoded sequence (15 amino acids in *B. subtilis*) and dissociation of the ribosome from the non-stop mRNA. The SsrA tag sequence promotes proteolytic elimination of the non-stop polypeptide via targeting to cellular proteases. *Trans*-translation is essential for the growth of some bacteria<sup>5,12</sup>. The essentiality lies in the liberation of the ribosome from the non-stop mRNA, but not in proteolytic degradation of the translation products<sup>13,14</sup>. Bacterial species that can survive without *trans*-translation often possess one or more alternative ribosome rescue factor(s), such as ArfA, ArfB, or ArfT, which are involved in stop-codon-independent cleavage of the non-stop peptidyl-tRNA<sup>5</sup>.

ArfA was identified in *E. coli* by a genetic screening for a mutation showing synthetic lethality with the loss of *ssrA*<sup>15</sup>. ArfA is an RF-dependent ribosome rescue factor, which recruits RF2, but not RF1, to the non-stop stalled ribosome complexes to induce hydrolysis of the dead-end peptidyl-tRNA<sup>16</sup>. Interestingly, ArfA itself is produced from a non-stop mRNA, such that it is strongly down-regulated by *trans*-translation in wild-type cells and only induced significantly upon dysfunction of *trans*-translation. Thus, it has been suggested that tmRNA-SmpB is the

primary rescue factor, and the ArfA-RF2 system serves as a backup system<sup>17,18</sup>. ArfB (YaeJ), identified as a multicopy suppressor of the *ssrA/arfA* double mutant<sup>19,20</sup>, contains its own GGQ catalytic motif, enabling it to act as an RF-independent ribosome rescue factor<sup>21</sup>. Although the physiological role of ArfB in *E. coli* is unknown, its homologs are widely distributed among both Gram-positive and -negative bacteria<sup>5,20,22</sup> as well as eukaryotic mitochondria<sup>23</sup>. ArfT in *Francisella tularensis*, a member of  $\gamma$ -proteobacteria that lacks both ArfA and ArfB homologs<sup>24</sup>, is essential in the absence of tmRNA. Like ArfA, ArfT is an RF-dependent ribosome rescue factor, although ArfT can function with either RF1 or RF2. Phylogenetic distribution of ArfA is limited to a subset of  $\beta$ - and  $\gamma$ -proteobacteria whereas that of ArfT is limited to a subset of  $\gamma$ -proteobacteria. To date, RF-dependent ribosome rescue factors have only been reported in Gram-negative bacteria.

*Bacillus subtilis*, a Gram-positive bacterium, can also survive without *ssrA*<sup>25</sup>, but no alternative factor for ribosome rescue has been reported in this organism, raising the question of whether the ribosome rescue function is non-essential or alternative factors have escaped identification in *B. subtilis*. In this study, we have addressed this question and identified BrfA (*Bacillus* ribosome rescue factor *A*; formerly YqkK) as a ribosome rescue factor. BrfA has no obvious sequence similarity to other Arf proteins. We show that BrfA is an RF2-dependent ribosome rescue factor, which induces hydrolysis of peptidyl-tRNA in non-stop translation complexes. BrfA is produced naturally from a non-stop mRNA and is thus negatively regulated by *trans*-translation, revealing a conceptually similar regulatory crosstalk as documented for *E. coli* ArfA. Lastly, using single-particle cryo-electron microscopy (cryo-EM), we reveal how BrfA recognizes the presence of truncated mRNAs and recruits and stabilizes an open conformation of RF2 to rescue the stalled ribosomes. BrfA uses a mechanism that is similar but distinct from ArfA. Collectively, our findings lead us to suggest that Gram-positive and -negative bacteria have independently acquired their own unique RF-dependent ribosome rescue systems equipped with a convergent scheme of regulation.

## Results

**BrfA and *trans*-translation exhibit synthetic lethality.** The dispensability of *trans*-translation in *B. subtilis* raises the possibility that it contains an alternative ribosome rescue factor. With the reasoning that the loss of such a factor would make the bacterial growth dependent on *trans*-translation proficiency, we searched for the chromosomal gene knockouts that cause synthetic lethality with the deficiency of *trans*-translation. We used a strain with chromosomal deletion of *smpB*, which encodes the *trans*-translation co-factor but having a plasmid carrying the wild-type *smpB* as well as *lacZ* genes (Fig. 1a). This rescue plasmid was a derivative of pLOSS\*<sup>26</sup> driven by a temperature sensitive (Ts) replicon, such that it is lost frequently at high temperature. We prepared chromosomal DNA from a mixture of the BKE library strains, a collection of mutants individually disrupted for the 3968 non-essential *B. subtilis* genes by replacements with the erythromycin resistance marker (*ery*)<sup>27</sup>, and used it to transform (by homologous recombination) the strain for the screening described above. Transformant mixtures were then incubated at 50 °C to destabilize the rescue plasmid and plated on selective agar containing X-Gal (see Methods). Whereas clones that did not depend on SmpB had segregated out the plasmid and formed white colonies, those requiring SmpB survived only when they had retained the plasmid and formed blue colonies due to the plasmid-encoded  $\beta$ -galactosidase (Fig. 1a). Among ~74,000 transformants, we picked up 42 blue colonies and determined the

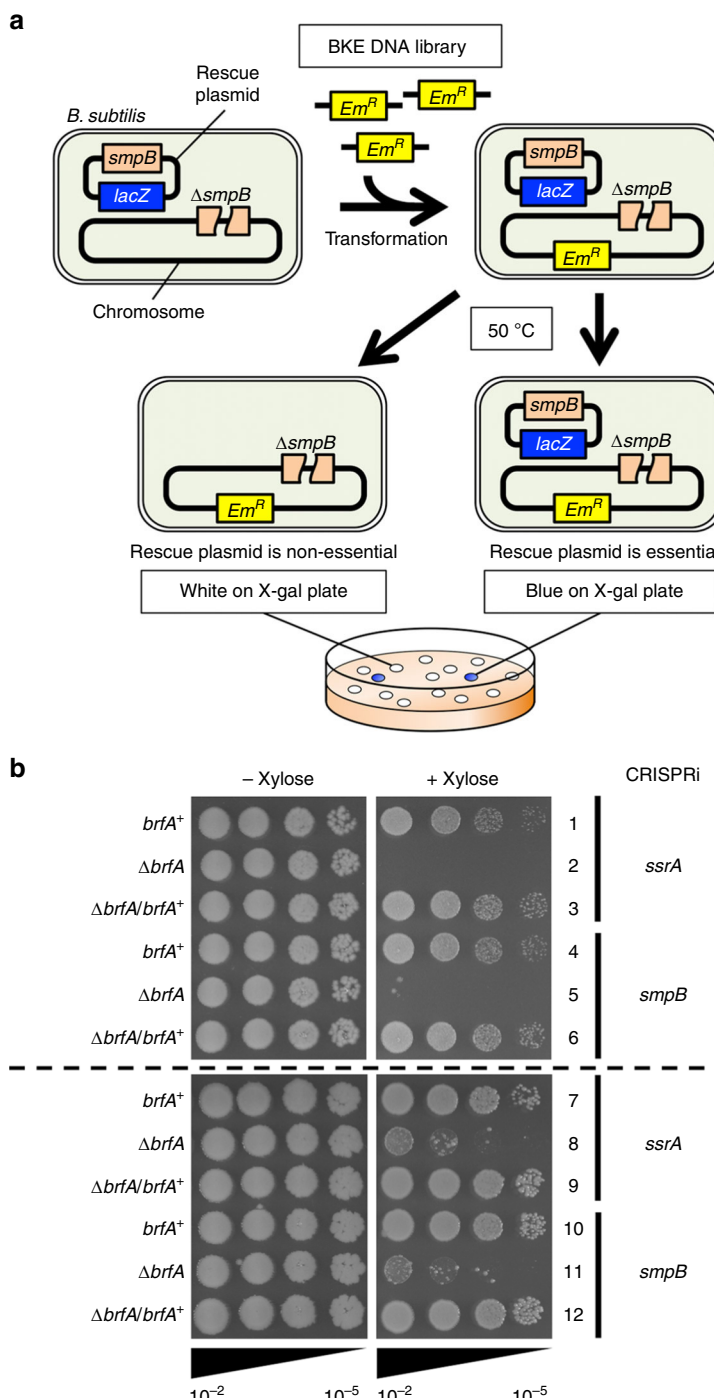


**Fig. 1** Simultaneous loss of BrfA and *trans*-translation leads to synthetic growth defects. **a** A schematic representation of the synthetic lethal screening to identify genes whose absence causes synthetic lethal phenotype with the deficiency of *trans*-translation. **b** Xylose-inducible CRISPRi was targeted to *ssrA* (lines 1–3, 7–9) or *smpB* (lines 4–6, 10–12) in the *B. subtilis* strains indicated at the left by the genotypes of the *brfA* gene (*ΔbrfA/brfA*<sup>+</sup> signifies the presence of *brfA*<sup>+</sup> in an ectopic locus). Cultures prepared in the absence of xylose were serially diluted (from 10<sup>-2</sup> to 10<sup>-5</sup>) and spotted onto LB agar plates with or without 1% xylose, as indicated at the top, for incubation at 30 °C (upper) or 37 °C (lower) for 17 h.

chromosomal locations of the *ery* inserts by DNA sequencing, followed by elimination of false-positive clones by retransformation experiments. These procedures left clones with an *ery* disruption of *yqkK* (renamed *brfA*, see below), which makes SmpB indispensable for survival.

We validated the growth requirement features of *B. subtilis* for BrfA and the *trans*-translation system by an independent approach. We used CRISPR interference (CRISPRi)<sup>28</sup> to conditionally silence either *ssrA* or *smpB* (Fig. 1b). To do this,

the catalytically inactive and xylose-inducible variant of Cas9 (dCas9) was integrated into the chromosomal *lacA* locus of the wild type (WT) and the *ΔbrfA* strains. In addition, the constitutively expressed small guide RNA (sgRNA) that targets either *ssrA* or *smpB* was integrated into the *amyE* locus of the same strains. The bacterial strains grew normally when dCas9 was uninduced in the absence of xylose (Fig. 1b, left panels). Growth of the *brfA*<sup>+</sup> (WT) cells was not affected by 1% xylose, which induced dCas9 to silence *ssrA* or *smpB* (lanes 1, 4, 7, and 10, right

panels). By contrast, growth of the  $\Delta brfA$  strain was severely impaired in the presence of xylose, which led to CRISPR-mediated repression of *ssrA* or *smpB* (lanes 2, 5, 8, and 11, right panels). Expression of *brfA* from an ectopic locus restored the growth defect associated with the *trans*-translation deficiency, substantiating that BrfA is the responsible factor for the synthetic growth phenotype (lanes 3, 6, 9, and 12). These results indicate that BrfA is required for optimal growth in the absence of sufficient activity of *trans*-translation in *B. subtilis*.

**BrfA expression is regulated by *trans*-translation.** The *brfA* gene contains 71 sense codons followed by a stop codon. We note that it contains a typical rho-independent transcription terminator sequence within the coding region, raising an intriguing possibility that BrfA is translated naturally from a non-stop mRNA lacking the 3' region including the stop codon (Fig. 2a). If this is the case, the translation product should initially consist of approximately 62 amino acids in the form of peptidyl-tRNA. However, translation of such mRNAs is likely dealt with by the *trans*-translation mechanism of ribosome rescue, which would add the SsrA tag sequence of 15 amino acids to the BrfA non-stop product. It follows then that the BrfA product would be rapidly degraded by cellular proteases, such that the protein level should be strongly down-regulated in *trans*-translation proficient cells.

To test this possibility, we examined the impact of *trans*-translation on the accumulation of a series of BrfA-derived proteins. We constructed a translational gene fusion consisting of the coding sequences for green fluorescence protein (GFP), BrfA (full length), and FLAG that are connected in-frame in this order from the N-terminus to the C-terminus. We also constructed transcriptional fusions, in which independently translatable *lacZ* follows *gfp-brfA-flag* to verify the occurrence of transcription termination in *brfA* (Fig. 2b). We expressed GFP-BrfA-FLAG in the wild type and the  $\Delta smpB$  cells and detected the products with anti-GFP and anti-FLAG immunoblotting. Strikingly, the wild-type cells did not produce any anti-GFP detectable protein from the *gfp-brfA(WT)-flag* construct (Fig. 2c, lane 1, upper panel). By contrast, the  $\Delta smpB$  cells produced a product that formed an intense band near the 37 kDa marker (Fig. 2c, lane 2, upper panel). This species of protein did not react with anti-FLAG (lane 2, lower panel), indicating that it lacked the C-terminal region. These results are consistent with the notion that the mRNA ends within *brfA* due to internal termination. The translation products are SsrA-tagged and degraded rapidly in the wild-type strain, while they accumulate in the *trans*-translation-deficient  $\Delta smpB$  cells.

To examine the above scenario further, we disrupted the transcription terminator either by internal deletion or by synonymous substitutions (Fig. 2a, b). In the former, we deleted the codons 63–71 of *brfA* in the context of GFP-BrfA-FLAG to eliminate the 3' T stretch of the transcriptional terminator (GFP-BrfA62-FLAG). In the latter, we introduced synonymous mutations to disrupt the secondary structure required for transcription termination (GFP-BrfA(no\_term)-FLAG) (Fig. 2a, b). Both of these terminator-less mutant forms of GFP-BrfA-FLAG accumulated equally in the wild type and  $\Delta smpB$  strains and are reactive with both anti-GFP and anti-FLAG (Fig. 2c, lanes 3–6).

We then confirmed the occurrence of internal transcription termination by examining the expression of *lacZ* attached at a 3' region of the transcription unit. If the terminator within *brfA* indeed functions, the downstream *lacZ* would not be expressed. As expected, cells harboring the construct with the wild-type *brfA* sequence exhibited very low levels of  $\beta$ -galactosidase activity (Fig. 2d, columns 1 and 2), as compared with those having the terminator mutations, which exhibited high levels of

$\beta$ -galactosidase activity (Fig. 2d, columns 3–6). These data establish that the internal transcription termination indeed occurs for *brfA*, indicating that it is a major element that triggers the BrfA down-regulation by the SsrA tag-dependent degradation.

These results show that *B. subtilis* is equipped with at least two layers of ribosome rescue mechanisms, *trans*-translation and BrfA-dependent peptidyl-tRNA hydrolysis (see below). The *trans*-translation-dependent down-regulation indicates that BrfA is the secondary ribosome rescue factor that is only produced upon dysfunction of *trans*-translation, the primary ribosome rescue mechanism. Thus, the internal transcription terminator in BrfA provides the means for this bacterium to accomplish the compensatory and vectorial regulation for the maintenance of ribosome rescue capability. In this context, BrfA bears a striking similarity to the *E. coli* alternative rescue factor, ArfA, which is also synthesized from a non-stop mRNA<sup>17,18</sup>.

**BrfA recruits RF2 to hydrolyze non-stop peptidyl-tRNAs.** We characterized BrfA biochemically by examining whether it could induce polypeptide release, as expected for an alternative ribosome rescue factor. To do this, we purified BrfA in the form of BrfA62-His<sub>6</sub>, which lacks the C-terminal 9 amino acid residues encoded by the *brfA* gene but not by the *brfA* mRNA (see above); a hexahistidine (His<sub>6</sub>) tag was attached to the C-terminus to aid purification. We considered that the absence of the C-terminal 9 amino acids was physiological. Also, the absence of the 3' coding region of *brfA* should disrupt the internal transcription terminator signal and enable the attachment of the His<sub>6</sub> tag. Since BrfA lacks a GGQ motif critical for peptidyl-tRNA hydrolysis, we hypothesized that BrfA requires an RF to hydrolyze peptidyl-tRNA. Therefore, we also purified *B. subtilis* RF1 and RF2. For in vitro translation with defined translation components, we used the *Bs* hybrid PURE system<sup>29</sup>, a modified version of the PURE coupled transcription–translation system<sup>30</sup>, in which the original *E. coli* ribosomes were replaced with *B. subtilis* ribosomes. We omitted RFs in the *Bs* hybrid PURE system unless otherwise stated.

We used DNA fragments encoding GFP but without an in-frame stop codon (GFP-ns) to direct in vitro transcription and translation with *Bs* hybrid PURE system and separated the translation products by neutral pH SDS-PAGE, which preserved the peptidyl-tRNA ester bond<sup>31</sup>. The major product, migrating between the 42 and the 55 kDa markers, represents the peptidyl-tRNA (GFP-tRNA; Fig. 3a, lane 1), as treatment of the sample with RNase A before electrophoresis down-shifted this band to the position near the 28 kDa marker, indicative of tRNA removal (GFP; lane 2). Thus, the non-stop template indeed produced a translation-arrested state of ribosome-nascent chain complex, which was unaffected when the reaction mixture included *B. subtilis* RF1 or RF2 (lanes 3–6), as expected from the absence of a stop codon in the template. We then addressed the effects of BrfA. Neither BrfA by itself nor its combination with *B. subtilis* RF1 affected the production of GFP-tRNA (lanes 7–10). By contrast, the addition of both BrfA and *B. subtilis* RF2 to the *Bs* hybrid PURE system resulted in the production of the hydrolyzed GFP band with a concomitant decrease in the level of GFP-tRNA (lanes 11 and 12). Thus, BrfA and RF2 cooperatively catalyze peptide release from the non-stop stalled ribosome.

**Distinct requirements of RF2 for rescue and termination.** Given that BrfA and RF2 cooperatively induce hydrolysis of non-stop peptidyl-tRNA, the role of RF2 would be to execute the catalysis. Consistent with this expectation, a catalytically inactive RF2 variant, RF2(GAQ), whose GGQ active site had been mutated to GAQ, no longer stimulated hydrolysis of GFP-tRNA

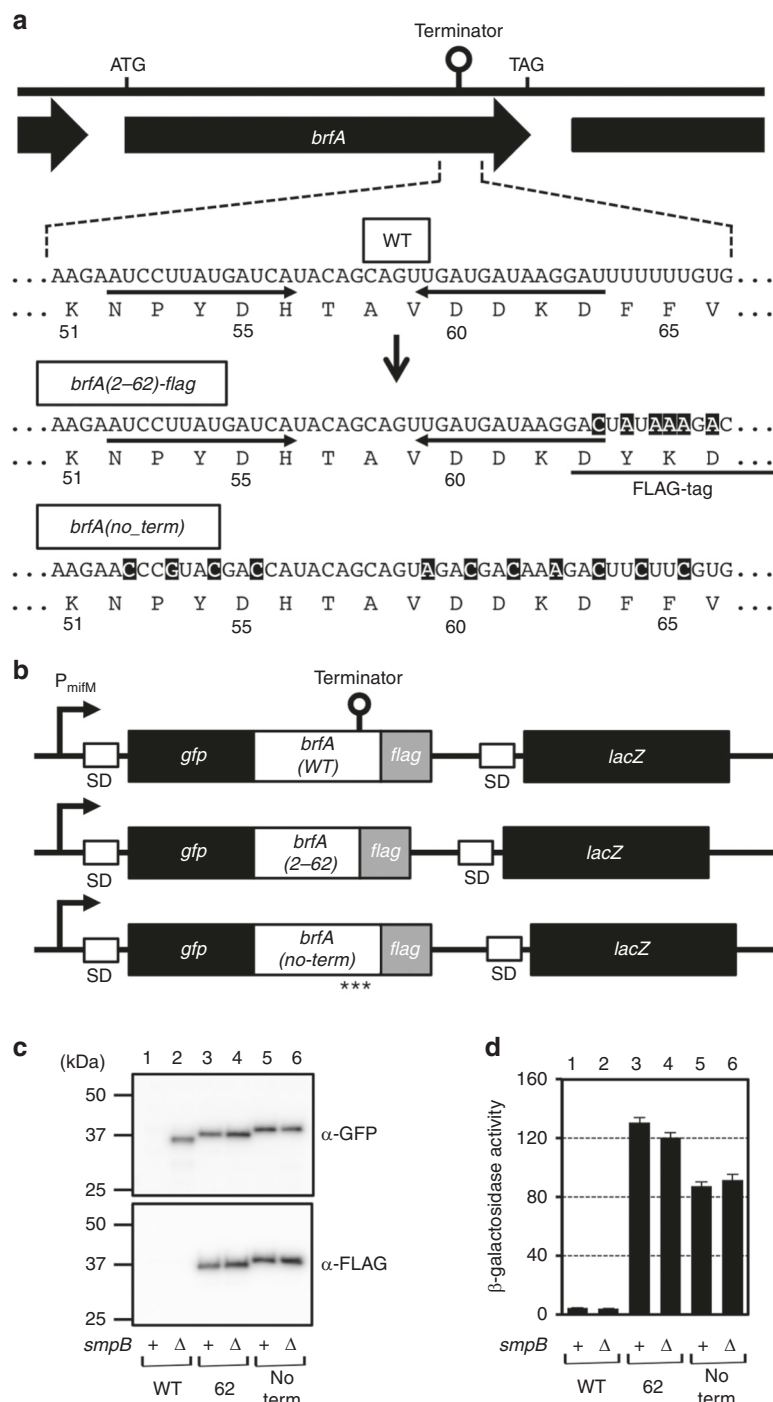


**Fig. 2** The cellular abundance of BrfA is negatively regulated by trans-translation. **a** A schematic representation of the *brfA* open reading frame, showing the intrinsic transcriptional terminator sequence within the coding region (indicated by “terminator” at the top and the wild type (WT) enlarged view below). Shown also are the corresponding sequences of the *gfp-brfA(2-62)-flag* and *gfp-brfA(no\_term)-flag* constructs (see **b**), in which nucleotide substitutions and the FLAG tag are indicated by reverse and underline, respectively. **b** Schematic representations of the *gfp-brfA-flag* constructs with wild-type terminator sequence (*gfp-brfA(2-71)-flag*) and its derivatives with defective terminator signals. These *gfp-brfA* derivatives were placed under the constitutive *mifM* promoter. The *lacZ* gene is also placed downstream of the *gfp-brfA* derivatives. “SD” and asterisks indicate Shine-Dalgarno sequence and synonymous mutations, respectively. **c** Cellular accumulation of the products of the wild-type construct (lanes 1, 2) as well as the *brfA(2-62)* (lanes 3, 4) and the *brfA(no\_term)* (lanes 5, 6) constructs. They were expressed in the *smpB*<sup>+</sup> (odd numbers) or the  $\Delta smpB$  (even numbers) strains and analyzed by anti-GFP (upper) or anti-FLAG (lower) immunoblotting. **d**  $\beta$ -Galactosidase activities (mean  $\pm$  s.d.,  $n = 3$ ) of the cells harboring *lacZ* at the downstream of wild type (columns 1, 2), the *brfA(2-62)* (columns 3, 4), or the *brfA(no\_term)* (columns 5, 6) derivatives of the *gfp-brfA* in the presence (odd numbers) or absence (even numbers) of *smpB*. “s.d.” indicates standard deviation. Source data are provided as a Source Data file.

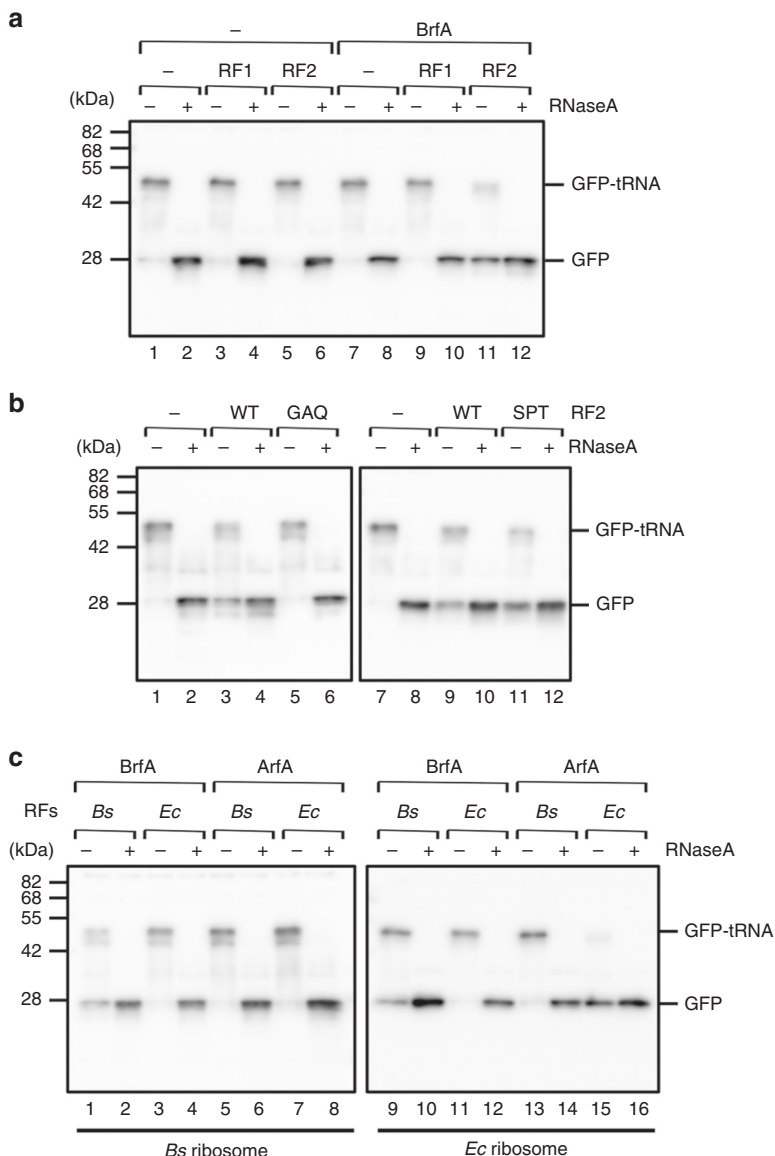


**Fig. 3** In vitro activity of BrfA to hydrolyze non-stop peptidyl-tRNA. **a** BrfA in combination with RF2 cleaves the GFP-tRNA non-stop translation product. In vitro translation using *Bs* hybrid PURE system was directed by the *gfp-ns* template. The reaction mixtures contained purified BrfA62-His<sub>6</sub> (lanes 7–12), purified *B. subtilis* RF1 (lanes 3, 4, 9, and 10), and RF2 (lanes 5, 6, 11, and 12), as indicated. Translation was allowed to proceed at 37 °C for 20 min, and the products were divided into two parts, one of which was treated with RNase A, as indicated. Samples were then analyzed by SDS-PAGE under neutral pH conditions, followed by anti-GFP immunoblotting. **b** BrfA-dependent peptidyl-tRNA hydrolysis activity of RF2 requires its GGQ active site but not SPF stop codon recognition motif. In vitro translation using *Bs* hybrid PURE system was directed by the *gfp-ns* template in the presence of combinations of BrfA, wild-type RF2 (lanes 3, 4, 9, and 10), RF2(GAQ) (lanes 5 and 6), and RF(SPT) (lanes 11 and 12), as indicated. The translation products were analyzed by anti-GFP immunoblotting as described above. **c** Interspecies compatibility of the RF-dependent rescue factor functions. In vitro translation of *gfp-ns* was carried out using *Bs* hybrid PURE system (lanes 1–8) or *Ec* PURE system (lanes 9–16) in the presence of combinations of purified BrfA (lanes 1–4, 9–12), *E. coli* ArfA (lanes 5–8, 13–16), RFs (RF1 plus RF2) purified from *B. subtilis* (lanes 1, 2, 5, 6, 9, 10, 13, and 14), and RFs purified from *E. coli* (lanes 3, 4, 7, 8, 11, 12, 15, and 16). The translation products were analyzed by anti-GFP immunoblotting as described above. Source data are provided as a Source Data file.

even in the presence of BrfA (Fig. 3b, lanes 5 and 6). RF2 possesses the conserved SPF motif as an essential element for the stop codon recognition in termination<sup>32</sup>. We addressed whether this motif is required for the ribosome rescue function of RF2 by mutating it to SPT, which abolishes the termination activity<sup>32</sup>. In the *in vitro* peptidyl-tRNA hydrolysis assay, the RF2(SPT) was as active as the wild-type RF2 in the BrfA-dependent cleavage of GFP-tRNA (Fig. 3b, lanes 9–12), in comparison with the parallel control reaction without RF2 (lanes 7 and 8). These results demonstrate that the stop codon recognition motif of RF2 is dispensable for the ribosome rescue function.

Ribosome stalling can also be induced by specific amino acid sequences of nascent polypeptides for regulatory purposes. Such regulatory nascent polypeptides include *E. coli* SecM, *B. subtilis* MifM, and *Vibrio alginolyticus* VemP<sup>33,34</sup>. Ribosome stalling in these cases needs to be adequately regulated, such that it is subject to conditional and specific mechanisms of cancellation<sup>35,36</sup>. Unregulated rescue could be counterproductive in these cases. Our *in vivo* and *in vitro* analyses show that the *B. subtilis* MifM stalling is refractory to both the *trans*-translation and the BrfA mechanisms of ribosome rescue (Supplementary Fig. 1). Thus, we conclude that BrfA is an RF-dependent ribosome rescue factor in

*B. subtilis* that rescues stalling on non-stop mRNAs, but not regulatory stalling peptides, leading us to suggest the renaming of YqkK to BrfA (*Bacillus* ribosome rescue factor A). To our knowledge, RF-dependent ribosome rescue factors have not been reported previously in Gram-positive bacteria.

**Low interspecies compatibility of ribosome rescue systems.** BrfA homologs are conserved among a subset of *Bacillaceae* family members, mainly among those belonging to the *Bacillus* genus. Although we do not rule out the possibility that BrfA and ArfA share the same evolutionary origin, their distinct phylogenetic distributions and the unique sequence features (Supplementary Fig. 2) seem to favor the notion that BrfA and ArfA have evolved independently of each other and independently from ArfT and ArfB. The narrow phylogenetic distributions of the RF-dependent rescue factors also implies that they emerged relatively late in evolution. Translation components are largely conserved across the species, but they have undergone some micro diversifications. If the alternative rescue factors evolved more recently than the translation factors, their interactions with the translation components, such as the ribosome and an RF, might be species-specific. Indeed, *Francisella tularensis* ArfT can work with *F. tularensis* RF1 or RF2, but not *E. coli* RFs<sup>24</sup>. Also, *E. coli* ArfA fails to recruit *Thermus thermophilus* RF2 (refs. <sup>37,38</sup>). We tested the compatibility of *B. subtilis* BrfA and *E. coli* ArfA with heterologous RFs in vitro. While BrfA efficiently hydrolyzed GFP-tRNA in the *Bs* PURE system supplemented with RF1 and RF2 of *B. subtilis* (Fig. 3c, lanes 1 and 2), it did not work with the *E. coli* RFs (lanes 3 and 4). Interestingly, BrfA was functional when the substrate was translated by the *E. coli* ribosome, provided that the *B. subtilis* RFs were available (lanes 9–10). These results suggest that BrfA interaction with RF2 is species-specific, but its interaction with the ribosome is rather promiscuous.

By contrast, we could show that *E. coli* ArfA requires both the RF2 as well as the ribosomes to be derived from *E. coli*. Specifically, ArfA did not work if combined with the *E. coli* RF2 when the substrate was translated by the *B. subtilis* ribosomes (Fig. 3c, lanes 7 and 8), nor did it work with *B. subtilis* RF2 (lanes 5 and 6), even if the substrate was translated by *E. coli* ribosomes (lanes 13 and 14). The *E. coli* ArfA-mediated hydrolysis of GFP-tRNA was only observed when the ribosomes and RFs were both derived from *E. coli* (lanes 15 and 16). Thus, *E. coli* ArfA is incompatible with the *B. subtilis* ribosomes and RF2, analogously to what was previously observed between *E. coli* ArfA and *T. thermophilus* RF2 (refs. <sup>37,38</sup>). The high specificity of molecular interactions involving the RF-dependent rescue factors is in contrast to the broader interactions in the tmRNA- and ArfB-based rescue pathways (see Discussion).

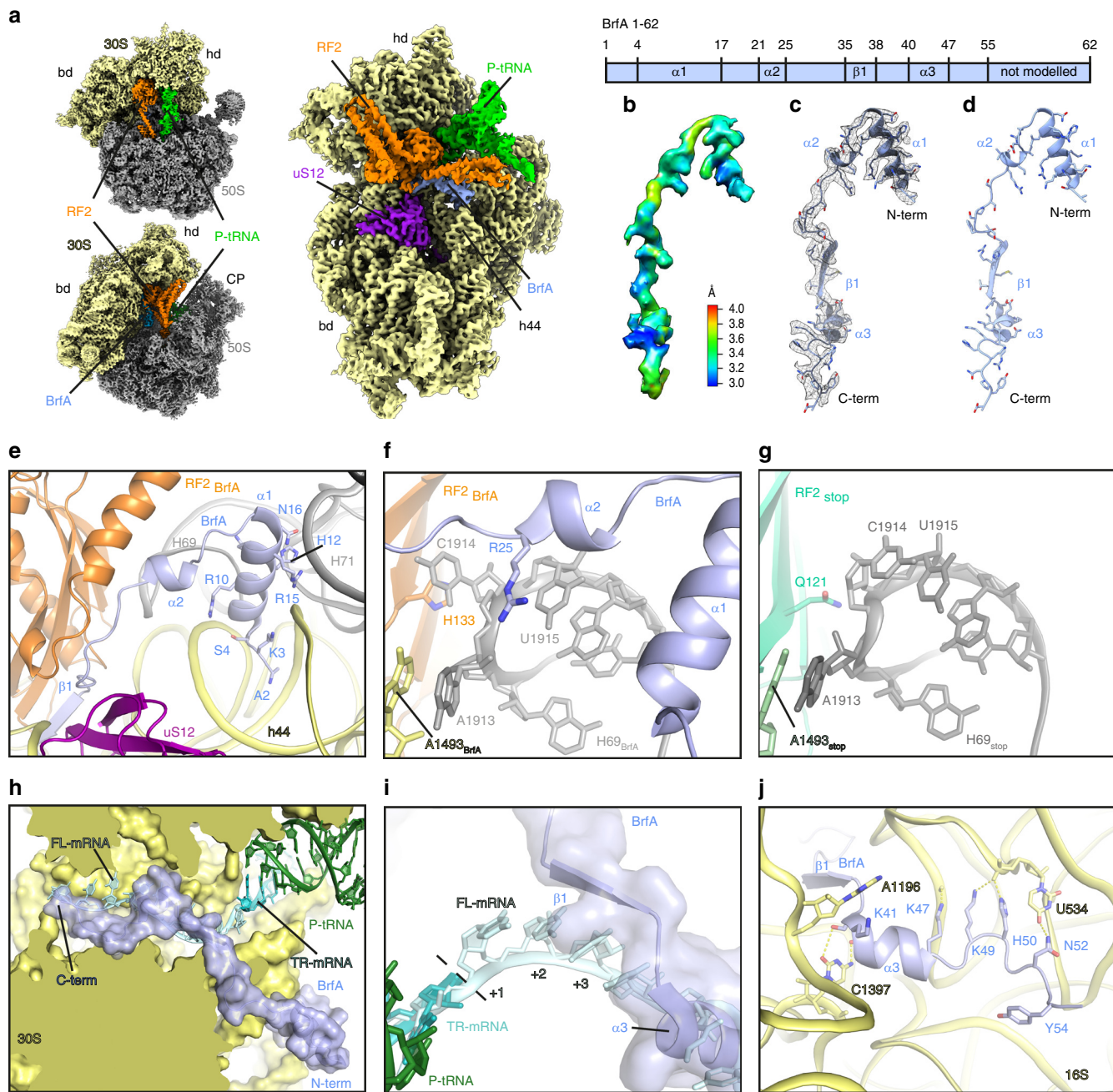
**Cryo-EM structure of a BrfA-RF2-non-stop-ribosome complex.** Since *B. subtilis* BrfA and RF2 can rescue *E. coli* ribosomes stalled on truncated non-stop mRNAs (Fig. 3c, Supplementary Fig. 3), we formed BrfA-RF2-non-stop 70S ribosome (ns70S) complexes by incubating *B. subtilis* BrfA and RF2 with *E. coli* ns70S complexes used previously for ArfA<sup>39</sup>. By substituting the wild-type *B. subtilis* RF2 with a catalytically inactive GGP mutant<sup>40,41</sup>, peptidyl-tRNA hydrolysis and therefore recycling of the ns70S complex was prevented (Supplementary Fig. 3). Cryo-EM analysis of the BrfA62His-RF2-GGP-ns70S complex (herein referred as BrfA-RF2-ns70S) and extensive in silico sorting of this dataset yielded a major subpopulation of ribosomal particles (>80%) that contained stoichiometric occupancy of BrfA, RF2 and P-site tRNA (Supplementary Fig. 4). Refinement of this subpopulation led to a final cryo-EM reconstruction of the BrfA-RF2-ns70S (Fig. 4a), with an average resolution of 3.06 Å (Supplementary

Fig. 4, Supplementary Table 1). The cryo-EM density for BrfA was well-resolved with local resolution ranging between 3.0–3.6 Å (Fig. 4b), enabling residues 2–55 of BrfA to be modeled de novo (Fig. 4c, d). BrfA contains an N-terminal  $\alpha$ -helix  $\alpha$ 1 (residues 4–17) followed by a short  $\alpha$ -helical turn ( $\alpha$ 2, residues 21–25) and  $\beta$ -strand ( $\beta$ 1, residues 35–38) as well as a short C-terminal  $\alpha$ -helix ( $\alpha$ 3, 40–47) followed by a positively charged region (residues 48–55) (Fig. 4d).

**Interaction of BrfA with the non-stop 70S ribosome.** The binding site of BrfA is located predominantly on the 30S subunit in the vicinity of the decoding center, where it spans from the top of helix 44 (h44) of the 16S rRNA past the ribosomal protein uS12 and reaches into the mRNA channel formed by the head and body of the 30S (Fig. 4a). The overall binding site of BrfA on the ribosome (Fig. 4a) is similar, but distinct, to that observed previously for *E. coli* ArfA<sup>37–39,42–44</sup>. The N-terminal helix  $\alpha$ 1 of BrfA resides within the intersubunit space, where highly conserved charged residues (Supplementary Fig. 2) establish interactions with the major groove of h44 and the minor groove of H71 of the 23S rRNA (Fig. 4e). In addition, Arg25 within helix  $\alpha$ 2 of BrfA, which is conserved in all BrfA sequences (Supplementary Fig. 2), stacks upon U1915 and flips C1914 out of H69, where it stacks upon His133 of RF2 (Fig. 4f). This contrasts with the canonical conformation of C1914 within H69 that is observed during translation termination (Fig. 4g) as well as ArfA-mediated ribosome rescue. Indeed, these N-terminal  $\alpha$ -helices have no counterpart in ArfA, instead the N-terminus of ArfA is unstructured and folds back to interact with uS12 (refs. <sup>37–39,42–44</sup>) (Supplementary Fig. 5a–c).

The C-terminal region of BrfA extends from the decoding center into the mRNA channel and would be incompatible with the presence of a full-length mRNA (Fig. 4h), but compatible with a truncated non-stop mRNA (Fig. 4i). BrfA exhibits a modest overlap with the second (+2) and third (+3) nucleotide of the A-site codon, but extensive steric clashes would be expected for the subsequent positions (+4 onwards) (Fig. 4i), similar to that observed previously for ArfA<sup>37–39,42–44</sup> (Supplementary Fig. 5d–i). Thus, BrfA may also recycle ribosomes stalled on non-stop mRNAs with 1–3 nucleotides extending into the A-site, as shown experimentally for ArfA<sup>45–47</sup>. The positively charged C-terminus of BrfA can form multiple hydrogen bond interactions with 16S rRNA nucleotides that comprise the mRNA channel (Fig. 4j). While the interaction network is generally distinct from that observed for ArfA, we note that the mode of contact between the side chains of Lys49 and His50 of BrfA with U534 of the 16S rRNA appears to be shared by ArfA<sup>37–39,42–44</sup> (Supplementary Fig. 5j–l).

**BrfA stabilizes an open conformation of RF2 on the ribosome.** The structure of the BrfA-RF2-ns70S reveals that BrfA recruits RF2 by establishing an extensive interaction surface, specifically encompassing the central portion (residues 30–40) of BrfA and domain 2 (d2) of RF2 (Fig. 5a). Similar to ArfA<sup>37–39,42–44</sup> (Supplementary Fig. 6A–C), BrfA also donates the small  $\beta$ -strand ( $\beta$ 1) to augment the  $\beta$ -sheet of the superdomain d2/d4 of RF2 (Fig. 5a). The overall position of RF2 in BrfA-RF2-ns70S is similar, but slightly shifted, compared to that observed during canonical translation termination<sup>40,48</sup> (Fig. 5b, Supplementary Fig. 6d–f). The shift is larger and more global than reported previously for ArfA<sup>37–39,42–44</sup> (Supplementary Fig. 6a–c), which may arise in part due to the differences between *B. subtilis* and *E. coli* RF2s. The shift affects the loop between the  $\beta$ 4 and  $\beta$ 5 strands of d2 bearing the SPF (*B. subtilis* 202-Ser-Pro-Phe-204) motif, which is involved in the specificity of recognition of the first and second positions of UGA/UAA stop codons<sup>32,40,48</sup>.



**Fig. 4** Cryo-EM structure of BrfA-RF2-ns70S complex. **a** Different views of the cryo-EM map of the BrfA-RF2-ns70S complex with isolated densities highlighting the 30S (yellow: hd, head; bd, body) and 50S (gray: CP, central protuberance) subunits, P-site tRNA (green), RF2 (orange), and BrfA (blue). **b, c** Isolated electron density for BrfA (**b**) colored according to local resolution and (**c**) shown as mesh (gray) with fitted molecular model for BrfA. **d** Model for BrfA with features highlighted corresponding to the schematic of BrfA protein, including  $\alpha$ -helical and  $\beta$ -strand regions. **e** The N-terminus of BrfA (blue) interacts both h44 of the 16S rRNA (yellow) and H69 and H71 of the 23S rRNA (gray). **f** The conserved R25 of BrfA (blue) stacks upon U1915 and causes C1914 to flip out and stack upon H133 of RF2. **g** Same view as **f** but showing the RF2<sub>stop</sub> (lime) and the conformation of H69 for a canonical termination complex (PDB ID 4V5E<sup>48</sup>). **h** Transverse section of the 30S subunit (yellow) to reveal the mRNA channel showing a superimposition of full-length mRNA (FL-mRNA, cyan) with truncated non-stop mRNA (TR-mRNA, teal), P-site tRNA (green), and surface representations of BrfA (blue). **i** Superimposition of FL-mRNA (cyan) with TR-mRNA (teal), P-site tRNA (green), and transparent surface representation of BrfA (blue). The first (+1), second (+2), and third (+3) nucleotides of the A-site codon of the FL-mRNA are indicated. **j** Interaction of the C-terminus of BrfA (blue) with the 16S rRNA showing potential hydrogen bonds with yellow dashed lines.

(Fig. 5c). Importantly, the structure illustrates that BrfA, like ArfA, does not interact with the SPF motif and therefore does not directly mimic the presence of a stop codon (Fig. 5c, Supplementary Fig. 6g–i), which is consistent with our observation that mutations in the SPF motif that impair RF2 termination activity do not affect BrfA-RF2-mediated ribosome rescue (Fig. 3b).

During canonical termination, recognition of the stop codon by RF2 (and RF1) is proposed to stabilize a distinct conformation of the switch loop that directs domain 3 into the PTC<sup>1,49</sup>. The switch loop conformation is stabilized by stacking interactions between Trp318 (*B. subtilis* numbering) of RF2 and A1492 (h44) as well as between A1493 (h44) and A1913 in H69 (refs. 40,48)

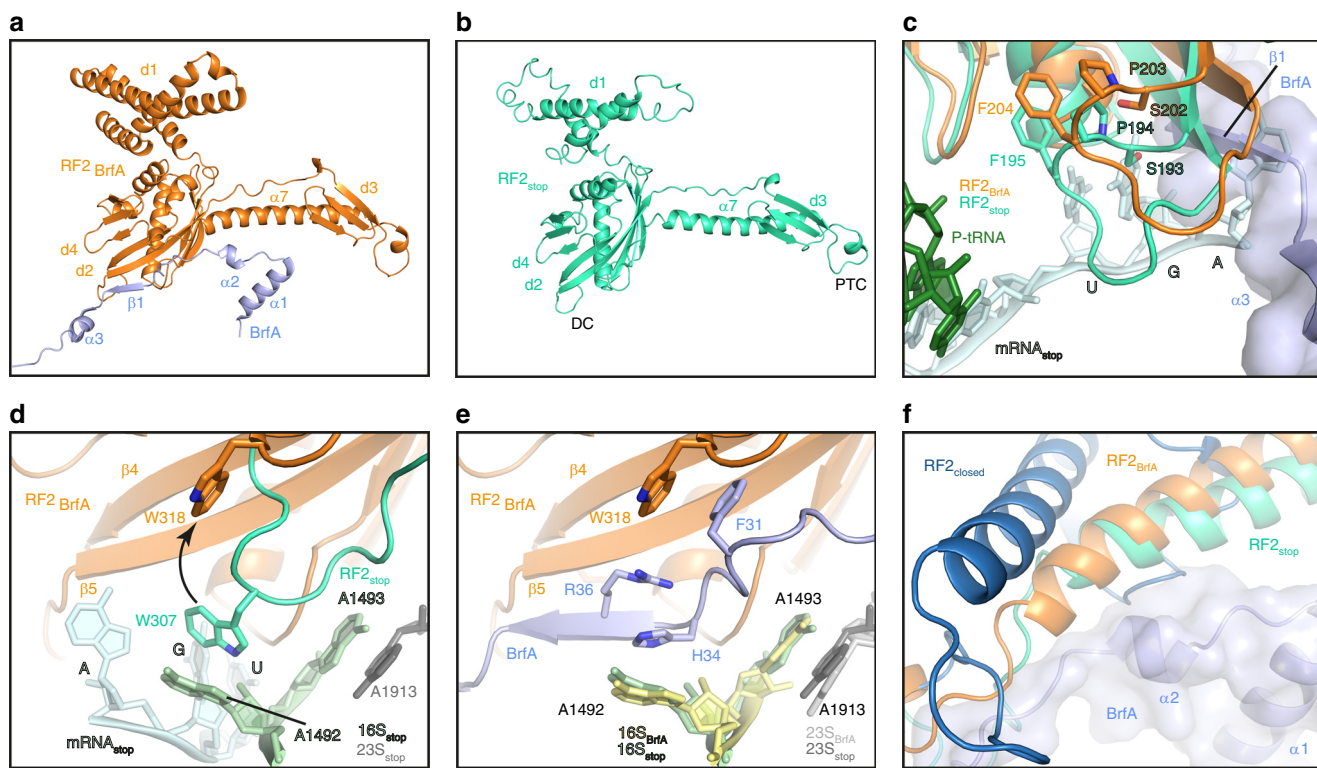


**Fig. 5** BrfA recruits and stabilizes the open conformation of RF2 on the ribosome. **a, b** Overview of the interaction of BrfA (blue) with **(a)** RF2 (RF2<sub>BrfA</sub>, orange) from the BrfA-RF2-ns70S and with **(b)** RF2 (RF2<sub>stop</sub>, lime, PDB ID 4V5E) from a canonical termination complex<sup>48</sup>. RF2 domains 1-4 (d1-d4) and relative positions of the decoding center (DC) and peptidyltransferase center (PTC) are indicated. **c** Comparison of the relative positions of the SPF motif of RF2<sub>stop</sub> (lime) and RF2<sub>BrfA</sub> (orange) with BrfA (blue), P-site tRNA (green), and truncated non-stop mRNA (TR-mRNA, cyan) shown for reference. **d** Interaction between Trp307 (W307, equivalent to *B. subtilis* Trp318 (W318)) of the switch region of *Thermus thermophilus* RF2<sub>stop</sub> (lime) and A1492 of the 16S rRNA (green) during decoding of the UGA stop codon of the mRNA (cyan). W318 in the switch loop of *B. subtilis* RF2 (RF2<sub>BrfA</sub>, orange) observed upon BrfA binding is superimposed and arrowed. **e** Same view as in **d**, but showing the conformation of the switch loop of RF2<sub>BrfA</sub> (orange) and A1492/A1493 (yellow) when BrfA (blue) is present. **f** Superimposition of the conformation of  $\alpha$ -helix  $\alpha$ 7 of RF2 from the crystal structure of the closed form of RF2 (RF2<sub>closed</sub>; dark blue, PDB ID 1GQE) with RF2<sub>stop</sub> (lime) and RF2<sub>BrfA</sub> (orange), with BrfA (blue) shown for reference.

(Fig. 5d). In the BrfA-RF2-ns70S, the presence of BrfA precludes a direct interaction between Trp318 and A1492 (Fig. 5e). Rather, BrfA appears to stabilize a similar conformation of A1492 through stacking interactions with His34 and Arg36 (Fig. 5e), whereas a completely distinct conformation of A1492 (and A1493) is adopted in the presence of ArfA (Supplementary Fig. 7a-c). Additional stacking interactions are also observed between Phe31 of BrfA and Trp318 within the switch region of RF2 (Fig. 5e), which we suggest facilitates the transition from the closed to the open form of RF2 (Fig. 5f, Supplementary Fig. 7d-j) and thereby enables placement of the GGQ motif within domain 3 (d3) of RF2 at the PTC of the ribosome.

## Discussion

We have shown that Gram-positive bacteria, such as *Bacillus*, possess an RF-dependent ribosome rescue pathway, which had previously been known to occur only in Gram-negative bacteria (Fig. 6a). In this pathway in *B. subtilis*, BrfA plays a critical role in the hydrolytic release of the incomplete polypeptide from the non-stop stalled ribosomes. It does so by recruiting RF2 in a stop-codon-independent manner to the otherwise dead-end translation complex, as shown by our biochemical experiments using purified components. Our cryo-EM structure also reveals that BrfA recognizes the empty mRNA channel of a non-stop ribosome complex to recruit and stabilize the active (open)

conformation of RF2 on the ribosome (Fig. 6b), in a similar but distinct manner to ArfA<sup>37–39,42–44</sup> (Fig. 6c).

*In vivo*, the *brfA* deletion mutation exhibits a synthetic lethal phenotype when combined with CRISPRi-mediated knock-down or deletion of either SsrA or SmpB. Thus, BrfA is essential for growth in the absence of *trans*-translation activity. These findings answer the long-standing question of why the *trans*-translation system is not essential in *B. subtilis*, which lacks ArfA, ArfB and ArfT. Instead, BrfA is the alternative ribosome rescue factor in this organism and some other *Bacillus* species. The growth requirement of *B. subtilis* for BrfA and *trans*-translation is observed under normal growth conditions without the imposition of proteotoxic stresses. Thus, clearing of constitutively produced aberrant states of translation might be critical for cell survival, and BrfA and *trans*-translation components are the major players in this basic quality control. In this regard, the recently reported RqcH pathway, which adds a protein-degrading polyalanine sequence to the arrested polypeptide on the split 50S subunit of the ribosome<sup>50</sup>, appears to play a minor role in ribosome rescue under normal growth conditions, since RqcH is dispensable for *trans*-translation deficient strains to grow in the absence of stress. By contrast, RqcH appears to be required under more harsh conditions, such as high temperature and the presence of translation-disturbing drugs<sup>50</sup>.

During BrfA-mediated ribosome rescue, peptidyl-tRNA hydrolysis depends on an intact GGQ motif of RF2, indicating

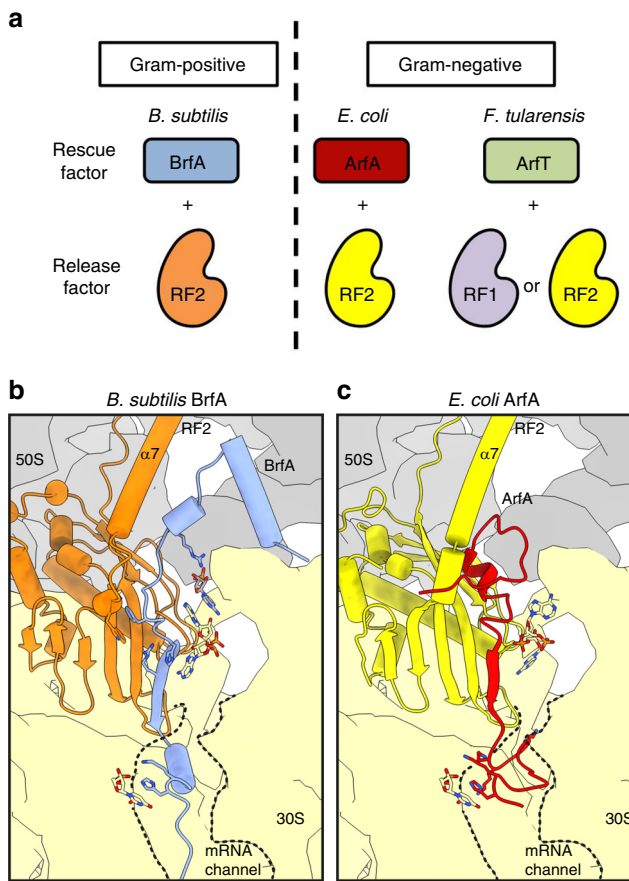


**Fig. 6** RF-dependent ribosome rescue factors in bacteria. **a** Independent evolution of the RF-dependent ribosome rescue factors. ArfA and BrfA are unrelated in their amino acid sequences despite the same partner (RF2) specificity. ArfT forms a still distinct group and cooperates with either of RF1 or RF2. They show narrow distributions among bacterial species. **b, c** A schematic model highlighting the similarities and differences between **(b)** BrfA- and **(c)** ArfA-mediated ribosome rescue mechanism.

that RF2 plays the catalytic role. The role of BrfA is rather to recruit RF2 to the ns70S complex to initiate the events of stop codon-independent translation termination and thereby allow the subsequent ribosome recycling process. We used the *Bs* PURE system containing only a minimal set of essential translation components from *E. coli* together with *B. subtilis* ribosomes to recapitulate the rescue reaction in vitro, making it unlikely that other unknown cellular factors, especially those from *B. subtilis*, are required for the process. Moreover, we could show structurally that BrfA alone is sufficient to recruit and induce an active (open) conformation of *Bs*RF2 on the non-stop ribosome complex. Taken together, we propose that BrfA is an RF-dependent ribosome rescue factor in Gram-positive bacteria, such as *Bacillus* (Fig. 6a).

In the process of canonical translation termination, stop codon recognition by the SPF motif of RF2 is a prerequisite for the process in which RF2 is accommodated into the A-site of the ribosome and adopting a catalytically active (open) conformation where the GGQ motif is directed into the PTC<sup>40,48,51,52</sup>. However, our structural data show that BrfA does not directly mimic the stop codon in the A-site (Fig. 5c), consistent with our observations that the stop codon recognition motif SPF is not required for ribosome rescue (Fig. 3b; see ref. 16 for the similar situation in *E. coli* ArfA). Instead, the role of BrfA is to induce an open conformation of RF2, despite the absence of a stop codon.

BrfA appears to facilitate ribosome rescue using a different mechanism than reported previously for ArfA<sup>37–39,42–44</sup>. For example, during stop codon decoding, the switch loop Trp stacks directly upon A1492 of the 16S rRNA (Fig. 5d, Supplementary Fig. 7a), whereas during BrfA-mediated recycling, a series of stacking interactions appear to indirectly relay this information—specifically, Phe31 of BrfA stacks upon the switch loop Trp318 of RF2, while His34 (and Arg36) of BrfA stacks upon A1492 (Fig. 5e, Supplementary Fig. 7b). By contrast, during ArfA-mediated rescue, the equivalent Trp residue inserts into a hydrophobic pocket created by ArfA and A1492 adopts a completely unrelated conformation (Supplementary Fig. 7c)<sup>37–39,42–44</sup>.

Perhaps the most dramatic difference between BrfA and ArfA is found in the N-terminal region, where BrfA contains two short  $\alpha$ -helices that establish multiple interactions with H69 and H71 of the 23S rRNA, whereas the N-terminus of ArfA is unstructured and does not establish any interactions with the 50S subunit (Supplementary Fig. 5a–c). Despite this lack of sequence and structural homology, there are some common features between the two rescue systems: Firstly, both ArfA and BrfA (as well as SmpB and ArfB) appear to utilize positively charged C-terminal extensions to interact with the negatively charged 16S rRNA comprising the mRNA channel. Although the details of the interactions are unrelated, we identified a Lys-His (K49-H50 in *B. subtilis*) motif that is conserved between BrfA and ArfA, which is used to establish contacts to the backbone of nucleotide U534 of the 16S rRNA (Supplementary Fig. 5j–l). Secondly, both ArfA and BrfA contain short  $\beta$ -strands that augment the  $\beta$ -sheet in domain 2/4 of RF2, which we presume is important to recruit RF2 to the ribosome (Supplementary Fig. 5a–c).

Here we show that BrfA works with RF2, but not RF1, reminiscent of the partner selectivity described previously for ArfA<sup>16</sup>. Analysis of the contacts between BrfA and RF2 within the BrfA-RF2-ns70S complex, and comparison with the sequence alignments between *B. subtilis* RF2 and RF1, indicated that there are two main regions in the RFs that are likely to be responsible for the selectivity of BrfA (Supplementary Fig. 8). These encompass residues within the  $\beta$ -sheet of domain 2/4 of RF2 that are in proximity of Phe31 of BrfA. For example, in RF2 residues 197 and 216 are generally Val and Phe, respectively, whereas in RF1 the equivalent residues are replaced with the smaller Ala and Thr residues, respectively (Supplementary Fig. 8a). More dramatic, however, is the lack of sequence conservation between the switch loops of *B. subtilis* RF1 and RF2. In fact, the switch loop of RF1 is one residue longer than in RF2 (Supplementary Fig. 8b, d). We also note that the RF-dependent rescue factors show low interspecies compatibility (Fig. 3c). The incompatibility of BrfA to work with *E. coli* RF2 is not surprising given the relatively low sequence conservation observed within the switch region (Supplementary Fig. 8d). Moreover, sequence differences are also observed with  $\alpha$ -helix 7 between *B. subtilis* and *E. coli* RF2 that could contribute to the interactions with BrfA (Supplementary Fig. 8c). Collectively, these differences suggest that even if BrfA could recruit *B. subtilis* RF1 or *E. coli* RF2 to the ns70S, the sequence differences in the switch loop are unlikely to stabilize the open conformation of RF2 on the ribosome. The lack of interspecies compatibility of BrfA (and ArfA) contrasts with other, more ubiquitous ribosome rescue factors. For example, *B. subtilis* tmRNA is functional in *E. coli*, albeit with lower efficiency<sup>25</sup>, and the human mitochondrial ArfB homolog, ICT1, is functional in *C. crescentus* and vice versa<sup>23</sup>. This low interspecies compatibility of the RF-dependent rescue factors reinforces the notion that these rescue systems emerged late in evolution.

It is crucial for the ribosome rescue factors not to intervene during normal translation, nor when translation is arrested by nascent polypeptides for regulatory purposes<sup>33</sup>. Our cryo-EM

structure of the BrfA-RF2-ns70 reveals that BrfA uses its C-terminal region to monitor the vacancy of the ribosomal mRNA channel, a hallmark of the ribosomes stalled on the 3' end of mRNA, and thereby discern non-stop translation complexes from those of ongoing translation<sup>42</sup>. Consistently, we have shown that neither BrfA, nor *trans*-translation, can resolve the MifM-programmed elongation arrest complexes (Supplementary Fig. 1). In this case, the mRNA channel should remain occupied by the *mifM* mRNA. Also, the cryo-EM structures of the MifM-stalled ribosomes reveal altered conformations of 23S rRNA residues near the peptidyltransferase center (PTC) such that they block accommodation of aminoacyl-tRNAs or mimics thereof into the A-site<sup>53</sup> explaining why MifM stalling is refractory to the BrfA-RF2 and the SmpB-tmRNA actions, too.

We have shown that *brfA* is transcribed as a non-stop mRNA because of the terminator sequence within the coding region. Thus, *brfA* itself is subject to a futile type of translation, producing a non-stop polypeptide that is extended by the SsrA tag sequence and rapidly eliminated by proteolysis. BrfA accumulates only when *trans*-translation is impaired, and in the form of peptidyl-tRNA. However, once some free BrfA product is generated by spontaneous hydrolysis of the BrfA peptidyl-tRNA, or by the presence of residual BrfA in the cell, it actively liberates in *trans* the BrfA peptide in a self-perpetuating manner. We have shown clearly using biochemical assays that a liberated form of the non-stop BrfA peptide (residues 1–62) is active in mediating the RF2-dependent peptidyl-tRNA hydrolysis.

Because BrfA is not effectively produced in *trans*-translation proficient cells, but induced strikingly upon dysfunction of *trans*-translation, it is likely to represent a secondary, back-up rescue system that compensates for defects in *trans*-translation. This scenario reinforces the notion that the proteolytic function characteristically associated with the SmpB-tmRNA system is not essential for growth, as reported previously<sup>13,14</sup>. Indeed, the GFP-*ns* product accumulates in the *ssrA*-deleted cell (Supplementary Fig. 1a), indicating that the products of the BrfA system are not necessarily toxic. Thus, the growth-essential roles of *trans*-translation and BrfA are in their ribosome recycling functions, rather than in the tagging-proteolysis that the BrfA system lacks. Cell viability would require a sufficient pool of the uncompromised ribosomes, which maintains the translation capacity of the cell. Whereas the two pathways share the essential function required for growth-supporting ribosome rescue, the proteolytic functions of the *trans*-translation and that of the RqCH tail-adding system could become more important under more severe stress conditions<sup>50</sup>.

The regulatory scheme of BrfA expression is strikingly similar to that elucidated for ArfA regulation in *E. coli*<sup>17,18</sup>; the *arfA* mRNA is also subject to RNase III-dependent cleavage and/or transcription termination such that ArfA only accumulates when *trans*-translation is defective. Assuming that BrfA and ArfA are evolutionarily unrelated, it is noteworthy that they employ a similar scheme of regulation. Convergent acquisition of such regulatory mechanisms may be more common for factors that have evolved recently and which have functions related to the firmly established and relatively rigid constituent of the cell, such as the ribosome and translation factors.

In summary, our study reveals that bacteria, both Gram-negative and Gram-positive, have RF-dependent mechanisms of ribosome rescue that allow for the stop-codon-independent liberation of the polypeptide from the ribosome on the non-stop mRNA (Fig. 6a). However, the crucial adapter proteins, ArfA, ArfT, and BrfA, are unrelated in amino acid sequence (Supplementary Fig. 2). The modes of their interactions with the catalytic RF partner(s) are also divergent, indicative of the tailored nature of their evolution in different species. It remains possible that

many more factors in this category exist in different organisms. As the present study suggests that sequence similarity alone cannot be used to identify additional factors that exist in the domains of life, we need better strategies to address this question. Further studies on the generality and diversity of independently evolved rescue factors and their manner of interaction with the ribosome and translation factor would provide invaluable insights into regulatory mechanisms of translation processes in the cell.

## Methods

**Bacterial strains and plasmids.** *B. subtilis* and *E. coli* strains, plasmids, DNA oligonucleotides used in this study are listed in Supplementary Tables 2, 3, 4 and 5, respectively. The *B. subtilis* strains were derivatives of PY79 (wild-type; ref. <sup>54</sup>) and constructed by transformation that involves homologous recombination with plasmids listed in Supplementary Table 6. These plasmids carried an engineered *B. subtilis* gene to be integrated, which was flanked by sequences from the integration target loci, and were constructed by standard cloning methods including PCR, PrimeSTAR mutagenesis (Takara), and Gibson assembly<sup>55</sup>. The plasmid pCH747 was constructed by cloning a *SphI*-*SpeI* fragment of pCH735 into pycjG21. Plasmids pCH735 and pycjG21 were constructed as described<sup>35</sup>. Successful integration of a gene into the chromosome was accomplished by double crossing-over at the target loci. The resulting recombinant clones were checked for their antibiotic-resistance markers, including the absence of those originally present on the plasmid backbone, and inactivation of the *amyE*, *lacA*, or *thrC* target locus. The marker-less deletion mutants of *smpB*, *yesZ*, and *lacA* were constructed by excising the drug resistance gene cassette by the Cre-loxP system as described previously<sup>27</sup> with some modification as follows. The *B. subtilis* strains were transformed with pMK2, a pLOSS\*-based Ts plasmid harboring *cre*. The resulting strain was grown at 37 °C overnight in LB agar medium supplemented with 1 mM IPTG (isopropyl β-D-1-thiogalactopyranoside) and 100 µg/mL spectinomycin to excise the drug marker flanked by *loxP*<sup>27</sup>. The strain was then grown at 37 °C overnight to drop off pMK2 on LB agar medium without spectinomycin. The absence of the drug resistance confirmed the absence of plasmid pMK2. The *B. subtilis* strain KFB792 was constructed by transformation of PY79 with a DNA fragment prepared by Gibson assembly with three PCR fragments, one of which was amplified from pCH1142 using a pair of primers SP89/SP90, and the other two of which were amplified from PY79 genomic DNA using pairs of primers SP91/SP92 and SP93/SP94, respectively.

**Growth conditions and general procedures.** For western blotting in Fig. 2c, *B. subtilis* cells were cultured at 37 °C in LB medium with or without 0.5% xylose until OD<sub>600</sub> reached ~0.5. Bacterial culture (1 mL) was treated with 5% trichloroacetic acid (TCA), and precipitates formed were washed with 0.75 mL of 1 M Tris-HCl (pH 8.0) and resuspended in 50 µL of buffer L (33 mM Tris-HCl, 1 mM EDTA, pH 8.0) containing 1 mg/mL lysozyme, followed by incubation at 37 °C for 10 min. Proteins were then solubilized with an equal volume of 2× SDS-loading buffer containing 5 mM dithiothreitol (DTT) with incubation at 65 °C for 5 min and subjected to SDS-PAGE and immunoblotting. One hundred microliters portions of the bacterial cultures were used for assay of β-galactosidase activity, presented in Fig. 2d as follows and also as described previously<sup>31</sup>. The cultures were transferred to individual wells of another 96-well plate for a Thermo Scientific Multiskan Go microplate spectrophotometer and OD<sub>600</sub> was recorded. Cells were then lysed by adding 50 µL of Y-PER reagent (Thermo Scientific) and incubating for 20 min at room temperature. Thirty microliters of *o*-nitrophenyl-β-D-galactopyranoside (ONPG) in Z-buffer (60 mM Na<sub>2</sub>HPO<sub>4</sub>, 40 mM NaH<sub>2</sub>PO<sub>4</sub>, 10 mM KCl, 1 mM MgSO<sub>4</sub>, 38 mM β-mercaptoethanol) was added to each well. The reaction solution was mixed thoroughly and then OD<sub>420</sub> and OD<sub>550</sub> were measured every 5 min over 60 min at 28 °C. Arbitrary units [AU] of β-galactosidase activity were calculated by the formula [(1000 × V<sub>420</sub> – 1.3 × V<sub>550</sub>) / OD<sub>600</sub>], where V<sub>420</sub> and V<sub>550</sub> are the first-order rate constants, OD<sub>420</sub>/min and OD<sub>550</sub>/min, respectively.

**Synthetic lethal screening using the BKE strain library.** To isolate *B. subtilis* mutants whose viability depends on *trans*-translation, we used the BKE library (a collection of single-gene knockout mutants covering the 3968 non-essential genes, which had been disrupted by replacement with the erythromycin resistance marker) as the source of gene knockouts. We pooled the BKE strains and prepared a genomic DNA mixture using Wizard genome DNA purification kit (Promega). We used this DNA preparation to transform an *smpB*-deleted strain of *B. subtilis* that harbored a rescue plasmid carrying *smpB*<sup>+</sup> and *lacZ*<sup>+</sup> (pNAB1286), which was constructed from pLOSS\* with a temperature sensitive (Ts) replication system. Transformant mixture was then incubated at 50 °C overnight to segregate out the Ts plasmid from bacteria that did not need the rescue plasmid, followed by further growth at 37 °C overnight and plating on LB agar containing 40 µg/mL X-Gal (5-bromo-4-chloro-3-indolyl β-D-galactopyranoside), 1 mM IPTG, 12.5 µg/mL lincomycin, and 1 µg/mL erythromycin. We picked up blue (*lacZ*<sup>+</sup>) colonies to obtain transformants that retained the *smpB*<sup>+</sup>-*lacZ*<sup>+</sup> rescue plasmid even after the high-temperature incubation and prepared chromosomal DNA from them. Genes that had been disrupted by the erythromycin resistance marker were determined by

PCR amplification and DNA sequencing of the mutant-specific barcode sequence, using appropriate primers<sup>27</sup>.

**CRISPR interference.** The CRISPRi was performed as described previously<sup>56</sup> with some modification. A gene encoding dCas9 under the xylose-inducible promoter was integrated into the *lacA* site on the chromosome of a *brfA*-deleted *B. subtilis* strain, into which an *ssrA*-targeted or an *smpB*-targeted sgRNA gene under a constitutive promoter was further integrated at the *amyE* site. The guide sequences for CRISPRi were designed on the basis of information provided by the previous study<sup>56</sup> as well as CHOPCHOP, a web tool for the CRISPR/Cas9 experiments<sup>57,58</sup>. The target gene knock-down was induced by addition of 1% xylose.

**Protein purification.** Hexahistidine-tagged proteins (*B. subtilis* BrfA62-His<sub>6</sub>, RF1-His<sub>6</sub>, RF2-His<sub>6</sub>, *E. coli* His<sub>6</sub>-ArfA60, and their derivatives) were expressed in *E. coli* strain BL21(DE3) from the pET28b-based plasmid. *E. coli* cells were grown in LB-kanamycin (25 µg/mL) medium. At a mid-log phase, IPTG (final concentration, 1 mM) was added, and cells were grown for an additional 3 h to express and accumulate the target protein. Cells were then harvested, washed with ice-cold 50 mM HEPES-NaOH (pH 7.6) buffer, and stored at -80 °C. They were suspended in binding buffer (50 mM HEPES-KOH pH 7.6, 5 mM imidazole, 300 mM NaCl, 1 mg/mL Pefabloc) and disrupted by passing through a microfluidizer LV1 (Microfluidics) at 16,000 psi three times. After removal of debris by centrifugation (4 °C, 15,000 r.p.m. for 15 min), Ni-NTA agarose was added to the sample, which was then incubated at 4 °C for 1 h. The Ni-NTA agarose was loaded on a spin column and washed seven times with wash buffer (50 mM HEPES-KOH pH 7.6, 20 mM imidazole, 0.1% Triton-X). Protein was eluted with the elution buffer (20 mM HEPES-KOH pH 7.6, 300 mM NaCl, 300 mM imidazole). Purified RFs were dialyzed against dialysis buffer A (50 mM HEPES-KOH pH 7.6, 100 mM potassium acetate, 1 mM DTT, 30% glycerol). Purified BrfA62-His<sub>6</sub> and His<sub>6</sub>-ArfA (2–60) were dialyzed against dialysis buffer B (50 mM HEPES-KOH pH 7.6, 100 mM potassium acetate, 1 mM DTT, 300 mM NaCl, 30% glycerol).

For the structural analysis, the wild-type *B. subtilis* RF2 and variant RF2-GGP protein were expressed from pET11a vectors incorporating a C-terminal hexahistidine tag (His<sub>6</sub>) for purification and detection purposes. The inactive RF2-GGP mutant was generated by site-directed mutagenesis. The wild-type RF2 and RF2-GGP proteins were over-expressed in *E. coli* BL21 (DE3) at 37 °C for 1.5 h after induction with 1 mM IPTG. Cells were collected and the pellet was resuspended in lysis buffer (50 mM NaH<sub>2</sub>PO<sub>4</sub>, 300 mM NaCl, 5 mM imidazole, pH 7.5). Lysis was performed using a microfluidizer (Microfluidics M-110L) by passing cells three times (at 18,000 psi). The cell debris was removed upon centrifugation and the proteins were purified from the supernatant by His-tag affinity chromatography using Ni-NTA agarose beads (Clontech). The bound proteins were washed with lysis buffer containing 10 mM imidazole and then eluted with lysis buffer containing 250 mM imidazole. The proteins RF2, RF2-GGP, and BrfA62-His<sub>6</sub> were purified by size-exclusion chromatography using HiLoad 16/600 Superdex 75 (GE Life Sciences) in gel filtration buffer (50 mM HEPES, pH 7.4, 50 mM KCl, 100 mM NaCl, 2% glycerol, 5 mM β-mercaptoethanol). The proteins were concentrated using Amicon Ultracel-30 Centrifugal Filter Units (Merck Millipore) for wild-type RF2 and RF2-GGP and Ultracel-3 for BrfA62-His<sub>6</sub> hereafter referred to as BrfA.

**In vitro translation using PURE system.** The *E. coli*-based coupled transcription–translation system with purified components (PUREflex 1.0; GeneFrontier) was used for in vitro translation as described previously<sup>29–31</sup> with some modifications. To maximize transcription, we added 2.5 U/µL of T7 RNA polymerase (Takara) further to the reaction mixture. Whereas the original reaction mixture, referred to as *E. coli* PURE system, contained the *E. coli* ribosome, we also used the *B. subtilis* hybrid PURE system containing the *B. subtilis* ribosomes at a final concentration of 1 µM. Unless otherwise noted, we omitted RF1, RF2, and RF3 from the reaction. However, we included purified RF or its derivatives derived either from *B. subtilis* or *E. coli* at a final concentration of 1 µM as indicated in each experiment. *E. coli* RFs were purchased from GeneFrontier. Purified BrfA or ArfA was added to the final concentration of 1 µM when indicated. The reaction was primed with an appropriate DNA fragment prepared by PCR (Supplementary Table 7) and allowed to continue at 37 °C for 20 min. Samples were then mixed with the same volume of 2× SDS-PAGE loading buffer. When indicated, they were further treated with 0.2 mg/mL RNase A (Promega) at 37 °C for 15 min before electrophoresis. Samples for SDS-PAGE were heated at 65 °C for 5 min, separated by 10% wide range gel (Nacalai Tesque)<sup>31</sup> and transferred on to a PVDF membrane. Translation products were detected by immunoblotting using anti-GFP (A-6455; Thermo) or anti-DYKDDDDK (anti-FLAG tag; Wako) as described previously<sup>31</sup>. Images were obtained and analyzed using an Amersham Imager 600 (GE Healthcare) luminoimager. Uncropped immunoblotting data are shown in the Source Data file.

**Generation of BrfA-RF2-ns70S complex.** Generation of the BrfA-RF2-ns70S complex was similar to that previously described for the ArfA-RF2-70S complex<sup>39</sup>. Briefly, the truncated nlpD template containing an N-terminal His<sub>6</sub> and HA-tag was first amplified from pET21b-r1nlpD using T7-promotor and

nucleotides 133–159 of nlpD as reverse primer. Following PCR purification via spin column (Qiagen), in vitro translation (PURExpress, NEB 6800) was started by adding the truncated nlpD PCR product at 37 °C for 20 min, shaking at 1000 r.p.m. The ribosomes were first isolated from the in vitro reaction mix by centrifugation through a sucrose cushion (50 mM HEPES-KOH pH 7.2, 250 mM potassium acetate, 25 mM magnesium acetate, 750 mM sucrose, 0.1% DDM) for 180 min at 72,000 × g using a TLA120.2 rotor (Beckman Coulter). The pellet was resuspended in buffer B250 (50 mM HEPES-KOH pH 7.2, 250 mM potassium acetate, 25 mM magnesium acetate, 0.1% DDM) and the ns70S complex was isolated using Talon cobalt-chelate affinity resin (Clontech). ns70S complex bound to the Talon matrix by the N-terminal His<sub>6</sub> tag of NlpD was washed with buffer B500 (50 mM HEPES-KOH pH 7.2, 500 mM potassium acetate, 25 mM magnesium acetate, 0.1% DDM) and eluted using buffer B250i (50 mM HEPES-KOH pH 7.2, 250 mM potassium acetate, 25 mM magnesium acetate, 250 mM imidazole, 0.1% DDM). The eluted ns70S complex was loaded onto a linear sucrose gradient (10–40% (w/v) sucrose in B250 buffer) for 18 h at 43,000 × g in a SW28 rotor (Beckman Coulter). The isolated 70S peak was pelleted by centrifugation for 3 h at 139,000 × g using a Ti70.1 rotor (Beckman Coulter). The pellet was resuspended in ns70S complex buffer (50 mM HEPES pH 7.2, 250 mM potassium acetate, 10 mM magnesium acetate, 0.05% DDM). The purified non-stop ribosome complex was then incubated together with a 10× excess of BrfA and RF2-GGP mutant for 5 min at 37 °C before being applied to cryo-EM grids.

**Cryo-EM and single-particle reconstruction.** Three microliters (4.5 OD<sub>260nm</sub> per mL) of BrfA-RF2-ns70S complex was applied to 2 nm pre-coated Quantifoil R3/3 holey carbon supported grids and vitrified using the Vitrobot Mark IV (FEI, Holland). Data collection was performed using EM-TOOLS (TVIPS GmbH) on a Titan Krios transmission electron microscope equipped with a Falcon III direct electron detector (FEI, Holland) at 300 keV at a pixel size of 1.065 Å and a defocus range of 0.4–2.2 µm. Forty frames (dose per frame of 2 e<sup>-</sup> Å<sup>-2</sup>) were aligned using Motion Correction software<sup>59</sup>. Power spectra and defocus values were determined using the GCTF software<sup>60</sup>. Micrographs showing thin rings beyond 3.2 Å were manually inspected for good areas and automatic particle picking was performed using the Gautomatch software (<http://www.mrci.mrc.ac.uk/kzhang/>). Single particles were then imported and processed in Relion 3 (ref. <sup>61</sup>). In total, 514,119 particles were first subjected to 2D classification (60 classes for 100 rounds) and 389,381 particles showing ribosome-like features were then selected for 3D refinement using an *E. coli* 70S ribosome as a reference structure (Supplementary Fig. 4a). 3D classification was then performed, resulting in 317,095 particles containing P-site tRNA and RF2 (Supplementary Fig. 4b) that were further selected for focus sorting on the RF2 (Supplementary Fig. 4c). Focus sorting yielded a major population of 154,405 particles containing stoichiometric amounts of BrfA, P-site tRNA, RF2, which after CTF-refinement and a final round of 3D refinement produced a final cryo-EM reconstruction with an average resolution of 3.06 Å according to FSC<sub>0.143</sub> criterion (Supplementary Fig. 4d). The final cryo-EM maps were sharpened by dividing the maps by the modulation transfer function of the detector and applying an automatically determined negative B factor in Relion 3 (ref. <sup>61</sup>). The final cryo-EM map was also filtered according to local resolution using SPHIRE<sup>62</sup>.

**Molecular modeling of the BrfA-RF2-ns70S complex.** The molecular model for the ribosomal proteins and rRNA core was based on the molecular model from the recent cryo-EM reconstructions of the *E. coli* 70S ribosome (PDB ID 6H4N<sup>63</sup> and 5MGP<sup>39</sup>). The models were rigid body fitted into the cryo-EM density map using UCSF Chimera followed by refinement in Coot<sup>64</sup>. Proteins L1, L10, L11 protein, and the L7/L12 stalk were not included in the final model due to the poor quality of density in the final cryo-EM map. For *B. subtilis* RF2, a homology model was generated using HHpred<sup>65</sup> based on an *E. coli* RF2 template (PDB ID 5MGP<sup>39</sup>). Domains 1 and 3 of RF2 were less well-resolved due to high flexibility (Supplementary Fig. 4e) and therefore only the backbone was modeled. Residues 2–55 of BrfA were built de novo using an HHpred model<sup>65</sup> as an initial starting point to determine the placement of the central helical regions. The complete atomic model of the BrfA-RF2-ns70S complex was manually adjusted using Coot<sup>64</sup> and refined with phenix real\_space\_refine for cryo-EM<sup>64</sup> using restraints obtained by phenix secondary\_structure\_restraints<sup>64</sup>. The model refinement and statistics of the refined model were obtained using MolProbity<sup>66</sup> (Supplementary Table 1).

**Figure preparation.** Figures showing electron densities and atomic models were generated using either UCSF Chimera, UCSF ChimeraX<sup>67</sup> or PyMol (Version 1.8 Schrödinger). The comparison of BrfA with full-length mRNA (PDB ID 4V5E<sup>48</sup>), ArfA (PDB ID 5MGP<sup>39</sup>, 5MDV<sup>37</sup>, 5U9P<sup>44</sup>), RF2<sub>closed</sub> (PDB ID 1GQE), and RF2<sub>stop</sub> (PDB ID 4V5E<sup>48</sup>) was obtained by alignment of the 16S rRNAs from the respective structures using PyMol (Version 1.8 Schrödinger).

**Reporting summary.** Further information on research design is available in the Nature Research Reporting Summary linked to this article.

## Data availability

The cryo-EM map of the BrfA-RF2-ns70S complex is available through the EMDB code EMD-10353 and the associated molecular model is deposited in the Protein Data Bank with the entry code 6SZS (<https://doi.org/10.2210/pdb6SZS/pdb>). The data that support the findings of this study are available from the corresponding authors on request. The source data underlying Figs 2c, d and 3a-c and Supplementary Figs 1a, 1b and 3 are provided as a Source Data file.

Received: 2 August 2019; Accepted: 7 November 2019;

Published online: 27 November 2019

## References

- Youngman, E. M., McDonald, M. E. & Green, R. Peptide release on the ribosome: mechanism and implications for translational control. *Annu. Rev. Microbiol.* **62**, 353–373 (2008).
- Petry, S., Weixlbaumer, A. & Ramakrishnan, V. The termination of translation. *Curr. Opin. Struct. Biol.* **18**, 70–77 (2008).
- Ito, K. et al. Nascentome analysis uncovers futile protein synthesis in *Escherichia coli*. *PLoS ONE* **6**, e28413 (2011).
- Buskirk, A. R. & Green, R. Ribosome pausing, arrest and rescue in bacteria and eukaryotes. *Philos. Trans. R. Soc. Lond. B Biol. Sci.* **372**, <https://doi.org/10.1098/rstb.2016.0183> (2017).
- Keiler, K. C. & Feaga, H. A. Resolving nonstop translation complexes is a matter of life or death. *J. Bacteriol.* **196**, 2123–2130 (2014).
- Inada, T. The ribosome as a platform for mRNA and nascent polypeptide quality control. *Trends Biochem. Sci.* **42**, 5–15 (2017).
- Joazeiro, C. A. P. Ribosomal stalling during translation: providing substrates for ribosome-associated protein quality control. *Annu. Rev. Cell Dev. Biol.* **33**, 343–368 (2017).
- Himeno, H., Nameki, N., Kurita, D., Muto, A. & Abo, T. Ribosome rescue systems in bacteria. *Biochimie* **114**, 102–112 (2015).
- Giudice, E. & Gillet, R. The task force that rescues stalled ribosomes in bacteria. *Trends Biochem. Sci.* **38**, 403–411 (2013).
- Keiler, K. C., Waller, P. R. & Sauer, R. T. Role of a peptide tagging system in degradation of proteins synthesized from damaged messenger RNA. *Science* **271**, 990–993 (1996).
- Karzai, A. W., Susskind, M. M. & Sauer, R. T. SmpB, a unique RNA-binding protein essential for the peptide-tagging activity of SsrA (tmRNA). *EMBO J.* **18**, 3793–3799 (1999).
- Brunel, R. & Charpentier, X. Trans-translation is essential in the human pathogen *Legionella pneumophila*. *Sci. Rep.* **6**, 37935 (2016).
- Thibonniere, M., Thibierge, J. M. & De Reuse, H. Trans-translation in *Helicobacter pylori*: essentiality of ribosome rescue and requirement of protein tagging for stress resistance and competence. *PLoS ONE* **3**, e3810 (2008).
- Huang, C., Wolfgang, M. C., Withey, J., Koomey, M. & Friedman, D. I. Charged tmRNA but not tmRNA-mediated proteolysis is essential for *Neisseria gonorrhoeae* viability. *EMBO J.* **19**, 1098–1107 (2000).
- Chadani, Y. et al. Ribosome rescue by *Escherichia coli* ArfA (YhdL) in the absence of trans-translation system. *Mol. Microbiol.* **78**, 796–808 (2010).
- Chadani, Y., Ito, K., Kutsukake, K. & Abo, T. ArfA recruits release factor 2 to rescue stalled ribosomes by peptidyl-tRNA hydrolysis in *Escherichia coli*. *Mol. Microbiol.* **86**, 37–50 (2012).
- Chadani, Y. et al. trans-translation-mediated tight regulation of the expression of the alternative ribosome-rescue factor ArfA in *Escherichia coli*. *Genes Genet. Syst.* **86**, 151–163 (2011).
- Schaub, R. E., Poole, S. J., Garza-Sanchez, F., Benbow, S. & Hayes, C. S. Proteobacterial ArfA peptides are synthesized from non-stop messenger RNAs. *J. Biol. Chem.* **287**, 29765–29775 (2012).
- Chadani, Y., Ono, K., Kutsukake, K. & Abo, T. *Escherichia coli* YaeJ protein mediates a novel ribosome-rescue pathway distinct from SsrA- and ArfA-mediated pathways. *Mol. Microbiol.* **80**, 772–785 (2011).
- Handa, Y., Inaho, N. & Nameki, N. YaeJ is a novel ribosome-associated protein in *Escherichia coli* that can hydrolyze peptidyl-tRNA on stalled ribosomes. *Nucleic Acids Res.* **39**, 1739–1748 (2011).
- Gagnon, M. G., Seetharaman, S. V., Bulkley, D. & Steitz, T. A. Structural basis for the rescue of stalled ribosomes: structure of YaeJ bound to the ribosome. *Science* **335**, 1370–1372 (2012).
- Feaga, H. A., Viollier, P. H. & Keiler, K. C. Release of nonstop ribosomes is essential. *MBio* **5**, e01916 (2014).
- Feaga, H. A., Quicke, M. D., Hankey-Giblin, P. A. & Keiler, K. C. Human cells require non-stop ribosome rescue activity in mitochondria. *PLoS Genet.* **12**, e1005964 (2016).
- Goralski, T. D. P., Kirimanjeswara, G. S. & Keiler, K. C. A new mechanism for ribosome rescue can recruit RF1 or RF2 to nonstop ribosomes. *MBio* **9**, <https://doi.org/10.1128/mBio.02436-18> (2018).
- Muto, A. et al. Requirement of transfer-messenger RNA for the growth of *Bacillus subtilis* under stresses. *Genes Cells* **5**, 627–635 (2000).
- Claessen, D. et al. Control of the cell elongation-division cycle by shuttling of PBP1 protein in *Bacillus subtilis*. *Mol. Microbiol.* **68**, 1029–1046 (2008).
- Koo, B. M. et al. Construction and analysis of two genome-scale deletion libraries for *Bacillus subtilis*. *Cell Syst.* **4**, 291–305 e297 (2017).
- Qi, L. S. et al. Repurposing CRISPR as an RNA-guided platform for sequence-specific control of gene expression. *Cell* **152**, 1173–1183 (2013).
- Chiba, S. et al. Recruitment of a species-specific translational arrest module to monitor different cellular processes. *Proc. Natl. Acad. Sci. USA* **108**, 6073–6078 (2011).
- Shimizu, Y. et al. Cell-free translation reconstituted with purified components. *Nat. Biotechnol.* **19**, 751–755 (2001).
- Fujiwara, K., Ito, K. & Chiba, S. MifM-instructed translation arrest involves nascent chain interactions with the exterior as well as the interior of the ribosome. *Sci. Rep.* **8**, 10311 (2018).
- Ito, K., Uno, M. & Nakamura, Y. A tripeptide ‘anticodon’ deciphers stop codons in messenger RNA. *Nature* **403**, 680–684 (2000).
- Ito, K. & Chiba, S. Arrest peptides: cis-acting modulators of translation. *Annu. Rev. Biochem.* **82**, 171–202 (2013).
- Ito, K., Mori, H. & Chiba, S. Monitoring substrate enables real-time regulation of a protein localization pathway. *FEMS Microbiol. Lett.* **365**, <https://doi.org/10.1093/femsle/fny109> (2018).
- Chiba, S., Lamsa, A. & Pogliano, K. A ribosome-nascent chain sensor of membrane protein biogenesis in *Bacillus subtilis*. *EMBO J.* **28**, 3461–3475 (2009).
- Chiba, S. & Ito, K. MifM monitors total YidC activities of *Bacillus subtilis*, including that of YidC2, the target of regulation. *J. Bacteriol.* **197**, 99–107 (2015).
- James, N. R., Brown, A., Gordiyenko, Y. & Ramakrishnan, V. Translational termination without a stop codon. *Science* **354**, 1437–1440 (2016).
- Zeng, F. et al. Structural basis of co-translational quality control by ArfA and RF2 bound to ribosome. *Nature* **541**, 554–557 (2017).
- Huter, P. et al. Structural basis for ArfA-RF2-mediated translation termination on mRNAs lacking stop codons. *Nature* **541**, 546–549 (2017).
- Korostelev, A. et al. Crystal structure of a translation termination complex formed with release factor RF2. *Proc. Natl. Acad. Sci. USA* **105**, 19684–19689 (2008).
- Santos, N., Zhu, J., Donohue, J. P., Korostelev, A. A. & Noller, H. F. Crystal structure of the 70S ribosome bound with the Q253P mutant form of release factor RF2. *Structure* **21**, 1258–1263 (2013).
- Huter, P., Muller, C., Arenz, S., Beckert, B. & Wilson, D. N. Structural basis for ribosome rescue in bacteria. *Trends Biochem. Sci.* **42**, 669–680 (2017).
- Ma, C. et al. Mechanistic insights into the alternative translation termination by ArfA and RF2. *Nature* **541**, 550–553 (2017).
- Demo, G. et al. Mechanism of ribosome rescue by ArfA and RF2. *Elife* **6**, e23687 (2017).
- Shimizu, Y. ArfA recruits RF2 into stalled ribosomes. *J. Mol. Biol.* **423**, 624–631 (2012).
- Kurita, D., Chadani, Y., Muto, A., Abo, T. & Himeno, H. ArfA recognizes the lack of mRNA in the mRNA channel after RF2 binding for ribosome rescue. *Nucleic Acids Res.* **42**, 13339–13352 (2014).
- Zeng, F. & Jin, H. Peptide release promoted by methylated RF2 and ArfA in nonstop translation is achieved by an induced-fit mechanism. *RNA* **22**, 49–60 (2016).
- Weixlbaumer, A. et al. Insights into translational termination from the structure of RF2 bound to the ribosome. *Science* **322**, 953–956 (2008).
- Zhou, J., Korostelev, A., Lancaster, L. & Noller, H. F. Crystal structures of 70S ribosomes bound to release factors RF1, RF2 and RF3. *Curr. Opin. Struct. Biol.* **22**, 733–742 (2012).
- Lytvynenko, I. et al. Alanine tails signal proteolysis in bacterial ribosome-associated quality control. *Cell* **178**, 76–90 e22 (2019).
- Laurberg, M. et al. Structural basis for translation termination on the 70S ribosome. *Nature* **454**, 852–857 (2008).
- Korostelev, A., Zhu, J., Asahara, H. & Noller, H. F. Recognition of the amber UAG stop codon by release factor RF1. *EMBO J.* **29**, 2577–2585 (2010).
- Sohmen, D. et al. Structure of the *Bacillus subtilis* 70S ribosome reveals the basis for species-specific stalling. *Nat. Commun.* **6**, 6941 (2015).
- Youngman, P., Perkins, J. B. & Losick, R. A novel method for the rapid cloning in *Escherichia coli* of *Bacillus subtilis* chromosomal DNA adjacent to Tn917 insertions. *Mol. Gen. Genet.* **195**, 424–433 (1984).
- Gibson, D. G. et al. Enzymatic assembly of DNA molecules up to several hundred kilobases. *Nat. Methods* **6**, 343–345 (2009).
- Peters, J. M. et al. A comprehensive, CRISPR-based functional analysis of essential genes in bacteria. *Cell* **165**, 1493–1506 (2016).
- Montague, T. G., Cruz, J. M., Gagnon, J. A., Church, G. M. & Valen, E. CHOPCHOP: a CRISPR/Cas9 and TALEN web tool for genome editing. *Nucleic Acids Res.* **42**, W401–W407 (2014).

58. Labun, K., Montague, T. G., Gagnon, J. A., Thyme, S. B. & Valen, E. CHOPCHOP v2: a web tool for the next generation of CRISPR genome engineering. *Nucleic Acids Res.* **44**, W272–W276 (2016).
59. Li, X. et al. Electron counting and beam-induced motion correction enable near-atomic-resolution single-particle cryo-EM. *Nat. Methods* **10**, 584–590 (2013).
60. Zhang, K. Gctf: real-time CTF determination and correction. *J. Struct. Biol.* **193**, 1–12 (2016).
61. Zivanov, J. et al. New tools for automated high-resolution cryo-EM structure determination in RELION-3. *Elife* **7**, e42166 (2018).
62. Moriya, T. et al. High-resolution single particle analysis from electron cryo-microscopy images using SPHIRE. *J. Vis. Exp.*, <https://doi.org/10.3791/55448> (2017).
63. Beckert, B. et al. Structure of a hibernating 100S ribosome reveals an inactive conformation of the ribosomal protein S1. *Nat. Microbiol.* **3**, 1115–1121 (2018).
64. Adams, P. D. PHENIX: a comprehensive Python-based system for macromolecular structure solution. *Acta Crystallogr. D Biol. Crystallogr.* **66**, 213–221 (2010).
65. Soding, J., Biegert, A. & Lupas, A. N. The HHpred interactive server for protein homology detection and structure prediction. *Nucleic Acids Res.* **33**, W244–W248 (2005).
66. Chen, V. B. et al. MolProbity: all-atom structure validation for macromolecular crystallography. *Acta Crystallogr. D Biol. Crystallogr.* **66**, 12–21 (2010).
67. Goddard, T. D. et al. UCSF ChimeraX: meeting modern challenges in visualization and analysis. *Protein Sci.* **27**, 14–25 (2018).

## Acknowledgements

We thank Dr. Hyouta Himento of Hirosaki University for the *B. subtilis* *ssrA* mutant strain; Dr. Jiří Nováček (CEITEC, Brno, Czech Republic) for help with high-resolution cryo-EM data collection; Dr. Allen Buskirk for discussion; and Yuko Sumino, Saori Amano, Sakika Otani, Toru Irie, S. Rieder, and C. Ungewickell for expert technical support. We are also thankful to the National BioResource Project for providing the BKE strain library. This work was supported by grants from MEXT and JSPS Grant-in-Aid for Scientific Research (Grant No. 25291006 and 16H04788 to S.C., 26116008 to S.C. and K.I., 19K16044 to K.F.) and the Deutsche Forschungsgemeinschaft (SPP1879-WI3285/5-2 to D.N.W.).

## Author contributions

N.S.-C., K.F., and S.C. performed biochemical experiments and C.M., B.B., and D.N.W. performed structural experiments. N.S.-C., K.F., K.I., S.C., C.M., B.B., and D.N.W. designed experiments, analyzed data, and were involved in writing the manuscript.

## Competing interests

The authors declare no competing interests.

## Additional information

Supplementary information is available for this paper at <https://doi.org/10.1038/s41467-019-13408-7>.

**Correspondence** and requests for materials should be addressed to D.N.W. or S.C.

**Peer review information** *Nature Communications* thanks the anonymous reviewers for their contribution to the peer review of this work. Peer reviewer reports are available.

**Reprints and permission information** is available at <http://www.nature.com/reprints>

**Publisher's note** Springer Nature remains neutral with regard to jurisdictional claims in published maps and institutional affiliations.



**Open Access** This article is licensed under a Creative Commons Attribution 4.0 International License, which permits use, sharing, adaptation, distribution and reproduction in any medium or format, as long as you give appropriate credit to the original author(s) and the source, provide a link to the Creative Commons license, and indicate if changes were made. The images or other third party material in this article are included in the article's Creative Commons license, unless indicated otherwise in a credit line to the material. If material is not included in the article's Creative Commons license and your intended use is not permitted by statutory regulation or exceeds the permitted use, you will need to obtain permission directly from the copyright holder. To view a copy of this license, visit <http://creativecommons.org/licenses/by/4.0/>.

© The Author(s) 2019

## Supplementary Information

### **Release factor-dependent ribosome rescue by BrfA in the Gram-positive bacterium *Bacillus subtilis***

Shimokawa-Chiba et al.

## Supplementary Tables

**Supplementary Table 1. Data collection, refinement and validation statistics**

<b>BrfA-RF2-ns70S</b>	
<b>Data collection</b>	
Particles	154,405
Microscope	Titan Krios
Detector	Falcon III
Pixel size (Å)	1.065
Defocus range (μm)	0.4-2.2
Voltage (keV)	300
Electron dose (e <sup>-</sup> / Å <sup>2</sup> )	2.0
<b>Model composition</b>	
Protein residues	6100
RNA nucleotides	4646
Hydrogens	0
<b>Refinement</b>	
Resolution (Å)	3.06
Map sharpening B factor (Å <sup>2</sup> )	-73.0479
CC map/model	0.85
<b>Validation: proteins</b>	
Poor rotamers (%)	0.54
Ramachandran outliers (%)	0.22
Bad backbone bonds (%)	0.01
Bad backbone angels (%)	0.05
<b>Validation: RNA</b>	
Correct sugar pockers (%)	99.31
Good backbone conformations (%)	79.88
Bad bonds (%)	0.00
Bad angels (%)	0.02
<b>Scores</b>	
MolProbity	1.74 (88 <sup>th</sup> percentile)
Clash score, all atoms	4.98 (93 <sup>nd</sup> percentile)

**Supplementary Table 2. *E. coli* strains**

Name	Description	Reference
BL21(DE3)	F <sup>+</sup> , <i>ompT</i> , <i>hsdS</i> (r <sub>s</sub> m <sub>s</sub> ), <i>gal</i> (λcI 857, <i>ind1</i> , <i>Sam7</i> , <i>nin5</i> , <i>lacUV5-T7gene1</i> ), <i>dcm</i> (DE3)	Promega
NAE970	BL21(DE3)/pNAR913 ( <i>Bs_prfA-his</i> )	This study
NAE972	BL21(DE3)/pNAR915 ( <i>Bs_prfB-his</i> )	This study
NAE973	BL21(DE3)/pNAR916 ( <i>brfA62-his</i> )	This study
NAE982	BL21(DE3)/pNAR917 ( <i>his-arfA(2-60)</i> )	This study
NAE1003	BL21(DE3)/pCH2307 ( <i>Bs_prfB(GAQ)-his</i> )	This study
NAE1017	BL21(DE3)/pNAR939 ( <i>Bs_pfrB(SPT)-his</i> )	This study

**Supplementary Table 3. *B. subtilis* strains and construction**

Name	Description	Reference	Construction	
			Host	DNA
PY79	WT	ref. <sup>1</sup>		
BKE23540	Δ <i>brfA</i> :: <i>erm</i>	ref. <sup>2</sup>		
BKE33600	Δ <i>smpB</i> :: <i>erm</i>	ref. <sup>2</sup>		
D1	Δ <i>ssrA</i> :: <i>cat</i>	ref. <sup>3</sup>		
TSB2	Δ <i>ssrA</i> :: <i>cat</i> :: <i>tet</i>	This study	SCB2582	pCm::Tc
NAB1196	<i>thrC</i> :: <i>P<sub>xytA</sub></i> GFPΩ <i>erm</i>	This study	PY79	pNAR778
NAB1198	<i>thrC</i> :: <i>P<sub>xytA</sub></i> GFP-nsΩ <i>erm</i>	This study	PY79	pNAR780
NAB1200	Δ <i>ssrA</i> :: <i>cat</i> , <i>thrC</i> :: <i>P<sub>xytA</sub></i> GFPΩ <i>erm</i>	This study	SCB2582	pNAR778
NAB1202	Δ <i>ssrA</i> :: <i>cat</i> , <i>thrC</i> :: <i>P<sub>xytA</sub></i> GFP-nsΩ <i>erm</i>	This study	SCB2582	pNAR780
NAB1280	Δ <i>smpB</i> :: <i>erm</i>	This study	PY79	BKE33600
NAB1281	Δ <i>yesZ</i> :: <i>loxP</i> , Δ <i>lacA</i> :: <i>loxP</i> , Δ <i>smpB</i> :: <i>erm</i>	This study	KFB793	NAB1233
NAB1282	Δ <i>smpB</i> :: <i>loxP</i>	This study	NAB1280	pMK2
NAB1283	Δ <i>yesZ</i> :: <i>loxP</i> , Δ <i>lacA</i> :: <i>loxP</i> , Δ <i>smpB</i> :: <i>loxP</i>	This study	NAB1281	pMK2
NAB1286	Δ <i>yesZ</i> :: <i>loxP</i> , Δ <i>lacA</i> :: <i>loxP</i> , Δ <i>smpB</i> :: <i>loxP</i> / pNAR813	This study	NAB1283	pNAR813
NAB1298	Δ <i>brfA</i> :: <i>erm</i>	This study	PY79	BKE23540
NAB1346	Δ <i>brfA</i> :: <i>kan</i>	This study	PY79	pNAR903
NAB1509	<i>amyE</i> :: <i>P<sub>mifM</sub></i> <i>rbsm1</i> -GFP- <i>brfA</i> -FLAGΩ <i>lacZ</i> Ω <i>cat</i>	This study	PY79	pNAR1036
NAB1510	<i>amyE</i> :: <i>P<sub>mifM</sub></i> <i>rbsm1</i> -GFP- <i>brfA62</i> -FLAGΩ <i>lacZ</i> Ω <i>cat</i>	This study	PY79	pNAR1037
NAB1511	<i>amyE</i> :: <i>P<sub>mifM</sub></i> <i>rbsm1</i> -GFP- <i>brfA</i> (no_term)-FLAGΩ <i>lacZ</i> Ω <i>cat</i>	This study	PY79	pNAR1038
NAB1514	Δ <i>smpB</i> :: <i>erm</i> , <i>rbsm1</i> -GFP- <i>brfA</i> -FLAGΩ <i>lacZ</i> Ω <i>cat</i>	<i>amyE</i> :: <i>P<sub>mifM</sub></i>	This study	NAB1280 pNAR1036
NAB1515	Δ <i>smpB</i> :: <i>erm</i> ,,Δ <i>amyE</i> :: <i>P<sub>mifM</sub></i> <i>rbsm1</i> -GFP- <i>brfA62</i> -FLAGΩ <i>lacZ</i> Ω <i>cat</i>		This study	NAB1280 pNAR1037
NAB1516	Δ <i>smpB</i> :: <i>erm</i> ,,Δ <i>amyE</i> :: <i>P<sub>mifM</sub></i> <i>rbsm1</i> -GFP- <i>brfA</i> (no_term)-FLAGΩ <i>lacZ</i> Ω <i>cat</i>		This study	NAB1280 pNAR1038
SCB851	<i>amyE</i> :: <i>P<sub>mifM</sub></i> <i>rbsm1</i> -GFP- <i>mifM35-flag-yidC2'-lacZ</i> Ω <i>cat</i>	ref. <sup>4</sup>		
SCB2582	Δ <i>ssrA</i> :: <i>cat</i>	This study	PY79	D1
SCB4122	<i>amyE</i> :: <i>P<sub>mifM</sub></i> <i>rbsm1</i> GFP- <i>brfA62</i> -FLAGΩ <i>cat</i>	This study	PY79	pCH2240
SCB4126	Δ <i>smpB</i> :: <i>erm</i> , <i>amyE</i> :: <i>P<sub>mifM</sub></i> <i>rbsm1</i> GFP- <i>brfA62</i> -FLAGΩ <i>cat</i>	This study	NAB1280	pCH2240
SCB4141	<i>amyE</i> :: <i>P<sub>mifM</sub></i> <i>rbsm1</i> -GFP- <i>brfA</i> -FLAGΩ <i>cat</i>	This study	PY79	pCH2239
SCB4142	<i>amyE</i> :: <i>P<sub>mifM</sub></i> <i>rbsm1</i> -GFP- <i>brfA</i> (no_term)-FLAGΩ <i>cat</i>	This study	PY79	pCH2241
SCB4144	Δ <i>smpB</i> :: <i>erm</i> , <i>amyE</i> :: <i>P<sub>mifM</sub></i> <i>rbsm1</i> -GFP- <i>brfA</i> -FLAGΩ <i>cat</i>		This study	NAB1280 pCH2239

SCB4145	$\Delta smpB::erm$ , $rbsm1-GFP-brfA(\text{no term})$ -FLAG-Qcat	$amyE::P_{mifM}$	This study	NAB1280	pCH2241
SCB4153	$lacA::P_{xylA}$ dCas9-Qerm, $amyE::P_{veg}$ sgRNA-smpB-Qcat		This study	KFB946	pCH2264
SCB4191	$lacA::P_{xylA}$ dCas9-Qerm, $\Delta brfA::kanR$		This study	KFB946	NAB1346
SCB4194	$amyE::P_{veg}$ sgRNA-smpB-Qcat, $lacA::P_{xylA}$ dCas9-Qerm, $\Delta brfA::kanR$		This study	SCB4191	pCH2264
SCB4199	$amyE::P_{veg}$ sgRNA-ssrA-Qcat, $lacA::P_{xylA}$ dCas9-Qerm, $\Delta brfA::kanR$		This study	SCB4191	pCH2302
SCB4205	$lacA::P_{xylA}$ dCas9-Qerm, $amyE::P_{veg}$ sgRNA-ssrA-Qcat		This study	KFB946	pCH2302
SCB4215	$amyE::P_{veg}$ sgRNA-smpB-Qcat, $lacA::P_{xylA}$ dCas9-Qerm, $\Delta brfA::kanR, thrC::PbrfA brfA-Qspc$		This study	SCB4194	pCH2293
SCB4217	$amyE::P_{veg}$ sgRNA-ssrA-Qcat, $lacA::P_{xylA}$ dCas9-Qerm, $\Delta brfA::kanR, thrC::PbrfA brfA-Qspc$		This study	SCB4199	pCH2293
SCB4218	$amyE::P_{mifM}$ rbsm1-GFP-mifM35-flag-yidC2'-lacZ-Qcat, ssrA::cat::tet		This study	SCB851	TSB2
KFB792	$\Delta lacA::loxP-kanR$		This study	PY79	DNA fragment
KFB793	$\Delta yesZ::loxP, \Delta lacA::loxP$		This study	KYB112	KFB792, pMK2
KFB946	$lacA::P_{xylA}$ dCas9-Qerm		This study	PY79	pJMP1
KFB948	$\Delta yesZ::loxP, lacA::Pxyl$ -dCas9-Qerm		This study	KYB112	pJMP1
KYB112	$\Delta yesZ::loxP$		This study	PY79	pKY13, pMK2

**Supplementary Table 4. Plasmids**

Name	Description	Source
pCm::Tc	<i>Cm::Tc</i>	ref. <sup>5</sup>
pDG1664	<i>thrC::erm</i> integration vector	ref. <sup>6</sup>
pET28b	vector	Novagen
pLOSS*	Ts vector	ref. <sup>7</sup>
pyqjG21	$amyE::P_{mifM}$ <i>mifM-yidC2-gfp</i>	ref. <sup>4</sup>
pJMP1	$lacA::Pxyl$ dCas9-Qerm	ref. <sup>8</sup>
pNAR756	$P_{xylA}$ <i>yidC2</i>	This study
pNAR758	$P_{xylA}$ <i>yidC2-non_stop</i>	This study
pNAR778	$thrC::P_{xylA}$ GFP-Qerm	This study
pNAR780	$thrC::P_{xylA}$ GFP-ns-Qerm	This study
pNAR809	$P_{spac}$ <i>smpB</i>	This study
pNAR813	$P_{spac}$ <i>smpB-FLAG</i>	This study
pNAR869	<i>brfA-his6</i>	This study
pNAR879	$amyE::P_{mifM}$ rbsm1-GFP- <i>brfA-Qcat</i>	This study
pNAR901	upstream region of <i>brfA</i>	This study
pNAR903	$\Delta brfA::kan$	This study
pNAR913	<i>Bs_prfA-his6</i>	This study
pNAR915	<i>Bs_prfB-his6</i>	This study

pNAR916	<i>brfA62-his<sub>6</sub></i>	This study
pNAR917	<i>his<sub>6</sub>-arfA(2-60)</i>	This study
pNAR939	<i>Bs_pfrB(SPT)</i>	This study
pNAR1036	<i>amyE::P<sub>mifM</sub> rbsm1-GFP-brfA-FLAGΩlacZΩcat</i>	This study
pNAR1037	<i>amyE::P<sub>mifM</sub> rbsm1-GFP-brfA62-FLAGΩlacZΩcat</i>	This study
pNAR1038	<i>amyE::P<sub>mifM</sub> rbsm1-GFP-brfA(no_term)-FLAGΩlacZΩcat</i>	This study
pCH735	<i>amyE::P<sub>mifM</sub> mifM-lacZΩcat</i>	ref. <sup>4</sup>
pCH747	<i>amyE::P<sub>mifM</sub> mifM-gfpΩcat</i>	This study
pCH805	<i>amyE::P<sub>mifM</sub> GFP-mifM35-yidC2'-lacZΩcat</i>	ref. <sup>4</sup>
pCH913	<i>amyE::P<sub>mifM</sub> rbsm1-GFP-mifM35-yidC2'-lacZΩcat</i>	ref. <sup>4</sup>
pCH1141	<i>thrC::P<sub>xylA</sub>Ωerm</i>	ref. <sup>9</sup>
pCH1142	<i>kanΩspc</i>	ref. <sup>10</sup>
pCH1517	<i>amyE::PyqzJ rbsm1-GFP-mifM35-95-lacZΩcat</i>	ref. <sup>10</sup>
pCH2238	<i>his<sub>6</sub>-Bs_pfrB</i>	This study
pCH2239	<i>amyE::P<sub>mifM</sub> rbsm1 GFP-brfA-FLAGΩcat</i>	This study
pCH2240	<i>amyE::P<sub>mifM</sub> rbsm1 GFP-brfA62-FLAGΩcat</i>	This study
pCH2241	<i>amyE::P<sub>mifM</sub> rbsm1 GFP-brfA(no_term)-FLAGΩcat</i>	This study
pCH2264	<i>amyE::P<sub>veg</sub> sgRNA-smpBΩcat</i>	This study
pCH2293	<i>thrC::P<sub>brfA</sub> brfAΩspc</i>	This study
pCH2302	<i>amyE::P<sub>veg</sub> sgRNA-ssrAΩcat</i>	This study
pCH2307	<i>Bs_pfrB(GAQ)-his<sub>6</sub></i>	This study
pKIG855	<i>amyE::P<sub>veg</sub> sgRNA-rfpΩcat</i>	This study
pMK2	<i>Pspac cre</i>	This study
pKY13	<i>ΔyesZ::loxP-kan-loxP</i>	This study
pNR1	<i>amyE::P<sub>xylA</sub> rbsm1 mifM-GFPΩcat</i>	This study

### Supplementary Table 5. Primers

Name	Sequence
SP1	TATTTTAAGGGGAAATCACATAAAAGGAGGAGAACAAA
SP2	GAAGCTTATCGAATTCACTAGTTCAGCCATGATAAACACAAGACTG
SP3	AGTCTTCTCATGGCTGAAGTAGTGAATTGATAAGCTTC
SP4	TTTGTTCTCCTCTTTATGTGATTCCCCCTAAAAATA
SP5	GTGAAAAATAAAAGCAACCCCGTGCAAAAG
SP6	GGGGTTGCTTTATTTTACCGACTCAGTAAGAGC
SP7	GAACAAAATTGTTAAAACATATGGATCCAAGCTTACTAGTAGT
SP8	GAAGCTTATCGAATTCACTAGTTCACGCCGTTGTATAGTCATC



SP45 GGCCTGGTGCCGCGCGCAGCAGTCGATATCAGCATACTAAA  
SP46 GGCTTGTAGCACCGGATCTTAGTGATTACTTCTTGCCTACT  
SP47 GATCCGGCTGCTAACAAAGCC  
SP48 GCTGCCGCGCGCACCAGGCC  
SP49 GTGCGGATCTCACCAACAGATTCATCAGGCCGCC  
SP50 GCGGC GGCTGATGAATCTGTTGGTGAGATCCGACAAAG  
SP51 GGCCTGGTGCCGCGCGCAGCGAATTATCAGAAATTAGAGCAG  
SP52 AGGTCAAGAGACCCCCCTAAAGTCCGC  
SP53 AGGGGGTCTCTGACCTCGAATCAAAGGA  
SP54 GGCTTGTAGCACCGGATCTTATGAAAGCTTAGAACGCAG  
SP55 TATAAAGACGACGACGACAATAGAGATCCGATCAGACCAGT  
SP56 GTCGTCGTCGTCTTATAGTCGGCGGCTTTGGGGCACAAAAAAATC  
SP57 GTCGTCGTCGTCTTATAGTCCTTATCATCAACTGCTGTATG  
SP58 ACCATACAGCAGTAGACGACAAGACTCTCGTGCCTCAAAAG  
SP59 TCGTCTACTGCTGTATGGTCGTACGGTTCTTATGCTCCGTTAT  
SP60 GCTCGTGTGTACAATAATGTAGGAATCCTTAAGGTTACGGTTTAGAGCTAGAAATAGC  
AAGTAAAATAAGGC  
SP61 ACATTATTGTACAACACGAGCC  
SP62 TTCGATAAGCTCTAGGATCCCATGCAGCTTACAGCAGTG  
SP63 GGCCAAAAAAACTGCTGCCTCCTAGGCGGCTTTGGGCAC  
SP64 GAAGGCAGCAGTTTTGGCCTTC  
SP65 GGATCCTAGAAGCTTATCGAA  
SP66 GCTCGTGTGTACAATAATGTGTGTTACGAGATCGCCTCTGTTAGAGCTAGAAATAGC  
AAGTAAAATAAGGC  
SP67 GGC GGGCGCACAGCACGTCAATACGACG  
SP68 GCCCGCGCCGCTTGCACGGTA  
SP69 GATCCTAGAAGCTTATCGAATTCC  
SP70 GCAGTCTAGACTCGAGTAAGG  
SP71 CCTTACTCGAGTCTAGACTGCTCGAATTCTCATGTTGACAG  
SP72 GGAATTGATAAGCTCTAGGATCCGATCA  
SP73 TTAACTAATAAGGAGGACAAACATGTCCAATTACTGACCGT  
SP74 CCGGTTATTACTAATGCCATCTCCA  
SP75 CGATTAGTAATAATAACCGGGCAGGCCATG  
SP76 TTGTCCTCCTTATTAGTTAATCAATTCAAGCTTAATTGTTAT  
SP77 AAGCTTGGCGTAATCATGGTC  
SP78 GAGCTCGAATTCTGCAGCTG  
SP79 GGTACCCGGGATCCACTAGT  
SP80 GCATGCCTCGAGGGGCCGCC

SP81 CAGCTGCAGGAATCGAGCTCATCTCACCCGCCACTGTTTT  
 SP82 ACTAGTGGATCCCCGGGTACCCACATTTCACCTTCTTGA  
 SP83 GGGCGGCCCTCGAGGCATGCTCTTGTATCGAATCAGCTT  
 SP84 GACCATGATTACCCAAGCTTTTCCGGTCCGTTTGACAG  
 SP85 GTGAATTGATAAGCTCTAGAAGCTAGGAGGAGGTGATGACAATGTTGT  
 SP86 CACACAAATTAAAAACTGGTCT  
 SP87 AGACCAGTTTAATTGTGTG  
 SP88 TAGAAGCTTATCGAATTCA  
 SP89 GGTACCCGGGATCCACTAGT  
 SP90 GCATGCCTCGAGGGGCCGCC  
 SP91 CAGCTGCAGGAATCGAGCTCTAAATTGACAATGCAGTCCAG  
 SP92 ACTAGTGGATCCCCGGGTACCATTCTCCTCCTGTTCTTA  
 SP93 GGGCGGCCCTCGAGGCATGCGCTGATGCTCCGCTCGATATG  
 SP94 GACCATGATTACCCAAGCTTATTCATGCCATGCCATC  
 SP95 TAACTTAAGAAGGAGGAGATACCAATGACAATGTTGTGGGATC  
 SP96 TTTGTATAGTTCATCCATGCC  
 SP97 TTATTATAAAAGAAGAGAAC  
 SP98 GAAATTAATACGACTCACTATAGGGAGACCACAACGGTTCCCTCTAGAAATAATTTGTT  
 AACTTAAGAAGGAG  
 SP99 TAACTTAAGAAGGAGGATTAGAATGACCATGATTACGGATTCA  
 SP100 AAAACTGGTCTGATGGATCTTATTTGACACCAGACCAACTG  
 SP101 AGATCCGATCAGACCAGTTT  
 SP102 AAATCCTCCTCTTAAAGTTACTATTGTCGTCGTCGCTTT  
 nlpD CGGCGGTCTAACACATAC  
 rev

---

**Supplementary Table 6.**

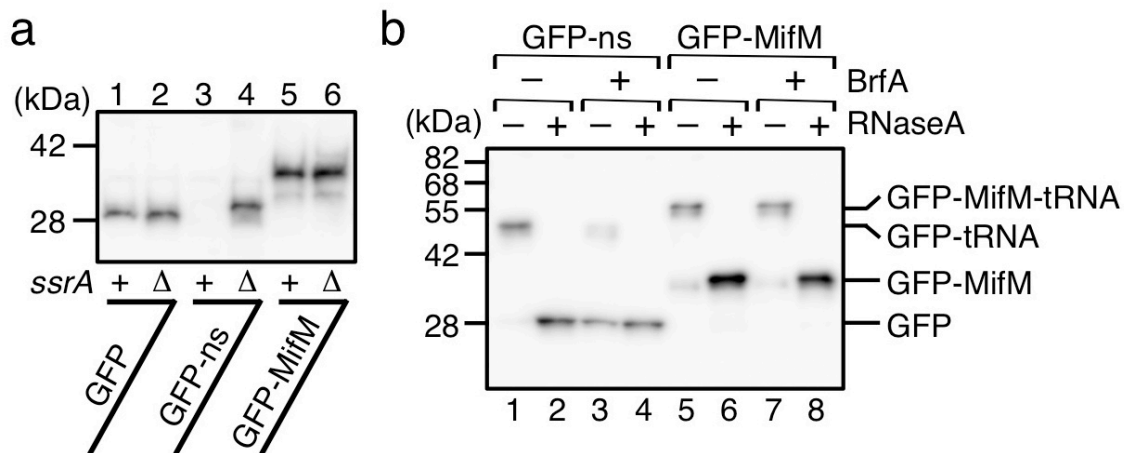
Plasmid name	Combinations of primers and template DNAs for plasmid construction			
pNAR756	SP1, 2	/PY79 DNA	SP3, 4	/pCH1141
pNAR758	SP5, 6	/pNAR756		
pNAR778	SP7, 8	/pNR1	SP9, 10	/pNAR756
pNAR780	SP7, 11	/pNR1	SP10, 12	/pNAR758
pNAR809	SP13, 14	/PY79 DNA	SP15, 16	/pLOSS*
pNAR813	SP17, 18	/pNAR809		
pNAR869	SP19, 20	/PY79 DNA	SP21, 22	/pET28b
pNAR879	SP23, 24	/PY79 DNA	SP25, 26	/pCH913
pNAR901	SP27, 28	/PY79 DNA	SP29, 30	/pCH1142

pNAR903	SP31, 32	/PY79 DNA	SP33, 34	/pNAR901			
pNAR913	SP35, 36	/PY79 DNA	SP37, 38	/pET28b			
pNAR915	SP39, 40	/pCH2238	SP37, 38	/pET28b			
pNAR916	SP41, 42	/pNAR869	SP43, 44	/pNAR869			
pNAR917	SP45, 46	/JM109 DNA	SP42, 47	/pET28b	SP43, 48	/pET28b	
pNAR939	SP49, 50	/pNAR915					
pNAR1036	SP99, 100	/pCH1517	SP101, 102	/pCH2239			
pNAR1037	SP99, 100	/pCH1517	SP101, 102	/pCH2240			
pNAR1038	SP99, 100	/pCH1517	SP101, 102	pCH2241			
pCH2238	SP51, 52	/PY79 DNA	SP53, 54	/PY79 DNA	SP47, 48	/pET28b	
pCH2239	SP55, 56	/pNAR879					
pCH2240	SP55, 57	/pNAR879					
pCH2241	SP58, 59	/pCH2239					
pCH2264	SP60, 61	/pKIG855					
pCH2293	SP62, 63	/PY79 DNA	SP64, 65	/pDG1731			
pCH2302	SP61, 66	/pKIG855					
pCH2307	SP67, 68	/pNAR915					
pKIG855	SP69, 70	/synthetic DNA	SP71, 72	/pDG1662			
pMK2	SP73, 74	/P1 phage DNA	SP75, 76	/pLOSS*			
pKY13	SP77, 78	/pCH1142	SP79, 80	/pCH1142	SP81, 82	/PY79 DNA	SP86, 87 /PY79 DNA
pNR1	SP85, 86	/pCH747	SP87, 88	/pCH1130			

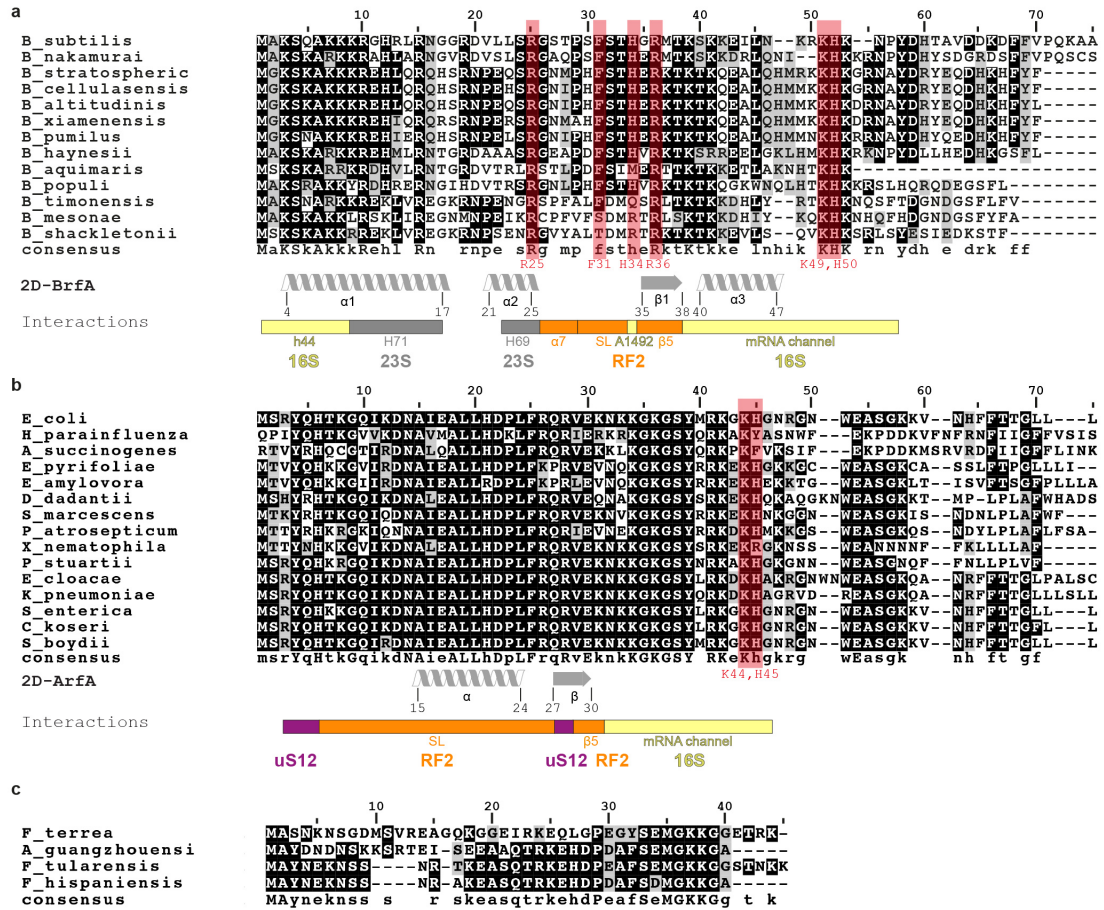
**Supplementary Table 7. PCR templates and primers for preparation of in vitro translation templates**

Gene name	1st PCR			2nd PCR		
	Primers		template	Primers		template
GFP-ns	SP95	SP96	pCH805	SP98	SP96	1st PCR product
GFP- <i>mifM</i>	SP95	SP97	pCH805	SP98	SP97	1st PCR product

## Supplementary Figures

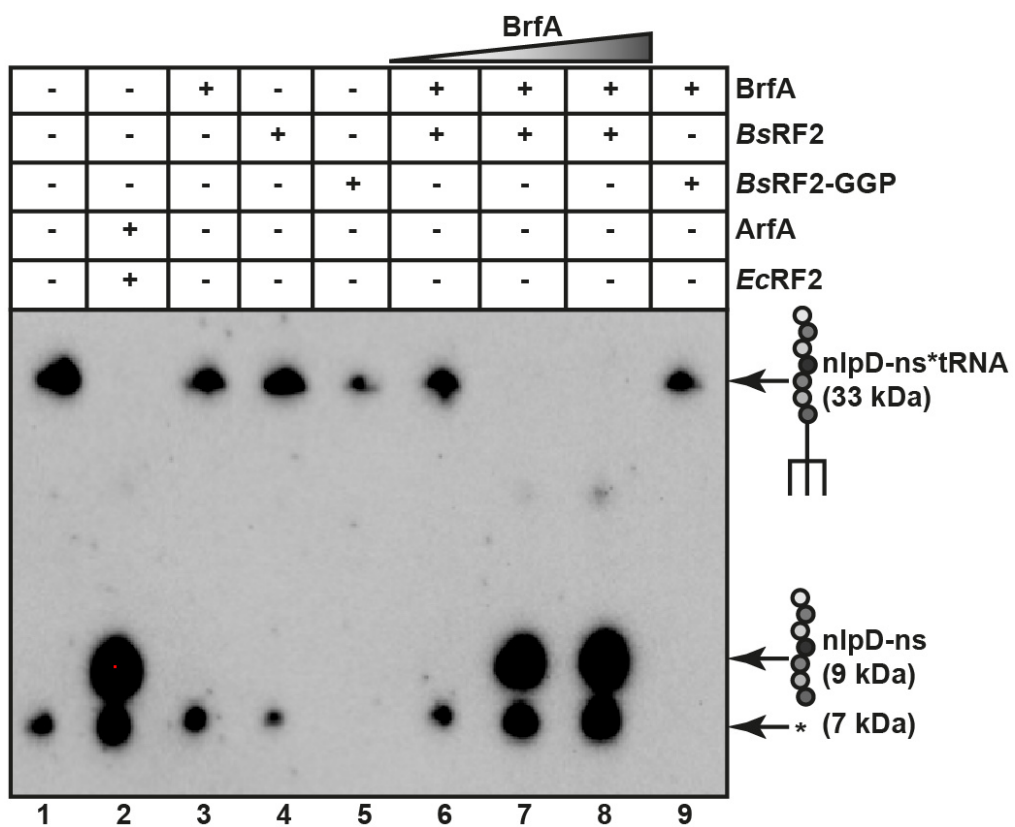


**Supplementary Fig. 1 | Nascent-chain mediated ribosome stalling is refractory to the ribosome rescue systems in *B. subtilis*.** **a**, MifM is refractory to *trans*-translation. Cellular accumulation of GFP-MifM was examined in the wild type and *ssrA*-deficient mutant strains. GFP (lanes 1, 2), GFP-ns (lanes 3, 4) and GFP-MifM (lanes 5, 6) were expressed in the wild type (odd number) and  $\Delta$ *ssrA* (even number) strains of *B. subtilis*, separated by SDS-PAGE and detected with anti-GFP immunoblotting. **b**, Inability of BrfA to induce RF2 hydrolysis of the elongation-arrested MifM-tRNA. In vitro translation using *Bs* hybrid PURE system with RF2 was directed by the *gfp-ns* (lanes 1-4) or *gfp-mifM* (lanes 5-8) template in the presence (lanes 3, 4, 7, 8) or the absence (lanes 1, 2, 5, 6) of purified BrfA62-His<sub>6</sub>. The translation products were analyzed by anti-GFP immunoblotting as described above.



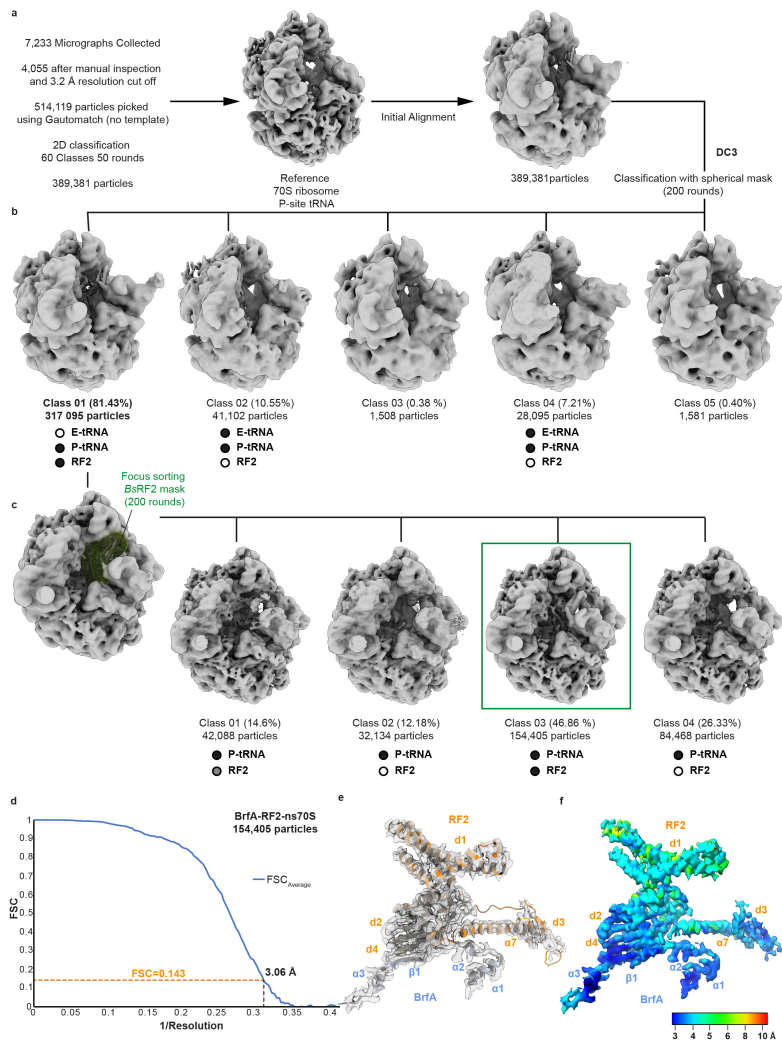
**Supplementary Fig. 2 | Multiple sequence alignments of BrfA, ArfA, and ArfT homologs.**

**a-c**, Multiple sequence alignments of (a) BrfA, (b) ArfA and (c) ArfT generated with Clustal W<sup>11</sup> and Boxshade with residues shaded that are identical (black) or similar (grey). Below each alignment, the consensus sequence with capital letters indicating 100% conservation and lower-case letters indicating less conservation. The known secondary structure is shown for *B. subtilis* BrfA (2D-BrfA) in (a) and *E. coli* ArfA (2D-ArfA) in (b), as well as interaction regions between (a) BrfA and (b) ArfA with the ribosome (16S rRNA, yellow, 23S rRNA, grey and uS12, violet) and RF2 (orange).



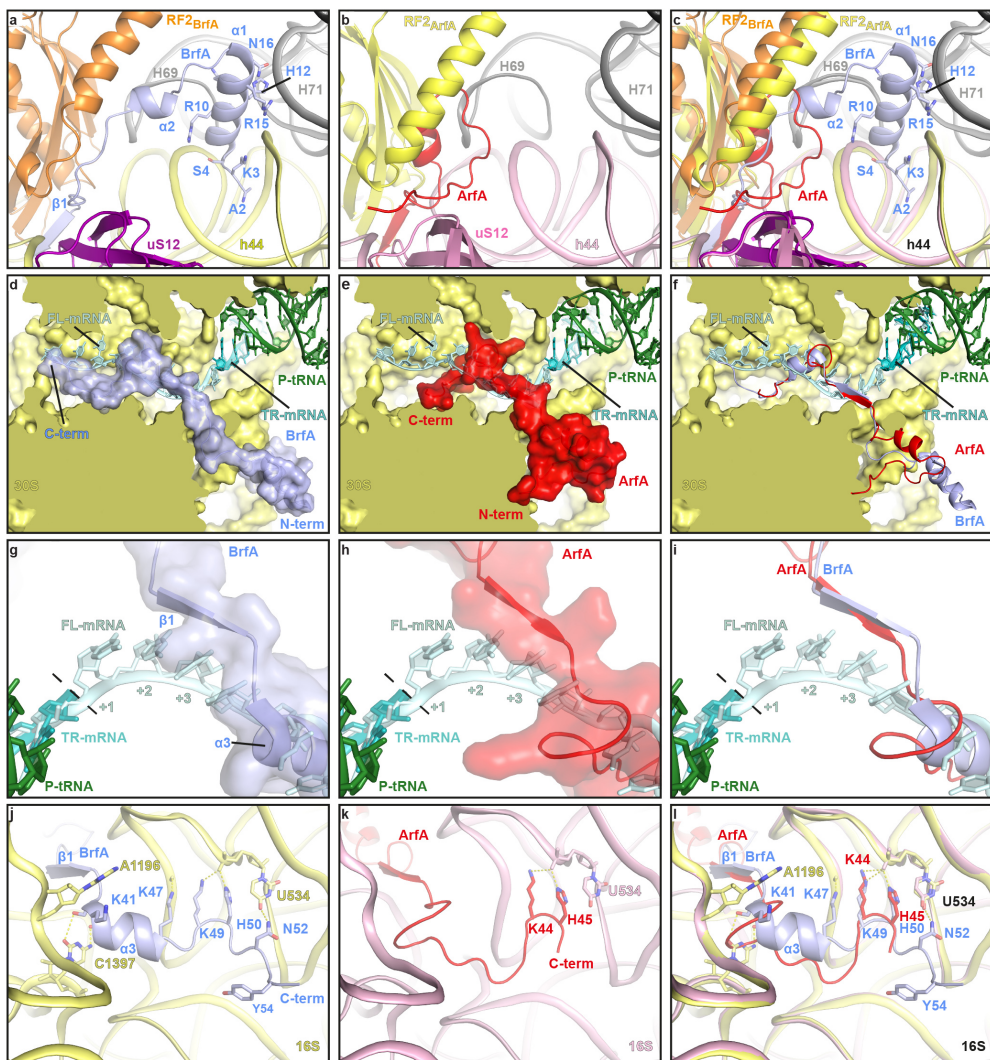
**Supplementary Fig. 3 | Recycling of non-stop ribosomes by BrfA and RF2.**

*In vitro* translation assays using the *E. coli* PURE systemΔRF123 kit (lacking all RFs) were performed with truncated non-stop *nlpD* DNA template, in the presence of BrfA, wildtype *B. subtilis* RF2 (*BsRF2*) and the RF2-GGP mutant (*BsRF2-GGP*) alone (lanes 3-5), or *BsRF2* (20 pmol) with increasing concentrations (12-100 pmol) of BrfA (lanes 6-8), or BrfA (100 pmol) in the presence of 100 pmol *BsRF2-GGP* (lane 9). As a positive control, reactions were performed with *E. coli* ArfA and RF2 (*EcRF2*), as described previously (lane 2) <sup>12</sup>. A negative control was also performed where reactions lacked all RFs and rescue factors (lane 1). Western blotting of NuPAGE gels using an antibody against the HA-tag present in the N-terminus of the NlpD peptide detected the presence of the non-stop NlpD-peptidyl-tRNA (33 kDa) and released NlpD peptide (9 kDa). The asterisk (\*) indicates a mysterious band that cross-reacts with the HA-antibody, but is also present in the negative control and was therefore not examined further. As expected, the negative control (lane 1), as well as reactions performed in the presence of BrfA, *BsRF2* or *BsRF2GGP* alone (lanes 3-5), show a strong band for the NlpD-peptidyl-tRNA and no evidence for the released NlpD peptide. By contrast, the positive control with ArfA and *EcRF2* (lane 2), as well as the reactions with *BsRF2* and increasing concentrations of BrfA (lanes 7 and 8) shows no NlpD-peptidyl-tRNA and only the presence of released NlpD peptide. As expected, substitution of wildtype *BsRF2* with the inactive *BsRF2-GGP* mutant led to a loss the band for the released NlpD peptide and the presence of NlpD-peptidyl-tRNA was restored (lane 9). Source data are provided as a Source Data file.

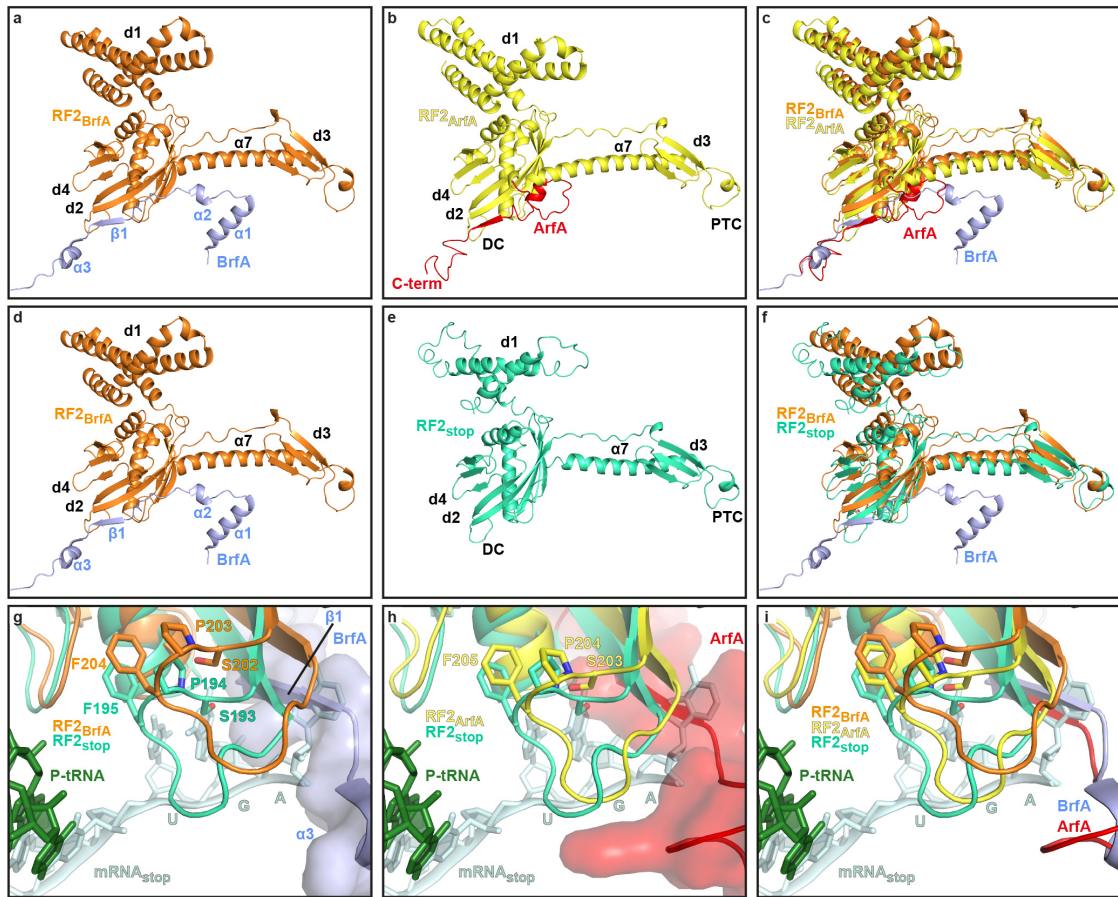


**Supplementary Fig. 4 | In silico sorting of the BrfA-RF2-ns70S complex.**

**a**, After particle picking and extensive 2D classification, the complete dataset of 389,381 particles was initially aligned against a P-site tRNA containing *E. coli* 70S ribosome. **b**, Following 3D classification for 200 rounds in Relion, five classes were generated. The majority (317,095 particles; 81.43%) of particles were found in class 1 and contained the BrfA-RF2-ns70S complex. The second major (41,102 particles; 10.55%) class 2 contained a fully programmed ribosome, but without the presence of RF2. In addition, three minor classes 4-6 (class 3; 1,508 particles; 0.38 %, class 4; 28,095 particles; 7.21%; class 5; 1,581 particles; 0.4%) containing damaged and/or poorly aligning particles were observed. **c**, The 317,095 particles from the class 1 were further sorted using a focus sorting mask around RF2, resulting in four additional classes, of which class 3 (154,405 particles, 46.86%) contained stoichiometric occupancy of P-site tRNA, RF2 and BrfA. Class 3 was then refined to yield a (**d**) final reconstruction of the BrfA-RF2-ns70S complex with an average resolution of 3.15 Å (0.143 FSC). **e-f**, Isolated electron density for BrfA and RF2 **e**, shown as grey mesh with fitted model and **(f)** colored according to local resolution

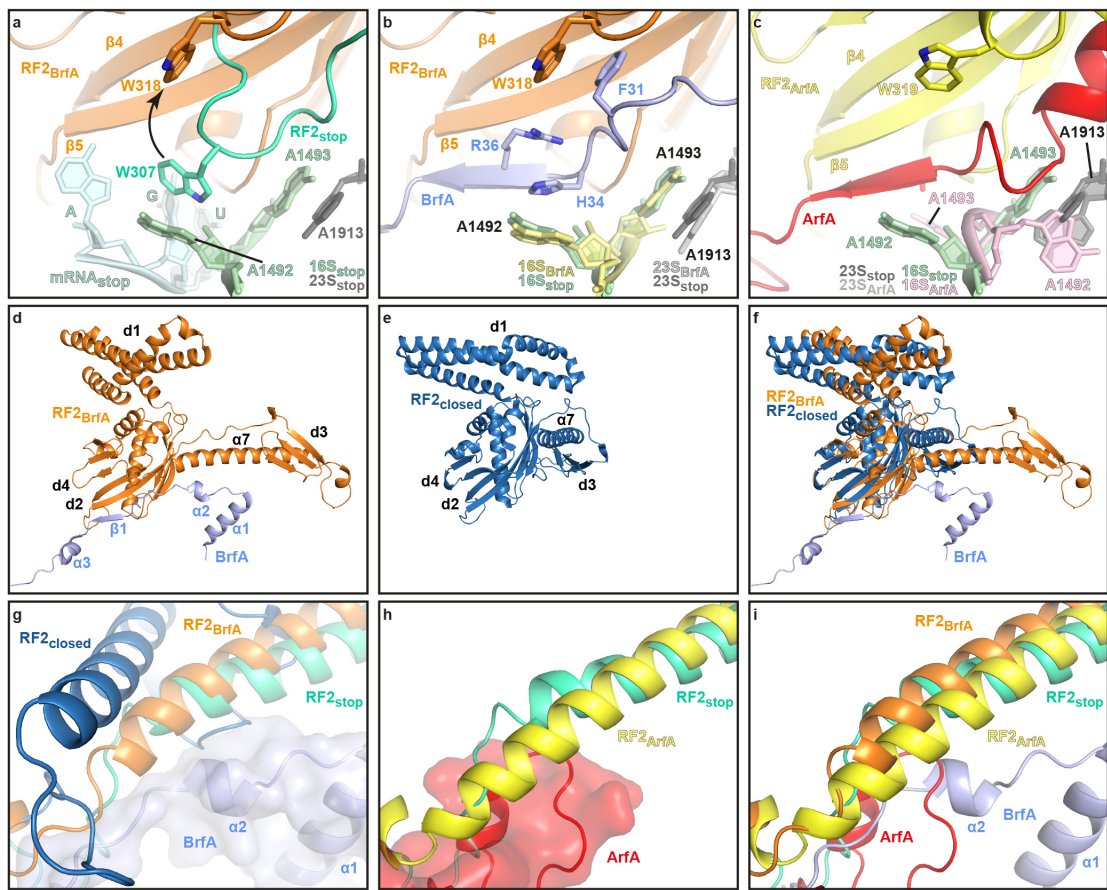


**Supplementary Fig. 5 | Interactions of BrfA and ArfA on the ribosome.** **a**, Interaction of the N-terminus of BrfA (blue) with RF2 (orange), uS12 (violet), helix 44 (h44) of the 16S rRNA (yellow) and helix 69 (H69) and H71 of the 23S rRNA (grey). **b**, Same view as (a), but for the ArfA-RF2-70S complex, with ArfA (red), RF2 (yellow) and 16S rRNA (pink). **c**, Overlay of (a) and (b). **d-e**, Transverse section of the 30S subunit (yellow) to reveal the mRNA channel showing a superimposition of full-length mRNA (FL-mRNA, cyan) with truncated non-stop mRNA (TR-mRNA, teal), P-site tRNA (green) and surface representations of (d) BrfA (blue) and (e) ArfA (red). **f**, Overlay of (d) and (e) with cartoon representations of BrfA (blue) and ArfA (red). **g-h**, Superimposition of full-length mRNA (FL-mRNA, cyan) with truncated non-stop mRNA (TR-mRNA, teal), P-site tRNA (green) and transparent surface representations of (g) BrfA (blue) and (h) ArfA (red). The first (+1), second (+2) and third (+3) nucleotides of the A-site codon of the FL-mRNA are indicated. **i**, Overlay of (g) and (h) with cartoon representations of BrfA (blue) and ArfA (red). **j-k**, Interaction of the C-terminus of (j) BrfA (blue) and (k) ArfA (red) with the 16S rRNA with potential hydrogen bonds indicated with yellow dashed lines. **l**, Overlay of (j) and (k).



**Supplementary Fig. 6 | Interaction of BrfA and ArfA with RF2 on the ribosome.**

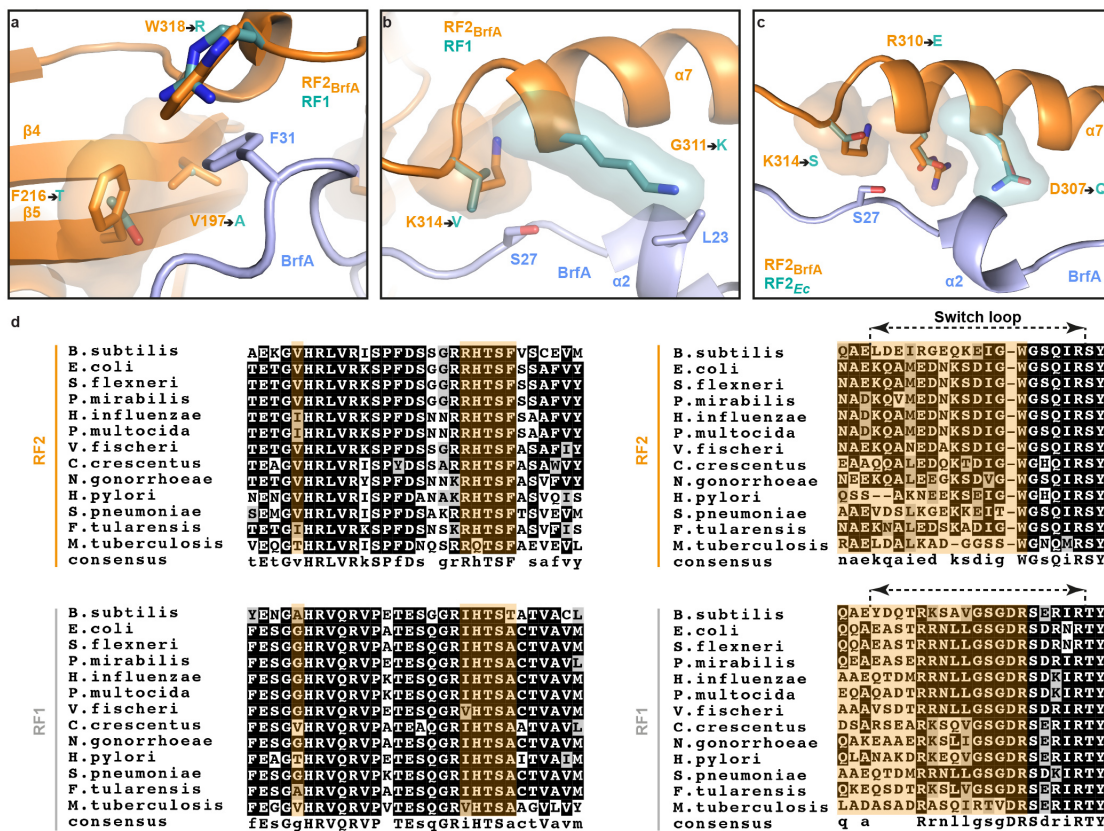
**a-b**, Interaction between (a) BrfA (blue) and RF2<sub>BrfA</sub> (orange) in the BrfA-RF2-ns70S complex compared with (b) ArfA (red) and RF2<sub>ArfA</sub> (yellow) in the ArfA-RF2-ribosome complex <sup>12</sup>. The approximate positions of the decoding center (DC) and peptidyltransferase center (PTC) on the ribosome are indicated. **c**, Superimposition of (a) and (b). **d-e**, The binding position of (d) RF2<sub>BrfA</sub> (orange) and BrfA (blue) in the BrfA-RF2-ns70S complex, compared with (e) RF2<sub>stop</sub> (lime) in a canonical termination complex <sup>13</sup>. The approximate positions of the decoding center (DC) and peptidyltransferase center (PTC) on the ribosome are indicated. **f**, Superimposition of (d) and (e). **g-h**, Superimposition of the SPF motif of RF2<sub>stop</sub> (lime) and UGA codon of the mRNA (cyan) (PDB ID 4V5E, <sup>13</sup>) with (g) the SPF motif of RF2<sub>BrfA</sub> (orange) and BrfA (blue), and (h) with the SPF motif of RF2<sub>ArfA</sub> (yellow) and ArfA (red) <sup>12</sup>. **i**, Overlay of (g) and (h) with BrfA (blue) and ArfA (red) as cartoon representations.



**Supplementary Fig. 7 | BrfA induces an open conformation of RF2 on the ribosome.**

**a**, Interaction between Trp307 (W307, which is equivalent to *B. subtilis* Trp318 (W318)) of the switch region of *Thermus thermophilus* RF2<sub>stop</sub> (lime) and A1492 of the 16S rRNA (green) during decoding of the UGA stop codon of the mRNA (cyan; PDB ID 4V5E<sup>13</sup>). W318 in the switch loop of RF2 (RF2<sub>BrfA</sub>, orange) observed upon BrfA binding is superimposed and arrowed.

**b**, Same view as in (a), showing the conformation of the switch loop of RF2<sub>BrfA</sub> (orange) and A1492/A1493 (pale yellow) when BrfA (blue) is present. **c**, Same view as in (a) and (b), showing the conformation of A1492/A1493 in comparison to (a) and the switch loop in the presence of ArfA (red, PDB ID 5MVGP<sup>12</sup>). **d**, Open conformation observed for RF2<sub>BrfA</sub> (orange) when in complex with BrfA on the ribosome, compared with (e) the closed conformation of RF2<sub>closed</sub> (dark blue, PDB ID 1GQE<sup>14</sup>) when not bound to the ribosome. **f**, Superimposition of (d) and (e). **g**, Superimposition of the conformation of helix α7 of RF2 from the crystal structure of the closed form of RF2<sub>closed</sub> with RF2<sub>stop</sub> (lime) and RF2<sub>BrfA</sub> (orange), with BrfA (blue) shown for reference. **h-i**, Same view as in (g) showing the conformation of helix α7 of RF2<sub>stop</sub> superimposed with (h) RF2<sub>ArfA</sub>, and ArfA (red) and (i) including RF2<sub>BrfA</sub> (orange) and BrfA (blue).



## Supplementary Fig. 8 | Basis for the species-specificity of BrfA

**a-b**, Potential species-specific interactions between BrfA (blue) and *B. subtilis* RF2 (orange) compared with a homology model for *B. subtilis* RF1 (green) aligned to the BrfA-RF2-ns70S. **a**, The BrfA interface with  $\beta$ 4 and  $\beta$ 5 strands of *B. subtilis* RF2 (orange) consists of hydrophobic residues Val197 and Phe216, which are substituted by Ala and Thr, respectively in *B. subtilis* RF1. **b**, The BrfA interface with the switch loop and helix  $\alpha$ 7 of *B. subtilis* RF2 (orange) consists of multiple residues that are distinct *B. subtilis* RF2 and RF1, for example, G311, K314 and W318 (seen in **(a)**) of RF2 that are substituted with Lys, Val and Arg, respectively, in *B. subtilis* RF1. **c**, Potential sequence differences between *B. subtilis* RF2 (orange) and *E. coli* RF2 (green) that could come within close proximity of BrfA and could explain the species-specific activity of BrfA. **d**, Sequence alignments of RF1 and RF2 for the corresponding regions shown in **(a)-(c)**.

## Supplementary References

- 1 Youngman, P., Perkins, J. B. & Losick, R. A novel method for the rapid cloning in *Escherichia coli* of *Bacillus subtilis* chromosomal DNA adjacent to Tn917 insertions. *Mol Gen Genet* **195**, 424-433, (1984).
- 2 Koo, B. M. *et al.* Construction and Analysis of Two Genome-Scale Deletion Libraries for *Bacillus subtilis*. *Cell Syst* **4**, 291-305 e297, (2017).
- 3 Muto, A. *et al.* Requirement of transfer-messenger RNA for the growth of *Bacillus subtilis* under stresses. *Genes Cells* **5**, 627-635, (2000).
- 4 Chiba, S., Lamsa, A. & Pogliano, K. A ribosome-nascent chain sensor of membrane protein biogenesis in *Bacillus subtilis*. *EMBO J* **28**, 3461-3475, (2009).
- 5 Steinmetz, M. & Richter, R. Plasmids designed to alter the antibiotic resistance expressed by insertion mutations in *Bacillus subtilis*, through in vivo recombination. *Gene* **142**, 79-83, (1994).
- 6 Guerout-Fleury, A. M., Frandsen, N. & Stragier, P. Plasmids for ectopic integration in *Bacillus subtilis*. *Gene* **180**, 57-61, (1996).
- 7 Claessen, D. *et al.* Control of the cell elongation-division cycle by shuttling of PBP1 protein in *Bacillus subtilis*. *Mol Microbiol* **68**, 1029-1046, (2008).
- 8 Peters, J. M. *et al.* A Comprehensive, CRISPR-based Functional Analysis of Essential Genes in Bacteria. *Cell* **165**, 1493-1506, (2016).
- 9 Saito, A. *et al.* Post-liberation cleavage of signal peptides is catalyzed by the site-2 protease (S2P) in bacteria. *Proc Natl Acad Sci U S A* **108**, 13740-13745, (2011).
- 10 Sohmen, D. *et al.* Structure of the *Bacillus subtilis* 70S ribosome reveals the basis for species-specific stalling. *Nat Commun* **6**, 6941, (2015).
- 11 Larkin, M. A. *et al.* Clustal W and Clustal X version 2.0. *Bioinformatics* **23**, 2947-2948, (2007).
- 12 Huter, P. *et al.* Structural basis for ArfA-RF2-mediated translation termination on mRNAs lacking stop codons. *Nature* **541**, 546-549, (2017).
- 13 Weixlbaumer, A. *et al.* Insights into translational termination from the structure of RF2 bound to the ribosome. *Science* **322**, 953-956, (2008).
- 14 Vestergaard, B. *et al.* Bacterial polypeptide release factor RF2 is structurally distinct from eukaryotic eRF1. *Mol Cell* **8**, 1375-1382, (2001).

# Structural basis for ArfA–RF2–mediated translation termination on mRNAs lacking stop codons

Paul Huter<sup>1\*</sup>, Claudia Müller<sup>1\*</sup>, Bertrand Beckert<sup>1,2</sup>, Stefan Arenz<sup>1</sup>, Otto Berninghausen<sup>1</sup>, Roland Beckmann<sup>1</sup> & Daniel N. Wilson<sup>1,2</sup>

**In bacteria, ribosomes stalled on truncated mRNAs that lack a stop codon are rescued by the transfer-messenger RNA (tmRNA), alternative rescue factor A (ArfA) or ArfB systems<sup>1</sup>. Although tmRNA–ribosome and ArfB–ribosome structures have been determined<sup>2–7</sup>, how ArfA recognizes the presence of truncated mRNAs and recruits the canonical termination release factor RF2 to rescue the stalled ribosomes is unclear. Here we present a cryo-electron microscopy reconstruction of the *Escherichia coli* 70S ribosome stalled on a truncated mRNA in the presence of ArfA and RF2. The structure shows that the C terminus of ArfA binds within the mRNA entry channel on the small ribosomal subunit, and explains how ArfA distinguishes between ribosomes that bear truncated or full-length mRNAs. The N terminus of ArfA establishes several interactions with the decoding domain of RF2, and this finding illustrates how ArfA recruits RF2 to the stalled ribosome. Furthermore, ArfA is shown to stabilize a unique conformation of the switch loop of RF2, which mimics the canonical translation termination state by directing the catalytically important GGQ motif within domain 3 of RF2 towards the peptidyl-transferase centre of the ribosome. Thus, our structure reveals not only how ArfA recruits RF2 to the ribosome but also how it promotes an active conformation of RF2 to enable translation termination in the absence of a stop codon.**

Premature transcription termination or truncation of a full-length mRNA can lead to mRNAs lacking a stop codon. Ribosomes translating these truncated mRNAs become trapped at the 3' end of the mRNA because translation elongation or termination cannot occur. In bacteria, these stalled ribosomes are recognized and recycled by the tmRNA rescue system (reviewed in ref. 1). A subset of bacteria, such as *E. coli*, can survive without the tmRNA system owing to the presence ArfA<sup>8</sup>. The synthetic lethality arising from inactivation of both the tmRNA and ArfA rescue systems can be alleviated by overexpression of ArfB<sup>9</sup>. Collectively, these studies illustrate the physiological importance that the rescue of stalled ribosomes has for cell viability. Structural studies have revealed how ribosomes stalled on truncated mRNA are recognized and recycled by the tmRNA–SmpB complex<sup>6,7</sup> or ArfB<sup>5</sup>. In the case of ArfB, the empty mRNA channel of the ribosome is probed by the C-terminal helix, positioning the N-terminal catalytic GGQ-containing domain at the peptidyl-transferase centre (PTC) to trigger peptidyl-tRNA hydrolysis<sup>5</sup>. Similarly, in the tmRNA–SmpB complex, the C-terminal helix of SmpB recognizes the empty mRNA channel and positions the tRNA-like domain of tmRNA at the PTC to enable peptidyltransfer<sup>6,7</sup>. Translation then continues on the mRNA-like domain of tmRNA, which encodes a short peptide targeting the incompletely translated nascent polypeptide chain for degradation<sup>1</sup>. Biochemical studies have demonstrated that ArfA represents a back-up system for tmRNA<sup>10,11</sup>. The *arfA* mRNA contains a stem-loop that acts as a transcription terminator as well as a substrate for RNase III

cleavage<sup>10–12</sup>. In the presence of tmRNA, the short ArfA product produced from the truncated *arfA* mRNA is tagged by tmRNA and targeted for degradation. However, in the absence of tmRNA, the short ArfA product is not degraded and assumes the role of recycling ribosomes stalled on truncated mRNAs<sup>10,11</sup>. The full-length *E. coli* ArfA protein is 72 amino acids long and contains a C-terminal hydrophobic region that leads to aggregation of the protein *in vivo*<sup>10</sup>. Shorter forms of ArfA that result from truncated *arfA* mRNAs and lack the terminal 17–18 amino acids retain full recycling activity<sup>10,11</sup>. ArfA alone is insufficient to recycle ribosomes stalled on truncated mRNAs and requires the assistance of the canonical termination release factor RF2 to hydrolyse the peptidyl-tRNA on the ribosome<sup>13,14</sup> (Fig. 1a–c). A mechanistic understanding of how ArfA recognizes ribosomes stalled on truncated mRNAs, recruits RF2 and stabilizes the active conformation of RF2 has so far been hampered by the lack of an ArfA–RF2–ribosome structure.

To generate a suitable complex for structural analysis, *in vitro* translation reactions were performed with a truncated mRNA in the presence and absence of ArfAΔ17 (lacking residues 56–72) and/or RF2. As reported previously<sup>13,14</sup>, the presence of both ArfA and RF2 was required for efficient recycling of the peptidyl-tRNA (Extended Data Fig. 1). By contrast, replacing wild-type RF2 with the catalytically inactive RF2-GAQ mutant (in which the tripeptide Gly-Gly-Gln is converted to Gly-Ala-Gln) prevented peptidyl-tRNA hydrolysis and recycling (Extended Data Fig. 1), as described previously<sup>13</sup>. Cryo-electron microscopy (cryo-EM) analysis of the ArfAΔ17–RF2–GAQ–stalled ribosomal complex (hereafter referred to as ArfA–RF2–SRC) and *in silico* sorting of this dataset yielded a major subpopulation of ribosomal particles that contained stoichiometric occupancy of P-tRNA, ArfA and RF2 (Extended Data Fig. 2). Subsequent refinement resulted in a final reconstruction of ArfA–RF2–SRC (Fig. 1d) with an average resolution of 3.1 Å (Extended Data Fig. 3 and Extended Data Table 1). The electron density for most of ArfA was well-resolved with local resolution mostly within the range of 3.0 to 3.5 Å (Fig. 1e), enabling a molecular model to be built *de novo* for residues 2–46 of ArfA (Fig. 1f, g). The lack of density for the C-terminal 9 amino acids of ArfA prevented these residues from being included in the final model.

The ArfA-binding site is located on the 30S subunit within the decoding A-site, where it is sandwiched between helices 18 (h18), h34 and h44 of the 16S rRNA and ribosomal protein S12 (Fig. 2a). ArfA establishes two contact sites with the β-hairpin of S12, namely, from the N terminus in which potential hydrogen bonds are possible between Thr38 of S12 and the backbone of Arg3 of ArfA, and between two highly conserved arginines (Arg26 and Arg28) of ArfA and Lys43 and Ser46 of S12 (Fig. 2b and Extended Data Fig. 3f). The large interaction surface that ArfA establishes with the 30S subunit may explain how ArfA can interact with the ribosome in the absence of RF2 (ref. 15). The C terminus of

<sup>1</sup>Gene Center, Department of Biochemistry and Center for integrated Protein Science Munich (CiPSM), Ludwig-Maximilians-Universität München, Feodor-Lynen-Strasse 25, 81377 Munich, Germany. <sup>2</sup>Institute for Biochemistry and Molecular Biology, University of Hamburg, Martin-Luther-King-Pl. 6, 20146 Hamburg, Germany.

\*These authors contributed equally to this work.

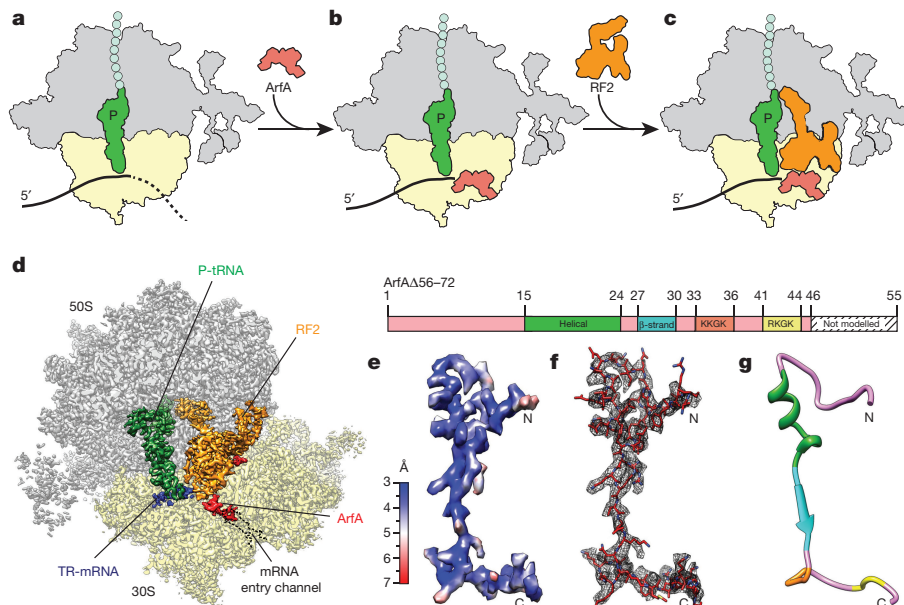


**Figure 1 | Cryo-EM structure of ArfA-RF2-SRC.** **a–c**, Schematic representation of ArfA–RF2-mediated rescue of ribosomes stalled on truncated mRNA (TR-mRNA). **d**, Transverse section of the cryo-EM map of ArfA–RF2–SRC, highlighting the 30S (yellow) and 50S (grey) subunits, P-tRNA (green), TR-mRNA (blue), RF2 (orange) and ArfA

(red). **e**, Electron density for ArfA, coloured according to local resolution. **f**, Electron density (mesh) with molecular model for ArfA (red). **g**, Model for ArfA with features highlighted corresponding to the schematic of the ArfA protein, including helical region (green),  $\beta$ -strand (blue) and KKGK (orange) and RKGK (yellow) motifs.

ArfA extends from the decoding A-site into the mRNA entry channel, where it occupies the space that would be normally house the 3' end of a full-length mRNA (Fig. 2c). The lack of density for the C-terminal residues of ArfA suggests that they are less important for binding, which is consistent with their poor conservation across ArfA from different species<sup>8,12</sup>. By contrast, two positively charged motifs, KKGK (residues 33–36) and RKGK (residues 41–44), are highly conserved and provide multiple interaction opportunities with the surrounding negatively charged rRNA forming the mRNA channel (Fig. 2d). We note that mutation of any single residue in ArfA, including within the K(R)KGK motifs, to cysteine is reported to have little effect on the recycling activity of ArfA<sup>15</sup>, suggesting a redundancy in the importance of the interactions of ArfA with the ribosome. Biochemical studies have demonstrated that the efficiency of ArfA–RF2-mediated ribosome recycling decreases with increasing length of the 3' end of the mRNA extending into the A-site<sup>14–16</sup>. Specifically, recycling occurred,

albeit with reduced efficiency, when the mRNA was extended by up to 3–4 A-site nucleotides, whereas almost no recycling was observed on artificially stalled ribosomes with mRNAs extended by six or more A-site nucleotides<sup>14–16</sup>. Consistently, superimposition of a full-length mRNA and the ArfA binding position suggests that only three nucleotides can be accommodated in the A-site without notable clashes with ArfA (Fig. 2e).

The location of the C terminus of ArfA within the mRNA channel of the 30S subunit observed in the Arf–RF2–SRC structure is also compatible with hydroxyl-radical probing experiments performed in the absence of RF2 (ref. 15; Extended Data Fig. 4), suggesting that ArfA initially uses a similar conformation to monitor the vacant mRNA channel. By contrast, 16S rRNA cleavages indicate that the N terminus of ArfA is flexible and only adopts a defined conformation contacting h18 upon binding of RF2 (ref. 15), as observed in the Arf–RF2–SRC structure (Extended Data Fig. 4). The ArfA–RF2–SRC structure also

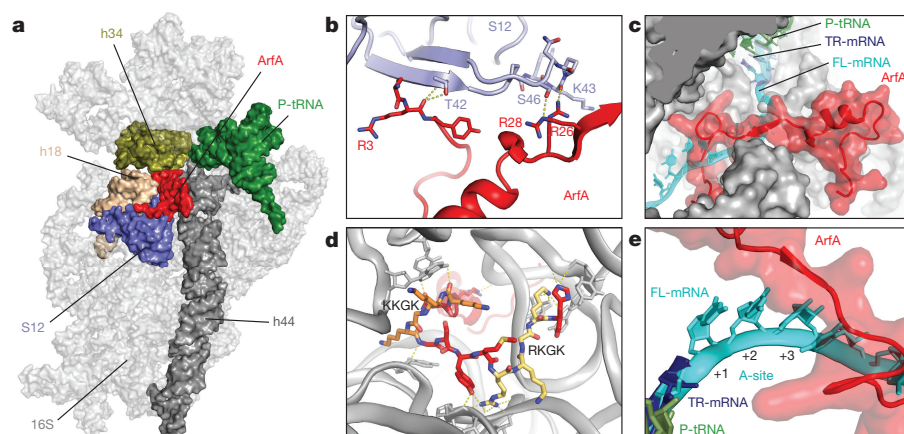


**Figure 2 | Interaction of ArfA with the small subunit.** **a**, Overview of ArfA (red) and 30S (16S rRNA, grey) interaction partners; h18 (tan), h34 (olive), h44 (dark grey), S12 (blue) and P-tRNA (green). **b**, Contacts between ArfA (red) and S12 (blue). **c**, Superimposition of ArfA (red) and truncated mRNA (TR-mRNA, blue), with full-length mRNA (FL-mRNA;

cyan, PDB code 4V6F)<sup>25</sup> within the mRNA entry channel (grey). **d**, Interaction of the KKGK (orange) and RKGK (yellow) motifs of ArfA with surrounding rRNA (grey ribbons). **e**, As in c, but highlighting the relative position of ArfA (red) with the A-site codon of the FL-mRNA (cyan).

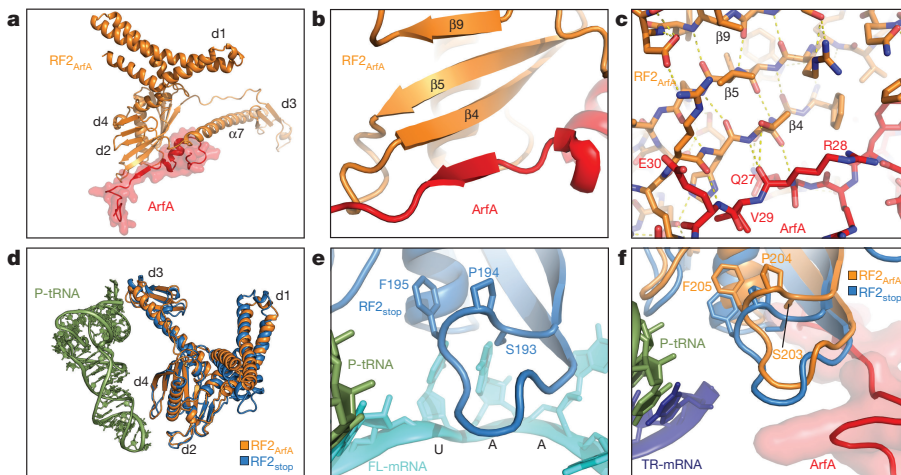


**Figure 3 | Interaction of ArfA with RF2 on the ribosome.** **a**, Overview of the interaction surface of ArfA (red) with RF2 (orange). **b**, **c**, ArfA (red) donates a  $\beta$ -strand to augment the  $\beta$ -sheet of RF2 (orange). In **c**, potential hydrogen bonds are shown with dashed yellow lines. **d**, Superimposition of the relative positions of the RF2 on the ribosome when decoding a stop codon (RF2<sub>stop</sub>; blue, PDB code 4V5E)<sup>18</sup> or interacting

provides insight into how ArfA recruits RF2 despite the absence of a stop codon in the mRNA. ArfA has a large interaction interface with RF2, encompassing the central portion (residues 15–31) of ArfA that contacts the distal end of  $\alpha$ -helix  $\alpha$ 7 of domain 3 as well as the  $\beta$ 4–35 strands of domain 2 of RF2 (Fig. 3a, b and Extended Data Fig. 3g). The nature of the backbone interactions between ArfA and RF2 suggest that residues 27–30 of ArfA donate a small  $\beta$ -strand to the  $\beta$ -sheet of domain 2/4 (Fig. 3b, c). The overall position of RF2 in ArfA-RF2-SRC is similar to that observed during canonical translation termination<sup>17,18</sup> (Fig. 3d), although a slight shift in the position of the decoding domain 2/4 is observed. The shift affects the loop between the  $\beta$ 4– $\beta$ 5 strands of domain 2 bearing the SPF (*E. coli* 205-Ser-Pro-Phe-207) motif, which is involved in the specificity of recognition of the first and second positions of the UGA/UAA stop codons<sup>17,18,19</sup> (Fig. 3e, f). Importantly, the structure illustrates that ArfA does not interact with the SPF motif and therefore does not directly mimic the presence of a stop codon (Fig. 3f).

with ArfA (RF2<sub>ArfA</sub>, orange), with P-tRNA (green) shown for reference. **e**, Interaction of the SPF motif of RF2<sub>stop</sub> with the UAA stop codon of the full-length mRNA (cyan) in the A-site<sup>18</sup>. **f**, Superimposition of RF2<sub>stop</sub> from **e** with ArfA (red) and RF2 (RF2<sub>ArfA</sub>, orange) from the ArfA-RF2-SRC structure.

This observation is consistent with a previous report that demonstrates that mutations in the SPF motif impairing RF2 termination activity do not affect ArfA-RF2-mediated recycling activity<sup>13</sup>. Furthermore, RF1 mutants bearing the SPF instead of PAT motif, conferring termination activity at UGA, are inactive in the ArfA-mediated recycling system<sup>13</sup>. An analysis of the ArfA–RF2 interaction network, together with *E. coli* RF1/RF2 sequence alignments (Extended Data Fig. 5) and models for *E. coli* RF1–ArfA on the ribosome (Extended Data Fig. 6), identified several regions in domain 2 of RF2 (Q133, V198 and G210–F221) and within the switch loop (K307–S321) that could potentially explain the specificity of ArfA for RF2.

During canonical termination, recognition of the stop codon by RF1 and RF2 is proposed to stabilize a rearranged conformation of the switch loop, which directs domain 3 into the PTC<sup>20,21</sup>. The switch loop conformation is stabilized by specific interactions with A1492 and A1493, which, in the case of RF2, involves stacking interactions

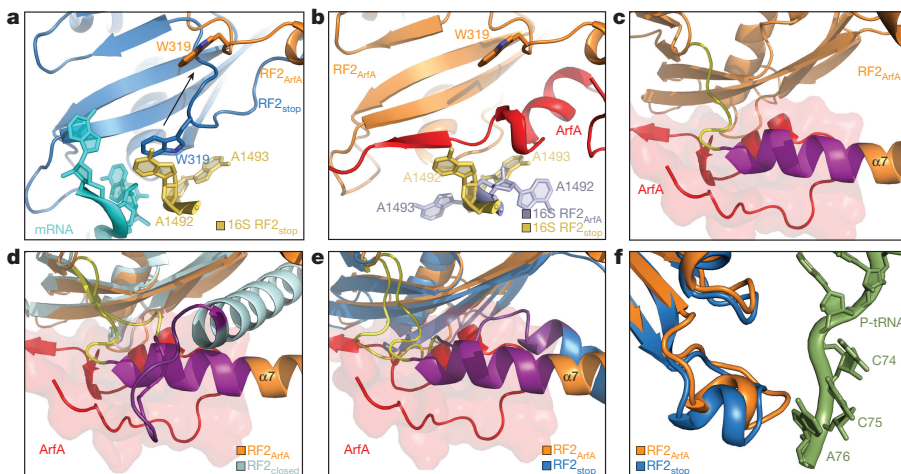


**Figure 4 | ArfA stabilizes a unique conformation of the RF2 switch loop.** **a**, Interaction between W319 (W307 in *Thermus thermophilus* RF2) of the switch region of RF2<sub>stop</sub> and A1492 of the 16S rRNA (yellow) during decoding of the UAA stop codon of the mRNA (cyan; PDB code 4V5E)<sup>18</sup>. The switch loop conformation of RF2 (RF2<sub>ArfA</sub>, orange) observed upon ArfA binding is superimposed and arrowed. **b**, Same view as in **a**, showing the distinct conformation of the switch loop of *E. coli* RF2 (orange) and A1492/A1493 (pale blue) when ArfA (red) is present. **c**, ArfA

(red) induces conformational changes within the switch loop (yellow) of RF2 (orange), leading to an extension (purple) of  $\alpha$ -helix  $\alpha$ 7 of the RF2 domain 3 by 2–3 helical turns. **d**, **e**, Superimposition of **c** with the switch loop and  $\alpha$ -helix  $\alpha$ 7 conformation in the crystal structure of the closed form of RF2 (RF2<sub>closed</sub>; cyan, PDB code 1GQE)<sup>22</sup> (**d**) and during canonical termination<sup>18</sup> (**e**). **f**, Superimposition of domain 3 of RF2<sub>stop</sub> (blue)<sup>18</sup> and RF2<sub>ArfA</sub> (orange), with P-tRNA (green) shown for reference.

of W319 (*E. coli* numbering) of RF2 with A1492 of the 16S rRNA<sup>17,18</sup> (Fig. 4a). In the ArfA-RF2-SRC structure, the conformation of A1492 and A1493 are distinct from those observed during canonical translation termination, and the presence of ArfA precludes the interaction between the switch loop and A1492 (Fig. 4a, b). Instead, ArfA itself appears to stabilize a distinct conformation of the switch loop in RF2 that extends the  $\alpha$ -helix  $\alpha$ 7 of domain 3 of RF2 by three helical turns when compared to the crystal structure of the free (closed) form of RF2 (ref. 22) (Fig. 4c, d, Supplementary Video 1). The extension of helix  $\alpha$ 7 is analogous to that observed during canonical translation termination with RF2 (refs 17, 18) (Fig. 4e, Supplementary Video 2). As observed for canonical termination<sup>17,18</sup>, the open conformation of RF2 on the ribosome in the presence of ArfA also directs the GGQ motif of domain 3 into the PTC (Fig. 4f), although the density for the GAQ motif is poorly resolved, possibly owing to the inactivity of the mutation. The A18T mutation that led to the discovery of ArfA does not interfere with ribosome binding<sup>8</sup> or RF2 recruitment, but prevents peptidyl-tRNA hydrolysis<sup>14</sup>. This can be rationalized on the basis of the ArfA-RF2-SRC structure since the A18T mutation is not located at the ArfA–ribosome or ArfA–RF2 interfaces, but would rather perturb the conformation of the N terminus of ArfA and thereby interfere indirectly with the correct placement of domain 3 of RF2 at the PTC (Extended Data Fig. 7).

In conclusion, our findings indicate that ArfA not only provides an interface to recruit RF2 to the ribosome in the absence of a stop codon, but also, by interacting with the switch loop of RF2, induces conformational changes that lead to the accurate placement of domain 3 at the PTC. Structurally, the bacterial recycling systems are similar in that they use tmRNA–SmpB<sup>6,7</sup>, ArfB<sup>5</sup> or ArfA (Extended Data Fig. 8) to monitor the mRNA channel and release the nascent polypeptide before ribosome splitting. This contrasts with the eukaryotic recycling of ribosomes stalled on truncated mRNAs, in which ribosome splitting by Dom34–Hbs1 and ABCE1 occurs before nascent polypeptide chain release<sup>23,24</sup>.

**Online Content** Methods, along with any additional Extended Data display items and Source Data, are available in the online version of the paper; references unique to these sections appear only in the online paper.

Received 26 September; accepted 25 November 2016.

Published online 1 December 2016.

- Keiler, K. C. Mechanisms of ribosome rescue in bacteria. *Nat. Rev. Microbiol.* **13**, 285–297 (2015).
- Valle, M. *et al.* Visualizing tmRNA entry into a stalled ribosome. *Science* **300**, 127–130 (2003).
- Fu, J. *et al.* Visualizing the transfer-messenger RNA as the ribosome resumes translation. *EMBO J.* **29**, 3819–3825 (2010).
- Weis, F. *et al.* tmRNA–SmpB: a journey to the centre of the bacterial ribosome. *EMBO J.* **29**, 3810–3818 (2010).
- Gagnon, M. G., Seetharaman, S. V., Bulkley, D. & Steitz, T. A. Structural basis for the rescue of stalled ribosomes: structure of YaeJ bound to the ribosome. *Science* **335**, 1370–1372 (2012).
- Neubauer, C., Gillet, R., Kelley, A. C. & Ramakrishnan, V. Decoding in the absence of a codon by tmRNA and SmpB in the ribosome. *Science* **335**, 1366–1369 (2012).
- Ramrath, D. J. *et al.* The complex of tmRNA–SmpB and EF-G on translocating ribosomes. *Nature* **485**, 526–529 (2012).
- Chadani, Y. *et al.* Ribosome rescue by *Escherichia coli* ArfA (YhdL) in the absence of *trans*-translation system. *Mol. Microbiol.* **78**, 796–808 (2010).

- Chadani, Y., Ono, K., Kutsukake, K. & Abo, T. *Escherichia coli* YaeJ protein mediates a novel ribosome-rescue pathway distinct from SsrA- and ArfA-mediated pathways. *Mol. Microbiol.* **80**, 772–785 (2011).
- Chadani, Y. *et al.* *trans*-translation-mediated tight regulation of the expression of the alternative ribosome-rescue factor ArfA in *Escherichia coli*. *Genes Genet. Syst.* **86**, 151–163 (2011).
- Garza-Sánchez, F., Schaub, R. E., Janssen, B. D. & Hayes, C. S. tmRNA regulates synthesis of the ArfA ribosome rescue factor. *Mol. Microbiol.* **80**, 1204–1219 (2011).
- Schaub, R. E., Poole, S. J., Garza-Sánchez, F., Benbow, S. & Hayes, C. S. Proteobacterial ArfA peptides are synthesized from non-stop messenger RNAs. *J. Biol. Chem.* **287**, 29765–29775 (2012).
- Chadani, Y., Ito, K., Kutsukake, K. & Abo, T. ArfA recruits release factor 2 to rescue stalled ribosomes by peptidyl-tRNA hydrolysis in *Escherichia coli*. *Mol. Microbiol.* **86**, 37–50 (2012).
- Shimizu, Y. ArfA recruits RF2 into stalled ribosomes. *J. Mol. Biol.* **423**, 624–631 (2012).
- Kurita, D., Chadani, Y., Muto, A., Abo, T. & Himeno, H. ArfA recognizes the lack of mRNA in the mRNA channel after RF2 binding for ribosome rescue. *Nucleic Acids Res.* **42**, 13339–13352 (2014).
- Zeng, F. & Jin, H. Peptide release promoted by methylated RF2 and ArfA in nonstop translation is achieved by an induced-fit mechanism. *RNA* **22**, 49–60 (2016).
- Korostelev, A. *et al.* Crystal structure of a translation termination complex formed with release factor RF2. *Proc. Natl. Acad. Sci. USA* **105**, 19684–19689 (2008).
- Weixlbaumer, A. *et al.* Insights into translational termination from the structure of RF2 bound to the ribosome. *Science* **322**, 953–956 (2008).
- Ito, K., Uno, M. & Nakamura, Y. A tripeptide ‘anticodon’ deciphers stop codons in messenger RNA. *Nature* **403**, 680–684 (2000).
- Youngman, E. M., McDonald, M. E. & Green, R. Peptide release on the ribosome: mechanism and implications for translational control. *Annu. Rev. Microbiol.* **62**, 353–373 (2008).
- Zhou, J., Korostelev, A., Lancaster, L. & Noller, H. F. Crystal structures of 70S ribosomes bound to release factors RF1, RF2 and RF3. *Curr. Opin. Struct. Biol.* **22**, 733–742 (2012).
- Vestergaard, B. *et al.* Bacterial polypeptide release factor RF2 is structurally distinct from eukaryotic eRF1. *Mol. Cell* **8**, 1375–1382 (2001).
- Franckenberg, S., Becker, T. & Beckmann, R. Structural view on recycling of archaeal and eukaryotic ribosomes after canonical termination and ribosome rescue. *Curr. Opin. Struct. Biol.* **22**, 786–796 (2012).
- Simms, C. L., Thomas, E. N. & Zaher, H. S. Ribosome-based quality control of mRNA and nascent peptides. *Wiley Interdiscip. Rev. RNA* <http://dx.doi.org/10.1002/wrna.1366> (2016).
- Jenner, L. B., Demeshkina, N., Yusupova, G. & Yusupov, M. Structural aspects of messenger RNA reading frame maintenance by the ribosome. *Nat. Struct. Mol. Biol.* **17**, 555–550 (2010).

**Supplementary Information** is available in the online version of the paper.

**Acknowledgements** We thank H. Sieber, S. Rieder and C. Ungewickell for technical assistance and L. Bischoff and R. Green for providing expression plasmids for *E. coli* ArfA $\Delta$ 17 and RF2, respectively. This research was supported by grants from the Deutsche Forschungsgemeinschaft WI3285/4-1, SPP-1879 (to D.N.W.), GRK 1721 and FOR1805 (to R.B. and D.N.W.).

**Author Contributions** D.N.W. designed the study. C.M. and P.H. prepared the cryo-EM sample. P.H., C.M. and B.B. processed the cryo-EM data. P.H., S.A. and D.N.W. built and refined the molecular models. O.B. collected the cryo-EM data. P.H., C.M., R.B. and D.N.W. interpreted the results and D.N.W. wrote the paper.

**Author Information** Reprints and permissions information is available at [www.nature.com/reprints](http://www.nature.com/reprints). The authors declare no competing financial interests. Readers are welcome to comment on the online version of the paper. Correspondence and requests for materials should be addressed to D.N.W. (daniel.wilson@chemie.uni-hamburg.de).

**Reviewer Information** *Nature* thanks T. Abo, Y. Hashem, K. Keiler and the other anonymous reviewer(s) for their contribution to the peer review of this work.

## METHODS

No statistical methods were used to predetermine sample size. The experiments were not randomized and investigators were not blinded to allocation during experiments and outcome assessment.

**Protein expression and purification.** *Escherichia coli* RF2 was expressed from a pET11a vector incorporating a C-terminal hexa-histidine tag (His<sub>6</sub>) for purification and detection purposes. An inactive RF2-GAQ mutant was generated by site-directed mutagenesis. *E. coli* ArfA without 17 C-terminal amino acids (ArfAΔ17) was cloned into pBAD vector with a N-terminal His<sub>6</sub> and 3C protease cleavage site. The wild-type RF2, RF2-GAQ and ArfAΔ17 proteins were over-expressed in *E. coli* BL21 (DE3) at 37 °C for 1.5 h after induction with 1 mM IPTG or 0.2% arabinose as required. Cells were collected and the pellet was re-suspended in lysis buffer (50 mM NaH<sub>2</sub>PO<sub>4</sub>·2H<sub>2</sub>O, 300 mM NaCl, 5 mM imidazole, pH 7.5). Lysis was performed using a microfluidizer (Microfluidics M-110L) by passing cells three times at 18,000 p.s.i. The cell debris was removed upon centrifugation and the proteins were purified from the supernatant by His-tag affinity chromatography using Ni-NTA agarose beads (Clontech). The bound proteins were washed with lysis buffer containing 10 mM imidazole and then eluted with lysis buffer containing 250 mM imidazole. The proteins were purified by size-exclusion chromatography using HiLoad 16/600 Superdex 75 (GE Life Sciences) in gel filtration buffer (50 mM HEPES, pH 7.4, 50 mM KCl, 100 mM NaCl, 2% glycerol, 5 mM β-mercaptoethanol). The proteins were concentrated using Amicon Ultra-4 Centrifugal Filter Units (Merck Millipore), Ultracel-3 for ArfAΔ17 and Ultracel-30 for wild-type RF2 and RF2-GAQ.

**Template preparation for in vitro translation.** Truncated *nlpD* template containing an N-terminal His<sub>6</sub> and a HA tag was amplified from pET21b-<sub>R1</sub>*nlpD*<sup>26</sup> using primers binding to pET21b upstream of the T7-promotor (GATCGAGA TCTCGATCCCGCG) and to nucleotides 133–159 of *nlpD* (ATCAACATACAGAATTAGTATTGTC). PCR products were purified via spin columns (Qiagen).

**ArfA peptidyl-tRNA recycling assays.** The recycling activity of the purified ArfAΔ17 and RF2 (wild-type and GAQ mutant) was monitored by independent triplicate experiments using PURExpress ΔRF123 *In Vitro* Protein Synthesis Kit (NEB E6850S) (Extended Data Fig. 1). Reactions of 6 μl were performed according to the manual protocol by mixing 250 ng of truncated *nlpD* PCR template, 5 μM of anti-ssrA oligo, 2 μM of ArfAΔ17 and/or wild-type RF2 or RF2-GAQ. The reactions were incubated at 37 °C for 15 min with shaking at 1,000 r.p.m. The translation reactions were stopped by adding 6 μl of tricine sample buffer (200 mM Tris-HCl pH 6.8, 40% glycerol, 2% SDS, 0.04% Coomassie Blue G-250) and then applied to 16.5% tricine-SDS-PAGE gels. The products were detected by western blotting using anti-haemagglutinin-peroxidase (Roche 11667475001) at 1:1,000 in 2.5% milk/TBS (2.5% (w/v) skim milk powder, 20 mM Tris, pH 7.5, 150 mM NaCl).

**Generation of ArfA-RF2-SRC.** *In vitro* translation was carried out using PURExpress *In Vitro* Protein Synthesis Kit (NEB 6800). The translation reaction (750 μl in total) was prepared according to the protocol of the PURExpress *In Vitro* Protein Synthesis Kit supplemented with 5 μM anti-ssrA oligo. Translation was started by adding the truncated *nlpD* PCR product at 37 °C for 20 min, shaking at 1,000 r.p.m. The ribosomes were first isolated from the *in vitro* reaction mix by centrifugation through a sucrose cushion (50 mM HEPES KOH pH 7.2, 250 mM potassium acetate, 25 mM magnesium acetate, 750 mM sucrose, 0.1% DDM) for 180 min at 72,000g using a TLA120.2 rotor (Beckman Coulter). The pellet was resuspended in buffer B250 (50 mM HEPES KOH pH 7.2, 250 mM potassium acetate, 25 mM magnesium acetate, 0.1% DDM) and the stalled ribosomal complexes (SRC) were isolated using Talon matrix by the N-terminal His<sub>6</sub> tag of NlpD were washed with buffer B500 (50 mM HEPES KOH pH 7.2, 500 mM potassium acetate, 25 mM magnesium acetate, 0.1% DDM) and eluted using buffer B250i (50 mM HEPES KOH pH 7.2, 250 mM potassium acetate, 25 mM magnesium acetate, 250 mM imidazole, 0.1% DDM). The eluted SRC was loaded onto a linear sucrose gradient (10–40% (w/v) sucrose in B250 buffer) for 18 h at 43,000g in a SW28 rotor (Beckman Coulter). The isolated 70S peak was pelleted by centrifugation for 3 h at 139,000g using a Ti70.1 rotor (Beckman Coulter). The pellet was re-suspended in SRC buffer (50 mM HEPES pH 7.2, 250 mM potassium acetate, 10 mM magnesium acetate, 0.05% DDM). The purified SRC was then incubated together with a 2.5× excess of ArfAΔ17 and RF2-GAQ mutant for 5 min at 37 °C before being applied to EM grids.

**Cryo-electron microscopy and single particle reconstruction.** Five microlitres (4.5 OD) of *E. coli* ArfA-RF2-SRC at OD<sub>260 nm</sub> was applied to 2 nm pre-coated Quantifoil R3/3 holey carbon supported grids and vitrified using the Vitrobot Mark IV (FEI, Holland). Data collection was performed using EM-TOOLS (TVIPS GmbH) on a Titan Krios transmission electron microscope equipped with a Falcon II direct electron detector (FEI, Holland) at 302 kV at a pixel size of 1.084 Å and a

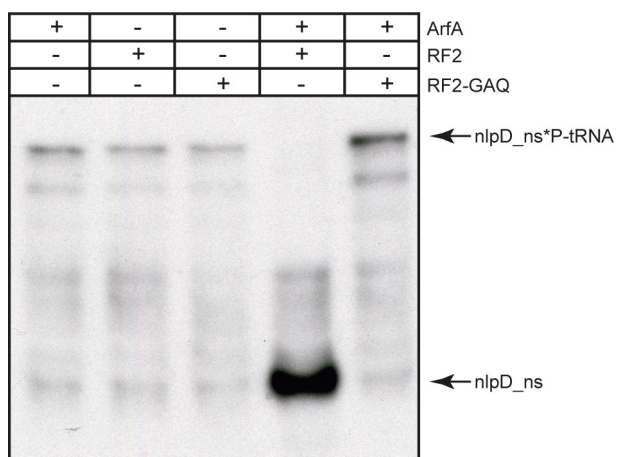
defocus range of 0.7–2.2 μm. Ten frames (dose per frame of 2.5 e<sup>−</sup> Å<sup>−2</sup>) were aligned using Motion Correction Software<sup>27</sup>. Power-spectra, defocus values and astigmatism were determined with CTFIND4 software<sup>28</sup>. Micrographs showing Thon rings beyond 3.5 Å were manually inspected for good areas and power-spectra quality. Automatic particle picking was performed using SIGNATURE<sup>29</sup> and single particles were processed using RELION 1.4 (ref. 30). 227,608 particles were first subjected to 3D refinement using *E. coli* 70S ribosome as reference structure<sup>31</sup> and movie particle extraction was performed as described before<sup>30</sup> (Extended Data Fig. 2). The 227,608 polished particles were finally subjected to 3D classification and refinement using FREALIGN resulting in a final reconstruction of 3.11 Å (0.143 FSC) average resolution containing 69,089 particles (Extended Data Figs 2 and 3). Local resolution was finally calculated using ResMap<sup>32</sup>.

**Molecular modelling and refinement of the ArfA-RF2-SRC.** The molecular model for the ribosomal proteins and rRNA of the 70S ribosome of the ArfA-RF2-SRC was based on the molecular model from the recent cryo-EM reconstruction of the *E. coli* 70S ribosome (PDB code 5AFI)<sup>33</sup>. The molecular model was initially fitted as a rigid body into the cryo-EM density map of the corresponding stalled complex using UCSF Chimera<sup>34</sup>. Owing to flexibility and poor density, the L1, L10, L11 protein and the L7/L12 stalk were not included in the final model. For *E. coli* RF2, a homology model was generated using HHpred<sup>35</sup> based on a template from *T. thermophilus* RF2 (PDB code 4V5E)<sup>18</sup>. Owing to flexibility and poor density, the GAQ motif, domain I, and the linker between domains 3 and 4 of RF2 were based on PDB code 2WH1. Residues 2–46 of ArfAΔ17 were built *de novo* using an HHpred model as an initial starting point in terms of placement of the central helical region. The complete atomic model of the ArfA-RF2-SRC was manually adjusted using Coot<sup>36</sup> and refined using phenix.real\_space\_refine<sup>37</sup>, with restraints obtained by phenix.secondary\_structure\_restraints<sup>37</sup>. The model and refinement statistics are presented in Extended Data Table 1. To reduce the clash score the model was refined using REFMAC<sup>38</sup>. The statistics of the refined model were calculated using MolProbity<sup>39</sup> and the validation of the model was performed as previously described<sup>40</sup>.

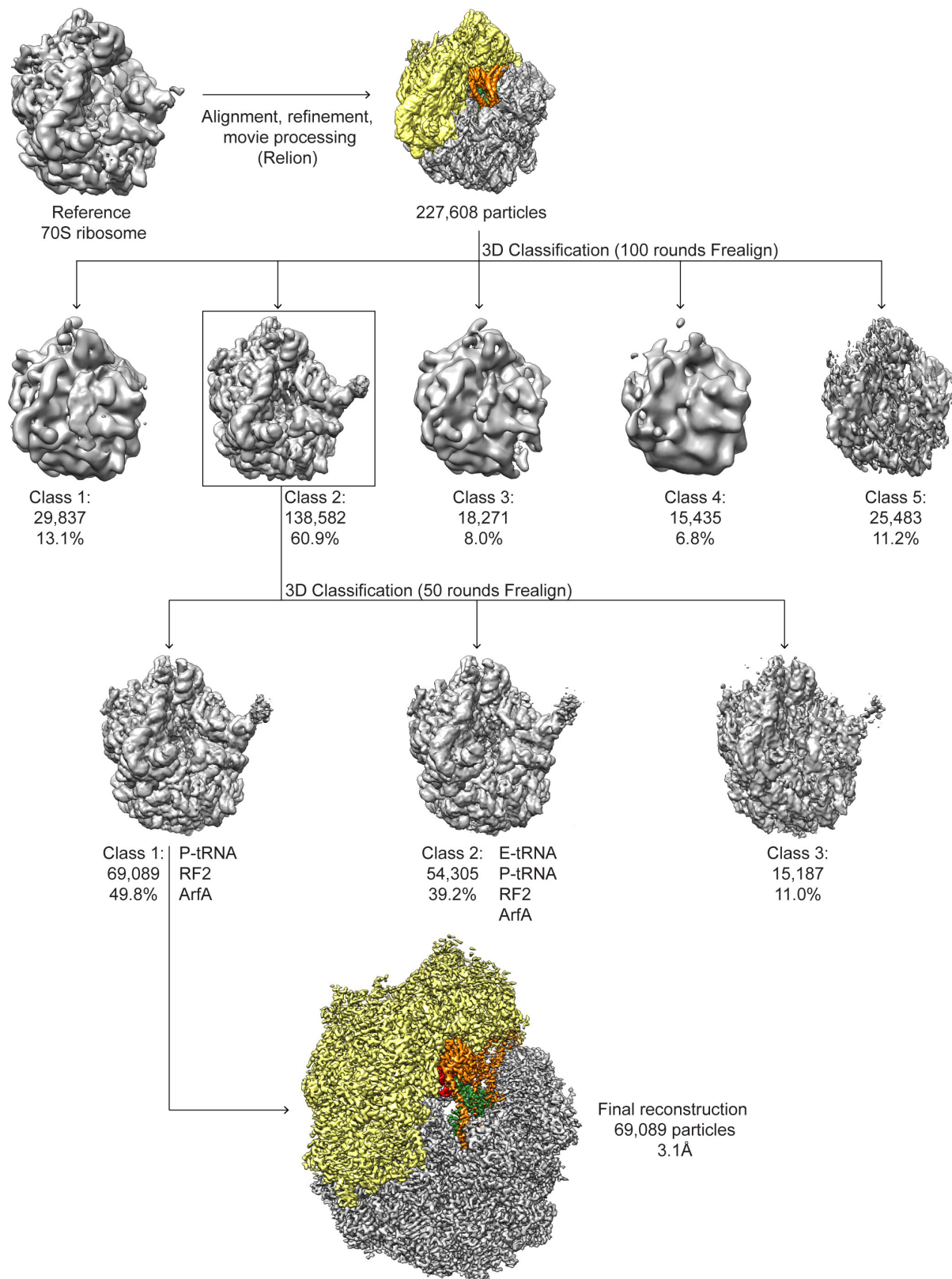
**Figure preparation.** Figures showing electron densities and atomic models were generated using either UCSF Chimera<sup>34</sup> or PyMol Molecular Graphic Systems (version 1.8 Schrödinger).

**Data availability.** The cryo-electron microscopy map for the ArfA-RF2-SRC has been deposited in the Electron Microscopy Data Bank (EMDB) with the accession code EMD-3508. The respective coordinates for electron-microscopy-based model of the ArfA-RF2-SRC are deposited in the Protein Data Bank (PDB) under the accession code 5MGP. All other data are available from the corresponding author upon reasonable request.

26. Starosta, A. L. *et al.* Translational stalling at proline stretches is modulated by the sequence context upstream of the stall site. *Nucleic Acids Res.* **42**, 10711–10719 (2014).
27. Li, X. *et al.* Electron counting and beam-induced motion correction enable near-atomic-resolution single-particle cryo-EM. *Nat. Methods* **10**, 584–590 (2013).
28. Rohou, A. & Grigorieff, N. CTFFIND4: Fast and accurate defocus estimation from electron micrographs. *J. Struct. Biol.* **192**, 216–221 (2015).
29. Chen, J. Z. & Grigorieff, N. SIGNATURE: a single-particle selection system for molecular electron microscopy. *J. Struct. Biol.* **157**, 168–173 (2007).
30. Scheres, S. H. RELION: implementation of a Bayesian approach to cryo-EM structure determination. *J. Struct. Biol.* **180**, 519–530 (2012).
31. Arenz, S. *et al.* The stringent factor RelA adopts an open conformation on the ribosome to stimulate ppGpp synthesis. *Nucleic Acids Res.* **44**, 6471–6481 (2016).
32. Kucukelbir, A., Sigworth, F. J. & Tagare, H. D. Quantifying the local resolution of cryo-EM density maps. *Nat. Methods* **11**, 63–65 (2014).
33. Fischer, N. *et al.* Structure of the *E. coli* ribosome-EF-Tu complex at <3 Å resolution by Cs-corrected cryo-EM. *Nature* **520**, 567–570 (2015).
34. Pettersen, E. F. *et al.* UCSF Chimera—a visualization system for exploratory research and analysis. *J. Comput. Chem.* **25**, 1605–1612 (2004).
35. Söding, J., Biegert, A. & Lupas, A. N. The HHpred interactive server for protein homology detection and structure prediction. *Nucleic Acids Res.* **33**, W244–W248 (2005).
36. Emsley, P. & Cowtan, K. Coot: model-building tools for molecular graphics. *Acta Crystallogr. D* **60**, 2126–2132 (2004).
37. Adams, P. D. *et al.* PHENIX: a comprehensive Python-based system for macromolecular structure solution. *Acta Crystallogr. D* **66**, 213–221 (2010).
38. Vagin, A. A. *et al.* REFMAC5 dictionary: organization of prior chemical knowledge and guidelines for its use. *Acta Crystallogr. D* **60**, 2184–2195 (2004).
39. Chen, V. B. *et al.* MolProbity: all-atom structure validation for macromolecular crystallography. *Acta Crystallogr. D* **66**, 12–21 (2010).
40. Brown, A. *et al.* Tools for macromolecular model building and refinement into electron cryo-microscopy reconstructions. *Acta Crystallogr. D* **71**, 136–153 (2015).

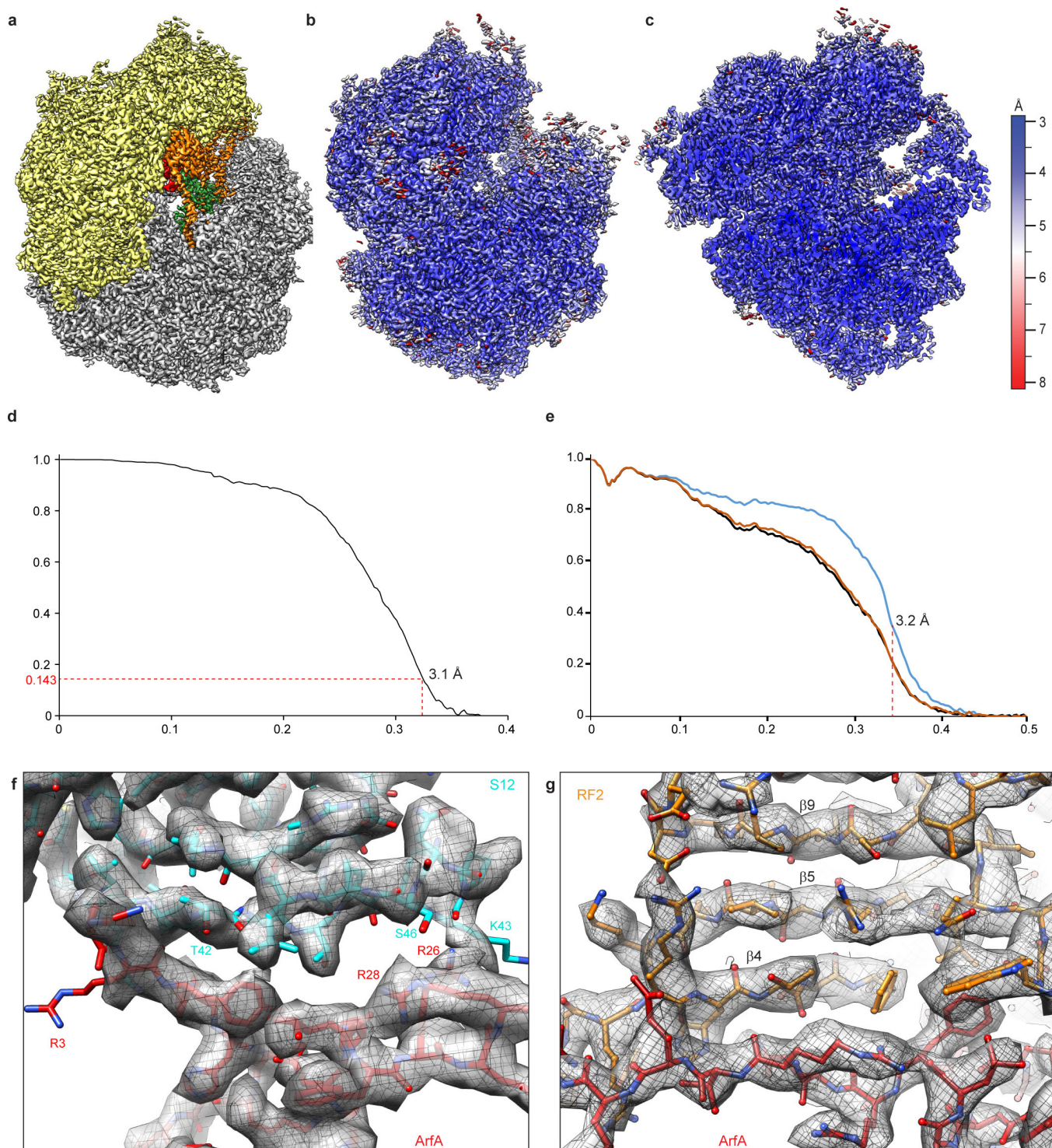


**Extended Data Figure 1 | Recycling of ribosomes stalled on truncated mRNA by ArfA and RF2.** *In vitro* translation assay of the truncated *nlpD* template was performed in the presence of ArfA, RF2 or RF2-GAQ, revealing a peptidyl-tRNA band (nlpD\_ns\*P-tRNA), whereas the peptidyl-tRNA was absent and free *nlpD* peptide (nlpD\_ns) was observed when the reaction was performed with ArfA and RF2. Replacing wild-type RF2 with the inactive RF2-GAQ mutant led to the reappearance of the peptidyl-tRNA band and loss of the free *nlpD* peptide.



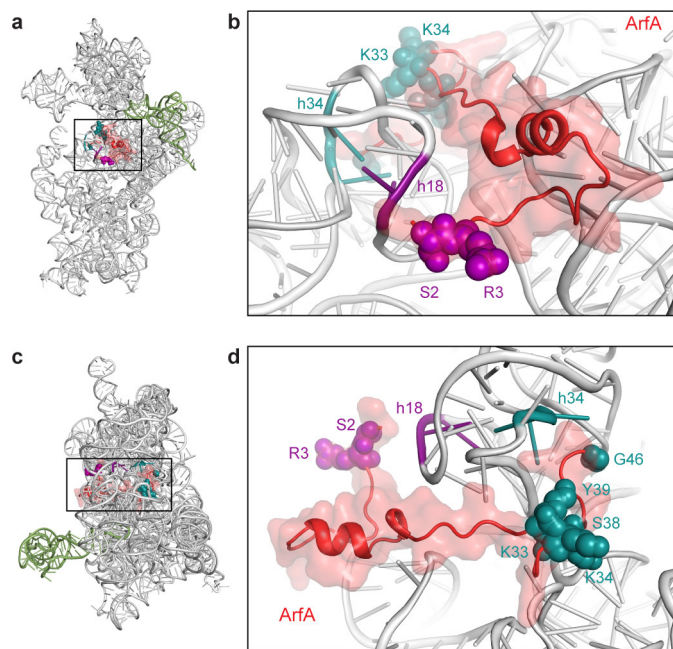
**Extended Data Figure 2 | Classification of the ArfA-RF2-SRC.** The complete dataset of 227,608 particles was initially aligned against a vacant *E. coli* 70S ribosome, refined with RELION using 3D auto-refine and the movie particles were extracted. The polished particles were then subjected to a 3D refinement and 3D classification using FREALIGN. The class 2 (138,582 particles) resulting from the 100 rounds of 3D classification

with 3× binned images using a ribosomal mask was then further refined and classified with 2× binned images. The remaining 69,089 particles containing ArfA-RF2-SRC were then 3D-refined, resulting in a final reconstruction of 3.1 Å (0.143 Fourier shell correlation (FSC) average resolution).

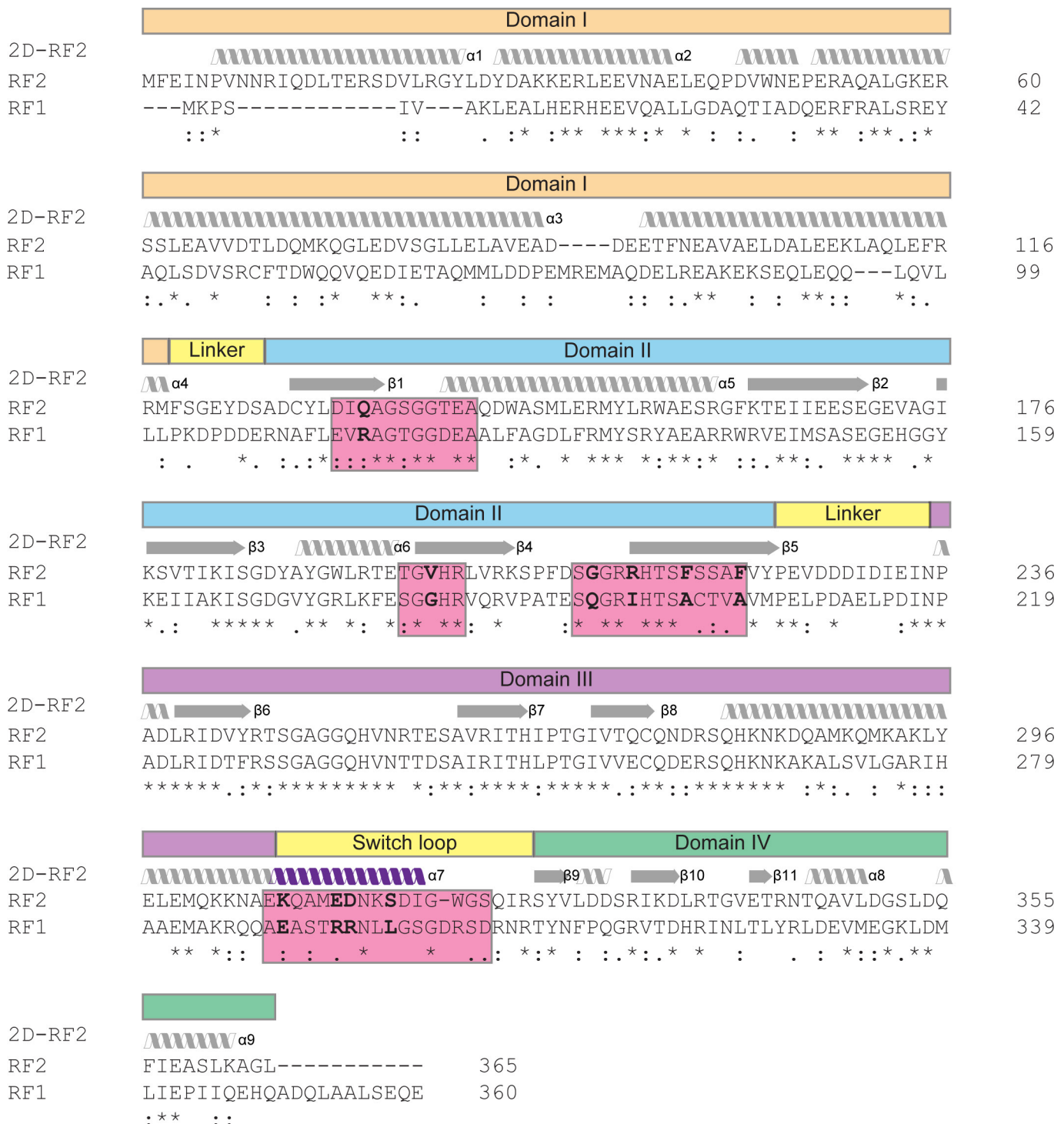


**Extended Data Figure 3 | Resolution of the ArfA-RF2-SRC.** **a**, Overview of the final refined cryo-EM map of the ArfA-RF2-SRC with separated densities for small (yellow) and large (grey) ribosomal subunit, as well as ArfA (red), RF2 (orange) and P-tRNA (green). **b**, Same view as in **a** but coloured according to local resolution. **c**, Transverse section of **b** showing local resolution in the core of the ribosomal subunits. **d**, FSC curve of the refined final map, indicating that the average resolution of the ArfA-RF2-SRC is 3.1 Å (at 0.143). **e**, Fit of models to maps. FSC curves calculated between

the refined model and the final map (blue), with the self- and cross-validated correlations in orange and black, respectively. Information beyond 3.2 Å was not used during refinement and preserved for validation. **f, g**, Selected examples illustrating the quality of fit of the molecular models to the unsegmented cryo-EM map (grey mesh) for the ArfA (red) interaction with S12 (blue), related to Fig. 2b (f), and with RF2 (orange), related to Fig. 3c (g).

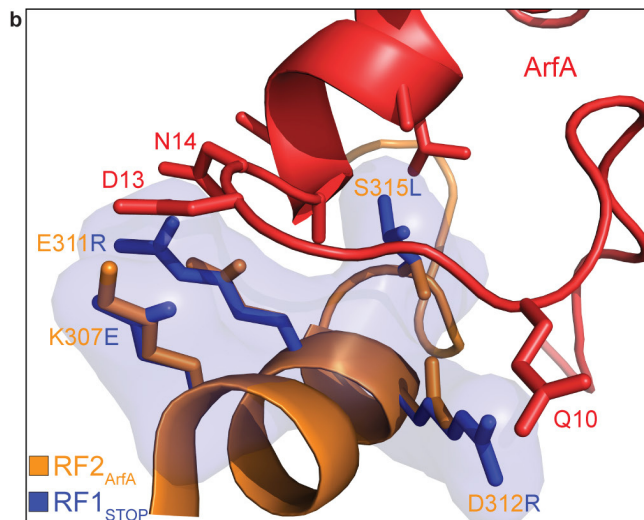
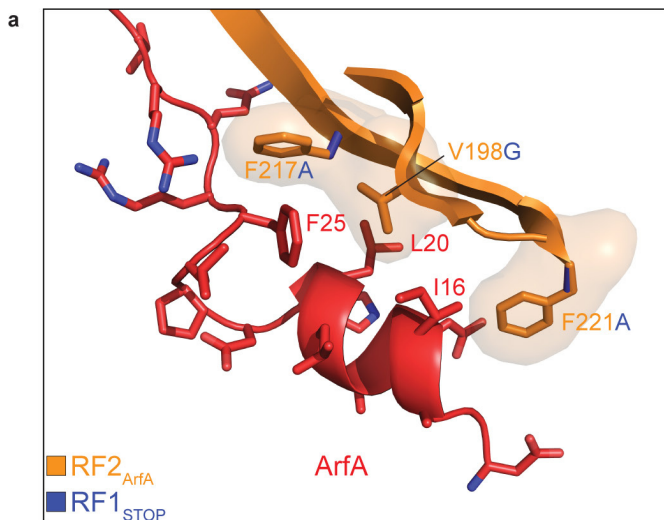


**Extended Data Figure 4 | Hydroxyl radical probing of ArfA on the ribosome.** a–d, Hydroxyl-radical probing data<sup>15</sup> of ArfA in complex with RF2 on the ribosome reveal that tethers linked to the N-terminal region of ArfA, for example, residues S2 and R3 (magenta), cleave the 16S rRNA within the vicinity of helices h18, whereas tethers linked to the C-terminal region of ArfA, such as residues 33–34/38–39 and 46 (teal), cleave the 16S rRNA within the vicinity of helices h34 (ref. 15). These findings are in excellent agreement with the position of ArfA (red) within the ArfA–RF2–SRC structure reported here. In the overview panels a and c, P-tRNA (green) is shown for reference.



**Extended Data Figure 5 | Sequence alignment of *E. coli* RF1 and RF2 with secondary structure assignments.** Sequence alignment of *E. coli* RF1 and RF2 generated using ClustalX with secondary structure (helices and strands) and domain (I–IV) assignments based on the crystal structures of *E. coli* RF2 (ref. 22), except for the switch loop (yellow) and extension to helix  $\alpha$ 7 (purple), which was based on the ArfA-RF2-SRC structure.

The pink boxes indicate regions of RF2 that form an interface with ArfA, with residues in bold predicted to prevent interaction of RF1 with ArfA. Asterisk (\*) or colon (:) and full stop (.) indicate a single, fully conserved residue or residues with strong (>0.5 in the Gonnet PAM 250 matrix) and weakly (>0.5) similar properties, respectively.



**c**

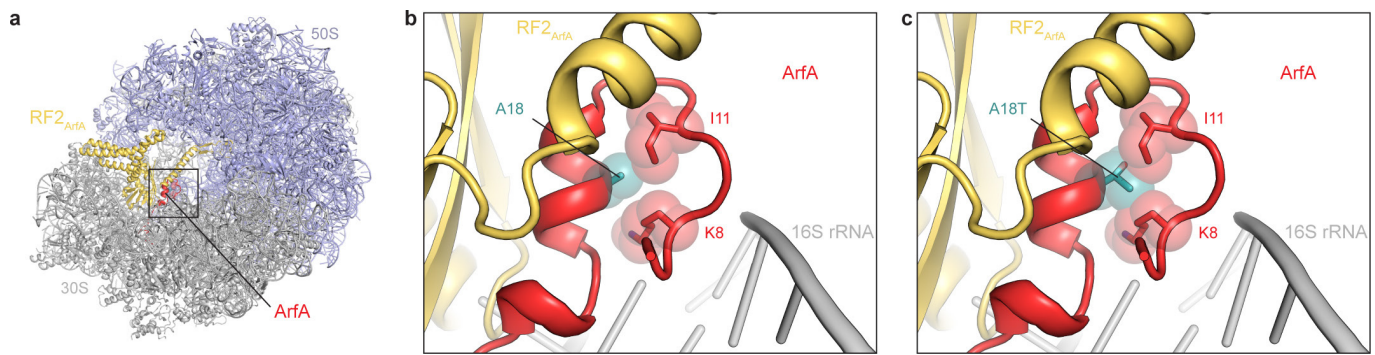
	RF2	RF1
<b>E. coli</b>	TETG <span style="background-color: pink;">V</span> HLVRKSPFD <span style="background-color: pink;">S</span> GGRRHTSFSSA <span style="background-color: pink;">F</span> VY 223	
<b>S. flexneri</b>	TETG <span style="background-color: pink;">V</span> HLVRKSPFD <span style="background-color: pink;">S</span> GGRRHTSFSSA <span style="background-color: pink;">F</span> VY 223	
<b>P. mirabilis</b>	TETG <span style="background-color: pink;">V</span> HLVRKSPFD <span style="background-color: pink;">S</span> GGRRHTSFSSA <span style="background-color: pink;">F</span> VY 223	
<b>H. influenzae</b>	TETG <span style="background-color: pink;">I</span> HLVRKSPFD <span style="background-color: pink;">S</span> NNRRHTSFSAAE <span style="background-color: pink;">F</span> VY 223	
<b>P. multocida</b>	TETG <span style="background-color: pink;">I</span> HLVRKSPFD <span style="background-color: pink;">S</span> NNRRHTSFSAAE <span style="background-color: pink;">F</span> VY 223	
<b>V. fischeri</b>	TETG <span style="background-color: pink;">V</span> HLVRKSPFD <span style="background-color: pink;">S</span> GRRRHTSFASAFIY 223	
<b>C. crescentus</b>	TEAGVHLVRV <span style="background-color: pink;">R</span> ISPFDS <span style="background-color: pink;">S</span> ARRHTSFASAFVY 218	
<b>N. gonorrhoeae</b>	TETGVHLVRV <span style="background-color: pink;">R</span> ISPFDS <span style="background-color: pink;">S</span> ARRHTSFASAFVY 223	
<b>H. pylori</b>	NENGVHLVRV <span style="background-color: pink;">R</span> ISPFDS <span style="background-color: pink;">S</span> ARRHTSFASAFVY 225	
<b>S. pneumoniae</b>	SEMGVHLVRV <span style="background-color: pink;">R</span> ISPFDS <span style="background-color: pink;">S</span> ARRHTSFITS <span style="background-color: pink;">V</span> EVM 220	
<b>B. subtilis</b>	AEKGVHLVRV <span style="background-color: pink;">R</span> ISPFDS <span style="background-color: pink;">S</span> GRRRHTSFV <span style="background-color: pink;">S</span> CEVM 222	
<b>M. tuberculosis</b>	VEQGT <span style="background-color: pink;">H</span> LRV <span style="background-color: pink;">R</span> ISPFDS <span style="background-color: pink;">S</span> QRQTS <span style="background-color: pink;">F</span> AEVEVL 224	
	*: * * * * * * * * : * : * * * * : :	
<b>E. coli</b>	FESGGH <span style="background-color: pink;">R</span> QRV <span style="background-color: pink;">P</span> ATE <span style="background-color: pink;">S</span> Q <span style="background-color: pink;">G</span> R <span style="background-color: pink;">I</span> HTS <span style="background-color: pink;">A</span> CTV <span style="background-color: pink;">A</span> VM 206	
<b>S. flexneri</b>	FESGGH <span style="background-color: pink;">R</span> QRV <span style="background-color: pink;">P</span> ATE <span style="background-color: pink;">S</span> Q <span style="background-color: pink;">G</span> R <span style="background-color: pink;">I</span> HTS <span style="background-color: pink;">A</span> CTV <span style="background-color: pink;">A</span> VM 206	
<b>P. mirabilis</b>	FESGGH <span style="background-color: pink;">R</span> QRV <span style="background-color: pink;">P</span> ATE <span style="background-color: pink;">S</span> Q <span style="background-color: pink;">G</span> R <span style="background-color: pink;">I</span> HTS <span style="background-color: pink;">A</span> CTV <span style="background-color: pink;">A</span> VL 206	
<b>H. influenzae</b>	FESGGH <span style="background-color: pink;">R</span> QRV <span style="background-color: pink;">P</span> KTE <span style="background-color: pink;">S</span> Q <span style="background-color: pink;">G</span> R <span style="background-color: pink;">I</span> HTS <span style="background-color: pink;">A</span> CTV <span style="background-color: pink;">A</span> VM 206	
<b>P. multocida</b>	FESGGH <span style="background-color: pink;">R</span> QRV <span style="background-color: pink;">P</span> KTE <span style="background-color: pink;">S</span> Q <span style="background-color: pink;">G</span> R <span style="background-color: pink;">I</span> HTS <span style="background-color: pink;">A</span> CTV <span style="background-color: pink;">A</span> VM 206	
<b>V. fischeri</b>	FESGGH <span style="background-color: pink;">R</span> QRV <span style="background-color: pink;">P</span> PTE <span style="background-color: pink;">S</span> Q <span style="background-color: pink;">G</span> R <span style="background-color: pink;">I</span> HTS <span style="background-color: pink;">A</span> CTV <span style="background-color: pink;">A</span> VM 208	
<b>C. crescentus</b>	FESGVHLVRV <span style="background-color: pink;">R</span> QRV <span style="background-color: pink;">P</span> PTE <span style="background-color: pink;">S</span> Q <span style="background-color: pink;">G</span> R <span style="background-color: pink;">I</span> HTS <span style="background-color: pink;">A</span> ATV <span style="background-color: pink;">A</span> VL 202	
<b>N. gonorrhoeae</b>	FESGVHLVRV <span style="background-color: pink;">R</span> QRV <span style="background-color: pink;">P</span> PTE <span style="background-color: pink;">S</span> Q <span style="background-color: pink;">G</span> R <span style="background-color: pink;">I</span> HTS <span style="background-color: pink;">A</span> ATV <span style="background-color: pink;">A</span> VM 206	
<b>H. pylori</b>	FEAGTH <span style="background-color: pink;">R</span> QRV <span style="background-color: pink;">P</span> PTE <span style="background-color: pink;">S</span> Q <span style="background-color: pink;">G</span> R <span style="background-color: pink;">I</span> HTS <span style="background-color: pink;">A</span> ITV <span style="background-color: pink;">A</span> IM 205	
<b>S. pneumoniae</b>	YESGAH <span style="background-color: pink;">R</span> QRV <span style="background-color: pink;">P</span> PTE <span style="background-color: pink;">S</span> Q <span style="background-color: pink;">G</span> R <span style="background-color: pink;">I</span> HTS <span style="background-color: pink;">A</span> ITV <span style="background-color: pink;">A</span> VM 208	
<b>B. subtilis</b>	YENGAH <span style="background-color: pink;">R</span> QRV <span style="background-color: pink;">P</span> PTE <span style="background-color: pink;">S</span> Q <span style="background-color: pink;">G</span> R <span style="background-color: pink;">I</span> HTS <span style="background-color: pink;">A</span> ITV <span style="background-color: pink;">A</span> CL 205	
<b>M. tuberculosis</b>	FEGGVHLVRV <span style="background-color: pink;">R</span> QRV <span style="background-color: pink;">P</span> PTE <span style="background-color: pink;">S</span> Q <span style="background-color: pink;">G</span> R <span style="background-color: pink;">I</span> HTS <span style="background-color: pink;">A</span> AGV <span style="background-color: pink;">L</span> VY 207	
	: * * * * * * * * : * : * * * * : *	

**d**

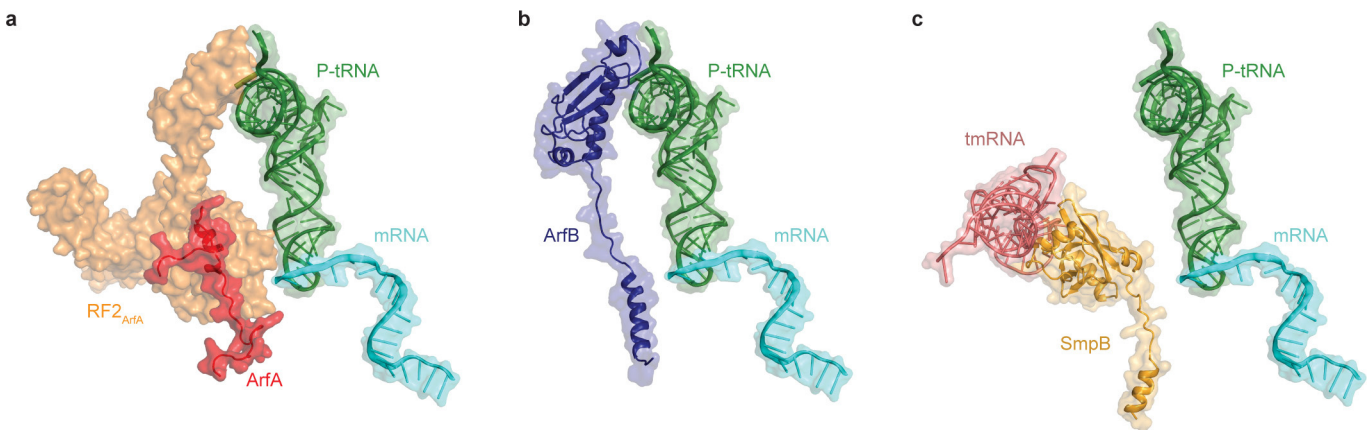
	RF2	RF1
<b>E. coli</b>	NAE <span style="background-color: pink;">K</span> QAM <span style="background-color: pink;">E</span> DNK <span style="background-color: pink;">S</span> DIG-WGSQIRSY 326	
<b>S. flexneri</b>	NAE <span style="background-color: pink;">K</span> QAM <span style="background-color: pink;">E</span> DNK <span style="background-color: pink;">S</span> DIG-WGSQIRSY 326	
<b>P. mirabilis</b>	NAD <span style="background-color: pink;">K</span> QVM <span style="background-color: pink;">E</span> DNK <span style="background-color: pink;">S</span> DIG-WGSQIRSY 326	
<b>H. influenzae</b>	NAD <span style="background-color: pink;">K</span> QAM <span style="background-color: pink;">E</span> DNK <span style="background-color: pink;">S</span> DIG-WGSQIRSY 326	
<b>P. multocida</b>	NAD <span style="background-color: pink;">K</span> QAM <span style="background-color: pink;">E</span> DNK <span style="background-color: pink;">S</span> DIG-WGSQIRSY 326	
<b>V. fischeri</b>	NAE <span style="background-color: pink;">K</span> QAN <span style="background-color: pink;">E</span> DAK <span style="background-color: pink;">S</span> DIG-WGSQIRSY 326	
<b>C. crescentus</b>	EAA <span style="background-color: pink;">Q</span> QALE <span style="background-color: pink;">E</span> DQK <span style="background-color: pink;">T</span> DIG-WGHQIRSY 321	
<b>N. gonorrhoeae</b>	NEEK <span style="background-color: pink;">Q</span> AL <span style="background-color: pink;">E</span> E <span style="background-color: pink;">G</span> K <span style="background-color: pink;">S</span> DVG-WGSQIRSY 328	
<b>H. pylori</b>	QSSA <span style="background-color: pink;">A</span> -KNEEK <span style="background-color: pink;">S</span> EIG-WGHQIRSY 323	
<b>S. pneumoniae</b>	AAE <span style="background-color: pink;">V</span> D <span style="background-color: pink;">S</span> T <span style="background-color: pink;">L</span> K <span style="background-color: pink;">G</span> E <span style="background-color: pink;">K</span> E <span style="background-color: pink;">I</span> EIG-WGSQIRSY 323	
<b>B. subtilis</b>	QAE <span style="background-color: pink;">L</span> DEI <span style="background-color: pink;">R</span> GE <span style="background-color: pink;">K</span> E <span style="background-color: pink;">I</span> G-WGSQIRSY 325	
<b>M. tuberculosis</b>	RAE <span style="background-color: pink;">L</span> DA <span style="background-color: pink;">L</span> KAD <span style="background-color: pink;">G</span> GSS-WGNQMRSY 326	
	** * : * * * *	
<b>E. coli</b>	QQAE <span style="background-color: pink;">A</span> EST <span style="background-color: pink;">R</span> RNLL <span style="background-color: pink;">G</span> SGDR <span style="background-color: pink;">S</span> DRNRTY 310	
<b>S. flexneri</b>	QQAE <span style="background-color: pink;">A</span> EST <span style="background-color: pink;">R</span> RNLL <span style="background-color: pink;">G</span> SGDR <span style="background-color: pink;">S</span> DRNRTY 310	
<b>P. mirabilis</b>	QFA <span style="background-color: pink;">E</span> ASER <span style="background-color: pink;">R</span> RNLL <span style="background-color: pink;">G</span> SGDR <span style="background-color: pink;">S</span> DRNRTY 310	
<b>H. influenzae</b>	AAE <span style="background-color: pink;">Q</span> TDM <span style="background-color: pink;">R</span> RNLL <span style="background-color: pink;">G</span> SGDR <span style="background-color: pink;">S</span> DRNRTY 310	
<b>P. multocida</b>	EQ <span style="background-color: pink;">A</span> QADT <span style="background-color: pink;">R</span> RNLL <span style="background-color: pink;">G</span> SGDR <span style="background-color: pink;">S</span> DRNRTY 310	
<b>V. fischeri</b>	AAA <span style="background-color: pink;">V</span> SDT <span style="background-color: pink;">R</span> RNLL <span style="background-color: pink;">G</span> SGDR <span style="background-color: pink;">S</span> DRNRTY 312	
<b>C. crescentus</b>	DS <span style="background-color: pink;">A</span> R <span style="background-color: pink;">S</span> E <span style="background-color: pink;">K</span> R <span style="background-color: pink;">S</span> Q <span style="background-color: pink;">V</span> G <span style="background-color: pink;">G</span> SGDR <span style="background-color: pink;">S</span> DRNRTY 304	
<b>N. gonorrhoeae</b>	QAE <span style="background-color: pink;">K</span> AAE <span style="background-color: pink;">R</span> SL <span style="background-color: pink;">I</span> G <span style="background-color: pink;">S</span> G <span style="background-color: pink;">G</span> DR <span style="background-color: pink;">S</span> DRNRTY 310	
<b>H. pylori</b>	QIA <span style="background-color: pink;">N</span> AKD <span style="background-color: pink;">R</span> KE <span style="background-color: pink;">Q</span> V <span style="background-color: pink;">G</span> SGDR <span style="background-color: pink;">S</span> DRNRTY 308	
<b>S. pneumoniae</b>	QDE <span style="background-color: pink;">Q</span> DAER <span style="background-color: pink;">K</span> ST <span style="background-color: pink;">I</span> G <span style="background-color: pink;">T</span> GDR <span style="background-color: pink;">S</span> DRNRTY 311	
<b>B. subtilis</b>	QAE <span style="background-color: pink;">Y</span> DQT <span style="background-color: pink;">R</span> KA <span style="background-color: pink;">S</span> V <span style="background-color: pink;">G</span> SGDR <span style="background-color: pink;">S</span> DRNRTY 308	
<b>M. tuberculosis</b>	LAD <span style="background-color: pink;">A</span> SAD <span style="background-color: pink;">R</span> ASQ <span style="background-color: pink;">I</span> RT <span style="background-color: pink;">V</span> DR <span style="background-color: pink;">S</span> DRNRTY 311	
	* . : : * * * : * * *	

**Extended Data Figure 6 | Potential specificity determinants for ArfA-mediated ribosome recycling.** **a**, **b**, ArfA (red) and *E. coli* RF2 (orange) compared to homology model of *E. coli* RF1 (blue) aligned to RF2 in the ArfA-RF2-SRC. **a**, The ArfA interface with  $\beta_4$  and  $\beta_5$  strands of *E. coli* RF2 (orange) consists of hydrophobic residues V198, F217 and F221, which are mutated to Gly, Ala and Ala, respectively, in RF1 (blue). **b**, The ArfA interface with  $\alpha$ -helix  $\alpha_7$  of RF2 (orange). Replacing negatively charged residues such as E311 and D312 in RF2 with Arg in RF1 is also likely to disrupt the interaction with ArfA. **c**, **d**, Sequence alignments for the

regions of RF1 and RF2 corresponding to **a** and **b**, respectively. The pink boxes indicate regions of RF2 that form an interface with ArfA, including residues in bold predicted to prevent interaction of RF1 with ArfA and therefore could provide the basis for RF2-specificity of ArfA action. Organisms in bold contain ArfA, whereas others have no detectable ArfA homologue. Asterisk (\*), colon (:) or full stop (.) indicate a single, fully conserved residue or residues with strong ( $>0.5$  in the Gonnet PAM 250 matrix) and weakly ( $>0.5$ ) similar properties, respectively.



**Extended Data Figure 7 | Location of the ArfA-A18T mutation relative to RF2.** **a**, Overview of ArfA (red) and RF2 (gold) on the ribosome (30S, grey; 50S, slate). **b**, **c**, Zoom of boxed region in **a** showing the environment of A18 (teal) of ArfA in close proximity to I11 and K8 in the N terminus of ArfA (red) (**b**), and A18T (teal) of ArfA in sterically clashing with I11 and K8 in the N terminus of ArfA (red) (**c**).



**Extended Data Figure 8 | Comparison of ArfA with other ribosome rescue systems.** **a–c**, Relative orientation on the ribosome with truncated mRNAs and ArfA (red) and RF2 (orange) (a), ArfB (purple, PDB code 4V95)<sup>5</sup> (b) or tmRNA (brown) and SmpB (yellow) (PDB code 4V8Q)<sup>6</sup> (c). In all cases, the mRNA and P-tRNA are coloured cyan and green, respectively.

Extended Data Table 1 | Data collection and refinement statistics

ArfA-RF2-SRC	
<b>Data collection</b>	
Particles	69,089
Pixel size (Å)	1.084
Defocus range (μm)	0.7-2.2
Voltage (kV)	302
Electron dose (e <sup>-</sup> /Å <sup>2</sup> )	24
<b>Model composition</b>	
Protein residues	6,480
RNA nucleotides	4,642
<b>Refinement</b>	
Resolution (Å)	3.11
Map sharpening B factor (Å <sup>2</sup> )	-60.34
FSC <sub>Average</sub>	0.85
<b>Validation proteins</b>	
Poor rotamers (%)	4.67
Ramachandran outliers (%)	2.45
Ramachandran favored (%)	88.09
Bad backbone bonds (%)	0.02
Bad backbone angles (%)	0.02
<b>Validation RNA</b>	
Correct sugar pockers (%)	98.91
Good backbone conformations (%)	78.72
Bad bonds (%)	0.00
Bad angles (%)	0.14
<b>Scores</b>	
MolProbity	2.20 (99 <sup>th</sup> percentile)
Clash score, all atoms	3.04 (100 <sup>th</sup> percentile)

Special Issue: Ribosomes and Translation

## Review

## Structural Basis for Ribosome Rescue in Bacteria

Paul Huter,<sup>1</sup> Claudia Müller,<sup>1</sup> Stefan Arenz,<sup>1</sup> Bertrand Beckert,<sup>1,2</sup> and Daniel N. Wilson<sup>1,2,\*</sup>

Ribosomes that translate mRNAs lacking stop codons become stalled at the 3' end of the mRNA. Recycling of these stalled ribosomes is essential for cell viability. In bacteria three ribosome rescue systems have been identified so far, with the most ubiquitous and best characterized being the trans-translation system mediated by transfer-messenger RNA (tmRNA) and small protein B (SmpB). The two additional rescue systems present in some bacteria employ alternative rescue factor (Arf) A and release factor (RF) 2 or ArfB. Recent structures have revealed how ArfA mediates ribosome rescue by recruiting the canonical termination factor RF2 to ribosomes stalled on truncated mRNAs. This now provides us with the opportunity to compare and contrast the available structures of all three bacterial ribosome rescue systems.

## Bacterial Ribosome Rescue Systems

Ribosome rescue systems are necessary to recycle ribosomes that have become stalled at the 3' end of mRNAs, so-called non-stop ribosome complexes [1,2]. Translation on these non-stop mRNAs is blocked due to the absence of a sense or stop **codon** (see **Glossary**) in the ribosomal **A site**, which is crucial for elongation or termination to continue. These truncated or non-stop mRNAs can arise in the cell due to premature transcription termination or mRNA damage; for example, by the action of **RNases**. Additionally, non-programmed frameshifting events or nonsense suppression (readthrough of a stop codon) can also lead to accumulation of non-stop complexes. Ribosome rescue systems that deal with non-stop complexes are present in all species of life. In archaea and eukaryotes, non-stop complexes are rescued by the combined action of Dom34 and Hbs1, which are homologs of eukaryotic RF (eRF) 1 and eRF3 [2]. Bacteria have evolved completely unrelated pathways to deal with rescue of non-stop complexes (reviewed in [2–7]). These include the trans-translation system mediated by the tmRNA and SmpB as well as two more recently identified Arf systems involving ArfA and ArfB (formerly known in *Escherichia coli* as YhdL and YaeJ, respectively). The occurrence of non-stop complexes appears to be a frequent event in bacteria. Experiments in *E. coli* indicate that 0.4% of all transcripts undergo trans-translation [8] and that 2–4% of **peptidyl-tRNAs** remain non-hydrolyzed when ribosome rescue pathways are inactivated [9]. This explains why the presence of at least one of the bacterial ribosome rescue pathways is essential for cell viability [10]. While structural studies have provided much insight into the mechanism of tmRNA-SmpB- and ArfB-mediated rescue of non-stop ribosome complexes, structural insight into ArfA-mediated ribosome rescue has been lacking. Recently, five cryoelectron microscopy (cryo-EM) structures of ArfA-RF2-non-stop ribosome complexes were reported [11–15], providing the opportunity to not only compare the similarities and differences of the structures with one another, but also to contrast the findings with the structures of the other bacterial ribosome rescue systems.

## Trends

Bacterial ribosome rescue systems are ubiquitous in bacteria and essential for cell viability. Homologs of some rescue factors are also found in eukaryotic mitochondria and plant chloroplasts.

Bacterial ribosome rescue factors such as small protein B (SmpB), alternative rescue factor (Arf) A, and ArfB recognize ribosomes stalled on truncated mRNAs by using their positively charged C-terminal tails to probe whether the mRNA channel is vacant.

ArfA induces conformational changes within the 'switch' loop of release factor 2 (RF2) that promotes transition from a closed to an open conformation, placing the catalytically important glycine–glycine–glutamine (GGQ) motif of RF2 at the peptidyltransferase center of the ribosome.

The distinct pathways used to rescue bacterial and eukaryotic cytoplasmic non-stop ribosome complexes suggest that bacterial ribosome rescue may be a potential target for the development of new antimicrobial agents.

<sup>1</sup>Gene Center, Department of Biochemistry and Center for Integrated Protein Science Munich (CiPSM), Feodor-Lynenstr. 25, 81377 München, Germany

<sup>2</sup>Institute for Biochemistry and Molecular Biology, University of Hamburg, Martin-Luther-King-Platz 6, 20146 Hamburg, Germany

\*Correspondence:  
Daniel.wilson@chemie.uni-hamburg.de  
(D.N. Wilson).

## Trans-translation Mediated by tmRNA and SmpB

Genes encoding tmRNA (*ssrA*) and SmpB have been found in most if not all sequenced bacterial genomes, including the smallest genomes of *Mycoplasma* species as well as endosymbionts such as *Carsonella ruddii* [16]. Moreover, tmRNA is essential in many bacteria, including many pathogenic bacteria such as *Neisseria gonorrhoeae*, *Mycobacterium tuberculosis*, and *Legionella pneumophila* [6,17]. ArfB, and particularly ArfA, have more limited phylogenetic distributions, with ArfB being present in 34% of representatively sequenced bacterial genomes and ArfA limited to a subset of  $\beta$ - and  $\gamma$ -proteobacteria [18,19]. In many bacteria trans-translation is not essential, presumably due to the presence of redundant alternative rescue pathways. Nevertheless, the loss of trans-translation usually leads to reduction in fitness, particularly under various stress conditions, such as high or low temperature, ethanol or acid treatment, or nutrient deprivation, or in the presence of antibiotics [6,17]. Such stress conditions can lead to an increase in truncated mRNAs and stalled ribosomes, explaining the higher levels and importance of trans-translation under these circumstances. These findings also highlight that, although the presence of alternative rescue pathways is sufficient to maintain cell viability, they appear to be insufficient to optimally cope with the cellular demands for ribosome rescue in the absence of trans-translation.

In most bacteria, tmRNA comprises a single RNA molecule containing a tRNA-like domain (TLD), which resembles the acceptor stem of an alanyl-tRNA, and a messenger-like domain (MLD) encoding a short, 8–35-aa peptide [20]. The TLD and MLD are linked together by a series of **pseudoknots** (see inset in Figure 1) [20]. The TLD of tmRNAs can be charged with alanine by the canonical alanine tRNA synthetase (AlaRS), a reaction that is enhanced by the presence of SmpB, which interacts with AlaRS and stabilizes the tmRNA structure [20]. The alanine-charged TLD of the tmRNA is recognized by elongation factor (EF)-Tu, which delivers tmRNA to the A site of a non-stop ribosome (Figure 1A,B) [20]. The structure of the TLD of a tmRNA in complex with SmpB and EF-Tu-GDP stabilized on a 70S ribosome using the antibiotic **kirromycin** [21] (Figure 1C) reveals that the TLD of tmRNA interacts with EF-Tu on the ribosome, analogous to the acceptor arm of an **aminoacyl-tRNA (aa-tRNA)** being delivered to the ribosome by EF-Tu [22]. During canonical translation the complementarity between the codon in the A site and the **anticodon** stem-loop (ASL) of the aa-tRNA dictates which aa-tRNA is delivered by EF-Tu [23,24]. On non-stop ribosomes there is no codon in the A site, explaining why the TLD of tmRNA does not require an ASL. Instead, the globular domain of SmpB mimics the ASL of a tRNA and occupies the decoding site of the ribosome [21] (Figure 1B,C), as predicted based on previous X-ray [25,26] and cryo-EM [27,28] studies. The C-terminal tail of SmpB, which is unstructured in solution, adopts an  $\alpha$ -helical conformation on the ribosome that probes the mRNA channel (Figure 1B,C) [21], explaining how the tmRNA–SmpB complex can distinguish actively translating ribosomes with mRNA in the channel from ribosomes stalled on truncated mRNAs with a vacant channel [29]. Accommodation of the TLD at the A site of the **peptidyltransferase center (PTC)** of the large ribosomal subunit allows peptide bond formation between the truncated nascent polypeptide chain and the alanine of the TLD of the tmRNA (Figure 1D). Binding of EF-G translocates the TLD of the tmRNA from the A site to the **P site**, which together with SmpB places the first (resume) codon of the MLD into the A site ready to be decoded by the next aa-tRNA (Figure 1E,F) [30]. A cryo-EM structure of the translocated state reveals that the TLD and SmpB occupy a **hybrid A/P site** of the ribosome and the linking pseudoknots wrap around the swiveled head of the small subunit to facilitate positioning of the MLD for decoding (Figure 1E) [31]. Translation then continues on the MLD of the tmRNA incorporating a degradation tag into the C terminus of the truncated polypeptide, which targets it for proteolysis by Clp and other proteases (Figure 1G). Importantly, the MLD of the tmRNA contains a stop codon, such as UAA, which allows canonical translation termination via recruitment of RF1 or RF2 (Figure 1G). The **glycine–glycine–glutamine (GGQ) motif** of RF1 or RF2 then catalyzes the hydrolysis of the tagged polypeptide chain, allowing the

## Glossary

**Aminoacyl-tRNA (aa-tRNA):** tRNA charged at the 3' end with an amino acid.

**Anticodon:** the region of the tRNA that is complementary to the codon of the mRNA.

**Anti conformation:** nucleotide conformation where the ring of the nucleobase is nearly perpendicular to the furanose ring but projecting away from the furanose; contrasts with the *syn* conformation where the nucleobase ring is rotated around the glycosidic bond.

**A site:** the tRNA-binding site on the ribosome where aa-tRNAs are delivered by EF-Tu during translation.

**Codon:** a sequence of three RNA (or DNA) nucleotides that corresponds to a specific amino acid (or stop signal) during protein synthesis.

**Deacylated tRNA:** tRNA that is not charged with an amino acid.

**E site:** the tRNA-binding site on the ribosome where uncharged or deacylated tRNAs exit from the ribosome during translation.

**Glycine–glycine–glutamine (GGQ) motif:** conserved motif found in protein factors that catalyze PTH on the ribosome.

**Hybrid A/P site:** when the tRNA is in the A site on the small subunit and in the P site on the large subunit.

**Hydroxyl radical probing:** chemical probing method that relies on the cleavage of RNA (or DNA) molecules by hydroxyl radicals, which can be generated from site-specific tethers located on neighboring proteins or factors.

**Kirromycin:** an antibiotic that binds and traps EF-Tu on the ribosome.

**Peptidyltransferase center (PTC):** the highly conserved region in the large subunit of the ribosome where peptide bond formation occurs.

**Peptidyl-tRNA:** a tRNA bearing the growing nascent polypeptide chain.

**Peptidyl-tRNA hydrolysis (PTH):** the activity of hydrolyzing and thereby breaking the ester linkage between the polypeptide chain and the tRNA to which it is attached.

**Proline–alanine–threonine (PAT) motif:** motif in *Escherichia coli* RF1 that is involved in recognition of the stop codon of the mRNA.

**Pseudoknot:** a nucleic acid secondary structure containing at least two stem-loop structures in which half of one stem is intercalated

ribosome to be subsequently recycled for the next round of translation. It has been demonstrated that it is the recycling of the stalled ribosomes, rather than tagging of the truncated polypeptide chains for degradation, that makes trans-translation essential for bacterial survival [20,32]. This is consistent with the observation that inactivation of trans-translation in bacteria such as *E. coli* is not lethal, due to the presence of back-up systems such as ArfA [33].

### Interplay between the Trans-translation, ArfA, and ArfB Rescue Systems

While the deletion of either the *ssrA* or the *arfA* gene in *E. coli* does not significantly affect viability, deletion of both genes ( $\Delta\text{ssrA}\Delta\text{arfA}$ ) is synthetic lethal [33], illustrating the importance of having at least one ribosome rescue for bacterial survival [5,10]. Biochemical studies have demonstrated that ArfA represents a back-up system for trans-translation [34,35]. The *arfA* mRNA contains a stem-loop structure that acts as a transcription terminator and/or a substrate for RNase III cleavage [18,34,35] (Figure 2A). In the presence of tmRNA, the short ArfA protein produced from the truncated *arfA* mRNA is tagged by tmRNA and targeted for degradation (Figure 2A). However, in the absence of tmRNA the short ArfA protein product is not degraded and assumes the role of recycling ribosomes stalled on truncated mRNAs [34,35] (Figure 2B). The full-length *E. coli* ArfA protein is 72 aa in length and contains a C-terminal hydrophobic region that leads to aggregation of the protein *in vivo* [34] (Figure 2A). By contrast, shorter forms

between the two halves of another stem.

**P site:** the tRNA-binding site for the peptidyl-tRNA on the ribosome.

**RNase:** a type of nuclease that catalyzes the degradation of RNA; for example, RNase III is an endonuclease that cleaves dsRNA.

**Serine-proline-phenylalanine motif (SPF):** motif in *E. coli* RF2 that is involved in recognition of the stop codon of the mRNA.

**Translocation:** the process of moving the A and P site tRNAs as well as the associated mRNA through the ribosome into the P and E sites, respectively. This reaction is catalyzed by EF-G in bacteria.

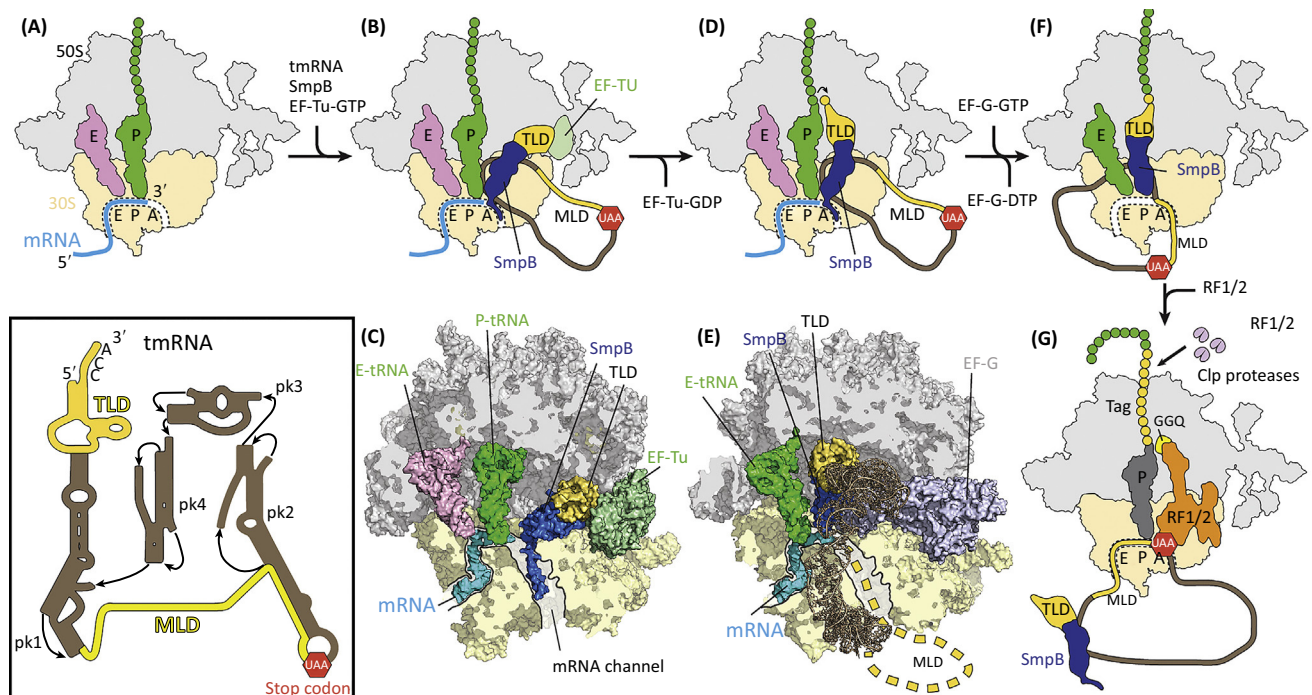
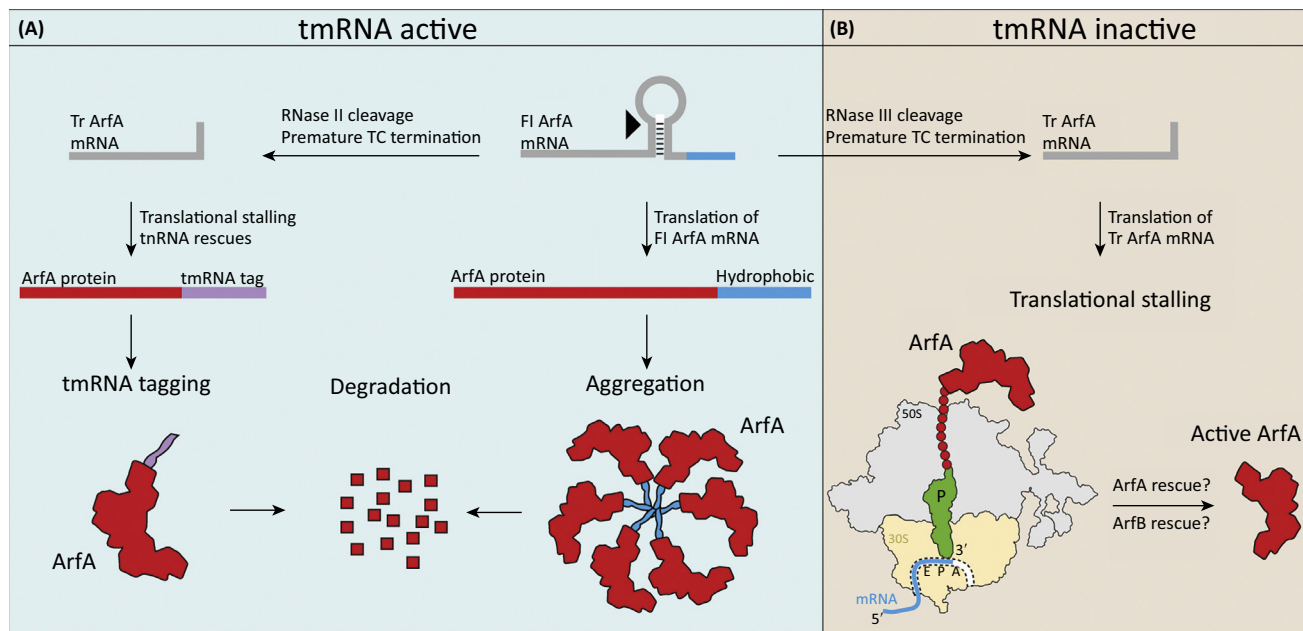


**Figure 1. Rescue of Non-stop Ribosomal Complexes by Trans-translation.** (A) Ribosomes stall on truncated mRNAs (cyan) with vacant A sites. (B) The tRNA-like domain (TLD) (yellow) of transfer-messenger RNA (tmRNA) (brown) is recognized by elongation factor (EF)-Tu (pale green) and delivered together with small protein B (SmpB) (blue) to the ribosomal A site. The globular domain of SmpB occupies the decoding site, while the C-terminal tail of SmpB probes the vacant mRNA channel of the small (30S) subunit. (C) Overview of the structure of the TLD of tmRNA (yellow), with SmpB and EF-Tu bound to the ribosome (PDB ID: 4V8Q) [70]. (D) Accommodation of the TLD at the A site of the large (50S) subunit allows peptide bond formation between the TLD and the nascent polypeptide chain, resulting in transfer from P-tRNA (green) to the TLD. (E) Cryo-electron microscopy (cryo-EM) structure of a translocated state of tmRNA-SmpB with bound EF-G (light blue; PDB ID: 4V6T) [31]. (F) After translocation of TLD by EF-G, the first codon of the mRNA-like domain (MLD) (yellow) is positioned at the A site. (G) Canonical translation termination mediated by release factor (RF) 1 or RF2 (orange) on encountering the UAA stop codon of the MLD at the A site. The translated degradation tag (yellow) is recognized by Clp proteases, leading to degradation of the incompletely translated nascent chain (green). Inset shows the secondary structure of tmRNA, with the TLD and MLD highlighted in yellow.



Trends in Biochemical Sciences

**Figure 2. Alternative Rescue Factor A (ArfA) Is a Back-Up System for Trans-translation.** (A) Full-length (Fl) ArfA mRNA (gray) forms a stem-loop structure that acts as a transcription terminator and/or is recognized and cleaved by RNase III, generating a truncated (Tr) mRNA. Ribosomes stall on the truncated mRNAs, inducing trans-translation, leading to tmRNA tagging (purple) and degradation of the ArfA protein (red). In the case that full-length ArfA protein is translated, the C-terminal region contains a hydrophobic stretch (cyan) that leads to aggregation and degradation of the full-length ArfA. (B) If trans-translation is impaired (or overwhelmed), the short ArfA protein is not tagged or degraded and the active ArfA assumes the role of rescuing non-stop ribosome complexes.

of ArfA resulting from truncated *arfA* mRNA lack the terminal 17–18 aa but retain full rescue activity [34,35].

Curiously, *ssrA* is essential in *Neisseria gonorrhoeae*, despite the presence of an *arfA* gene [32], although *N. gonorrhoeae* ArfA is active when expressed in *E. coli* [18]. By contrast, tmRNA is not essential in *Bacillus subtilis* [36] despite the apparent absence of both the ArfA and ArfB systems, raising the question of additional alternative rescue systems existing in some bacteria [10]. The synthetic lethality of *E. coli* due to the  $\Delta ssrA \Delta arfA$  double deletion occurs despite the presence of *arfB*, but overexpression of ArfB can rescue the lethality of the  $\Delta ssrA \Delta arfA$  strain [37]. This finding indicates that endogenous levels of ArfB are insufficient to cope with the level of ribosome rescue needed when tmRNA and ArfA are both absent [7]. It also raises the question of whether there are specific growth or stress conditions where ArfB is more important or whether ArfB is simply less important in *E. coli* than in other species due to the additional presence of ArfA.

### Ribosome Rescue by ArfB

The globular N-terminal domain (NTD) of ArfB is evolutionarily related to domain 3 of RF1 and RF2 [38,39], which contain a conserved GGQ motif that is critical for **peptidyl-tRNA hydrolysis (PTH)** activity [40]. In contrast to RF1 and RF2, ArfB lacks the domain 2/4 responsible for stop codon recognition and instead has an extended C-terminal tail (Figure 3A–C). In agreement with the finding that overexpression of ArfB can rescue *E. coli* lacking tmRNA and ArfA rescue systems [37], ArfB can efficiently catalyze PTH on ribosomes stalled at the 3' ends of non-stop mRNAs *in vivo* [19,37,41,42] (Figure 3A,B). The crystal structure of ArfB on the ribosome reveals that the NTD interacts with the large subunit such that the GGQ motif is positioned at the PTC (Figure 3C) [43], consistent with the reports that mutations of the GGQ

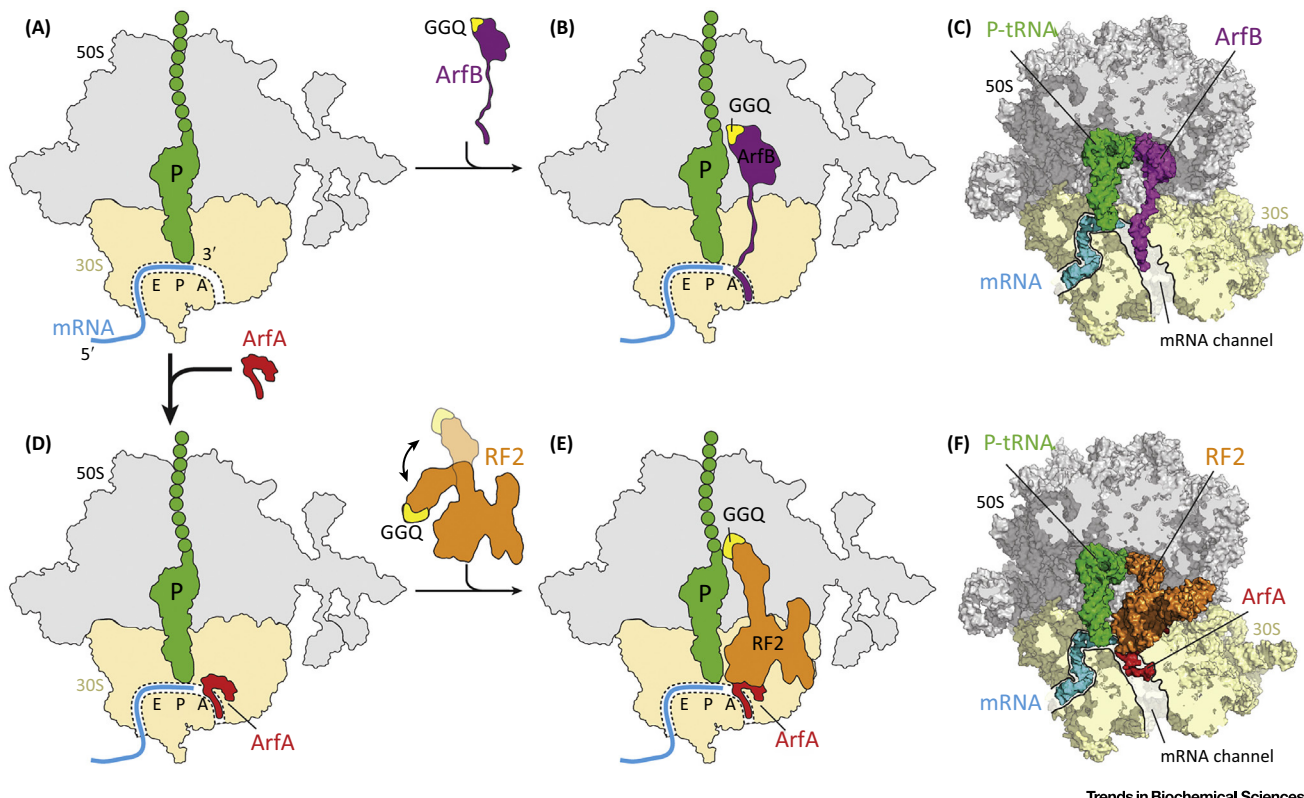


**Figure 3. Rescue of Non-stop Ribosomal Complexes by Alternative Rescue Factor (Arf) B and ArfA.** (A) Ribosomes stall on truncated mRNAs (cyan) resulting in vacant A sites. (B) These non-stop ribosomes are recognized by the C-terminal tail of ArfB (purple), which probes the vacant mRNA channel. The N-terminal domain of ArfB containing the glycine–glycine–glutamine (GGQ) motif (yellow) catalyzes the hydrolysis of polypeptide from the P-tRNA (green). (C) Overview of the structure of ArfB (purple) bound to the ribosome (PDB ID: 4V95) [43]. (D) Non-stop ribosomes are also recognized by the C-terminal tail of ArfA (red), which also probes the vacant mRNA channel. (E) ArfA recruits release factor 2 (RF2) (orange) to the non-stop ribosome to catalyze peptidyl-tRNA (green) hydrolysis. (F) Overview of the structure of ArfA (red) and RF2 (orange) bound to a non-stop ribosome (PDB ID: 5MGP) [12].

motif of ArfB impair the rescue activity of ArfB both *in vitro* [19,37] and *in vivo* [37]. The C-terminal tail of ArfB, which was disordered in previous unbound ArfB structures [38,39,44], adopts a  $\alpha$ -helical conformation that reaches into the mRNA channel of the small subunit (Figure 3B,C) [43]. This suggests that, like SmpB, ArfB also utilizes the C-terminal tail to distinguish actively translating ribosomes from those stalled on truncated mRNAs. Truncation of ten residues or more from the C terminus of ArfB leads to a severe reduction in ribosome binding and PTH activity as well as the ability to rescue the  $\Delta$ ssrA $\Delta$ arfA strain [19,37,39]. The NTD and C-terminal helix are connected by a flexible linker of  $\sim$ 12 aa that adopts an extended conformation on the ribosome (Figure 3B,C). Deletion of one or two residues within the linker of ArfB led to progressive loss of PTH activity although the ribosome interaction remained unaffected [39], suggesting that the linker is important for positioning of the NTD at the PTC of the ribosome.

While ArfB rescue is most efficient on non-stop ribosomes, it maintains some rescue activity on longer mRNAs that extend into the A site [19,42]. The ArfB rescue activity decreases with increasing length of the 3' end, such that little activity is observed when the 3' end extends  $>14$  nucleotides from the P site [42]. This suggests that the C-terminal tail of ArfB can efficiently compete and may even displace short mRNA 3' ends from the channel and that longer mRNAs encompassing the entire mRNA channel are resilient to displacement by ArfB, explaining why ArfB does not interfere with canonical translation elongation.

ArfB homologs are present in most, if not all, eukaryotes, where they are targeted to mitochondria [45]. In addition, some plants also encode ArfB homologs with chloroplast-targeting signals. By contrast, there is no evidence for ArfA genes in eukaryotes and tmRNA/SmpB genes are found only in some protist mitochondria [46]. The best-characterized organellar ArfB homolog is the human mitochondrial immature colon carcinoma transcript-1 (ICT1) (reviewed in [47]). Like other ArfB homologs, ICT1 displays excellent rescue activity on non-stop ribosomal complexes from either *E. coli* [39,42,48] or mammalian mitochondria [49]. The rescue activity is dependent on an intact GGQ motif and the presence of a C-terminal tail [39,48,49]. Loss or knockdown of ICT1 leads to a loss of cell viability [38,48], which can be rescued by the expression of a bacterial ArfB homolog [42]. Likewise, ICT1 supported the viability of a bacterial  $\Delta$ ssrA $\Delta$ arfA strain, suggesting that ICT1 and ArfB are functionally interchangeable [42]. However, unlike bacterial ArfB, ICT1 was shown to be an integral component of the mitochondrial large subunit [48], where it is located at the base of the central protuberance [50]. Subsequent *in vitro* experiments demonstrated that the integrated ICT1 does not appear to display any rescue activity on non-stop complexes, but rather exogenous ICT1 is required [49]. So far, ribosome-free ICT1 has not been detected in mitochondria [48], raising the question of whether ICT1 is released from the mitoribosome to rescue stalled ribosomes or whether ICT1 expression is upregulated under specific stress conditions.

### Ribosome Rescue by ArfA and RF2

ArfA was originally identified in a screen for factors that are essential for viability of *E. coli* when the *ssrA* gene is disabled [33]. The loss-of-function mutation identified had an Ala-to-Thr substitution at position 18 (A18T) in ArfA [33]. ArfA, as well as the ArfA-A18T mutant, were both shown to co-localize with ribosomes *in vivo*, but only the wild-type ArfA could rescue non-stop ribosomes [33]. Interestingly, recombinant ArfA was effective at rescuing non-stop ribosomes *in vitro* when an *E. coli*-extract-based system was used [33] but displayed no rescue activity with purified non-stop ribosome complexes [37]. This indicated that ArfA requires an additional cellular factor present in the *E. coli* extract to mediate ribosome rescue [37]. Subsequent *in vitro* studies using a reconstituted cell-free translation system revealed that RF2, but not RF1, cooperates with ArfA to hydrolyze the peptidyl-tRNA and rescue non-stop ribosomes [41,51] (Figure 3D,E). ArfA does not interact with RF2 in solution [51,52] but rather interacts with non-stop ribosomes [52] (Figure 3D) before recruiting RF2 to the complex (Figure 3E). Initial binding assays observed interaction of ArfA with the large ribosomal subunit [33], whereas subsequent **hydroxyl radical probing** experiments indicated a binding site located on the 30S subunit in the vicinity of the mRNA channel [52]. The five cryo-EM structures of ArfA–RF2–non-stop ribosome complexes [11–15] (Figure 3F) revealed that ArfA interacts almost exclusively with the small subunit. Overall, the structures are in excellent agreement with each other and enable most of the available biochemical data to be rationalized. The structures provide much-needed structural insight into the mechanisms of action of ArfA and RF2 in rescuing non-stop ribosome complexes, which are discussed in detail in the following sections.

### Monitoring the mRNA Channel of the Non-stop Ribosome

Full-length *E. coli* ArfA is 72 aa in length but is aggregation prone; therefore, C-terminally truncated ArfA variants were used for the structural analysis that lacked either 12 [11,15] or 17 residues [12–14]. In each case, however, the flexibility of the C terminus permitted only 46–48 of the 55–60 aa of ArfA to be modeled. The absence of electron density for the very-C terminus of ArfA suggests that these residues are less important for binding, which is consistent with their poor conservation across ArfA from different species [18,33]. In all five cryo-EM structures [11–15], the C-terminal part of ArfA extends from the decoding A site into the mRNA entry channel (Figure 4A), analogous to the C-terminal tails of SmpB [21] (Figure 4B) and ArfB [43] (Figure 4C) as well as the 3' end of a full-length mRNA [53] (Figure 4D). The location of the C terminus of ArfA within the mRNA channel is also compatible with hydroxyl radical probing experiments

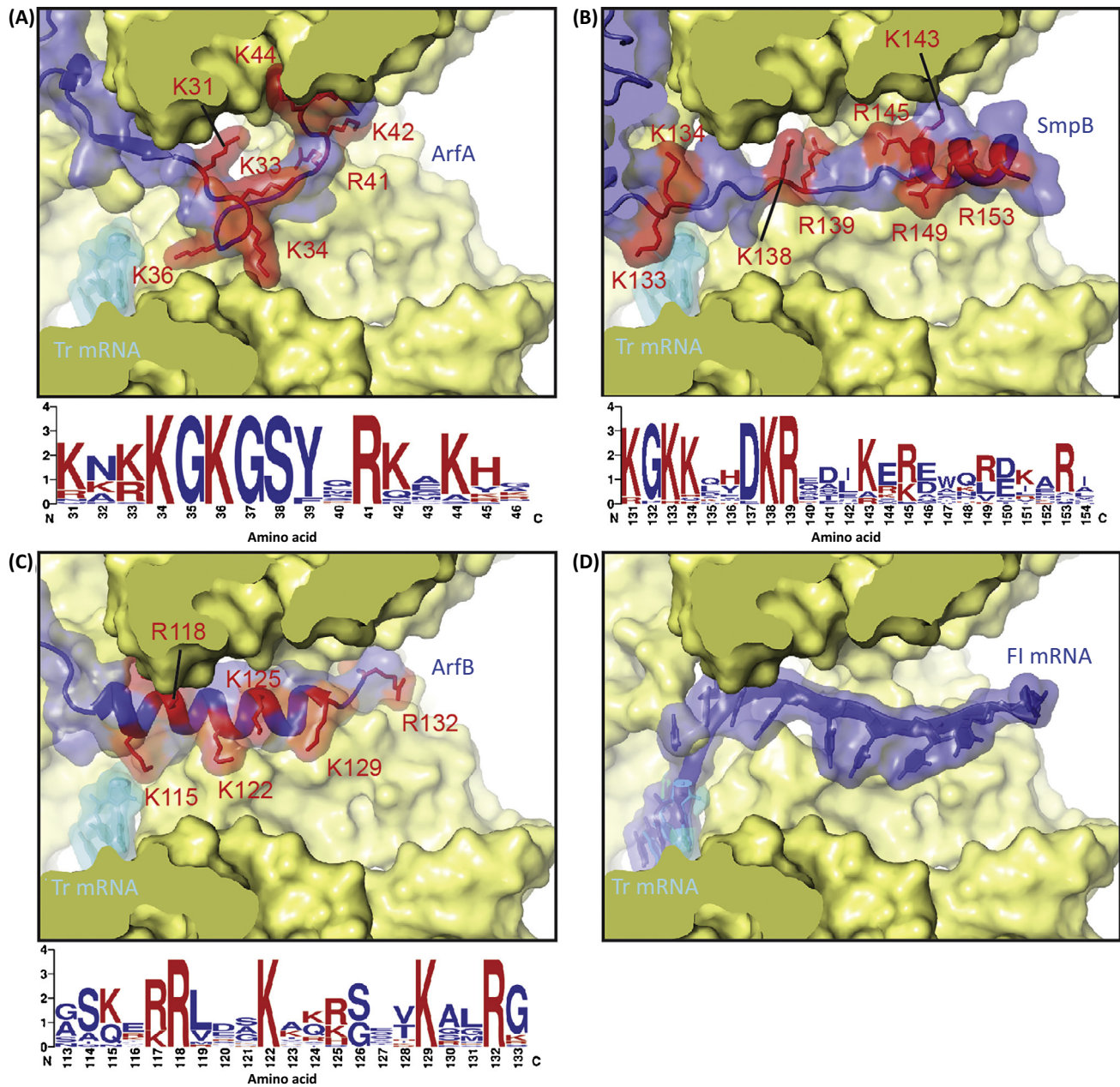


**Figure 4. Monitoring of the mRNA Channel by Ribosome Rescue Factors.** The mRNA channel of the ribosome is probed by the C-terminal tail of (A) alternative rescue factor (Arf) A (PDB ID: 5MGP) [12], (B) small protein B (SmpB) (PDB ID: 4V8Q) [70], or (C) ArfB (PDB ID: 4V95) [43]. The interaction is mediated via positively charged amino acids (red), the conservation of which is presented as a WebLogo [71] below the respective panels. (D) For comparison, the path of a full-length (Fl) mRNA is indicated (PDB ID: 4V6F) [53].

performed in the absence of RF2 [52], suggesting that ArfA initially uses a similar conformation to monitor the vacant mRNA channel.

Like SmpB and ArfB, the C terminus of ArfA also contains several highly conserved positively charged arginine and lysine residues that establish interactions with the negatively charged 16S rRNA comprising the walls of the mRNA channel [11–15] (Figure 4A–C). There appears to be

some redundancy in the interaction of these conserved residues of ArfA, since individual point mutations had little to no effect on the recycling activity of ArfA [13,52], although some reduction was reported for K34C and R41C mutations in a recent study [14]. The C-terminal tail of SmpB is also rich in positively charged residues and includes several highly conserved stretches, such as  $_{131}\text{KGKK}_{134}$  and  $_{137}\text{DKR}_{139}$  (Figure 4B). Although single mutations within the  $_{137}\text{DKR}_{139}$  motif had little effect, a triple alanine substitution abolished SmpB's ability to support tmRNA activity *in vivo* [54,55]. Similar loss of activity was observed when the C-terminal helix of SmpB was truncated [56]. Single mutations within the C-terminal tail of *E. coli* ArfB, such as K122A, K129A, and R132A, as well as the equivalent residues in ICT1, dramatically decreased the rescue activity of the respective factors [39] (Figure 4C). Similar to ArfB [19,37,39], C-terminal truncations in human ICT1 that remove these residues also abolished rescue activity [39,49].

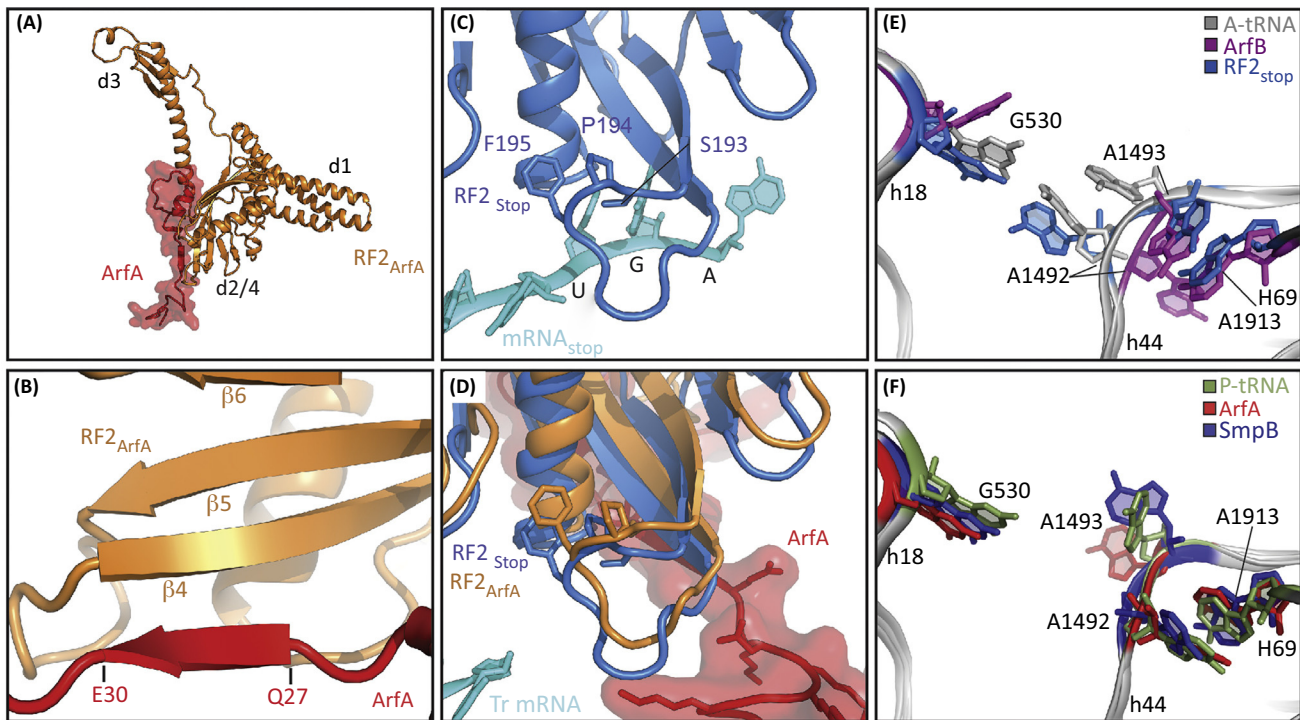
Biochemical studies have demonstrated that the efficiency of ArfA–RF2-mediated ribosome rescue decreases with increasing length of the 3' end of the mRNA that extends into the A site [41,57]. Specifically, rescue was observed, although with reduced efficiency, when mRNA extended by up to three or four A-site nucleotides was used [41,57]. Almost no rescue occurred on artificially stalled ribosomes with mRNAs extended by six or more A-site nucleotides [41,57]. This is consistent with the overlap in the binding position of ArfA [11–15] (Figure 4A) and a full-length mRNA (Figure 4D), which indicates that three nucleotides (but not more) can be accommodated in the A site without significant clashes with ArfA. By contrast, the tmRNA–SmpB trans-translation system is less sensitive to mRNA length, with the most dramatic reductions in trans-translation activity being observed when mRNAs with 12 or more A-site nucleotides were used [29,58,59]. mRNA length dependence for the rescue activity of ArfB has also been reported and appears to be intermediate to the ArfA and trans-translation systems [41]. It remains to be determined whether the length dependencies of the different rescue systems correlate with the ability of C-terminal extensions of the respective rescue factors to displace the 3' portion of the mRNA from the mRNA channel, or whether the factors utilize different binding modes when the mRNA channel is occupied.

#### Recruitment of RF2 to the Ribosome by ArfA

The recent cryo-EM structures also provide insight into how ArfA recruits RF2 to the ribosome despite the absence of a stop codon in the mRNA [11–15]. ArfA establishes a large interaction interface with RF2 encompassing the central portion (residues 15–31) of ArfA and the distal end of  $\alpha$  helix  $\alpha$ 7 of domain 3 as well as the  $\beta$ 4– $\beta$ 5 strands of domain 2 of RF2 (Figure 5A). Residues 27–30 of ArfA form a small  $\beta$  strand that complements the  $\beta$  sheet of RF2 domain 2/4 (Figure 5B). The overall position of RF2 in the ArfA–RF2–non-stop complex is similar to that observed during canonical translation termination [60,61], although the decoding domain 2/4 is slightly shifted. The shift affects the loop between the  $\beta$ 4– $\beta$ 5 strand of domain 2 of RF2 bearing the **serine–proline–phenylalanine (SPF) motif** (*E. coli* Ser205–Pro206–Phe207), which is involved in the specificity of recognition of the first and second positions of the UGA and UAA stop codons [60–62] (Figure 5C,D). Importantly, the structures illustrate that ArfA does not interact with the SPF motif and therefore does not directly mimic the presence of a stop codon (Figure 5D). Consistently, mutations in the SPF motif that impair RF2 termination activity do not affect ArfA–RF2-mediated rescue activity [51] whereas RF1 mutants bearing the SPF motif instead of the **proline–alanine–threonine (PAT) motif** (which confers termination activity at UGA) remain inactive in the ArfA-mediated rescue system [51].

#### Distinct Conformations of the Decoding Site during Ribosome Rescue

During canonical termination G530 of the 16S rRNA adopts an **anti conformation** that stacks on the A3 nucleotide of a stop codon [40]. The same flipped *anti* conformation of G530 is also stabilized during ribosome rescue via interaction with E30 of ArfA [11–15] or by stacking interactions with Y126 of SmpB [21] and Arg118 of ArfB [43]. G530, together with A1492 and



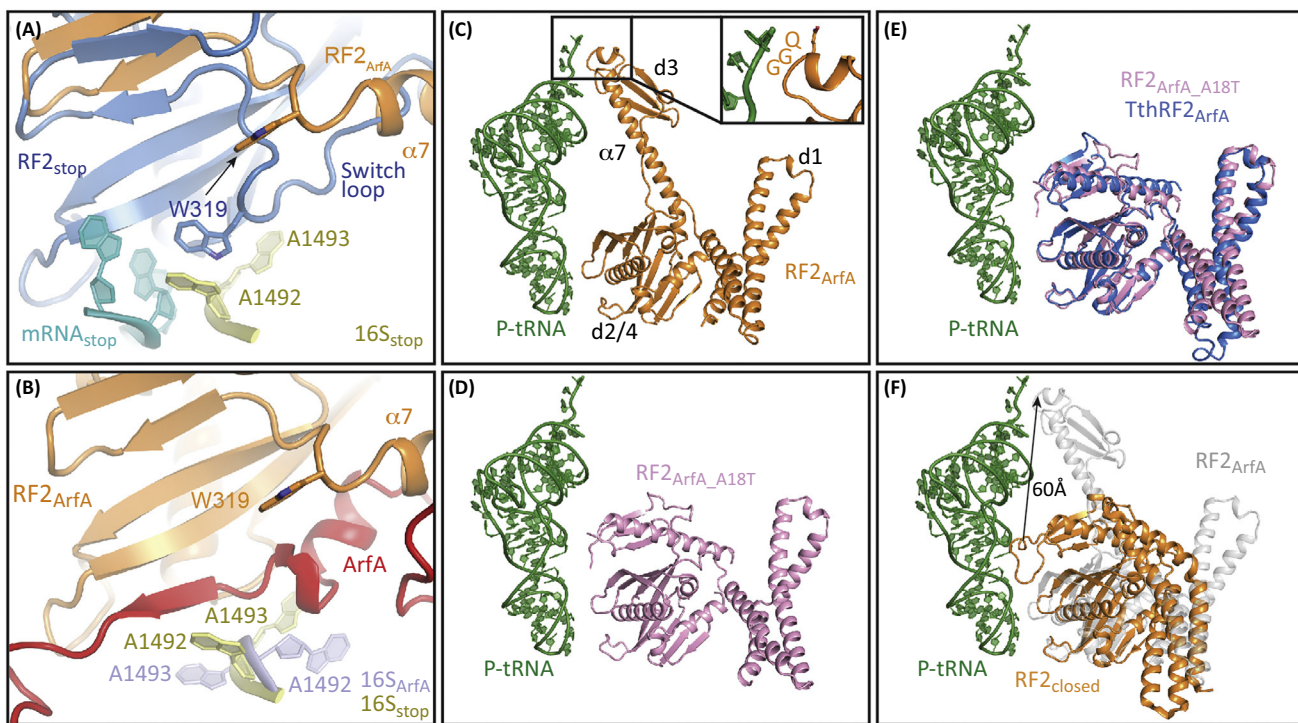
Trends in Biochemical Sciences

**Figure 5. Recruitment of Release Factor 2 (RF2) to Non-stop Ribosomes by Alternative Rescue Factor A (ArfA).** (A) Interaction surface between ArfA (red) and RF2 (orange). (B) ArfA donates a  $\beta$  strand to the  $\beta$  sheet of domain 2/4 of RF2 (orange). (C) Interaction of the serine–proline–phenylalanine (SPF) motif of RF2 with the A-site UGA stop codon of an mRNA ( $\text{mRNA}_{\text{stop}}$ , cyan; PDB ID: 4V5E) [60]. (D) Same view as (C) but superimposed with the ArfA–RF2–non-stop ribosome complex containing ArfA (red), RF2 (orange), and the truncated (Tr) mRNA (cyan; PDB ID: 5MGP) [12]. (E,F) Superimposition of decoding center showing 16S rRNA nucleotides G530, A1492, and A1493 as well as the 23S rRNA nucleotide A1913 from ribosomes bound with (E) A-tRNA (grey; PDB ID: 4V6F) [53], RF2<sub>Stop</sub> with a UGA codon (marine blue; PDB ID: 4V5E) [60], ArfB (purple; PDB ID: 4V95) [43], (F) P-tRNA (green; PDB ID: 4V9B) [64], ArfA (red; PDB ID: 5MGP) [12], or small protein B (SmpB) (blue; PDB ID: 4V8Q) [70].

A1493, is critical for monitoring the interaction between the codon of the mRNA and the anticodon of the A-site tRNA [23,63]. While both A1492 and A1493 are flipped out of helix 44 (h44) during decoding of sense codons [23,63], only A1492 is flipped during termination by RFs while A1493 stacks on A1913 in H69 of the 23S rRNA (Figure 5E) [40]. In the presence of ArfB, A1492 is only partially flipped out and A1493 is stacked with A1913 (Figure 5E) and Pro110 of ArfB [43]. The opposite occurs with ArfA or SmpB; namely, A1493 is flipped out of h44 whereas A1492 stacks on A1913 [11–15,21] (Figure 5F). This is similar to the conformation observed when tRNA is bound at the P site but the A site is vacant [64] (Figure 5F). Thus, the flexibility of the decoding site is manipulated in various ways to accommodate binding of the rescue factors on the ribosome. While mutations with the decoding center of the ribosome (G530A, A1492G, or A1493G) have a dramatic effect (1000-fold reduction) on aa-tRNA accommodation at the PTC, only a twofold reduction was observed on peptidyl-transfer to Ala-tmRNA [55]. It remains to be determined to what extent such mutants influence factor binding and accommodation at the PTC during ArfA- and ArfB-mediated ribosome rescue.

#### ArfA Induces the Active Open Conformation of RF2 on the Ribosome

During canonical termination, recognition of the stop codon by RF1 and RF2 stabilizes a rearranged conformation of the switch loop that directs domain 3 into the PTC [40,65]. The switch loop conformation is stabilized via specific interactions with A1492 and A1493 that, in the case of RF2, involve stacking interactions of W319 of RF2 with A1492 [60,61] (Figure 6A). In



Trends in Biochemical Sciences

**Figure 6. Alternative Rescue Factor A (ArfA) Induces a Closed-to-Open Transition in Release Factor 2 (RF2).** (A) Interaction between Trp319 (W307 in *Thermus thermophilus* RF2) of the switch region of RF2<sub>Stop</sub> (sky blue) and A1492 of the 16S rRNA (yellow) during decoding of the UGA stop codon (cyan; PDB ID: 4V5E) [60]. The switch loop conformation of RF2 (RF2<sub>ArfA</sub>, orange) observed on ArfA binding is superimposed and arrowed. (B) Same view as (A) showing the distinct conformation of the switch loop of *Escherichia coli* RF2 (orange) and A1492/A1493 (pale blue) when ArfA (red) is present. (C) The open conformation of RF2 (orange) in the non-stop complex with ArfA (PDB ID: 5MGF) [12] compared with the closed RF2 conformations observed when using (D) RF2 (pink) in the presence of ArfA A18T (PDB ID: 5MDW) [11], (E) *T. thermophilus* RF2 (blue; PDB ID: 5MDY) [11], or (F) the free RF2 structure (orange; PDB ID: 1GQE) [66], which was aligned with the ribosome-bound RF2 (gray) on the basis of domain 2/4 (d2/4). In (C–F) the P-tRNA (green) is shown for reference.

the cryo-EM structures, ArfA precludes the interaction between the switch loop and A1492 [11–15] (Figure 6B). Instead, ArfA itself appears to stabilize a distinct conformation of the switch loop in RF2 that extends the  $\alpha$  helix  $\alpha$ 7 of domain 3 of RF2 by two to three helical turns, analogous to that observed during canonical translation termination with RF2 [60,61]. As observed for canonical termination [60,61], the open conformation of RF2 on the ribosome in the presence of ArfA also directs the GGQ motif of domain 3 into the PTC (Figure 6C). The A18T mutation that led to the discovery of ArfA does not interfere with ribosome binding [33] or with RF2 recruitment, but prevents PTH [41]. Consistently, the cryo-EM structure of the ArfA–A18T non-stop complex reveals that RF2 is recruited to the ribosome but adopts a closed rather than an open conformation [11] (Figure 6D). The A18T mutation appears to destabilize the interaction of the N terminus of ArfA and the switch loop of RF2, preventing the transition from the closed to the open conformation [11]. A closed conformation of RF2 was also observed when *Thermus thermophilus* RF2 replaced *E. coli* RF2 [11] (Figure 6E), suggesting an incompatibility between *T. thermophilus* RF2 and *E. coli* ArfA (note: *T. thermophilus* does not have an ArfA homolog). The ribosome-bound closed conformations resemble the closed conformation observed previously in the structures of the unbound form of RF2 [66,67] (Figure 6F). The closed conformation may reflect a *bona fide* intermediate during ribosome rescue, since this state represented a major population in the cryo-EM analysis of Demo *et al.* [15], where wild-type RF2 was employed. The open conformation and positioning of domain 3 of RF2 at the PTC observed in the different cryo-EM structures are very similar despite two of

the structures reflecting pre-hydrolysis states (obtained using either a GAQ mutant or a non-hydrolyzable P-tRNA) [11,12] and the other three representing post-hydrolysis states (assembled with **deacylated tRNA** in the P site) [13–15].

### Concluding Remarks

The availability of structures of ArfA and RF2 on the non-stop ribosome has provided much needed mechanistic insight into this bacterial ribosome rescue system and enabled comparisons with the tmRNA/SmpB and ArfB systems to be made. The structures have also provided initial insights into specificity determinants in ArfA and RF2 that allow ArfA to cooperate with RF2 but not RF1; however, this needs to be validated biochemically (see Outstanding Questions). Similarly, the species specificity of ArfA–RF2 action has so far not been addressed systematically. The apparent absence of Arfs in some species where trans-translation is not essential raises the possibility of other novel, unidentified Arf systems. Will novel ArfA or ArfA-like systems emerge in bacteria where RF1, rather than RF2, is recruited to the stalled ribosomes? Perhaps bacteria exist where entirely different GGQ-containing factors (ArfB-like?) or even non-GGQ factors are recruited to non-stop ribosomes to mediate PTH. The wider distribution of ArfB/ICT1 compared with ArfA suggests that it may play a more important role in other bacteria and organelles than it does in *E. coli*. Distinguishing the division of labor of alternative rescue systems in different bacteria will provide much needed insight into their importance under different environmental and stress conditions. The importance of ribosome rescue in bacteria, coupled with the distinct pathways used by eukaryotic ribosomes, suggests that ribosome rescue may be a possible target for the development of novel antimicrobial agents. Small molecules have already been discovered that specifically target trans-translation [68,69]. Can similar approaches be used to identify lead compounds that selectively target the Arf systems?

### Acknowledgments

The work from the Wilson laboratory described in this review is funded by grants from the Deutsche Forschungsgemeinschaft (DFG).

### References

1. Harigaya, Y. and Parker, R. (2010) No-go decay: a quality control mechanism for RNA in translation. *Wiley Interdiscip. Rev. RNA* 1, 132–141
2. Buskirk, A.R. and Green, R. (2017) Ribosome pausing, arrest and rescue in bacteria and eukaryotes. *Philos. Trans. R. Soc. Lond. B Biol. Sci.* Published online January 30, 2017. <http://dx.doi.org/10.1098/rstb.2016.0183>
3. Giudice, E. and Gillet, R. (2013) The task force that rescues stalled ribosomes in bacteria. *Trends Biochem. Sci.* 38, 403–411
4. Shimizu, Y. (2014) Biochemical aspects of bacterial strategies for handling the incomplete translation processes. *Front. Microbiol.* 5, 170
5. Keiler, K.C. (2015) Mechanisms of ribosome rescue in bacteria. *Nat. Rev. Microbiol.* 13, 285–297
6. Himeno, H. et al. (2015) Ribosome rescue systems in bacteria. *Biochimie* 114, 102–112
7. Abo, T. and Chadani, Y. (2014) The fail-safe system to rescue the stalled ribosomes in *Escherichia coli*. *Front. Microbiol.* 5, 156
8. Moore, S.D. and Sauer, R.T. (2005) Ribosome rescue: tmRNA tagging activity and capacity in *Escherichia coli*. *Mol. Microbiol.* 58, 456–466
9. Ito, K. et al. (2011) Nascentome analysis uncovers futile protein synthesis in *Escherichia coli*. *PLoS One* 6, e28413
10. Keiler, K.C. and Feaga, H.A. (2014) Resolving nonstop translation complexes is a matter of life or death. *J. Bacteriol.* 196, 2123–2130
11. James, N.R. et al. (2016) Translational termination without a stop codon. *Science* 354, 1437–1440
12. Huter, P. et al. (2017) Structural basis for ArfA–RF2-mediated translation termination on mRNAs lacking stop codons. *Nature* 541, 546–549
13. Zeng, F. et al. (2017) Structural basis of co-translational quality control by ArfA and RF2 bound to ribosome. *Nature* 541, 554–557
14. Ma, C. et al. (2017) Mechanistic insights into the alternative translation termination by ArfA and RF2. *Nature* 541, 550–553
15. Demo, G. et al. (2017) Mechanism of ribosome rescue by ArfA and RF2. *Elife* 6, e23687
16. Gueneau de Novoa, P. and Williams, K.P. (2004) The tmRNA website: reductive evolution of tmRNA in plastids and other endosymbionts. *Nucleic Acids Res.* 32, D104–D108
17. Brunel, R. and Charpentier, X. (2016) Trans-translation is essential in the human pathogen *Legionella pneumophila*. *Sci. Rep.* 6, 37935
18. Schaub, R.E. et al. (2012) Proteobacterial ArfA peptides are synthesized from non-stop messenger RNAs. *J. Biol. Chem.* 287, 29765–29775
19. Handa, Y. et al. (2011) YaeJ is a novel ribosome-associated protein in *Escherichia coli* that can hydrolyze peptidyl-tRNA on stalled ribosomes. *Nucleic Acids Res.* 39, 1739–1748
20. Moore, S.D. and Sauer, R.T. (2007) The tmRNA system for translational surveillance and ribosome rescue. *Annu. Rev. Biochem.* 76, 101–124
21. Neubauer, C. et al. (2012) Decoding in the absence of a codon by tmRNA and SmpB in the ribosome. *Science* 335, 1366–1369
22. Schmeing, T.M. et al. (2009) The crystal structure of the ribosome bound to EF-Tu and aminoacyl-tRNA. *Science* 326, 688–694

### Outstanding Questions

What are the specificity determinants in ArfA and RF2 that allow only RF2, and not RF1, to be recruited by ArfA to non-stop ribosomes?

Are there other, as-yet-unidentified alternative rescue factor systems in bacteria, particularly in those bacteria where tmRNA does not appear to be essential?

Will ArfA or ArfA-like systems emerge in bacteria where RF1, and not RF2, is recruited to non-stop ribosomes?

What is the role of ArfB? When is ArfB expressed? Is ArfB action more important under specific stress or growth conditions or in different bacterial species?

Is it possible to develop specific antibiotics that selectively target the alternative rescue factor systems?

23. Ogle, J.M. and Ramakrishnan, V. (2005) Structural insights into translational fidelity. *Annu. Rev. Biochem.* 74, 129–177
24. Rozov, A. *et al.* (2016) New structural insights into translational miscoding. *Trends Biochem. Sci.* 41, 798–814
25. Gutmann, S. *et al.* (2003) Crystal structure of the transfer-RNA domain of transfer-messenger RNA in complex with SmpB. *Nature* 424, 699–703
26. Bessho, Y. *et al.* (2007) Structural basis for functional mimicry of long-variable-arm tRNA by transfer-messenger RNA. *Proc. Natl. Acad. Sci. U. S. A.* 104, 8293–8298
27. Cheng, K. *et al.* (2010) tmRNA-SmpB complex mimics native aminoacyl-tRNAs in the A site of stalled ribosomes. *J. Struct. Biol.* 169, 342–348
28. Weis, F. *et al.* (2010) Accommodation of tmRNA–SmpB into stalled ribosomes: a cryo-EM study. *RNA* 16, 299–306
29. Kurita, D. *et al.* (2014) Rejection of tmRNA–SmpB after GTP hydrolysis by EF-Tu on ribosomes stalled on intact mRNA. *RNA* 20, 1706–1714
30. Weis, F. *et al.* (2010) tmRNA–SmpB: a journey to the centre of the bacterial ribosome. *EMBO J.* 29, 3810–3818
31. Ramrath, D.J. *et al.* (2012) The complex of tmRNA–SmpB and EF-G on translocating ribosomes. *Nature* 485, 526–529
32. Huang, C. *et al.* (2000) Charged tmRNA but not tmRNA-mediated proteolysis is essential for *Neisseria gonorrhoeae* viability. *EMBO J.* 19, 1098–1107
33. Chadani, Y. *et al.* (2010) Ribosome rescue by *Escherichia coli* ArfA (YhdL) in the absence of trans-translation system. *Mol. Microbiol.* 78, 796–808
34. Chadani, Y. *et al.* (2011) Trans-translation-mediated tight regulation of the expression of the alternative ribosome-rescue factor ArfA in *Escherichia coli*. *Genes Genet. Syst.* 86, 151–163
35. Garza-Sanchez, F. *et al.* (2011) tmRNA regulates synthesis of the ArfA ribosome rescue factor. *Mol. Microbiol.* 80, 1204–1219
36. Wiegert, T. and Schumann, W. (2001) SsrA-mediated tagging in *Bacillus subtilis*. *J. Bacteriol.* 183, 3885–3889
37. Chadani, Y. *et al.* (2011) *Escherichia coli* YaeJ protein mediates a novel ribosome-rescue pathway distinct from SsrA- and ArfA-mediated pathways. *Mol. Microbiol.* 80, 772–785
38. Handa, Y. *et al.* (2010) Solution structure of the catalytic domain of the mitochondrial protein ICT1 that is essential for cell vitality. *J. Mol. Biol.* 404, 260–273
39. Kogure, H. *et al.* (2014) Identification of residues required for stalled-ribosome rescue in the codon-independent release factor YaeJ. *Nucleic Acids Res.* 42, 3152–3163
40. Zhou, J. *et al.* (2012) Crystal structures of 70S ribosomes bound to release factors RF1, RF2 and RF3. *Curr. Opin. Struct. Biol.* 22, 733–742
41. Shimizu, Y. (2012) ArfA recruits RF2 into stalled ribosomes. *J. Mol. Biol.* 423, 624–631
42. Feaga, H.A. *et al.* (2016) Human cells require non-stop ribosome rescue activity in mitochondria. *PLoS Genet.* 12, e1005964
43. Gagnon, M.G. *et al.* (2012) Structural basis for the rescue of stalled ribosomes: structure of YaeJ bound to the ribosome. *Science* 335, 1370–1372
44. Singarapu, K.K. *et al.* (2008) NMR structure of the peptidyl-tRNA hydrolase domain from *Pseudomonas syringae* expands the structural coverage of the hydrolysis domains of class 1 peptide chain release factors. *Proteins* 71, 1027–1031
45. Duarte, I. *et al.* (2012) Evolution and diversification of the organellar release factor family. *Mol. Biol. Evol.* 29, 3497–3512
46. Hudson, C.M. *et al.* (2015) Islander: a database of precisely mapped genomic islands in tRNA and tmRNA genes. *Nucleic Acids Res.* 43, D48–D53
47. Wesolowska, M.T. *et al.* (2014) Overcoming stalled translation in human mitochondria. *Front. Microbiol.* 5, 374
48. Richter, R. *et al.* (2010) A functional peptidyl-tRNA hydrolase, ICT1, has been recruited into the human mitochondrial ribosome. *EMBO J.* 29, 1116–1125
49. Akabane, S. *et al.* (2014) Ribosome rescue and translation termination at non-standard stop codons by ICT1 in mammalian mitochondria. *PLoS Genet.* 10, e1004616
50. Brown, A. *et al.* (2014) Structure of the large ribosomal subunit from human mitochondria. *Science* 346, 718–722
51. Chadani, Y. *et al.* (2012) ArfA recruits release factor 2 to rescue stalled ribosomes by peptidyl-tRNA hydrolysis in *Escherichia coli*. *Mol. Microbiol.* 86, 37–50
52. Kurita, D. *et al.* (2014) ArfA recognizes the lack of mRNA in the mRNA channel after RF2 binding for ribosome rescue. *Nucleic Acids Res.* 42, 13339–13352
53. Jenner, L.B. *et al.* (2010) Structural aspects of messenger RNA reading frame maintenance by the ribosome. *Nat. Struct. Mol. Biol.* 17, 555–560
54. Sundermeier, T.R. *et al.* (2005) A previously uncharacterized role for small protein B (SmpB) in transfer messenger RNA-mediated trans-translation. *Proc. Natl. Acad. Sci. U. S. A.* 102, 2316–2321
55. Miller, M.R. *et al.* (2011) The role of SmpB and the ribosomal decoding center in licensing tmRNA entry into stalled ribosomes. *RNA* 17, 1727–1736
56. Jacob, Y. *et al.* (2005) Function of the SmpB tail in transfer-messenger RNA translation revealed by a nucleus-encoded form. *J. Biol. Chem.* 280, 5503–5509
57. Zeng, F. and Jin, H. (2016) Peptide release promoted by methylated RF2 and ArfA in nonstop translation is achieved by an induced-fit mechanism. *RNA* 22, 49–60
58. Ivanova, N. *et al.* (2004) Ribosome rescue by tmRNA requires truncated mRNAs. *J. Mol. Biol.* 338, 33–41
59. Asano, K. *et al.* (2005) Competition between trans-translation and termination or elongation of translation. *Nucleic Acids Res.* 33, 5544–5552
60. Weixlbaumer, A. *et al.* (2008) Insights into translational termination from the structure of RF2 bound to the ribosome. *Science* 322, 953–956
61. Korostelev, A. *et al.* (2008) Crystal structure of a translation termination complex formed with release factor RF2. *Proc. Natl. Acad. Sci. U. S. A.* 105, 19684–19689
62. Ito, K. *et al.* (2000) A tripeptide 'anticodon' deciphers stop codons in messenger RNA. *Nature* 403, 680–684
63. Rozov, A. *et al.* (2015) Structural insights into the translational infidelity mechanism. *Nat. Commun.* 6, 7251
64. Jenner, L. *et al.* (2013) Structural basis for potent inhibitory activity of the antibiotic tigecycline during protein synthesis. *Proc. Natl. Acad. Sci. U. S. A.* 110, 3812–3816
65. Youngman, E.M. *et al.* (2008) Peptide release on the ribosome: mechanism and implications for translational control. *Annu. Rev. Microbiol.* 62, 353–373
66. Vestergaard, B. *et al.* (2001) Bacterial polypeptide release factor RF2 is structurally distinct from eukaryotic eRF1. *Mol. Cell.* 8, 1375–1382
67. Zoldák, G. *et al.* (2007) Release factors 2 from *Escherichia coli* and *Thermus thermophilus*: structural, spectroscopic and microcalorimetric studies. *Nucleic Acids Res.* 35, 1343–1353
68. Ramadoss, N.S. *et al.* (2013) Small molecule inhibitors of trans-translation have broad-spectrum antibiotic activity. *Proc. Natl. Acad. Sci. U. S. A.* 110, 10282–10287
69. Alumasa, J.N. and Keiler, K.C. (2015) Clicking on trans-translation drug targets. *Front. Microbiol.* 6, 498
70. Neubauer, C. *et al.* (2009) The structural basis for mRNA recognition and cleavage by the ribosome-dependent endonuclease RelE. *Cell* 139, 1084–1095
71. Crooks, G.E. *et al.* (2004) WebLogo: a sequence logo generator. *Genome Res.* 14, 1188–1190